8-2015

Experimental and Ab initio Computational Study of Azobenzene and Several of its Derivatives

Mohammadreza Rezaee
University of Tennessee - Knoxville, mrezaee@vols.utk.edu

To the Graduate Council:

I am submitting herewith a dissertation written by Mohammadreza Rezaee entitled "Experimental and Ab initio Computational Study of Azobenzene and Several of its Derivatives." I have examined the final electronic copy of this dissertation for form and content and recommend that it be accepted in partial fulfillment of the requirements for the degree of Doctor of Philosophy, with a major in Physics.

Robert Compton, Major Professor

We have read this dissertation and recommend its acceptance:

Marianne Breinig, Shawn R. Campagna, Joseph Macek

Accepted for the Council:

Carolyn R. Hodges

Vice Provost and Dean of the Graduate School

(Original signatures are on file with official student records.)

Experimental and Ab initio Computational Study of Azobenzene and Several of its Derivatives

A Dissertation Presented for the

Doctor of Philosophy

Degree

The University of Tennessee, Knoxville

Mohammadreza Rezaee

August 2015

To my parents

Acknowledgements

I greatly appreciate Dr. Robert N. Compton's kind attention and help during this extremely difficult time. Without his help and trust this was not possible. I am thankful to Dr. Peter B. Armentrout for his kind help with experimental collision induced dissociation data analysis part and many helpful discussions. I am also grateful to Dr. John E. Bartmess which he helped us with computational challenges.

Abstract

In this dissertation we studied azobenzene and seven of its derivatives experimentally in addition to comprehensive *ab initio* computational investigation. Gas phase ion chemistry studies sre a rich and important area of chemical physics. We used an energy resolved collision induced dissociation technique to study the chemical bonding of these molecule negative or positive ions. We studied the fragment ions which we have detected in the mass spectrum computationally as well. Doing so we experimentally measured the bond dissociation energies and compared them with those resulting from the quantum chemistry computations. We also performed other experiments such as Raman spectroscopy, NMR spectroscopy and UV-Vis spectroscopy to experimentally study the electronic structure of these molecules. We have utilized state of the art computational algorithms such as high accuracy multi-level calculations to study thermochemical properties of the parent neutral molecules as well as precursor and fragment negative and positive ions and neutrals. We have calculated electron affinities and compared results from different methods such as density functional theory methods and perturbative methods such as MP2 with multi-level high accuracy calculations to compare their performances. Many high accuracy multi-level calculations which we have done results compared with the experimental results can provide an accurate benchmark for comparing the performance of different theoretical methods for different molecules and ions. Comparing our experimental results for electron affinities and bond dissociation energies with theoretically obtained results, we have proved the ab initio computational results can be accurate and close to those can be measured experimentally.

Table of Contents

List of Tables

List of Figures

List of Abbreviations

BIRD – Blackbody Infrared-Radiative Dissociation

CID – Collision-induced dissociation

CE – Collision energy

DOF – Degrees of Freedom

ESI – Electrospray Ionization

$H^{\ddagger}$ – enthalpy of activation

IRMPD – Infrared Multiphoton Dissociation

k – rate constant

k_B – Boltzmann's constant

KER – Kinetic Energy Release

MS/MS – Tandem Mass Spectrometer / Tandem Mass Spectrometry

RRK – Rice-Ramsperger-Kassel reaction rate theory

RRKM – Rice-Ramsperger-Kassel-Marcus reaction rate theory

TCID – Threshold Collision-Induced Dissociation

ZPE – Zero Point Energy

SY – Survival Yield

T – Temperature

aug-cc-pVnZ Augmented, correlation-consistent, polarized valence n zeta basis sets,

where n = double (D), triple (T), quadruple (Q)

B3LYP Becke 3-parameter (exchange), Lee, Yang and Parr (correlation) DFT functional

BDE - Bond Dissociation Energy

CBS - Complete Basis Set

CC - Coupled Cluster theory

CCSD(T) - Coupled Cluster Singles, doubles, and perturbative triples

CI - Configuration Interaction

D_0, 0K Total Atomization or dissociation energy

DFT - Density Functional Theory

AEA – Adiabatic Electron affinity

eV – electron Volts

EA - Electron Affinity

ΔE_{ZPE} - Zero point energy correction to the total atomization energy

Gn - Gaussian-n theory, n = 2, 3

Gn(MP2) - Gn calculation using a reduced Møller-Plesset order

$\Delta H_{f,0K}$ - Heat of formation at 0 K

$\Delta H_{f,298K}$ - Heat of formation at 298 K

HF - Hartree-Fock

ΔH_{rxn} - Reaction enthalpy change

MO - Molecular Orbital

MP2 - 2nd order Møller-Plesset perturbation theory

NBO - Natural Bond Order

NIST - National Institute of Standards

NMR - Nuclear Magnetic Resonance

ΔS - Entropy change

SCF - Self-Consistent Field

VDE – Vertical Detachment Energy

VEA – Vertical Electron Affinity

ZPVE – Zero Point Vibrational Energy

NBO – Natural Bond Orbital

EA – Electron Affinity

BDE – Bond dissociation Energy

μ - Reduced mass

σ - Cross section

APA – Adiabatic Proton Affinity

PES – Potential Energy Surface

ORD – Optical Rotatory Dispersion

Chapter 1 / Introduction

1.1 Introduction

Understanding the electronic structure of molecules and their corresponding ions is extremely important to reveal different aspects of their possible applications and provide us valuable physical and chemical information. In this regard quantum chemistry calculations represent a versatile tool and over many years these calculations have reached a point that the results can be considered as accurate as experiment. The areas of physics and chemistry which can be explored and studied utilizing computational quantum chemistry are vast. In this dissertation we mostly focus on molecular and thermochemical properties such as electron affinities, vertical detachment energies, proton affinities and bond dissociation energies of azobenzene and some of its derivatives. We also study some of the optical properties of molecules of interest by utilizing experimental methods such as UV-Vis spectroscopy, Raman spectroscopy, circular dichroism spectroscopy and optical rotatory dispersion. In many cases theoretical calculations are compared with experimental results for completeness. Ab intio calculations are necessary to make sense of the CID experiments. Ab initio calculations can provide the vibrational frequencies and rotational constants which are needed to evaluate the internal energy of the reactant complex and required for the statistical calculations of rate constants used to estimate kinetic and competitive shifts.[1]

Our main focus in this dissertation was the study of negative ions of the azobenzene molecule and some of its derivatives. In general negative ions and computational studies related to such complex molecules are challenging topics in theoretical chemistry. Selecting the best method for calculation and appropriate basis set is important to obtain reliable and accurate results. We must consider the fact that the extra electron often is loosely bound and occasionally further away from the parent molecule (dipole bound anions) and the basis set should reliably address this diffuse nature of such diffuse orbitals and remote electrons. In the Pople basis set we can address this by adding the ++

sign before the basis set, i.e. 6-311++G(2d,2p). Only one, +, plus adds diffuse s and p functions for non-hydrogen atoms and ++ add diffuse function for hydrogen atoms as well. The Dunning basis set use the abbreviation "aug" before the basis set name which stands for augmented such as aug-cc-pVTZ. In general basis sets are mathematical functions we use to explain the molecular orbitals. Not all of the available theoretical chemistry methods are cable to take into account the nature of how the extra electron is bound and the fact that negative ions can be temporary and in some cases they are not even stable or in case of dipole bound anions barely bound with energies in order of magnitude of few milli electron volts. Because temporary anion states lie in the continuum of the neutral species plus free electron, they cannot be treated in general by means of a straightforward variational calculation.[2] Often in studying negative ions we are calculating very small energy differences between the ground state of the neutral and the negative ion and if we want the calculated values to be reliable, we need to use high level, high accuracy theoretical methods which are capable of treating the complications which occur upon addition of an extra electron. This of course comes with a high price of computational power resources. That means we need long computational hours which can be months in case of large size molecules such as the molecules which we studied in this thesis. Methods such as coupled clusters CCSD[3-5] and its triple excitation variation, CCSD(T)[4, 6, 7], which do take into account electron correlation and quadratic configuration interaction QCISD[8], corrects for size-consistency errors in single and double excitation CI methods (CISD), which is a variation of the configuration interaction (CI) method and its triple excitation version[9, 10] can yield reliable results for electron affinities and other properties related to negative ions. Also high accuracy energy calculation methods such as high accuracy complex energy computations, Gaussian Gn[11-14] algorithms (G1, G2, G3, G4) and their variations such as G2MP2, G3MP2, G3MP2B3 and G4MP2[15] can result in highly reliable electron affinities and other thermochemical properties. All of these methods take into account electron correlation and do the optimizations at lower level but add the correlation calculated using MP2 or MP4 and QCI level of theory to the final results. They usually consider all electrons in energy calculations and also the scaled zero-point energy (ZPE) is calculated and added which drastically improves the accuracy for subtle purposes such as negative ions. In order to have an exact solution for the electronic energy of a molecule, we need to solve the Schrodinger equation for an infinitely large size basis set but we know this is practically impossible. That being said, we do have methods such as Complete Basis Set (CBS) methods[16-19] which emulate an infinitely large size basis set.

There several variation of this available for computations using the Gaussian computational program such as 4M, QB3 and APNO. We mostly used the CBS-QB3 method for our high level calculations. The APNO (Atomic Pair Natural Orbital) version is the most accurate method in the CBS family. CBS-APNO can calculate the heat of formation with an average error of 0.5 kcal/mol. The reason we used the QB3 version is that it is much faster (APNO is almost twice as accurate as QB3). When we use these predefined methods, it is not necessary to specify any keyword or basis set except for the method name. The other family of computational methods in this regards which are capable of calculating energy with accuracy of 0.3 kcal/mol is the Weizmann family[20, 21] (W1U, W1BD and W1RO). The W1U keyword specifies the W1 method modified to use UCCSD instead of ROCCSD for open shell molecules.[22] The Wizmann 1[20] (W1) and Wizmann 2 (W2) methods use extrapolations to complete the basis set treatment for SCF and correlation energies. The accuracies of the W-methods are in the order of magnitude of 0.24 kcal/mol for thermochemical properties. The accuracy of this method results from using a large and diffuse basis set such as cc-pV5Z + 2d1f and using methods like CCSD and CCSD(T) for energy calculations. This method is extremely time consuming and we were able to only perform this type calculations for one of the fragment anions, $[C_6H]^-$. The average error in calculation of enthalpies of formation using G2 method is 1.6 kcal/mol and this is as small as 0.9 kcal/mol for G3[23] method. G3 is almost twice as fast as G2 and more accurate than G2.[24] A particular feature of the CBS method which makes it particularly interesting for our purposes is the inclusion of an empirical correction for spin contamination in open shell molecules for which unrestricted treatment sensitive to this contamination are used.[24] We should emphasize that in order to have an accurate and reliable value for a theoretical electron affinity we need to use a large basis set with diffuse functions. Electron affinities and ionization potentials theoretically obtained by using these multilevel calculations, such as the ones we mentioned above, are accurate on the order of less than 1 kcal/mol. In addition to multi-level calculations we used density functional methods to calculate the electron affinities, proton affinities as well as bond dissociation energies. Density functional methods[25, 26] are fast and reliable results for electron affinities and can be obtained provided that we use a suitable basis set and increase the accuracy of calculations using tight convergence criteria for the optimization process and during the self-consistent field (SCF) procedure. Instead of dealing with wave function or probability density in this work, we use the electron density and integrate over that to represent the total number electrons and take into account electron-electron interactions as well as the

electron interaction with a positive potential which mimics the nuclei. The Hohenberg-Kohn-Sham theorem is one of the main foundation of this theory which states that the ground-state energy of a many-body system is a unique functional of the electron density. The exact exchange (HF) for a single determinant is replaced by a more general expression, the exchange-correlation functional which can include terms accounting for both the exchange and the electron correlation energies.[22] We extensively used methods such as B3LYP, different variation of wB97[27, 28] which include long range corrections and hybrid functional M06[29] methods in order to optimize the molecular structures and obtain their thermodynamically properties. Through these methods we have attempted to obtain reliable and accurate values for electron affinities, proton affinities and bond dissociation energies. Performing these ab initio computations is absolutely necessary to make sure the experimental results for BDE which are obtained from CID experiments make sense and are in a reasonable agreement.

Jack Simons et al.[2] introduced these expressions for the exact nonrelativistic electron affinity (EA) and ionization potential (IP):

$$EA = -\varepsilon_{\alpha} - E_{-}(R) + XE_{EA}(corr) \quad (1.1)$$

$$IP = -\varepsilon_{i} - E_{+}(R) + XE_{IP}(corr) \quad (1.2)$$

where $XE_{IP}(corr)$ is $E_{+}(corr) - E_{N}(corr)$ and $XE_{EA}(corr) = E_{N}(corr) - E_{-}(corr)$ are the correlation corrections to the IP and EA, respectively. ε_i and ε_{α} are related to Koopmans' theorem (KT) approximations to the EA and ionization potential (IP) according to:

$$IP_{KT} = E_{+}(KT) - E_{N}(SCF) = -\varepsilon_{i} \quad (1.3)$$

$$EA_{KT} = E_{N}(SCF) - E_{-}(KT) = -\varepsilon_{\alpha} \quad (1.4)$$

where ε_i and ε_{α} are respectively the energies of the appropriate occupied and unoccupied orbitals of the neutral molecule. In the case of negative ions, the correlation energy difference, $E_{EA}(corr)$, is usually positive but now the relaxation correction enters as a positive quantity. The result is that the correlation and relaxation corrections tend to reinforce in the EA case.[2] The webbook of NIST introduced the following definition for the electron affinity: it is equal to the energy difference between the enthalpy of formation of a neutral species and the enthalpy of formation of the

negative ion of the same structure or the negative of the 0 K enthalpy change for the electron attachment reaction:[30-32]

$$M + e^- \rightarrow M^-; \quad \Delta H_{rxn} = -EA \tag{1.5}$$

$$-EA = \Delta_f H(M^-) - \Delta_f H^0(M) - \Delta_f H(e^-) \tag{1.6}$$

Within the limitations of the HF, frozen orbital model, the ionization potentials (IPs) and electron affinities (EAs) are given as the negative of the occupied and virtual spin-orbital energies, repectively.[33]

The other main aspect of this dissertation is the experimental investigations on the negative ion of azobenzene molecule and some of its derivatives. The major experimental portion is the collision induced dissociation (CID) experiments. CID experiments description according to IUPAC[34] is an ion/neutral species interaction wherein the projectile ion is dissociated as a result of interaction with a target neutral species. This is brought about by conversion of part of the translation energy of the ion to internal energy in the ion during collision. In all of our experiments the neutral reactant was argon atom. Originally we were interested in collision induced dissociation (CID) experiments on cis and trans isomers of this interesting light sensitive molecule and we were predicting that due to the considerable difference in ground state electronic energy between the cis and trans isomer we might be able to detect this difference in CID experiment threshold energy measurements. Even though this experiment was attempted many times using different approaches to generate the cis isomer of azobenzene and its fluorinated derivative, tetrafluoroazobenzene, (using high power, 2 W, green LED light source or second harmonic of Nd-YAG laser) we were unable to detect difference in the threshold energy from the CID experiments. This might be simply due to the inherent high temperature of the ion source used at atmospheric pressure and/or the small energy difference between the ground state of cis and trans is not large enough to be detected using this method. Other experiments such as NMR spectroscopy and UV-Vis spectroscopy results clearly showed the trans to cis isomerization happens successfully. Using a high power (2W) green LED it takes almost 20 minutes to convert more than 90% of trans tetrafluoroazobenzene to cis isomer. One of the challenges in CID experiments is the ability to ionize the molecule of interest. This is basically step one in the experimental procedure. Our initial efforts to make negative ions of azobenzene using the electro spray ionization (ESI) method was not successful. Electrospray

mass spectrometry (ESMS) is a technique that allows ions present in solution to be transferred to the gas phase with minimal fragmentation, followed by conventional ion-molecule techniques and eventual mass-spectrometric characterization.[35] Consequently we changed the ionization method to atmospheric pressure chemical ionization (APCI) method which is a somewhat more direct method compared with ESI. APCI generates the ions at high temperature (300-500 ºC) and by vaporizing the sample before electron attachment occurs. The heated nebulizer source which we used generates the ions by first nebulizing the sample in a heated tube and vaporize the sample drops while in keeps the sample molecule structure intact. The sample and solvent molecules which now are in gas phase after being vaporized are transported by help of an axillary gas (nitrogen in our case) in a second tube.

Azobenzene or 1,2 - Diphenyldiazene, (C6H5)–N=N–(C6H5), with an average mass of 182.221 Da and monoisotopic mass182.08 Da can change its geometry and undergo cis/trans isomerization upon irradiation with light with proper wavelength. It is envisaged that inversion proceeds *via* a linear transition state (TS) in which the N–N double bond remains intact, whereas rotation proceeds *via* a twisted transition state in which the N–N p-bond is broken. Frequently the interpretation of experimental data has been based on the argument (from resonance structures) that the rotational TS would be dipolar but the inversion TS would not.[36] The absorbed photon can excite an electron from the ground state to a π^* orbital. According to the Britannica Encyclopedia, most aromatic azo compounds are prepared by the reaction of a diazonium salt with an organic substance that contains easily replaced hydrogen atoms.[37] Azobenzene which has been known for centuries now has interesting and novel applications besides being used as a commercial dye. It can be used as a photochromic switch and data storage material. Recently its applications in biology and biophysics has been studied intensively. First described by the German chemist Eilhard Mitscherlich[38] in 1834, azobenzene and its derivatives include more than 70% of commercial dyes owing to their vibrant, chemically tunable colors and extreme durability even upon continuous irradiation.[39] Azobenezene and its derivatives are photo-responsive and its cis/trans geometry can be mechanically changed upon irradiation, making them excellent candidates for photo-switching. Photochromic switches that are able to quickly transmit information have attracted a growing interest because of their potential applicability as active data storage and communication elements in many devices, such as optical systems for opto-electronics, holographic materials and multi-color displays during the last few decades.[40] The cis

isomer of azobenzene has been known since 1937 when Hartley[41] performed photometric studies of azobenzene and observed that the solubility of azobenzene changed after being irradiated with sunlight. The photo-isomerization can change the geometry of azobenzene from trans to the thermodynamically less stable cis isomer quickly using UV light (300-400 nm) and the backward reaction occurs using light (visible blue light > 400 nm) or thermally on the timescale of minutes.[42] Azobenzene and its derivatives have attracted much interest because of the large-amplitude structural changes between their cis and trans isomers, the reversibility of their transformations and since high photo-stabilities guarantee large numbers of switching cycles.[43] The azobenzene family represents promising candidates for future molecular switches, light harvesting materials, photonic devices, and photo-controllable materials.[44] They also have remarkable biological applications such as the ability to remotely control the cellular functions.[45] Designing an azobenzene amino acid opens the possibilities for biological incorporation of photo-switches *in situ*.[46] Azobenzene doped polymers and liquid crystals have fascinating potential applications in biology, photonic, biophysics, nonlinear optics that have been intensively investigated.[47-49] Fluorinated azobenzene derivatives have been recently synthesized and analyzed. Bushuyev et al.[50] studied fluorinated azobenzene and showed that these solids can directly convert visible light into mechanical motion with high isomerization efficiency and chemical stability under multiple isomerization cycles. Functionalizing azobenzene eliminates the need for employing UV light for photo-switching making it more thermally stable and favorable in bio-applications. Recently Gan et al.[51] studied a series of fluorinated azobenzene esters and found that trans–cis isomerization occurs after 4 minutes and cis–trans isomerization occurred after 22 hours under the same conditions. Cis azobenzene can convert to trans isomer by absorbing photon or by heating it since the cis isomer is thermodynamically less stable than the trans isomer. In chapter 2 we will discuss the theoretically calculated properties of azobenzene itself and 7 other azobenzene derivatives.

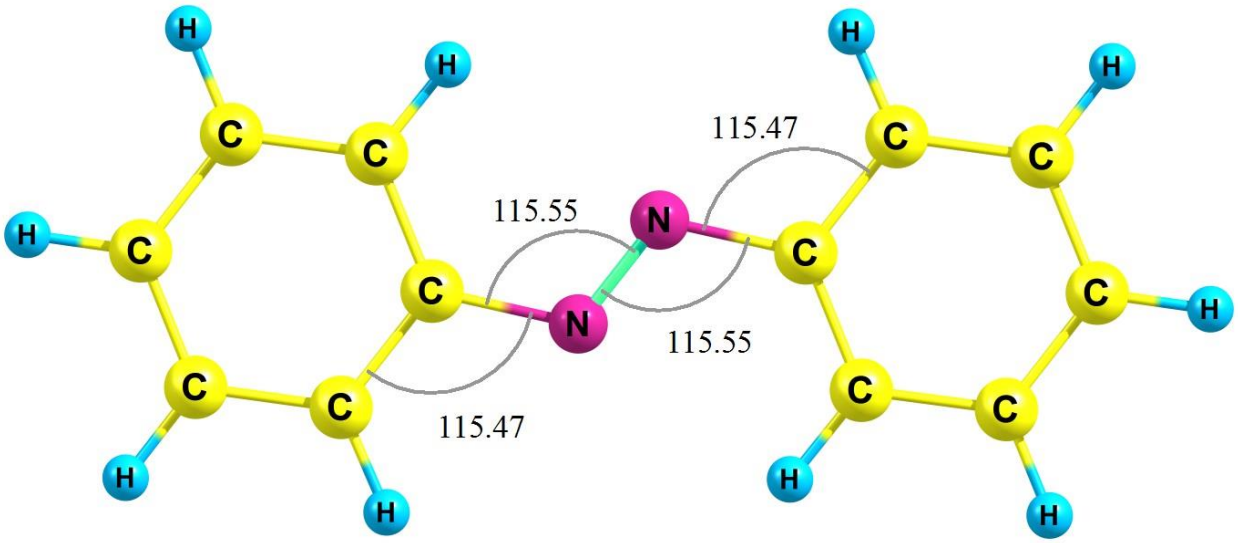

Figure 1.1: Trans azobenzene geometry which is optimized at B3LYP level of theory with aug-cc-pVTZ basis set. The bond angles are shown and CCNN dihedral angle and CNNC are both 180.0 which indicates this molecule in neutral form is planar. Dipole moment of this molecule is 0 Debye.

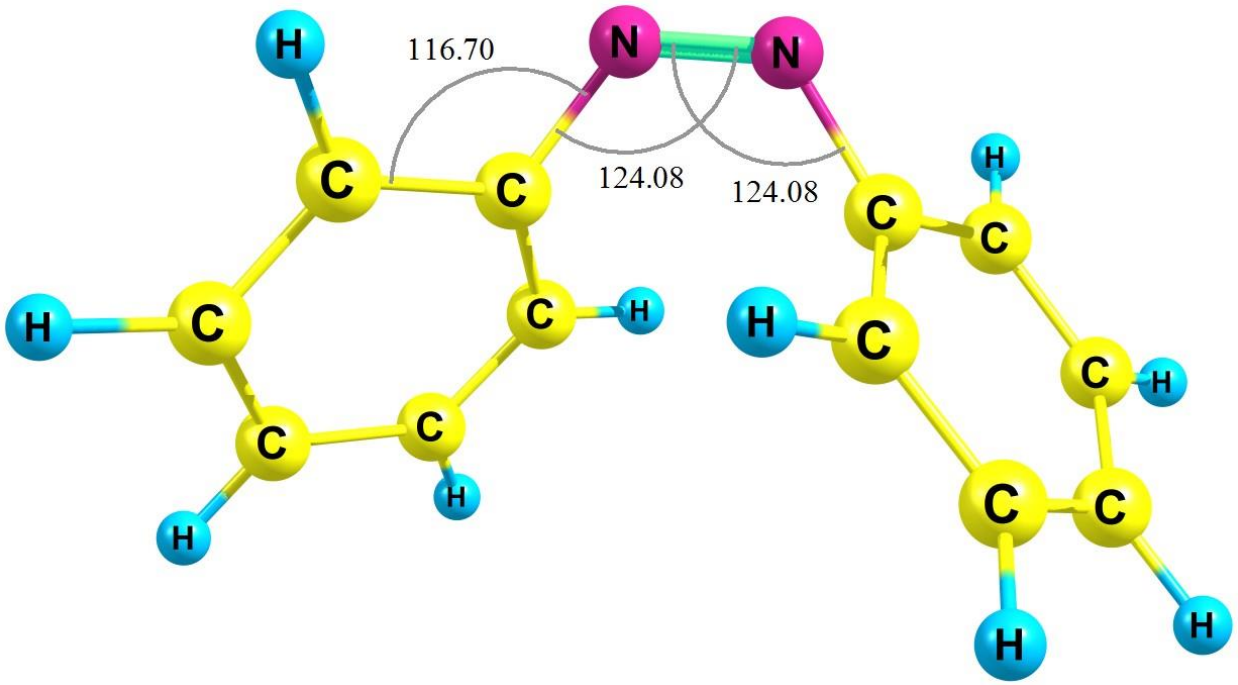

Figure 1.2: cis azobenzene geometry optimized at B3LYP level of theory with 6-311++G(2d,2p) level of theory. Dipole moment is 3.2 Debye and CCNN dihedral is 136.9 degree and CNNC dihedral is -9.1 degree.

We have performed CID experiments and theoretical calculations for 8 different samples including azobenzene ($C_{12}H_{10}N_2$), 2,2́,6,6́-tetrafluoro-azobenzene ($C_{12}H_6N_2F_4$), (2,2',6,6') tetramethyl-(4,4') dinitro-azobenzene ($C_{16}H_{16}N_4O_4$), (4,4') dinitro-azobenzene ($C_{12}H_8N_4O_4$), (2,2',6,6') tetramethyl-azobenzene ($C_{16}H_{18}N_2$), 4-Methoxyazobenzene ($C_{13}H_{12}N_2O$), 2,4-Dihydroxyazobenzene,4-(Phenylazo) resorcinol ($C_{12}H_{10}N_2O_2$), 4-Dimethylamino-2-methylazobenzene ($C_{15}H_{17}N_3$). We studied the electronic structure of the cis and trans isomers for the neutral, positive and negative ions of these precursors and their fragments by means of quantum chemistry calculations. The rigid mesogenic shape of the molecule is well suited to spontaneous organization into liquid-crystalline phases, and hence polymers doped or functionalized with azobenzene-based chromophores (azo polymers) are common as liquid-crystalline media.[52]

Figure 1.3: Trans isomer structures of the samples we have studied in this dissertation. These structures are all optimized at B3LYP level of theory by using 6-311++G(d,p). (a) azobenzene (b) 2,2́,6,6́-tetrafluoro-azobenzene (c) (2,2',6,6') tetramethyl-(4,4') dinitro-azobenzene ($C_{16}H_{16}N_4O_4$) (d) (4,4') dinitro-azobenzene ($C_{12}H_8N_4O_4$) (e) 2,2',6,6'tetramethyl-azobenzene ($C_{16}H_{18}N_2$) (f) 4-Methoxyazobenzene ($C_{13}H_{12}N_2O$) (g) 2,4-Dihydroxyazobenzene,4-(Phenylazo) resorcinol ($C_{12}H_{10}N_2O_2$) (h) 4-Dimethylamino-2-methylazobenzene ($C_{15}H_{17}N_3$).

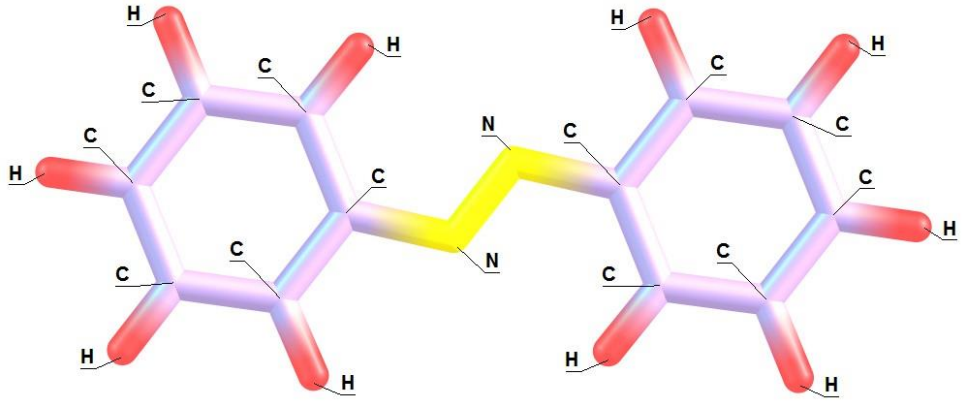

(a)

(b)

Figure 1.3: continued

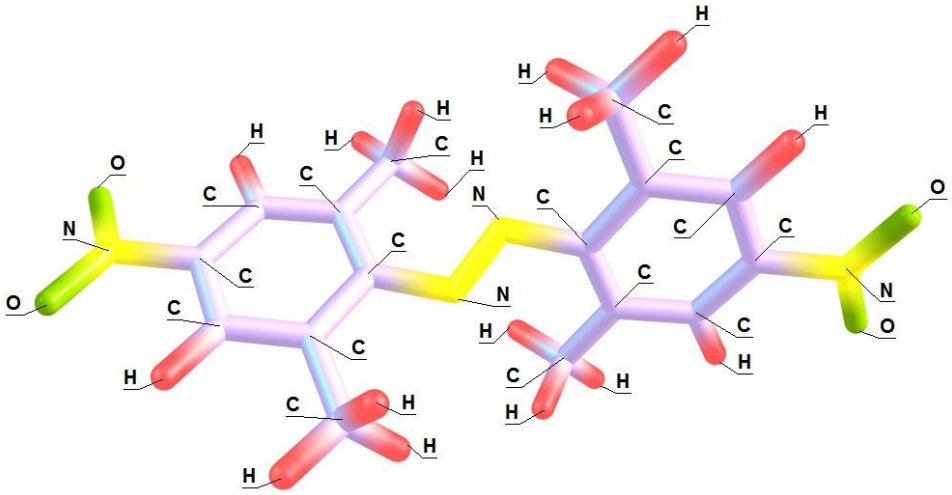

(c)

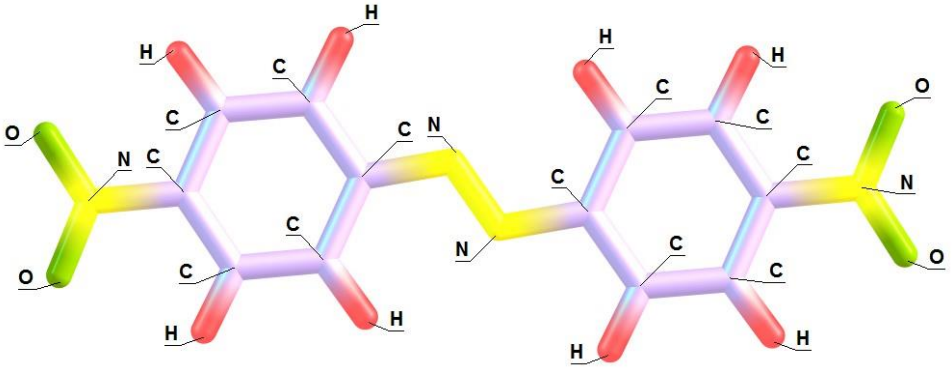

(d)

Figure 1.3: continued

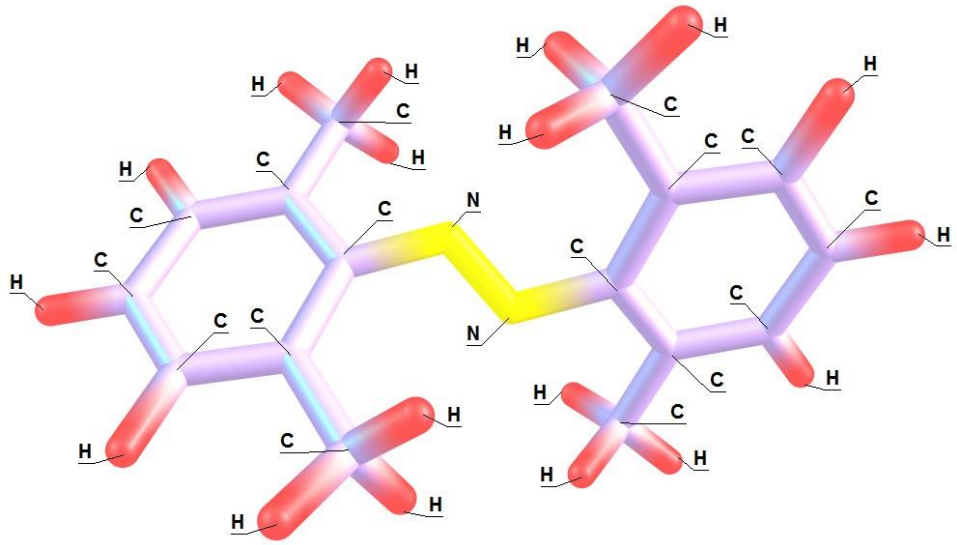

(e)

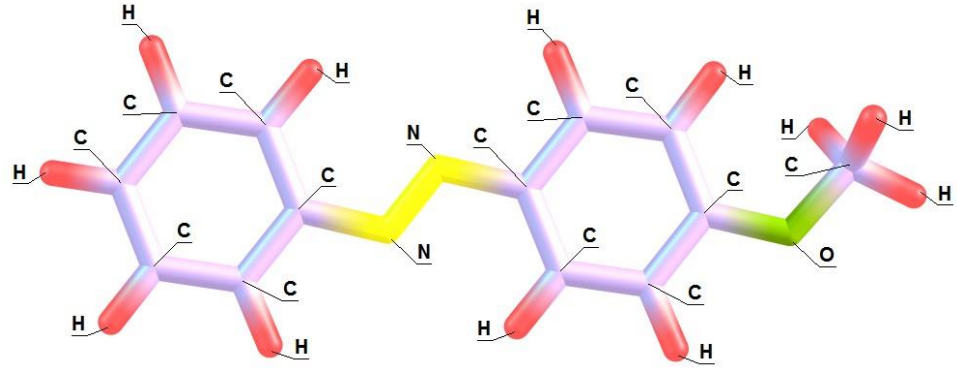

(f)

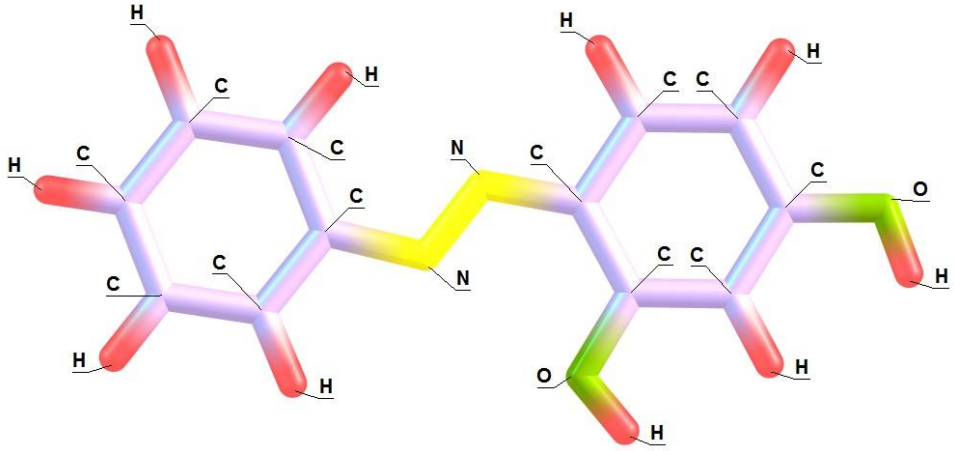

(g)

Figure 1.3: continued

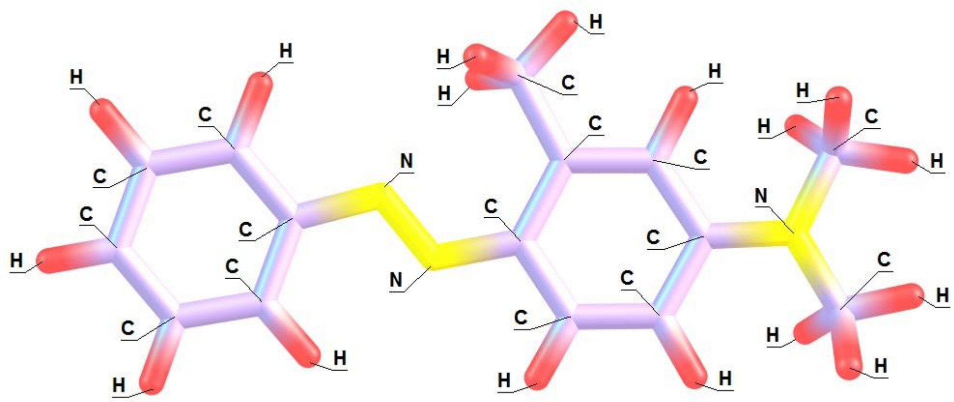

(h)

Figure 1.3: continued

High accuracy thermochemistry information including bond dissociation energy can be obtained from threshold collision induced dissociation experiments by analyzing the kinetic energy dependence of the dissociation reactions. Chemistry is fundamentally about making and breaking bonds,[53] so having accurate information in that regard is highly desirable. We used the AB SCIEX QSTAR Elite Hybrid LC/MS/MS apparatus which is a hybrid quadrupole time-of-flight mass spectrometer available in the chemistry department, UTK for all our experiments without any further modification. The precision and stability of this instrument allowed us to preform highly accurate and reliable accurate mass measurements of the precursor and fragment ions in the CID experiments. The voltage which determines the translational kinetic energy of the precursor ions can be changed in 0.1 V increment which is highly desirable in energy resolved collision induced dissociation experiment. We also can precisely control the pressure in the cell. The instrument is equipped with automatic syringe which can infuse the sample to the instrument with a desired rate. The steady rate of spray of solution is important to enter the mass spectrometer with a steady rate since we are measuring the intensities of precursor and fragment ions. CID type experiments which we will discuss in details in chapter 3 are straightforward experiments which can be a source of valuable thermodynamic information for different molecules if the experiment is done carefully and the appropriate procedures before and after data acquisition is done correctly step by step. In general CID experiments must be done at different pressure of collision gas and the precursor and fragment ion intensities must be extrapolated to the zero pressure condition (perhaps even a linear

extrapolation would result in most reliable results) and the cross sections of collision must be obtained under single collision condition. Multiple collisions definitely will render the threshold energy and the resulting bond dissociation energy unreliable. The problem due to multiple collisions along with added effects such as kinetic shift and Doppler broadening, makes it complicated to predict and quantify the effects of multiple collisions. Many other aspects should be taken into account such as the Doppler broadening and the internal energy of the anions, cations and the neutral target. We utilized the CRUNCH[54, 55] program and also the L-CID[56] program to extract the true threshold value for the dissociations. The CRUNCH program is state of the art in CID data analysis and it has been developed over many years by the Dr. Peter B. Armentrout group and L-CID code developed by Bach et al. at the Laboratory of Organic Chemistry ETH Zürich. We will discuss them in chapter 3 in some detail. L-CID uses a single effective frequency with a new model for the density-of-states function and eliminates the need to explicitly calculate the frequencies for the parent ion and the transition state. CID reactions are in general described as unimolecular reactions. There might be an energy barrier between the reactants and products which lead to tight transition state and there might be rearrangements in the product molecules or the reaction might be simply a bond cleavage and no energy barrier between reactants and products. We have encountered both types of bond dissociation in our experiments. Simple bond cleavage can occur which leaves the product intact with similar structure as the product. Also some experiments provide evidence that the fragment ions and neutrals exhibit rearrangement. Cis-trans isomerization reactions are another example of unimolecular reactions. The newest theoretical approaches to the unimolecular reaction is the RRKM theory (Rice–Ramsperger–Kassel–Marcus theory) which we will explain and discuss in details in chapter 3. RRKM is a microcanonical transition state theory which is described in details by Tomas Baer et al.[57] The RRKM theory includes quantum mechanical considerations in treating the unimolecular reactions along with different modes of energy available for the reaction. We have not wrote the code or algorithms in this regards but used the available programs which have been developed based on RRKM theory such as CRUNCH in performing the data analysis and the procedure to obtain the threshold energy of the dissociations.[1, 58, 59]

Chapter 2 / Computational Quantum Chemistry

2.1 Introduction to Computational Quantum Chemistry

Computational chemistry is an extremely important approach in today's chemical physics research and plays a major role in many different areas of science and technology. From designing new molecules for light harvesting to understanding how molecules move into and exit living cells. The rapid expansion of the computational chemistry society, codes and dedicated academics groups are good indicators of the vast capabilities of theoretical and computational chemistry. Sophisticated codes and methods are being developed all around the globe to simulate and predict the structure and properties of new materials before being synthesized in any laboratory. We can calculate chemical and physical properties of materials with accuracies close to the best available experimental values. These codes and methods, along with powerful computing machines, can solve the quantum mechanical problems, which are not an easy task even for a simple atom, for big molecules and predict their physical and chemical properties and structure. This new and exciting field has been explored extensively ever since the appearance of computers. Ab initio electronic structure calculations were first beginning to be carried out roughly 40 years ago, and since that time, all parts of theoretical chemistry have developed links to computation.[60] FORTRAN was primarily the initial language of computational chemistry but today C++ and Python are strong competitors. Most of these codes include the Hartree–Fock (HF) and some post-Hartree–Fock methods such as Coupled Cluster methods like CCSD, density functional methods and Moeller-Plesset perturbation (MPn) theory methods. In general we can categorize different quantum chemistry techniques into molecular mechanics, semi-empirical and ab initio methods. We used the molecular mechanics method as an initial optimization approach but for all other

calculations we employed ab initio techniques. For all of our calculations we used the Gaussian 09 quantum chemistry package.[61]

Computational chemistry is capable of investigating complicated chemical and physical problems on a computer with inexpensive to moderate price. It usually involves computing the correct molecular geometry with lowest possible energy. This ground state includes electronic energy as well as rotational and vibration energies. We also can compute and visualize molecular orbitals and quantify their energy levels. We can compute the zero point energy following a frequency analysis which also can yield the infrared (IR) spectrum. TD-DFT type calculations can yield UV-Vis spectrum of a molecule and some of the quantum chemistry packages have the capability to simulate the spectrum in different environments. For these calculations usual organic solvents are often available as defaults which can be added to the calculation. Thermochemical and physical properties of materials are perhaps the most important information which we can infer from computational quantum chemistry calculations since they are often very delicate to measure experimentally.

2.2 Potential Energy Surface:

Most of what we do in computational quantum chemistry starts with exploring the potential energy surface. The potential energy surface displays the relation between energy of a molecule or an ensemble of molecules as a function of its geometry. It is a mathematical function that shows energy as a function of change in any of the degrees of freedom. The central assumption here is the Born–Oppenheimer approximation. We can use this approximation simply because electrons are much lighter than nuclei. We can assume the nucleus stays stationary during the short time which it takes for an electron to move. This approximation makes life much easier and possible to apply quantum mechanics fundamentals to a molecule by allowing us separate the electronic and nuclear motion. The Born–Oppenheimer approximation makes it possible to apply the Schrodinger equation to a molecule. Figure 2.1 is a picture of a two dimensional potential energy surface for trans-tetrafluoroazobenzene in which the C-N bond has been increased 0.04 Angstrom in 140 steps. We can clearly see how the total energy of molecule increases by moving further and further

from the equilibrium point. This simple example can illustrate how change in bond length, bond angle or dihedral angle can change the total molecular energy. Transition states are basically saddle point on the PES.

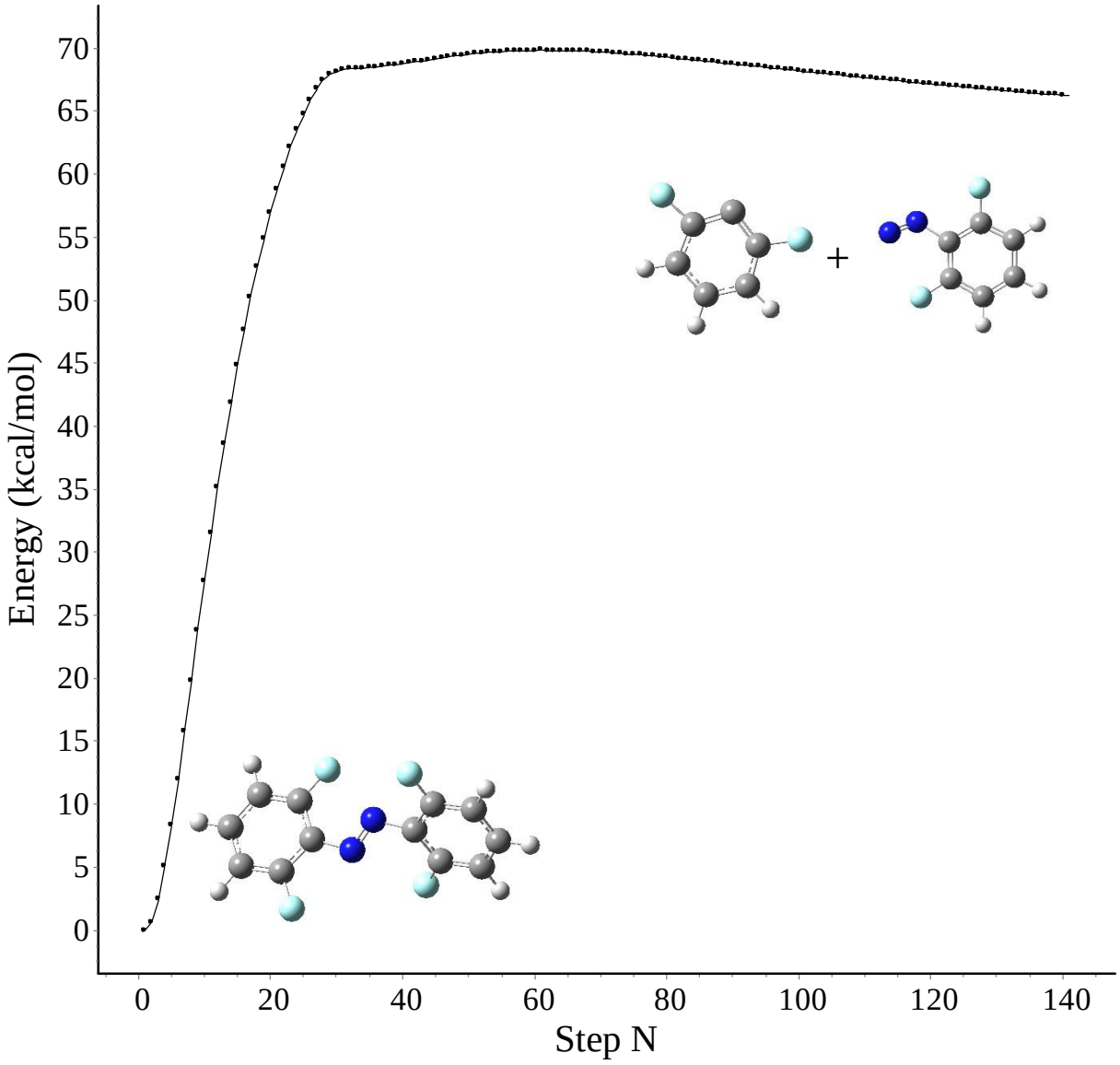

Figure 2.1: Two dimensional potential energy surface scan for the 2,2́,6,6́-tetrafluoroazobenzene anion when we increase the C-N bond length until it dissociate to $[C_6H_3F_2]^-$ and $C_6H_3N_2F_2$.

Here is another example of scanning potential energy surface and how it helps to understand the nature of a reaction. We scanned the potential energy surface for the dissociation of $C_6H_3N_2F_2$ to

a N_2 fragment and $C_6H_3F_2$. Figure 2.2 clearly visualizes how this reaction requires to overcome a barrier of almost ~ 0.56 eV and the products are ~ 0.3 eV higher in energy comparing to the reactants.

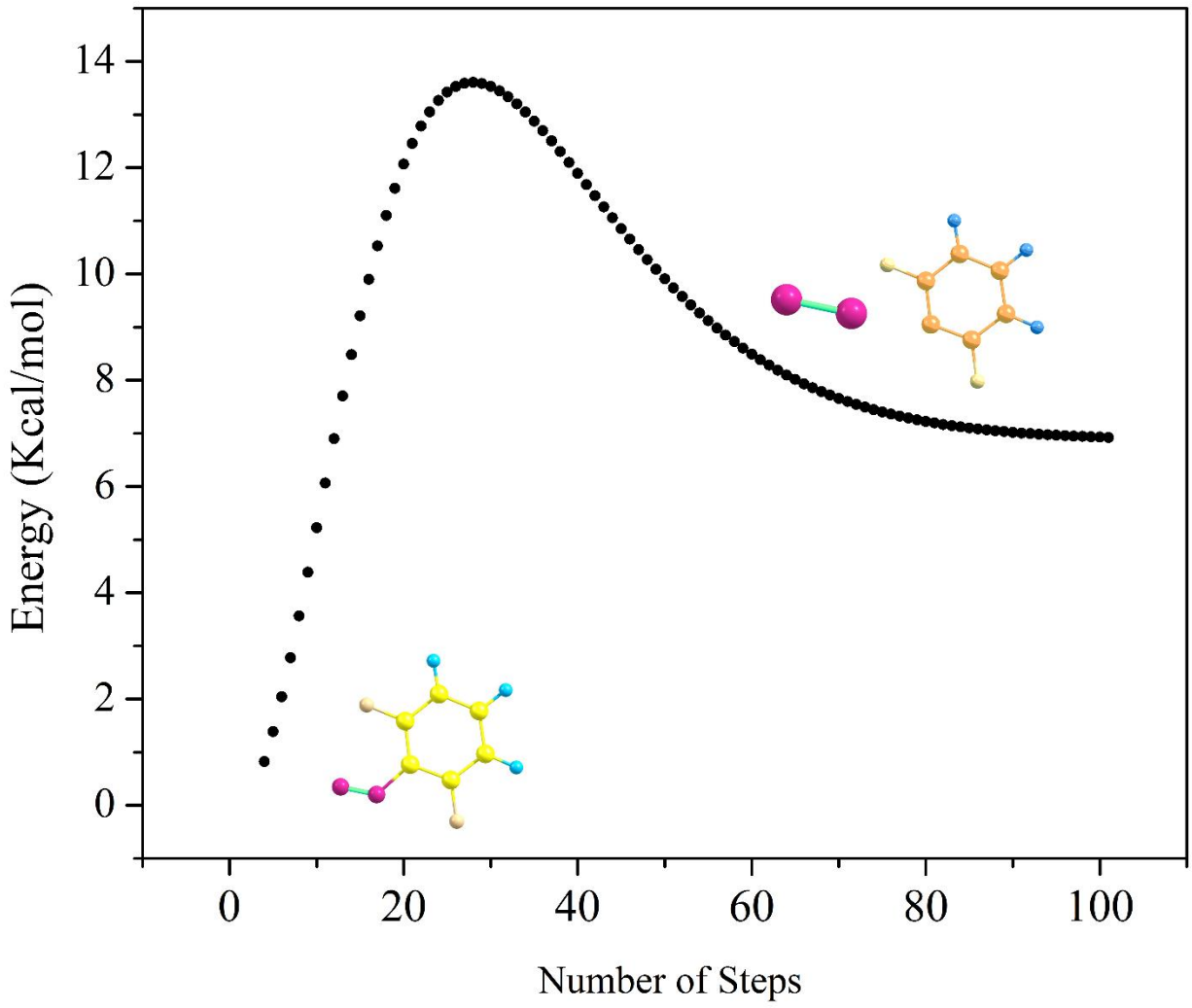

Figure 2.2: One dimensional potential energy surface scan for the dissociation reaction of $C_6H_3N_2F_2$ which yields N_2 and $C_6H_3F_2$ by increasing the C-N bond in 100 equal steps.

The simplest possible case to imagine is a two atom molecule (diatomic). We can model this system as two particles connected with a spring which follow Hooke's law.

$$F = -k(R - R_{eq}) \tag{2.1}$$

$$U = \frac{-1}{2}\left(R - R_{eq}\right)^2 \tag{2.2}$$

this potential is a harmonic potential and the motion due to this spring and ball system would represent simple harmonic motion. The total energy (potential plus kinetic energy) is constant during each period. Considering the concept of reduced mass μ, the solution for the above would be a harmonic motion:

$$R(t) = A\ \sin(\omega t) + B\cos(\omega t) + R_{eq} \tag{2.3}$$

where $\omega = \left(\frac{k}{\mu}\right)^{1/2}$ is the angular frequency. Then the total vibrational energy of the harmonically vibrating diatomic molecule would be:

$$E_{tot} = \frac{1}{2}\ k\ (x_2 - \ x_1)^2 + \frac{1}{2}\ m_1 {v_1}^2 + \frac{1}{2}\ m_2 {v_2}^2 \tag{2.4}$$

A better model for a real diatomic molecule would be the Morse potential since the *springs* between the atoms don't obey the Hooke's law when fully extended. The Morse potential can be written the form:

$$U(R) = \ D_e\ \left(1 - exp\left(-a(R - R_{eq})\right)\right)^2 \tag{2.5}$$

Here D_e is the thermodynamic dissociation energy which, as illustrate in Figure 2.3, is situated at the bottom of the well. From our physical knowledge we know the bottom of the well is merely a mathematical abstract and the total energy of the molecule is always above this value. We can see how the Morse potential deviates from a simple harmonic potential in regions away from equilibrium point. The force constant and the D_e parameter are related according to:

$$a = \frac{\omega_e}{2}\sqrt{\frac{2\mu}{D_e}} \tag{2.6}$$

The Morse potential in comparison to that of the simple harmonic potential has one extra variable which takes into account the anharmonicities of the potential. More advanced models exist with 5 and more variables (Linnett function) or potentials which do include the long range interactions (The Lennard-Jones potential).

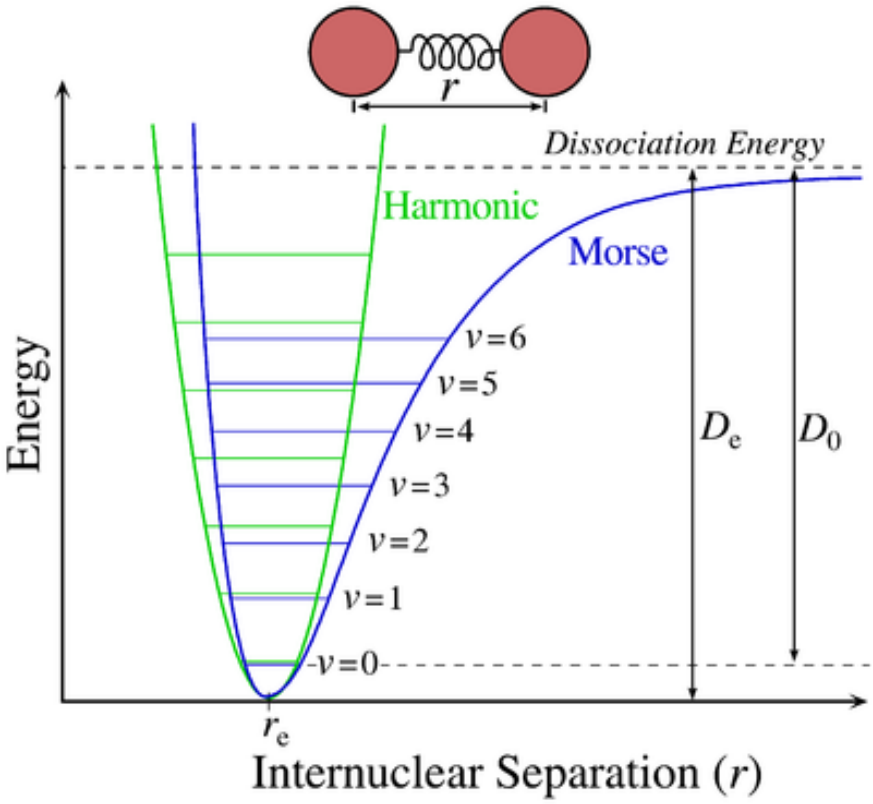

Figure 2.3: Morse potential vs Harmonic potential and the dissociation energy. Around the equilibrium they are similar but the further we go from equilibrium we can see the results change. Illustration courtesy of Wikipedia commons.

Most of our computational chemistry calculations start with exploring the potential energy surface. We can distinguish 3 different important point on a potential energy surface which include the non-stationary points and the stationary points which can be a global minimum or a local minimum. A molecule with N atom has 3N-6 degree of freedom (3N-5 if it is linear) and there are 3N Cartesian coordinates. The molecular potential energy U will include 3N −6 independent variables. [62] Considering these coordinate as q_i and their equilibrium values as q_{ie}:

$$q = \begin{pmatrix} q_1 \\ q_2 \\ . \\ . \\ . \\ q_p \end{pmatrix}, \qquad q_e = \begin{pmatrix} q_{1e} \\ q_{2e} \\ . \\ . \\ . \\ q_{pe} \end{pmatrix}, \qquad \xi = \begin{pmatrix} q_1 - q_{1e} \\ q_2 - q_{2e} \\ . \\ . \\ . \\ q_p - q_{pe} \end{pmatrix} \tag{2.7}$$

Taylor's expansion of potential around the equilibrium point would be:

$$U(R) - U(R_e) = (R - R_e)\left(\frac{dU}{dR}\right)_{R=R_e} + \frac{1}{2}(R - R_e)^2\left(\frac{d^2U}{dR^2}\right)_{R=R_e} + \cdots \tag{2.8}$$

$$U(q) - U(q_e) = \sum_{i=1}^{p} \xi_i \left(\frac{\partial U}{\partial q_i}\right)_{\xi_i=0} + \frac{1}{2}\sum_{i=1}^{p}\sum_{j=1}^{p} \zeta_i \zeta_j \left(\frac{\partial^2 U}{\partial q_i \partial q_j}\right)_{\zeta_i=0,\zeta_j=0} + \cdots \tag{2.9}$$

$$grad\ U = \begin{pmatrix} \frac{\partial U}{\partial q_1} \\ \frac{\partial U}{\partial q_2} \\ . \\ . \\ \frac{\partial U}{\partial q_p} \end{pmatrix} \tag{2.10}$$

Hessian matrix which is symmetric $p \times p$ matrix is our mathematical tool here which describes the local curvature of a function of many variables.

$$H = \begin{pmatrix} \frac{\partial^2 U}{\partial {q_1}^2} & \cdots & \frac{\partial^2 U}{\partial q_1 \partial q_n} \\ \vdots & \ddots & \vdots \\ \frac{\partial^2 U}{\partial q_n \partial q_1} & \cdots & \frac{\partial^2 U}{\partial {q_n}^2} \end{pmatrix} \tag{2.11}$$

We are interested in the gradient and the Hessian at the equilibrium point. We can write the transformation matrix from Cartesian coordinates to internal coordinate utilizing the rectangular Wilson B-matrix which has p rows and 3N columns as:

$$q = B\,X \tag{2.14}$$

A local or global minimum is an stationary point which the gradient of the potential with respect to each and every geometric parameter q is zero: [63]

$$\frac{\partial U}{\partial q_1} = \frac{\partial U}{\partial q_2} = \cdots = \frac{\partial U}{\partial q_N} = 0 \tag{2.15}$$

A transition point is also a stationary point (in this case it is called a saddle point) which the first derivative of energy is zero and the energy is a maximum along the reaction coordinate and a minimum in all other directions. In mathematical language we can represents these concepts as:

For a minimum (local or global)	for all q, $\frac{\partial^2 U}{\partial q^2} > 0$
For a transition state (saddle point)	for all q , $\frac{\partial^2 U}{\partial q^2} > 0$; except for the coordinate along the reaction coordinate which $\frac{\partial^2 U}{\partial q^2} < 0$

Thus in order to find the transition state we look for a negative or imaginary frequency (only one negative frequency). Since we are doing collision induced dissociation experiments and utilizing computational chemistry to analysis the results and make sense of the mass spectroscopic results we need to elaborate on the concept of a transition state and specifically the activated complex

concept. A transition structure is the saddle point on a theoretically calculated PES. [63] The transition structure is a saddle point on an enthalpy surface. The activated complex is the structure at the maximum energy point along the reaction path (first derivative of energy in respect to q is zero); the activation energy is the difference between the energies of the activated complex and the reactants. In our case this activation energy will be provided to the complex by a collision between the precursor negative ion with a neutral target such as argon. Thus the required energy is not simply the difference between reactants and the products (ΔH) but always more than that (activation energy).

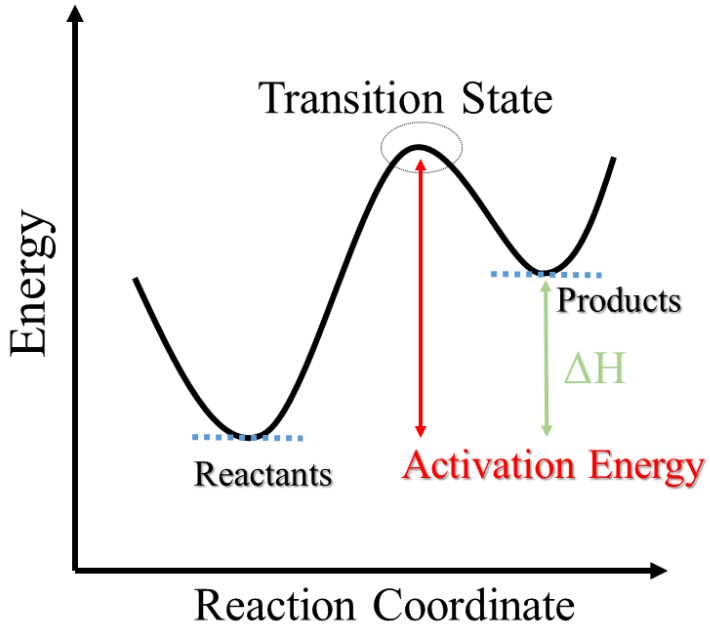

Figure 2.4: Generic energy diagram for unimolecular reactions.

Computational chemistry calculations begin with an optimization of the geometry of a molecule. That requires finding the minimums on a potential energy surface (PES). This process starts with a reasonable initial structure and then an algorithm changes all the available coordinates and iteratively calculates the energy until the minimum possible energy is found. The default algorithm for both minimizations (optimizations to a local minimum) and optimizations to transition states and higher-order saddle points is known as the Berny algorithm.[22] The Other common algorithm is the Newton-Raphson method. At each step of a Berny optimization the Hessian matrix which

has been explained before is updated unless an analytic Hessian has been computed or it is the first step. The algorithm performs a linear search between the latest point and the best previous point (the previous point having lowest energy). If the second derivatives are available at both points and a minimum is sought, a quintic polynomial fit is attempted first; if it does not have a minimum in the acceptable range or if second derivatives are not available, a constrained quartic fit is attempted. This fits a quartic polynomial to the energy and first derivative (along the connecting line) at the two points with the constraint that the second derivative of the polynomial just reach zero at its minimum, thereby ensuring that the polynomial itself has exactly one minimum. If this fit fails or if the resulting step is unacceptable, a simple cubic fit is performed.

2.3 Computational results for sample molecules:

Here we explain the fundamental computational results for the sample molecules we have studied in this dissertation. These results are obtained from various calculations and help us to better understand the nature of the electronic structure of these molecules and their negative and positive ions.

2.3.1 Azobenzene

Herein we report calculations on the trans and cis isomers of azobenzene and their negative and positive ions. We used different levels of theory and various basis sets in order to obtain a reliable understanding of this molecule and its electron affinity. Geometry optimization has been performed on the optimized structures shown in Figure 5 and Figure 6. The cis azobenezene is 0.66 eV higher in energy than the ground electron state in comparison to that of the trans isomer. The trans isomer has a dipole moment of 0 Debye which means it is planar and the cis isomer has a dipole moment of 3.34 Debye. In the collision induced dissociation (CID) experiments one of the most important information required for further analysis of the data obtained from the CID experiment involves the transition state of the reaction. It is necessary to have the frequencies of the transition state as well. Below is the intrinsic reaction coordinate calculation for the trans azobenzene isomerization reaction to convert from the trans to cis isomer. Calculating the optimized structure of the transition state is a tedious job. There are many states with potential energy surface derivate to be zero but only one of them is *THE* transition state of the reaction.

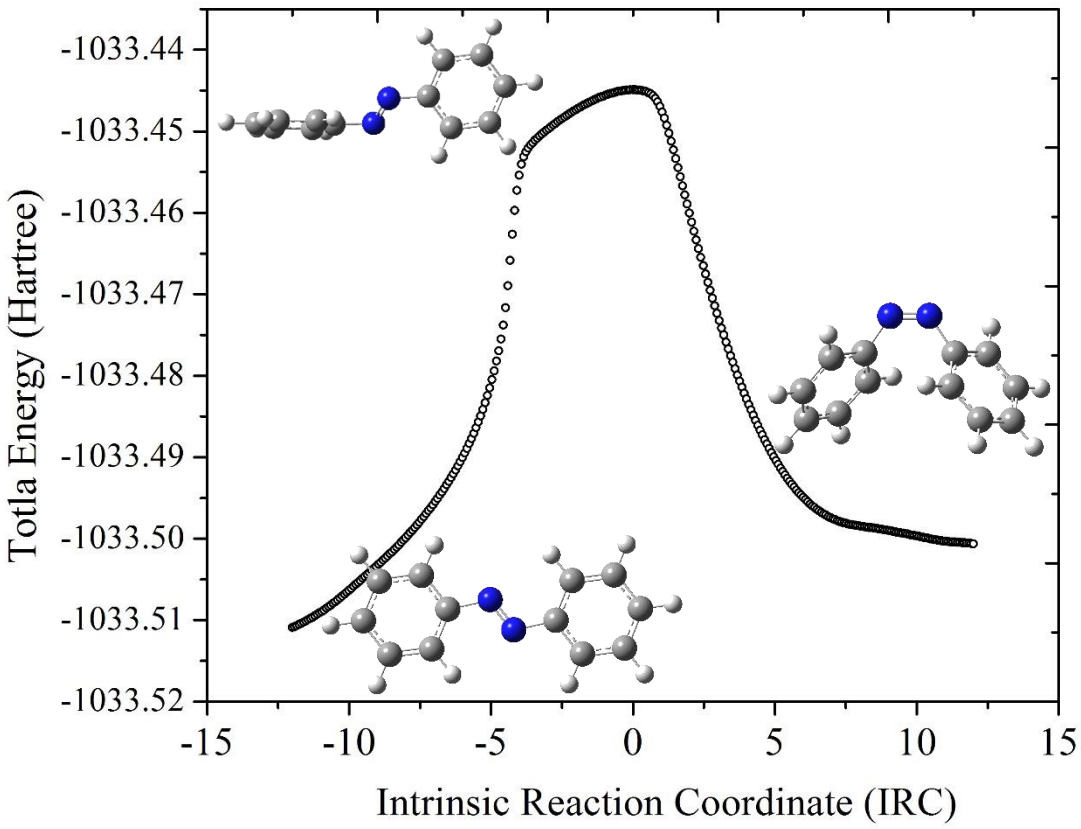

Figure 2.5: Intrinsic reaction coordinate of trans to cis isomerization reaction. We can also see the structure of the transition state of this reaction. The transition state must have only and only one negative frequency in its frequency spectrum. Calculations have been performed at the wB97XD level of theory.

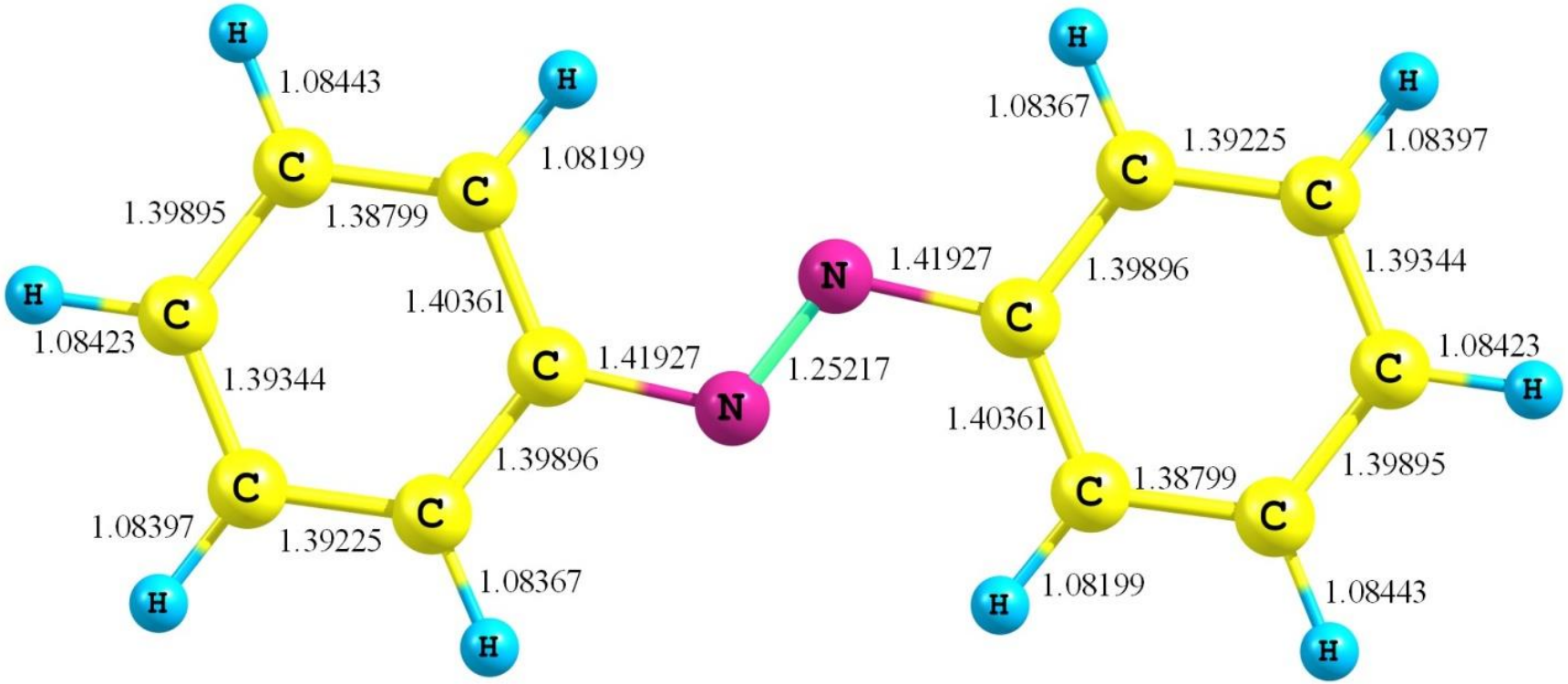

Figure 2.6: Trans azobenzene geometry optimized at B3LYP level of theory with 6-311++G(d,p). All the bond length are shown and the unit is Angstrom. The geometry optimization and the SCF procedure have been done using tight convergence criteria along with ultra-fine grid for the integrals which is recommended for optimizations of larger molecules.

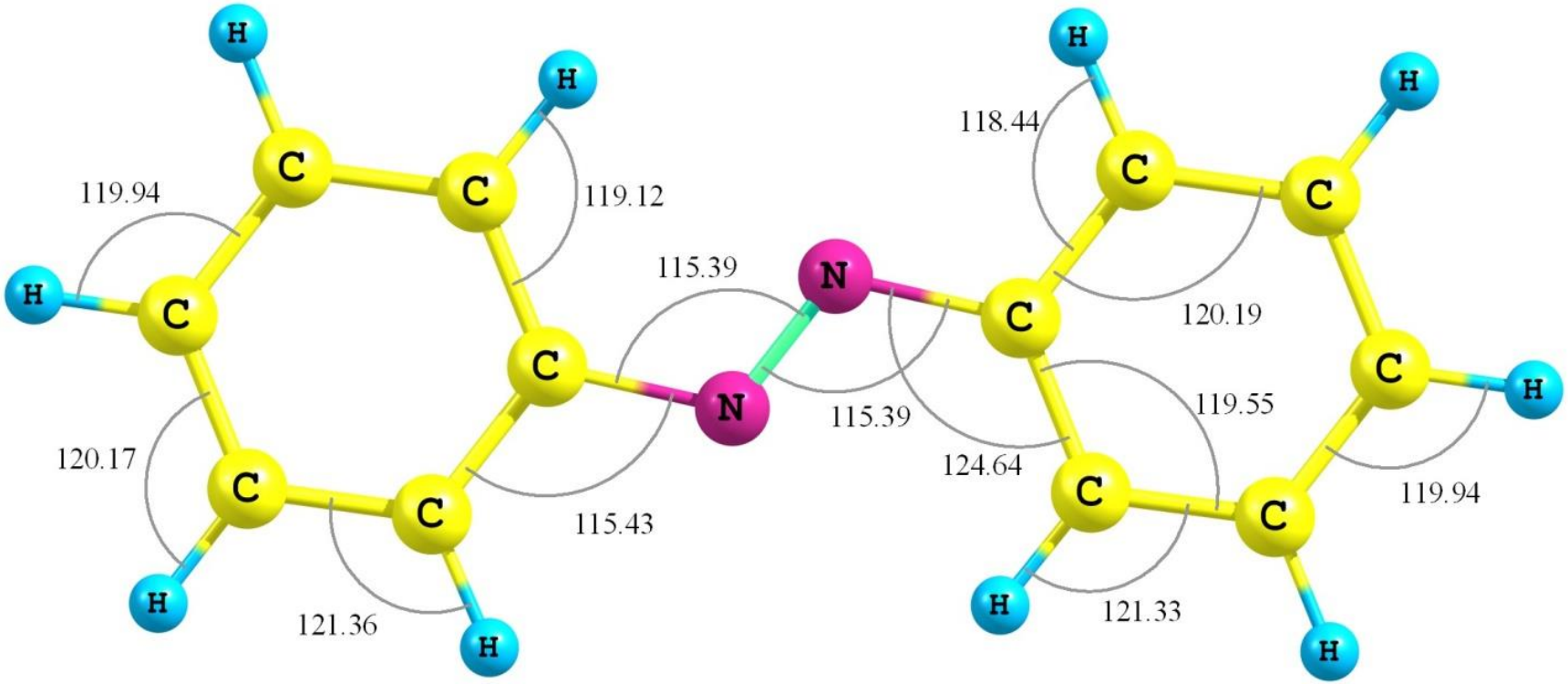

Figure 2.7: Trans azobenzene bond angles optimized at B3LYP level of theory with 6-311++G(d,p). All the bond angles are in degree. The geometry optimization and the SCF procedure have been done using tight convergence criteria along with ultra-fine grid for the integrals which is recommended for optimizations of larger molecules.

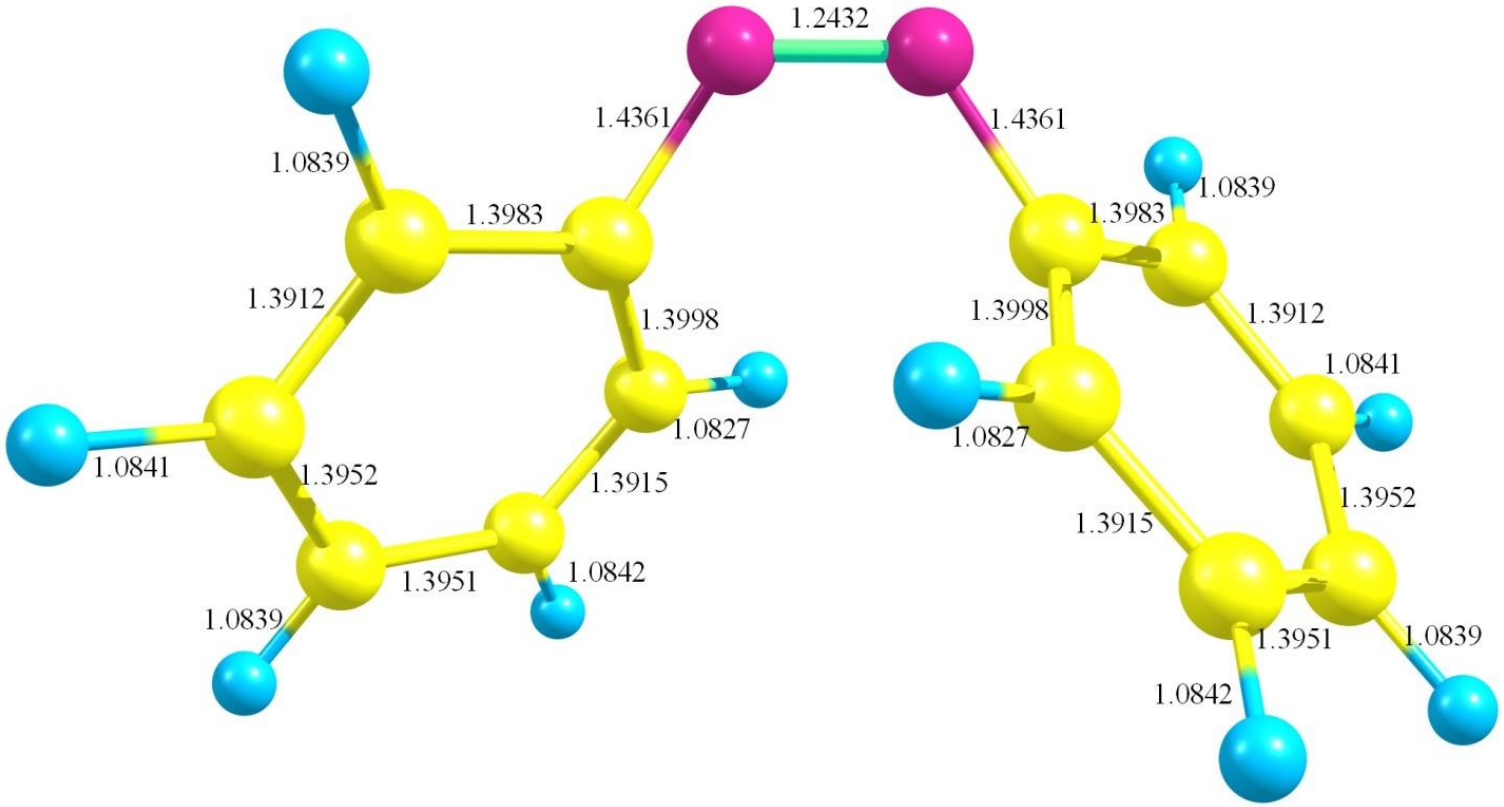

Figure 2.8: Cis azobenzene geometry optimized at B3LYP level of theory with 6-311++G(d,p). All the bond length are shown and the unit is Angstrom. The geometry optimization and the SCF procedure have been done using tight convergence criteria along with ultra-fine grid for the integrals which is recommended for optimizations of larger molecules.

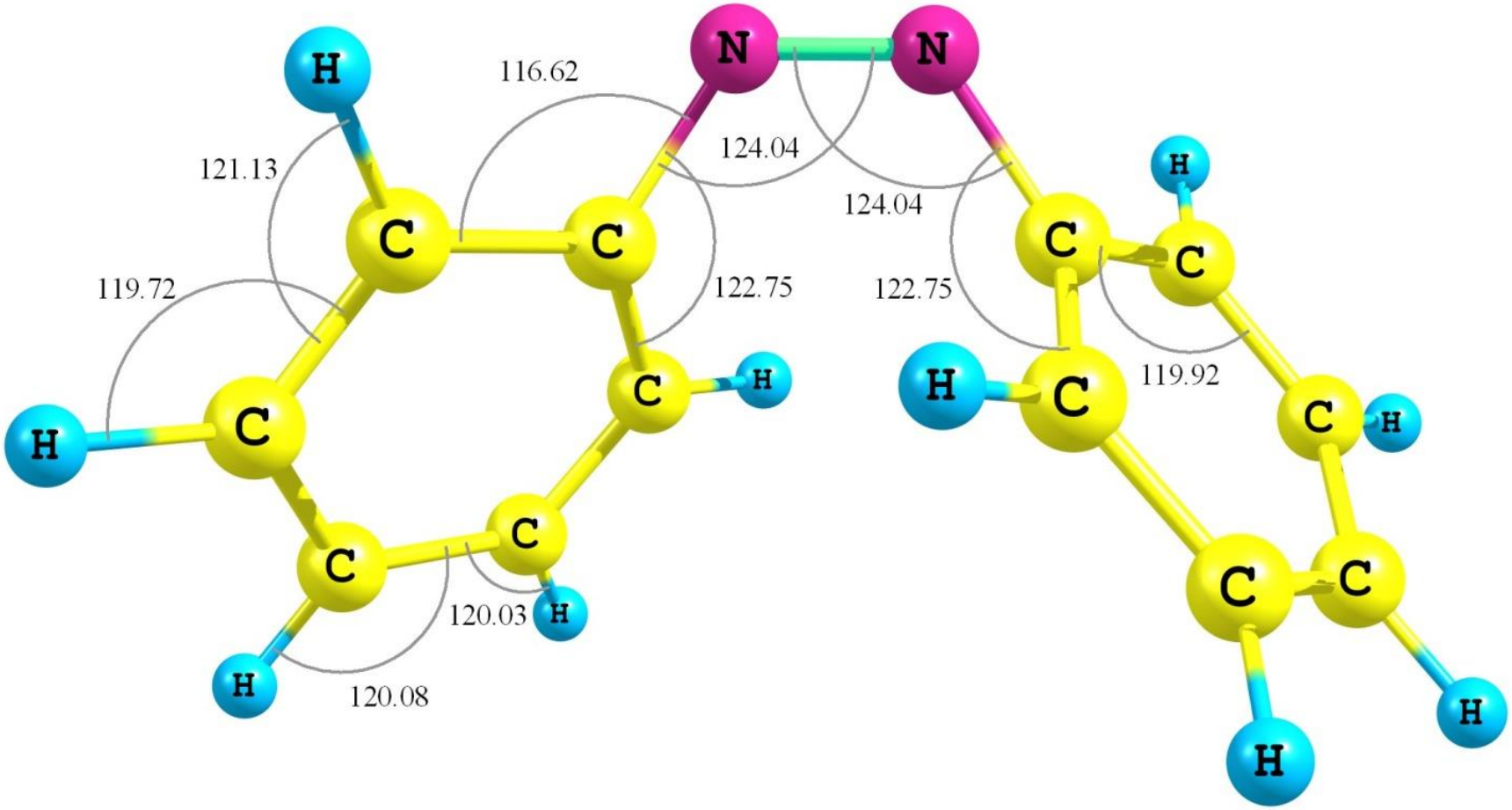

Figure 2.9: Cis azobenzene bond angles optimized at B3LYP level of theory with 6-311++G(d,p). All the bond angles are in degree. The geometry optimization and the SCF procedure have been done using tight convergence criteria along with ultra-fine grid.

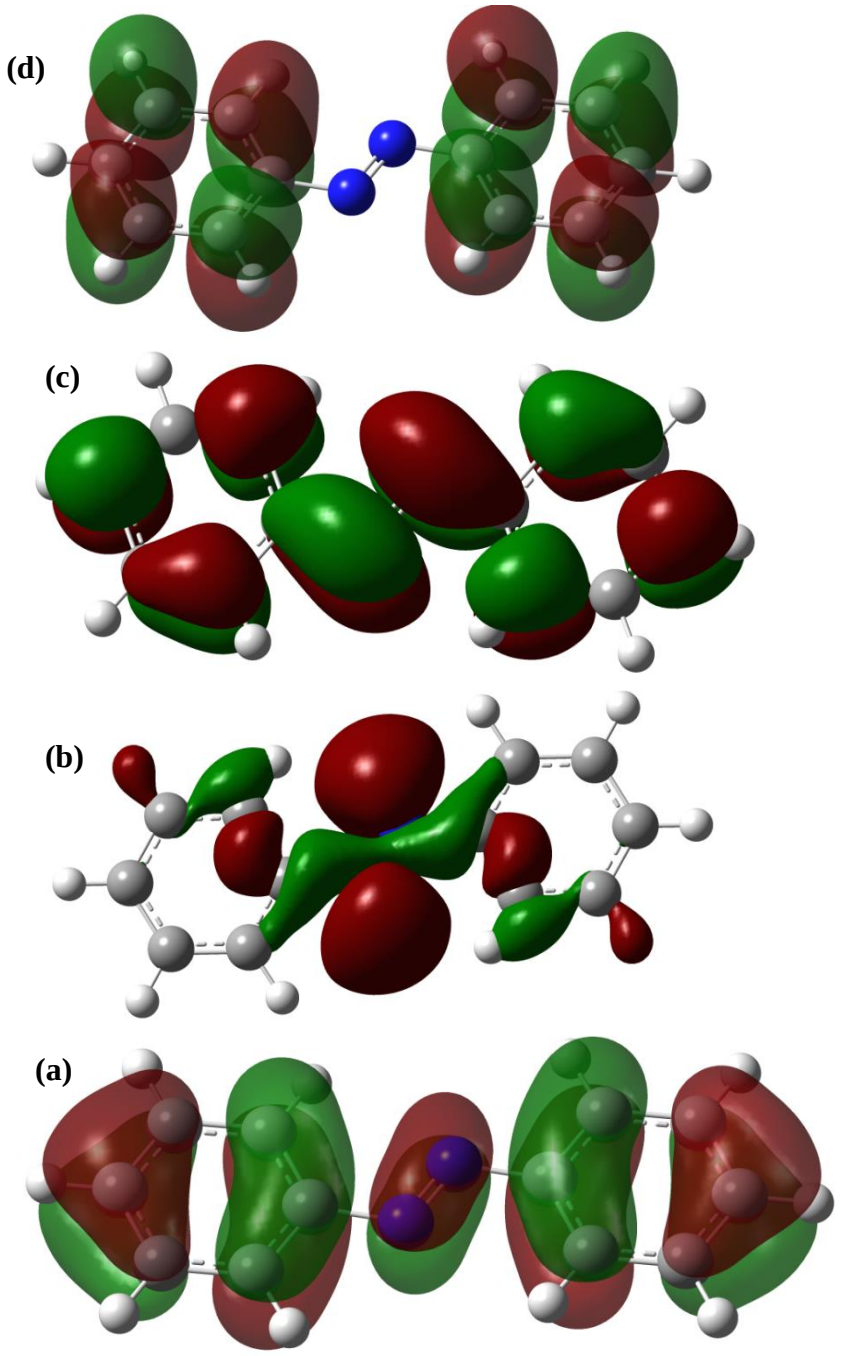

Figure 2.10: Population analysis and molecular orbitals of trans azobenzene. Calculations performed at B3LYP level of theory along with 6-311++G(d,p) basis set. The four orbitals which are illustrated include a) HOMO-1, b) HOMO, c) LUMO, d) LUMO+1, Isoval=0.02, Density 0.0004.

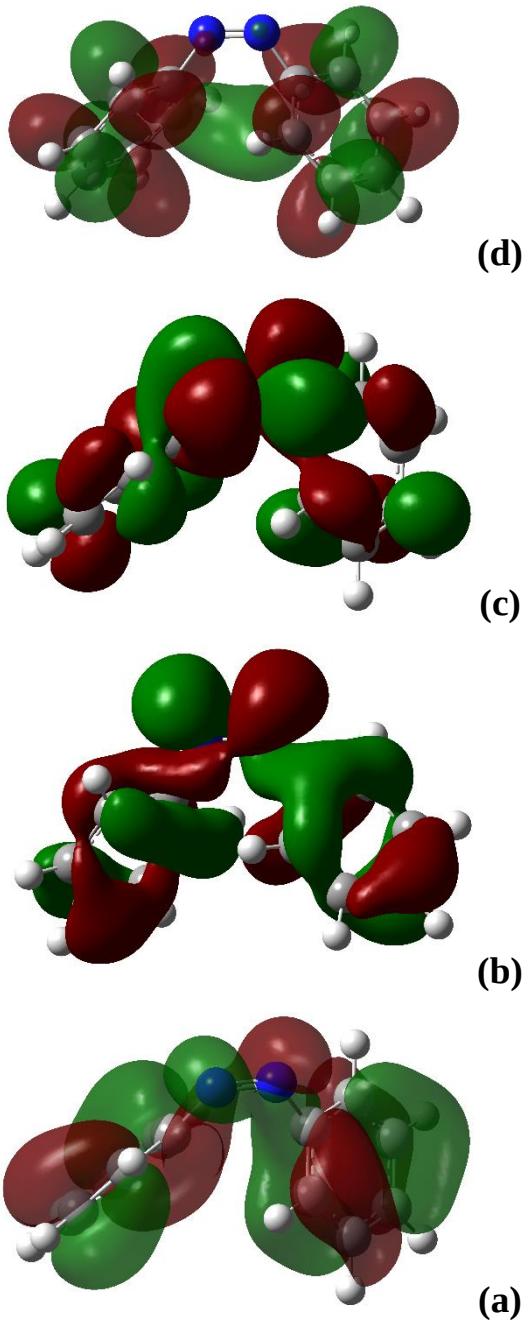

Figure 2.11: Population analysis and molecular orbitals of cis azobenzene. Calculations performed at B3LYP level of theory along with 6-311++G(d,p) basis set. The four orbitals which are illustrated include a) HOMO-1, b) HOMO, c) LUMO, d) LUMO+1, Isoval=0.02, Density 0.0004.

Table 2.1: Thermochemical information of **azobenzene**, trans and cis isomers. Temperature 298.150 Kelvin and Pressure 1.00000 Atm. Energy values are all in Hartree unit. Calculations has been done at B3LYP level of theory along with 6-311++G(d,p) basis set.

	(Trans)	(Cis)
Zero-point correction	0.1897 (Hartree/Particle)	0.189 (Hartree/Particle)
Thermal correction to Energy	0.200673	0.200305
Thermal correction to Enthalpy	0.201617	0.201249
Thermal correction to Gibbs Free Energy	0.151168	0.151496
Sum of electronic and zero-point Energies	-572.718348	-572.694077
Sum of electronic and thermal Energies	-572.707441	-572.683252
Sum of electronic and thermal Enthalpies	-572.706497	-572.682308
Sum of electronic and thermal Free Energies	-572.756945	-572.732060

Table 2.2: Optimized geometry of top) trans azobenzene bottom) cis azobenzene at B3LYP level of theory and using 6-311++G(d,p) as the basis set.

Center Number	Atomic Number	Atomic Type	Coordinates (Angstroms) X	Y	Z
1	6	0	-4.534251	-0.198491	0.000000
2	6	0	-3.672594	-1.300589	0.000001
3	6	0	-2.296598	-1.118529	0.000001
4	6	0	-1.770601	0.182795	0.000000
5	6	0	-2.633154	1.284203	-0.000001
6	6	0	-4.012276	1.093486	-0.000001
7	1	0	-4.082135	-2.304717	0.000002
8	1	0	-1.617644	-1.960973	0.000002
9	1	0	-2.201224	2.278070	-0.000002
10	1	0	-4.677064	1.949665	-0.000001
11	7	0	0.385691	-0.493180	0.000000
12	1	0	-5.607720	-0.350852	0.000000
13	7	0	-0.385691	0.493181	0.000000
14	6	0	1.770601	-0.182794	0.000000
15	6	0	2.633154	-1.284202	-0.000001
16	6	0	2.296598	1.118530	0.000001
17	1	0	1.617644	1.960974	0.000001
18	6	0	3.672594	1.300589	0.000001
19	1	0	4.082136	2.304717	0.000001
20	6	0	4.534251	0.198491	0.000000
21	1	0	5.607720	0.350852	0.000000
22	6	0	4.012276	-1.093486	-0.000001
23	1	0	4.677064	-1.949665	-0.000002
24	1	0	2.201224	-2.278069	-0.000002

Table 2.2: Continued

Center Number	Atomic Number	Atomic Type	Coordinates (Angstroms) X	Y	Z
1	6	0	3.243557	-1.347727	0.293652
2	6	0	2.175511	-1.245383	1.185399
3	6	0	1.261113	-0.202395	1.074114
4	6	0	1.427096	0.758363	0.069746
5	6	0	2.527961	0.688550	-0.789636
6	6	0	3.414985	-0.379101	-0.695825
7	1	0	2.052239	-1.982260	1.971114
8	1	0	0.433144	-0.125039	1.767389
9	1	0	2.670336	1.472570	-1.524422
10	1	0	4.253391	-0.443109	-1.380148
11	7	0	-0.621510	1.944480	0.011640
12	1	0	3.947316	-2.167432	0.380663
13	7	0	0.621514	1.944479	-0.011636
14	6	0	-1.427094	0.758364	-0.069745
15	6	0	-2.527953	0.688546	0.789645
16	6	0	-1.261119	-0.202386	-1.074122
17	1	0	-0.433156	-0.125026	-1.767402
18	6	0	-2.175521	-1.245372	-1.185409
19	1	0	-2.052255	-1.982242	-1.971131
20	6	0	-3.243560	-1.347722	-0.293655
21	1	0	-3.947321	-2.167425	-0.380668
22	6	0	-3.414980	-0.379103	0.695831
23	1	0	-4.253380	-0.443116	1.380160
24	1	0	-2.670321	1.472559	1.524439

2.3.2 2,2́,6,6́-tetrafluoroazobenzene:

Many different type of calculations using different methods and basis sets were employed to study this molecule thoroughly. Below are the results related to the population analysis of this molecule and its anion. We have calculated the electron affinity of this molecule employing more than 17 different levels of theory. We presented calculated energy values for this sample as well as the electron affinities and bond dissociation energy. Comparing to azobenzene itself this sample doesn't require using UV light for trans to cis isomerization to happen which is an important advantage. Figure 2.12 is the illustration of the population analysis of trans 2,2́,6,6́-tetrafluoroazobenzene. Population analysis which is the depiction of charge distribution around atoms in a molecule helps to understand its electronic structure better. An analysis in quantitative form is given here in terms of breakdowns of the electronic population into partial and total "gross atomic populations," or into partial and total "net atomic populations" together with "overlap populations." "Gross atomic populations" distribute the electrons almost perfectly among the various AOs (atomic orbitals) of the various atoms in the molecule.[64] Figure 2.13 is the illustration of population analysis of trans 2,2́,6,6́-tetrafluoroazobenzene anion and we can clearly see the difference between the charge distribution comparing with the neutral molecule. Figure 2.14 and 2.15 are the population analysis of cis 2,2́,6,6́-tetrafluoroazobenzene neutral and anion molecule respectively which is a reasonable way to visualize the difference in charge distribution between the cis and trans isomers. We have done a complete population analysis including natural bonding orbital analysis for all the samples we studied neutral and anion molecules. The results hve been provided in chapter 2, chapter 3 and also in the appendix B.

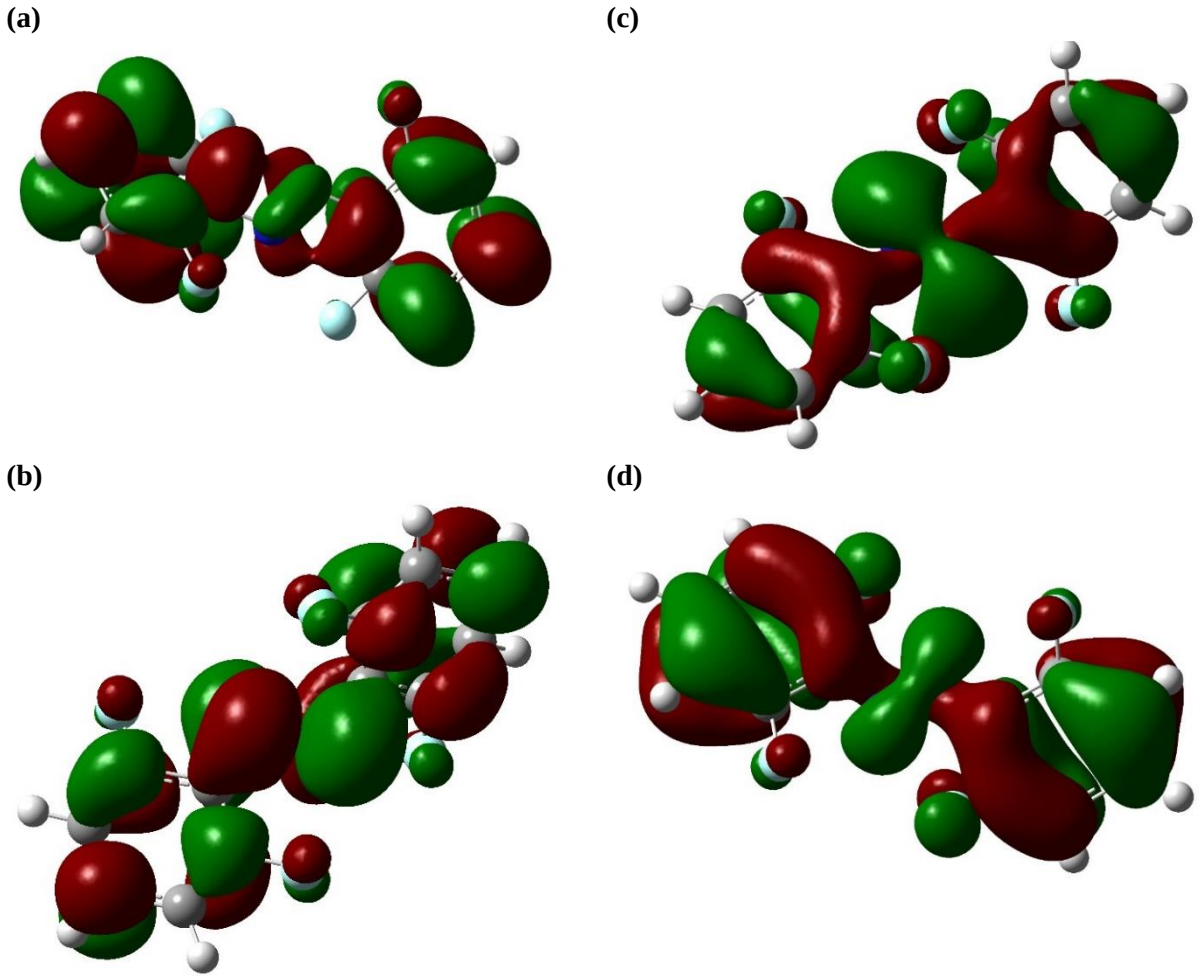

Figure 2.12: Population analysis of trans 2,2́,6,6́-tetrafluoroazobenzene. (a) LUMO + 1 (b) LUMO (c) HOMO (d) HOMO -1. Calculations have been done using B3LYP level of theory with 6-311++G(d,p) basis set. Isovalue = 0.02 and Density is 0.00040.

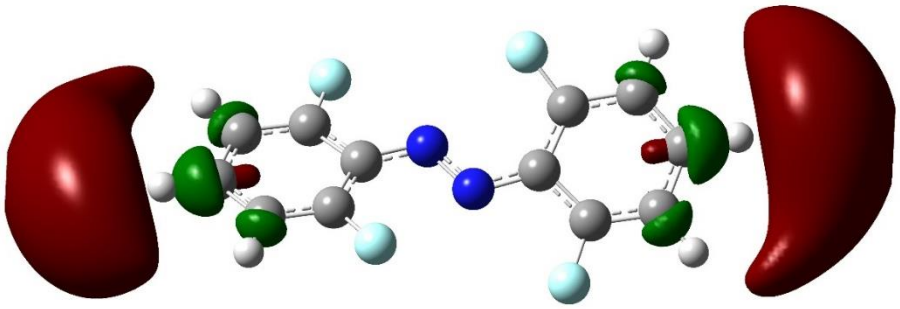

(a)

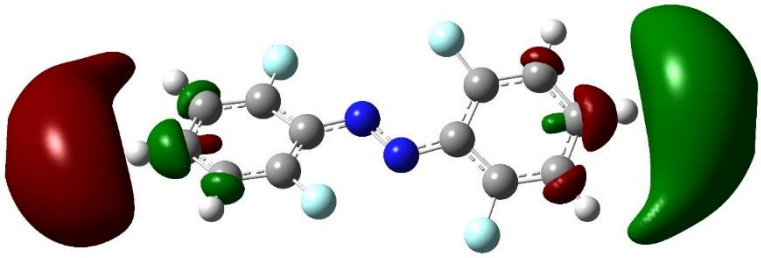

(b)

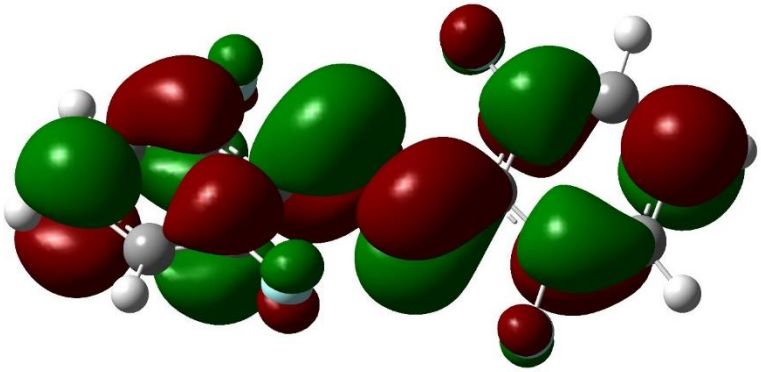

(c)

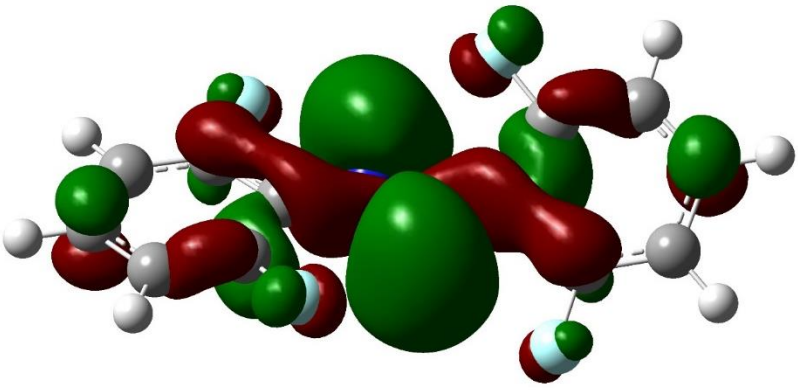

(d)

Figure 2.13: Population analysis of trans 2,2́,6,6-tetrafluoroazobenzene **anion**. (a) LUMO + 1 (b) LUMO (c) HOMO (d) HOMO -1. Calculations have been done using B3LYP level of theory with 6-311++G(d,p) basis set. Isovalue = 0.02 and Density is 0.00040.

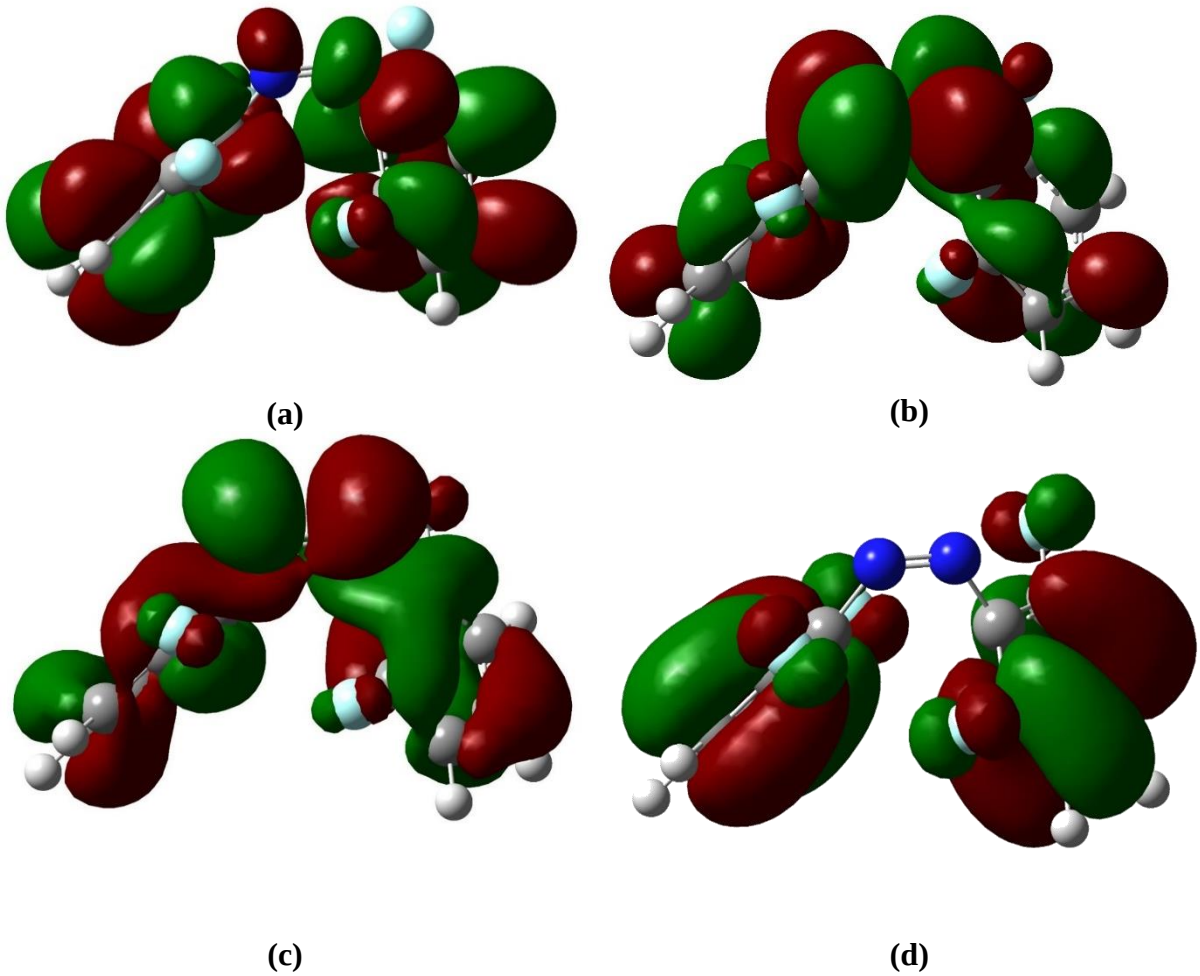

Figure 2.14: Population analysis of cis 2,2́,6,6́-tetrafluoroazobenzene. (a) MO=64; LUMO + 1 (b) MO=65; LUMO (c) MO=66 HOMO (d) MO=67 HOMO -1. Calculations have been done using B3LYP level of theory with 6-311++G(d,p) basis set. IsoValue = 0.02 and Density is 0.00040.

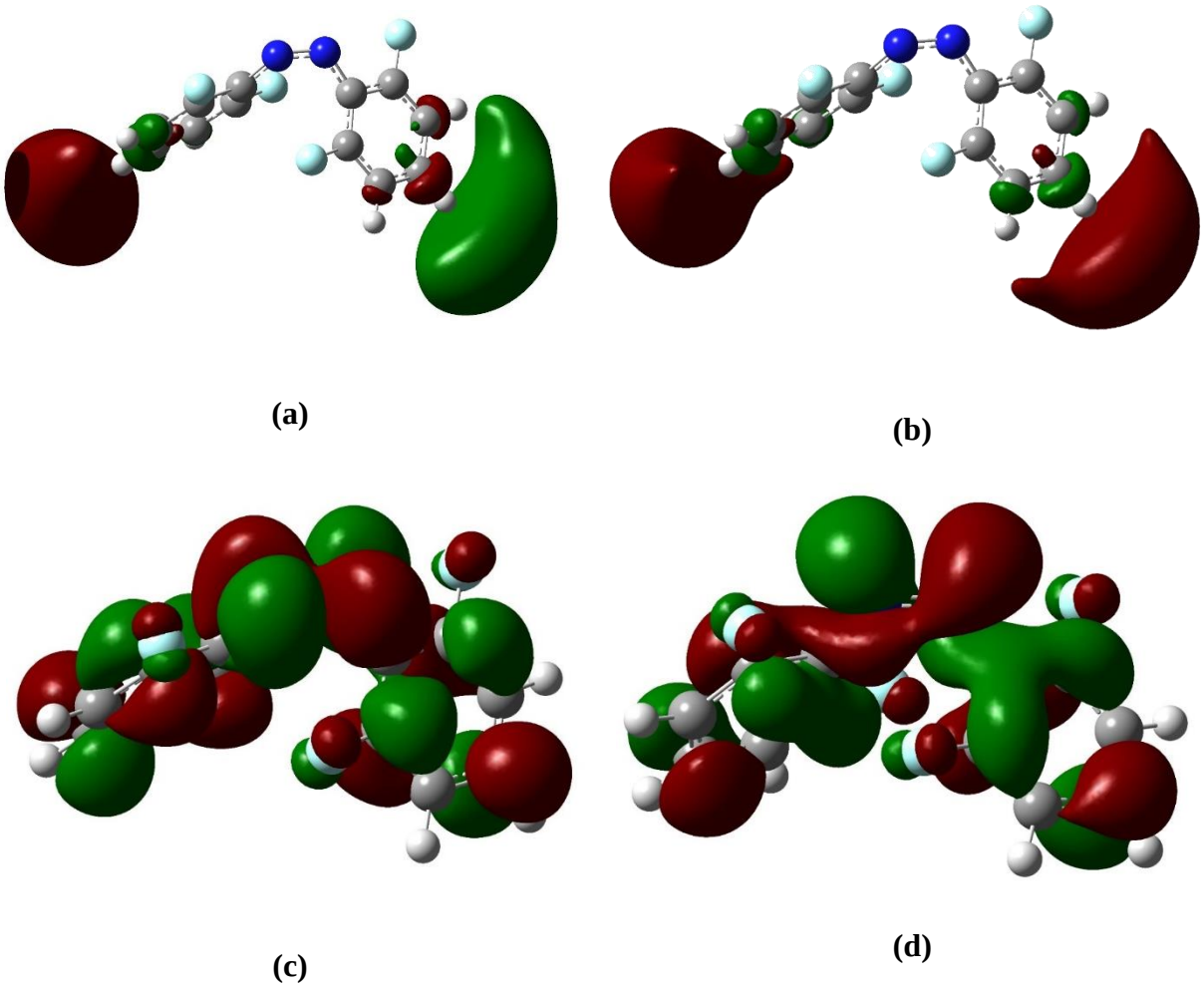

Figure 2.15: Population analysis of **cis** 2,2́,6,6́-tetrafluroazobenzene **anion**. (a) MO=64; LUMO+1 (b) MO=65; LUMO (c) MO=66 HOMO (d) MO=67 HOMO -1. The calculations were done using B3LYP level of theory with 6-311++G(d,p) basis set. IsoValue = 0.02 and Density is 0.00040.

We also extensively studied the electron affinities of 2,2́,6,6́-tetrafluoroazobenzene for which a summary of the results will be presented later in this chapter. This molecule was our main sample used in the collision induced dissociation (CID) experiments. Therefore extensive calculations were carried out on this system. These studies are integral parts of any CID experiment. It is necessary to find the exact isomer for each fragment ion. This requires consideration of different possibilities for the geometry and to find their minimum energies and global minima. We calculated different thermochemical, optical and electronic properties of it.

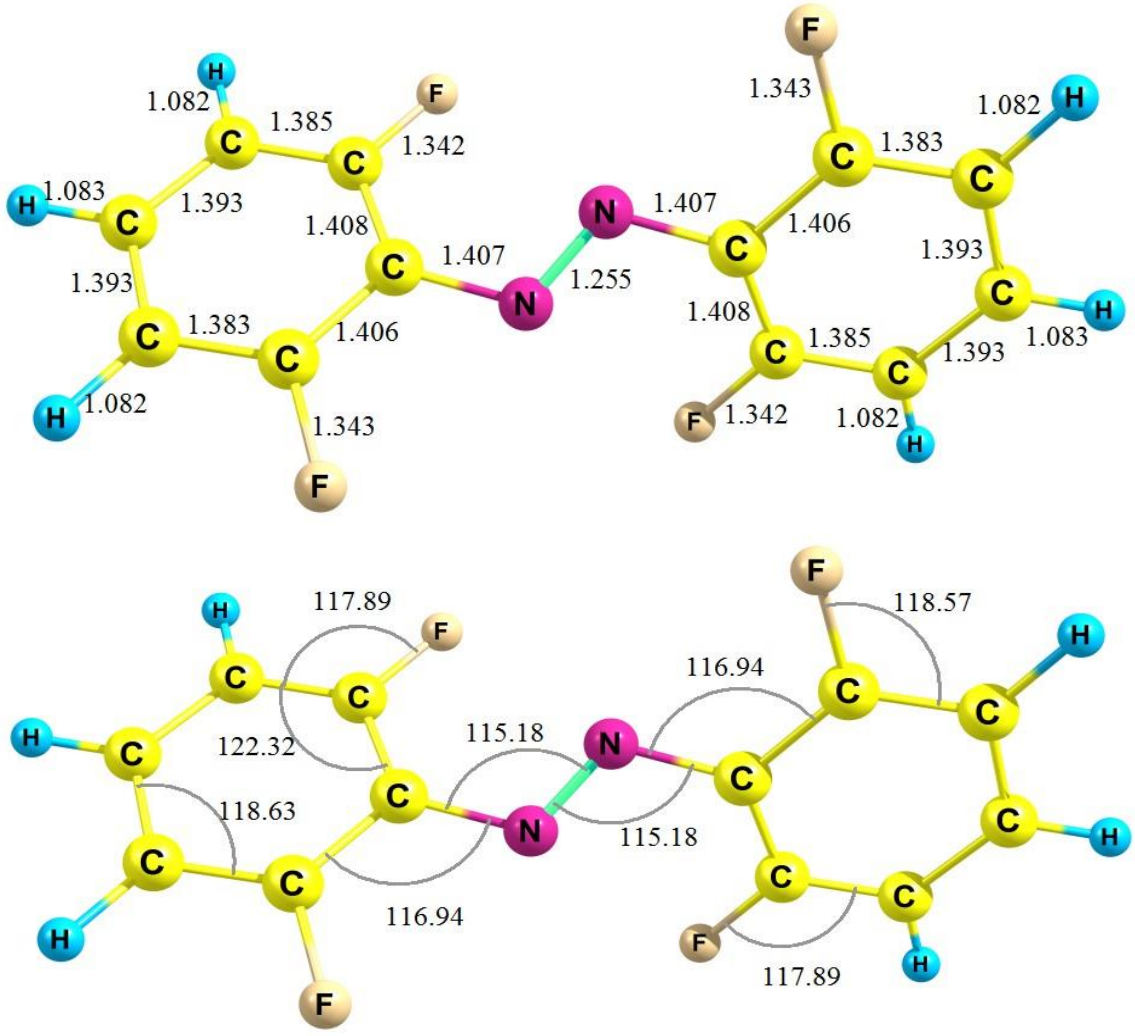

Figure 2.16: The optimized geometry of trans 2,2́,6,6́-tetrafluroazobenzene. The CNNC dihedral is -175.9 and the CCNN dihedral is 21.9. This molecule is optimized at the B3LYP level of theory with 6-311++G(d,p) as the basis set.

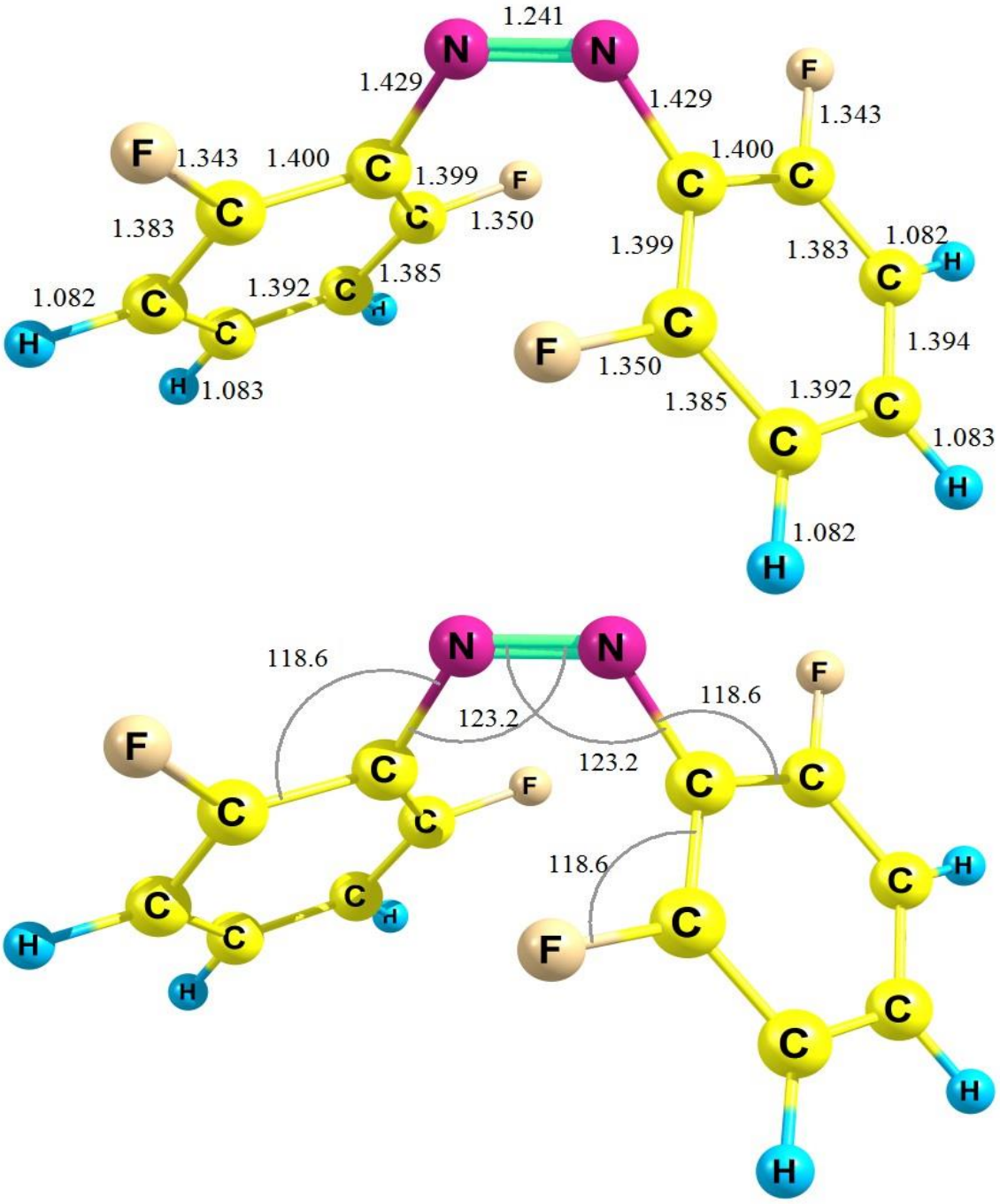

Figure 2.17: The optimized geometry of cis 2,2́,6,6́-tetrafluoroazobenzene. The CNNC dihedral is -172.327 and the CCNN dihedral is 133.2. This molecule is optimized at B3LYP level of theory with 6-311++G(d,p) as the basis set.

2.4 Introduction to Raman Spectroscopy

Raman spectroscopy is a highly quantitative nondestructive analytical method which became popular and feasible after lasers had been invented and commercially available. Without a coherent intense laser light, detecting Raman signals is a tedious task. Raman spectroscopy which is based on inelastic scattering of intense monochromatic light from vibrational states of molecules first was suggested by Sir Chandrasekhara Raman. Rayleigh scattering which is elastic scattering of light was known a long time before Raman suggest the inelastic scattering should exist as well. In Rayleigh scattering atoms and molecules re-radiated a photon with same frequency as the incident photon. On the other hand, in Raman scattering, the re-radiated photons gain or loss energy from the molecules of the sample. The change in photon energy is added or subtracted from the vibrational or rotational energy of the molecule which shows a finger print of that molecule. A small amount of the photon energy of the incident light wave is modulated by the molecular scattering system. An energy transfer occurs as a result of the coupling between the incident radiation and the quantized states of the scattering system. Depending on the coupling, the incident photons either gain or lose energy. The light, which has less energy than the incident laser light, is named Stokes–Raman scattering, and the radiation, which has gained energy, is referred to as anti-Stokes Raman scattering [65].

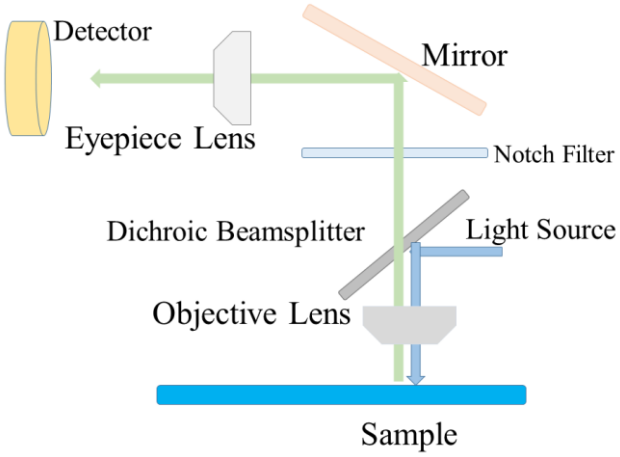

Figure 2.18: A typical Raman system. It usually involves an excitation source such as lasers, illumination system and light collection optics, a Spectrophotometer as the wavelength selector and a detector such has CCSD or PMT tube.

One technical problem with Raman spectroscopy is the Rayleigh scattering which is approximately 1000 times more intense than the stokes or anti stokes scattering. Thus in order to detect the inelastic scattering a strong coherent light source is required. In addition, a good filtering mechanism is necessary to eliminate the Rayleigh scattered background. Reduction of the Rayleigh line was accomplished the first time in 1929 by using a 435.83 nm mercury line and filtering the rest of the mercury spectrum. Photographic plates had been used as a detector (today CCD or ICCD detectors are used). Argon and Kripton ion laser, He-Ne, Cd and ruby laser are widely used as the source of excitation due to their intensity and reliable stability.

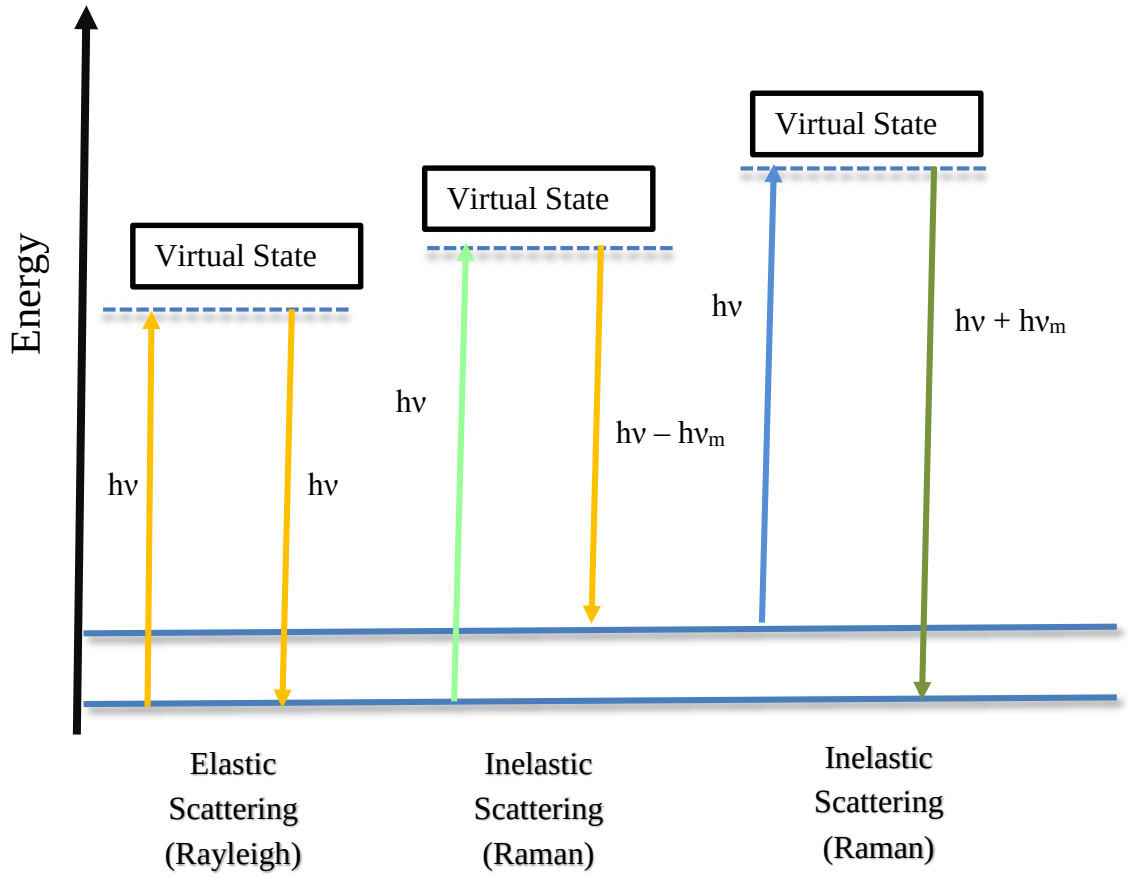

Figure 2.19: Energy-level diagram which illustrates the Stokes, anti-Stokes (Raman) and inelastic scattering (Rayleigh) mechanism. Inelastically scattered photons which can have either lower (Stokes) or higher (anti-Stokes) energy comparing to the incoming light source photon (usually laser light).

A classical treatment of Raman spectroscopy can be briefly summarized in the following: The incident light with the electric filed can be written as:

$$E = E_0 \cos(\omega t) \tag{2.16}$$

This incident field induces a dipole moment μ in the sample molecule which can be formulated as:

$$\mu = \alpha E \tag{2.17}$$

Where α is the polarizability tensor. In general we can write this in tensor language as:

$$\begin{aligned} \mu_x &= \alpha_{xx} E_x + \alpha_{xy} E_y + \alpha_{xz} E_z \\ \mu_y &= \alpha_{yx} E_x + \alpha_{yy} E_y + \alpha_{yz} E_z \\ \mu_z &= \alpha_{zx} E_x + \alpha_{zy} E_y + \alpha_{zz} E_z \end{aligned} \tag{2.18}$$

Plugging this into above relation we have:

$$\mu = \alpha E_0 \cos(\omega t) \tag{2.19}$$

To the find the normal modes of a molecule consider the atoms in a molecule as harmonic oscillators with the angular frequency ω_R. Then the time dependent amplitude would be:

$$q = q_0 \cos(\omega_R t) \tag{2.20}$$

A Taylor series expansion of the polarizability around the equilibrium gives:

$$\alpha = \alpha(q) = \alpha_0 \left(\frac{\partial \alpha}{\partial q}\right)_0 q + \cdots \tag{2.21}$$

have:

$$\mu = \left[\alpha_0 + \left(\frac{\partial \alpha}{\partial q}\right)_0 \; q_0 \; \cos(\omega_R t)\right] E_0 \; \cos(\omega_L t) \tag{2.22}$$

Which can be rewritten in more a informative form as:

$$\begin{aligned} \mu = \; \alpha \, E_0 \; \cos(\omega_L t) + \frac{1}{2}\left(\frac{\partial \alpha}{\partial q}\right)_0 \; q_0 E_0 \; \cos(\omega_L - \omega_R)\, t \\ + \; \frac{1}{2}\left(\frac{\partial \alpha}{\partial q}\right)_0 \; q_0 E_0 \; \cos(\omega_L + \omega_R)\, t \end{aligned} \tag{2.23}$$

The first term in this relation is simply due to Rayleigh scattering and the second and third terms are Stokes-Raman and Anti-Stokes Raman scattering, respectively. The Stokes term has lower frequency $\omega_S = \omega_L - \omega_R$ and the anti-Stokes has higher frequency $\omega_{AS} = \omega_R + \omega_L$. We can conclude from above relation that a mode would be Raman active if $\left(\frac{\partial \alpha}{\partial q}\right)_0 \neq 0$. As we can see, not all the modes are Raman active and that makes the Raman spectrum different from IR spectrum. For a nonlinear molecule with N atoms there will be 3N-6 (for a linear it would be 3N-5) IR active mode. For highly symmetric molecules Raman and IR transitions are mutually exclusive. Gaussian G09 quantum chemistry package which we have used for all our computational parts, gives the polarizability in a tensor form of xx, xy, xz, yy, yz, zz and the scalar polarizability can be obtained by averaging the diagonal elements, (xx+yy+zz) / 3.

2.5 Computational Raman Spectroscopy

Raman spectroscopy is one of those quantities which most of quantum chemistry codes can treat computationally. To do so we need to compute force constants and the resulting vibrational frequencies. The simplest possible model which is the fundamental assumption in most of the quantum chemistry codes is a harmonic oscillator model. Quantum mechanical description of harmonic oscillator tells us where the probability of finding an atom in the highest energy level is highest and also the fact that energy levels are quantized. Some of these codes can include other modes (beside the harmonic ones) such as anharmonic modes in the calculations. This is important if we need very high accuracy results. To compute anharmonic corrections to the vibrational frequencies is necessary to compute the higher order derivatives (from Hessian matrix)[66]. Harmonic force constants correspond to the eigenvalues of the Hessian calculated at the stationary point [62]. The force constants can be determined analytically, by single numerical differentiation for methods for which only first derivatives are available such as MP3 and CCD, and by double numerical differentiation for those methods for which only energies are available.[22] The sensitivity of Raman intensities to basis set and correlation is even larger than that for IR intensities[24]. To have a more reliable result we need to use a large basis set size with large polarized valence orbitals and consider the scaling factors which should be obtained for any level of theory and basis set. Considering the mean absolute errors in harmonic vibrational frequencies shows that the CCSD(T) level of theory as well as the B3LYP method provides the lowest error between all the available possibilities. Considering the simple fact that CCSD(T) calculations usually take an unacceptably long time and the error in results from B3LYP level of theory calculations are in acceptable margin, makes it a favorable method to perform this type of calculations. Some of these methods provide random errors which make it more complicated in comparison with methods such as HF which usually includes large error (10% higher) but exhibits the same behavior and can be improved by scaling the end results. The intensities of the computed lines are representative of the probability of a certain transition or absorption. To compute these probabilities we need to calculate the transition dipole moment from the wave function and so we should look into the time-dependent behavior of wave functions. The relation to provide us with the probability of transition (due to some external influence such as electromagnetic field or a collision) between the different stationary states is the famous Fermi's golden rule:

$$\omega_{m\to n} = \frac{2\pi}{\hbar} |\langle m|P|n\rangle|^2 \, \delta(E_m - E_n) \tag{2.24}$$

That is the transition rate which is defined as the probability per unit time for a quantum system to transit from stationary state m to another stationary state n. In this relation P is the time dependent external perturbation. As we know from our mathematical background, the closer this to states are, the higher the probability for the transition to occur which will yield a higher intensity transition. Often times in spectroscopy we encounter the case in which instead of one state we have several possible states which in this case the concept of density of states, $\rho(E_n)$, can be useful. In such case we can write the Fermi golden rule in the form:

$$\omega_{m\to n} = \frac{2\pi}{\hbar} |\langle m|P|n\rangle|^2 \rho(E_n) \tag{2.25}$$

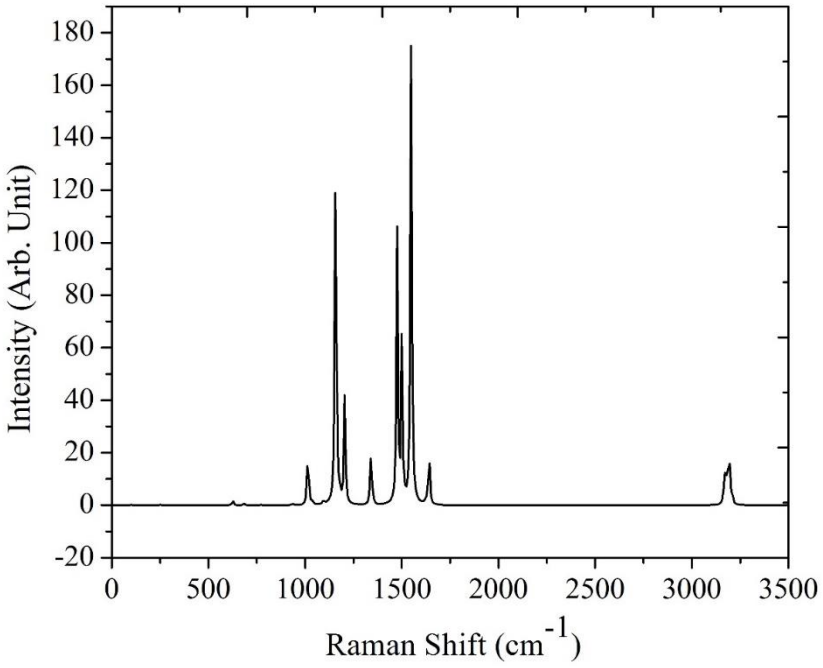

Figure 2.20: Computational Raman spectrum of **trans azobenzene**. The calculation was performed using the B3LYP level of theory with 6-311++G(d,p) as the basis set and the molecule was optimized with tight convergence criteria initially. Requested convergence on RMS density matrix=1.00D-08. Only harmonic frequencies being included in this calculation.

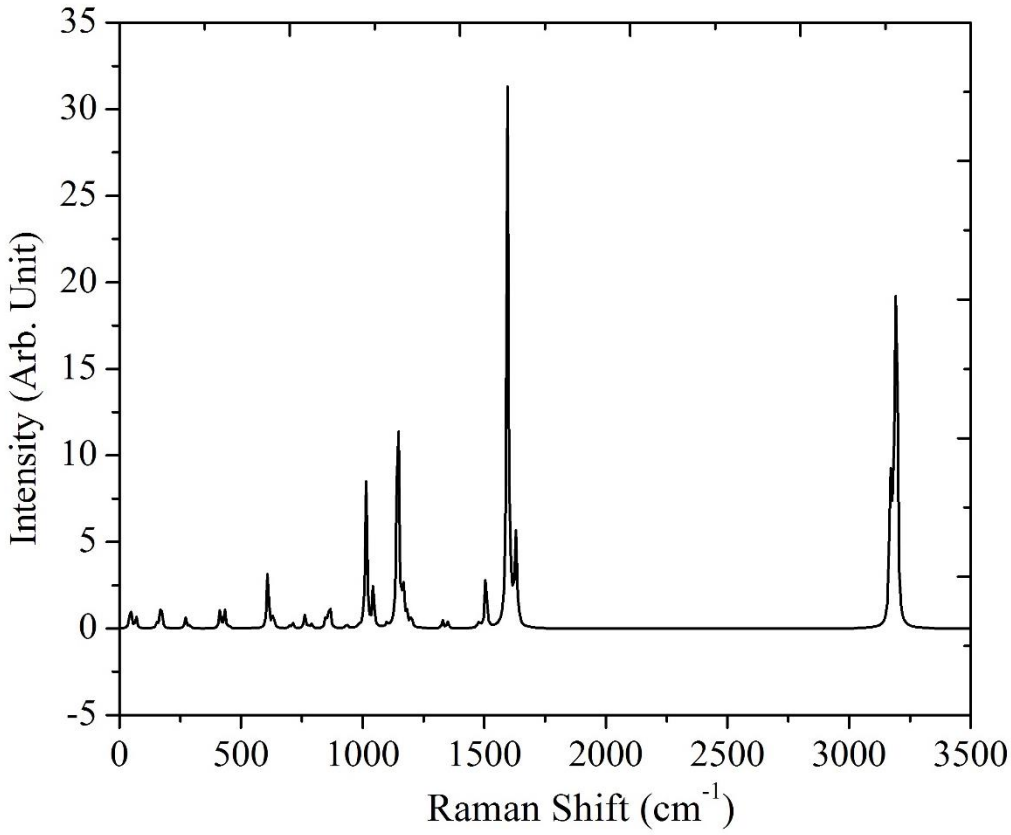

Figure 2.21: Computational Raman spectrum of **cis azobenzene**. Calculation has been performed using B3LYP level of theory with 6-311++G(d,p) as the basis set and the molecule is optimized with tight convergence criteria initially. Requested convergence on RMS density matrix=1.00D-08. Only harmonic frequencies being included in this calculation.

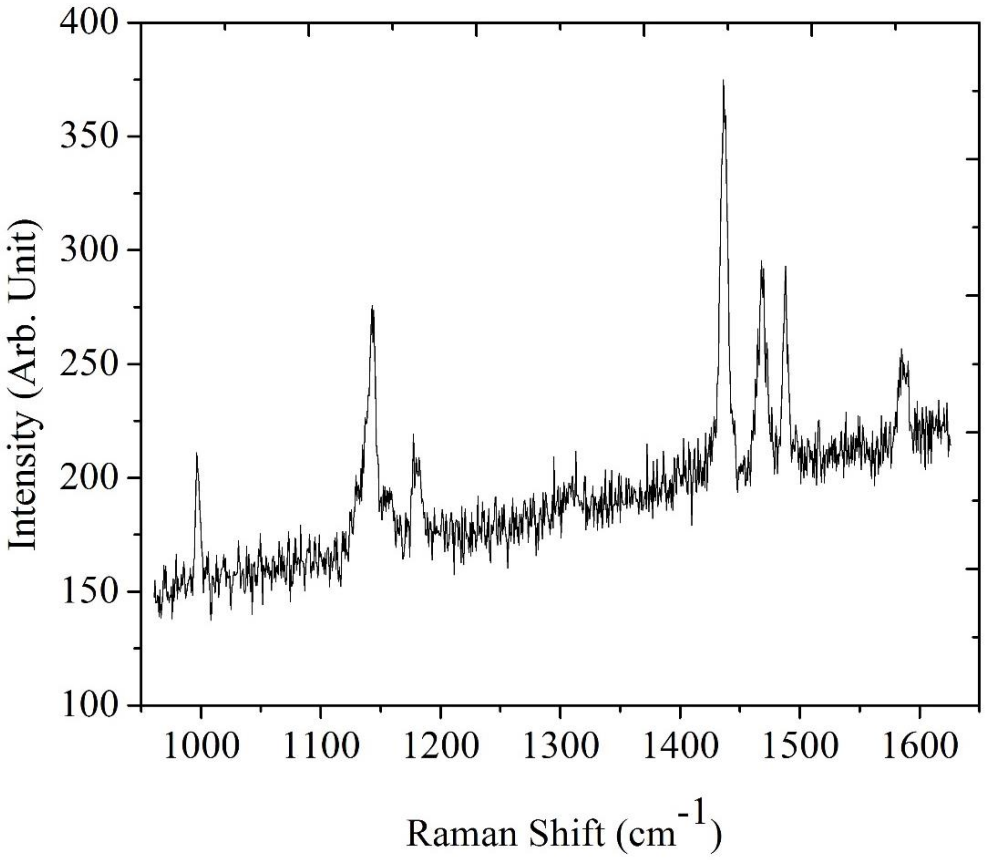

Figure 2.22: Experimental Raman spectrum obtained for trans azobenzene for small region in order to see the details of the spectrum clearly.

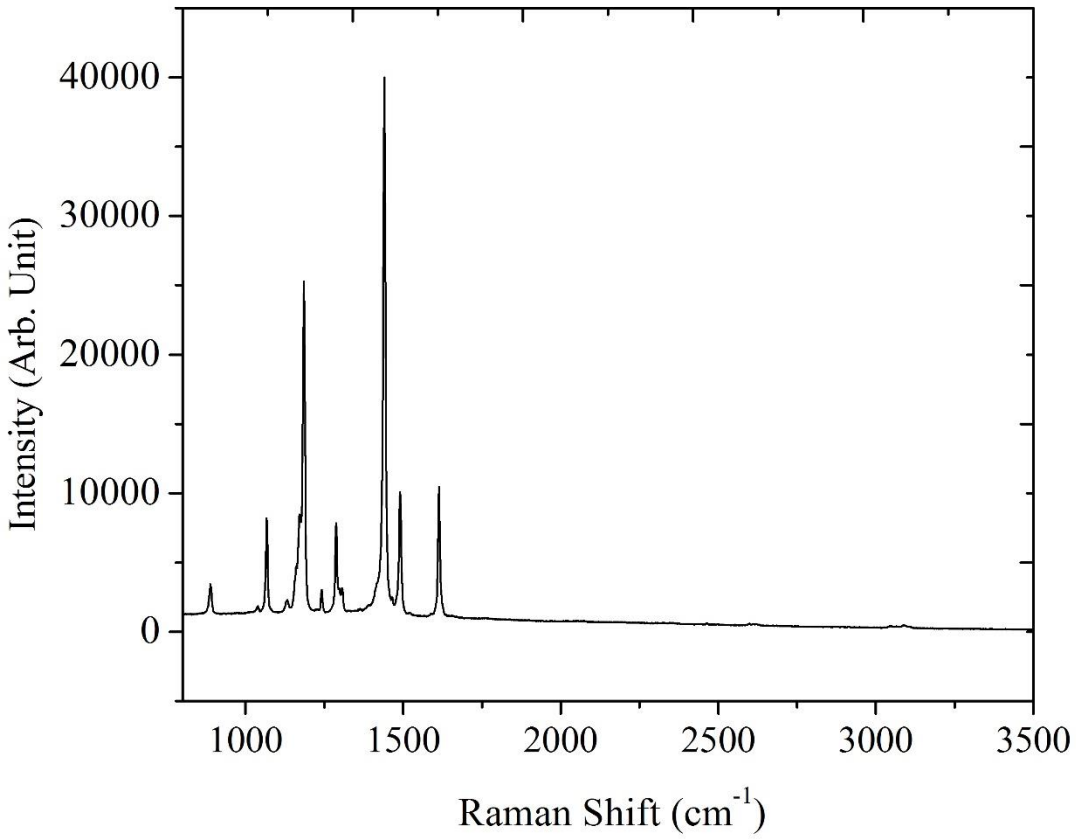

Figure 2.23: Experimental Raman spectrum for the trans 2,2́,6,6́-tetrafluoroazobenzene.

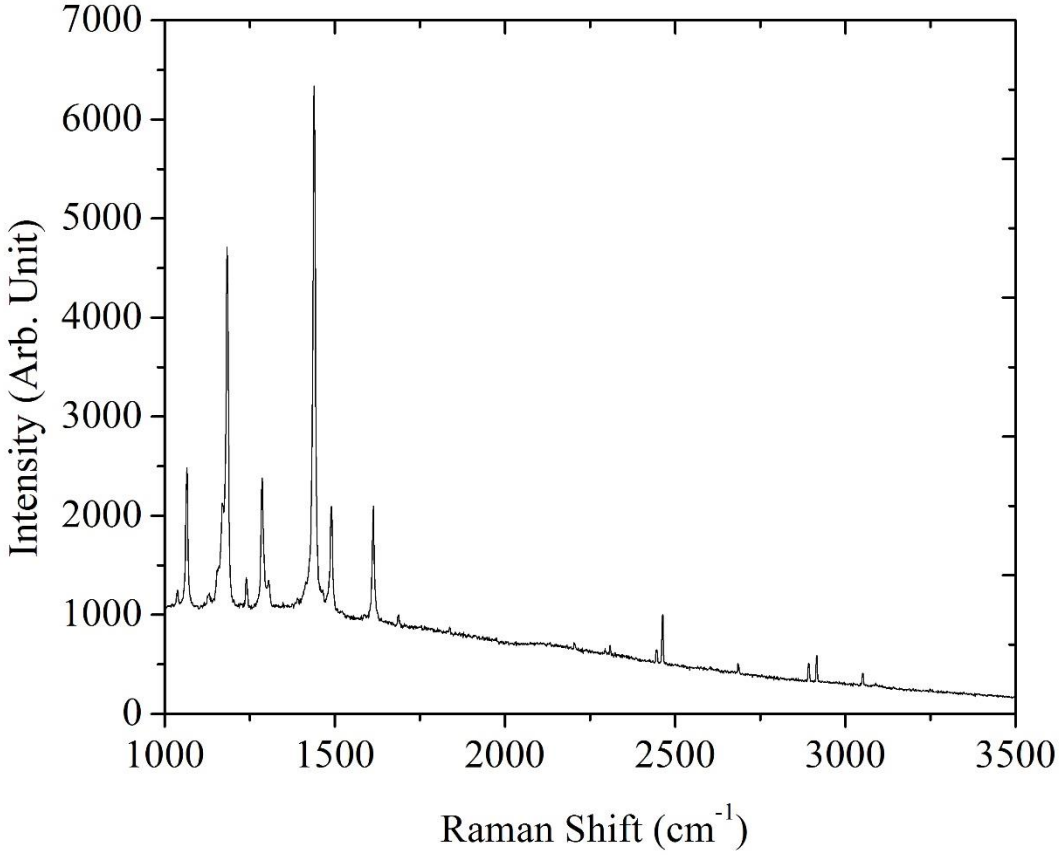

Figure 2.24: Experimental Raman spectrum for the trans 2,2́,6,6́-tetrafluoroazobenzene. The laser wavelength used in this experiment was 676.457 nm and the laser power was 4.5 mW.

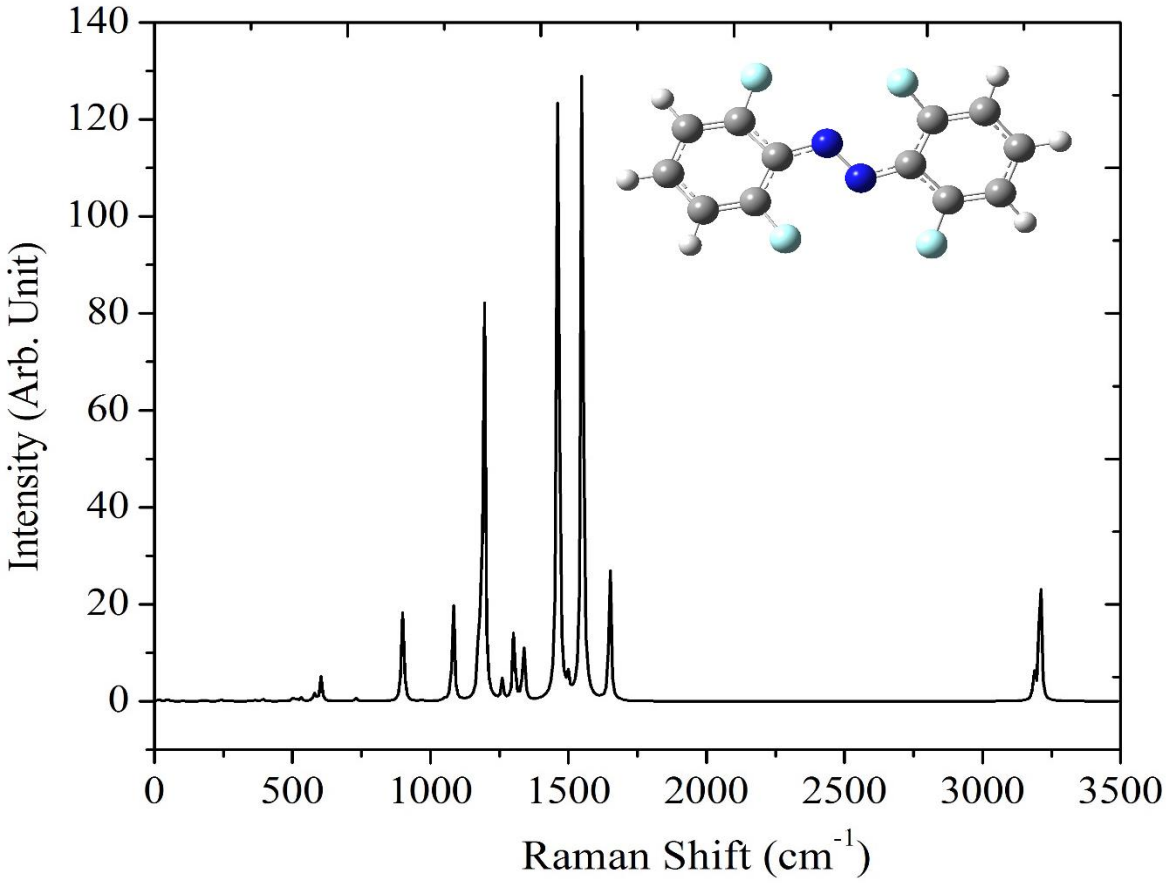

Figure 2.25: Computational Raman spectrum of trans 2,2́,6,6́-tetrafluoroazobenzene. The calculation was performed using B3LYP level of theory with 6-311++G(d,p) as the basis set and the molecule is optimized with tight convergence criteria initially. Requested convergence on RMS density matrix=1.00D-08. Only harmonic frequencies being included in this calculation.

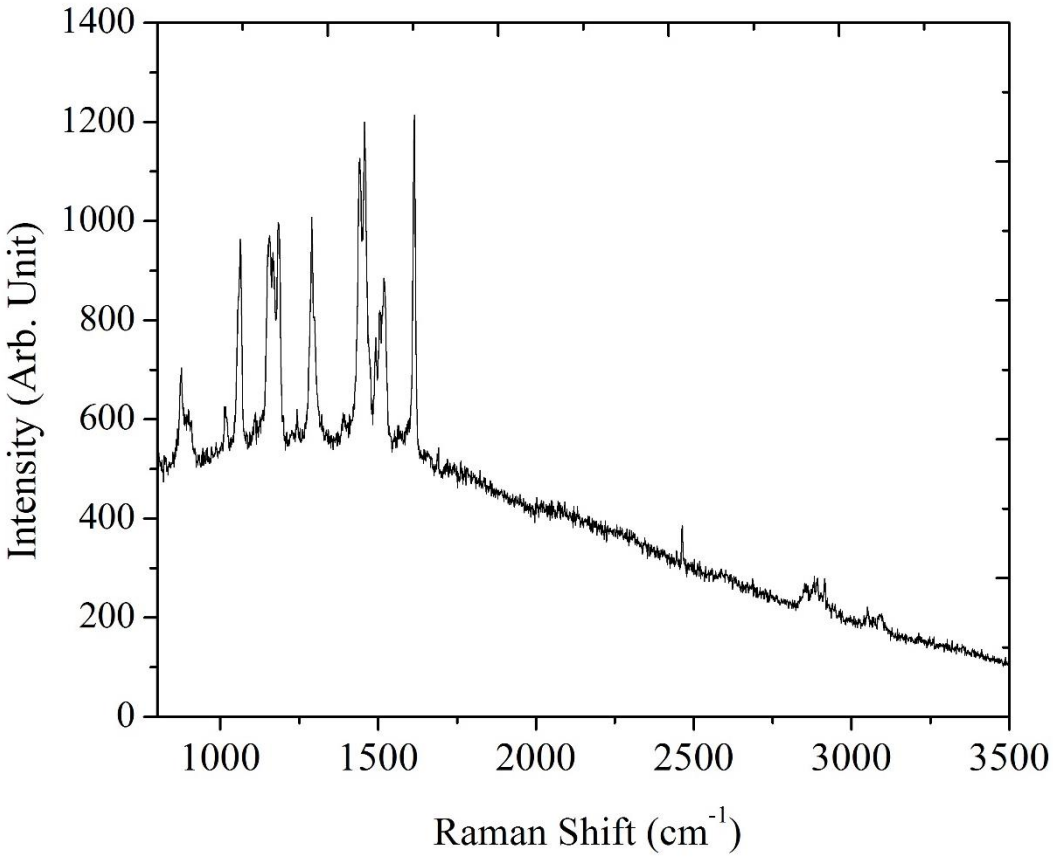

Figure 2.26: Experimental Raman spectrum for the cis 2,2́,6,6́-tetrafluoroazobenzene.

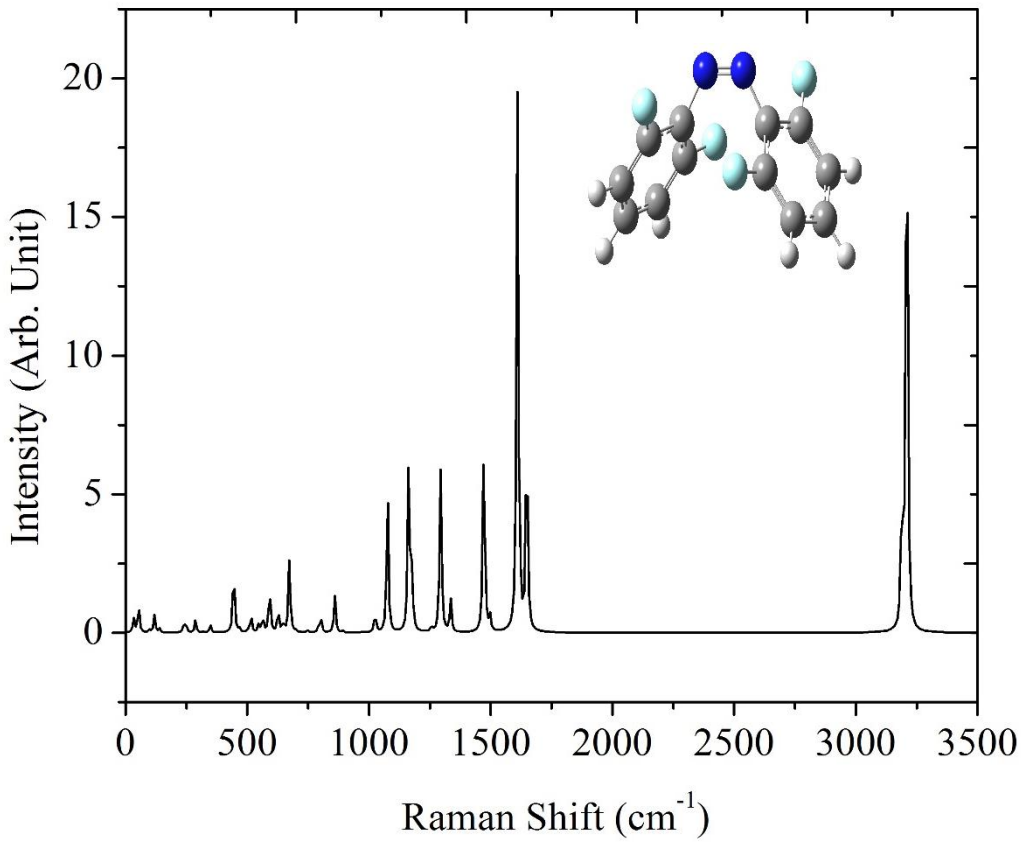

Figure 2.27: Computational Raman spectrum of cis 2,2́,6,6́-tetrafluoroazobenzene. The calculation was performed using B3LYP level of theory with 6-311++G(d,p) as the basis set and the molecule is optimized with tight convergence criteria initially. Requested convergence on RMS density matrix=1.00D-08. Only harmonic frequencies were included in the calculations.

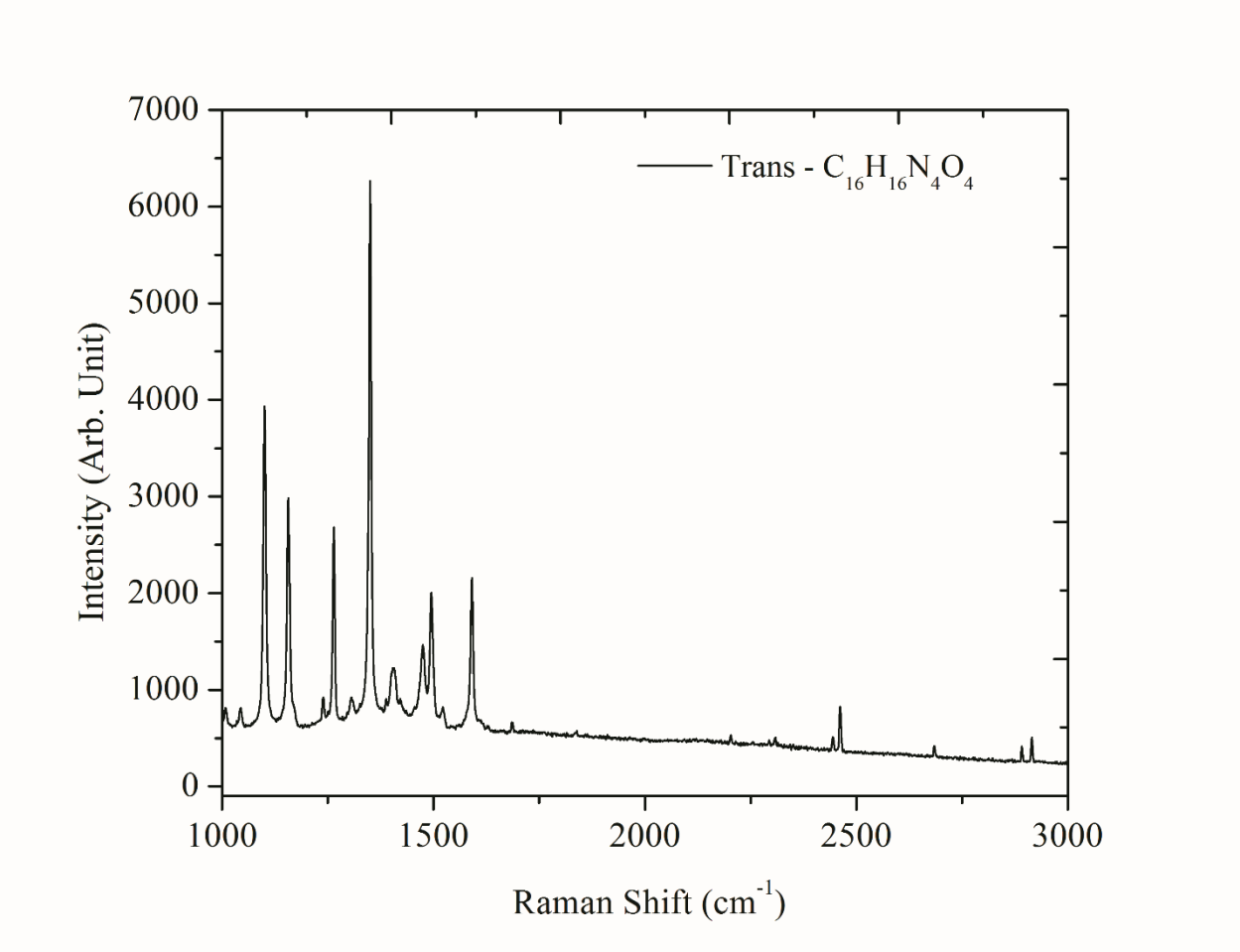

Figure 2.28: Experimental Raman spectrum of trans 2,2',6,6' tetramethyl-(4,4') dinitro-azobenzene, $C_{16}H_{16}N_4O_4$.

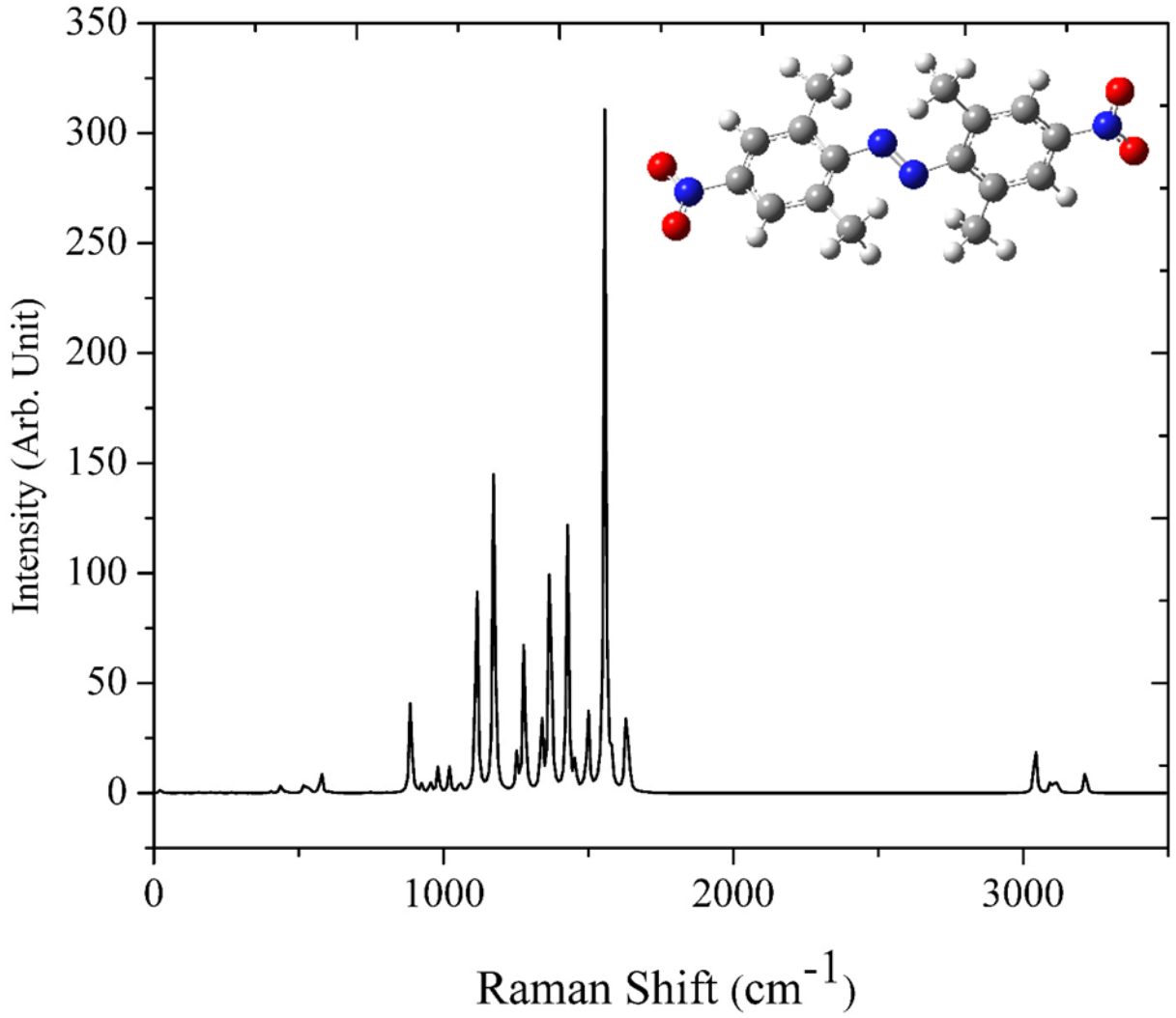

Figure 2.29: Computed Raman spectrum of trans 2,2',6,6' tetramethyl-(4,4') dinitro-azobenzene, $C_{16}H_{16}N_4O_4$. Computation has been done at B3LYP level of theory with 6-311++G(d,p) as basis set. The sample molecule is originally optimized with tight convergence criteria and ultra-fine grid for integrals.

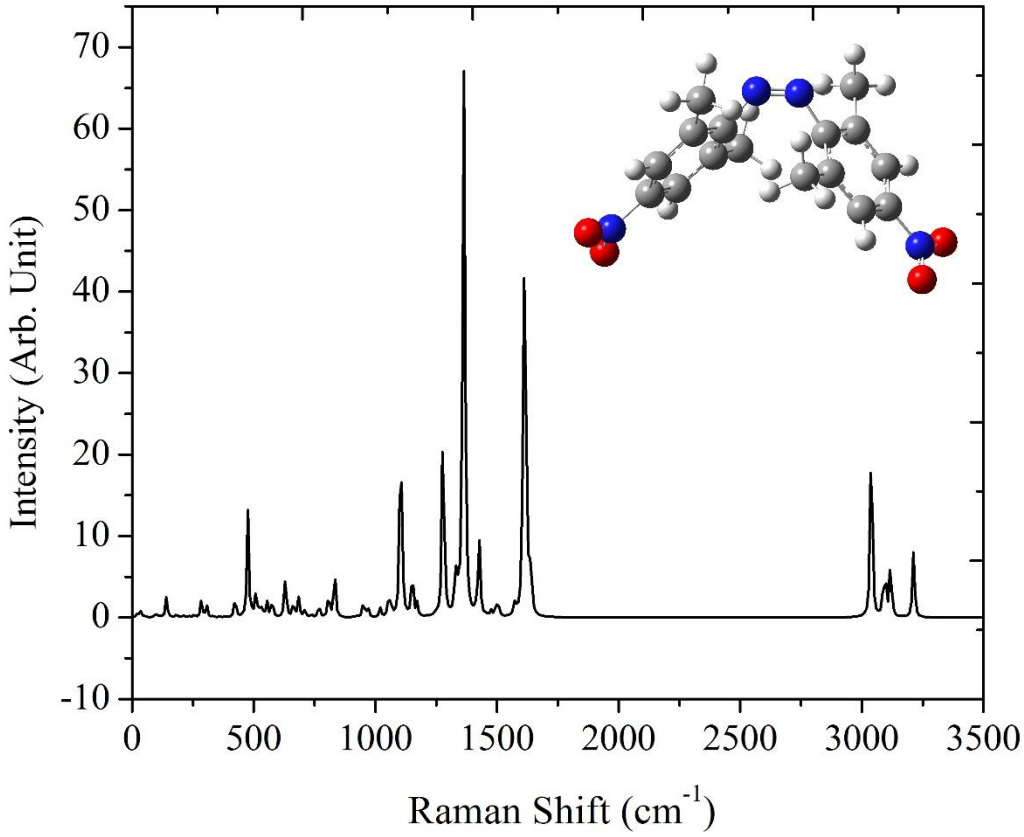

Figure 2.30: Computed Raman spectrum of **cis** 2,2',6,6' tetramethyl-(4,4') dinitro-azobenzene, $C_{16}H_{16}N_4O_4$. Computation has been done at B3LYP level of theory with 6-311++G(d,p) as basis set.

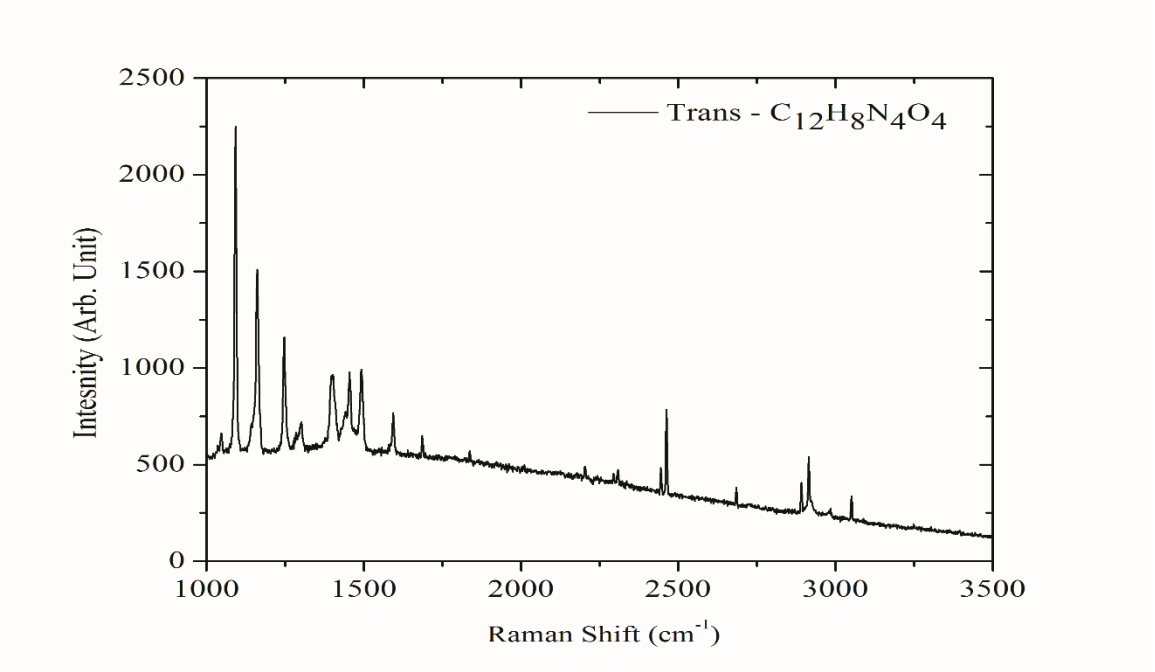

Figure 2.31: Experimental Raman spectrum of 4,4' dinitro-azobenzene; $C_{12}H_8N_4O_4$.

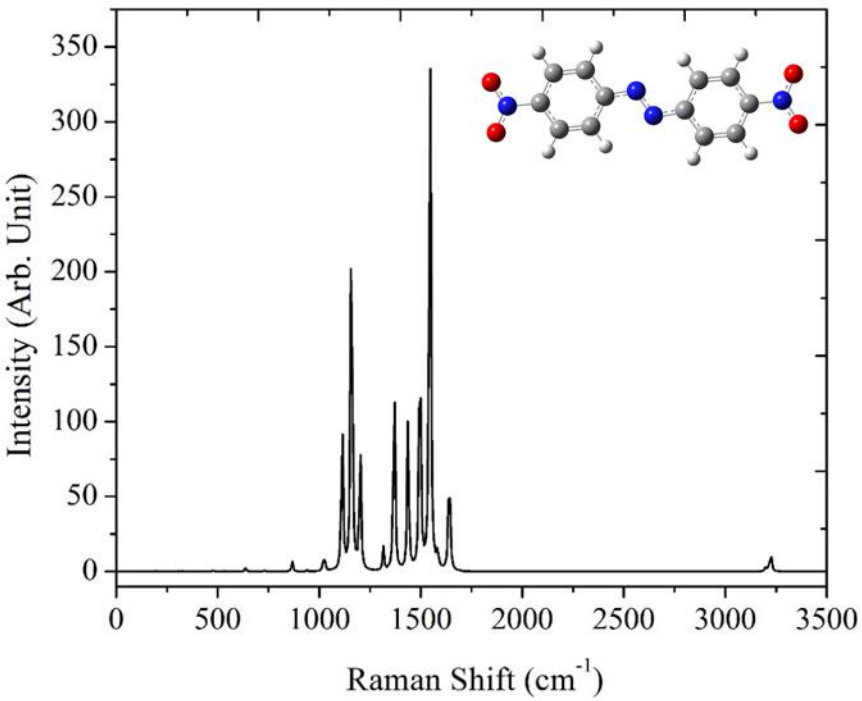

Figure 2.32: Computed Raman spectrum of **trans** 4,4' dinitro-azobenzene ($C_{12}H_8N_4O_4$). Computation has been done at B3LYP level of theory with 6-311++G(d,p) as the basis set.

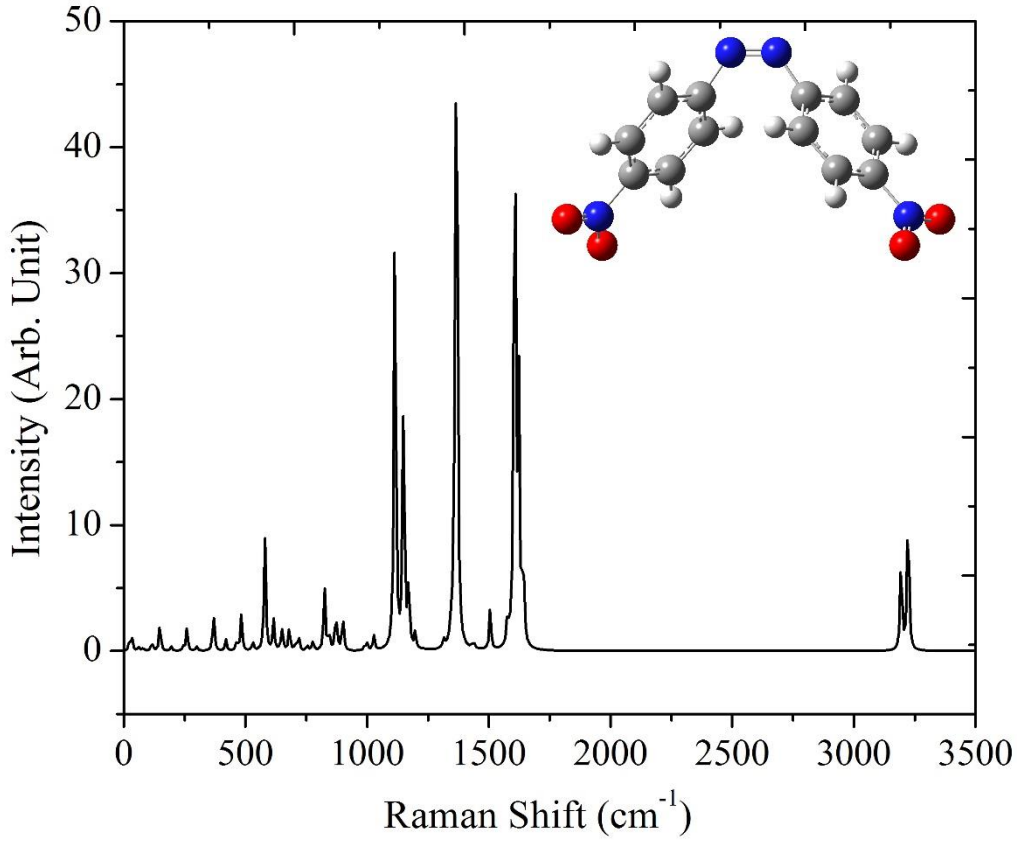

Figure 2.33: Computed Raman spectrum of cis 4,4' dinitro-azobenzene ($C_{12}H_8N_4O_4$). Computation has been done at B3LYP level of theory with 6-311++G(d,p) as basis set.

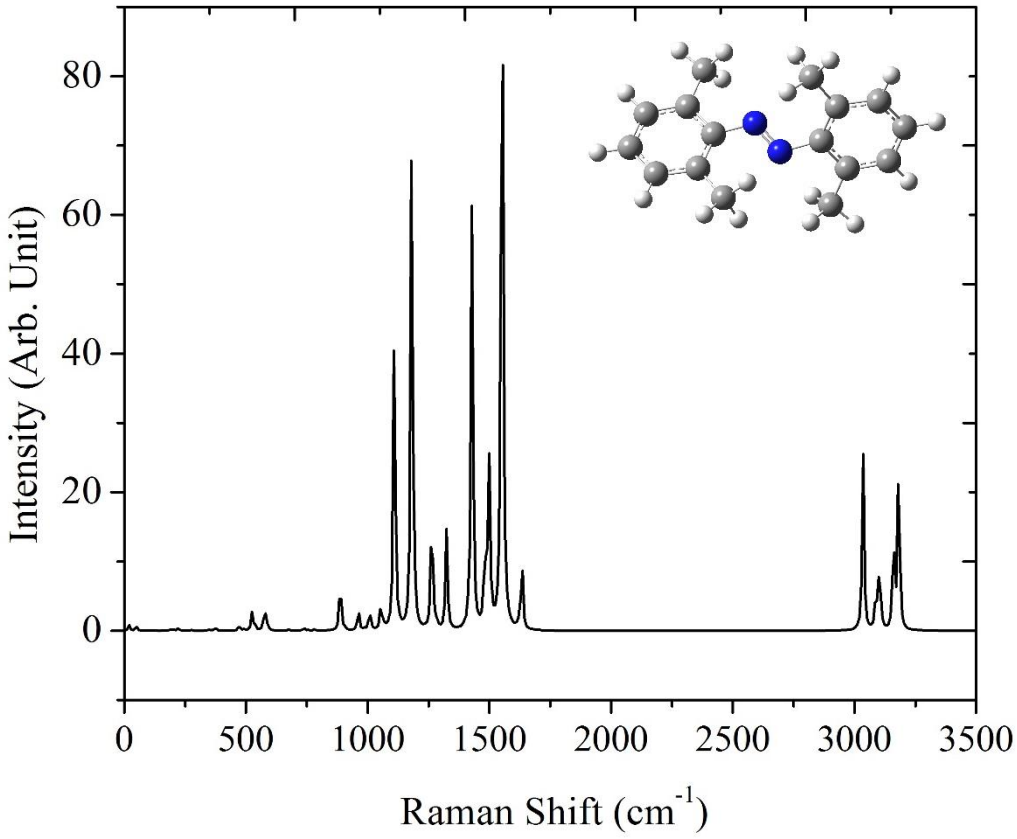

Figure 2.34: Computed Raman spectrum of trans 2,2',6,6' tetramethyl-azobenzene ($C_{16}H_{18}N_2$). Computation has been done at B3LYP level of theory with 6-311++G(d,p) as basis set. The sample molecule is originally optimized with tight convergence criteria and ultra-fine grid for integrals.

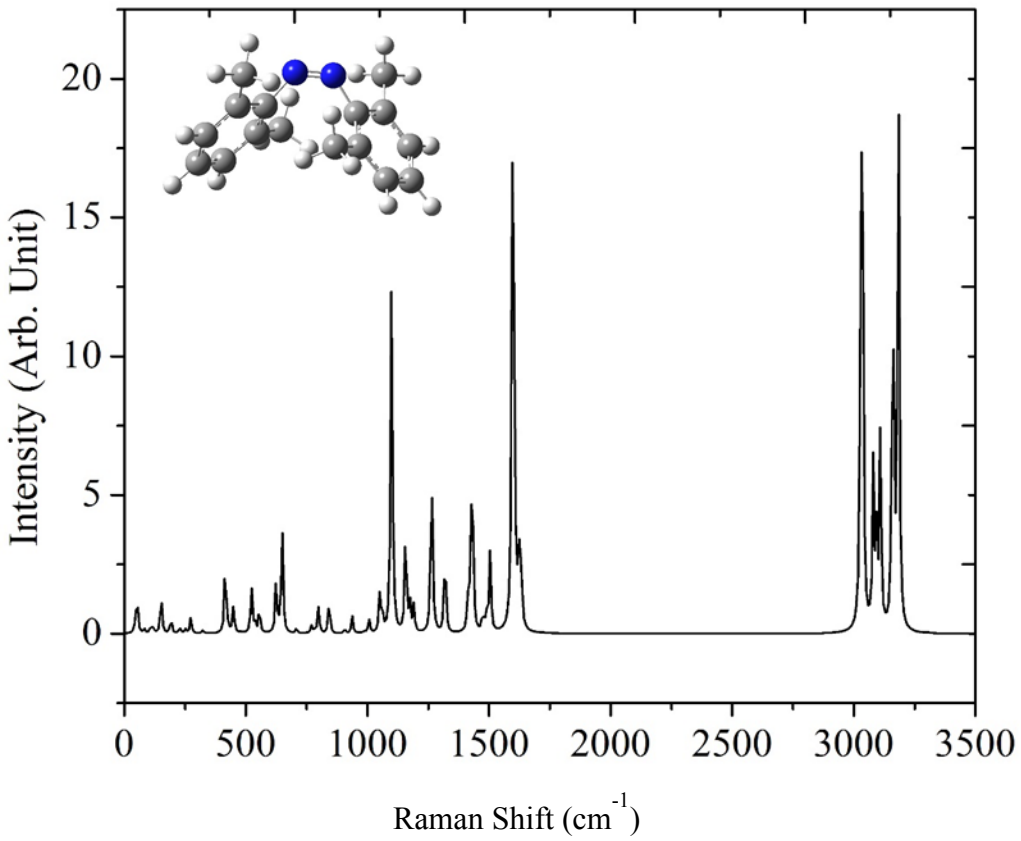

Figure 2.35: Computed Raman spectrum of **cis** 2,2',6,6' tetramethyl-azobenzene ($C_{16}H_{18}N_2$). The computation was done at B3LYP level of theory with 6-311++G(d,p) as basis set. The sample molecule is originally optimized with tight convergence criteria and ultra-fine grid for integrals.

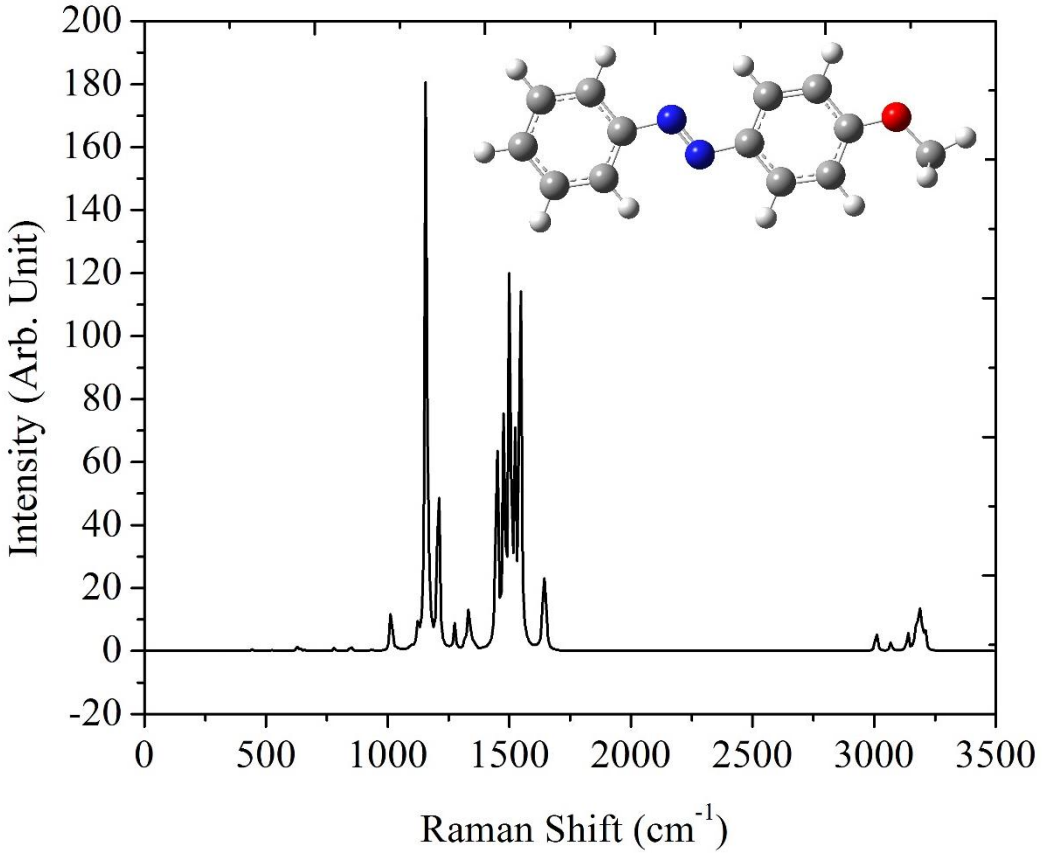

Figure 2.36: Computed Raman spectrum of trans 4-Methoxyazobenzene ($C_{13}H_{12}N_2O$). The computation was done at B3LYP level of theory with 6-311++G(d,p) as basis set. The sample molecule is originally optimized with tight convergence criteria and ultra-fine grid for integrals.

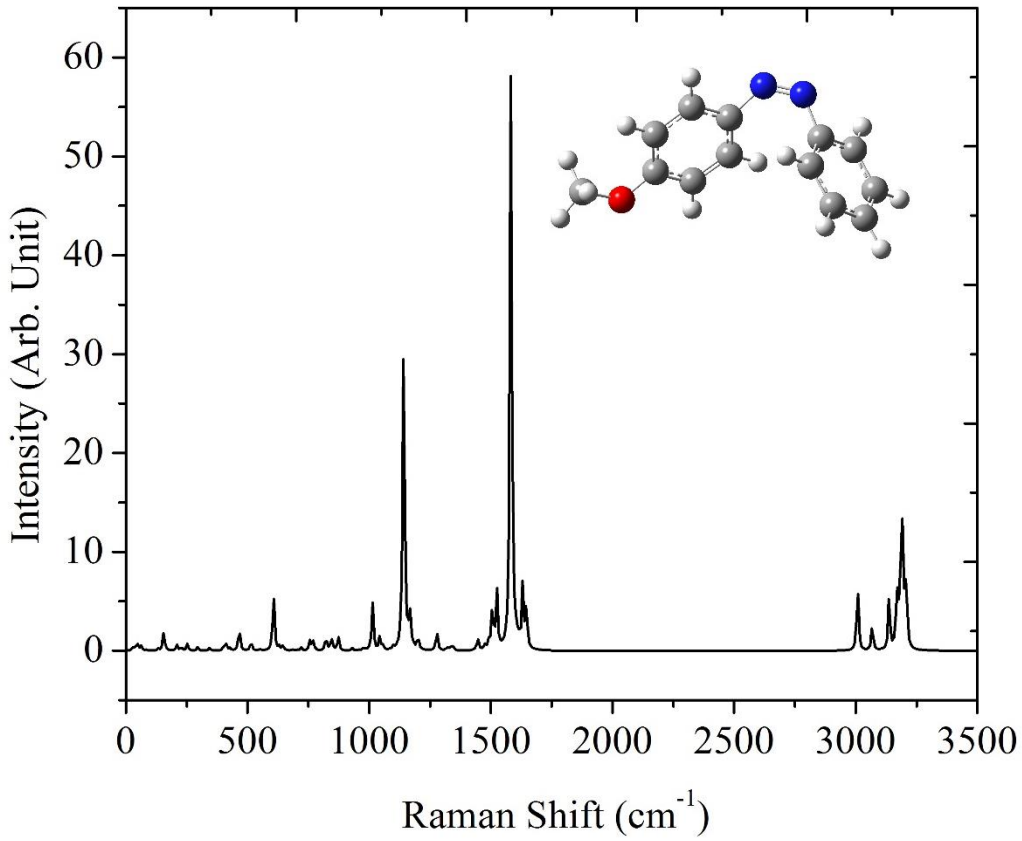

Figure 2.37: Computed Raman spectrum of cis 4-Methoxyazobenzene ($C_{13}H_{12}N_2O$). The computation was done at B3LYP level of theory with 6-311++G(d,p) as basis set. The sample molecule is originally optimized with tight convergence criteria and ultra-fine grid for integrals.

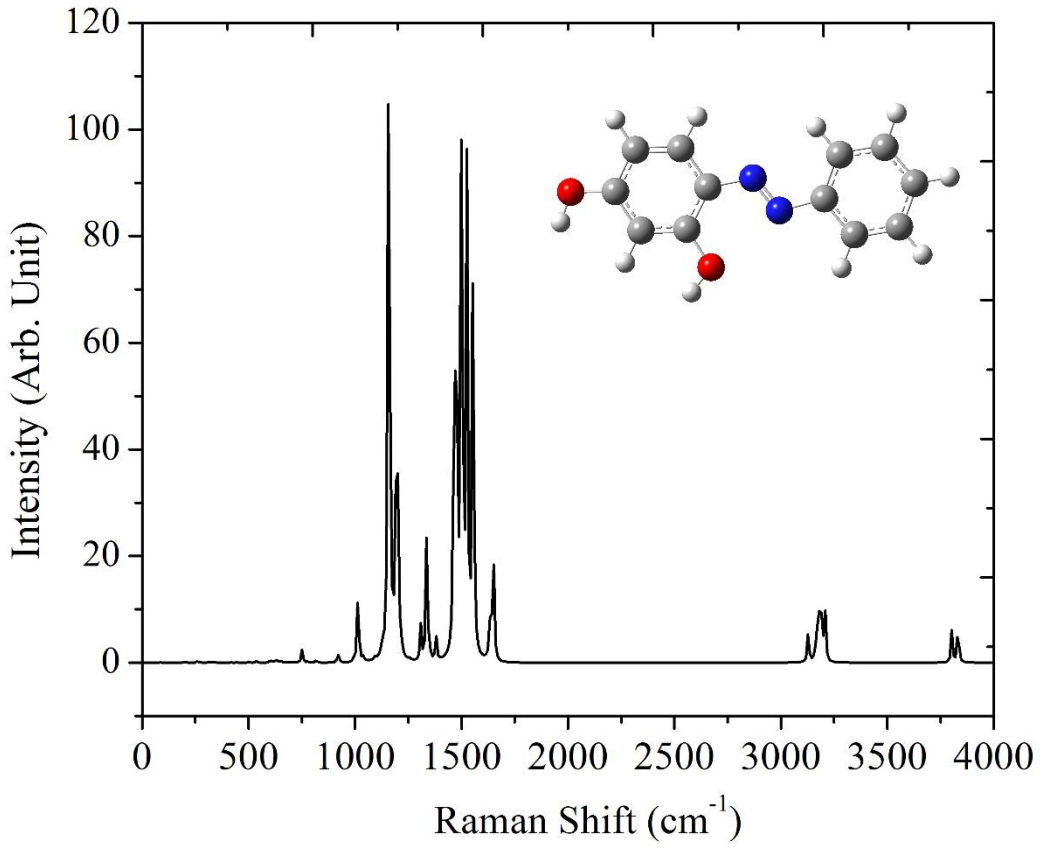

Figure 2.38: Computed Raman spectrum of trans 2,4-Dihydroxyazobenzene,4 - (Phenylazo) resorcinol ($C_{12}H_{10}N_2O_2$). The computation has been done at B3LYP level of theory with 6-311++G(d,p) as basis set. The sample molecule is originally optimized with tight convergence criteria and ultra-fine grid for integrals.

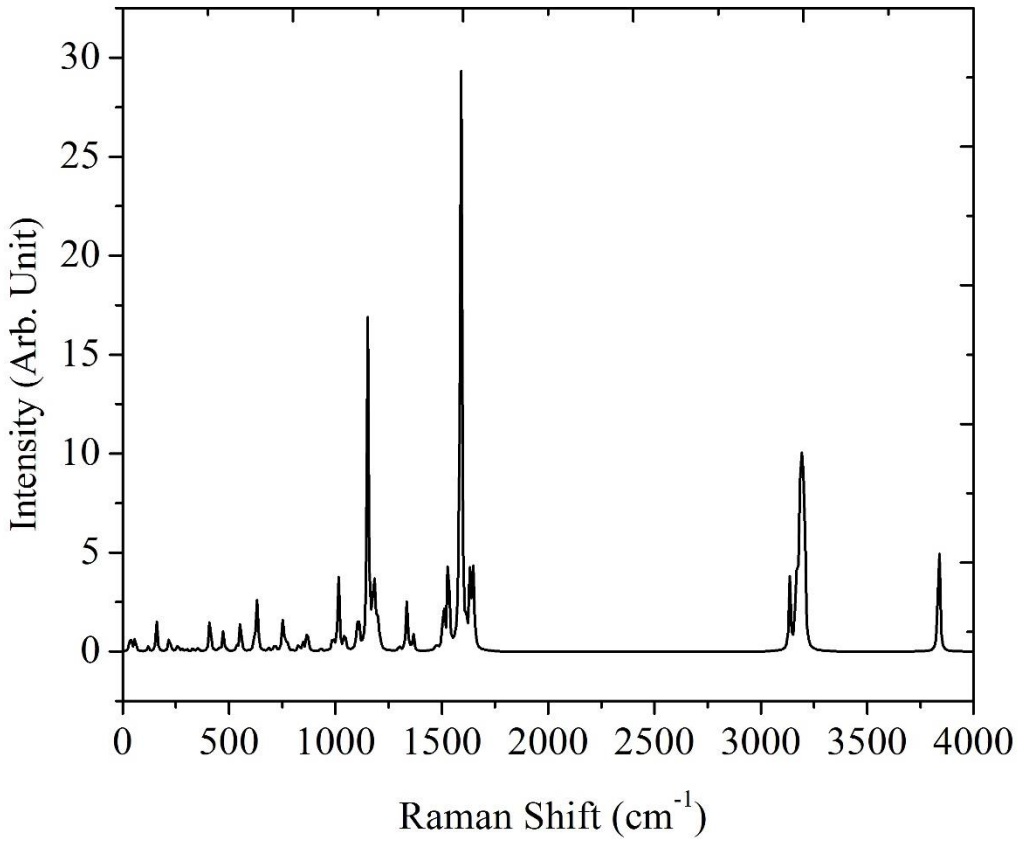

Figure 2.39: Computed Raman spectrum of cis 2,4-Dihydroxyazobenzene, 4-(Phenylazo) resorcinol ($C_{12}H_{10}N_2O_2$). The computation has been done at B3LYP level of theory with 6-311++G(d,p) as basis set. The sample molecule is originally optimized with tight convergence criteria and ultra-fine grid for integrals.

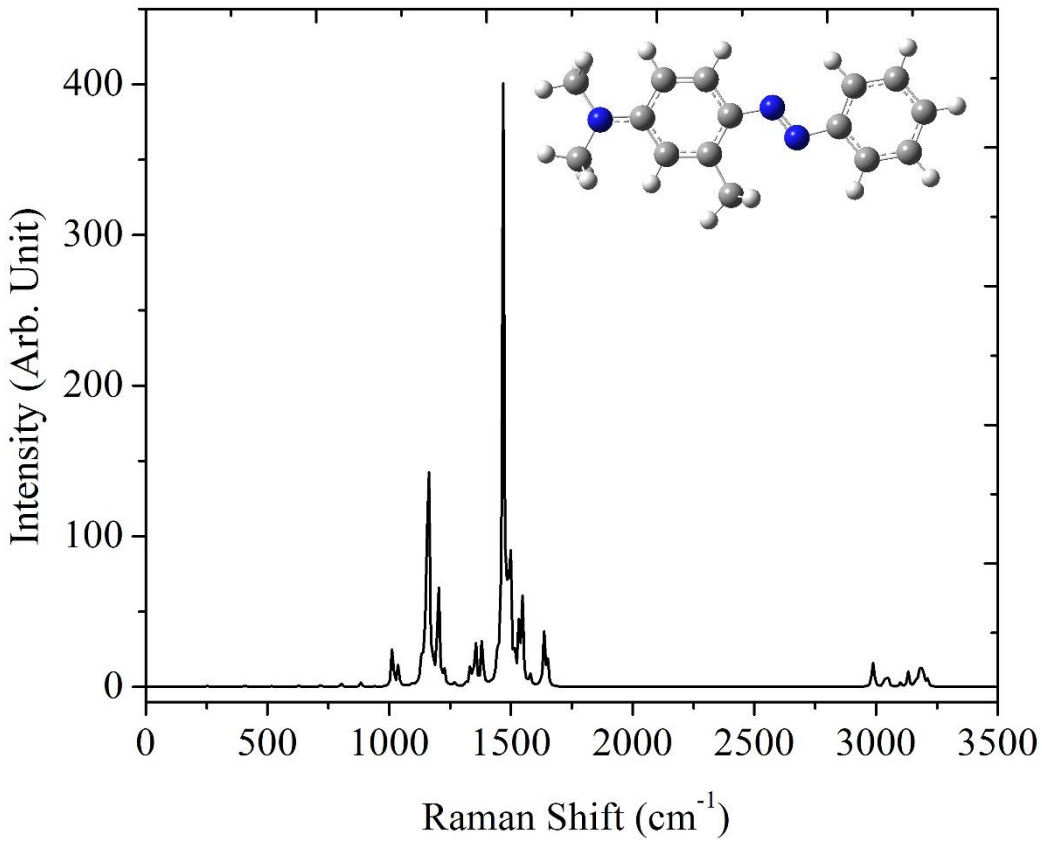

Figure 2.40: Computed Raman spectrum of trans 4-Dimethylamino-2-methylazobenzene ($C_{15}H_{17}N_3$). The computation has been done at B3LYP level of theory with 6-311++G(d,p) as basis set. The sample molecule is originally optimized with tight convergence criteria and ultra-fine grid for integrals.

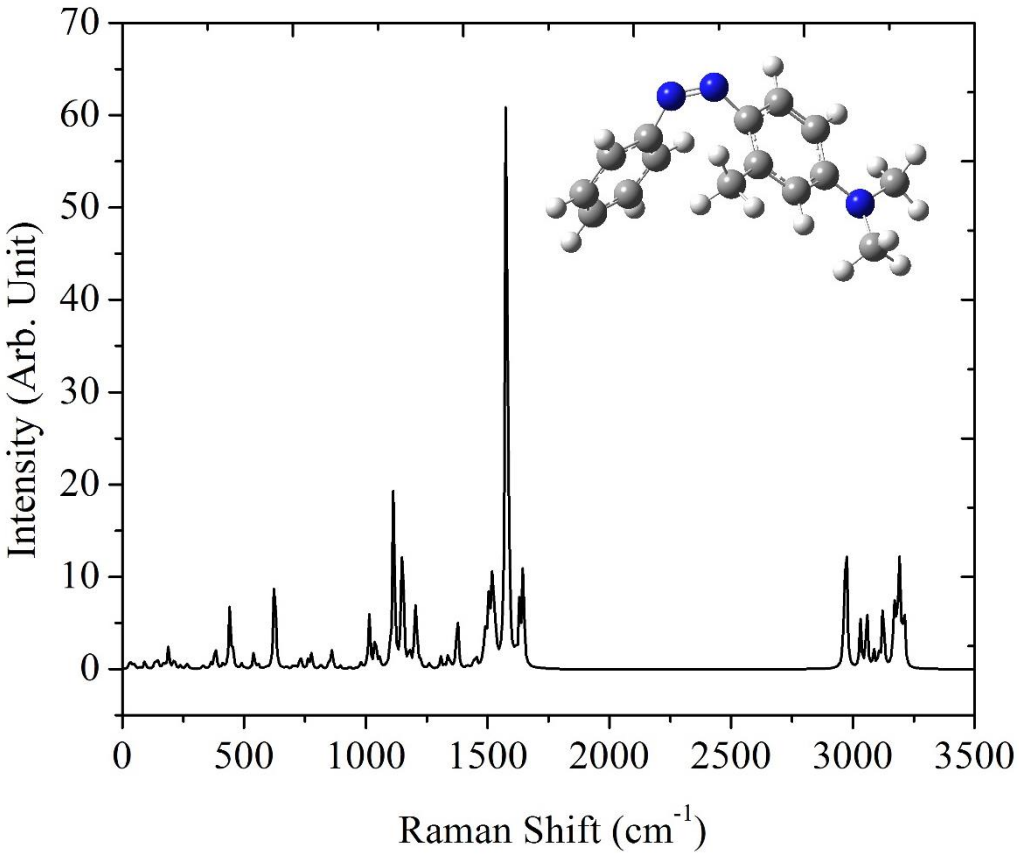

Figure 2.41: Computed Raman spectrum of cis 4-Dimethylamino-2-methylazobenzene ($C_{15}H_{17}N_3$). The computation was done at B3LYP level of theory with 6-311++G(d,p) as basis set. The sample molecule is originally optimized with tight convergence criteria and ultra-fine grid for integrals.

2.6 Computational UV-Vis Spectroscopy

Another interesting property which can be computed and described using quantum chemistry calculations is the UV-Vis spectrum. Also calculations can give the wavelength at which radiation should be used to induce the trans to cis isomerization in molecules. Regarding azobenzene itself this was known since from the literature we do know that UV light at ~300 nm is needed to transform the trans isomer into cis but this is unknown for other derivatives. Simulations of UV-Vis spectrum reveal the absorption region of the trans form. Photons in UV-Vis region of the electromagnetic spectrum have enough energy (1-4 eV) to induce transitions from filled and half-filled orbitals (even Rydberg states) and also to break a chemical bound. The UV-Vis region matches the electronic and vibrational transitions. Time dependent density functional theory methods made this type calculations readily possible. TD-DFT which is an ab initio method based on wave function works is based upon finding the optimized electronic structure of the ground and several excited states. By International Union of Pure and Applied Chemistry gold book definition TD-DFT is a method for computing accurate excitation energies at a low computational cost in large molecular species within the time-dependent scheme and the density functional theory. By applying an oscillating potential and varying its frequency, a resonance occurs whenever the frequency equals the difference between the two energy eigenvalues of the system. The basic idea is to apply time-dependent perturbation theory to first order and to describe the time dependent linear response of the one-particle density to a time-dependent oscillating electric field. Before the time-dependent electric field is applied, the molecular system is assumed to be in its electronic ground state, that is, to obey the ground-state Kohn–Sham equation[67]. We simulate the absorption spectrum which contains several absorption bands as a function of incident photon energy. The quantity of interest here is the extinction coefficient ε which is formulated as:

$$\varepsilon(\lambda) = \frac{A(\lambda)}{\beta d} \tag{2.26}$$

in this relation d is the optical path, β is the molar concentration (mol/lit) and the measured absorbance $A = -log(I/I_0)$. The molecular absorption cross-section can then be calculated from the experimental value of ε from:[68]

$$\sigma = \frac{2.303\varepsilon}{N_a} = 3.825 \times 10^{-19} \quad (2.27)$$

and σ has dimensions of cm^2. Experimental measurements of this absorbance spectrum have been performed for the trans and the cis isomers of several azobenzene derivatives. In addition, modeling of electronically excited states was performed to compute the UV-Vis spectrum. The Gaussian quantum chemistry code could also be used to model the effects of the solvent environment and compute the spectrum for different organic solvents by placing the solute in a cavity within the solvent reaction field. This is important since solvents can interact with the electronic spectral bands of the sample molecule. In fact solvation can change the ground state and the excited electronic states energy. This can be especially true for polar solvents since the cis-azobenzene derivatives possess a large dipole moment making solute-solvent interactions particularly important. The lines in the calculated results are basically single lines but we know that in reality there are always broadening due to Franck-Condon factors and ro-vibrational effects. Therefore we introduce this broadening to the calculated lines manually by applying a Lorentzian or Gaussian broadening to the lines. As a first approximation, to simulate the intensities of UV-Vis signals, the square of the transition dipole moment integral between the initial and the final electronic state has to be evaluated[67]. We need to compute the oscillator strength, $f_{0\to n}$, which is the probability of transition from ground state to n's exited states.

$$f = 2303 \frac{mc_0^2}{N_a \pi e^2 n} \int \varepsilon(\bar{v})\, d\bar{v} = \frac{4.32 \times 10^{-9}}{n} \int \varepsilon(\bar{v})\, d\bar{v} \quad (2.28)$$

The molecule is considered to be an oscillating dipole. In the above relation n is the refractive index and $\bar{v}$ is the wavenumber in cm^{-1} and the oscillator strength itself is a dimensionless quantity. The relation between the oscillator strength and the square of the transition moment integral is summarized as:

$$f = \frac{4\pi m v}{3\hbar e^2} \langle \Psi_1 | \boldsymbol{M} | \Psi_2 \rangle^2 \quad (2.29)$$

in which Ψ_1 and Ψ_2 are the initial and final states and **M** is the dipole moment operator.

The other interest here is the optical activity of our sample molecules. All of our samples are light sensitive and studying their optical properties was one of the initial goals. Optical activity is due to molecular chirality and can be observed experimentally through radiating sample with linearly polarized light. Optical activity is usually described as:

$$\alpha_{\lambda}^{T} = \frac{\alpha_{obs} \times 100}{\ell \times c} \tag{2.30}$$

where α_{obs} is the observed rotation in degrees which is the solution minus pure solvent and ℓ is optical path length in meters and c is the concentration in grams per 100 ml [69].

In general we can categorize the optical activities as vibrational circular dichroism (VCD), optical rotary dispersion (ORD) and circular dichroism (CD). ORD is the measurement, as a function of wavelength, of a molecule's ability to rotate the plane of linearly polarized light.[70] CD results from the fact that left-handed and right-handed circularly polarized light are absorbed differently in the absorption band regions of spectrum. VCD is particularly difficult to predict since the Born-Oppenheimer approximation is not valid in this case [66]. A CD graph includes the difference of the molar absorption for the right and left handed circularly polarized light ($\Delta\varepsilon = \varepsilon_L - \varepsilon_R$) as a function of wavelength. The Gaussian G09 quantum chemistry package which we use is able to compute the electronic circular dichroism as well.

$$CD = \varepsilon_L - \varepsilon_R = \frac{k_L - k_R}{c} \tag{2.31}$$

$$I = I_0\, 10^{-kd} \tag{2.32}$$

Considering above relations for CD, θ, the rotation angle would be:

$$\theta\ (rad/cm) = \frac{2.303\ (\varepsilon_L - \varepsilon_R)}{4d} \tag{2.33}$$

In this relation d is optical path length through the sample. Optical rotatory dispersion is related to the rotation of polarization axis of the linearly polarized light after passing through the sample. A difference in in refractive index for right-hand and left-hand polarization leads to this optical rotation. That again is due to different speed of propagation for right- and left-handed polarization. An ORD spectrum is the dependence of this angle (degree) of rotation as a function of incident linearly polarized light wavelength (nm). Specifically if the sample has n_R and n_L as the right and left handed polarized light index of refraction, respectively, the rotation angle can be described as:

$$\alpha = \frac{n_L - n_R}{\lambda} \tag{2.34}$$

and the optical rotation in ϕ which has the unit of rad/cm will be:

$$\phi = \frac{\pi}{\lambda}(n_L - n_R) \tag{2.35}$$

In this equation λ is the wavelength of the incident polarized light.

2.6.1 2,2́,6,6́-tetrafluoroazobenzene:

Below we present the results for electronic transition results including the UV-Vis spectrum and Circular Dichroism, Vibrational circular dichroism (VCD), and Optical rotatory dispersion (ORD) results related to our main sample, 2,2́,6,6́-tetrafluoroazobenzene. We also present the experimental results to compare how well the computational results can represents the experimental data.

The UV-Vis type calculations includes:

I) Carefully optimizing the sample molecule with a highly polarized basis set:

#p B3LYP/6-311++G(3df,3pd) Opt=(CalcFC,tight,MaxCycles=4000) SCF=(NoVa

rAcc,tight,MaxCycle=500,NoIncFock) Int=UltraFine

II) Performing a frequency calculation on the resulted geometry to make sure that there is no any negative frequency is available in the results:

#P Geom=AllCheck Guess=TCheck SCRF=Check GenChk

Freq RB3LYP/6-311++G(3df,3pd)

III) performing a TD-DFT calculation on the obtained results from previous computations:

#p B3LYP/6-311++G(3df,3pd) Geom=allcheck TD(Nstates=12,Root=1,50-50) S

CF=(NoVarAcc,tight,MaxCycle=500,NoIncFock) Int=UltraFine SCRF=(Solvent

=Acetonitrile)

In this calculation 12 excited states are included and the final state is the ground state (Root=1) and in this case the solvent is acetonitrile. The keyword 50-50 makes sure that both singlet states and triplet states are equally included in the calculations (this works only for closed-shell systems).

The main parts of data resulted from a TD-DFT computation for the cis 2,2́,6,6́-tetrafluoroazobenzene is provided below:

Polarizable Continuum Model (PCM)

==========

Model : PCM (using non-symmetric T matrix).

Atomic radii : UFF (Universal Force Field).

Polarization charges : Total charges.

Charge compensation : None.

Solution method : On-the-fly selection.

Cavity type : Scaled VdW (van der Waals Surface) (Alpha=1.100).

Cavity algorithm : GePol (No added spheres)

Default sphere list used, NSphG= 24.

Lebedev-Laikov grids with approx. 5.0 points / Ang**2.

Smoothing algorithm: Karplus/York (Gamma=1.0000).

Polarization charges: spherical gaussians, with

point-specific exponents (IZeta= 3).

Self-potential: point-specific (ISelfS= 7).

Self-field : sphere-specific E.n sum rule (ISelfD= 2).

Solvent : Acetonitrile, Eps= 35.688000 Eps(inf)= 1.806874

GePol: Number of generator spheres = 24

GePol: Total number of spheres = 24

GePol: Number of exposed spheres = 24 (100.00%)

GePol: Number of points = 2136

GePol: Average weight of points = 0.13

GePol: Minimum weight of points = 0.26D-07

GePol: Maximum weight of points = 0.20577

GePol: Number of points with low weight = 138

GePol: Fraction of low-weight points (<1% of avg) = 6.46%

GePol: Cavity surface area = 272.549 Ang**2

GePol: Cavity volume = 292.004 Ang**3

Excitation energies and oscillator strengths:

Excited State 1: Triplet-A 1.7568 eV 705.73 nm f=0.0000 <S**2>=2.000

60 → 65 0.21328

64 → 65 0.66229

This state for optimization and/or second-order correction.

Total Energy, E(TD-HF/TD-KS) = -969.952141170

Copying the excited state density for this state as the 1-particle RhoCI density.

Excited State 2: Singlet-A 2.7494 eV 450.95 nm f=0.0545 <S**2>=0.000

60 → 65 0.18361

64 → 65 0.67889

Excited State 3: Triplet-A 3.2629 eV 379.98 nm f=0.0000 <S**2>=2.000

61 → 65 0.57555

62 → 65 0.29063

62 → 67 -0.12574

63 → 69 -0.12077

64 →66 -0.15735

Excited State 4: Triplet-A 3.3073 eV 374.88 nm f=0.0000 <S**2>=2.000

51 →65 0.10707

58→65 -0.10381

60→65 0.58377

61 → 66 0.15301

62 → 69 0.12575

63 →67 0.13198

64 → 65 -0.19365

64→68 0.16324

Excited State 5: Triplet-A 3.4867 eV 355.59 nm f=0.0000 <S**2>=2.000

63 → 65 0.69011

Excited State 6: Triplet-A 3.6167 eV 342.81 nm f=0.0000 <S**2>=2.000

61 → 65 -0.28956

62 → 65 0.62107

63 → 66 -0.12776

Excited State 7: Singlet-A 3.7592 eV 329.82 nm f=0.0122 <S**2>=0.000

63 → 65 0.70081

Excited State 8: Singlet-A 3.8582 eV 321.36 nm f=0.0003 <S**2>=0.000

62 → 65 0.69843

Excited State 9: Triplet-A 4.0524 eV 305.96 nm f=0.0000 <S**2>=2.000

60→66 -0.10668

61 → 65 0.25083

61 → 68 0.22512

62 → 67 0.33755

63 → 66 -0.15197

63 → 69 0.29683

64 → 66 0.33980

Excited State 10: Singlet-A 4.0725 eV 304.44 nm f=0.0342 <S**2>=0.000

61 → 65 0.68196

64 → 66 0.12264

Excited State 11: Triplet-A 4.1039 eV 302.11 nm f=0.0000 <S**2>=2.000

51 → 65 -0.13439

58 → 65 0.11326

60 → 65 -0.22637

60 → 68 -0.12341

61 → 66 0.21438

62 → 69 0.30386

63 → 67 0.36503

63 → 68 -0.12211

64 → 68 0.26881

Excited State 12: Singlet-A 4.2304 eV 293.08 nm f=0.1967 <S**2>=0.000

60 → 65 0.67573

64 → 65 -0.18322

Excited State 13: Triplet-A 4.5911 eV 270.05 nm f=0.0000 <S**2>=2.000

51 → 65 -0.13061

58 → 65 0.16087

61 → 69 0.13832

62 → 66 0.18733

62 → 69 -0.19221

63 → 67 -0.31114

63 → 68 0.11178

64 → 67 0.27168

64 → 68 0.38051

Excited State 14: Triplet-A 4.6004 eV 269.51 nm f=0.0000 <S**2>=2.000

61 → 68 0.13287

62 → 67 -0.31963

62 → 68 0.13451

63 → 66 0.13533

63 → 69 -0.28450

64 → 66 0.49345

Excited State 15: Triplet-A 4.6750 eV 265.20 nm f=0.0000 <S**2>=2.000

60→67 -0.10201

61→66 -0.16856

61 → 69 0.15621

62 → 69 0.14032

64 → 67 0.55892

64 →68 -0.26956

Excited State 16: Triplet-A 4.7967 eV 258.48 nm f=0.0000 <S**2>=2.000

60 → 69 -0.12222

61→ 67 0.28811

62 → 65 0.11267

62→ 68 0.16490

63 → 66 0.24278

64 → 66 -0.10032

64 → 69 0.52800

Excited State 17: Singlet-A 5.0571 eV 245.17 nm f=0.0595 <S**2>=0.000

62 → 66 -0.15830

63 → 68 -0.13924

64 →67 0.65208

64 → 68 0.12575

Excited State 18: Triplet-A 5.0809 eV 244.02 nm f=0.0000 <S**2>=2.000

62 → 66 0.46397

62 → 69 0.15563

63 → 65 0.10908

63 → 67 0.16594

63 → 68 0.41478

64 → 67 -0.18129

Excited State 19: Singlet-A 5.1917 eV 238.81 nm f=0.0842 <S**2>=0.000

64 → 68 0.67407

Excited State 20: Singlet-A 5.2107 eV 237.94 nm f=0.0335 <S**2>=0.000

62 → 68 0.11602

63 → 66 0.18473

63 → 69 0.10015

64 → 66 0.53179

64 → 69 -0.36016

Excited State 21: Singlet-A 5.3378 eV 232.28 nm f=0.0323 <S**2>=0.000

62 → 68 -0.13608

63 → 66 -0.20998

64 → 66 0.41190

64 → 69 0.48819

Excited State 22: Singlet-A 5.7395 eV 216.02 nm f=0.0421 <S**2>=0.000

60 → 67 0.24317

61 → 66 0.13459

61 → 69 -0.25080

62 → 66 0.37186

63 → 67 0.25742

63 → 68 0.32005

64 → 67 0.19816

Excited State 23: Singlet-A 5.7447 eV 215.82 nm f=0.0000 <S**2>=0.000

60 → 69 0.17065

61 → 67 -0.37879

62 → 68 0.15177

63 → 66 0.42361

63 → 69 0.10763

64 → 69 0.31987

Excited State 24: Singlet-A 5.9186 eV 209.48 nm f=0.0143 <S**2>=0.000

62 → 66 -0.22763

63 → 67 0.27338

63 → 68 0.10801

64 → 70 0.54723

64 → 72 -0.21418

SavETr: write IOETrn= 770 NScale= 10 NData= 16 NLR=1 NState= 24 LETran= 442.

Electronic spatial extent (au): <R**2>= 3784.4348

Charge= 0.0000 electrons

Dipole moment (field-independent basis, Debye):

X= 0.0000 Y= 0.0008 Z= 6.9420 Tot= 6.9420

Quadrupole moment (field-independent basis, Debye-Ang):

XX= -80.5804 YY= -100.8657 ZZ= -101.9938

XY= 6.1737 XZ= -0.0007 YZ= -0.0001

Traceless Quadrupole moment (field-independent basis, Debye-Ang):

XX= 13.8996 YY= -6.3858 ZZ= -7.5138

XY= 6.1737 XZ= -0.0007 YZ= -0.0001

Octapole moment (field-independent basis, Debye-Ang**2):

XXX= -0.0007 YYY= 0.0041 ZZZ= 20.2838 XYY= 0.0014

XXY= 0.0064 XXZ= 52.9407 XZZ= -0.0012 YZZ= -0.0003

YYZ= 11.2441 XYZ= 5.9247

Hexadecapole moment (field-independent basis, Debye-Ang**3):

XXXX= -2784.6933 YYYY= -892.8633 ZZZZ= -840.0634 XXXY= -94.2226

XXXZ= 0.0081 YYYX= -34.8990 YYYZ= 0.0154 ZZZX= -0.0139

ZZZY= -0.0084 XXYY= -672.6291 XXZZ= -593.7978 YYZZ= -255.7534

XXYZ= 0.0092 YYXZ= 0.0102 ZZXY= 29.5179

N-N= 1.327802184526D+03 E-N=-4.934835878032D+03 KE= 9.663760182731D+02

The results of computationally calculated and some experimental results for the UV-Vis spectrum and other related properties for all the samples we have studied are provided below. We used GaussSum Version 3.0[71] to visualize some of the results.

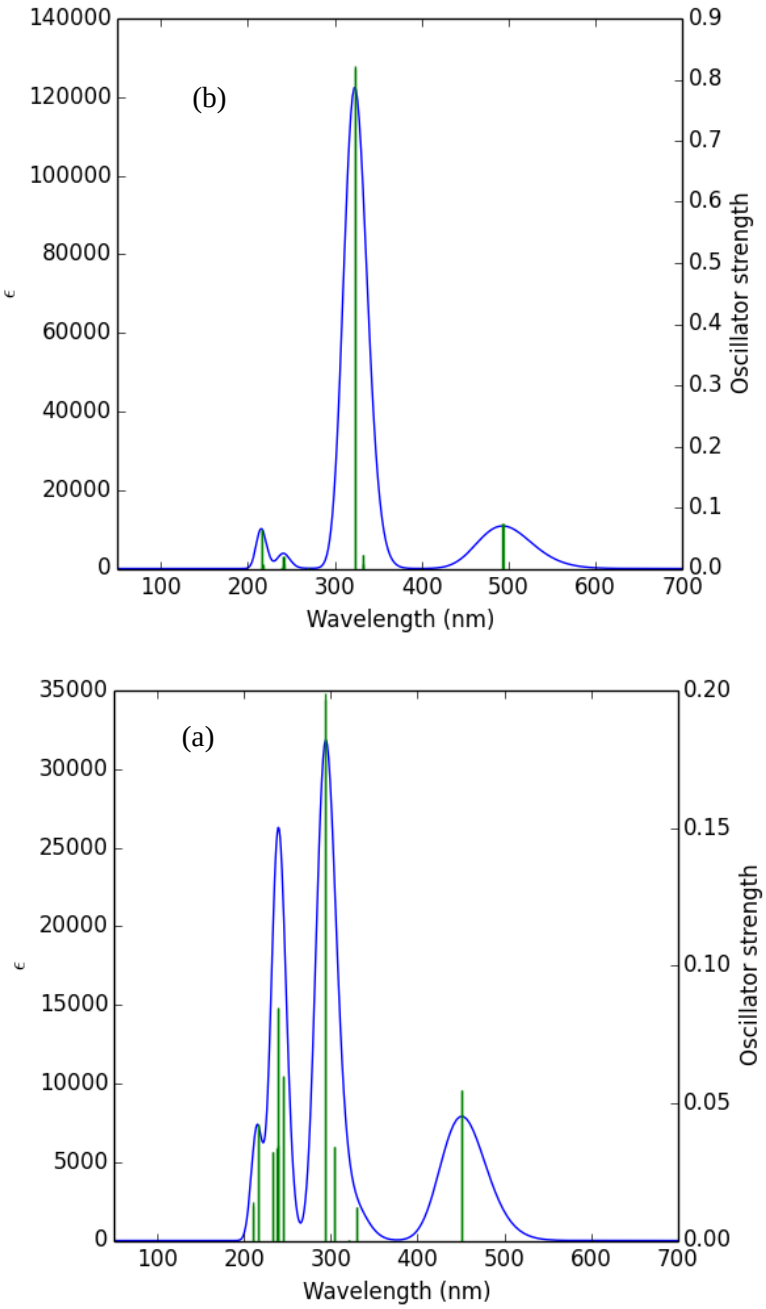

Figure 2.42: Computed UV-Vis spectrum for (a) cis and (b) trans 2,2́,6,6́-tetrafluoroazobenzene. Calculations were done using B3LYP level of theory and 6-311++G(3df,3dp) as the basis set. In this calculation acetonitrile is considered as the solvent.

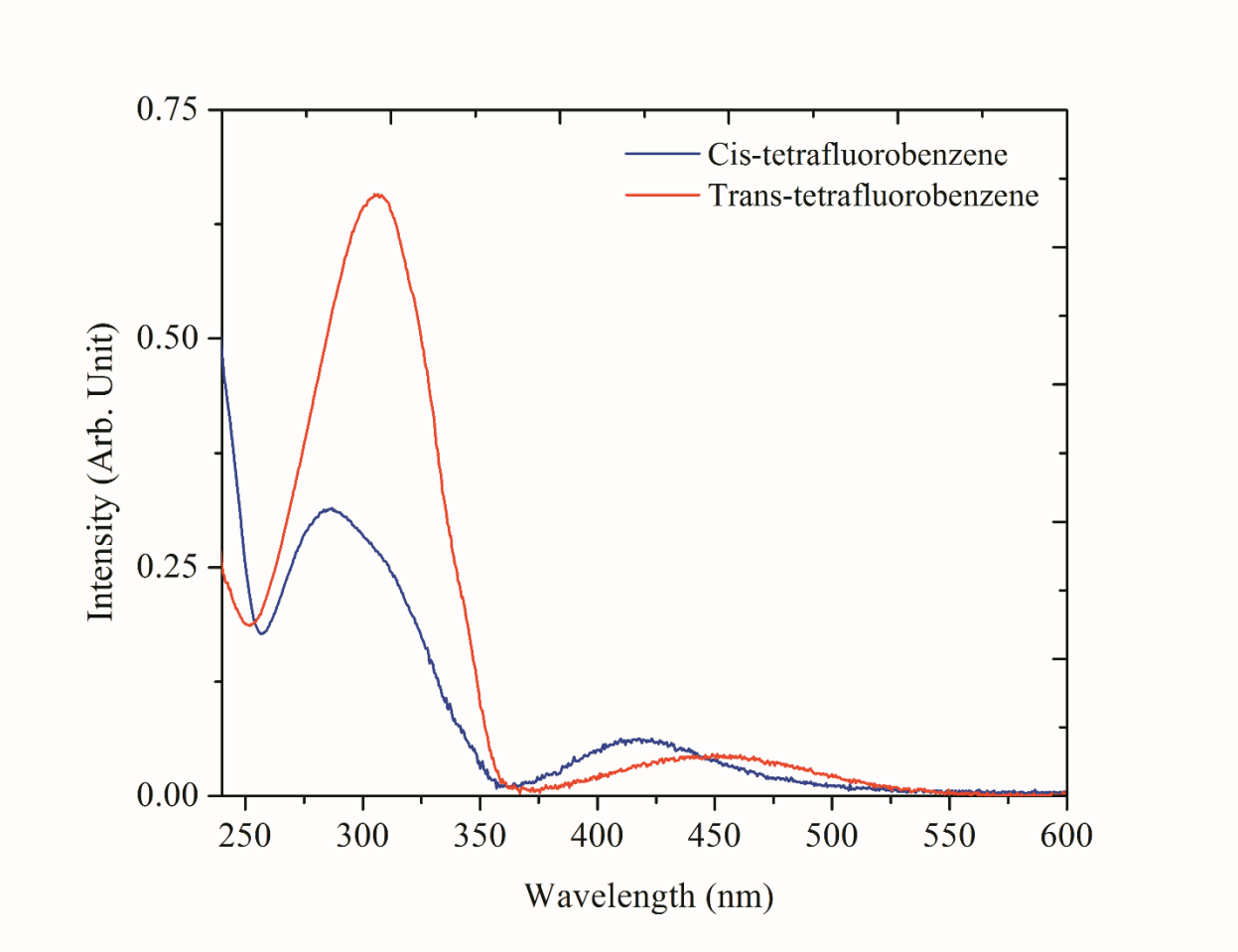

Figure 2.43: Experimental UV-Vis spectrum of cis and trans isomers of 2,2́,6,6́-tetrafluoroazobenzene in chloroform. The cis form is made by irradiating sample in solution using a high power green LED.

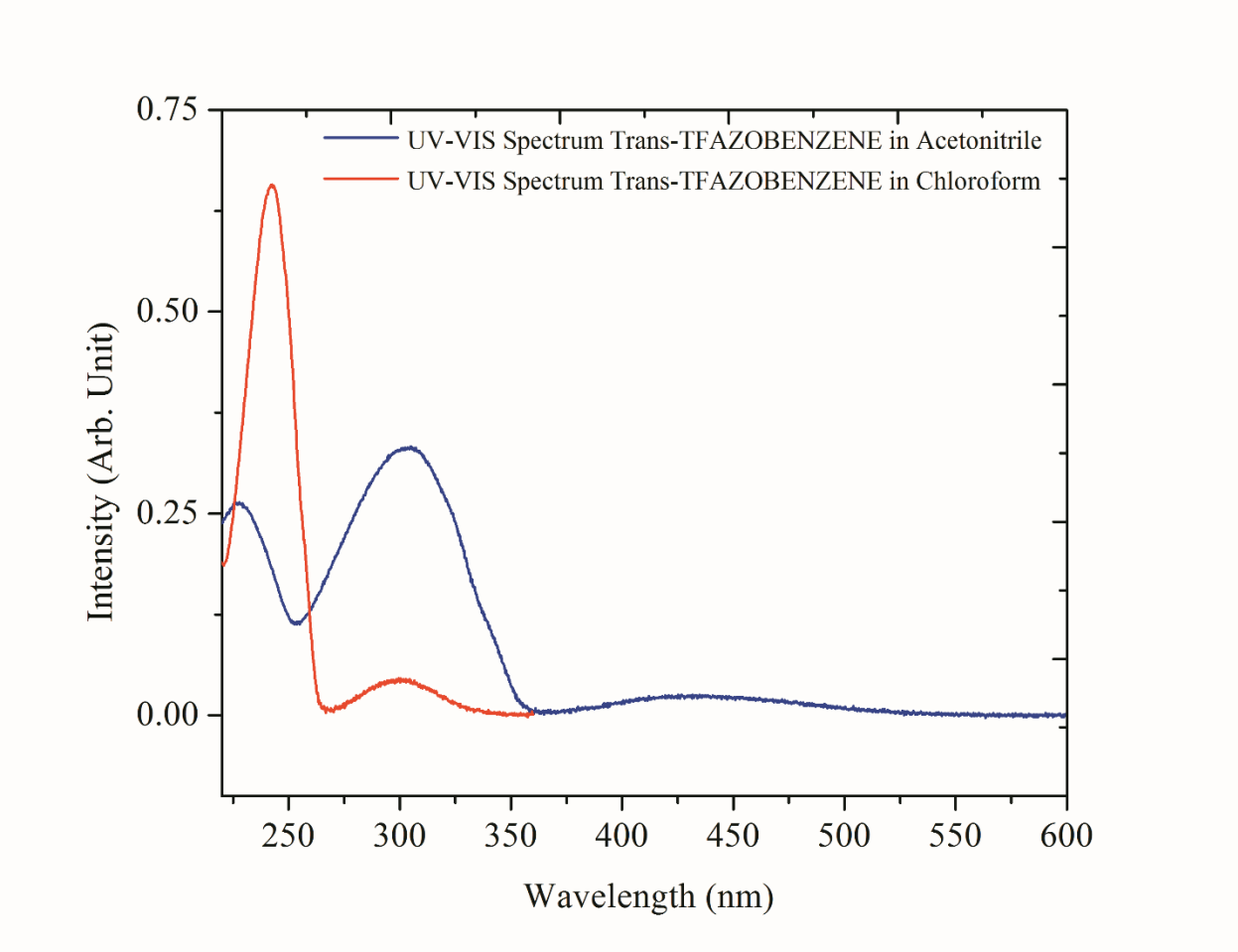

Figure 2.44: Effects of solvent. Comparison of two experimentally obtained UV-Vis spectrum Here we compared the trans 2,2́,6,6́-tetrafluoroazobenzene UV-Vis spectrum in two different organic solvent (acetonitrile and chloroform).

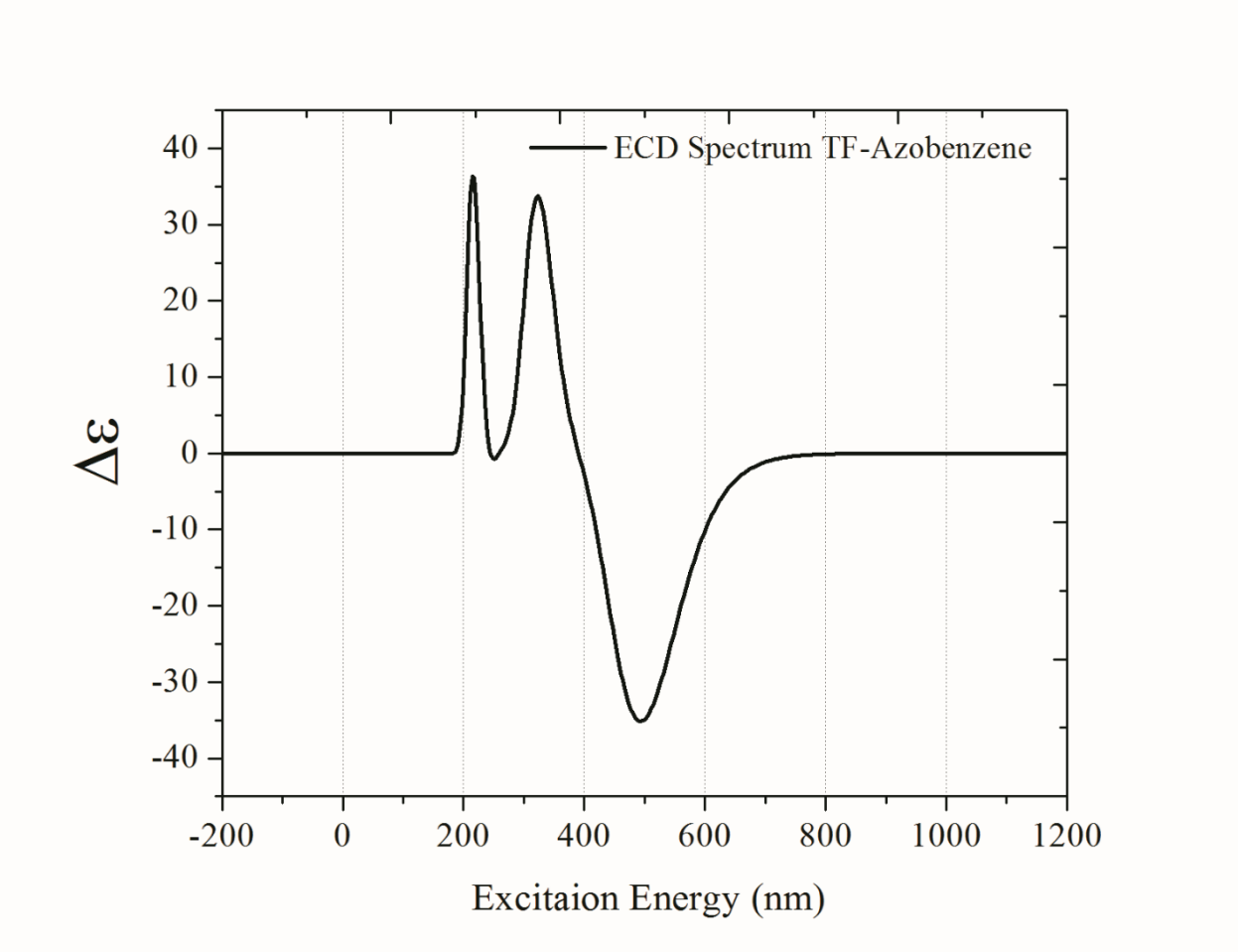

Figure 2.45: Computational Electronic Circular Dichroism (ECD) spectrum simulation of trans 2,2́,6,6́-tetrafluoroazobenzene, calculated at B3LYP with **6-311++G(3df,3dp)** as the basis set. Excitation energy (nm) = 746.85. This spectrum is the results of a time-dependent Density Functional Theory (TD-DFT). E(TD-HF/TD-KS) = -969.96828167 a.u. and Dipole Moment = 0.3511 Debye.

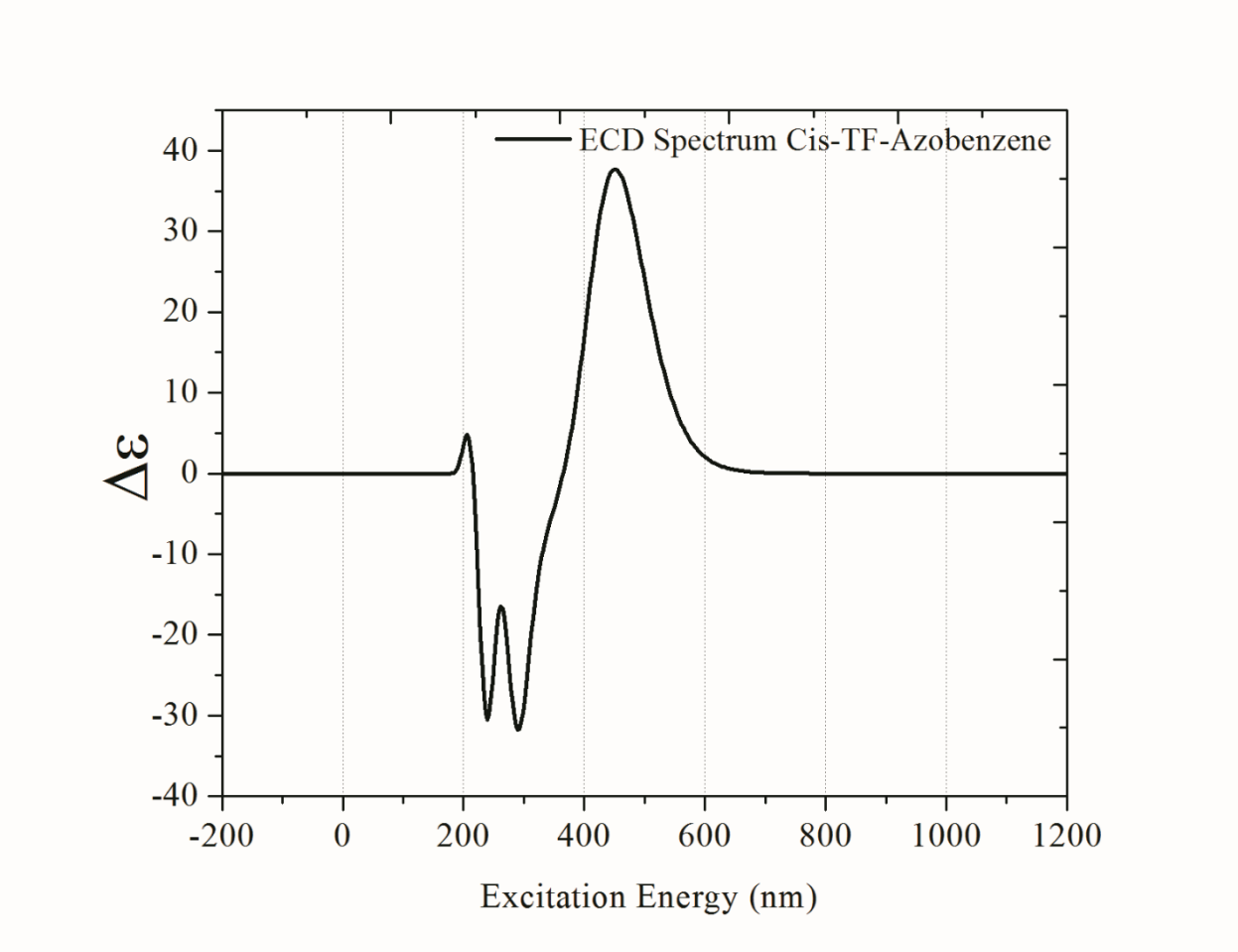

Figure 2.46: Computational electronic circular dichroism, ECD, spectrum of **cis** 2,2́,6,6́-tetrafluoroazobenzene calculated at B3LYP with **6-311++G(3df,3dp)** as the basis set. Excitation energy (nm) = 706.15. E(TD-HF/TD-KS) = -969.95197755 a.u. and dipole moment = 6.8953 Debye.

Another example of optical properties of molecules which can be simulated and visualized is the optical rotary dispersion (ORD) spectrum. Here we present an example of ORD spectrum which is simulated for trans 2,2́,6,6́-tetrafluoroazobenzene. We optimized the structure with B3LYP/6-311++G(d,p) level of theory and simulated the Optical Rotation Beta and [Alpha]D for the sample with Molar Mass=254.1864 grams/mole using 255 nm, 300 nm, 355 nm, 400 nm, 450 nm, 500 nm, 550 nm, 600 nm and 650 nm as the excitation wavelengths using keywords like Polar=OptRot

and CPHF= (RdFreq,Grid=Ultrafine). We fitted the simulated data points with a 7th order polynomial function to simulate the ORD spectrum.

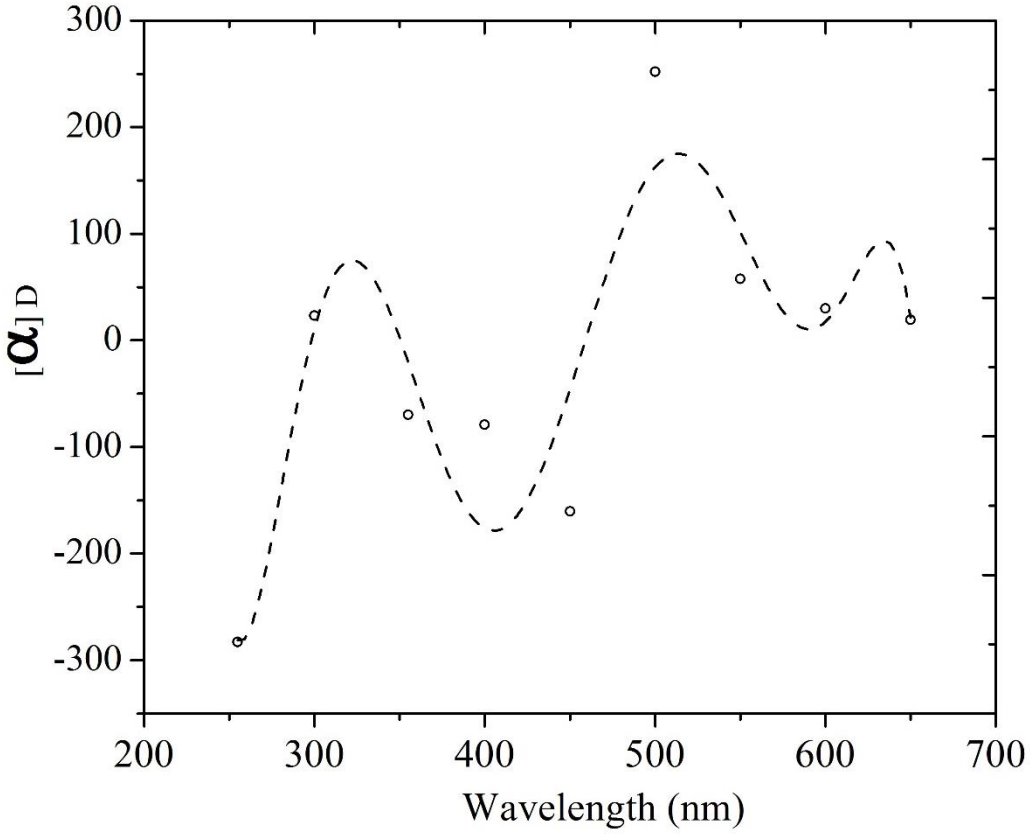

Figure 2.47: Optical rotary dispersion (ORD) spectrum of trans 2,2́,6,6́-tetrafluoroazobenzene simulated at B3LYP level of theory along with 6-311++G(d,p) as the basis set. Alpha of rotation (angle of rotation as a function of wavelength) is plotted as a function of excitation wavelength and fitted with a 7th order polynomial function.

2.6.2 Azobenzene:

Our original sample in this study was the azobenzene molecule. To induce the trans to cis isomerization we used the third harmonic of a Nd-YAG laser harmonic which is in UV region. The experimental UV-Vis spectroscopy has been performed using a commercial UV-Vis

spectrophotometers (Evolution 600 UV-Visible spectrophotometer). The experimental results is shown in Figure 48.

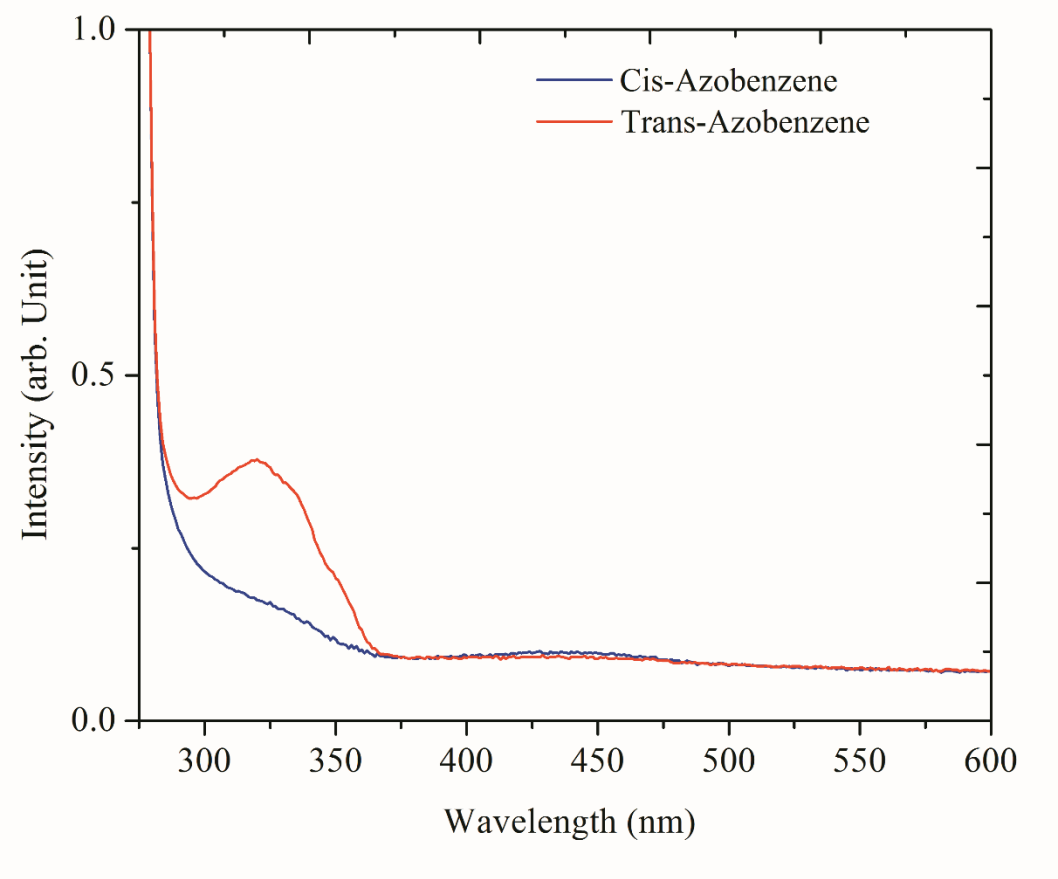

Figure 2.48: Experimental UV-Vis spectrum of cis and trans azobenzene solvated in benzene. To prepare the cis isomer we radiated trans azobenzene with 355 nm laser line for 15 minutes.

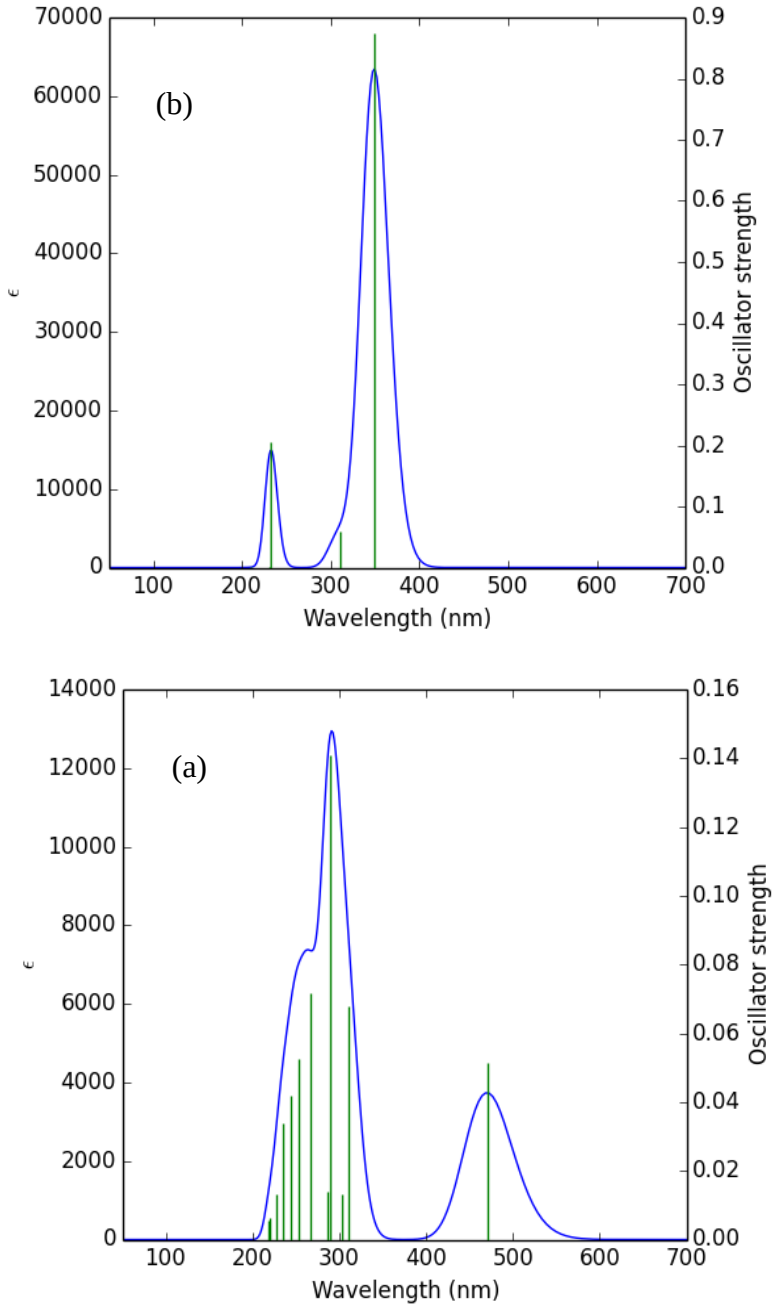

Figure 2.49: Computational UV-Vis spectrum of azobenzene. (a) Cis (b) Trans. The calculation was performed using B3LYP level of theory and 6-311++G(2d,2p) as the basis set. Solvent is acetonitrile.

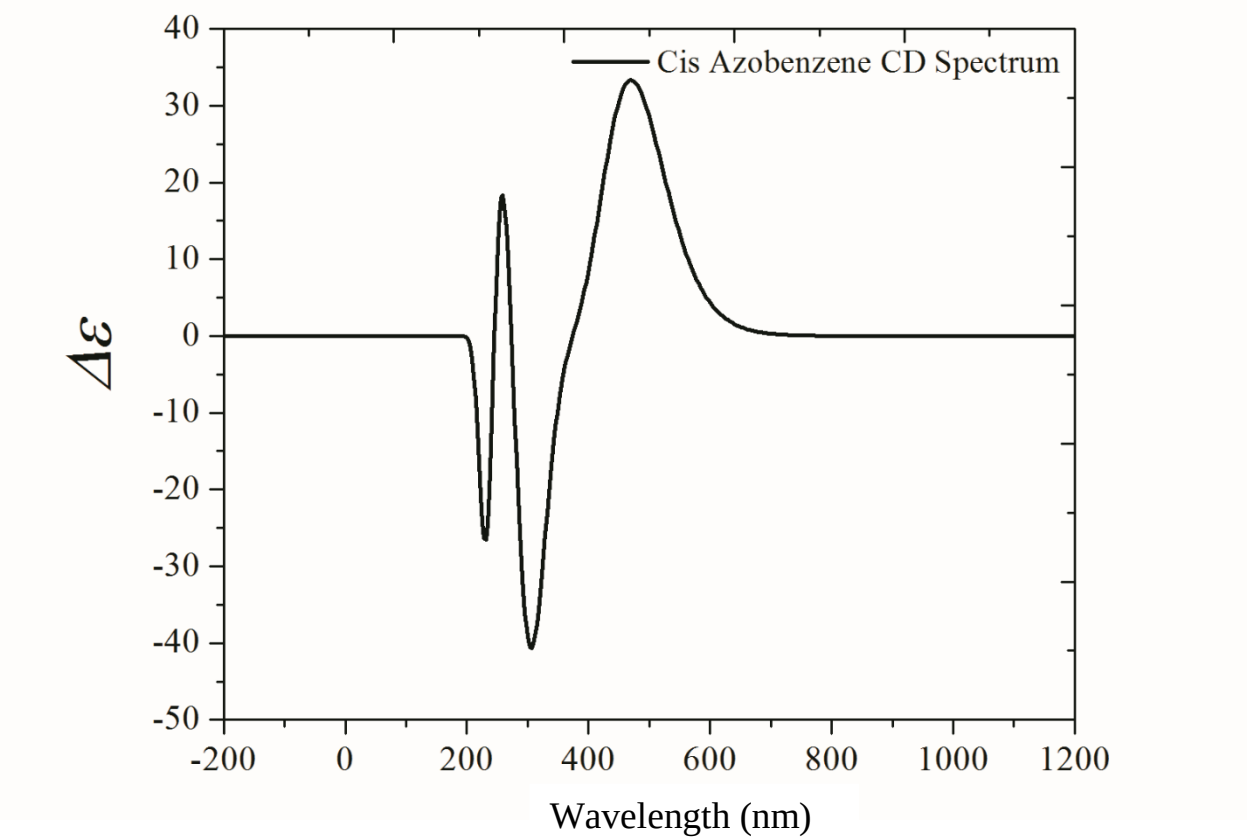

Figure 2.50: Circular dichroism spectrum of cis azobenzene. Excitation energy (nm)= 731.09 E(TD-HF/TD-KS) = -572.84999816 a.u. and dipole moment is 4.3516 Debye.

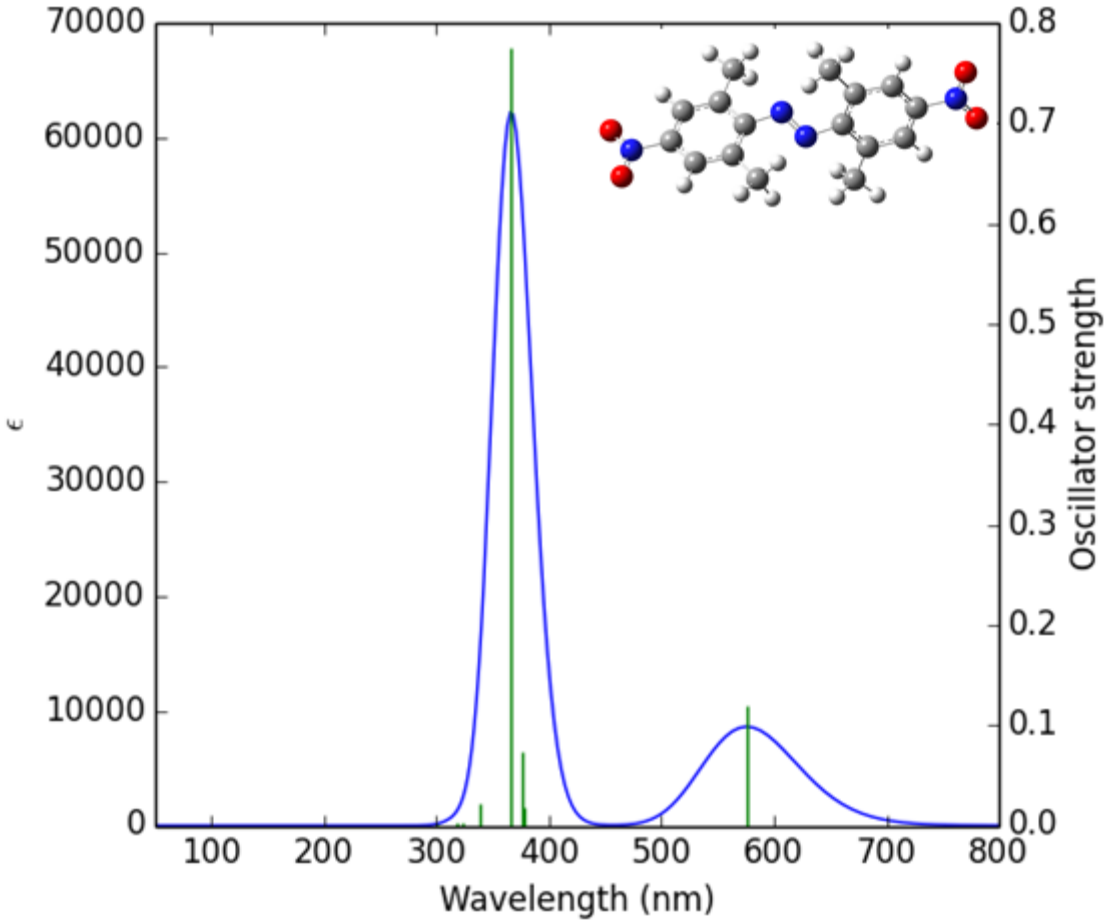

Figure 2.51: Computational UV-Vis Spectrum of 2,2',6,6' tetramethyl-(4,4') dinitro-azobenzene simulated at B3LYP level of theory using 6-311++G(d,p) basis set. Acetonitrile was considered in this computation as the solvent.

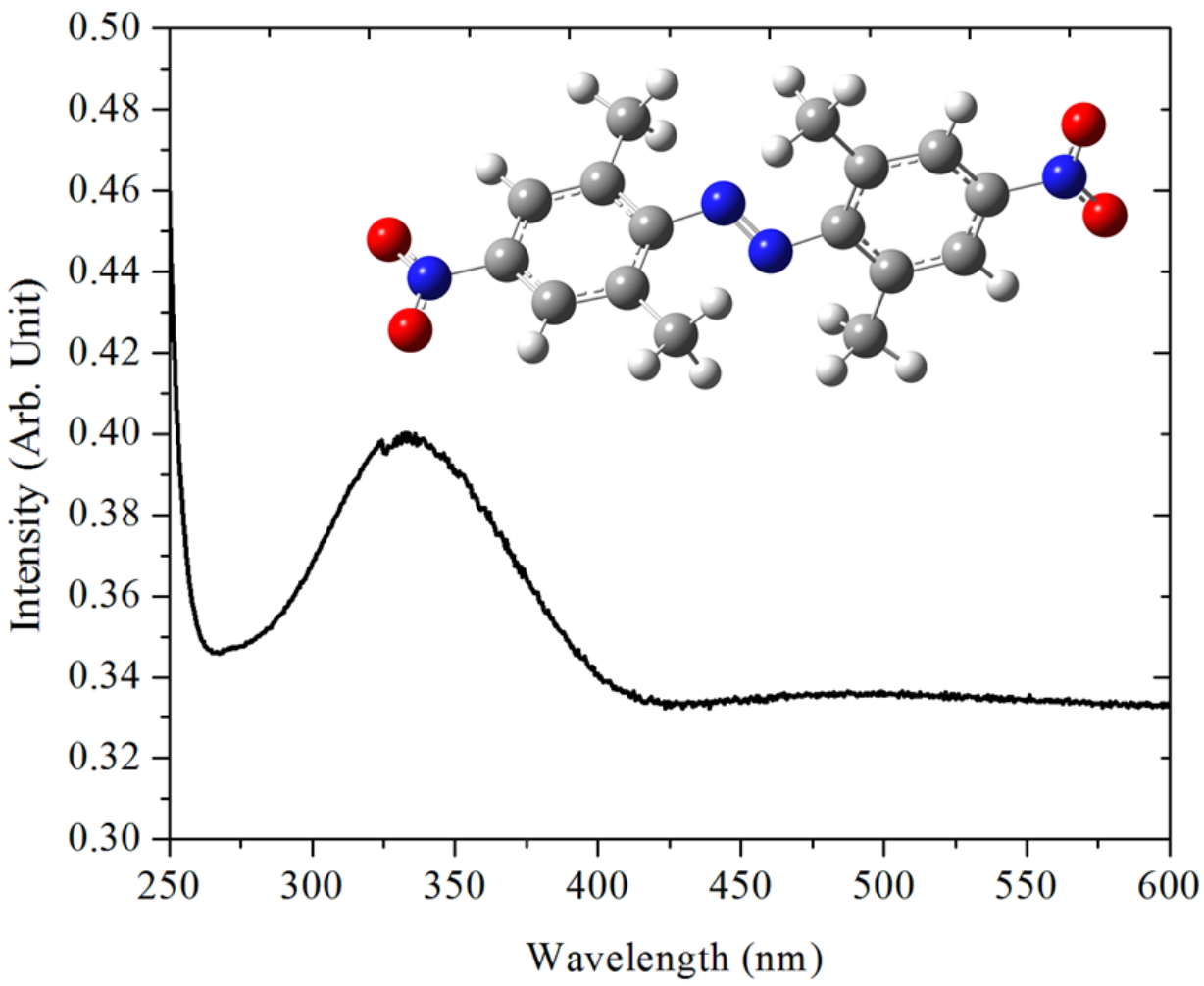

Figure 2.52: Experimental UV-Vis spectrum of trans 2,2',6,6' tetramethyl-(4,4') dinitro-azobenzene in Acetonitrile. Data was obtained using Evolution 600 Thermo Scientific UV-Visible spectrophotometer.

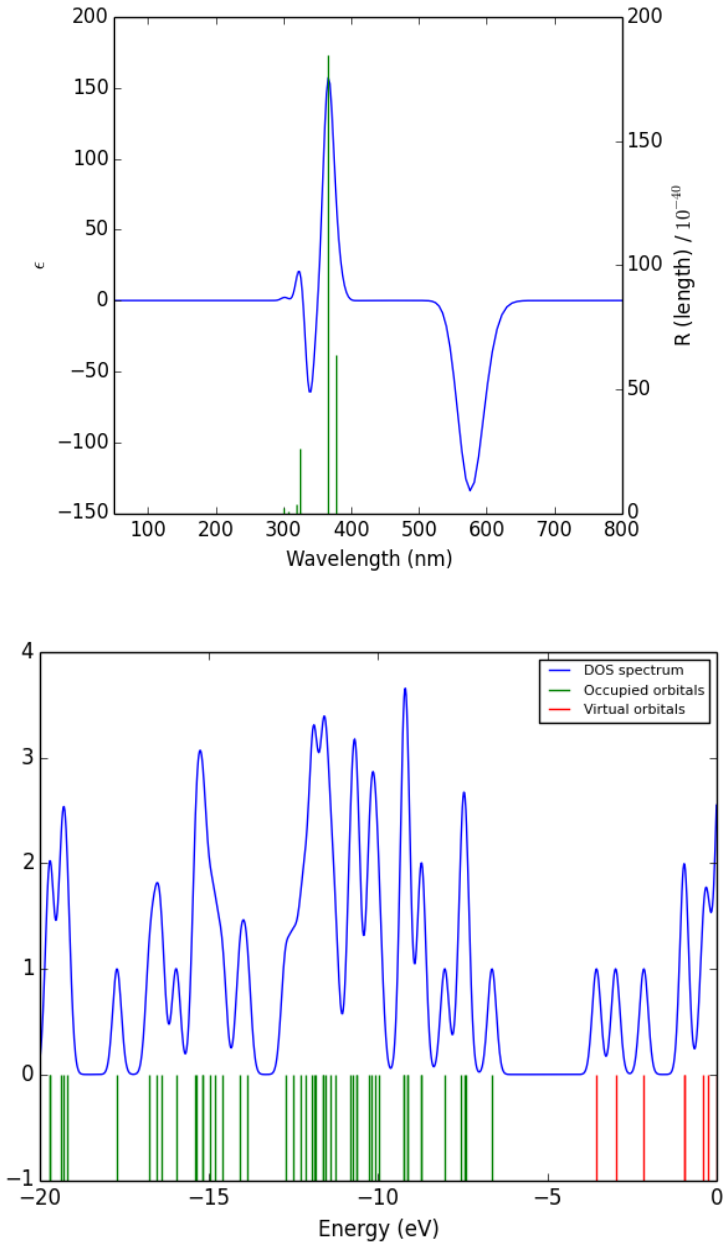

Figure 2.53: Top) Circular dichroism spectrum of trans 2,2',6,6' tetramethyl-(4,4') dinitro-azobenzene computed at B3LYP level of theory and 6-311++G(d,p) and acetonitrile is considered as the solvent. Bottom) Density of state (DOS) and energy levels of occupied and virtual orbitals computations has been performed at same level of theory.

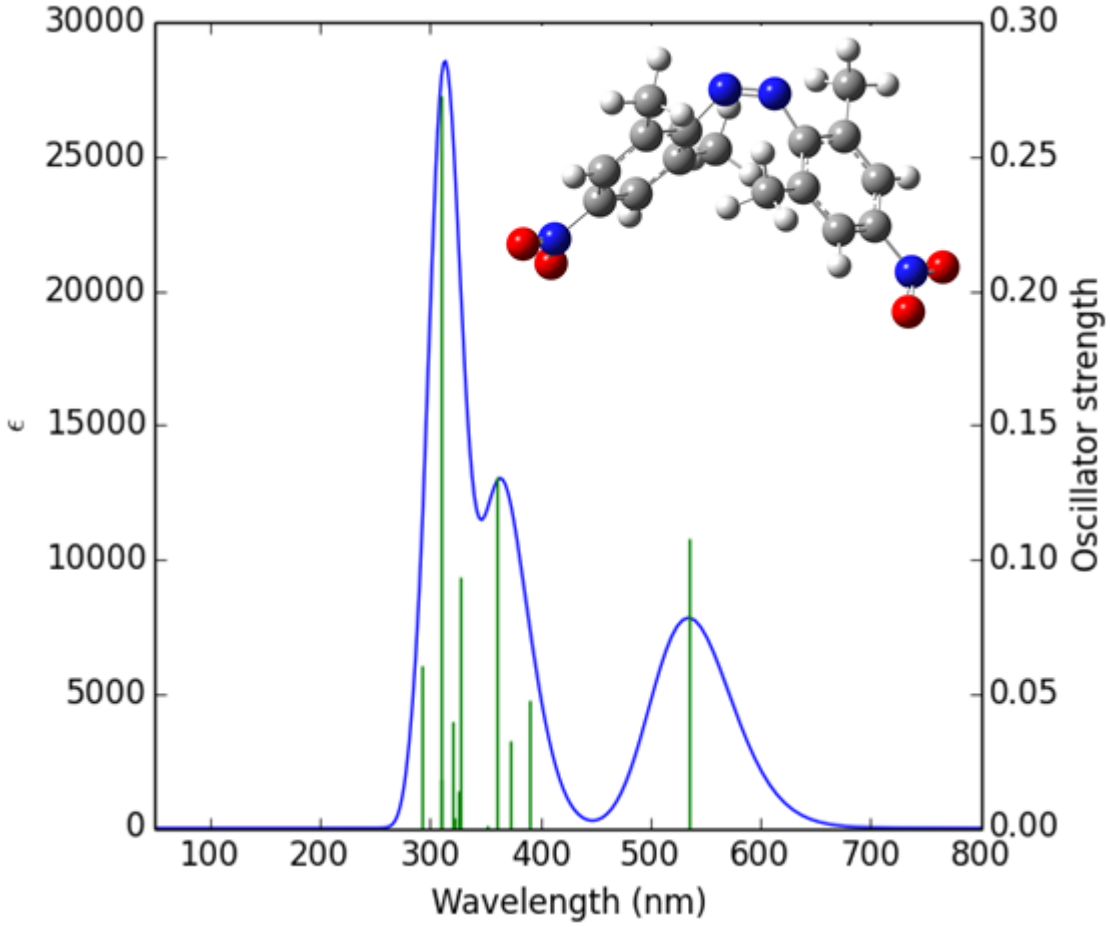

Figure 2.54: Computational UV-Vis Spectrum of cis 2,2',6,6' tetramethyl-(4,4') dinitro-azobenzene simulated at B3LYP level of theory using 6-311++G(d,p) basis set. Acetonitrile has been considered in this coputaions as the solvent.

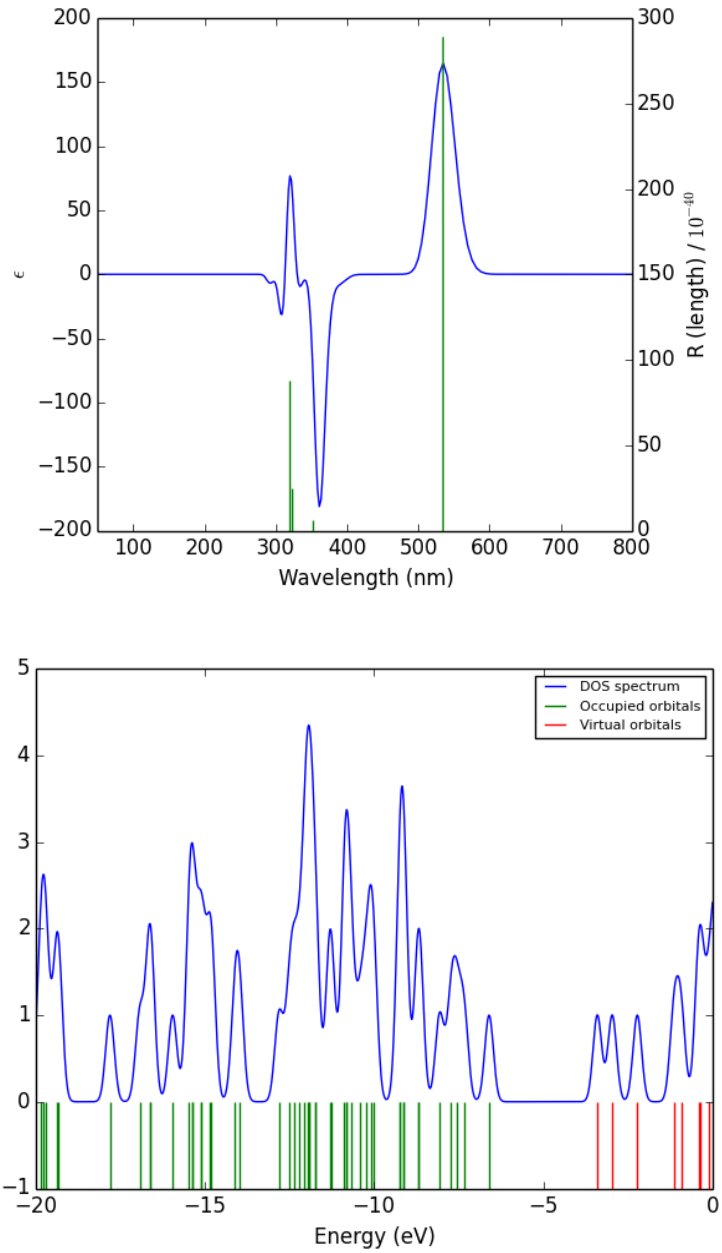

Figure 2.55: Circular dichroism spectrum of cis 2,2',6,6' tetramethyl-(4,4') dinitro-azobenzene computed at B3LYP level of theory and 6-311++G(d,p) and acetonitrile is considered as the solvent. Bottom) Density of state (DOS) and energy levels of occupied and virtual orbitals computations has been performed at same level of theory.

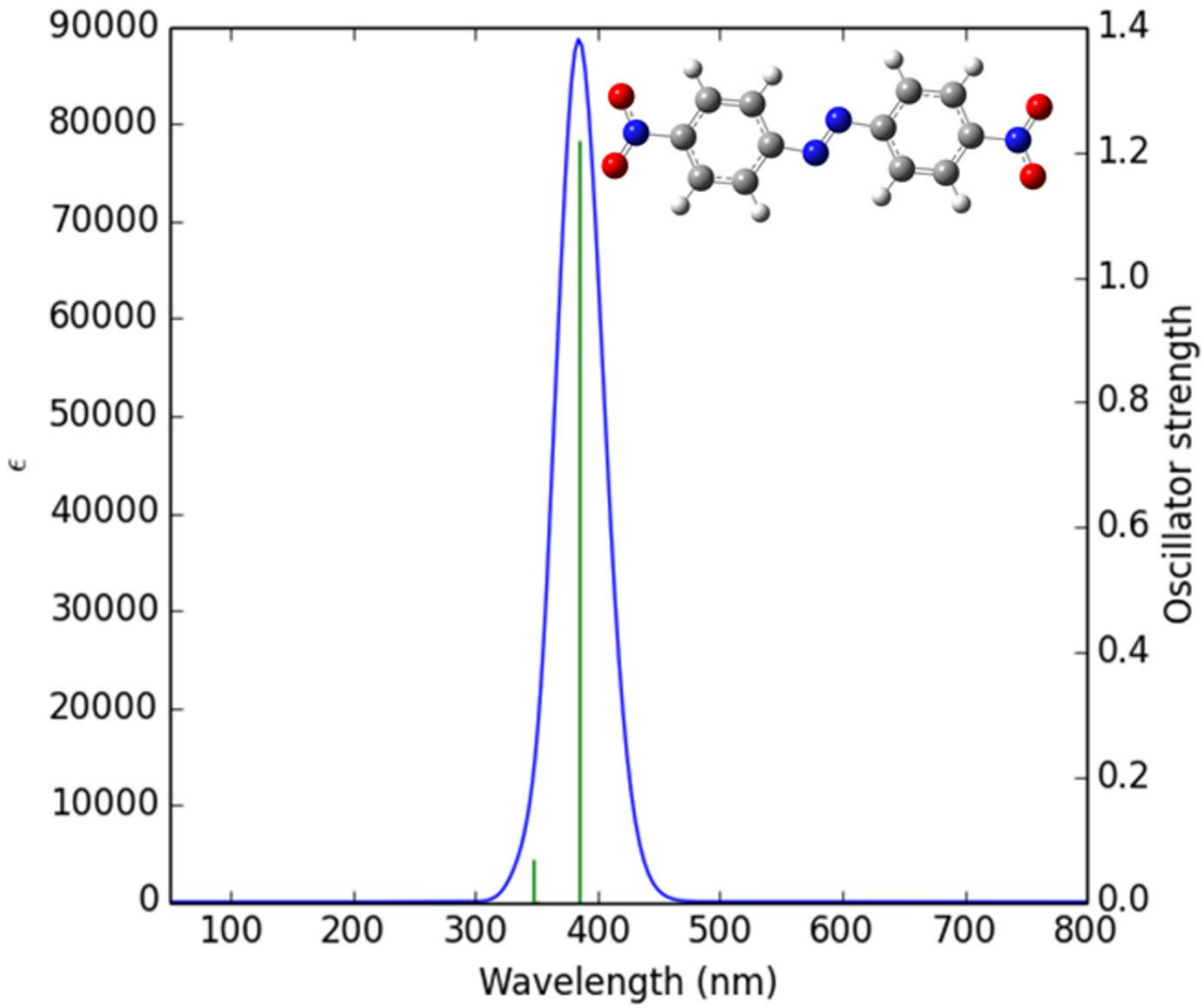

Figure 2.56: Computational UV-Vis Spectrum of 2,2',6,6' tetramethyl - (4,4') dinitro-azobenzene, $C_{16}H_{16}N_4O_4$.Computations has been at B3LYP level of theory using 6-311++G(d,p) basis set. Acetonitrile has been considered in this computations as the solvent. The peak wavelength is an educated guess for the required wavelength to make the cis isomer of this sample.

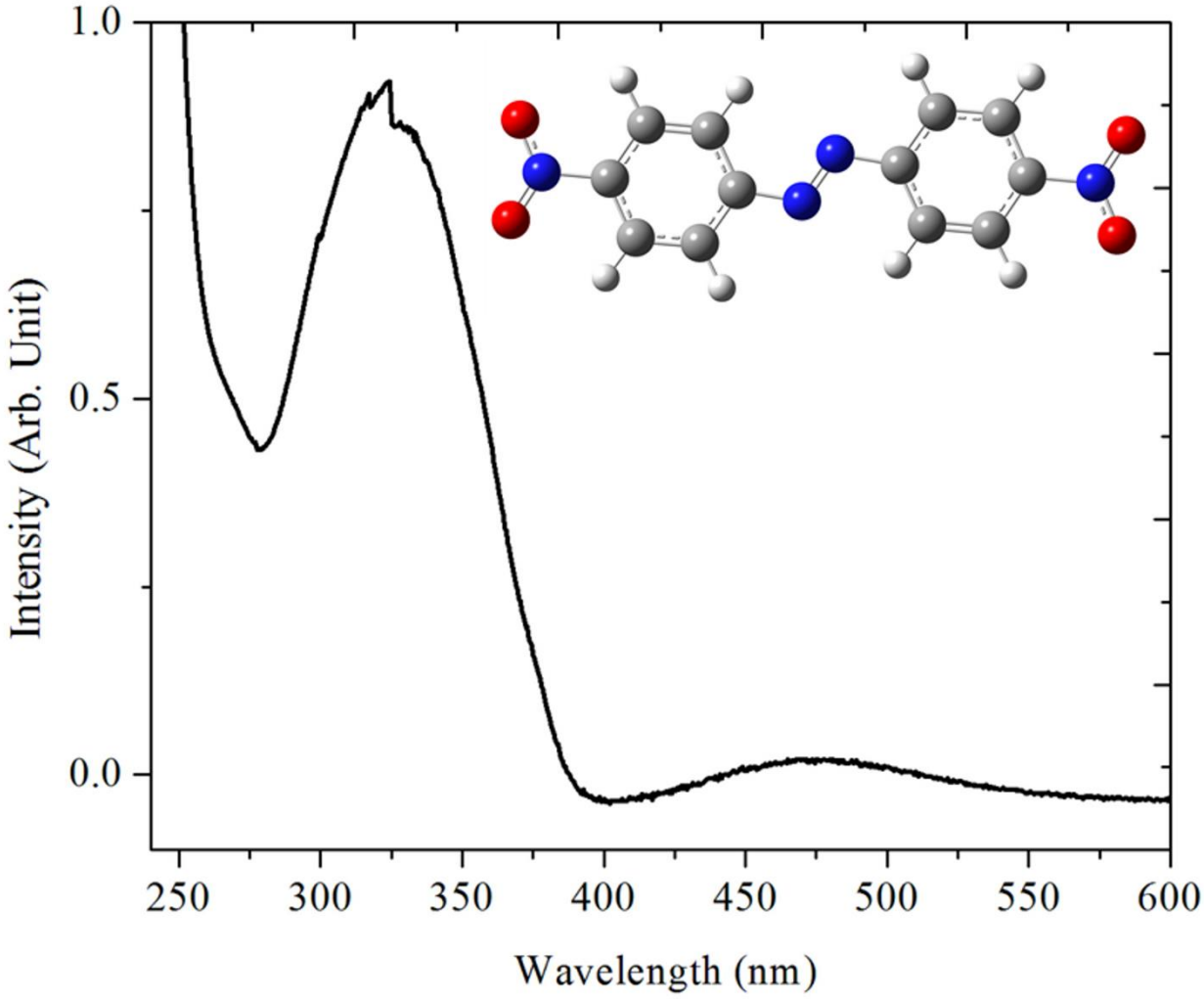

Figure 2.57: Experimental UV-Vis spectrum of trans 4,4' dinitro-azobenzene in Acetonitrile. Data was obtained using Evolution 600 Thermo Scientific UV-Visible spectrophotometer.

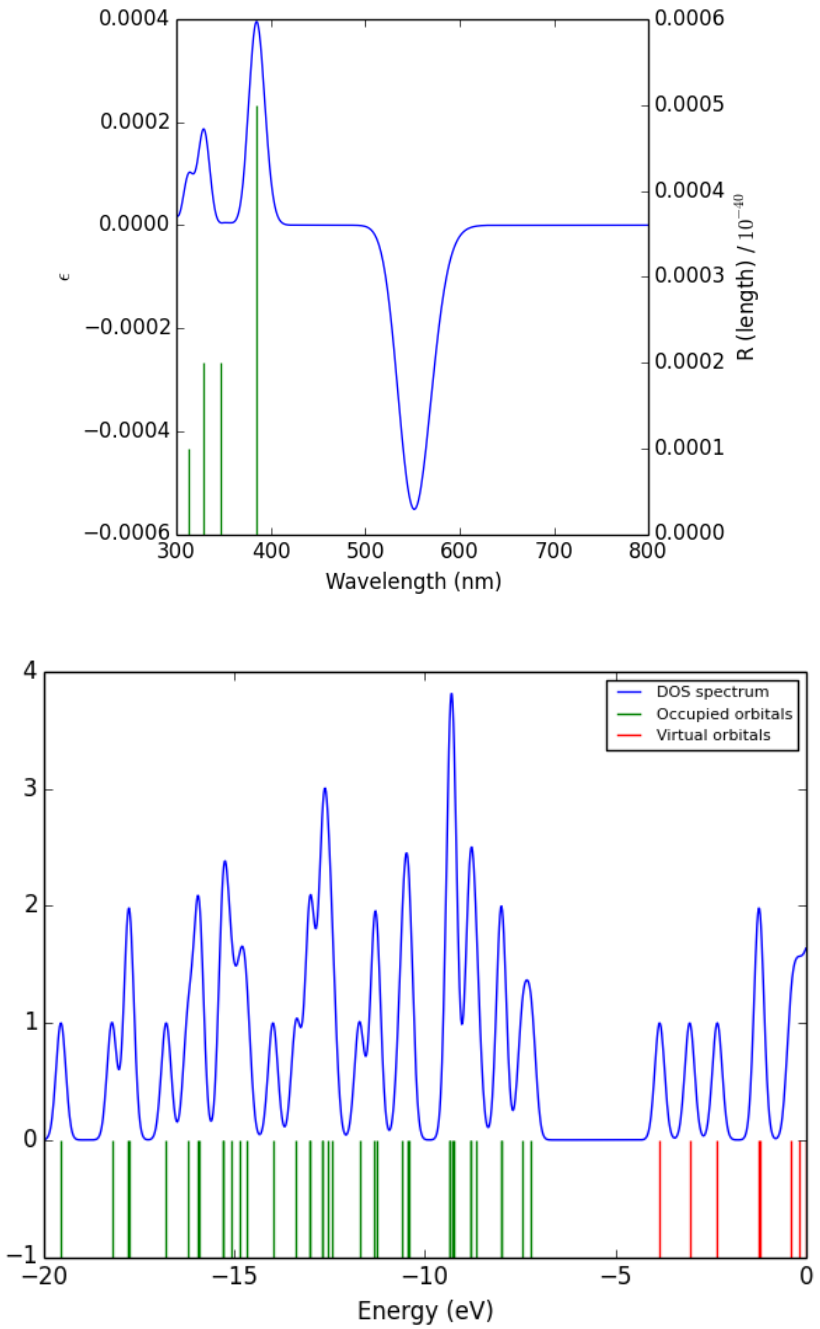

Figure 2.58: top) Circular dichroism spectrum of trans 4,4' dinitro-azobenzene computed at B3LYP level of theory and 6-311++G(d,p) and acetonitrile is considered as the solvent. Bottom) Density of state (DOS) and energy levels of occupied and virtual orbitals, computations has been performed at same level of theory.

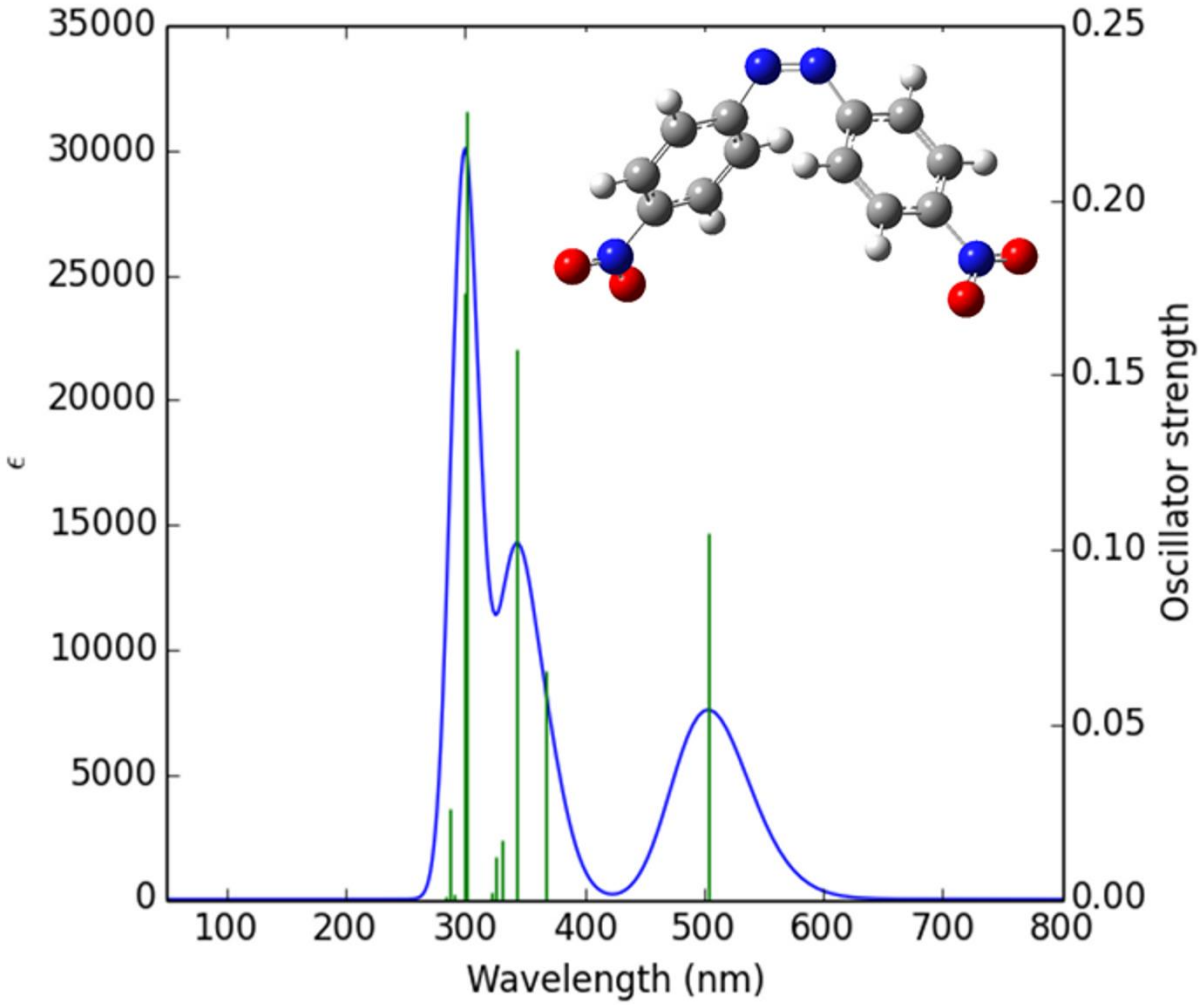

Figure 2.59: Computational UV-Vis Spectrum of cis 4,4' dinitro-azobenzene. Computations has been at B3LYP level of theory using 6-311++G(d,p) basis set. Acetonitrile has been considered in this computations as the solvent.

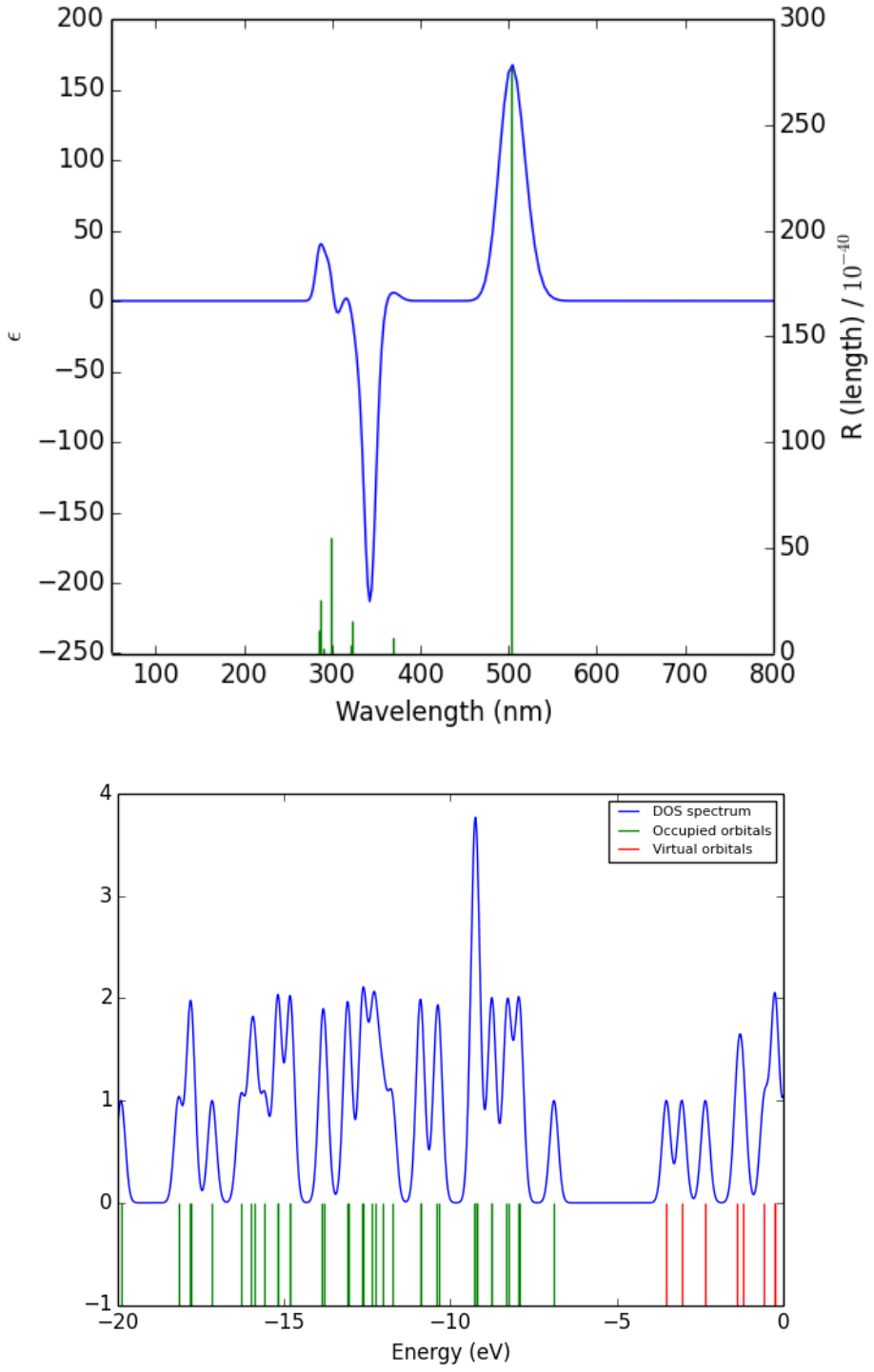

Figure 2.60: Top) Circular dichroism spectrum of **cis** 4,4' dinitro-azobenzene computed at B3LYP level of theory and 6-311++G(d,p) and acetonitrile is considered as the solvent. Bottom) Density of state (DOS) and energy levels of occupied and virtual orbitals computations has been performed at same level of theory.

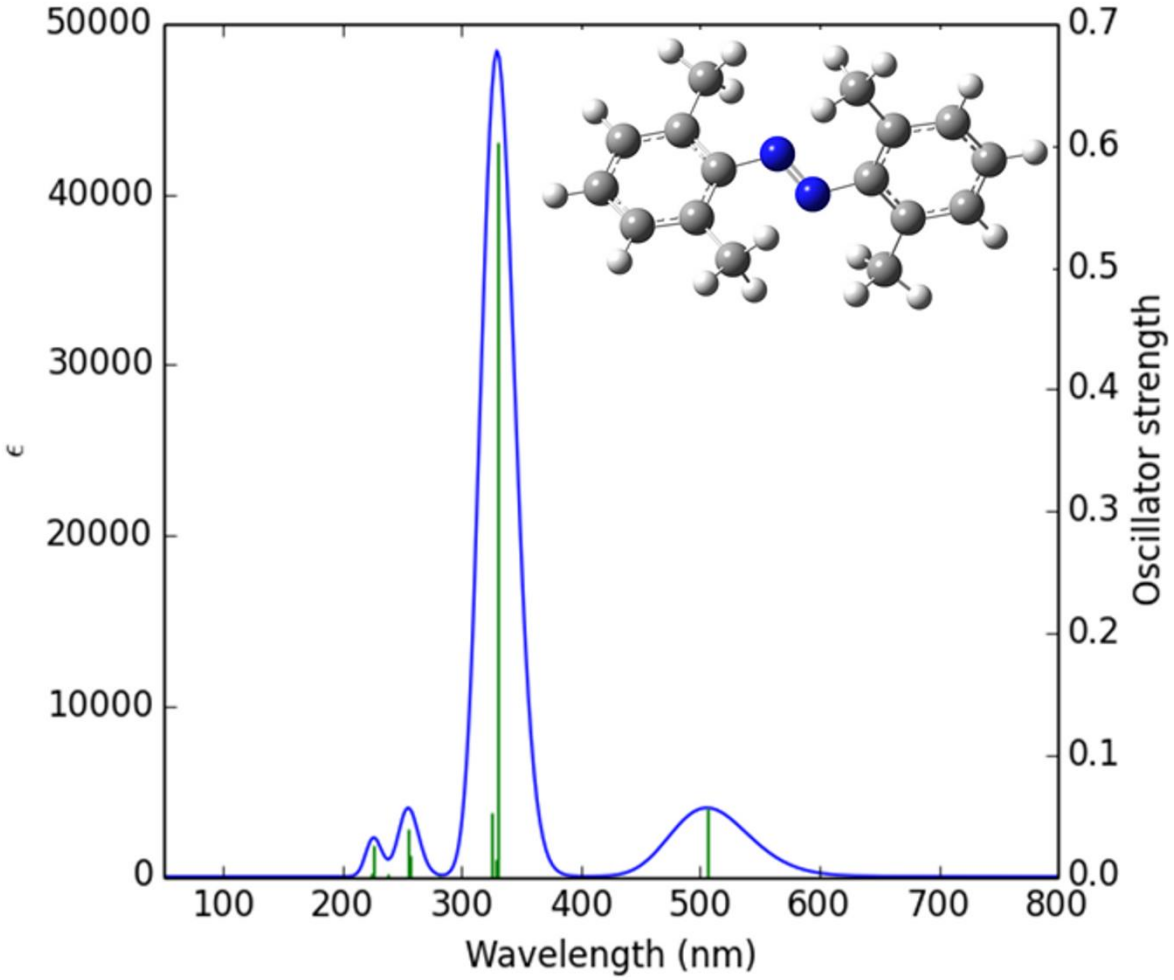

Figure 2.61: Computational UV-Vis Spectrum of trans 2,2',6,6' tetramethyl-azobenzene $C_{16}H_{18}N_2$. Computations has been at B3LYP level of theory using 6-311++G(d,p) basis set. Acetonitrile has been considered in this computations as the solvent.

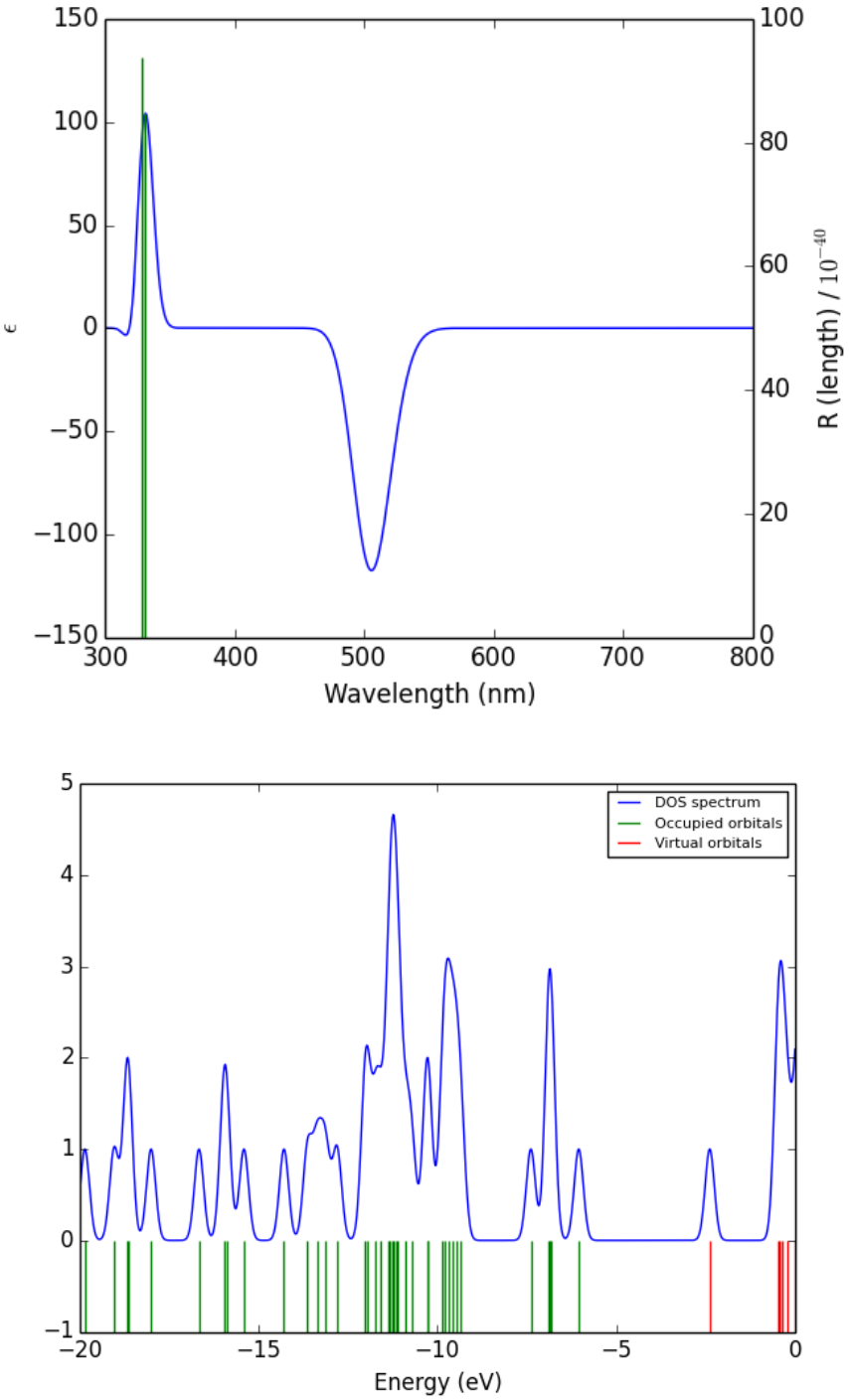

Figure 2.62: top) Circular dichroism spectrum of trans 2,2',6,6' tetramethyl-azobenzene computed at B3LYP level of theory and 6-311++G(d,p) and acetonitrile is considered as the solvent. Bottom) Density of state (DOS) and energy levels of occupied and virtual orbitals computations has been performed at same level of theory.

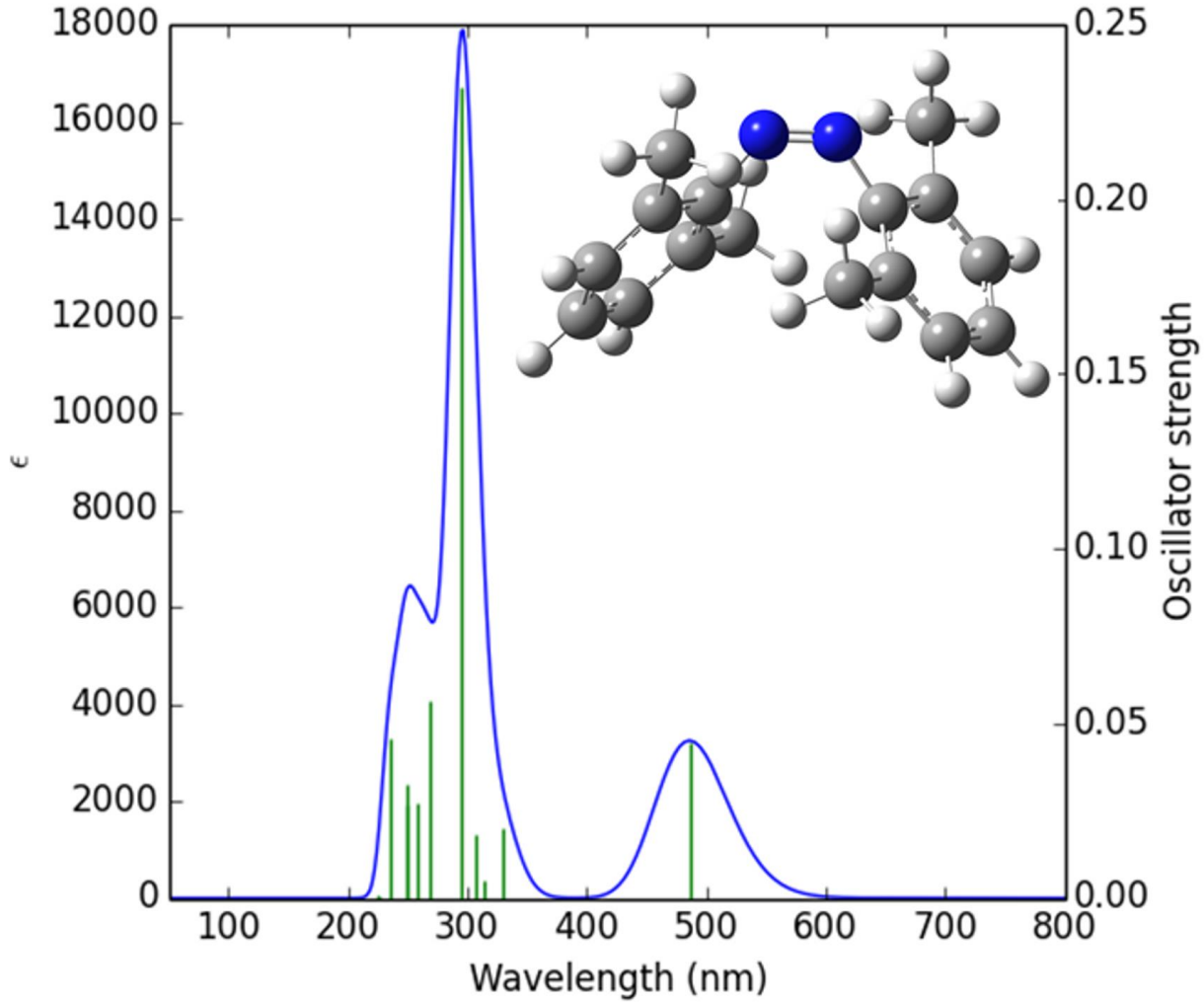

Figure 2.63: Computational UV-Vis Spectrum of cis 2,2',6,6' tetramethyl-azobenzene ($C_{16}H_{18}N_2$). The computations were performed at the B3LYP level of theory using 6-311++G(d,p) basis set. Acetonitrile has been considered in this computations as the solvent.

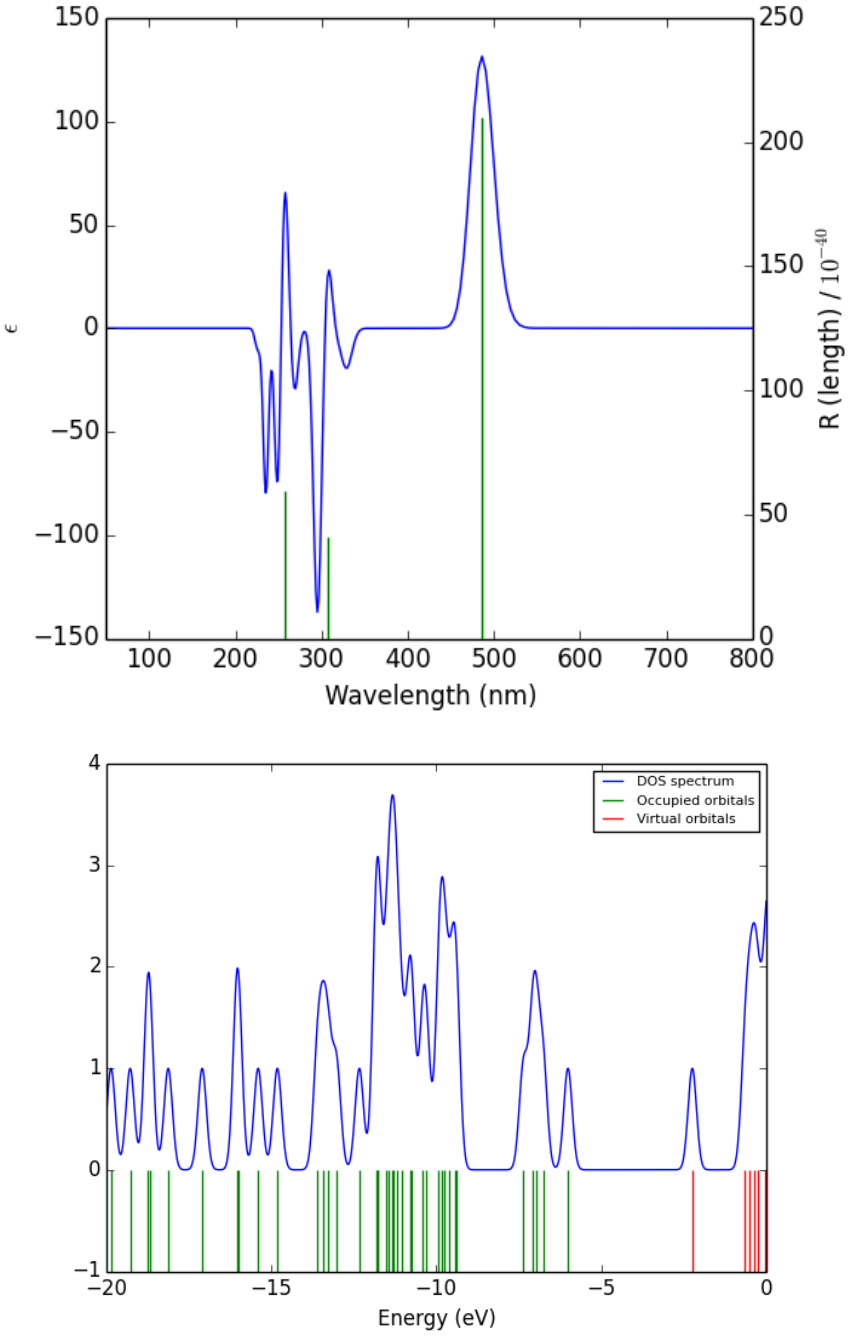

Figure 2.64: Top) Circular dichroism spectrum of cis 2,2',6,6' tetramethyl-azobenzene computed at B3LYP level of theory and 6-311++G(d,p) and acetonitrile is considered as the solvent. Bottom) Density of state (DOS) and energy levels of occupied and virtual orbitals computations has been performed at same level of theory.

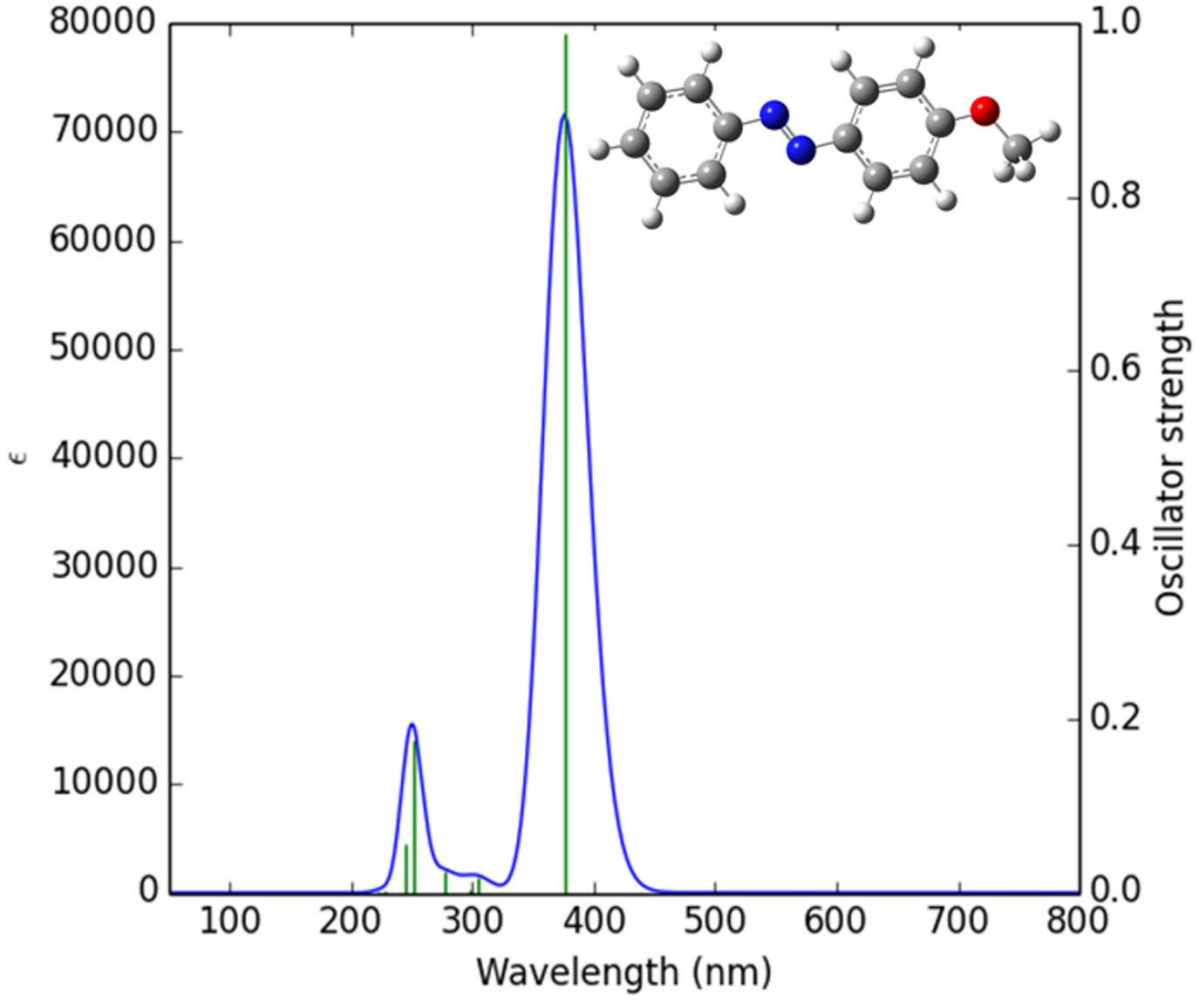

Figure 2.65: Computational UV-Vis Spectrum of trans 4-Methoxyazobenzene.Computations has been at B3LYP level of theory using 6-311++G(d,p) basis set. Acetonitrile has been considered in this computations as the solvent. This spectrum is a result of TD-DFT calculation.

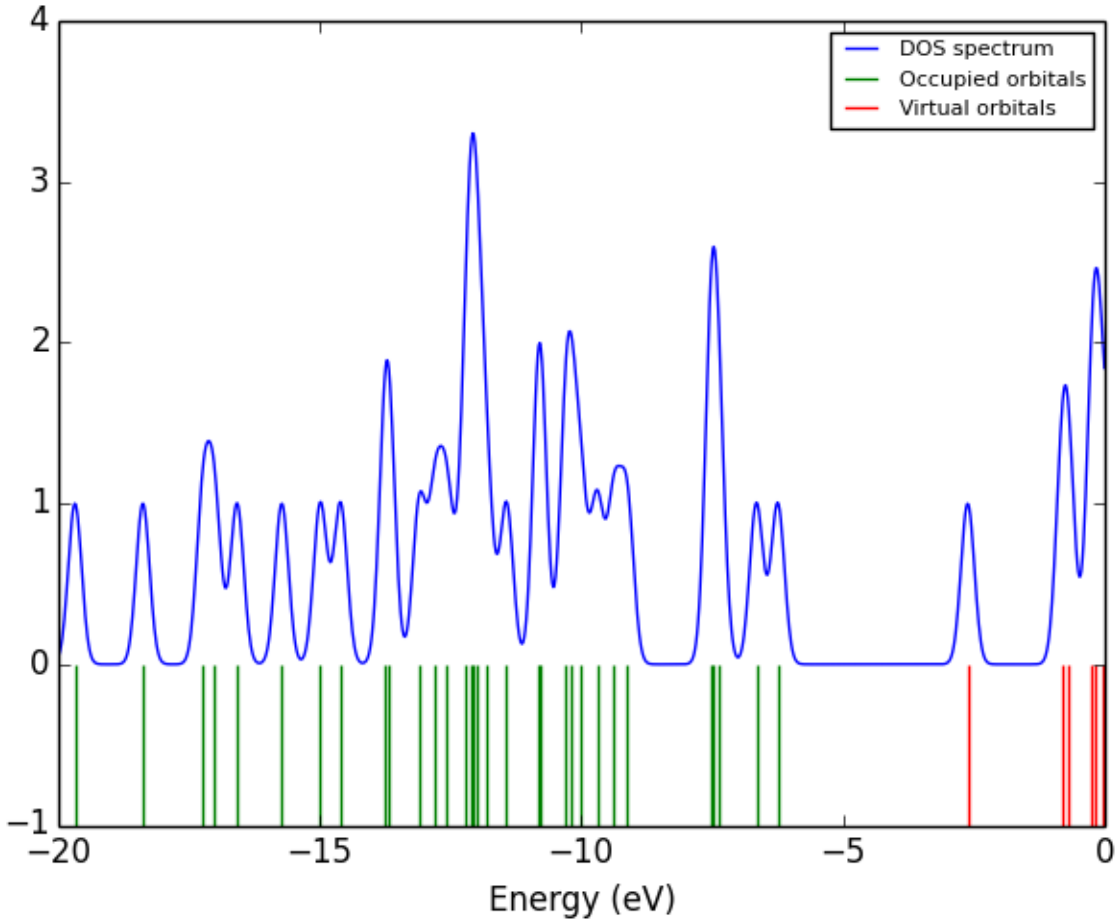

Figure 2.66: Density of state (DOS) and energy levels of occupied and virtual orbitals of trans 4-Methoxyazobenzene ($C_{13}H_{12}N_2O$). The computations were performed at the B3LYP level of theory along with a 6-311++G(d,p) basis set. This sample showed no any circular dichroism and that is the reason CD spectrum is not provided.

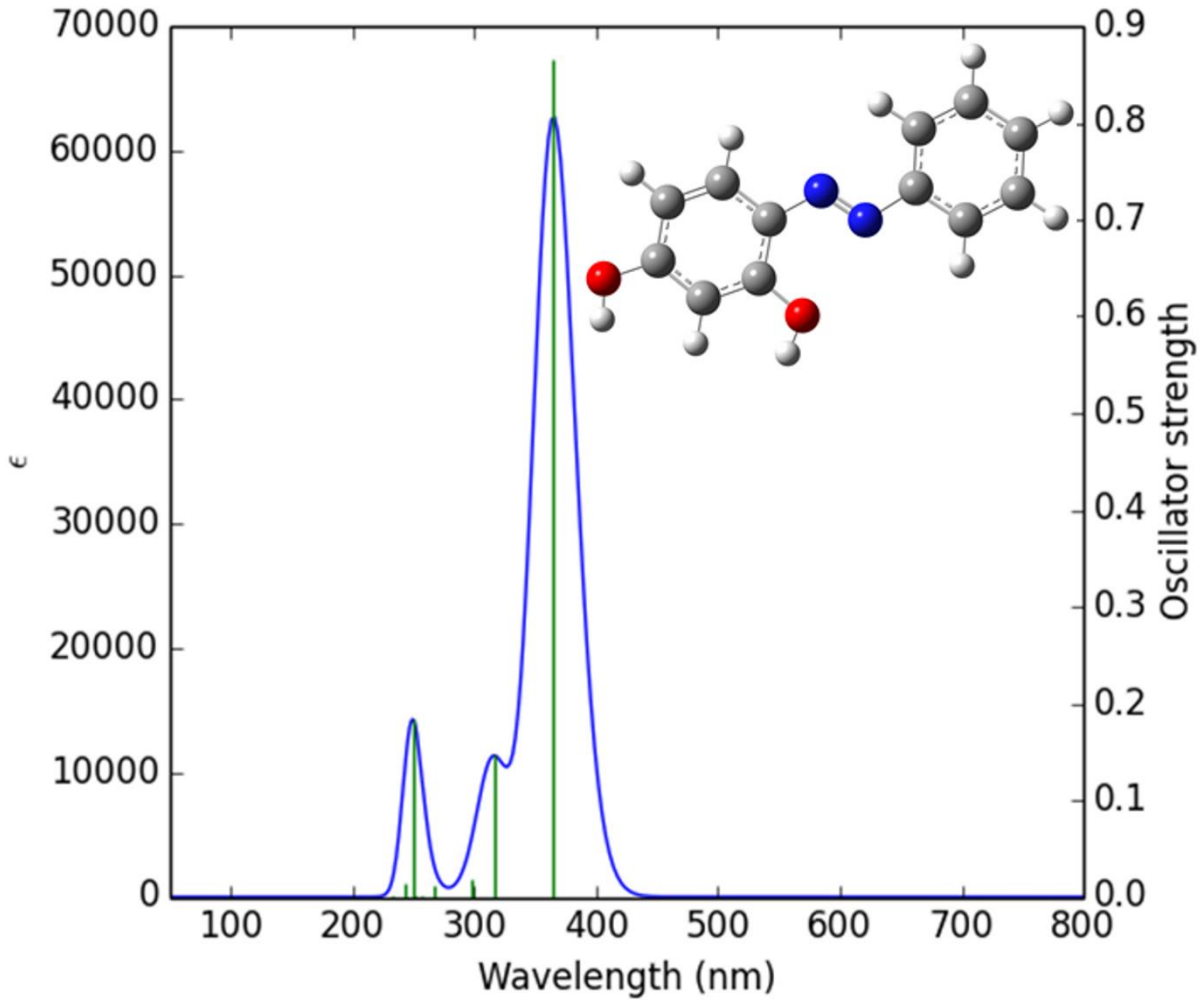

Figure 2.67: Computational UV-Vis Spectrum of trans 2,4-Dihydroxyazobenzene,4-(Phenylazo) resorcinol. Computations has been at B3LYP level of theory using 6-311++G(d,p) basis set. Acetonitrile has been considered in this computations as the solvent.

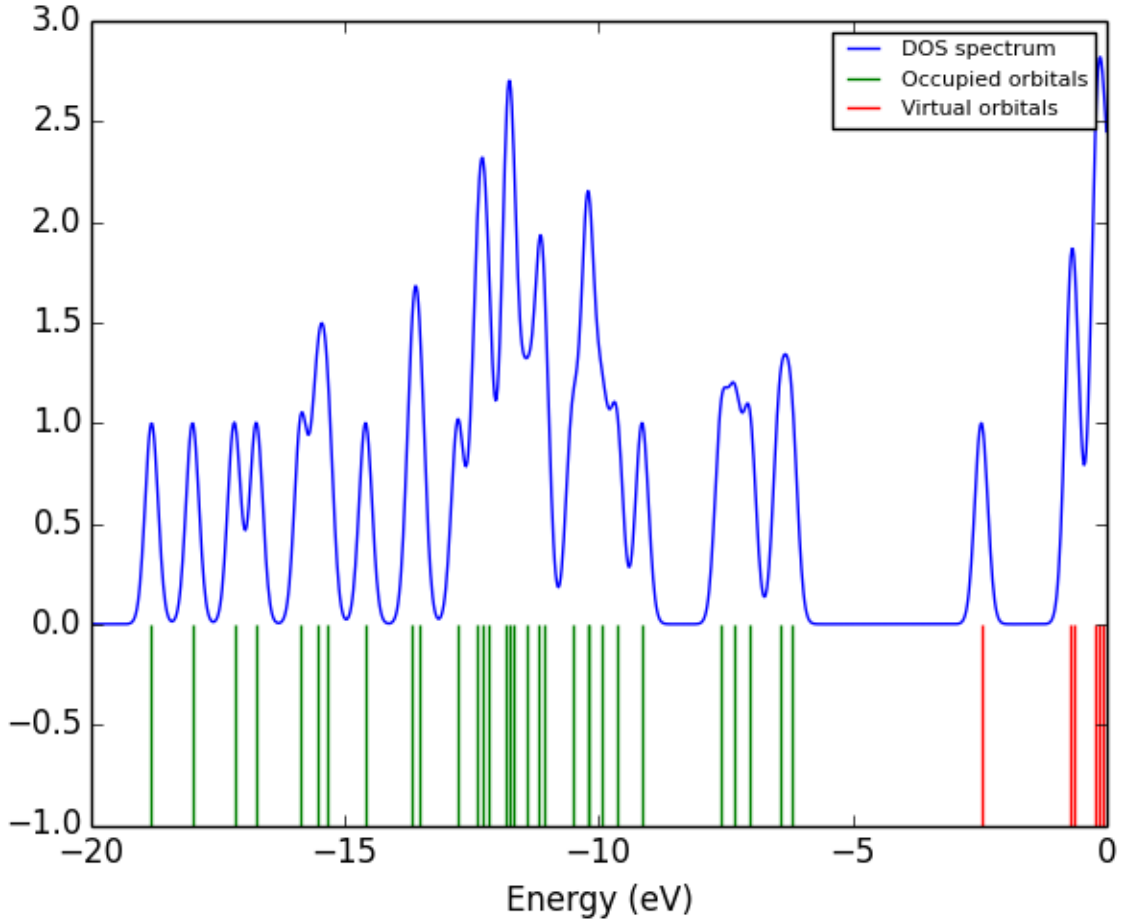

Figure 2.68: Density of state (DOS) and energy levels of occupied and virtual orbitals of 2,4-Dihydroxyazobenzene, 4-(Phenylazo) resorcinol ($C_{12}H_{10}N_2O_2$). Computations has been performed at B3LYP level of theory along with 6-311++G(d,p) basis set. This sample showed no any circular dichroism and that is the reason CD spectrum is not provided.

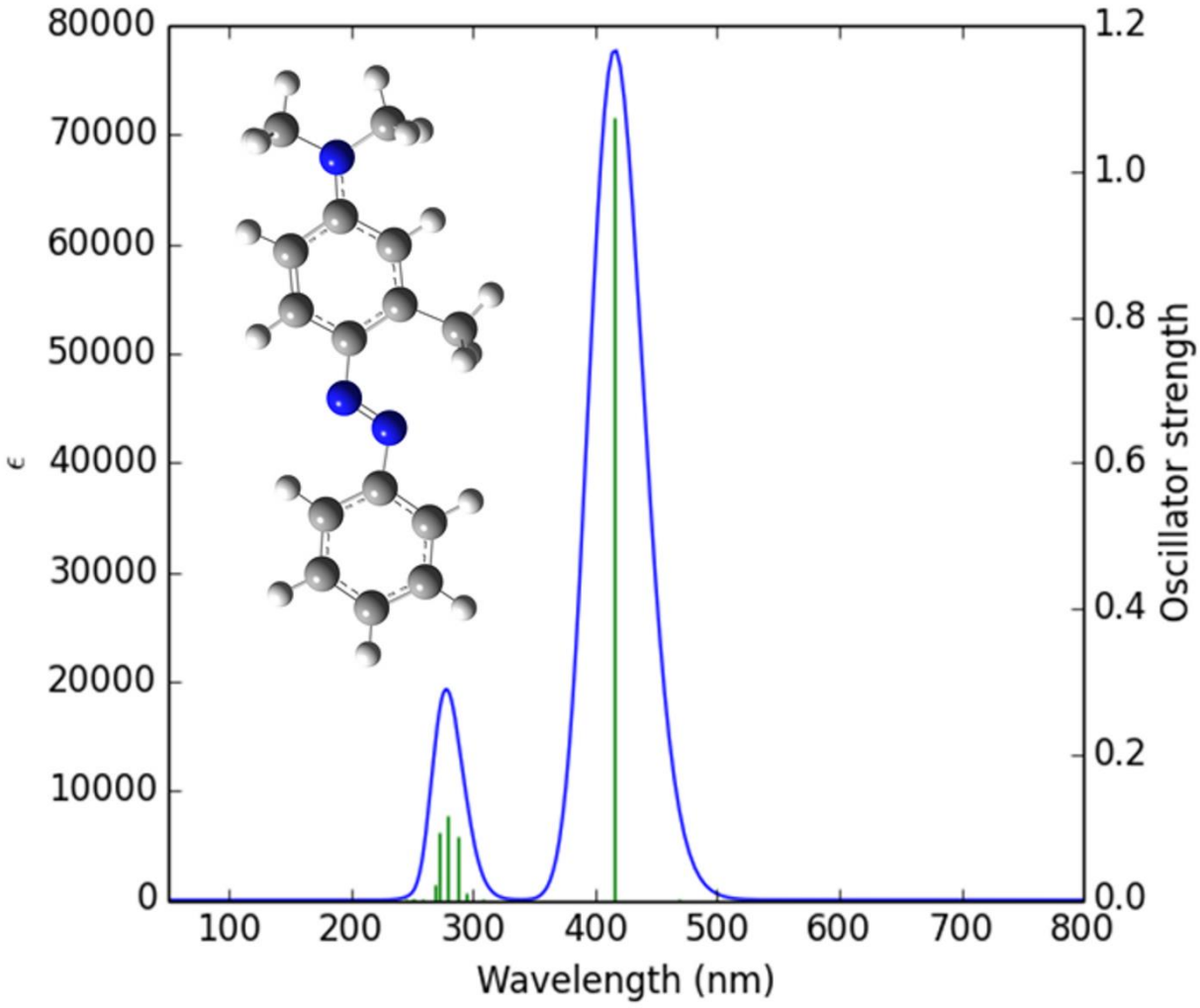

Figure 2.69: Computational UV-Vis Spectrum of trans 4-Dimethylamino-2-methylazobenzene. Computations has been at B3LYP level of theory using 6-311++G(d,p) basis set. Acetonitrile has been considered in this computations as the solvent.

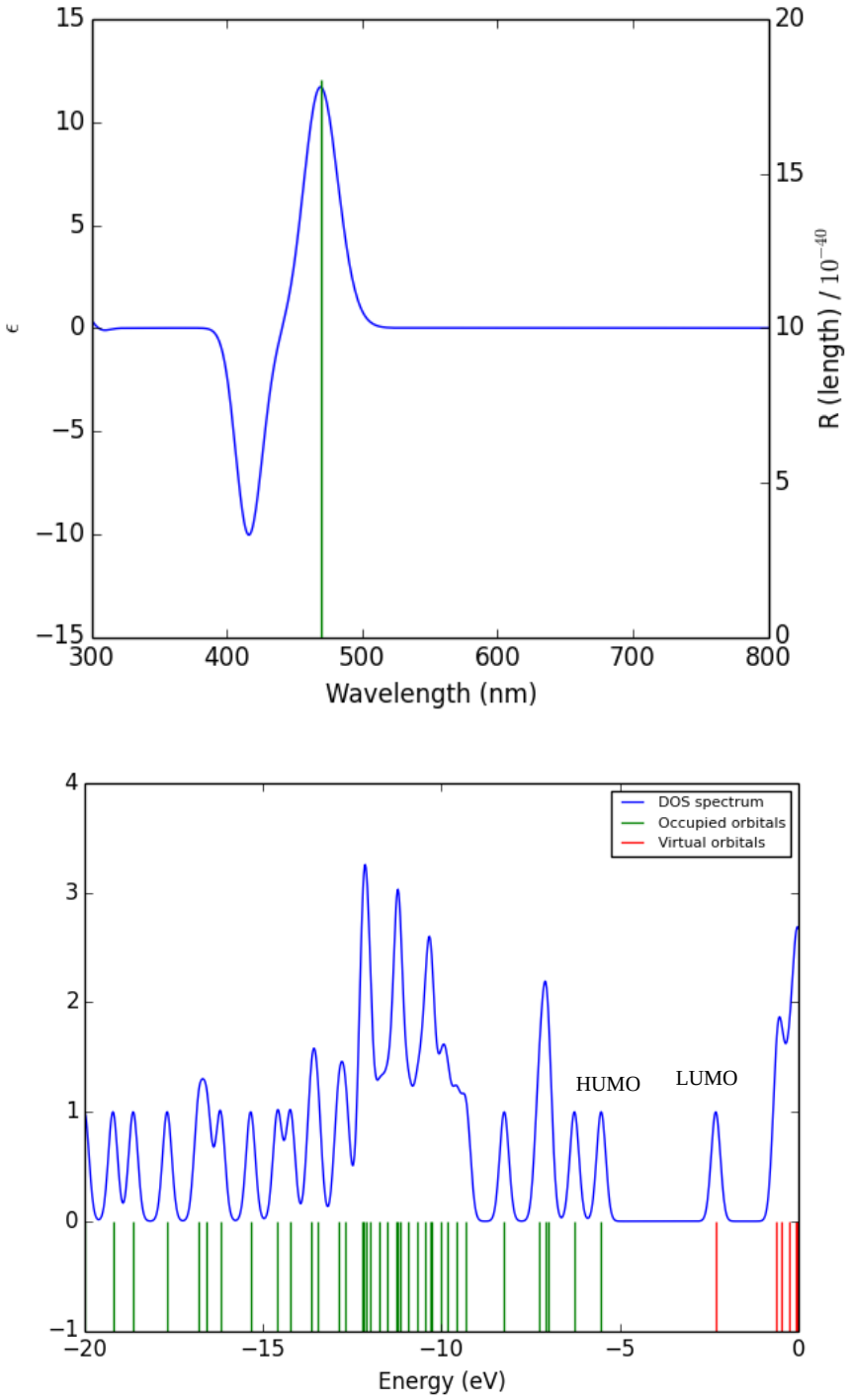

Figure 2.70: Top) Circular dichroism spectrum of trans 4-Dimethylamino-2-methylazobenzene computed at B3LYP level of theory and 6-311++G(d,p) and acetonitrile is considered as the solvent. Bottom) Density of state (DOS) and energy levels of occupied and virtual orbitals computations has been performed at same level of theory.

2.7 NMR Spectroscopy:

Nuclear Magnetic Resonance, NMR, spectroscopy is a robust analytical method in determining physical and chemical properties of molecules. NMR can be performed in a wide range of phases and states especially for the analysis of organic molecules. It is also possible to calculate NMR spectra using readily available quantum chemistry computational methods. The properties we can measure in an NMR experiment includes chemical shift, spin-spin splitting, linewidths, relaxation and chemical exchange. Proton NMR and ^{13}C are the most common type of characterization in organic chemistry. We have performed NMR experiments for several of the samples studied in this dissertation. NMR is able to distinguish between the cis and trans isomer of the sample molecule which will provide a proof of the conversion efficiency occurring upon irradiation. NMR spectra were recorded with 300, 500 and 600 MHz frequency. Constant frequency NMR was used to analyze the energy levels while the magnetic field is varied. Figure 2.71 illustrates a simple picture of the physics behind NMR spectroscopy.

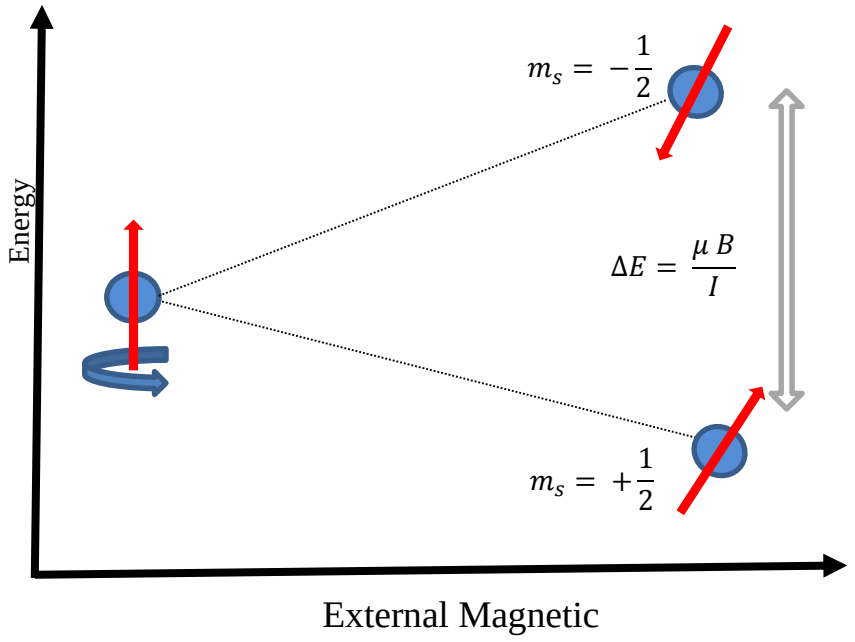

Figure 2.71: Basic physics of nuclear magnetic resonance (NMR) and the decoupling mechanism.

The chemical shift which is be obtained experimentally and computationally is the difference between the resonance frequency of the nucleus to a standard and is independent of the external magnetic field strength. This quantity is reported in part per million, ppm. According to the Larmor equation, the Larmor frequency of a specific magnetic field is:

$$\omega_0 = \gamma B_0 \tag{2.36}$$

$$\gamma = \frac{\mu\, \mu_N}{h\, I} \tag{2.37}$$

Where B_0 is the strength of the magnet and γ and μ are the gyromagnetic ratio of the sample nucleus and its magnetic moment respectively. I is the nucleus spin quantum number and μ_N is the nuclear magnetron.

$$\delta = \frac{\left(\nu_{sample} - \nu_{refrence}\right)}{\nu_{refrence}} \tag{2.38}$$

In this equation ν_{sample} is the resonant frequency of the sample and ν_{refrence} is the reference frequency. The reference frequency refers to that of tetramethylsilane (TMS) which provides an absolute resonance frequency for a standard reference compound. In ^{1}H NMR spectroscopy spin-spin splitting occurs only between nonequivalent protons on the same carbon or adjacent carbons. Herein we present experimental and theoretical NMR spectroscopy results for some of our samples. NMR spectroscopy had been used to study azobenzene photoisomerisation before.[72] Tait et al used ^{1}H NMR spectroscopy to study Cis–trans photoisomerisation of four azo dyes and the Ab initio calculation results for chemical shifts were in good agreement with the experimental results. We have done 1D and 2D NMR spectroscopy for several of our samples. Below we present the experimental results in Figure 2.72 to Figure 2.79.

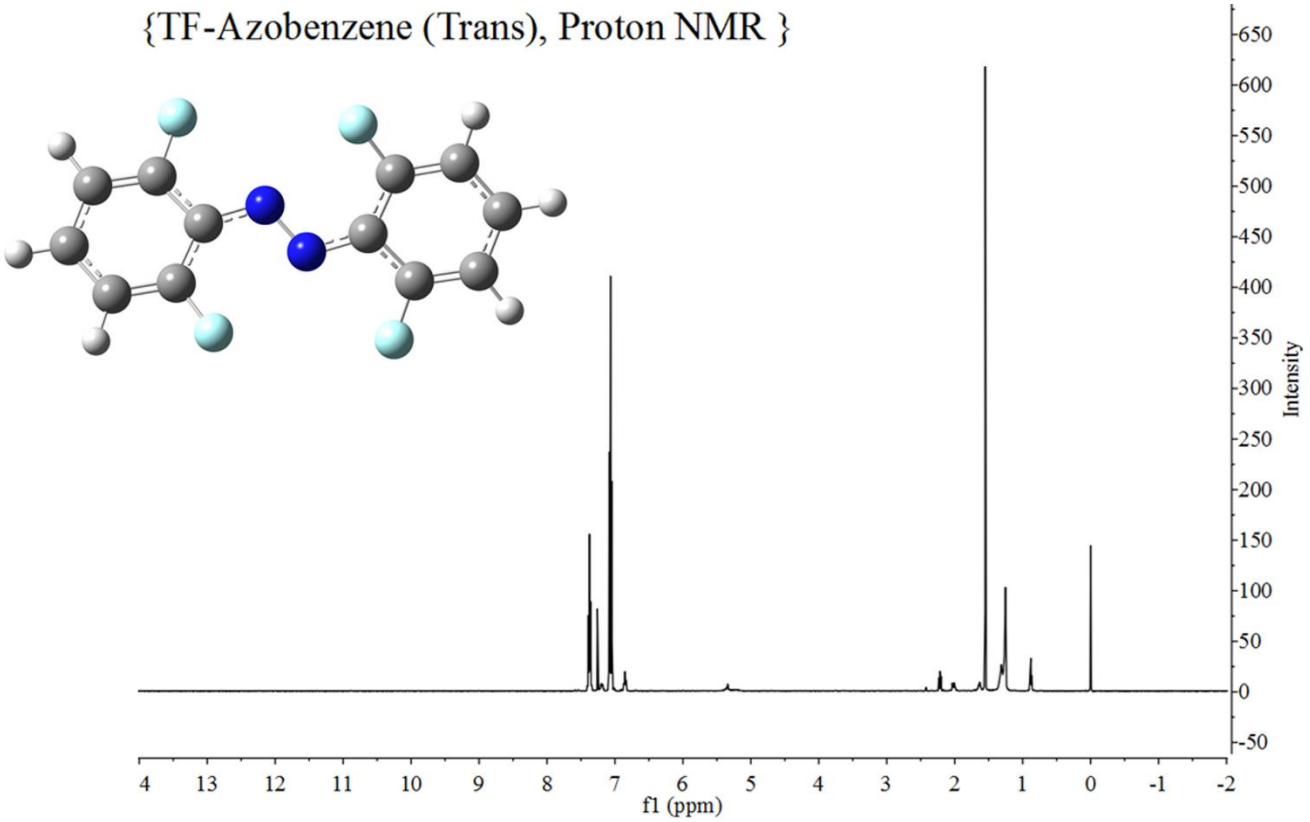

Figure 2.72: ^{1}H NMR (500 MHz, CDCl3), Experimental Proton NMR of trans 2,2́,6,6́-tetrafluoroazobenzene.

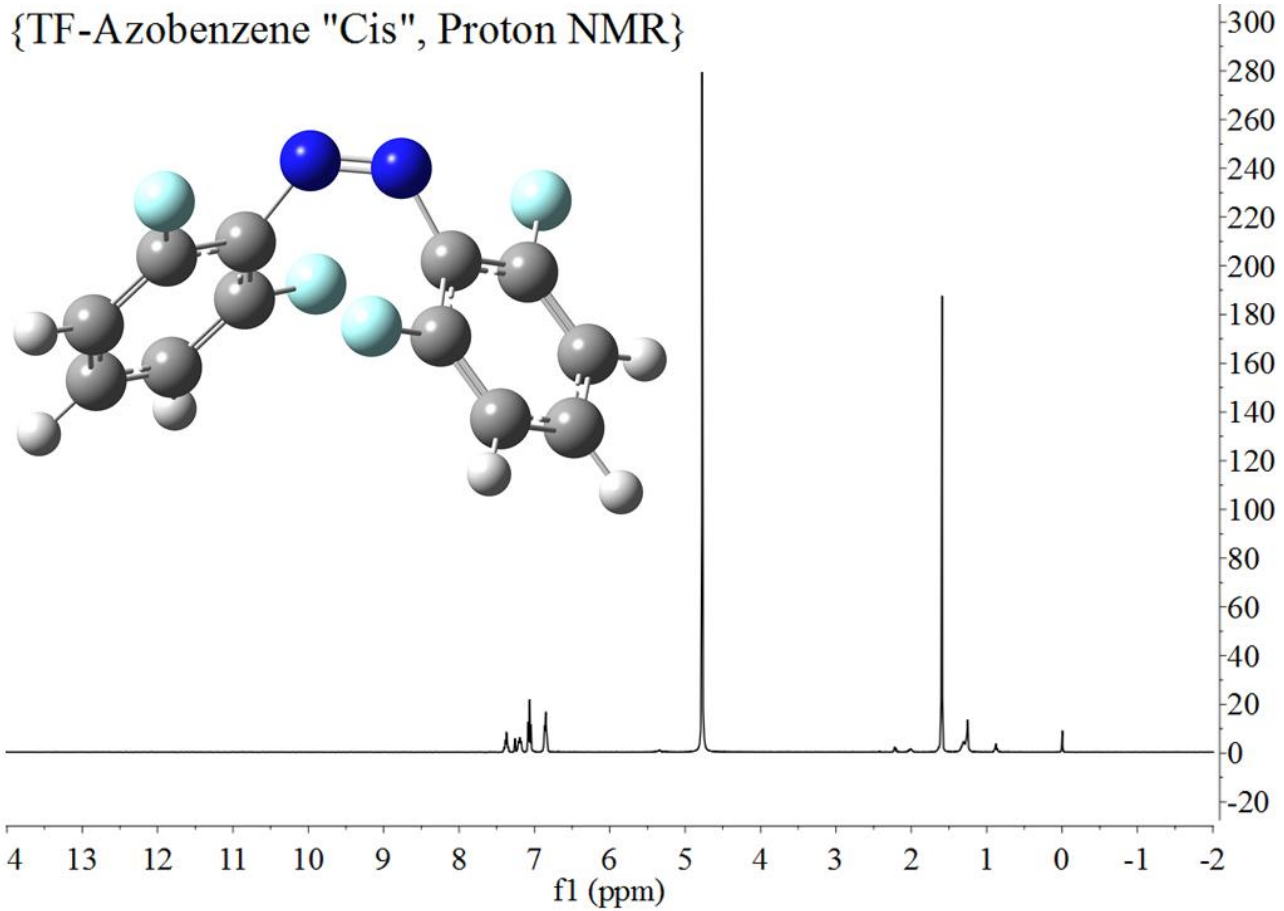

Figure 2.73: ^{1}H NMR (500 MHz, CDCl3), Experimental Proton NMR of cis 2,2́,6,6́-tetrafluoroazobenzene.

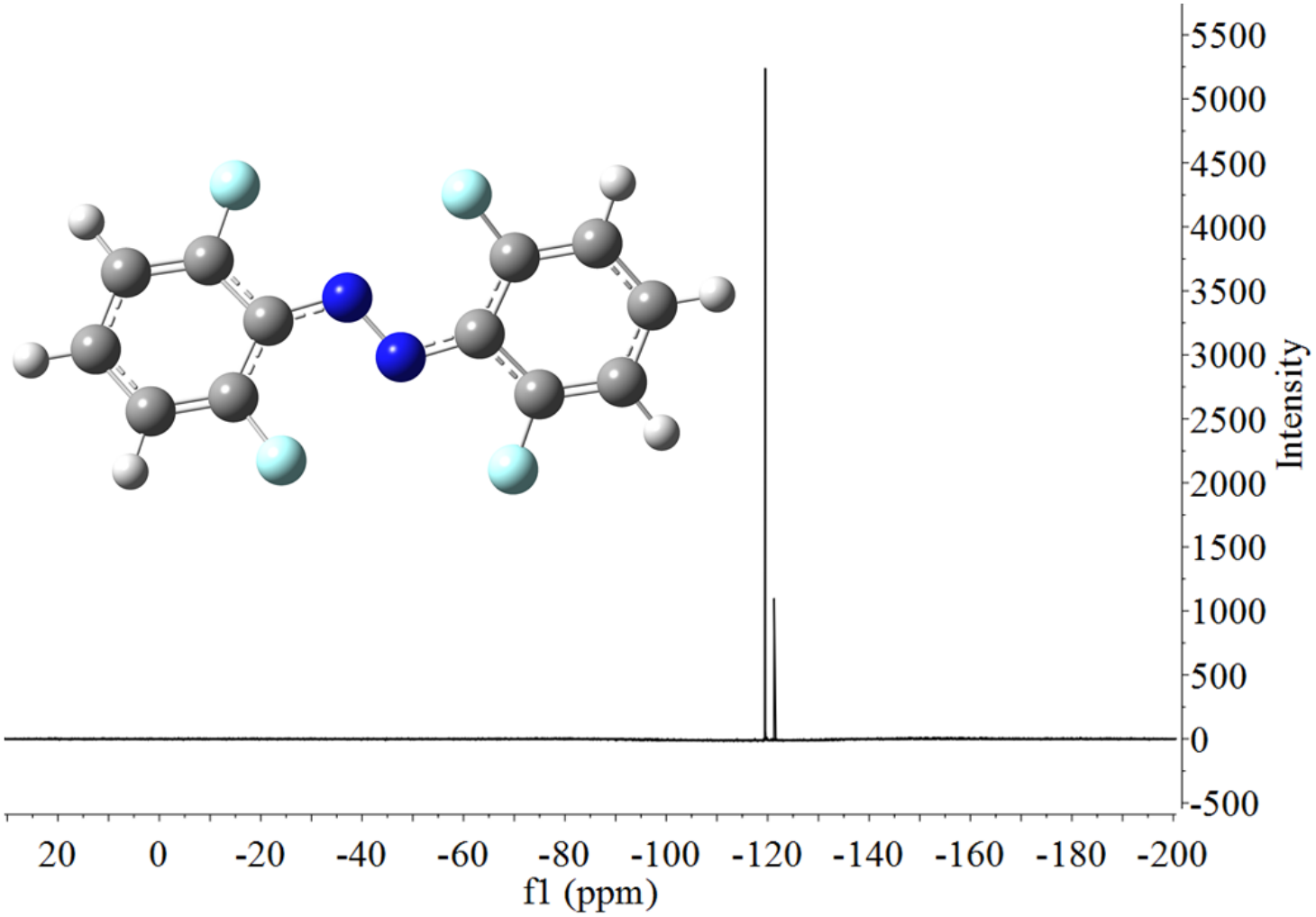

Figure 2.74: ^{13}C NMR (500 MHz, CDCl3), Experimental ^{13}C NMR of trans 2,2́,6,6́-tetrafluoroazobenzene.

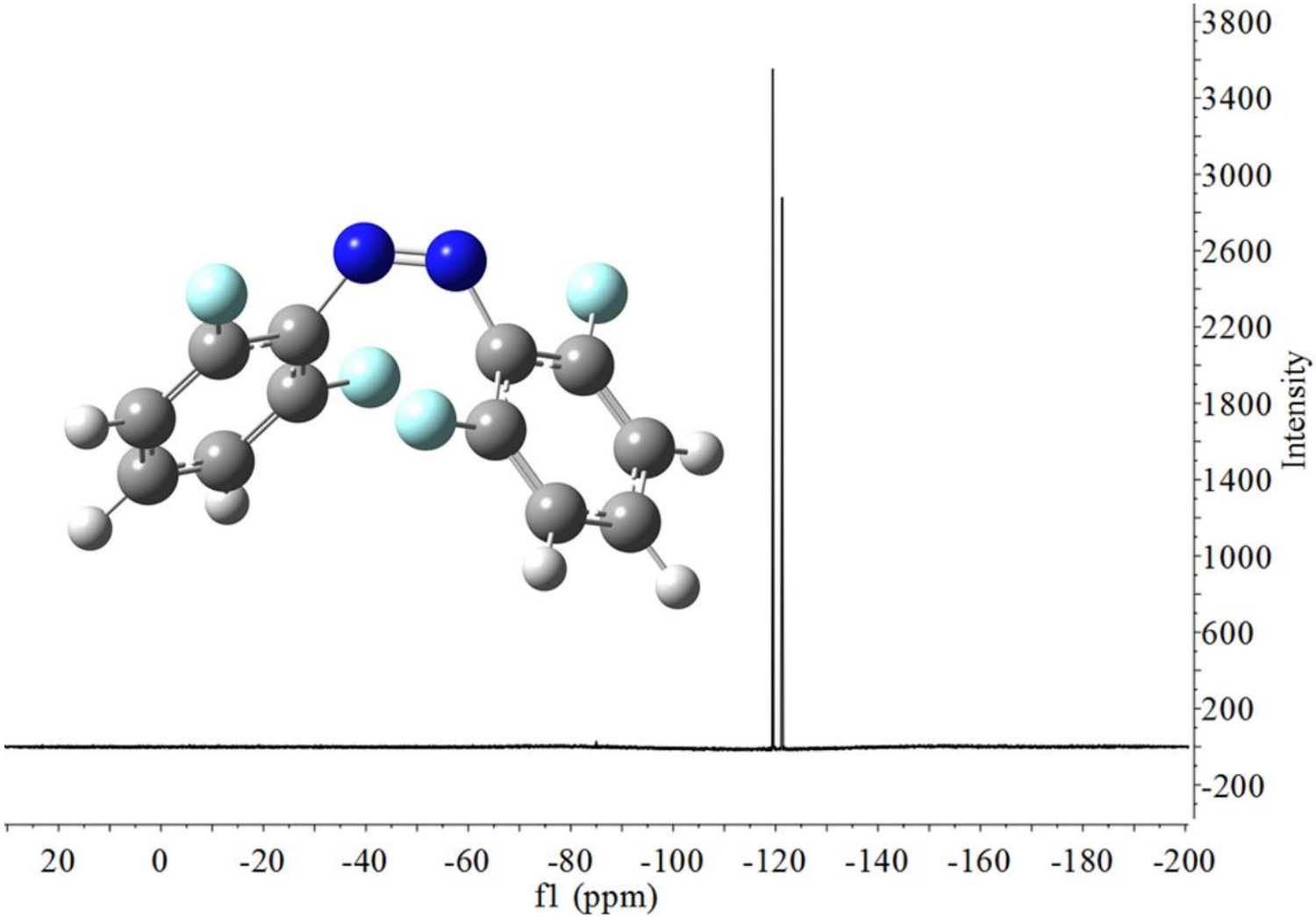

Figure 2.75: ^{13}C NMR (500 MHz, CDCl3), Experimental ^{13}C NMR of cis 2,2́,6,6́-tetrafluoroazobenzene.

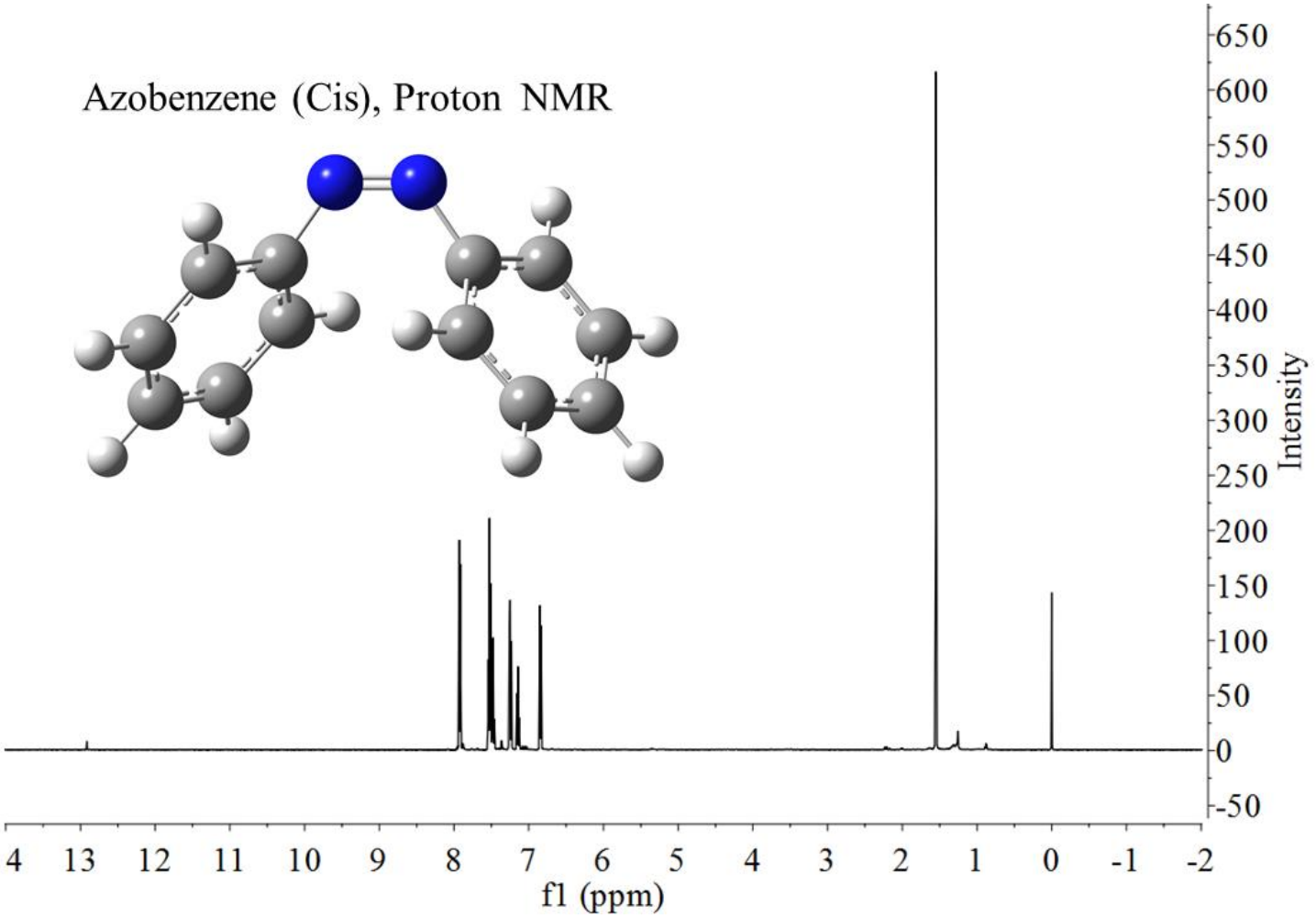

Figure 2.76: ^{1}H NMR (500 MHz, CDCl3), Experimental Proton NMR spectrum of cis azobenzene.

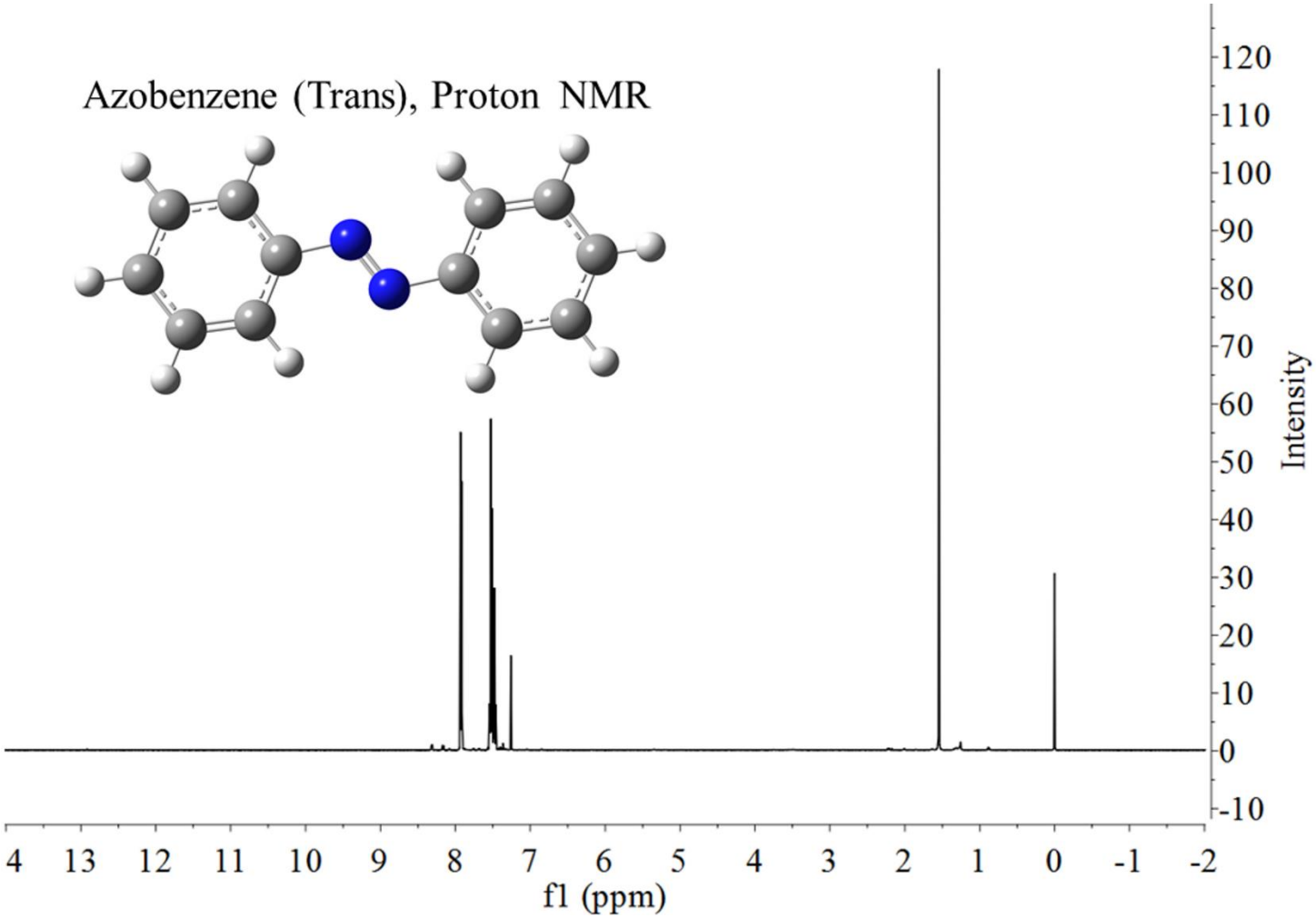

Figure 2.77: ^{1}H NMR (500 MHz, CDCl3), Experimental Proton NMR spectrum of trans azobenzene.

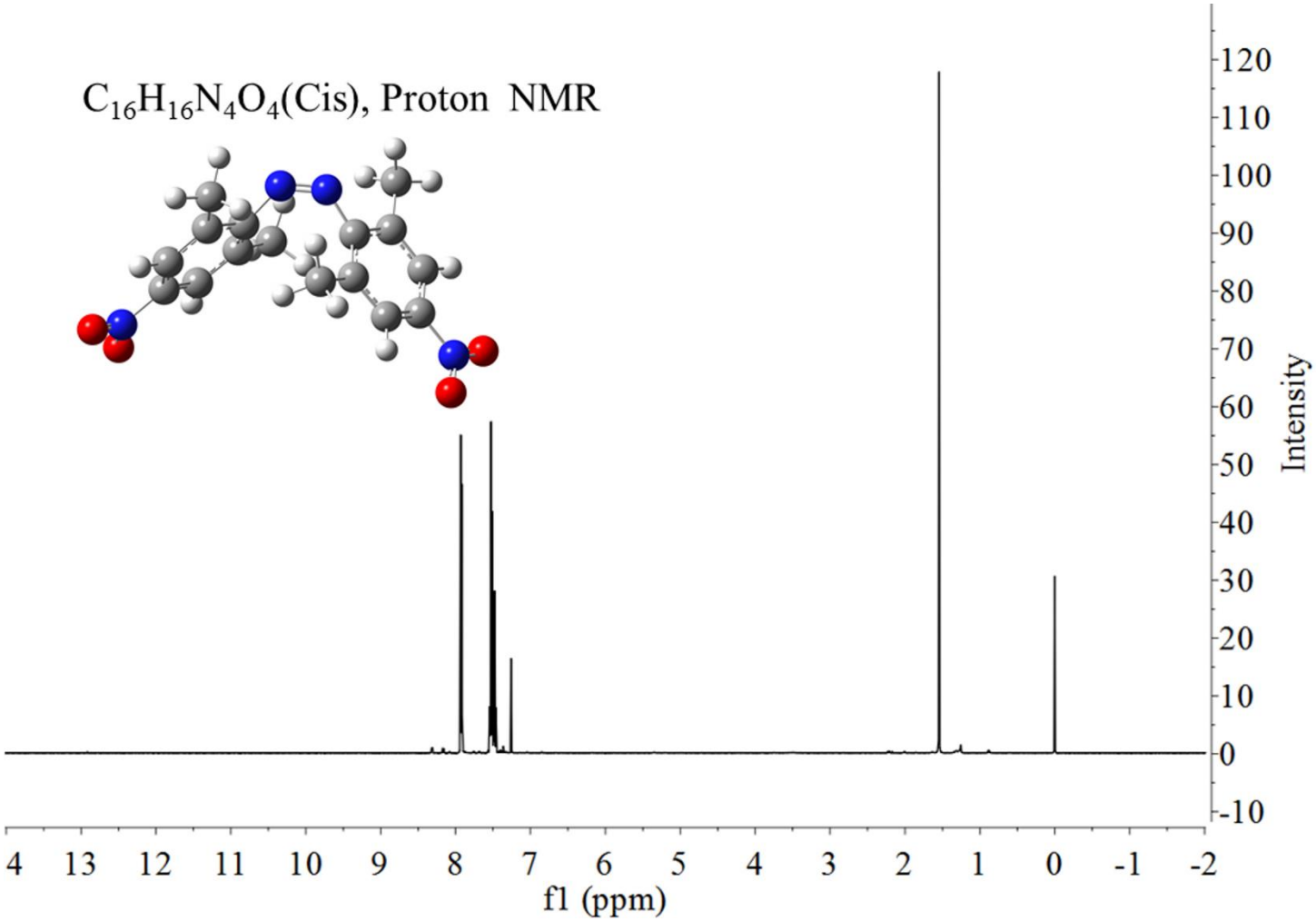

Figure 2.78: [1]H NMR (500 MHz, CDCl3), Experimental Proton NMR spectrum of cis 2,2',6,6' tetramethyl-(4,4') dinitro-azobenzene.

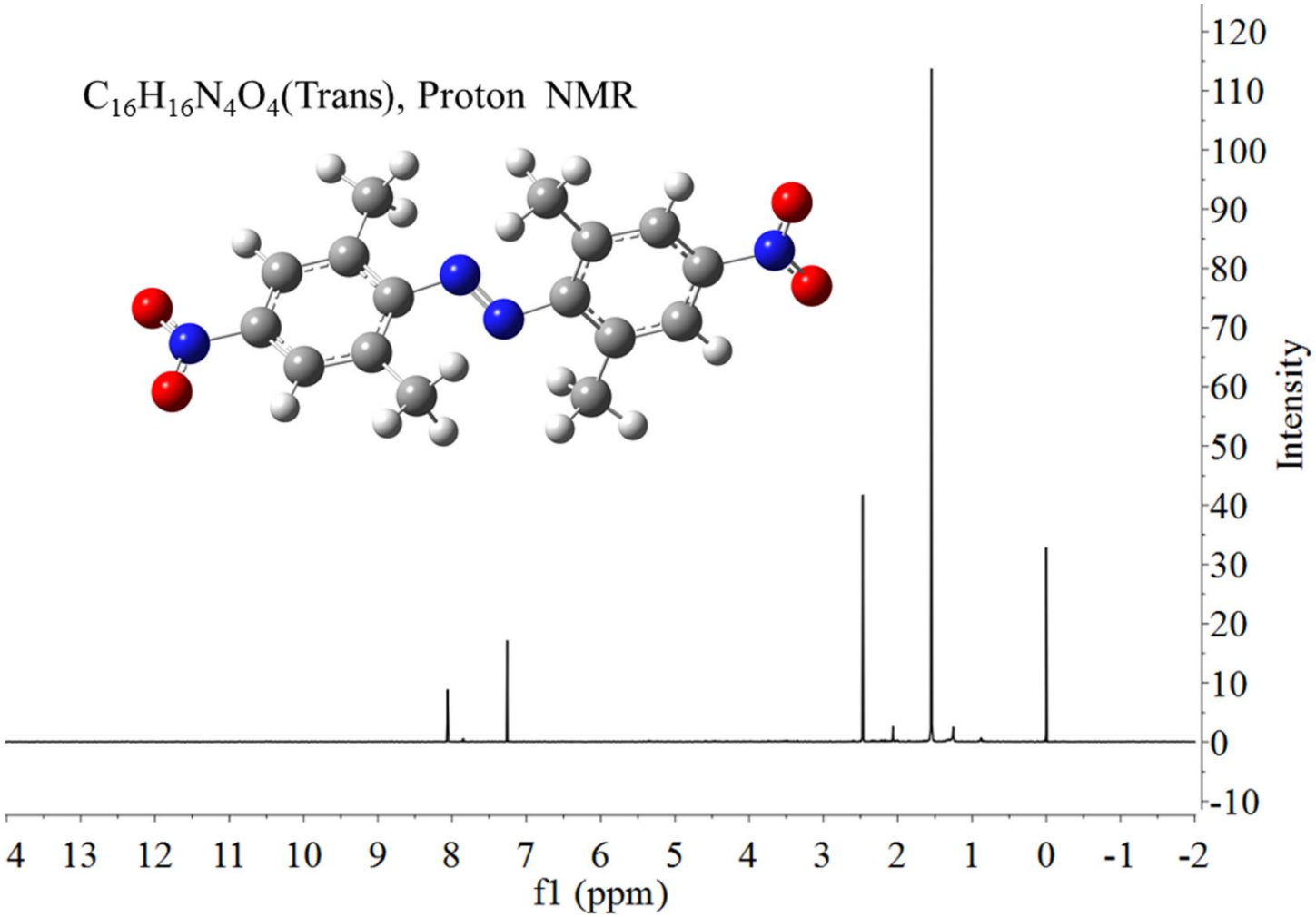

Figure 2.79: ^{1}H NMR (500 MHz, CDCl3), Experimental Proton NMR of trans 2,2',6,6' tetramethyl-(4,4') dinitro – azobenzene.

As an example of calculations for the NMR spectroscopy we present the simulated NMR spectrum data for the trans 2,2́,6,6́-tetrafluoroazobenzene. These results have been obtained following an optimization calculation with tight convergence criteria with B3LYP level of theory and no use of incremental Fock matrix formation, along with 6-311++G(d,p) level of theory.

Calculating GIAO nuclear magnetic shielding tensors.

SCF GIAO Magnetic shielding tensor (ppm):

1 N Isotropic = -344.4501 Anisotropy = 757.4317
XX= -188.1428 YX= -219.5564 ZX= 12.7764
XY= -87.3700 YY= -1003.9990 ZY= -22.8082
XZ= 36.0521 YZ= 40.5746 ZZ= 158.7916
Eigenvalues: -1032.0550 -161.7996 160.5044
2 N Isotropic = -344.4501 Anisotropy = 757.4317
XX= -188.1428 YX= -219.5564 ZX= -12.7764
XY= -87.3700 YY= -1003.9990 ZY= 22.8082
XZ= -36.0521 YZ= -40.5746 ZZ= 158.7916
Eigenvalues: -1032.0550 -161.7996 160.5044
3 C Isotropic = 43.3830 Anisotropy = 125.2883
XX= 31.5895 YX= 1.4086 ZX= 53.6950
XY= -2.3126 YY= 4.3695 ZY= 4.7164
XZ= 56.8240 YZ= 14.1008 ZZ= 94.1901
Eigenvalues: -3.9661 7.2066 126.9085
4 C Isotropic = 47.0739 Anisotropy = 191.7848
XX= 61.8563 YX= 20.2061 ZX= 62.4054
XY= 25.2372 YY= -58.3858 ZY= 7.5785
XZ= 64.9749 YZ= 1.3825 ZZ= 137.7512
Eigenvalues: -62.8286 29.1199 174.9304
5 C Isotropic = 24.2541 Anisotropy = 84.1200
XX= 0.9624 YX= -9.4247 ZX= 53.2342
XY= -21.8000 YY= 21.5151 ZY= 22.5057
XZ= 43.0748 YZ= 10.0767 ZZ= 50.2848

Eigenvalues: -36.6961 29.1242 80.3341

6 C Isotropic = 12.0243 Anisotropy = 106.4963

XX= -33.0630 YX= 12.1820 ZX= 65.4411

XY= 17.8947 YY= 18.9529 ZY= -2.4777

XZ= 55.4676 YZ= 5.1677 ZZ= 50.1830

Eigenvalues: -66.7258 19.7769 83.0219

7 C Isotropic = 66.7417 Anisotropy = 144.4295

XX= 50.1323 YX= -28.3185 ZX= 66.6298

XY= -23.4583 YY= 27.7719 ZY= 25.7993

XZ= 67.1492 YZ= 28.4680 ZZ= 122.3209

Eigenvalues: -18.4034 55.6004 163.0280

8 C Isotropic = 65.9277 Anisotropy = 143.1402

XX= 29.1348 YX= 22.3973 ZX= 74.9838

XY= 19.6777 YY= 52.3927 ZY= -1.2407

XZ= 77.8248 YZ= -3.0613 ZZ= 116.2557

Eigenvalues: -20.3866 56.8152 161.3545

9 C Isotropic = 43.3830 Anisotropy = 125.2883

XX= 31.5895 YX= 1.4086 ZX= -53.6950

XY= -2.3126 YY= 4.3695 ZY= -4.7164

XZ= -56.8240 YZ= -14.1008 ZZ= 94.1901

Eigenvalues: -3.9661 7.2066 126.9085

10 C Isotropic = 47.0739 Anisotropy = 191.7848

XX= 61.8563 YX= 20.2061 ZX= -62.4054

XY= 25.2372 YY= -58.3858 ZY= -7.5785

XZ= -64.9749 YZ= -1.3825 ZZ= 137.7512

Eigenvalues: -62.8286 29.1199 174.9304

11 C Isotropic = 24.2541 Anisotropy = 84.1200

XX= 0.9624 YX= -9.4247 ZX= -53.2342

XY= -21.8000 YY= 21.5151 ZY= -22.5057

XZ= -43.0748 YZ= -10.0767 ZZ= 50.2848

Eigenvalues: -36.6961 29.1242 80.3341

12 C Isotropic = 12.0243 Anisotropy = 106.4963

XX= -33.0630 YX= 12.1820 ZX= -65.4411

XY= 17.8947 YY= 18.9529 ZY= 2.4777

XZ= -55.4676 YZ= -5.1677 ZZ= 50.1830

Eigenvalues: -66.7258 19.7769 83.0219

13 C Isotropic = 66.7417 Anisotropy = 144.4295

XX= 50.1323 YX= -28.3185 ZX= -66.6298

XY= -23.4583 YY= 27.7719 ZY= -25.7993

XZ= -67.1492 YZ= -28.4680 ZZ= 122.3209

Eigenvalues: -18.4034 55.6004 163.0280

14 C Isotropic = 65.9277 Anisotropy = 143.1402

XX= 29.1348 YX= 22.3973 ZX= -74.9838

XY= 19.6777 YY= 52.3927 ZY= 1.2407

XZ= -77.8248 YZ= 3.0613 ZZ= 116.2557

Eigenvalues: -20.3866 56.8152 161.3545

15 F Isotropic = 296.8385 Anisotropy = 183.8035

XX= 258.2873 YX= 12.2449 ZX= -82.2040

XY= 53.8342 YY= 239.5110 ZY= 47.5349

XZ= -27.7622 YZ= 48.9281 ZZ= 392.7172

Eigenvalues: 189.0682 282.0730 419.3742

16 F Isotropic = 287.4701 Anisotropy = 162.4019

XX= 321.3452 YX= -4.3596 ZX= -37.9533

XY= 17.1795 YY= 203.8308 ZY= -4.3557

XZ= -92.7714 YZ= -13.0743 ZZ= 337.2344

Eigenvalues: 203.2101 263.4623 395.7381

17 F Isotropic = 296.8385 Anisotropy = 183.8035

XX= 258.2873 YX= 12.2449 ZX= 82.2040

XY= 53.8342 YY= 239.5110 ZY= -47.5349

XZ= 27.7622 YZ= -48.9281 ZZ= 392.7172

Eigenvalues: 189.0682 282.0730 419.3742

18 F Isotropic = 287.4701 Anisotropy = 162.4019

XX= 321.3452 YX= -4.3596 ZX= 37.9533

XY= 17.1795 YY= 203.8308 ZY= 4.3557

XZ= 92.7714 YZ= 13.0743 ZZ= 337.2344

Eigenvalues: 203.2101 263.4623 395.7381

19 H Isotropic = 24.7922 Anisotropy = 4.7226

XX= 24.9727 YX= -1.8634 ZX= -1.3819

XY= -1.3407 YY= 26.7590 ZY= 0.4742

XZ= -1.4393 YZ= 0.4240 ZZ= 22.6449

Eigenvalues: 21.9612 24.4748 27.9406

20 H Isotropic = 24.5601 Anisotropy = 4.3700

XX= 26.1103 YX= 0.1031 ZX= -2.3096

XY= 0.5911 YY= 24.4985 ZY= -0.4653

XZ= -2.2783 YZ= -0.8668 ZZ= 23.0716

Eigenvalues: 21.7722 24.4347 27.4734

21 H Isotropic = 24.8913 Anisotropy = 4.9330

XX= 24.1214 YX= 0.4797 ZX= -1.0627

XY= 0.3744 YY= 28.0427 ZY= -0.6524

XZ= -1.1544 YZ= -0.5225 ZZ= 22.5098

Eigenvalues: 21.9269 24.5670 28.1800

22 H Isotropic = 24.7922 Anisotropy = 4.7226

XX= 24.9727 YX= -1.8634 ZX= 1.3819

XY= -1.3407 YY= 26.7590 ZY= -0.4742

XZ= 1.4393 YZ= -0.4240 ZZ= 22.6449

Eigenvalues: 21.9612 24.4748 27.9406

23 H Isotropic = 24.5601 Anisotropy = 4.3700

XX= 26.1103 YX= 0.1031 ZX= 2.3096

XY= 0.5911 YY= 24.4985 ZY= 0.4653

XZ= 2.2783 YZ= 0.8668 ZZ= 23.0716

Eigenvalues: 21.7722 24.4347 27.4734

24 H Isotropic = 24.8913 Anisotropy = 4.9330

XX= 24.1214 YX= 0.4797 ZX= 1.0627

XY= 0.3744 YY= 28.0427 ZY= 0.6524

XZ= 1.1544 YZ= 0.5225 ZZ= 22.5098

Eigenvalues: 21.9269 24.5670 28.1800

2.8 Computational Electron Affinities

Electron affinities including adiabatic, vertical detachment energy and vertical electron affinity are of central importance in this research. To be able to perform a collision induced dissociation experiment, the very first step is to ionize the sample. To initially investigate the sample to determine whether it is possible to produce a negative ion from the neutral sample, it is helpful to calculate the electron affinity. Theoretical calculations related to negative ions are complicated since these calculations should address the extra electron which is generally loosely bound to the precursor neutral. For this reason the use of large size and diffuse basis sets are necessary. By definition the adiabatic electron affinity is the difference between the two ground electronic states of the neutral and anion (or cation). Finally it is necessary to include calculations of the zero-point energies to obtain the AEA.

One important issue in the calculation which needs to be treated and considered especially for structures with unpaired electron, is the spin contamination. It is necessary to check the value of this contamination in the output file of the calculations and make sure it is within the accepted range. Spin unrestricted calculations using density functional theory can yield wave functions with spin contamination.[73] The S^2 value in absence of spin contamination should be s(s+1) and s is half the number of unpaired electrons. As an example for a system with 1 unpaired electron it should be 0.75. We have observed this value to be around 1.5 for a UMP2 calculation of one of our fragment ions, $[C_6H]^-$, which means results from this calculation are not reliable and must be corrected. DFT calculations usually don't show large spin contamination. Gaussian has treatments for spin contamination and provides the value for it after spin contamination annihilation. Spin projection is another approach to minimize this.[66]

Using photoelectron spectroscopy (Johns Hopkins University) we were able to experimentally determine electron affinities and vertical detachment energies for two of our samples (trans-

azobenzene and trans-2,2',6,6' tetrafuoroazobenzene). Computational methods such as CCSD(T) along with a highly polar basis set such as aug-cc-pVnZ are able to predict an electron affinity with an error margin of few percent. In general these types of calculations are sensitive to the basis set size and how diffuse they are since they should be able to treat the extra electron binding to the neutral molecule correctly. Sophisticated quantum chemistry algorithm are able to predict the electron affinities with a reliable level of accuracy. Although from the point of view of practicality DFT methods are the only feasible possibility specially for molecules with more than 10 atoms, there are other techniques and possibilities such as Gn Gaussian methods (G1, G2, G2MP2, G3, G3MP2, G3B3, G3MP2B3, G4MP2 which are capable of energy calculations with error smaller than 2 kcal/mol), CBS method (CBS-QB3, CBS-4M, CBS-APNO) which are Complete Basis Set, W1U, W1BD[74] and W1RO which W1 method modified to use UCCSD instead of ROCCSD for open shell systems. These methods provide complex energy computations involving several pre-defined calculations on the specified molecular system.[22] W methods are more accurate but slower. The W1 theory has a mean absolute error of 0.016 eV in calculating electron affinities. This is even more improved in W2 method and the mean error is in the order of magnitude of 0.012 eV.[75] These methods are time consuming and considering our computational resources it was impossible to apply these methods to our samples which are molecules with more than 14 atoms. We did apply some of these methods to our fragment ions. Even for a structure as small as C_6H, W methods take days for completion.

Anion photodetachment techniques are currently the most accurate and reliable experimental methods for measuring electron affinities, and DFT is perhaps the only widely applicable and easily employed theoretical method in use today which achieves satisfactory accuracy (within 0.2 eV) in the prediction of EAs for large molecules[76]. By definition the electron affinity of a molecule which has been represented as R is the transition energy:

$$EA(R) = \Delta E(R \leftarrow R^{-}) \tag{2.39}$$

The electron affinity is equal to the energy difference between the enthalpy of formation of a neutral species and the enthalpy of formation of the negative ion of the same structure. The electron affinity is defined as the negative of the 0 K enthalpy change for the electron attachment reaction[77]:

$$M + e^- \rightarrow M^- \qquad \Delta H_{rxn} = -EAa \tag{2.40}$$

We can define the electron affinity as an adiabatic electron affinity which is the energy difference of the Born-Oppenheimer energy surfaces of the neutral and anionic species at their respective minima[78] and the vertical electron affinity. The value of the vertical electron affinity being greater than or equal to the adiabatic value. To calculate the adiabatic electron affinity we can simply subtract energies at equilibrium geometry of neutral and negative ion molecule. Considering the zero point energy are necessary in this calculation. As it has been illustrated in Figure 2.80 below, the reference for the energies are the ZPE corrected values and not the bottom of the electronic wells. Vertical electron affinities on the other hand are the difference in energy between optimized neutral in its equilibrium configuration and the negative ion in the neutral equilibrium geometry. From the technical point of view to compute this we need to perform a single point energy calculation on the neutral equilibrium geometry but charge and multiplicity of the anion should be considered. For the vertical detachment energy on the other hand we need to consider the negative ion in its equilibrium geometry and neutral molecule energy in the negative ion equilibrium geometry. To obtain the value of the neutral at optimized anion geometry, we perform a single point energy calculation on the anion optimized geometry but using the charge and multiplicity of the neutral. Quantum computational methods are extremely important and useful to investigate molecular properties such as the electron affinity since it is difficult to measure those experimentally with high accuracy. The adiabatic electron affinity is rather a theoretical concept and difficult to measure experimentally (since both neutral and anion must be at their equilibrium geometry configuration). In general for the numerical values for this quantities we can summarize as:

$$VAE < AEA < VDE \tag{2.41}$$

We need to calculate the vibrational zero point energy and add this to the minimum electron energy. To make this calculation results more accurate, the scaling factor must be applied to the zero point energy. There are standard resources such as NIST webbook to find this scaling factors for different levels of theory and basis sets. Electronic model chemistries are usually used to

compute vibrational frequencies by invoking the approximation that the potential energy in the vicinity of a minimum varies quadratically with respect to the nuclear coordinates[79].

$$ZPE = \frac{1}{2} \sum^{3n-6} h\omega_e \tag{2.42}$$

$$E_{tot}^{0K} = ZPE + E_{electronic}^{0K} \tag{2.43}$$

and ω_e is the harmonic frequency which there should be 3n-6 (or 3n-5 for linear molecule). $E_{electronic}^{0K}$ is the energy for the stationary point on the Born-Oppenheimer potential energy surface[24]. Often times since it is much less time consuming to only consider the harmonic frequencies (and disregard the anharmonic frequencies), the calculated ZPE is overestimated. One of the important considerations in this type of calculation is the utilization of diffuse basis sets. For the Dunning type basis set the aug- will suffice and for Gaussian type basis set it is necessary to use the ++ basis set such as 6-311++G(2d,2p). W1 and W2 methods can yield EAs with mean absolute errors in the range of 0.01 eV. B3LYP level of theory along with aug-cc-pVDZ can perform as good as 0.2 eV mean absolute errors[24]. Better accuracy usually requires electron correlation methods such as CCSD (or at least MPn methods) and large basis sets with extra-diffuse basis sets to take into account the diffuse electron density of anions. An important point here is to make sure frequency calculations are performed at the same level of theory and the exact same basis set as the geometry optimization has been done. The term vertical in this context refers to the concept of the Born-Oppenheimer approximation and simply means the electronic changes happens so fast that we can ignore any change in nuclear coordinates. Energy level diagram are illustrated schematically in Figure 81.[76]

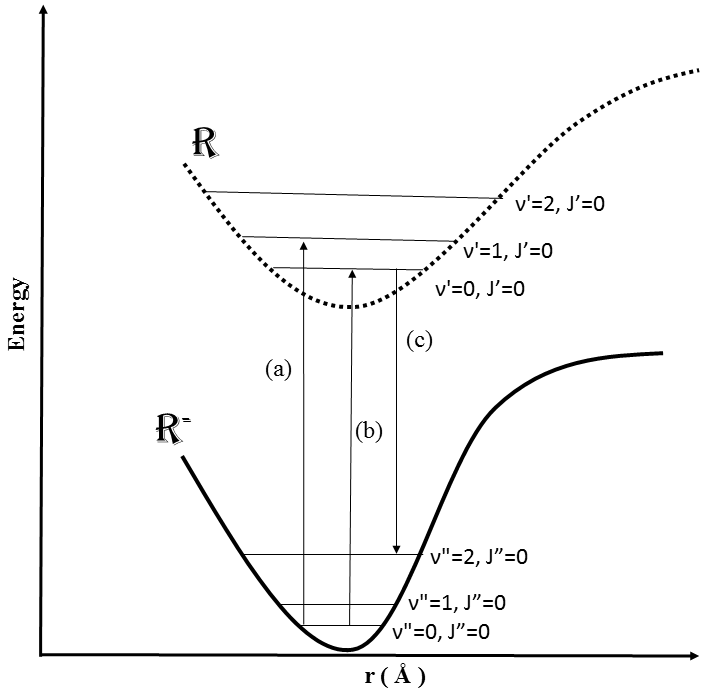

Figure 2.80: Schematic of energy level diagram of the potential energy surface for a molecule and its negative ion.

In general we used the following relations to calculate the vertical electron affinity (VEA), vertical detachment energy (VDE) and the adiabatic electron affinities (AEA).[76]

$$\mathrm{VEA} = \mathrm{E}(\text{optimized neut.}) - \mathrm{E}(\text{anion at optimized neut. geometry}) \tag{2.44}$$

$$VDE = E(\text{neut. at optimized anion geometry}) - E(\text{optimized anion}) \tag{2.45}$$

$$AEA = E(\text{optimized neut.}) - E(\text{optimized anion}) \tag{2.46}$$

Table 2.3: Summery of **CBS-QB3** calculations for the **trans** isomer of all of the samples we studied. These results are obtained at 298.15 K temperature and 1 atm pressure. Electron affinity is in eV unit and all other energies are in Hartree. (0 K) is the electronic energy at 0 K which the ZPE has been added to it.

	Neutral (CBS-QB3)				Anion (CBS-QB3)				
	(0 K)	Energy	Enthalpy	Free Energy	(0 K)	Energy	Enthalpy	Free Energy	AEA
Azobenzene	-571.7263	-571.7153	-571.7144	-571.7641	-571.7671	-571.7561	-571.7551	-571.8050	1.11
2,2´,6,6´-tetrafluoroazobenzene	-968.3711	-968.3567	-968.3557	-968.4140	-968.4233	-968.4084	-968.4075	-968.4687	1.42
2,2´,6,6´-tetramethyl-4,4´-dinitro-azobenzene									
4,4´-dinitro-azobenzene	-980.3111	-980.2949	-980.2940	-980.3586	-980.3999	-980.3839	-980.3829	-980.4458	2.41
2,2´,6,6´-tetramethyl-azobenzene	-728.6426	-728.6251	-728.6242	-728.6884	-728.6806	-728.6631	-728.6621	-728.7264	1.03
4-Methoxyazobenzene	-686.0877	-686.0741	-686.0732	-686.1295	-686.1247	-686.1109	-686.1100	-686.1670	1.00
Dihydroxyazobenzene,4-(Phenylazo)	-722.0173	-722.0039	-722.0030	-722.0589	-722.0485	-722.0345	-722.0336	-722.0910	0.85
4-Dimethylamino-2-methylazobenzene	-744.6678	-744.6507	-744.6497	-744.7147	-744.7007	-744.6838	-744.6829	-744.7473	0.89

Table 2.4: Summery of adiabatic electron affinity (AEA) calculated at B3LYP level of theory along with 6-311++G(d,p) for the **trans** isomer of all of the samples we studied. These results are obtained at 298.15 K temperature and 1 atm pressure. Electron affinity is in eV unit and all other energies are in Hartree. (a) Sum of electronic and zero-point Energies (b) Sum of electronic and thermal Energies (c) Sum of electronic and thermal Enthalpies (d) Sum of electronic and thermal Free Energies.

	Neutral				Anion				
	(a)	(b)	(c)	(d)	(a)	(b)	(c)	(d)	AEA
Azobenzene	-572.7183	-572.7074	-572.7064	-572.7569	-572.7673	-572.7563	-572.7554	-572.8060	1.33
2,2′,6,6′-tetrafluoroazobenzene	-969.7963	-969.7819	-969.7810	-969.8390	-969.8576	-969.8429	-969.8419	-969.9016	1.67
2,2′,6,6′-tetramethyl-4,4′-dinitro-azobenzene	-1139.0270	-1139.0041	-1139.003	-1139.0815	-1139.1271	-1139.1047	-1139.1037	-1139.1808	2.72
4,4′-dinitro-azobenzene	-981.8365	-981.8203	-981.8194	-981.8844	-981.9448	-981.9288	-981.9279	-981.9915	2.95
2,2′,6,6′-tetramethyl-azobenzene	-729.9052	-729.8878	-729.8868	-729.9509	-729.9483	-729.9310	-729.9300	-729.9942	1.17
4-Methoxyazobenzene	-687.2443	-687.2307	-687.2298	-687.2862	-687.2879	-687.2741	-687.2731	-687.3305	1.19
Dihydroxyazobenzene,4-(Phenylazo)	-723.1974	-723.1839	-723.1829	-723.2396	-723.2357	-723.2220	-723.2211	-723.2788	1.04
4-Dimethylamino-2-methylazobenzene	-745.9483	-745.9313	-745.9304	-745.9950	-745.9852	-745.9684	-745.9674	-746.0317	1.00

Table 2.5: Summery of adiabatic electron affinity calculated at **wB97XD** level of theory along with 6-311++G(d,p) for the **trans** isomer of all of the samples we studied. These results are obtained at 298.15 K temperature and 1 atm pressure. Electron affinity is in eV unit and all other energies are in Hartree. (a) Sum of electronic and zero-point Energies (b) Sum of electronic and thermal Energies (c) Sum of electronic and thermal Enthalpies (d) Sum of electronic and thermal Free Energies.

	Neutral				Anion				
	(a)	(b)	(c)	(d)	(a)	(b)	(c)	(d)	AEA
Azobenzene	-572.5008	-572.4900	-572.4891	-572.5390	-572.5463	-572.5353	-572.5344	-572.5849	1.24
2,2′,6,6′-tetrafluoroazobenzene	-969.4729	-969.4587	-969.4578	-969.5153	-969.5282	-969.5137	-969.5127	-969.5721	1.50
2,2′,6,6′-tetramethyl-4,4′-dinitro-azobenzene	-1138.6338	-1138.6112	-1138.6102	-1138.6882	-1138.7225	-1138.7009	-1138.6999	-1138.7747	2.41
4,4′-dinitro-azobenzene	-981.4840	-981.4679	-981.4670	-981.5324	-981.5821	-981.5662	-981.5653	-981.6281	2.67
2,2′,6,6′-tetramethyl-azobenzene	-729.6462	-729.6291	-729.6281	-729.6916	-729.6859	-729.6692	-729.6682	-729.7307	1.08
4-Methoxyazobenzene	-686.9904	-686.9770	-686.9760	-687.0325	-687.0303	-687.0168	-687.0158	-687.0728	1.08
Dihydroxyazobenzene,4-(Phenylazo)	-722.9346	-722.9213	-722.9203	-722.9772	-722.9680	-722.9538	-722.9529	-723.0118	0.91
4-Dimethylamino-2-methylazobenzene	-745.6786	-745.6618	-745.6609	-745.7250	-745.7133	-745.6964	-745.6955	-745.7621	0.94

Table 2.6: Summery of adiabatic electron affinity calculated at **B3LYP** level of theory along with 6-311++G(d,p) basis set for the **cis** isomer of all of the samples we studied. These results are obtained at 298.15 K temperature and 1 atm pressure. Electron affinity is in eV unit and all other energies are in Hartree. (a) Sum of electronic and zero-point Energies (b) Sum of electronic and thermal Energies (c) Sum of electronic and thermal Enthalpies (d) Sum of electronic and thermal Free Energies.

	Neutral				Anion				
	(a)	(b)	(c)	(d)	(a)	(b)	(c)	(d)	AEA
Azobenzene	-572.6940	-572.6832	-572.6823	-572.7320	-572.7420	-572.7311	-572.7301	-572.7804	1.31
2,2′,6,6′-tetrafluoroazobenzene	-969.7831	-969.7689	-969.7679	-969.8252	-969.8423	-969.8278	-969.8268	-969.8854	1.61
2,2′,6,6′-tetramethyl-4,4′-dinitro-azobenzene	-1139.0072	-1138.9846	-1138.9837	-1139.0601	-1139.1052	-1139.0829	-1139.0820	-1139.1578	2.67
4,4′-dinitro-azobenzene	-981.8126	-981.7966	-981.7957	-981.8595	-981.9186	-981.9027	-981.9017	-981.9651	2.88
2,2′,6,6′-tetramethyl-azobenzene	-729.8852	-729.8681	-729.8671	-729.9292	-729.9272	-729.9099	-729.9090	-729.9719	1.14
4-Methoxyazobenzene	-687.2187	-687.2053	-687.2043	-687.2602	-687.2619	-687.2482	-687.2473	-687.3042	1.17
Dihydroxyazobenzene,4-(Phenylazo)	-723.1769	-723.1635	-723.1626	-723.2174	-723.2151	-723.2010	-723.2001	-723.2571	1.04
4-Dimethylamino-2-methylazobenzene	-745.9229	-745.9061	-745.9051	-745.9680	-745.9618	-745.9451	-745.9442	-746.0075	1.06

Table 2.7: Summery of adiabatic electron affinity utilizing **wB97XD** level of theory calculations along with 6-311++G(d,p) for the **cis** isomer of all of the samples we studied. These results are obtained at 298.15 K temperature and 1 atm pressure. Electron affinity is in eV unit and all other energies are in Hartree. (a) Sum of electronic and zero-point Energies (b) Sum of electronic and thermal Energies (c) Sum of electronic and thermal Enthalpies (d) Sum of electronic and thermal Free Energies.

		Neutral				Anion				
		(a)	(b)	(c)	(d)	(a)	(b)	(c)	(d)	AEA
Azobenzene	$C_{12}H_{10}N_2$	-572.4816	-572.4710	-572.4700	-572.5194	-572.5234	-572.5127	-572.5118	-572.5615	1.137
2,2′,6,6′-tetrafluoroazobenzene	$C_{12}H_6N_2F_4$	-969.4646	-969.4507	-969.4497	-969.5064	-969.5163	-969.5022	-969.5012	-969.5589	1.41
2,2′,6,6′-tetramethyl-4,4′-dinitro-azobenzene	$C_{16}H_{16}N_4O_4$	-1138.6227	-1138.6002	-1138.5992	-1138.6763	-1138.7066	-1138.6850	-1138.6840	-1138.7582	2.281
4,4′-dinitro-azobenzene	$C_{12}H_8N_4O_4$	-981.4656	-981.4498	-981.4488	-981.5124	-981.5589	-981.5432	-981.5422	-981.6045	2.54
2,2′,6,6′-tetramethyl-azobenzene	$C_{16}H_{18}N_2$	-729.6354	-729.6186	-729.6177	-729.6789	-729.6709	-729.6542	-729.6532	-729.7147	0.97
4-Methoxyazobenzene	$C_{13}H_{12}N_2O$	-686.9696	-686.9564	-686.9555	-687.0109	-687.0073	-686.9939	-686.9930	-687.0493	1.03
Dihydroxyazobenzene,4-(Phenylazo)	$C_{12}H_{10}N_2O_2$	-722.9201	-722.9070	-722.9060	-722.9604	-722.9700	-722.9570	-722.9560	-723.0107	1.36
4-Dimethylamino-2-methylazobenzene	$C_{15}H_{17}N_3$	-745.6606	-745.6442	-745.6433	-745.7052	-745.6949	-745.6785	-745.6775	-745.7400	0.936

Table 2.8: Summery of vertical detachment energy (VDE), adiabatic electron affinity (AEA) and vertical electron affinity (VEA). B3LYP calculations along with 6-311++G(d,p) for the **trans** isomer of all of the samples. ZPE has been calculated and included in all of these results. These results are obtained at 298.15 K temperature and 1 atm pressure. Electron affinities are in eV unit and all other energies are in Hartree.

	Neutral	Anion	Anion in the equilibrium geometry of neutral	Neutral in the equilibrium geometry of anion	VEA (eV)	AEA (eV)	VDE (eV)
Azobenzene	-572.7183	-572.7673	-572.7591	-572.7109	1.11	1.33	1.53
2,2′,6,6′-tetrafluoroazobenzene	-969.7963	-969.8576	-969.8467	-969.7882	1.37	1.67	1.883
2,2′,6,6′-tetramethyl-4,4′-dinitro-azobenzene	-1139.0270	-1139.1271	-1139.1165	-1139.0167	2.43	2.73	2.99
4,4′-dinitro-azobenzene	-981.8365	-981.9448	-981.9364	-981.8277	2.72	2.95	3.17
2,2′,6,6′-tetramethyl-azobenzene	-729.9052	-729.9483	-729.9382	-729.8969	0.90	1.17	1.39
4-Methoxyazobenzene	-687.2443	-687.2879	-687.2791	-687.2367	0.95	1.19	1.39
Dihydroxyazobenzene,4-(Phenylazo)	-723.1974	-723.2357	-723.2267	-723.1899	0.80	1.04	1.24
4-Dimethylamino-2-methylazobenzene	-745.9483	-745.9852	-745.9745	-745.9369	0.71	1.00	1.31

Table 2.9: Summery of **B3LYP** calculations along with 6-311++G(d,p) for the **trans** isomer of all of the samples we studied. **Adiabatic Proton affinity (APA).** These results are obtained at 298.15 K temperature and 1 atm pressure. Proton affinities are in eV unit and all other energies are in Hartree. (a) Sum of electronic and zero-point Energies (b) Sum of electronic and thermal Energies (c) Sum of electronic and thermal Enthalpies (d) Sum of electronic and thermal Free Energies. These are the samples we studied their positive ions in our collision induced dissociation experiments.

	Neutral				Cation				
	(a)	(b)	(c)	(d)	(a)	(b)	(c)	(d)	APA
Azobenzene	-572.7183	-572.7074	-572.7064	-572.7569	-573.0704	-573.0593	-573.0584	-573.1092	**9.58**
2,2′,6,6′-tetramethyl-azobenzene	-729.9052	-729.8878	-729.8868	-729.9509	-730.267	-730.2497	-730.2488	-730.3125	**9.84**
4-Methoxyazobenzene	-687.2443	-687.2307	-687.2298	-687.2862	-687.6085	-687.5947	-687.5938	-687.6503	**9.91**
Dihydroxyazobenzene,4-(Phenylazo)	-723.1974	-723.1839	-723.1829	-723.2396	-723.5753	-723.5621	-723.5612	-723.6157	**10.28**
4-Dimethylamino-2-methylazobenzene	-745.9483	-745.9313	-745.9304	-745.995	-746.3295	-746.3125	-746.3116	-746.3757	**10.37**

Table 2.10: Summery of **Proton Affinities, wB97XD** calculations along with 6-311++G(d,p) for the **trans** isomer of some the samples we studied. These results are obtained at 298.15 K temperature and 1 atm pressure. Adiabatic proton affinity is in eV unit and all other energies are in Hartree. (a) Sum of electronic and zero-point Energies (b) Sum of electronic and thermal Energies (c) Sum of electronic and thermal Enthalpies (d) Sum of electronic and thermal Free Energies.

	Neutral				Cation				
	(a)	(b)	(c)	(d)	(a)	(b)	(c)	(d)	AEA
Azobenzene	-572.4816	-572.4710	-572.4700	-572.5194	-572.8510	-572.8409	-572.8399	-572.8876	**10.05**
2,2′,6,6′-tetramethyl-azobenzene	-729.6354	-729.6186	-729.6177	-729.6789	-730.0078	-729.9909	-729.9900	-730.0527	**10.13**
4-Methoxyazobenzene	-686.9696	-686.9564	-686.9555	-687.0109	-687.3520	-687.3384	-687.3374	-687.3938	**10.40**
Dihydroxyazobenzene,4-(Phenylazo)	-722.9201	-722.9070	-722.9060	-722.9604	-723.3120	-723.2990	-723.2980	-723.3524	**10.66**
4-Dimethylamino-2-methylazobenzene	-745.6606	-745.6442	-745.6433	-745.7052	-746.0482	-746.0315	-746.0306	-746.0934	**10.54**

Table 2.11: Summery and comparison of adiabatic electron affinity (AEA) and dipole moment for the **cis** and **trans** isomers of all of the samples. All of the calculations have been performed using **B3LYP** level of theory and 6-311++G(d,p) basis set and tight convergence criteria applied for the self-consistent field procedure as well as optimization along with ultra-fine grid for the integrals. Electron affinities are in eV unit and dipole moment in Debye.

	CIS		TRANS	
	AEA	Dipole moment	AEA	Dipole moment
Azobenzene	1.31	3.34	1.33	0.00
2,2′,6,6′-tetrafluoroazobenzene	1.61	5.45	1.67	0.29
2,2′,6,6′-tetramethyl-4,4′-dinitro-azobenzene	2.67	5.18	2.72	0.00
4,4′-dinitro-azobenzene	2.88	4.12	2.95	0.00
2,2′,6,6′-tetramethyl-azobenzene	1.14	2.22	1.17	0.09
4-Methoxyazobenzene	1.17	3.96	1.19	2.10
Dihydroxyazobenzene,4-(Phenylazo)	1.04	5.18	1.04	2.98
4-Dimethylamino-2-methylazobenzene	1.06	5.22	1.00	6.30

Table 2.12: Summary of the calculated vertical detachment energy (VDE), adiabatic electron affinity (AEA), vertical electron affinity (VEA) and the dipole moment for the trans 2,2´,6,6´-tetrafluoroazobenzene at 0 K.

Method/Basis set	VDE	AEA	VEA	Scale factor	Neutral Dipole moment	Anion Dipole moment
B3LYP/6-31+G(d)	1.75	1.61	1.25	0.98	0.27	0.30
B3LYP/6-311+G(d)	1.80	1.65	1.27	0.98	0.29	0.34
B3LYP/6-311++G(d)	1.80	1.66	1.27	0.98	0.26	0
B3LYP/6-311++G(d,p)	1.82	1.67	1.28	0.98	0.29	0.35
B3LYP/6-311++G(2d,2p)	1.77	1.63	1.24	0.98	0.27	0
B3LYP/6-311++G(3df,3pd)	1.76	1.62	1.24	0.981	0.26	0
B3LYP/LanL2DZ	1.88	1.73	1.38	0.98	0.33	0.49
B3LYP/aug-cc-pVDZ	1.79	1.65	1.29	0.98	0.24	0
M06/6-311++G(d,p)	1.84	1.66	1.27	0.971	0.25	0.38
M06L/6-311++G(d,p)	1.68	1.56	1.24	0.972	0.34	0.45
M062X/6-311++G(d,p)	1.80	1.57	1.10	0.98	0.20	0
wB97/6-311++G(d,p)	1.81	1.50	0.91	0.978	0.20	0
wB97X/6-311++G(d,p)	1.78	1.50	0.95	0.967	0.22	0
wB97XD/6-311++G(d,p)	1.74	1.50	1.00	0.971	0.26	0
B3PW91/6-311++G(d,p)	1.80	1.66	1.28	0.971	0.30	0.34
B3P86/6-311++G(d,p)	2.36	2.21	1.85	0.975	0.29	0.29
MP2/6-311++G(d,p)	1.63	0.96	0.69		0.27	0
CBS-QB3		1.41			0.20	0
Experimental	1.78	1.3±0.1	-		-	-

Beside the CBS method, we tried to do Gn (G1-G4) Gaussian methods for calculating accurate electron affinities. This methods are slow and for large molecules such as precursor we were dealing with not simply practical. Here we presents some of the results for G3[23] method and

compare it with density functional results. G3 is a complex energy calculation method which utilizes a series of ab initio calculations and properly scale the results from each step to conclude the final results for energies.[75] Below is a summary of levels of calculations in G3 algorithms and what is being calculated at each step:

1) Geometry optimization at HF/6-31G(d); RHF for the singlet states and UHF for other.
2) Scaled ZPE is calculated at HF/6-31G(d) and geometry optimization at MP2(Full) /6-31G(d). This will be the geometry which will be used for further calculations (single point).
3) A series of single point (SP) energy calculations at MP4/6-31G(d) level of theory. Corrections (for QCISD; diffuse function; higher polarization function; basis set effects) will be calculated according to:
   a) Correction EQCI for correlation beyond MP4 perturbation theory:

$$E_{QCI} = E_{QCISD(T)/d} - E_{MP4/d} \quad (2.47)$$

   b) Correction for diffuse functions (E_{plus} for the 6-31+G(d) diffuse function):

$$E_{plus} = E_{MP4/plus} - E_{MP4/d} \quad (2.48)$$

   c) Correction for higher polarization function $E_{2df,p}$:

$$E_{2df,p} = E_{MP4\,/\,2df,p} - E_{MP4/d} \quad (2.49)$$

   d) Correction for large basis set size effects

$$E_{G3Large} = E_{MP2(Full)\,/\,G3Large} - E_{MP2\,/\,2df,p} - E_{MP2\,/\,plus} + E_{MP2\,/\,d} \quad (2.50)$$

G3 include some core polarization functions as well as multiple sets of valance polarization functions.

4) For atomic species, the experimental or high accuracy calculation resulted spin-orbit correction term would be included.
5) To correct for remaining deficiencies in energy calculations, a correction term (E_{HLC}) will be calculated and added.

6) By adding all the energies and correction terms calculated above, the final value for the energy at 0 k is obtained.

$$E^{0}{}_{G3} = E_{MP4\,/\,d} + E_{QCI} + E_{plus} + E_{2df,p} + E_{G3Large} + E_{SO} + E_{HLC} + E_{ZPE} \qquad (2.51)$$

CBS (Complete Basis Set) method algorithm involves following calculations:

- Geomterty optimization at B3LYP level of theory along with 6-311++G(2d,d,p) basis set
- #P Geom=AllCheck Guess=TCheck SCRF=Check B3LYP/CBSB7 Freq
- #P Geom=AllCheck Guess=TCheck SCRF=Check CCSD(T)/6-31+G(d')
- #P Geom=AllCheck Guess=TCheck SCRF=Check MP4SDQ/CBSB4
- #P Geom=AllCheck Guess=TCheck SCRF=Check MP2/CBSB3 CBSExtrap=(NMin=10, MinPop)

When all above terms are ready, the final CBS energy is calculated according to:

$$E_{CBS-QB3} = \Delta E_{CCSD(T)} + \Delta E_{MP4} + E_{MP2} + \Delta E_{ZPE} + \Delta E_{CBS} + \Delta E_{emp} + \Delta E_{int}$$

Table 2.13: Summary of high accuracy energy calculations results for **azobenzene**. Here we compared results from DFT methods with the highly accurate multilevel energy calculation methods such as **G3** and **CBS-QB3**. Adiabatic electron affinities (AEA) are in eV unit and for 0 K and all other energies are in Hartree. (a) Sum of electronic and zero-point Energies (b) Sum of electronic and thermal Energies (c) Sum of electronic and thermal Enthalpies (d) Sum of electronic and thermal Free Energies.

Method / Basis set	NEUT				ANION				AEA
	(a)	(b)	(c)	(d)	(a)	(b)	(c)	(d)	
B3LYP/6-311++G(2d,2p)	-572.7385	-572.7276	-572.7267	-572.7772	-572.7868	-572.7759	-572.7749	-572.8255	1.31
B3LYP/aug-cc-pVTZ	-572.7749	-572.7641	-572.7631	-572.8135	-572.8230	-572.8121	-572.8112	-572.8615	1.31
wB97XD/6-311++G(2d,2p)	-572.5207	-572.5099	-572.5089	-572.5589	-572.5650	-572.5541	-572.5532	-572.6035	1.20
wB97XD/aug-cc-pVTZ	-572.5547	-572.5439	-572.5429	-572.5934	-572.5982	-572.5874	-572.5864	-572.6366	1.18
G3	-572.3349	-572.3237	-572.3227	-572.3731	-572.3751	-572.3636	-572.3626	-572.4133	1.09
CBS-QB3	-571.7263	-571.7153	-571.7144	-571.7641	-571.7671	-571.7561	-571.7551	-571.8050	1.11

Table 2.14: Summary of high accuracy energy calculations results for trans **2,2́,6,6́-tetrafluoroazobenzene**. Here we compared results from highly accurate multilevel energy calculation methods such as **G3, G3MP2**, **G4** and **CBS-QB3**. Adiabatic electron affinities (AEA) are in eV unit and for 0 K and all other energies are in Hartree. (a) Gn(0 K) (b) Gn Energy (c) Gn Enthalpy (d) Gn Free Energy.

Method / Basis set	NEUT				ANION				
	(a)	(b)	(c)	(d)	(a)	(b)	(c)	(d)	AEA
G3	-969.1360	-969.1213	-969.1204	-969.1789	-969.1837	-969.1684	-969.1674	-969.2281	**1.30**
G3MP2	-968.4300	-968.4153	-968.4144	-968.4730	-968.4740	-968.4586	-968.4577	-968.5183	**1.19**
G4	-969.3128	-969.2983	-969.2974	-969.3559	-969.3699	-969.3551	-969.3541	-969.4142	**1.55**
CBS-QB3	-968.3711	-968.3567	-968.3557	-968.4140	-968.4233	-968.4084	-968.4075	-968.4687	**1.42**

2.9 Computational Thermochemistry

Computational quantum chemistry methods are able to accurately determine the binding energies and many other thermochemical and physical properties of molecules. There has been considerable progress in the development of reliable quantum chemical methods for prediction of thermochemical data.[80] This is important since some of these properties are extremely tedious to measure experimentally. Not only bond length and angles, bond dissociation energies and equilibrium geometry but also free energy, enthalpy and entropy are possible to calculate. If we do the calculation carefully and successfully the errors could be in the order of magnitudes of the experimental error. The main thermodynamic property we can measure by performing the energy resolved collision induced dissociation is bond dissociation energy. Ab initio calculations are powerful techniques which use first principles techniques to compute properties such as bond dissociation energies. In this thesis we compare theoretical and experimental approaches and compare the results for BDEs. Bond dissociation energies provide a measure of both reactivity of a compound and the stability of the corresponding compound[75]. Theoretically it is necessary to compute the enthalpy of formation at 0 K and 298 K ($\Delta H^o_{f,0}\ and\ \Delta H^o_{f,298}$). Extensive treatment of electron correlation is required to compute reasonable BDEs.[53] The bond dissociation energy is obtained from calculations using the following relation[24] (Cramer, 2004):

$$\Delta H^o_{f,298}(M) = E(M) + ZPE(M) + [H_{298}(M) - H_0(M)] - \sum_{z}^{atoms} \{E(X_z) + [H_{298}(X_z) - H_0(X_z)]\} + \sum_{z}^{atoms} \Delta H^o_{298}(X_z) \quad (2.52)$$

By default Gaussian performs the calculations at 298.15 K and 1 atm of pressure. The vibrational internal energy is calculated according to:

$$U_{vib} = R \sum_{i=1}^{3N-6} \frac{h\upsilon_i}{k_B\left(exp\left(\frac{h\upsilon_i}{k_B T}\right) - 1\right)} \quad (2.53)$$

And the entropy from:

$$S_{vib} = R \left\{ \sum_{i=1}^{3N-6} \frac{h\nu_i}{k_B \left(exp\left(\frac{h\nu_i}{k_B T}\right) - 1 \right)} - \ln\left(1 - exp\left(\frac{h\nu_i}{k_B T}\right) \right) \right\} \quad (2.54)$$

The concept of entropy is fundamentally important for us in collision induced dissociation theory. An important part of data analysis requires us to know the nature of the transition state of the active complex and to know if the transition is loose or tight. A simple bond cleavage usually does not have a large activation barrier and this type of transition would be categorized as loose. If the entropy of the activated complex ($\Delta S^{\ddagger}$) is positive that is an indication that the transition is loose. That is valid for the cases which do not include rearrangement in molecular configuration. The contribution to the internal thermal energy from the rotational motion is equal to $\frac{3}{2}\ RT$. To calculate enthalpies of reaction we need to calculate heats of formation according to the following relation:

$$\Delta_r H^0\ (298\ K) = \sum_{products} \Delta_f H^0_{prod}(298\ K)\ - \sum_{react} \Delta_f H^0_{react}\ (298\ K) \quad (2.55)$$

The other important quantity for us is the atomization energy of the molecule. To calculate the atomization energy we need to know the ZPVE and using the following relation we can obtain the atomization energy[81]:

$$\sum D_0(M) = \sum_{atoms} x\varepsilon_0(X) - \ \varepsilon_0(M) - \ \varepsilon_{ZPE}(M) \quad (2.56)$$

In this relation x is the number of atoms, X, in molecule M. To calculate the heat of formation at 0 K (ΔH_f^0) from the total electronic energy there are several common methods[75] available. In the atomization method, the heat of formation of a radical is obtained by combining the calculated energy of the atomization reaction with the known heats of formation of the gaseous atoms (usually provided for us as standard tables). The other approach to this would be the formation method in which the heat of formation of the radical is obtained from the calculated energy of the formation reaction. To have a reliable BDE estimation we need high level calculations such as W1[20, 21] or

CBS[17, 19, 82-85] method. This method can provide highly accurate results for energy and electron affinities since the major error source in ab initio calculations is the truncation of the one-electron basis set which this method can be used to minimize. An open-shell complete basis set (CBS) model chemistry, based on the unrestricted Hartree-Fock (UHF) zero-order wave function, is defined to include corrections for basis set truncation errors. The total correlation energy for the first-row atoms is calculated using the unrestricted Moller-Plesset perturbation theory, the quadratic configuration interaction (QCI) method, and the CBS extrapolation. The agreement with experiment is in the order of 0.75 kcal/mol.[17]

What we measure as a result of collision induced dissociation is a bond dissociation energy (BDE) which is computed usually by considering the standard thermodynamic state in gas phase (0 K, pressure, 1 atm and main isotope). To make sure our experiments has been done accurately and the results are reliable it is necessary to perform high accuracy calculations to obtain a good estimation of the BDEs. As we discussed before the complex energy calculation methods such as Gn or CBS (complete basis set) family can be used to compute the heats of formation and from there we can determine the BDEs. The CBS method perform a geometry optimization at the UB3LYP level, ZPVE calculation at UB3LYP and energy calculations at UCCSD(T) level of theory. The mean absolute deviation of the thermochemical data from CBS method is in the order of 3.2 kJ/mol. The other experimentally available methods employed to measure the BDEs include Photoacoustic calorimetry, Acidity−oxidation potential method, estimation from kinetic measurements, Calorimetric method and Chemical Equilibrium (CE)[86]. The performance of the MP2 model is almost as good as B3LYP for calculating BDEs except for the fact that it is more time consuming than DFT methods. So from the practical point of view it is more feasible to just use DFT methods for large molecules such as those in this thesis. We often use the DFT or MP2 methods since HF which is faster but neglects the electron correlation which cause systematic error. Methods such as QCISD(T) on the other hand extensively include the electron correlation in computations. To have a reliable thermochemical property computation we defiantly need a highly accurate structure. In all of our calculation we tried to ensure this by using a tight convergence criteria or all of the optimization as well as using tight convergence for SCF procedure and using the ultrafine grid for calculating the integrals. Doing so increases the calculation time but more reliable results will be obtained.

The Gibbs free energy is related to the reaction constant k through:

$$\Delta G = -RTln\,(k) = \Delta H - T\,\Delta S \tag{2.57}$$

The rate constant which first was described by Arrhenius is simply a relation between the reaction temperature and rate:

$$k = A\exp\left(\frac{-(E_{transition\,state} - E_{reactants})}{RT}\right) = A\,e^{-E^{\ddagger}/RT} \tag{2.58}$$

We can rewrite this using the concept of Gibbs free energy, enthalpy and the entropy of the activated complex as:

$$k = \frac{kT}{h}\exp\left(-\frac{\Delta G^{\ddagger}}{RT}\right) = \frac{kT}{h}\exp\left(-\frac{\Delta H^{\ddagger}}{RT}\right)\exp\left(-\frac{\Delta S^{\ddagger}}{R}\right) \tag{2.59}$$

And the quantity $(E_{transition\,state} - E_{reactants})$ is often refred to as the activation energy (E_{act}). The activation energies of endothermic reactions (which includes all of CID reactions) can be calculated using:

$$E = \Delta H + 0.5\,RT \tag{2.60}$$

In general there is no experimental method to measure the activation barrier or to accurately predict the activation barrier energy (not a straightforward procedure). The same is true for the transition state. There might several points exist along the Born-Oppenheimer potential energy surface with exact properties of a transition state point but not THE transition state. Different level of theories yield very different results for an activation barrier. But as a rule of thumb we can say UB3LYP and CBS-QB3 methods give acceptable results at same margin.

Table 2.15: Calculated Bond Dissociation Energies (BDE) at 0 K for cleaving the C-N bond of the precursor ion yielding the $[C_6H_3F_2]^-$ anion and $C_6H_3F_2\,N_2$ neutral fragment in collision induced dissociation experiment of 2,2́,6,6́-tetrafluoroazobenzene.

Method/Basis set	Bond Dissociation Energy (eV)
B3LYP/6-31+G(d)	1.84
B3LYP/6-311+G(d)	1.79
B3LYP/6-311++G(d)	1.79
B3LYP/6-311++G(d,p)	1.79
B3LYP/6-311++G(2d,2p)	1.80
B3LYP/6-311++G(3df,3pd)	1.83
B3LYP/aug-cc-pVDZ	1.86
B3LYP/Lanl2DZ	2.14
M06/6-311++G(d,p)	2.08
M06-L/6-311++G(d,p)	2.10
M06-2X/6-311++G(d,p)	2.01
B3P86/6-311++G(d,p)	1.97
B3PW91/6-311++G(d,p)	1.88
wB97/6-311++G(d,p)	1.91
wB97X/6-311++G(d,p)	1.90
wB97XD/6-311++G(d,p)	1.95
CBS-QB3	1.90

Chapter 3 / Collision Induced Dissociation

3.1 Introduction to Collision Induced Dissociation

Collision induced dissociation (CID) experiments, computational quantum chemistry and the data analysis related to those, constitutes most of the experimental and theoretical sections of this dissertation. In this chapter we try to briefly introduce concepts and theories behind the important parts of CID experiments and data analysis and present some of our experimental data as well as a few examples of the analysis and the measurements we have performed. Highly accurate quantitative thermodynamic knowledge can be obtained through CID type experiments for molecular ions from small size to large clusters. Collisional dissociation and ionization are the most fundamental concept in mass spectrometry, therefore it is necessary to elaborate on theoretical and experimental aspects of this method.[87-89] Collision-induced dissociation also known as collisionally activated dissociation (CAD), is a tandem mass spectrometry technique used to induce fragmentation of molecular ions in the gas phase.[90, 91] There are several methods to determine the bond energies in chemistry which include threshold collision-induced dissociation (TCID), blackbody infrared radiative dissociation (BIRD) i.e. special case of infrared multiphoton dissociation wherein excitation of the reactant ion is caused by absorption of infrared photons radiating from heated blackbody surroundings, which are usually the walls of a vacuum chamber[92], surface-induced dissociation (SID) and kinetic methods.[93] Guided ion beam tandem mass spectrometry has proved to be a robust tool for the measurement of thermodynamic information as well.[87] CID by definition[92] involves the dissociation of an ion following collisional excitation. The collisional excitation results from the interaction of an ion with another gas-phase species in which part of the relative translational energy of the collision partners is converted into internal

energy. Two fundamental types of reactions can be used to acquire thermodynamic information: Bimolecular exchange reactions, process 1, and collision-induced dissociation (CID), process 2:

$$M^+ + AB \rightarrow MA^+ + B \quad (3.1)$$

$$MA^+ + Rg \rightarrow M^+ + A + Rg \quad (3.2)$$

in reaction (1), it can be exothermic or endothermic but reaction (2) is intrinsically endothermic since an stable bond is broken. To understand the quantum treatment of collision theory we essentially need to solve the time dependent Schrodinger equation [94]:

$$\hat{H}\,\Psi\,(\boldsymbol{R},t) = i\hbar\,\frac{\partial\Psi(\boldsymbol{R},t)}{\partial t} = \left(\sum_j \frac{\hbar^2}{2m_j}\,\nabla_j + V\big(\boldsymbol{R}(t)\big)\right)\Psi(\boldsymbol{R},t) \quad (3.3)$$

where, $\hat{H}$ is the Hamiltonian that corresponds to the sum of kinetic and potential energies, j designates every particle regardless of whether an electron or atomic nucleus, m_j is the mass of the respective particle, and the vector **R** is a variable that includes all positions. In other word this a type of unimolecular reaction in which the activation happens through collisions and some of the ions kinetic energy (E_{CM}) will be converted into internal energy and if this energy is high enough to overcome the barrier, then it can break a chemical bond.

We also need to consider the activation barrier in tight transition reactions. For a loose transition this can be very small and negligible but in tight transition cases we need more energy for the reaction than just the bond breaking energy requirements. To accurately determine the threshold energy of the collision induced dissociation it is extremely critical to know the all the energy available for the reaction and not only the kinetic part. All of the other partitions of energy including electronic, vibrational and rotational can contribute to the reaction and the bond dissociation energy inferred from CID experiments and need to be carefully included. Analysis of the data obtained from performing CID experiments without performing quantum chemistry computations is not practically possible and will lead to inaccurate conclusions. As a simple example of the quantitative values which are required to know before further analysis of cross sections of a CID experiments, the frequencies of vibrational modes of the transition state of the reaction are required. Also an accurate knowledge of energies of reactants and products of the

dissociation reaction is needed. The first step is to have an educated guess of the electron affinity or proton affinity of the sample molecule to see if it is possible to perform a CID (since ionization of the sample molecule is the first step in any CID experiment) experiment for the molecule of interest or which method of ionization we need to choose. These all required accurate theoretical calculations which were performed extensively in this thesis. We used high accuracy multilevel methods such as CBS-QB3 for all of the samples of interest and to obtain their electron or proton affinity and so we can select appropriate negative or positive mode for the CID experiments performed herein. Methods for determining absolute values of thermochemical quantities are rarely applicable, so relative values are typically measured by kinetic and equilibrium measurements on gas-phase ions.[95]

3.2 Mass Spectrometry: Experimental and Theoretical Aspects

3.2.1 Instrumentation:

An ABSciex QSTAR Elite Hybrid LC/MS/MS System was employed for all our mass spectroscopy purposes. This is not optimized for energy resolved collision induced dissociation measurements such as guided ion beam tandem mass spectrometers (GIBMS). Figure 3.1 shows the schematic of QSTAR. Here we briefly explain different parts and sections of this instrument. 1) multiple ion source including electro spray ionization (ESI) and atmospheric pressure chemical ionization sources. 2) turbo pumps. 3) LINAC collision cell which is almost 21 cm long. 4) ion mirrors and shields. 5) Razor ion detector. 6) Ion cooler guide which allows the collisional cooling of large, non-covalently bound complexes. Another schematic is provided in Figure 3.2, which contains more details for the interested reader. As the neutral collision gas we always used argon since it has no internal energy and also has high ionization potential.

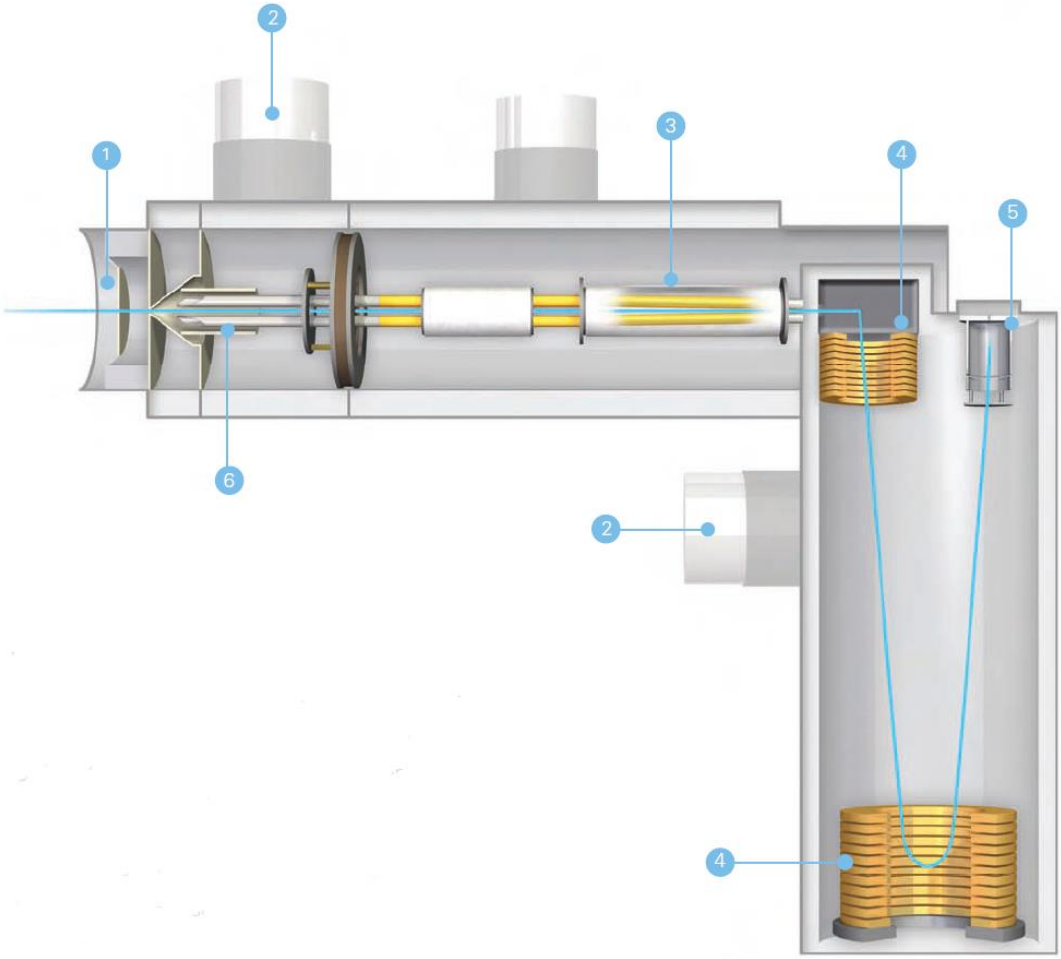

Figure 3.1: Schematic of ABSciex QSTAR Elite Hybrid LC/MS/MS. 1) ion source 2) turbo pump 3) collision cell 4) ion mirrors and shield 5) ion detector 6) optional Ion Cooler. Reprinted by written permission from ABSciex.

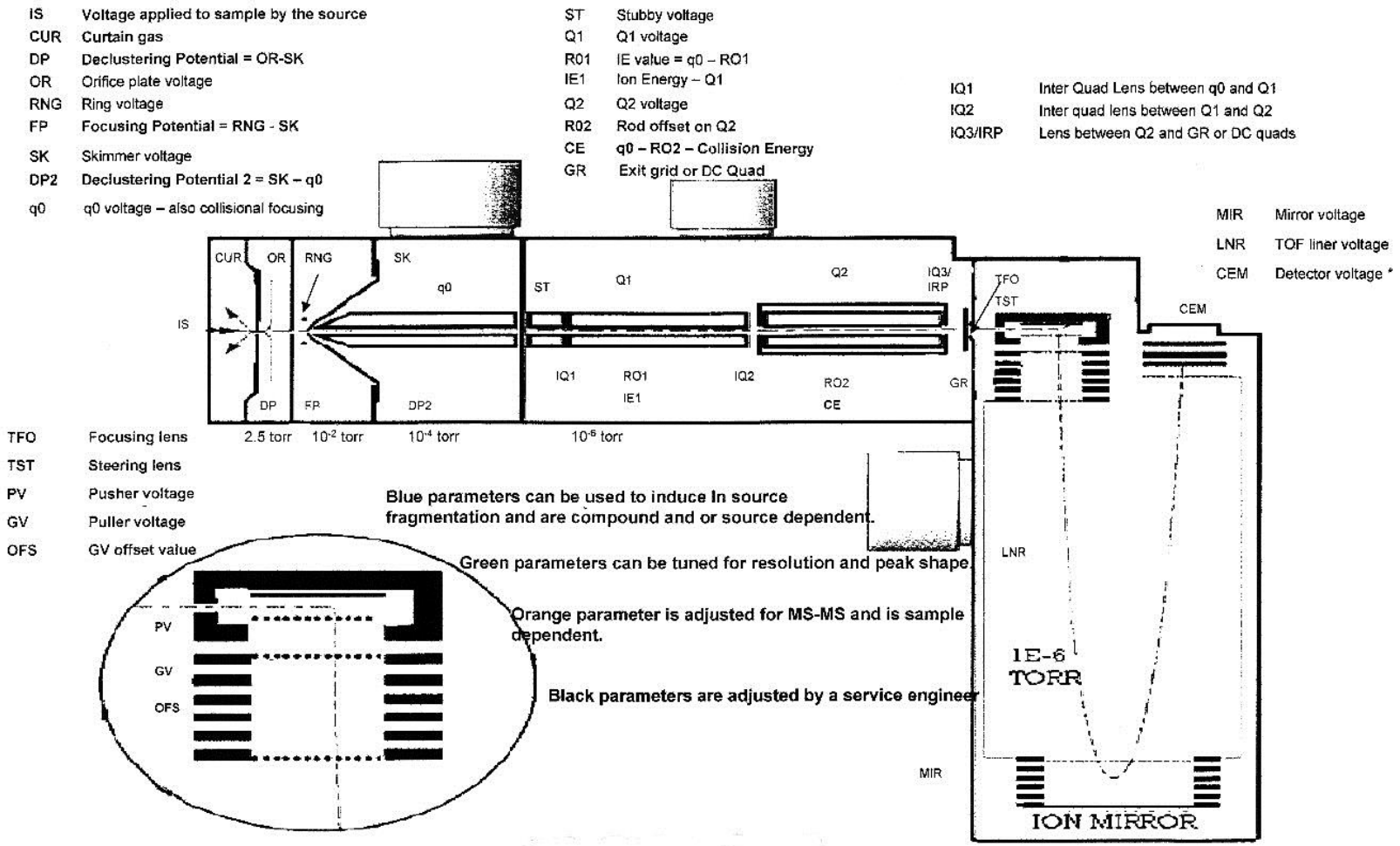

Figure 3.2: Detailed schematic of the mass spectrometer which is used to obtain mass spectrometry data.

3.2.2 Ion source:

We started our experiments using a more conventional ions source, Electrospray ionization (ESI), but this method was not successful in making anions for azobenzene and its derivatives which were the main ions of interest. Consequently, after a series of unsuccessful trials and errors a more direct “hard” ionization method was used, the so called atmospheric pressure chemical ionization method (APCI). In Atmospheric pressure chemical ionization (APCI) gas-phase ion-molecule reactions at atmospheric pressure is utilized to ionize parent neutral molecule via direct electron attachment followed by collisional relaxation. Negative ions are generated under atmospheric pressure conditions at high temperature, 573 K, using a corona discharge. ESI utilizes an electrospray in which a high voltage is applied to a liquid to create a charged aerosol. In the APCI technique on the other hand the combination of the heat and gas flow desolvates the nebulized droplets, producing dry vapor of solvent and analyte molecules. The solvent molecules are then ionized by a corona discharge. ESI is usually defined as a soft ionization technique which has the capability of controllable fragmentation and ionization of large molecules and produces intact and possibly multiple-charged non-covalent complexes, however ESI generally produces protonated or deprotonated ions. APCI is suitable for conditions which ESI does not work and the compounds which are not highly polar and thermally stable. Solvent molecules initially ionize and methanol is a good candidate.

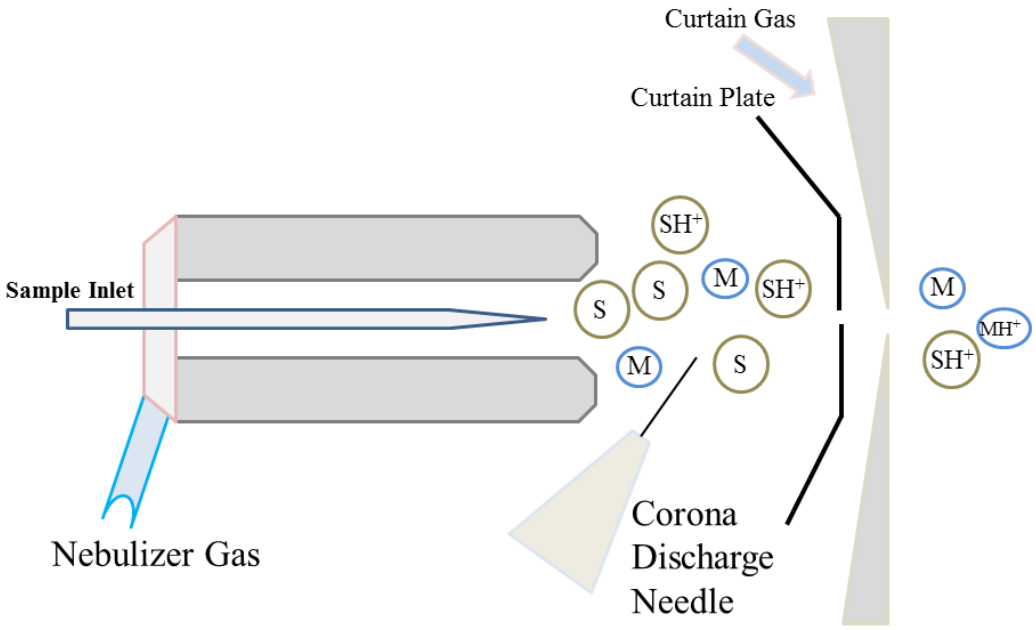

Figure 3.3: Schematic of Ion source which we used, APCI mechanism. Around the corona needle ionization mostly produced solvent ions but after that reagent ions react with the sample to form charged clusters. S represents the solvent and M is the sample molecule. SH^+ is the ionized solvent reagent.

In the positive ion mode which we have used for four of our samples to perform the collision induced dissociation experiment, the ionization procedure is predominantly proton transfer. In negative mode, ions can form by either proton removal or electron transfer.

One of the important aspects of threshold CID experiments is to have an a priori idea of the released ions kinetic energy distribution. The high temperature of APCI source makes this determination problematic. In addition, the zero of the ion energy scale is a crucial point which should be obtained doing accurate measurements. The potential difference that accelerates the ions into the collision cell area is not always easily determined. The potential difference experienced by the ions inside the ion optics is modulated by local potential disturbances. These include contact potentials and the buildup of surface charges which can increase significantly during experiments, necessitating regular determinations of the actual potential and the distribution of the kinetic energy during

intervals between experiments.[96] For example some calculations done using CRUNCH program[54, 87-89, 97-102], which represents a state of the art method for the deconvolution and data analysis in TCID experiments, and also experimental measurements performed previously obtained a value of ~ 0.4 V (Lab frame). That means when the Lab energy is shown by the Analyst software which controls the instruments shows 0 V potential difference which is the kinetic energy of ions, there is actually ~0.4 eV energy available (in Lab frame) for ions to enter the collision cell. This can be the result of contact potentials, field effects, space charge effects, and surface charging. Also a full width at half maximum for the kinetic energy distribution of ions had been measured to be ~ 0.5 eV (Lab frame). If the energy scale for reaction is to be known accurately, then it is clearly important that the zero of this scale be ascertained.[87]

3.3 Introduction to Unimolecular Ion Dissociation

A unimolecular reaction represents the simplest possible reaction in gas phase ion chemistry. Collision induced dissociation intrinsically is a unimolecular reaction which we are interested in studying product ions. The mass of the product ion is known accurately but we do not know the structure of the ion. Activation takes place by colliding the parent ion with a usually neutral Nobel gas like Argon or Xenon and in some cases a nitrogen molecule. Photo-dissociation would be another possibility but unavailable in these experiments. By IUPAC definition[92], unimolecular dissociation is a fragmentation reaction in which the molecularity of the reaction system is unity. The dissociation may arise from the extra energy acquired by a metastable ion produced in the ion source or that provided by collisional excitation of a stable ion.

Unimolecular reaction rates can be described by a statistical theory such as the Rice–Ramsperger–Kassel–Marcus (RRKM) theory.

Kinetic Energy Release (KER) is an important concept which needs to be discussed. KER is the total kinetic energy of the two particles in the center of mass system when a parent ion with mass

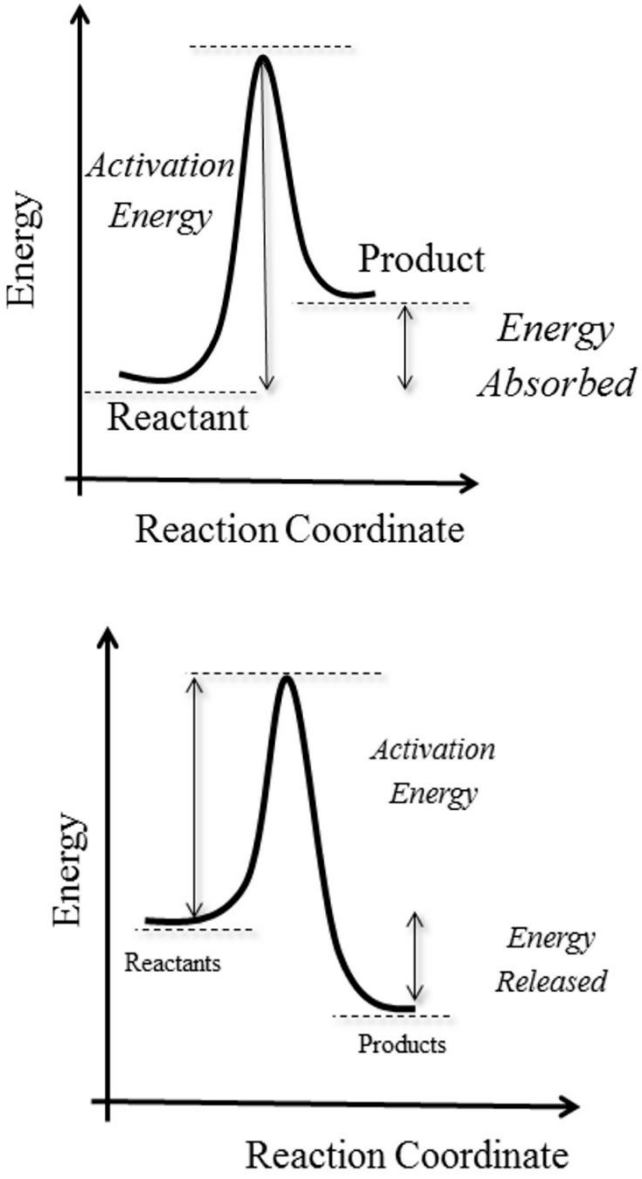

Figure 3.4: Energy diagram for unimolecular reactions and change in energy as the reaction proceeds. The activation energy which is the difference in energy between the reactant and the transition state is illustrated. The activated complex or ion/neutral complex transition states lies between the reactant ions and products on the reaction coordinate.

M dissociates into fragments of masses m and M-m. In other word the translational energy of fragments resulting from dissociation of a metastable ion measured relative to the center of mass.[92] The collision-driven dissociation in mass spectrometry can be regarded as an extremely fast excitation process combined with spontaneous dissociation.[94] As we know in the center of mass the two particles will have the same momentum but in opposite directions so the net momentum in center of mass is zero:

$$E_{CM} = \frac{1}{2}\, m_A\, V_A^2 + \frac{1}{2}\, m_B\, V_B^2 = \frac{m_A}{2}\left(\frac{\mu}{m_A}\, v_r\right)^2 + \frac{m_B}{2}\left(\frac{\mu}{m_B}\, v_r\right)^2 = \frac{1}{2}\, \mu\, v_r^2 \qquad (3.4)$$

The only energy available for the reactions such as dissociation or ionization is this center of mass energy. v_r is the relative velocity between the two fragments. The relative velocity in the center of mass based on the KER then would be:

$$v_r' = \sqrt{\frac{2\, KER}{\mu}} = \sqrt{\frac{2M\, KER}{m(M-m)}} \qquad (3.5)$$

In this relation m_A and m_B correspond to m and M-m. The energy in the laboratory system is related to KER according to the following relation:

$$\Delta E_{lab} = 2\left(\frac{4m(M-m)\, KER\, E_{lab}}{M^2}\right)^2 \qquad (3.6)$$

By defining the mass width d which is related to the Lab-system energy range ΔE_{lab}:

$$d = \frac{\Delta E_{lab}}{E_{lab}}\, M \qquad (3.7)$$

We can calculate the KER by considering the mass width d_0 of ion peaks of the incident particles as:

$$KER = \frac{E_{Inc}}{16m(M-m)}\left(d^2 - \left(\frac{m}{M}\, d_0\right)^2\right) \qquad (3.8)$$

In which E_{Inc} is the incident particle energy (precursor ion). Therefore the KER distribution $P\,(E, \epsilon_t)$ in collision induced dissociation would be:[94]

$$P\ (E, \epsilon_t) = \frac{G(E - E_0 - \epsilon_t)}{G(E - E_0)} = (s-1)\ \frac{(E - E_0 - \epsilon_t)^{s-2}}{(E - E_0)^{s-1}} \tag{3.9}$$

in this relation $\epsilon_t = KER$ is the kinetic energy released via dissociation and $P\ (E, \epsilon_t)$ is the monotonically decreasing function having its maximum at $\epsilon_t = 0$. The averaged KER can be obtained from the relation:

$$KER_{ave} = \int_0^{E-E_0} \epsilon_t\, P\ (E, \epsilon_t)\ d\epsilon_t = \frac{(E - E_0)}{s} \tag{3.10}$$

in which s is the number of harmonic oscillators.

3.4 Energy-Resolved Collision Induced Dissociation:

The kinetic energy dependence of a reaction especially the unimolecular reactions which describe the dissociation reaction is of interest and there is no simple method to describe the kinetic energy dependence. Armentrout[87, 103] introduced an empirical formula for this purpose:

$$\sigma_p(E_{cm}) = \sigma_0 \sum_i \frac{g_i(E_{CM} + E_i + E_0)^n}{(E_{CM})^m} \tag{3.11}$$

here $\sigma_p(E_{CM})$ is the collision cross section as a function of parent ion kinetic energy, σ_0 is the scaling factor, E_{CM} is the energy of the precursor ion in the center-of-mass frame of reference E_0 is the threshold (bond dissociation) energy which we are trying to infer and it represents the 0 K threshold for the reaction of ground electronic, vibrational, and rotational state reactants, g_i is the population of state *i* with, internal energy of a given vibrational state and n and m are adjustable parameters which we can find by fitting the experimental data points. Historically, the closest relation to describe the kinetic energy dependence of chemical reactions is the Arrhenius equation, $k(T) = A\ exp(-E_a/k_B\,T)$. In this equation A is the pre-exponential factor, k_B is the Boltzmann constant and Ea is the activation energy which is the energy barrier on the potential energy surface between the reactants and products. Arementrout[87] suggests m=1 in the above relation provides an

adequate treatment of the kinetic energy dependence of ion molecule reactions. Converting the line intensities to cross sections has been performed using the following relationship:

$$I_R = \left(I_R + \Sigma I_p\right) e^{-\sigma_{tot} nl} \tag{3.12}$$

where I_R is the parent ion intensity, I_P is the intensity of each product ion, σ_{tot} is the total cross section, l is the effective collision cell length and n is the density of particles in the collision cell which is related to the pressure and temperature of the neutrals, argon atoms, in the collision cell as $n = \frac{P}{k_B T}$. This is similar to the Beer-Lambert law. P and T in this equation are the collision gas pressure and temperature and k_B is the Boltzmann constant. This is valid only if there is no ion lost in the collision cell or in the path from the collision cell to the detector.

$$I_0 = I + \sum I_p \tag{3.13}$$

In general if the density of the particles in the collision cell is represented by ρ and the thickness of the target is x then for the intensity of the incident and transmitted particles we can write:

$$\frac{dI(x)}{I(x)} = -\sigma \rho dx \tag{3.14}$$

And if the length of the target is L then:

$$\exp(-\sigma L \rho) = \frac{I_{transmited}}{I_{incident}} \tag{3.15}$$

There are several uncertainties in this regards. For example the collision cell pressure is not exactly constant during the entire data acquisition time and also this pressure is not uniform since there is an entrance and an exit to the cell which is connected to the turbo pumps and causes a pressure profile along the collision cell length. The thin target approximation is valid if $nl\sigma_{tot} \ll 1$ then the above equation will be simplified to:

$$\sigma_{tot} = \frac{\sum I_P}{nl\ (I_R + \sum I_P)} \tag{3.16}$$

We used the original form for the sake of accuracy. After obtaining the total cross section we can convert it to cross section for each one of the product ions using the following relation:

$$\sigma_P = \sigma_{tot}\left(\frac{I_P}{\sum I_P}\right) = \frac{1}{n\,l}\,ln\left(\frac{I_0}{I}\right) = -\frac{1}{n\,l}\,ln\left(1-\frac{I_P}{I_0}\right) \quad (3.17)$$

The center-of-mass energy (energy available for a reaction) is obtained from:

$$E_{CM} = E_{lab}\frac{m_{Ar}}{(m_{Ar}+m_p)} \quad (3.18)$$

where m_{Ar} and m_p are the masses of an argon atom and the parent negative ion, respectively.[55, 87] E_{CM} is the amount of kinetic energy which is available for the chemical reaction to happen. This relation is the direct consequence of conservation of linear momentum. The entire translational energy in laboratory frame is not available for the chemical reaction (dissociation in our experiments) to take place, some of it should be available in the system for products to move and keep the linear momentum constants (conservation of linear momentum).

Another important issue which must be taking into account in any collision induced dissociation experiment and data analysis is the single collision condition. The available codes for deconvolution of data purposes such as the CRUNCH program all work based on this fundamental assumption that each dissociation reaction happens after a single collision between the parent ion and the neutral target gas. If more than one collision happens, then each collision adds some energy to the parent ion and this may lower the final dissociation energy. Since in multiple collision situations we don't know exactly how many collisions happened and how much energy each one added to the system there could be a large uncertainty in the resulting threshold energy. When multiple collisions occur, each collision leads to increased variability in the distribution of reactant velocities.[89] To investigate this for our system here we discuss the conditions required for single collision based on Armentrout's[89] explanation and formalism. Collison density which is defined as the number of collisions between molecules 1 and 2 is:

$$N_{12} = \rho_1\rho_2\,\sigma v_{12}\,V \quad (3.19)$$

where V is the collision volume and v_{12} is the mean relative speed of molecules 1 and 2, $\rho_m = P/k_B\,T = N_A P/RT$ number density and k_B is the Boltzmann constant. σ is the cross section with

unit of area. The ion beam with intensity of I, the number of ions observed per unit time, and undergoes collision with gas at pressure P and temperature T:

$$I_0 = I\ exp(-\rho\sigma l) = I\ exp\left(\frac{-P\sigma l}{RT}\right) \tag{3.20}$$

The cross section is in units of 10^{-16} cm^2 = $Å^2$. Then the intensity of ions which had a single collision would be:

$$I_1 = I\ \left[1 - exp\left(\frac{-P\sigma l}{RT}\right)\right] \tag{3.21}$$

The simple form of the above relation which is a thin target assumption would be:

$$I_1 = I\ \left(\frac{-P\sigma l}{RT}\right) \tag{3.22}$$

$$I\ =\ I_0\ +\ I_1 \tag{3.23}$$

The ion intensity can be converted into a cross section following this relation:

$$\sigma = \left(\frac{RT}{Pl}\right) ln\left(\frac{I_0}{I}\right) = \left(\frac{RT}{Pl}\right)\ ln\left[1 - \frac{I_1}{I}\right] \tag{3.24}$$

Multiple collisions shift the dissociation energies to lower energies in compare to single collision dissociation. For an ion undergoing x number of collisions the cross section to intensity relation would be:

$$I_x\ =\ \left[1 - exp\left(\frac{-P\sigma l}{RT}\right)\right]^x \tag{3.25}$$

3.5 RRKM/Quasi Equilibrium Theory:

Collision induced dissociation reactions can be statistically described and the unimolecular reaction of a molecule can be explained using the Rice–Ramsperger–Kassel–Marcus (RRKM) theory. In RRKM theory a molecule is considered as a set of harmonic oscillators which can interact with each other by exchanging energy freely.[94] Comparing to Rice–Ramsperger–Kassel

(RRK) theory, RRKM does not apply all the simplifying assumptions. The total internal energy is partitioned into active and inactive components, such that only the active component can flow freely among the internal modes and thus contribute to the reaction.[92] To perform RRKM analysis we need the vibrational frequencies of the parent ion. This is easiest to calculate using the keyword FREQ in Gaussian 09 route section. Also needed is an estimate of the transition state. A key assumption of statistical unimolecular theories such as the RRKM theory is that following excitation, rapid intramolecular vibrational and rotational energy redistribution occurs in a time which is short compared with the time for dissociation or isomerization.[104]

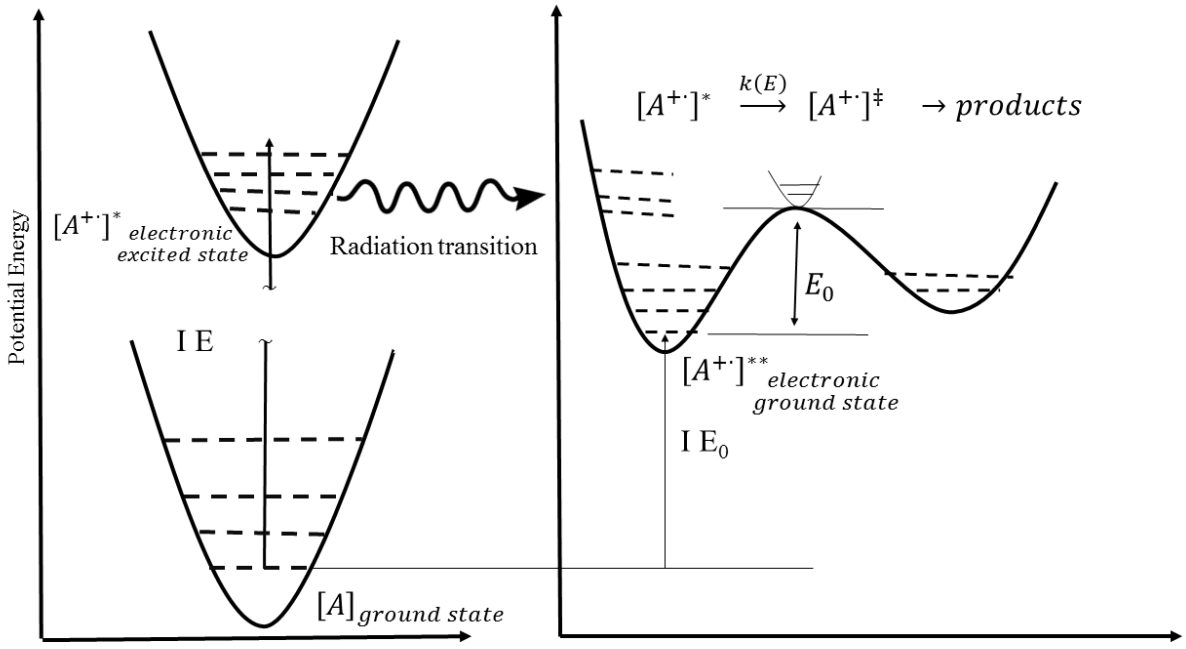

Figure 3.5: A schematic diagram of the unimolecular dissociation based on RRKM theory reproduced from the reference (fundamentals of mass spec). Internal energy of molecule A and the ionic ground state is represented by $[A^{+\cdot}]$.

The main assumptions here in the statistical treatment of reaction rate, k(ε), includes the fact that the activated molecule in the transition state can be in any internal energy state and dissociation will happen when it passes this critical point. Also the time it takes for redistribution of vibrational energy states in the activated complex at transition state is much shorter than the unimolecular

reaction time. This latter assumption is often known as the ergodic assumption. In physics the definition of an ergodic assumption is over long periods of time which is the time spent by a system in some region of the phase space of microstates with the same energy is proportional to the volume of this region which means that all accessible microstates are equally probable over a long period of time. So in active complex the redistribution of vibrational states is much faster than the dissociation interaction. The potential energy surface discussed in chapter 2 gives a static picture of a given reaction. But for a dissociation reaction we need a dynamic picture as well. To build this picture we construct a 2n-dimensional space (phase space) for the n internal degrees of freedom of the molecule, one dimension for each generalized coordinate $\mathbf{q} = (q_1,\ldots,q_n)$ and one for each conjugate momentum $\mathbf{p} = (p_1,\ldots,p_n)$. The importance and convince of this construction is that the instantaneous state or phase is represented by single point in ϕ_{2n} space, phase space, which during the temporal evolution of the parent molecule into products can be described as a trajectory in phase space.[105] To describe this system it is necessary to solve the Hamiltonian for this phase space:

$$H(\boldsymbol{q},\boldsymbol{p}) = E \tag{3.26}$$

Where E is the total energy and is a constant of motion. The important concept here is the transition state or in other words the activated complex. RRKM or the classical reaction rate, k(E) with the SI unit of mol/(dm^3s), describe how the rate of reactants transform to this state, transition state.

$$M \xrightarrow{k(E)} M^{\ddagger} \rightarrow products \tag{3.27}$$

Considering the concept of phase space we can write for the rate constant:

$$k(E) = \langle\Phi\rangle = \frac{\int_{X_{2n-2}} \ldots \int d\boldsymbol{q}d\boldsymbol{p}\, \rho(\boldsymbol{q},\boldsymbol{p})\Phi(\boldsymbol{q},\boldsymbol{p})}{\int_{S_{2n-1}} \ldots \int d\boldsymbol{q}d\boldsymbol{p}\, \rho(\boldsymbol{q},\boldsymbol{p})} \tag{3.28}$$

In this relation $\Phi(\boldsymbol{q},\boldsymbol{p})$ is the number of times a phase point passes through X_{2n-2} per unit time in the forward direction and $\rho(\boldsymbol{q},\boldsymbol{p})$ is the distribution of phase points in S_{2n-1}. The quantum treatment of this rate constant is more complicated. According to the Heisenberg uncertainty principle the momentum and position in phase space are related as $\Delta\boldsymbol{p}\Delta\boldsymbol{q} > \hbar$. Here the classical integration in

phase space would be basically counting the number of quantum states. If the reactant molecule has n degrees of freedom there will be n-1 degrees of freedom for the transition state:

$$\int_{0\leq H^{*}\leq E-E_0} \ldots \int dq^{*}dp^{*} \;=\; h^{n-1}G^{*}(E-E_0) \tag{3.29}$$

Here $G^{*}(E-E_0)$ is the total number of quantum states of the transition state in the interval $[0, E-E_0]$. Counting the states and defining $\delta G(E) = G(E+\delta E) - G(E)$:

$$\int_{E\leq H\leq E+\delta E} \ldots \int \frac{d\boldsymbol{q}d\boldsymbol{p}}{h^n} = \delta G(E) \tag{3.30}$$

The number of states, N, with momentum p and generalized position q in one dimension would be:

$$\frac{dpdq}{h} = N \tag{3.31}$$

The limit of of $\delta G(E)$, the difference between the total number of quantum states of the reactant at $E+\delta E$ and the E will be:

$$lim_{\delta E\to 0}\ \frac{\delta G(E)}{\delta E} = \rho(E) \tag{3.32}$$

and $\rho(E)$ is the density of states at energy E. The loose or tight transition state needs to be determined. Accounting for the vibrational degrees of freedom as those due to harmonic oscillators, the classical RRKM rate coefficient, k_{RRKM}, for unimolecular decomposition is:

$$k_{RRKM}(E) = \frac{G^{*}(E-E_0)}{h\rho(E)} \tag{3.33}$$

If the reaction path has a degeneracy of S then the above relation must be re-written as:[105]

$$k_{RRKM}(E) = S\frac{G^{*}(E-E_0)}{h\rho(E)} \tag{3.34}$$

where $G^*(E-E_0)$ is the total number of states between the E_0 and the E energy levels in the transition state and $\rho(E)$ is the density of states at energy E for the reactant.[106] In our case we used the RRKM and RRK algorithm embedded in the CRUNCH program or L-CID program. The RRKM theory is basically RRK theory in which the transition state theory has been included. Transition state theory describes how the reaction happens in potential energy surface space. The reactants must reach a certain level of energy before they can convert into products. The products might be in lower or higher energy states in respect to reactants which makes the reaction exothermic or endothermic. Also if the activated complex has much higher energy in comparison with the products the reaction would be tight. Usually in a loose transition there is little geometry change and difference between the active complex and the reactants. In tight reactions the activated complex has a geometry different from that of the reactants and products. The number of states grows more quickly for loose transition states than for tight transition states. If we ignore the ion's rotational energy the sum and the density of states refer only to the vibrational degrees of freedom.[107]

3.6 Internal Energy Distributions

In order to obtain a highly accurate bond dissociation energy from an energy-resolved collision-induced dissociation experiment the precursor ions should have a well-defined internal energy distribution and the FWHM of this energy which in optimum case should have a Gaussian or Maxwell-Boltzmann distribution shape is required for the deconvolution process to simulate the real threshold energy required for dissociation process.

The main methods to measure the internal energy of ions in mass spectrometry had been the thermometer molecule (TM) method, the deconvolution method and the survival yield method, later refined to include the kinetic shift.[106] The survival yield (M^+):

$$P \rightarrow F_1 + F_2 + \cdots \tag{3.35}$$

$$SY = \frac{I(P)}{I(P) + \sum I_{F_i}} \tag{3.36}$$

In this relation I(P) is the intensity of the parent ion and I_F is the intensity of the fragments. If the fragmentation can be viewed as a unimolecular decomposition reaction; then we can use the

experimental survival yields to calculate the rate coefficients. These rate coefficients can also be calculated using the Rice-Ramsperger-Kassel-Marcus (RRKM) theory for a particular internal energy of the ion. By projecting the experimental reaction coefficients on the RRKM curve[106], an estimate of the internal energy of the ions can be obtained. This method represents a simplification of the original survival yield method that has used additional assumptions on the functional form of the survival yield as a function of critical energy. According to the unimolecular kinetics valid for the ion source of a linear TOF-MS at low pressures, the survival yields were converted into experimental rate coefficients, $k_{exp}(E)$:

$$k_{exp} = -\frac{1}{\tau} \ln(SY) \tag{3.37}$$

Where τ is the reaction time in the accelerating region. Precursor ions subjected to threshold induced dissociation will need to have a well-defined internal energy following a Maxwell-Boltzmann distribution. Some uncertainty surrounds the amount of energy acquired by gas-phase ions created by electrospray ionization.[96] For larger precursor ions, additional internal energy is required to ensure that fragmentation occurs inside the collision cell, and a correction is applied to the apparent threshold for this kinetic shift, whose magnitude can be estimated from the unimolecular rate constant of the dissociation according to the Rice-Ramsperger-Kassel-Marcus (RRKM) theory.[55] A well-defined internal energy following a Maxwell-Boltzmann distribution for precursor ions is required for an accurate T-CID experiment. The distribution of the ion kinetic energy and absolute zero of the ion energy must be determined as accurately as experimentally possible. The derivative of the beam intensity yields the kinetic energy distribution of the parent ions. Chantry[108] discussed the FWHM of the distribution of relative kinetic energies at an energy E dependence to temperature as:

$$FWHM = (11.1k\gamma TE)^{0.5} \tag{3.38}$$

the parameter γ is described as:

$$\gamma = \frac{m}{M+m} \tag{3.39}$$

Where m is the mass of projectile particle and M is Mass of target molecule. The kinetic energy distribution of the ion and the Doppler broadening of the neutral reactant gas has been taken into

account in the deconvolution programs like CRUNCH program which has been developed by Peter B. Armentrout group over many years.

3.7 Data Analysis and Deconvolution Methods

The experimental cross section results are convoluted with the kinetic energy distributions of the ion and neutral reactants and that is why a deconvolution process is necessary. In our case we used two different available codes to do so. First and state of the art is the CRUNCH program developed by Armentrout group and the L-CID program.[56] The results for threshold dissociation energy for the bond dissociations were measured using both programs and are in close agreement. Here we briefly explain how the L-CID program works. Using L-CID is more convenient than other conventional methods since it only uses a single effective frequency with a new model for the density-of-states function and eliminates the need to explicitly calculate the frequencies for the parent ion and the transition state. Instead of conventional Marquardt-Levenburg least-squares routines, L-CID utilizes a Monte Carlo simulation and a sophisticated genetic algorithm to fit the data. L-CID uses a physical method to take into account the electrostatic potential for the two collision partners and properly consider the centrifugal barrier which is the direct result of the conservation of angular momentum. Input for L-CID requires the number of degrees of freedom, the looseness or tightness of the transition, number of free rotors, mass and polarizability of the target gas, experimental full width at half maximum (FWHM) of the ion kinetic energy distribution and the cross section data as a function of the energy in the center of mass or the laboratory frame. The individual processes modeled in L-CID is schematically illustrated in the figure below[56]. Here are the brief description of the relations implemented in L-CID:

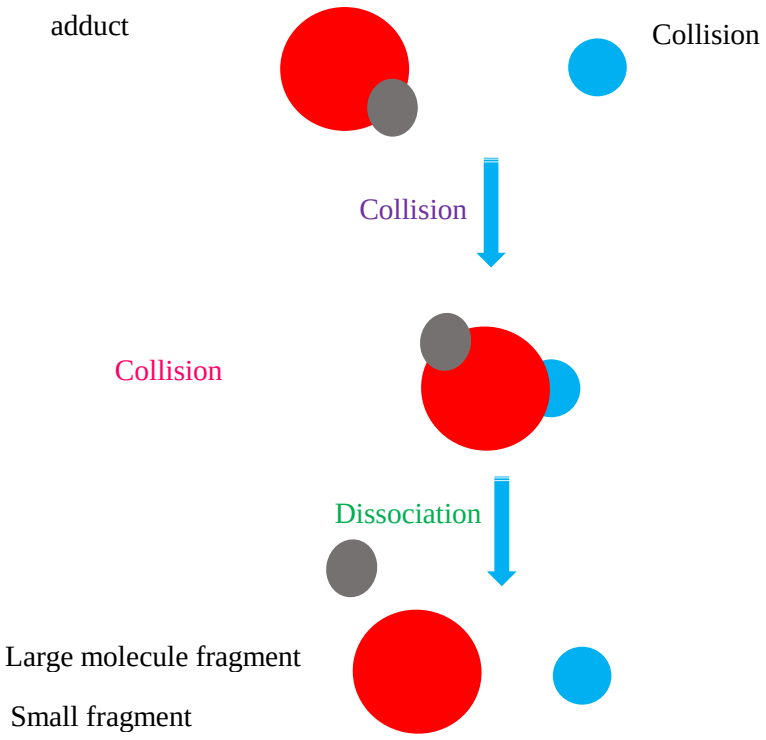

Figure 3.6: Component processes in L-CID and L-CID modeling method.

$$E_{coll} = \frac{\mu}{2}\left(\frac{dR}{dt}\right)^2 + \frac{E_{coll}b^2}{R^2} + V(R)$$ Ion-molecule collision dynamics

$$P(E_v) = \frac{\rho(E_v)}{Q(T)}\exp\left(\frac{-E_v}{RT}\right)$$ Heat content

Experimentally needs to be determined Kinetic Energy Distribution

$$FWHM_{Doppler} = \sqrt{11.1\,\gamma\,kTE_{c.o.m}}$$ Doppler Effect (collision gas)

$$P^0(\varepsilon, E_{conv}) = C(E_{conv})\,\varepsilon^{1/2}\,\rho_{(s+2)}\,(E_{conv} - \varepsilon\,)$$ Collison energy transfer

$$\sigma_{abs} = \sigma_0^{exp}\sum_{b=0}^{b=b_{max}} \pi b^2 P_{coll}(b)[1 - exp(-k\,(E_{deconv} - E_0)\,\tau)]$$ Reaction cross section

$$k(E_{deconv}) = \frac{1}{h\rho(E_{deconv})}\sum_{E=0}^{E_{deconv}-E_0}\rho^{\ddagger}\left(E^{\ddagger}\right) = \frac{W(E_{deconv} - E_0)}{h\rho(E_{deconv})}$$ Kinect shift

In L-CID the ion-molecule collision is treated using the electrostatic theory by Giomousis and Stevenson and properly treats a centrifugal barrier in the collision by partitioning the total collision energy between the fraction that is available for reaction and the remainder that is sequestered in overall rotation of the collision complex.[56] Here we reproduce the partitioning of the Incident velocity into a component along the line-of-centers and a centrifugal component from their publication and description describing L-CID:[56]

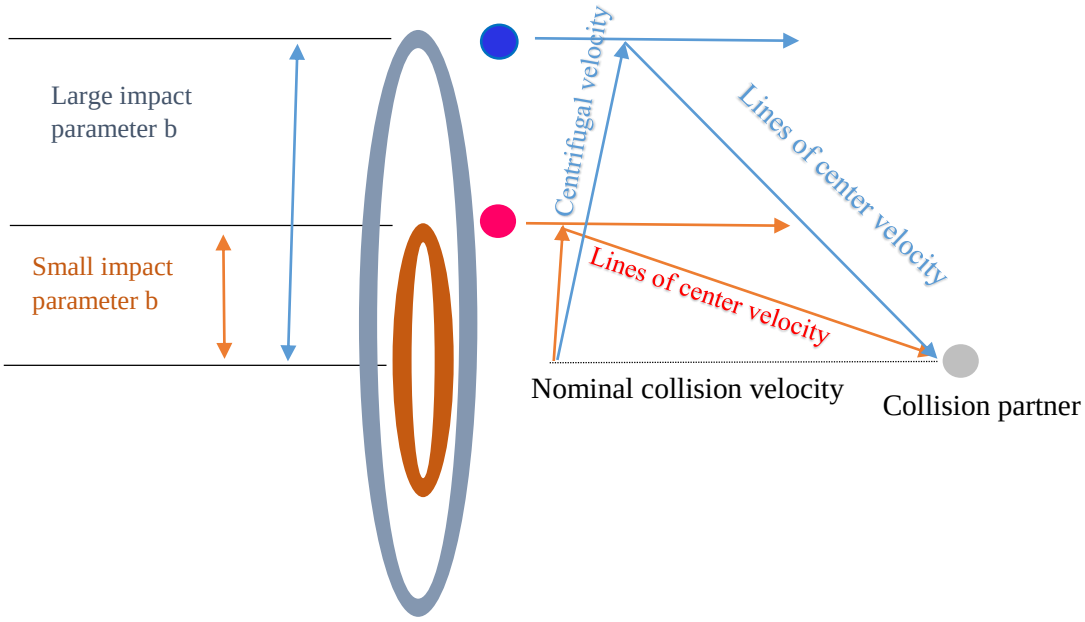

Figure 3.7: Schematic of how L-CID treat the collision process reproduced from Narancic et al.

To define the interaction between an ion and a nonpolar molecule we can use the Langevin theory. The effective interaction potential in Langevin theory is in the form:

$$V(r) = U(r) + \frac{L^2}{2\mu r^2} = -\frac{1}{2}\frac{\alpha\, e^2}{r^4} + \frac{L^2}{2\mu r^2} \tag{3.40}$$

Here r is the average inter distance between ion and neutral and L is the angular momentum. A is the polarizability of the neutral gas which in case of our experiments it was Argon and $\alpha = 1.6$ Å^3. $\frac{L^2}{2\mu r^2}$ is the repulsion term or the centrifugal barrier. For a reaction to happen reactants should have more energy than the centrifugal barrier. If b is the impact factor and E is the kinetic translational energy of the reactant then this centrifugal barrier (CB) will be:

$$CB = \frac{b^4\, E}{2\alpha e^2} \tag{3.41}$$

L-CID does not use any fit parameters (in contrast with CRUNCH program) and includes angular momentum effects in the collision dynamics. The other difference between L-CID and the

CRUNCH program, is the treatment of the density-of-state, $\rho(E)$. In general the density-of-state treatment procedure is an important issue in any data deconvolution process. The Crunch program uses the direct state count Beyer-Swinehart algorithm which requires the frequencies for the ion and the transition state while L-CID uses a single effective frequency to derive the density of states, $\rho(E)$. This is possible since in the canonical RRKM theorem in which the rate is related to the density of states and the sum of the states therefore the transition-states can be used as the only requirements here and the transition state is a two parameter model related to enthalpy and entropy of the transition state. Thus it is easy to see how it is possible to describe the density of state with two parameters which are threshold energy and an effective frequency. The density of state which Narancic[56] et al. introduce is:

$$\rho(E) = \exp\left[\left(\frac{E^2 s}{0.519\upsilon\left(E + \upsilon\, exp(1.546 - 0.1593\, rotors)\right)}\right)^{\frac{1}{2}}\right] \tag{3.42}$$

In this relation s is the number of vibrational degrees of freedom and energy, E, and frequency, ν are in cm^{-1} and we also need the number of free rotors. L-CID uses a genetic algorithm to fit the experimental convoluted data.

The data analysis and deconvolution also has been done using the CRUNCH program developed by the Armentrout group.[54, 55] The simplest form of line of center model to treat the cross section of CID experiments results and fit is[109]:

$$\sigma(E) = \sigma_0 \frac{(E - E_T)^n}{E^m} \tag{3.43}$$

Here n, m and σ_0 are adjustable parameters which should be well adjusted to fit the data as close as possible. Through this process we can find the threshold energy required for the dissociation process. The CRUNCH program utilizes the following relation to model the threshold regions of the reaction cross sections:

$$\sigma(E) = \sigma_0 \sum_i g_i\,(E + E_i - E_0)^n / E \tag{3.44}$$

in this relation σ_0 is an energy-independent scaling factor, E is the relative translational energy of the reactants, E_0 is the dissociation reaction threshold for 0 K and ro-vibrational state, and n is an adjustable parameter.[55] In the limit of hard sphere collisions n=1. The summation is over the ro-vibrational states of the reactant ions, i, where E_i is the excitation energy of each state and g_i is the population of those states (according to Maxwell-Boltzmann distribution at T = 300 K) which requires $\sum_i g_i = 1$. The CRUNCH program uses direct count Beyer-Swinehart algorithm to evaluate the density of the ro-vibrational states, and the relative populations. To include the statistical effects and the RRKM theory in calculations and data analysis, the CRUNCH program uses:

$$\sigma(E) = n\,\sigma_0/E\ \sum_i g_i \int_{E_0-E_i}^{E} \left(1 - e^{-k(E^{\ddagger})\tau}\right) \times (E-\varepsilon)^{n-1}\, d\varepsilon \qquad (3.45)$$

In this relation the dissociation probability, P_D, is represented by the term $1 - e^{-k(E^{\ddagger})\tau}$ and $E^{\ddagger}$ is the active or the transition state energy and ε is the energy transferred from translation into internal energy of the ion complex during the collision, τ is the experimental time for dissociation. The statistical unimolecular rate constant is shown with $k(E^{\ddagger})$. This was explained in some detail in the RRKM section. The total energy available to the reactants $E_T = E + E_i$ and the internal energy of the energized molecule after the collision is $E^* = E_T - \varepsilon$. The CRUNCH program treats the 2D external rotations as an adiabatic process so that partition of energy would not be available for the dissociation reaction. By statistically distributing E^* to all degrees of freedom including the 2D rotor, the average rotational energy would be:

$$\langle E_R \rangle = k_B\, T \qquad (3.46)$$

$$\langle E_R \rangle = E^* \left(\frac{2}{3N-3}\right) \qquad \text{equipartitioned} \qquad (3.47)$$

$$\langle E_R \rangle = \frac{\sum_{J=0}^{Jmax} E_R(J)\ g_J \rho\left(E^* - E_R(J)\right)}{\sum_{J=0}^{Jmax} g_J \rho\left(E^* - E_R(J)\right)} \qquad \text{statistical average} \qquad (3.48)$$

We used Gaussian G09[61] to find the vibrational frequencies, which are needed to be inputted in Crunch program, for different ions which we have studied. The best proposed treatment of single

channel CID processes is to average the entire dissociation probability over the statistical distribution of rotational quantum numbers:[110]

$$\langle 1 - e^{-k(E^*,J)\tau} \rangle = \frac{\sum_{J=0}^{J_{max}} \left[1 - e^{-k(E^*,J)\tau}\right] g_j \rho_{vr}\left(E^* - E_R(J)\right)}{\sum_{J=0}^{J_{max}} g_J \rho_{vr}\left(E^* - E_R(J)\right)} \tag{3.49}$$

in this relation $g_J = 2J + 1$ is the degeneracy of the 2D rotor and J_{max} is the maximum value possible for the rotational quantum number determined by energy conservation. J_{max} is possible to find through:

$$J_{max} = \frac{\left(\left(1 + \frac{4E^*}{hcB}\right)^{1/2} - 1\right)}{2} \tag{3.50}$$

here B is the rotational constants of the 2D rotors in the energized molecules and the transition state. Rotational energies can be found using $E_R(J) = hcBJ(J+1)$ and for the transition state $E_R^{\ddagger}(J) = hcB^{\ddagger}J(J+1)$. $B^{\ddagger}$ is the rotational constant of the transition state. Here the looseness or tightness of the transition comes into play. For a tight transition state $B^{\ddagger}$ is well defined but on the other hand for a loose transition $E_R^{\ddagger}(J)$ is a function of the height of the centrifugal barrier $V_{eff}(r^*)$. For an ion-induced dipole interaction this potential can be written as:

$$V_{eff}(r) = \frac{\alpha e^2}{8\pi\varepsilon_0}\frac{1}{r^4} + \frac{L^2}{2\mu r^2} \tag{3.51}$$

in this relation α is the polarizability of the neutral product r is the distance between the products, L is the orbital angular momentum of the products, and μ is the reduced mass of the products. The height of the centrifugal barrier can be found according to the following relation:

$$E_R^{\ddagger}(J) = V_{eff}(r^*) = \left(\frac{\pi\varepsilon_0}{2\,\alpha\,e^2\,\mu^2}\right)\left(\frac{\hbar^2 E_R(J)}{h\,c\,B}\right)^2 \tag{3.52}$$

3.8 Bond Dissociation Energy Determinations:

The experiments in this thesis the energy resolved collision induced dissociation is the bond dissociation energy (BDE). The BDE for a simple reaction such as the following which is cleavage of bond AB (no any rearrangement involve):

$$AB \rightarrow A + B \tag{3.53}$$

would be:

$$\Delta H^0_{f,298K} = \Delta H^0_{f,298K}(A) + \Delta H^0_{f,298K}(B) - \Delta H^0_{f,298K}(AB) \tag{3.54}$$

where the $\Delta H^0_{f,298K}$ is the standard state heat of formation at T = 298 K. The integrated heat capacity of a molecule, AB, from 0 to 298 K is equal to the heat content.[111]

$$\Delta H^0_{f,298\,K} - \Delta H^0_{f,0\,K} = \int_0^{298} [C_P(H)]dT \tag{3.55}$$

How to computationally obtain this was explained in details in chapter 2. The reactions of interests here can be a simple bond cleavage or involve rearrangement as well as bond cleavage.

As we can see from the above dissociation energy diagram at 0 K, the homolytic bond dissociation energy can be written as:

$$D_0(AB) = E_0(A) + E_0(B) - E_0(AB) \tag{3.56}$$

and $E_0 = E_{electronic} + ZPE$. The fine point here is the difference between bond enthalpy and bond dissociation energy. The bond dissociation energy is the energy required to break one mole of specific bonds in gas phase. Bond enthalpy is the average of a specific bond such as C-N. For a simple diatomic molecule these are basically the same.

A precursor ion can dissociate or undergo an isomerization to a more stable ion; and the same for fragments. Threshold collision-induced dissociations experiments needs accurate initial kinetic energy determinations to yield accurate BDE. We need to fit the experimental data such as parent ion intensity as a function of the center of-mass collision energy with the correct model to infer the threshold energy for bond cleavage. The other important consideration here is the single collision criteria. Each and every collision can deposit some energy in the available energy partitions (vibrational, rotational) and this will unpredictably convolute the experimental data in way that the obtained threshold energy (BDE) is unreliable. This can be done by extrapolating the cross sections measured under a series of low-pressure measurements conditions to zero pressure. CRUCNH or L-CID calculate the bond dissociation energy which is corresponding to T = 0 K and to convert that to T = 298 K we should add $(3/2)RT$. In Gaussian language starting from the partition function q(V;T) for the corresponding component of the total partition function we can see this 3/2 coming from the contribution to the internal thermal energy due to translation:[112]

$$\begin{aligned} E_T &= N_A k_B T^2 \left(\frac{\partial \ln q}{\partial T}\right)_V \\ &= RT^2 \left(\frac{3}{2T}\right) \\ &= \frac{3}{2} R\,T \end{aligned} \tag{3.57}$$

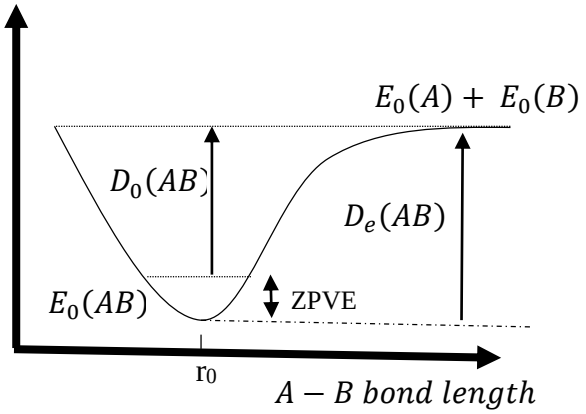

Figure 3.8: Bond dissociation energy diagram reproduced from reference 4. Energy required to dissociate molecule AB which is in its ground state (electronic + vibrational + rotational) fragment the molecule A and B in their ground state.

3.9 Kinetic shift

Kinetic shift is an important phenomena which must be considered in the data analysis and determining the threshold of bond dissociation energy. This is the direct result of finite lifetimes for dissociation. Chupka[113] and earlier Rosenstock et al.[114] described this phenomena. Chupka explained this phenomena even for the case of diatomic molecules, the occurrence of pre-dissociation and loss of energy by radiation or autoionization can lead to errors in interpretation. Basically we need more energy than the critical energy for fragmentation to be observed in the finite instrument time scale. For large molecules when the lifetime of the energized complex increases, it can eventually exceed the experimental timescale. Under these circumstances and for a given sensitivity, the onset for product formation is shifted to higher kinetic energies, resulting in a kinetic shift. Increasing the energy in such long-lived complexes increases the dissociation rate, enhancing the probability of seeing products.[87] Considering this which incorporates integration over a unimolecular dissociation probability:

$$\sigma(E) = (n\sigma_0/E) \sum_i g_i \int_0^{E+E_i-E_0} \left[1 - e^{-k(E+E_i-\Delta E)\tau}\right] \times (\Delta E)^{n-1}\, d(\Delta E) \qquad (3.58)$$

where ΔE is the energy that remains in translation after collision and τ is the average experimental time available for dissociation (the ion time-of-flight from the collision cell to the quadrupole mass analyzer. $k(E + E_i - \Delta E) = k(E^*)$ is the unimolecular dissociation rate constant, calculated using Rice-Ramsperger-Kassel-Marcus (RRKM) statistical theory. $k(E^*)$ is the dissociation rate. The accuracy of the estimated kinetic shift is limited by the models used, including the statistical RRKM theory, and the assumptions made regarding the transition states for the appropriate dissociation. In general the process of intramolecular energy transfer is expected to be more rapid for ions of higher energy of excitation for several reasons. On average, the density of electronic and vibrational energy levels increases rapidly with energy thus increasing the number of crossings of potential surfaces.[113] This is important phenomena and must be considered in the deconvolution process even for a diatomic molecule dissociation. In our case which we have very large floppy molecules the magnitude of this shift might be the same as the threshold energy itself. A Kinetic shift can shift the appearance of observed threshold energy since an ion can have energy high enough to be able to dissociate before it has the chance to be detected. It can be non-negligible for

large molecules with many vibrational degrees of freedom. Small or negligible kinetic shift means that all ions are expected to fragment immediately upon being activated to the dissociation threshold.[95]

3.10 Competitive Shifts

Whenever there is more than one reaction path available, there is the possibility of competition between the available possible paths. In other word more energy required than the actual TCID for the dissociation to be competitive with pathway of lower appearance energy. We have not observed this phenomenon in our experiments. Mostly what we have observed is the sequential dissociation. Statistically, the number of states available to the lower energy channel is much greater than to the higher energy channel, such that the cross section for the second channel rises slowly from its thermodynamic threshold, a victim of competition with the lower energy channel.[87] Whenever there is more than one reaction path available there is the possibility of competition between the available possible paths. In other words more energy is required than the actual TCID for the dissociation to be competitive with a pathway of lower appearance energy. We have not observed this phenomenon in our experiments. Primarily we have observed sequential dissociation. Statistically, the number of states available to the lower energy channel is much greater than to the higher energy channel, such that the cross section for the second channel rises slowly from its thermodynamic threshold, a victim of competition with the lower energy channel.[87] As an example of this:

$$(L_1)\,M^+\,(L_2) + Rg \rightarrow M^+(L_1) + L_2 + Rg \quad (3.59)$$

$$\rightarrow M^+(L_2) + L_1 + Rg \quad (3.60)$$

statistically, the number of states available to the lower energy channel is much greater than to the higher energy channel.

3.11 Azobenzene and its derivatives

Azobenzene and its derivatives are the main molecules which have been studied in this dissertation both for our computational investigations and also the CID experiments. Thus it is helpful to briefly describe these molecules here. We have done comprehensive theoretical and experimental studies on these molecules. Azobenzene exhibits a cis to trans isomerization following absorption of a light photon with the correct wavelength. The incident photon excites an electron to a Π^* orbital. This character can be used in many different basic and applied science and technology. Utilizing this photo isomerization phenomenon we can build molecular switches which can be turned on and off upon radiation with specific frequency and this frequency can be changed by functionalizing azobenzene with different functional groups. The trans to cis isomerization happens only by radiation with the correct wavelength but cis to trans can happen by heat or radiation with light. UV-Visible, NMR and Raman spectroscopies have been utilized to investigate the excited state dynamics of trans-azobenzene and its derivatives in solution after $\pi\pi^*$(S2) excitation. This interesting molecules and its derivative can simply convert the light energy into mechanical motion. *Ab initio* quantum molecular dynamics simulations of photo-induced cis-trans isomerization have been published recently[115-117]. We performed the threshold collision induced dissociation experiment for all of the samples and explained the details for the experiment performed on trans 2,2́,6,6́-tetrafluoroazobenzene. We could not do this for the cis isomer due to the high temperature in the ion source. Our experiments to measure the difference between bond dissociation energies for the trans and cis isomers of azobenzene and its depravities was not successful so we focused on the trans isomers for the CID experiments.

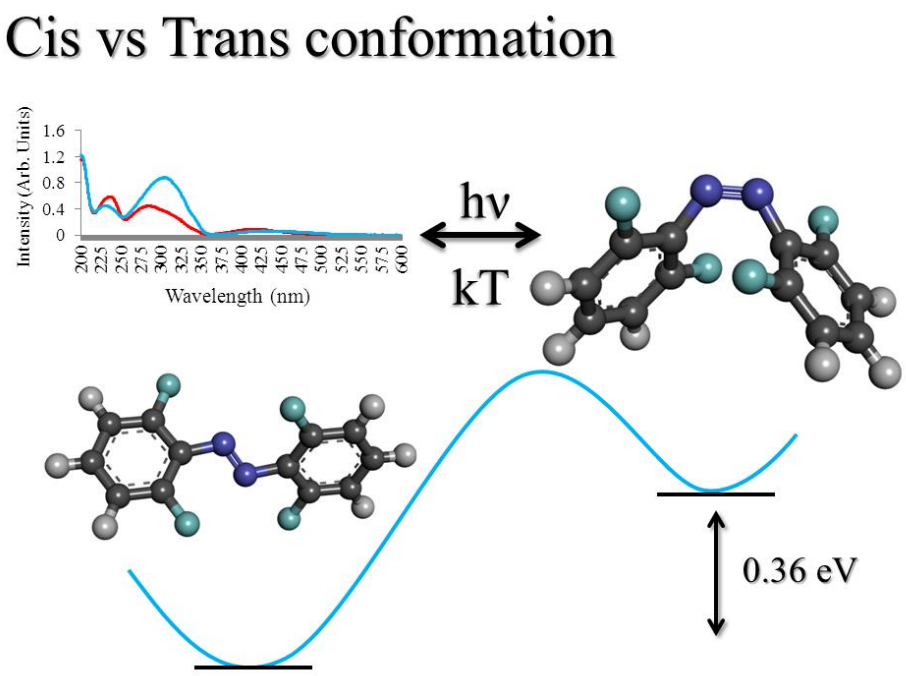

Figure 3.9: trans and cis isomers of 2,2',6,6'-tetrafluoro azobenzene. As a result of a B3LYP level of theory calculation with 6-311++G(d,p) basis set we can see that the cis isomer is 0.36 eV higher in energy comparing cis and trans isomers ground states. UV-Vis spectroscopy clearly proved that we can convert trans to cis isomers using green light and the reverse reaction can happen thermally or using light.

3.12 Collision Induced dissociation of trans-2,2',6,6'-tetrafluoro-azobenzene

3.12.1 Properties of trans-2,2',6,6'-tetrafluoro-azobenzene negative ion

Chemical bonding and the electronic structure of the trans-2,2′,6,6′-tetrafluoroazobenzene negative ion have been studied using collision-induced dissociation (CID) as well as photodetachment-photoelectron spectroscopy (PD-PES) and the experimental results were compared with *ab initio* calculations. The trans-2,2′,6,6′-tetrafluoroazobenzene anion was prepared by atmospheric pressure chemical ionization (APCI) for the CID experiment and through

thermal electron attachment in the PES experiments. The adiabatic electron affinity of trans-2,2′,6,6′-tetrafluoroazobenzene was measured to be 1.3 ± 0.1 eV and the vertical detachment energy was 1.78 ± 0.1 eV. Calculations of the adiabatic electron affinity employing different *ab initio* methods gave an average value of the adiabatic electron affinity of 1.6 eV and a vertical detachment energy of 1.81 eV, which are in reasonable agreement with the experimental results. Energy resolved CID studies of the precursor anion resulted in 1.73 ± 0.2 eV bond dissociation energy for the collision process yielding $[C_6H_3F_2]^-$ fragment ion and $C_6H_3F_2N_2$ neutral fragment. Calculations from 17 different *ab initio* methods resulted in a dissociation energy ranging from 1.7 to 2 eV at 0 K temperature. Two additional CID fragment ions appear at higher energy: $[C_6H_2F]^-$ and $[C_6H]^-$. The occurrence of $[C_6H]^-$ is of particular interest since it is the first anion to be observed in the interstellar medium.

In this research we studied tetrafluoroazobenzene. Figure 10 illustrates the cis and trans forms of 2,2′,6,6′-tetrafluoroazobenzene optimized at the B3LYP level of theory with 6-311++G(d,p) as the basis set. This calculation results in a 0.29 Debye dipole moment for the trans 2,2′,6,6′-tetrafluoroazobenzene and 5.45 Debye for the cis isomer. Notice that the trans isomer is slightly twisted and is not planar, which is the origin of the small dipole moment. Trans azobenzene is a planar molecule with zero dipole moment. The trans 2,2′,6,6′-tetrafluoroazobenzene is 0.36 eV lower in the ground state electronic energy in comparison to the cis isomer.

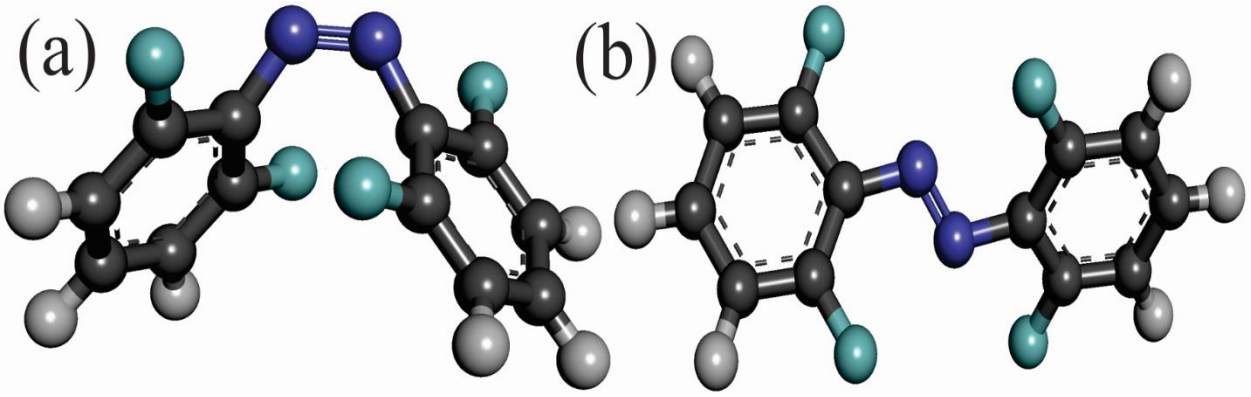

Figure 3.10: Optimized structure of 2,2′,6,6′-tetrafluoroazobenzene neutral molecule. (a) cis isomer, the CNNC dihedral is -9.2 and the CCNN dihedral angle is -58.4 (b) trans isomer, the CNNC dihedral is -175.9 and the CCNN dihedral angle is 153.9.

3.12.2 Collision induced dissociation experiment

Collision induced dissociation (CID) experiments are well established analytical methods based on tandem mass spectrometry to obtain important information about the thermochemical properties of ions. Combined with quantum chemistry computations, CID experiments can be an accurate source of information in gas phase thermochemistry. Analysis of the energy dependence of the cross sections for CID reactions has permitted the determination of quantitative thermodynamic information for a variety of molecular ions.[55] The main strengths of CID type experiments are the relatively direct manner of obtaining bond energies from dissociation thresholds, its broad dynamic range, and its ability to treat a diverse set of chemical species.[118] The CID experiments in this work were carried out using an AB SCIEX QSTAR Elite Hybrid LC-MS/MS apparatus consisting of a hybrid quadrupole/time-of-flight mass spectrometer equipped with an atmospheric pressure chemical ionization (APCI) source. Two figures and a schematic of this instruments are shown at the beginning of this chapter. The trans-2,2′,6,6′-tetrafluoroazobenzene sample is first dissolved in methanol as a dilute solution having 2 µg/ml concentration and injected into the instrument with 20 µL/min rate. The gaseous sample is then mixed with nitrogen gas at atmospheric pressure and passed through a short externally heated region. This gas then passes through a 5 cm tube at room temperature where a corona discharge was used to produce negative ions. Low energy electron attachment to the molecule is followed by collisional stabilization in a bath gas. The anions were expanded through a small orifice into the instrument using nitrogen as the curtain gas and through two regions of differential pumping. At the point of entrance into the mass spectrometer the ions are believed to be at or slightly below room temperature as a result of expansion into the vacuum. The precursor ion of mass m/z = 254 was transmitted through the first quadrupole mass spectrometer and injected into the collision cell. Argon was used as the neutral collision gas. The collision cell is 20.9 cm long and is at room temperature. The laboratory frame collision energy was varied from 0 eV to 25 eV in increments of 0.5 eV and data were recorded for one minute at each collision energy. The zero of the kinetic energy scale and the FWHM of distribution of the ion kinetic energy is determined by obtaining the derivative of precursor ion intensity in respect to the energy in the laboratory frame and fitting it to a Gaussian function. The FWHM of ion kinetic energy is ~2 eV (lab). The zero of energy is 2.7 eV (lab) and was used to calibrate the energy scale. Analysis of the recorded mass spectrum was performed by using the Analyst® QS 2.0 software

package. To convert the data from an instrument dependent ion intensity signal in an energy resolved CID experiment and extract the threshold energy E_0 many factors such as the transition state of the reaction and the finite temperature of the ions and the collision cell must be considered. We discussed in details how the conversion from precursor and fragment ions intensity to cross sections can be performed.

Input information for the CRUNCH program includes the number of degrees of freedom (34), number of free rotors (0), the polarizability of the target gas argon (1.6×10^{-24} cm^3), experimental full width at half maximum (FWHM) of the laboratory ion kinetic energy distribution which in this case is ~2 eV (0.27 CM). To analyze our experimental cross sections data, we used the CRUNCH program and also the L-CID program which the results from both will be presented here. To have a better idea of how the collision induced dissociation quantitative and qualitative data analysis procedure works here we presented the experimental mass spectrum in different collisional energy (in laboratory frame) and we can see how the intensity of fragment ions increase while the precursor ion intensity decline. We also provided the optimized molecular structure for precursor neutral, ion and fragment ions. We first need to identify all the possible fragment ions by recording the intensities of peaks available in the mass spectrum and see which ones intensity is changing in a reasonable matter by changing the translational energy. Then we record the intensity of those fragment ions and precursor at each energy step. We usually take data at each 0.5 eV increment. In this particular experiment we have 3 fragment ions. In low energy region the predominant ion is 113 m/z peak but at higher energy the 93 and 73 m/z ions appear and their intensities grow upon increasing the collision energy. The suggested mechanism to form the three negative product ions detected in the mass spectrum can be summarized as:

$$[C_{12}H_6F_4N_2]^- + Ar \rightarrow \ [C_6H_3F_2]^- + \ C_6H_3F_2N_2 + Ar \tag{3.61}$$

$$[C_6H_3F_2]^- + Ar \rightarrow \ [C_6H_2F]^- + HF + Ar \tag{3.62}$$

$$[C_6H_2F]^- + Ar \rightarrow \ [C_6H]^- + HF + Ar \tag{3.63}$$

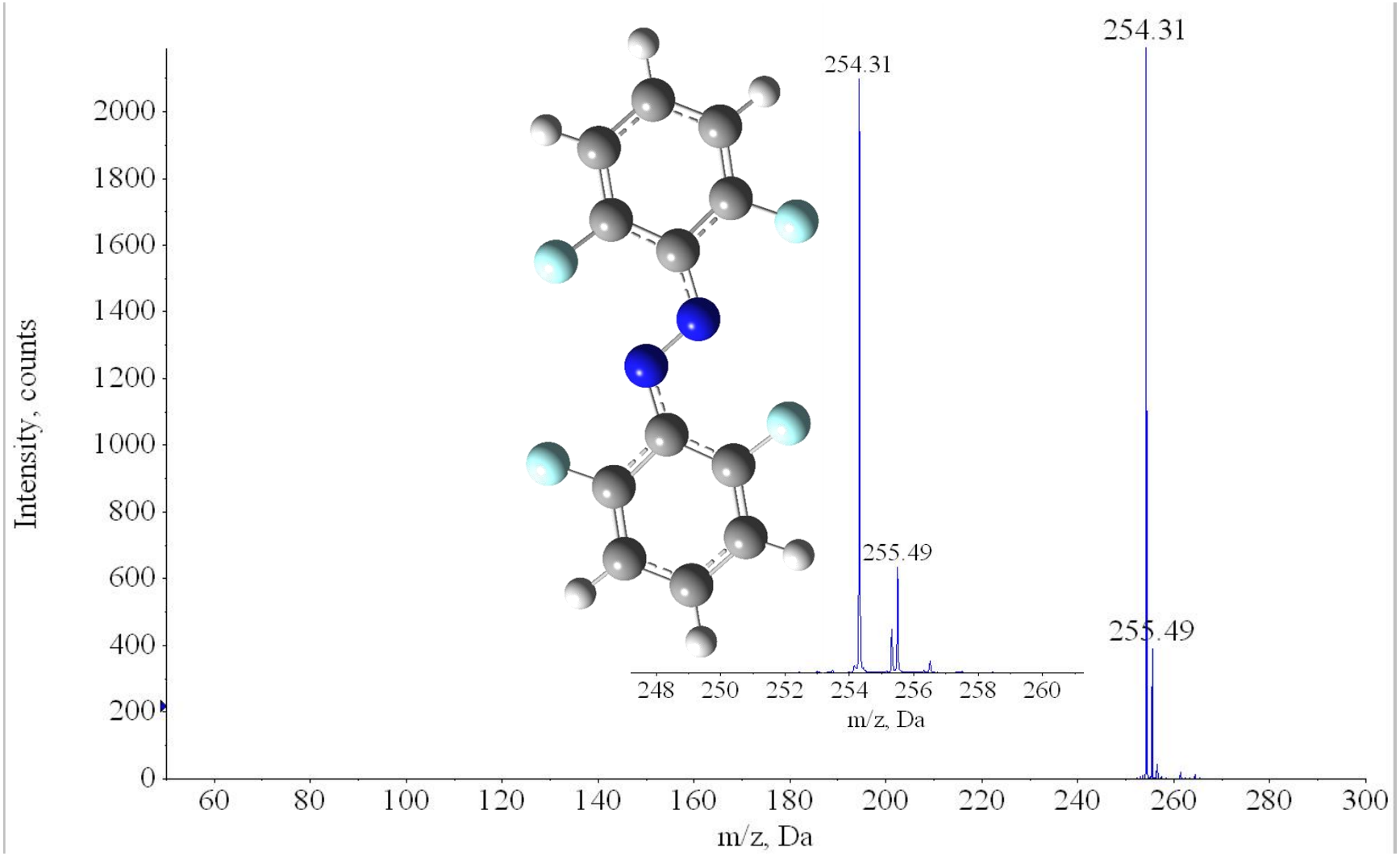

Figure 3.11: Mass spectrum of trans-2,2′,6,6′-tetrafluoroazobenzene ($C_{12}H_6N_2F_4$, precursor neutral Molecular Weight: 254.18 Da) at **5 eV** collision energy in the laboratory frame (CID experiment), negative mode and the precursor **anion** is illustrated. This is in negative mode and the precursor ion is an anion.

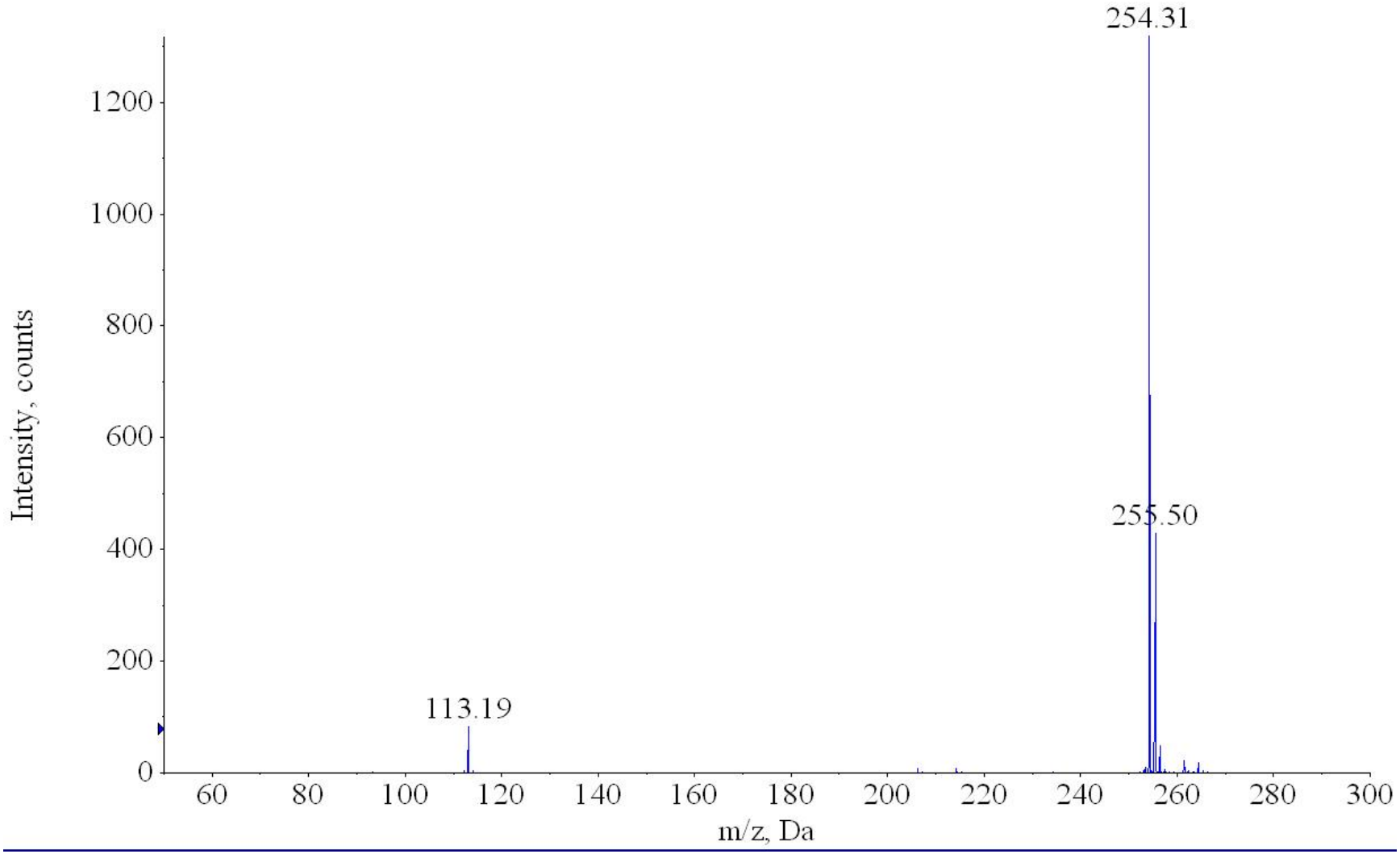

Figure 3.12: Mass spectrum of trans-2,2′,6,6′-tetrafluoroazobenzene at 10 eV translational collision energy in the laboratory frame. The fragment ions m/z = 113 and m/z =93 are present in the spectrum.

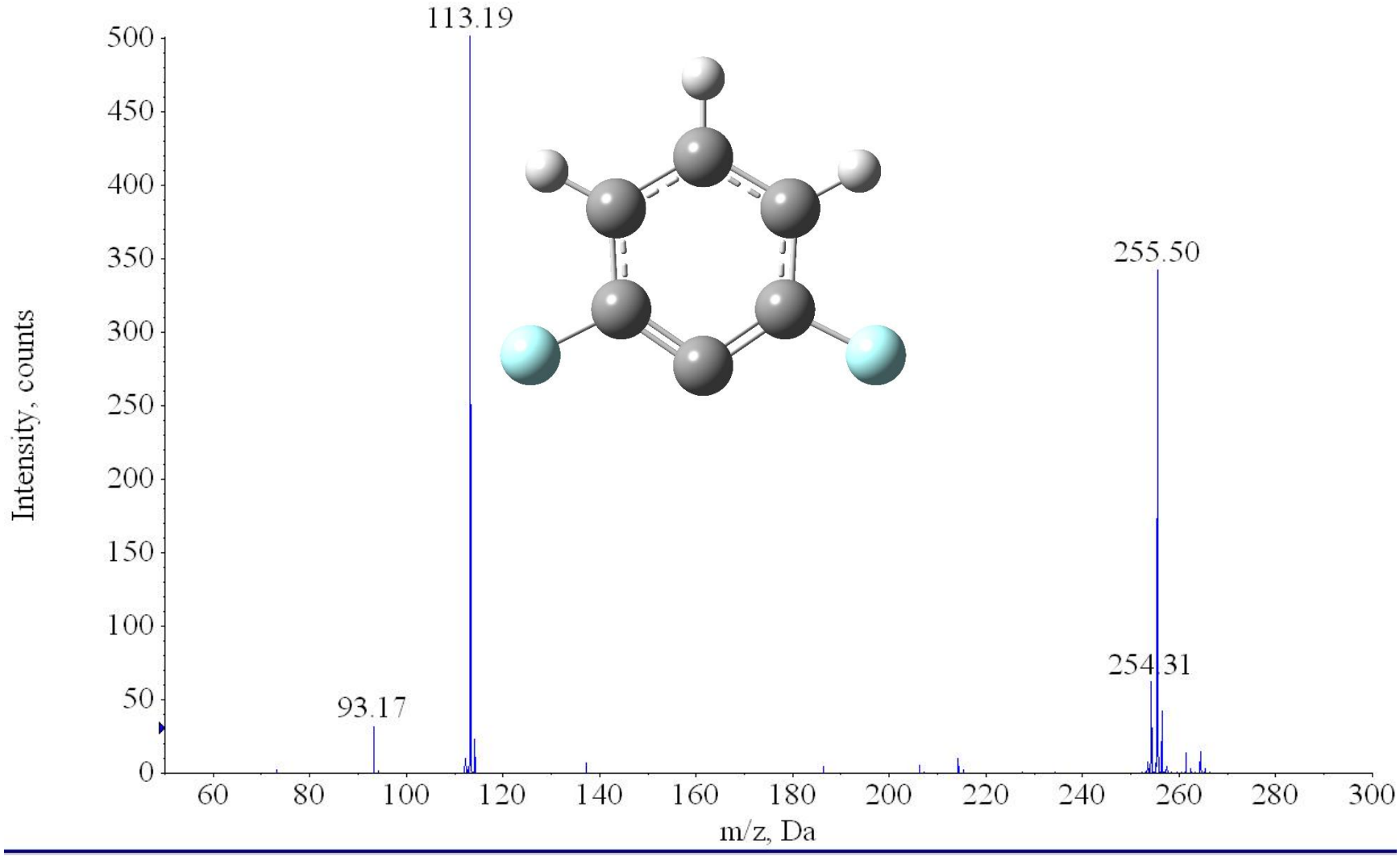

Figure 3.13: Mass spectrum of trans-2,2′,6,6′-tetrafluoroazobenzene at 15 eV translational collision energy in the laboratory frame. The fragment ion m/z = 113 is present in the spectrum.

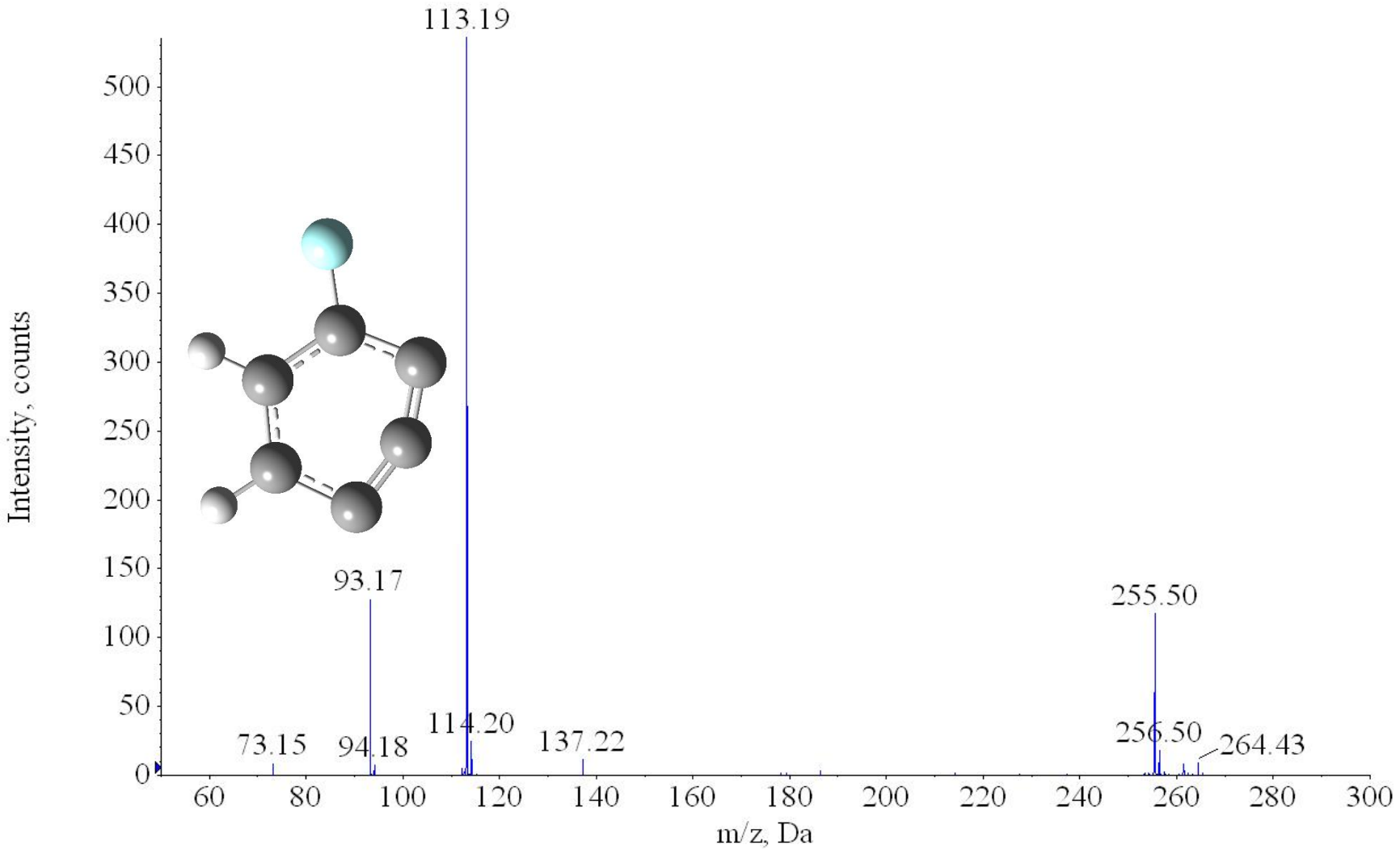

Figure 3.14: Mass spectrum of trans-2,2′,6,6′-tetrafluoroazobenzene at 20 eV translational collision energy in the laboratory frame. The fragment ion m/z = 93 is present in the spectrum.

The energy dependence of the ion peak intensities were initially analyzed using Analyst software and then converted into a relative cross section. Deconvolution of the energy resolved collision induced dissociation cross sections was performed using the L-CID program to fit the data points and find the threshold energy. Our quantum chemistry calculations showed the energy that it takes to produce the 93 m/z anion $[C_6H_2F]^-$ directly from the parent ion through a single collision is ~4.3 eV depending upon the method and the basis set. The fact that this anion exists and shows up in the spectrum around 2.1 eV (center of mass energy) of energy which is available for the reaction to take place suggests that it cannot be the result of a single collision interaction. This is possible since the fragment ion has enough translational energy to overcome the dissociation barrier to produce 93 m/z peak ion. Computations using B3LYP and 6-311++G(d,p) show that this reaction will take ~2.5 eV energy. Creating the 73 m/z ion from the 93 m/z product ion in a sequential dissociation would be easier and requires only 0.65 eV energy to take place. This has been calculated using B3LYP level of theory with 6-311++G(d,p) basis set. This can explain the resemblance of the cross section data for the 93 m/z and 73 m/z peaks. Thus we will only focus on the 113 m/z peak in order to obtain the bond dissociation enthalpy for breaking the C-N bond yielding the $[C_6H_3F_2]^-$ anion and assumed $[C_6H_3F_2N_2]$ fragment.

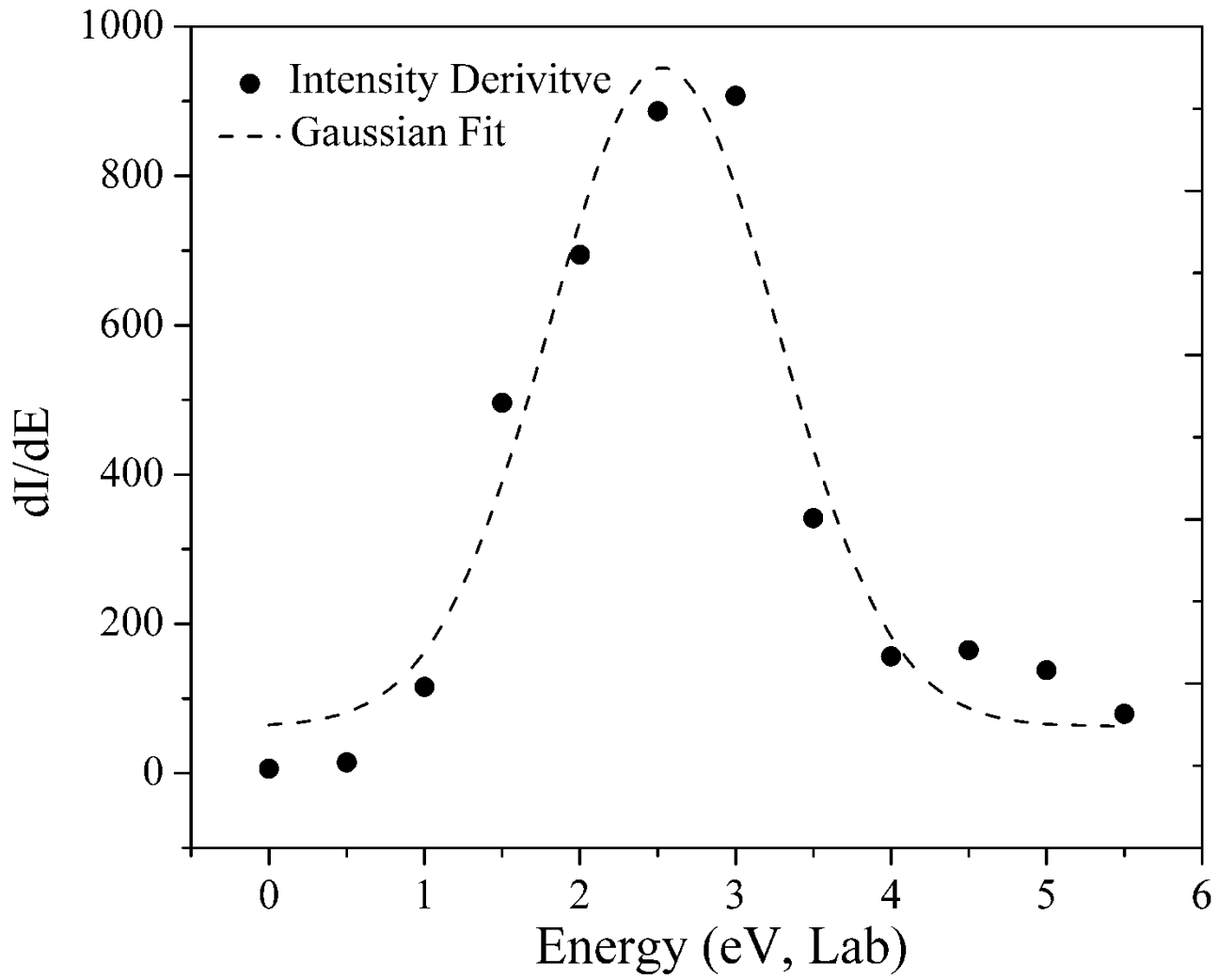

Figure 3.15: The derivative of precursor ion intensity with respect to energy in lab frame Gaussian fit FWHM is an accurate approximation of the FWHM of the precursor ion kinetic energy. This procedure shows that the true zero of energy is at 0.33 eV for this experiment.

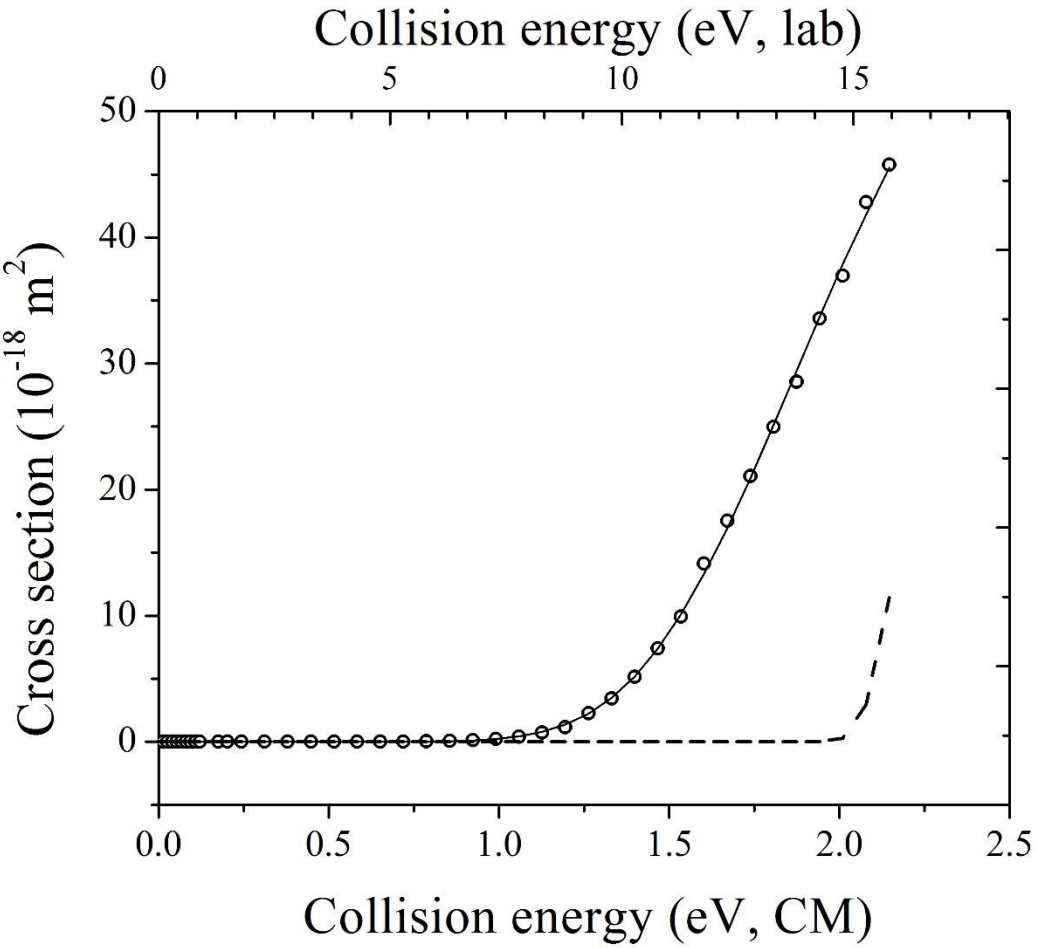

Figure 3.16: The experimental cross section for CID and the CRUNCH fit to the experimental data. The dashed line is the deconvoluted cross section when the broadening effects of experimental kinetic energy, target gas motion and anion temperature is corrected for reactants at 0 K. The energy scale is corrected for the measured 0.33 eV difference between the real and nominal energy. The threshold energy for dissociation after deconvolution of Doppler broadening of neutrals is 1.85 eV.

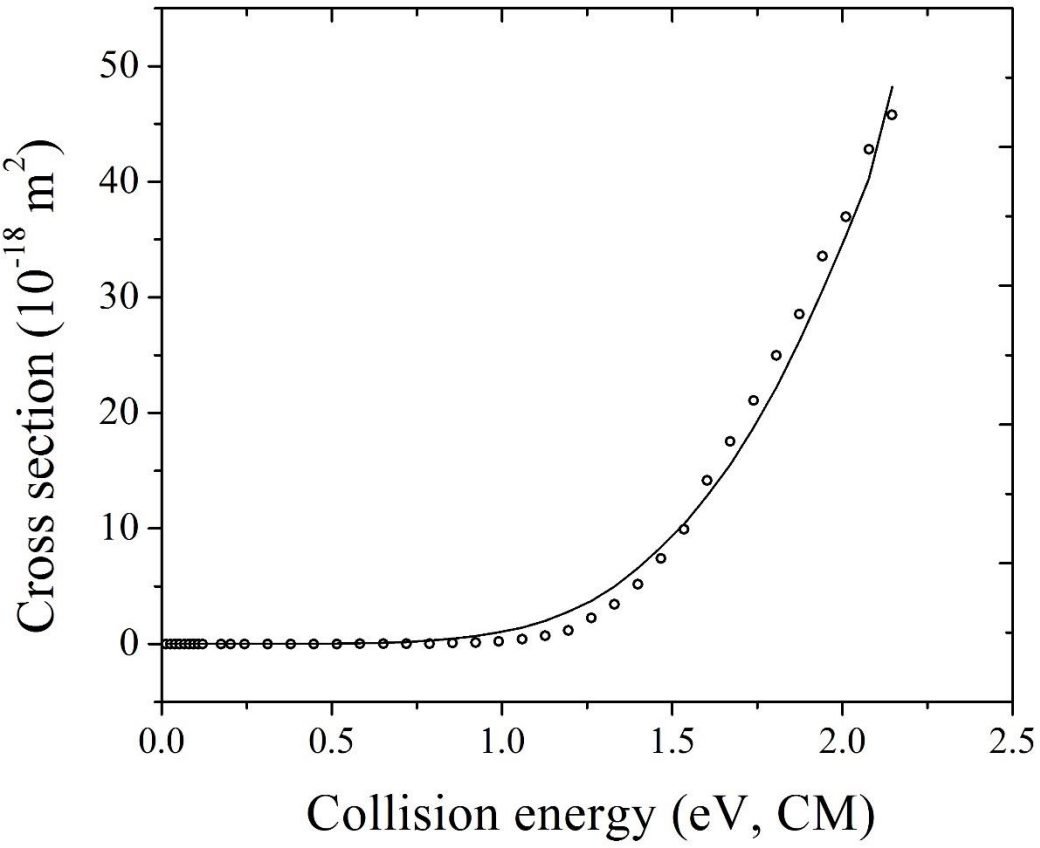

Figure 3.17: Experimental cross section and the fit generated by the L-CID program. This fitting resulted 2.00 eV for the C-N bond dissociation which yields the m/z = 113 fragment ion along with 8528 cm^{-1} for the effective frequency and 5.76×10^3 $cm^{-1}$for the ά.

Table 3.1: Calculated and experimentally measured Bond Dissociation Energies (BDE) at 0 K for cleaving the C-N bond of the precursor ion yielding the $[C_6H_3F_2]^-$ anion and $C_6H_3F_2\,N_2$ neutral fragment.

Method/Basis set	Bond Dissociation Energy (eV)
B3LYP/6-31+G(d)	1.84
B3LYP/6-311+G(d)	1.79
B3LYP/6-311++G(d)	1.79
B3LYP/6-311++G(d,p)	1.79
B3LYP/6-311++G(2d,2p)	1.80
B3LYP/6-311++G(3df,3pd)	1.83
B3LYP/aug-cc-pVDZ	1.86
B3LYP/Lanl2DZ	2.14
M06/6-311++G(d,p)	2.08
M06-L/6-311++G(d,p)	2.10
M06-2X/6-311++G(d,p)	2.01
B3P86/6-311++G(d,p)	1.97
B3PW91/6-311++G(d,p)	1.88
wB97/6-311++G(d,p)	1.91
wB97X/6-311++G(d,p)	1.90
wB97XD/6-311++G(d,p)	1.95
CBS-QB3	1.90
Experiment(CRUNCH program)	1.85 ± 0.20
Experiment (L-CID Program)	2.00 ± 0.20

Taking into account the estimated experimental uncertainty most of the calculations are compatible with the experimental result. The computations show the $(C_6H_3F_2 + N_2)$ complex is 0.33 eV more stable than $C_6H_3F_2N_2$.

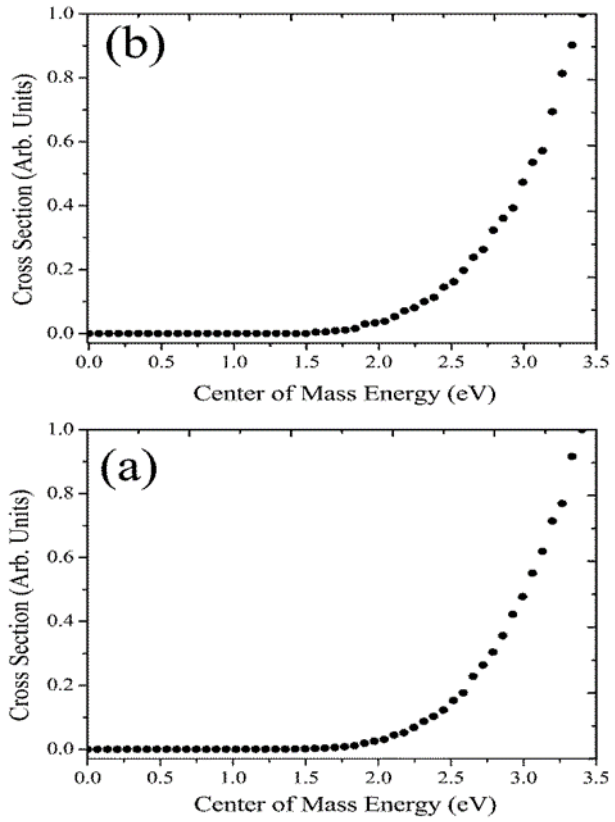

Figure 3.18: Experimental cross sections for collision-induced dissociation as a function of kinetic energy in the center of mass frame. These ions are the result of sequential dissociation of HF from $[C_6H_3F_2]^-$ into (a) 93 m/z peak $[C_6H_2F]^-$ (b) 73 m/z peak $[C_6H]^-$.

In Table 3.1 we summarize the bond dissociation energies at 0 K based on the suggested mechanism to create the other ions through a sequential dissociation from the primary product ion, $[C_6H_3F_2]^-$, and their dipole moments. The studied ions have been optimized with tight convergence criteria using aug-cc-pVTZ as the basis set and the ZPE was included. BDEs are in electron volt and the dipole moments are in Debye.

Table 3.2: summary of the product ions properties and the bond dissociation energies to yield (1) $[C_6H_2F]^-$ and (2) $[C_6H]^-$ product anions. BDEs are in electron volts unit and the dipole moments in Debye.

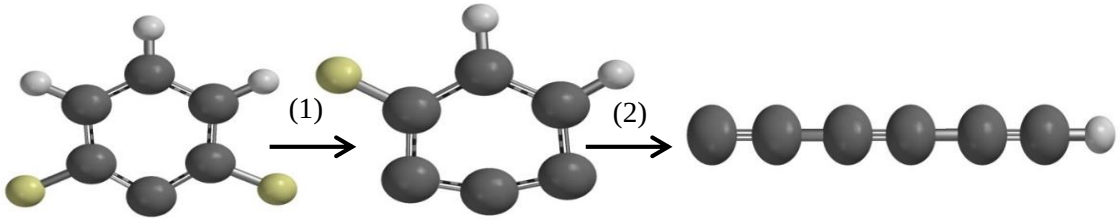

Method/basis set	BDE (1)	BDE (2)	113 m/z Dipole Moment (D)	93 m/z Dipole moment (D)
B3LYP	2.52	0.64	4.86	3.83
wB97XD	2.64	1.15	4.97	4.02
MP2(Full)	2.54	0.78	5.28	4.01

As we discussed before since the presence of $[C_6H_2F]^-$ and $[C_6H]^-$ ions are not believed to result from single collision reactions, we are not analyzing the experimental cross section data related to those anions. Instead we present the bond dissociation energies for the reactions suggested to be reasonable for their production which are the calculated values using high level calculations. The 73 m/z peak, $[C_6H]^-$, which showed up in the spectrum at laboratory energies more than 25 eV is an especially interesting anion especially since it and other C_nH^- anions represents the first negative ion observed in the interstellar medium. McCarthy et al.[119] described the detection of $[C_6H]^-$ in the radio band in the laboratory and has been identified in the molecular envelope of IRC +10216 and in the dense molecular cloud TMC-1.

3.12.3 $[C_6H]^-$ Negative Ion:

One of the important results of this experiment was the existence of $[C_6H]^-$ ion. This ion is the first negative ion to be found in the interstellar medium. This negative ion has a ground electronic state which is represented as $X^2\Pi$ and a close state to this $A^2\Sigma^+$ which is ~0.82 eV higher in energy. The ground state has a dipole moment of ~4.72 Debye which is the main reason to have a strong IR transition which is helpful to be detected in interstellar medium. The other close state ($A^2\Sigma^+$) has 0.82 Debye dipole moment. Murakami et al[120] studied the molecular constants, rotational constants and related quantities of this molecule using restricted Hartree-Fock method (RHF) and reported 5 and 1 Debye for these configurations dipole moment, respectively. The linear polyynyl radicals, C_nH (n=1-8), has been detected in interstellar medium using radio astronomy and the negative ion detection has been done in 2006 by McCarthy et al.[119] which he reported the $[C_6H]^-$ detection in the radio band in the laboratory and has been identified in the molecular envelope of IRC +10216 and in the dense molecular cloud TMC-1. Here we used some high level calculations to predict the equilibrium geometry and electronic structure of physical and chemical properties of this ion.

Since the neutral ground state has a large dipole moment (in comparison to 2.5 Debye which is the theoretical value to form a Dipole bound anion) I suggest that beside the valance bound anion there should be a dipole bound anion state as well. All the effort to find any results in literature about the dipole bound negative ion of $[C_6H]^-$ was not successful and we think it worth the effort to find this dipole bound state which we know is barely bound (the binding energy is in the order of few meV). To find this dipole bound anion there are some technical issues. Usually to find a dipole bound anion a high level calculation which includes the electron correlation such as CCSD and CCSD(T), we need to include diffuse basis sets. Such basis sets are usually constructed as combination of a standard valence-type basis, designed to describe the neutral molecular core, and an extra diffuse set designed to describe the charge distribution of the extra electron.[121] The exponents of the extra diffuse basis set should be small enough to describe the diffuse charge distribution of the excess electron. To do this I designed an extra diffuse basis set based on cc-pVDZ and cc-pVTZ. Finding the adequate extra diffuse coefficient and avoiding the linearity problem in the basis set is important in constructing an extra diffuse basis set.

Extra diffuse aug-cc-pVDZ coefficient:[122]

For H: d-aug-cc-pVDZ + 2 S + 2 P

For C: d-aug-cc-pVDZ + 2 S + 2 P + 2D

****

H 0

S 3 1.00

13.0100000 0.0196850

1.9620000 0.1379770

0.4446000 0.4781480

S 1 1.00

0.1220000 1.0000000

S 1 1.00

0.0297400 1.0000000

S 1 1.00

0.0072500 1.0000000

S 1 1.00

0.001767401 1.0000000

S 1 1.00

0.000430856 1.0000000

P 1 1.00

0.7270000 1.0000000

P 1 1.00

0.1410000 1.0000000

P 1 1.00

0.0273000 1.0000000

P 1 1.00

0.005285745 1.0000000

P 1 1.00

0.00102341 1.0000000

****

C 0

S 8 1.00

6665.0000000 0.0006920
1000.0000000 0.0053290
228.0000000 0.0270770
64.7100000 0.1017180
21.0600000 0.2747400
7.4950000 0.4485640
2.7970000 0.2850740
0.5215000 0.0152040
S 8 1.00
6665.0000000 -0.0001460
1000.0000000 -0.0011540
228.0000000 -0.0057250
64.7100000 -0.0233120
21.0600000 -0.0639550
7.4950000 -0.1499810
2.7970000 -0.1272620
0.5215000 0.5445290
S 1 1.00
0.1596000 1.0000000
S 1 1.00
0.0469000 1.0000000
S 1 1.00
0.0138000 1.0000000
S 1 1.00
0.004060554 1.0000000
S 1 1.00
0.00119479 1.0000000
S 1 1.00
0.000351559 1.0000000
P 3 1.00
9.4390000 0.0381090

```
      2.0020000           0.2094800
      0.5456000           0.5085570
P   1   1.00
      0.1517000           1.0000000
P   1   1.00
      0.0404100           1.0000000
P   1   1.00
      0.0108000           1.0000000
P   1   1.00
      0.002886414         1.0000000
P   1   1.00
     0.000771425          1.0000000
D   1   1.00
      0.5500000           1.0000000
D   1   1.00
      0.1510000           1.0000000
D   1   1.00
      0.0415000           1.0000000
D   1   1.00
      0.011405629         1.0000000
D   1   1.00
      0.00313466          1.0000000
****
```

To use our specifically designed basis set using the Gaussian quantum chemistry computation code we can use Gen keyword and the route line would be: #p CCSD(T)/Gen. Our effort to obtain this dipole bound state is not successful as yet. But we have made successful high level computation with results which we were not able to find anywhere in the literature. The neutral C_6H is an open-shell doublet state. This caused a major problem in optimization of this molecule using MP2 level of theory and aug-cc-pVDZ. This doublet state should have a sigma symmetry orbital on the carbon atom on the right as it's a singly occupied SOMO. However, it may indeed be possible that there

is a low-lying state in which one electron is moved from the pi-orbital manifold into the sigma orbital on the rightmost carbon atom to produce a doublet state of Π symmetry. If there is such a state and if it is close to the sigma ground state in energy, this could produce a bending symmetry vibration having imaginary frequency (i.e., a second order Jahn Teller instability). The extra electron could enter the half-filled sigma symmetry orbital on the rightmost C atom to form a closed-shell singlet state (this is similar to HCC, whose anion HCC- has the extra electron in the rightmost C atom's sigma orbital) or B. The extra electron could enter a dipole bound orbital localized on the left side of C_6H. This is because the ground state neutral is doublet and its description by a single determinant is probably not correct. The ground anionic state seems to be easy to obtain, as the excess electron closes the shell in this case and the closed-shell singlet is the product. However, the dipole-bound anionic state will have its excess electron on a different orbital. Hence, the shell will remain open which means that the dipole-bound state will be either open-shell singlet or triplet.[123] Figure 3.19 is the illustration of the population analysis of the $[C_6H]^-$ which resembles the dipole bound anion molecular orbital features.

Table 3.3: Optimized geometry of the ground state of neutral and negative ion of C_6H, obtained from different types of calculations and using different size basis sets. In all calculations the Int=UltraFine and SCF = (NoVarAcc,tight,NoIncFock) conditions has been applied.

	Method/basis set	Equilibrium geometry
Neutral	UMP2(FUll)/cc-pVDZ	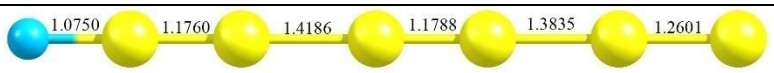
	UMP2(Full)/aug-cc-pVDZ	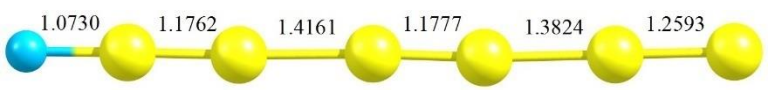
	UMP2/6-311++G(2d,2p)	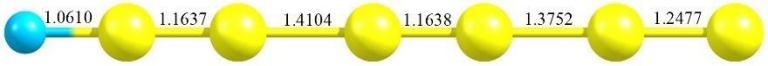
	MP2(Full)/aug-cc-pVTZ	
	B3LYP/aug-cc-pVTZ	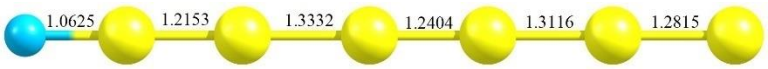
	UB3LYP/6-311++G(3df,3pd)	
	CBS-QB3	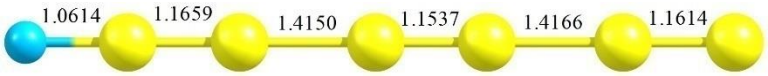
	CBS-APNO	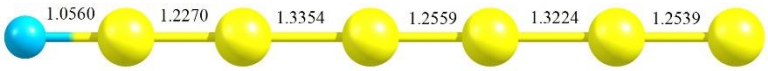
	W1RO	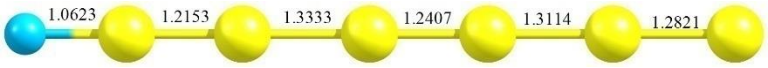
	MP2(Full)/aug-cc-pV5Z	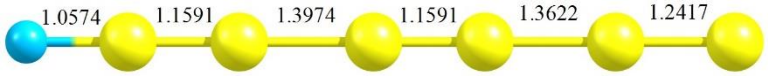
	UMP2(Full)/6-311++G(3df,3pd)	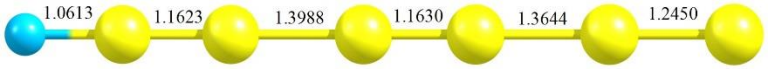
Anion	MP2(Full)/aug-cc-pVTZ	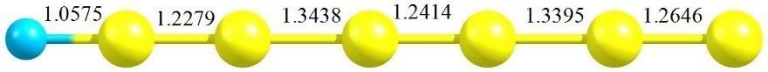
	UMP2(Full)/aug-cc-pVTZ	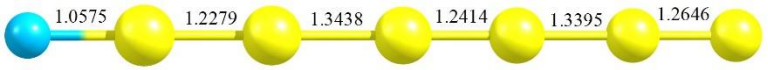
	CBS-QB3	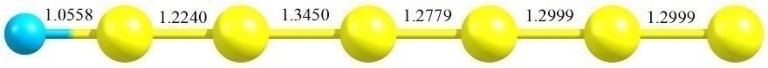
	CBS-APNO	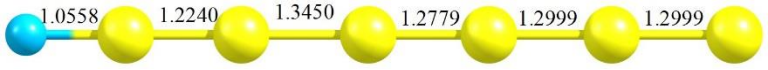
	UB3LYP/6-311++G(3df,3pd)	
	wB97XD/aug-cc-pVTZ	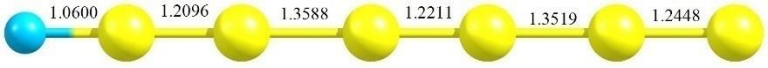

Table 3.4: W1RO energy components for top C_6H and bottom $[C_6H]^-$ for Temperature = 298.15 and Pressure = 1.00 Pa. Adiabatic electron affinity according to this calculation is 3.87 eV.

	SCF	CCSD	CCSD(T)
AVDZ+2d	-227.515519	-228.264919	-228.309524
AVTZ+2df	-227.569258	-228.444509	-228.502821
AVQZ+2df	-227.581157	-228.493568	
	NR/FC	DKH/Full	
MTsmall	-228.517001	-228.906375	

Extrapolated Energy Components

SCF	CCSD	CCSD(T)
-227.584859	-0.936775	-0.063407

Core + Scalar Relativistic Component: -0.389374

W1RO Electronic Energy -228.974416

E(ZPE)=	0.034320	E(Thermal)=	0.040691
W1RO (0 K)=	-228.940096	W1RO Energy=	-228.933725
W1RO Enthalpy=	-228.932781	W1RO Free Energy=	-228.968028

	SCF	CCSD	CCSD(T)
AVDZ+2d	-227.617858	-228.396687	-228.444195
AVTZ+2df	-227.671301	-228.580435	-228.642406
AVQZ+2df	-227.683223	-228.631002	
	NR/FC	DKH/Full	
MTsmall	-228.651082	-229.040903	

Extrapolated Energy Components

SCF	CCSD	CCSD(T)
-227.686932	-0.973115	-0.067347

Core + Scalar Relativistic Component: -0.389821

W1RO Electronic Energy -229.117216

E(ZPE)=	0.034854	E(Thermal)=	0.041084
W1RO (0 K)=	-229.082362	W1RO Energy=	-229.076132
W1RO Enthalpy=	-229.075187	W1RO Free Energy=	-229.109252

Table 3.5: CBS-APNO calculations for top C_6H and bottom $[C_6H]^-$ for Temperature = 298.15 K and Pressure = 1.00 Pa. Adiabatic electron affinity according to this calculation is 4.11 eV.

E(ZPE)	0.029998	E(Thermal)	0.036834
E(SCF)	-227.614189	DE(SCF)	-0.002362
DE(MP2)	-0.773216	DE(CBS)	-0.060873
DE(QCI)	-0.132273	DE(Int)	0.021257
DE(Core)	-0.325168	DE(Empirical)	-0.009122
CBS-APNO (0 K)	-228.865949	CBS-APNO Energy	-228.859113
CBS-APNO Enthalpy	-228.858169	CBS-APNO Free Energy	. -228.894070
E(ZPE)	0.036051	E(Thermal)	0.041985
E(SCF)	-227.683055	DE(SCF)	-0.002300
DE(MP2)	-0.932555	DE(CBS)	-0.070017
DE(QCI)	-0.058313	DE(Int)	0.027474
DE(Core)	-0.324384	DE(Empirical)	-0.009937
CBS-APNO (0 K)	-229.017037	CBS-APNO Energy	-229.011103
CBS-APNO Enthalpy	-229.010159	CBS-APNO Free Energy	-229.043747

Table 3.6: CBS-QB3 calculations for top C_6H and bottom $[C_6H]^-$ for Temperature = 298.15 K and Pressure = 1.00 Pa. Adiabatic electron affinity according to this calculation is 4.10 eV.

E(ZPE) =	0.037378	E(Thermal) =	0.043037
E(SCF) =	-227.598410	DE(MP2) =	-0.738639
DE(CBS) =	-0.071016	DE(MP34) =	-0.051787
DE(CCSD) =	-0.076569	DE(Int) =	0.023353
DE(Empirical) =	-0.045667		
CBS-QB3 (0 K) =	-228.521357	CBS-QB3 Energy =	-228.515698
CBS-QB3 Enthalpy =	-228.514753	CBS-QB3 Free Energy =	-228.548424

E(ZPE)=	0.034877	E(Thermal)=	0.041176
E(SCF)=	-227.665020	DE(MP2)=	-0.900003
DE(CBS)=	-0.082851	DE(MP34)=	-0.009901
DE(CCSD)=	-0.044374	DE(Int)=	0.030746
DE(Empirical)=	-0.035731		
CBS-QB3 (0 K)=	-228.672257	CBS-QB3 Energy=	-228.665958
CBS-QB3 Enthalpy=	-228.665014	CBS-QB3 Free Energy=	-228.699163

Table 3.7: Summary of dipole moment and adiabatic electron affinity for C_6H and $[C_6H]^-$.

Method/Basis set	Dipole Moment (**Debye**)		Rotational constant (**GHZ**)		Ground state electronic energy + ZPE (Hartree)		Adiabatic electron affinity (eV)
	NEUT	NI	NEUT	NI	NEUT	NI	
UMP2(FUll)/cc-pVDZ	4.5593	8.4423	1.371260	1.333976	-228.1306	-228.3333	**5.51**
MP2(Full)/aug-cc-pVTZ	4.7210	8.7887	1.412205	1.377984	-228.4452	-228.6587	**5.81**
UMP2(Full)/aug-cc-pVTZ	4.7209	8.7887	1.412203	1.3779913	-228.4452	-228.6587	**5.81**
B3LYP/aug-cc-pVTZ	6.0532	8.2617	1.396004	1.387451	-228.9889	-229.1226	**3.64**
UB3LYP/6-311++G(3df,3pd)	6.0557	8.2481	1.396869	1.388003	-228.9822	-229.1163	**3.65**
UMP2(Full)/6-311++G(3df,3pd)	4.7074	8.8009	1.408165	1.373302	-228.4607	-228.6733	**5.78**
wB97XD/aug-cc-pVTZ	5.9279	9.0368	1.39753	1.387313	-228.8727	-229.0061	**3.63**
B3LYP/6-311++G(3df,3pd)	6.0493	8.2480	1.39662	1.388016	-228.9826	-229.1163	**3.64**
CBS-QB3	5.8683	7.7775	1.3902078	1.3818995	-228.529711	-228.67221	**3.88**
W1RO	5.9877	8.0500	1.3957147	1.3876993	-228.9401	-229.08236	**3.87**
W1BD	5.9877	8.0500	1.3957164	1.3876981	-228.93988	-229.0820	**3.87**
W1U	5.9877	8.0500	1.3957147	1.3877013	-228.941101	-229.08236	**3.84**

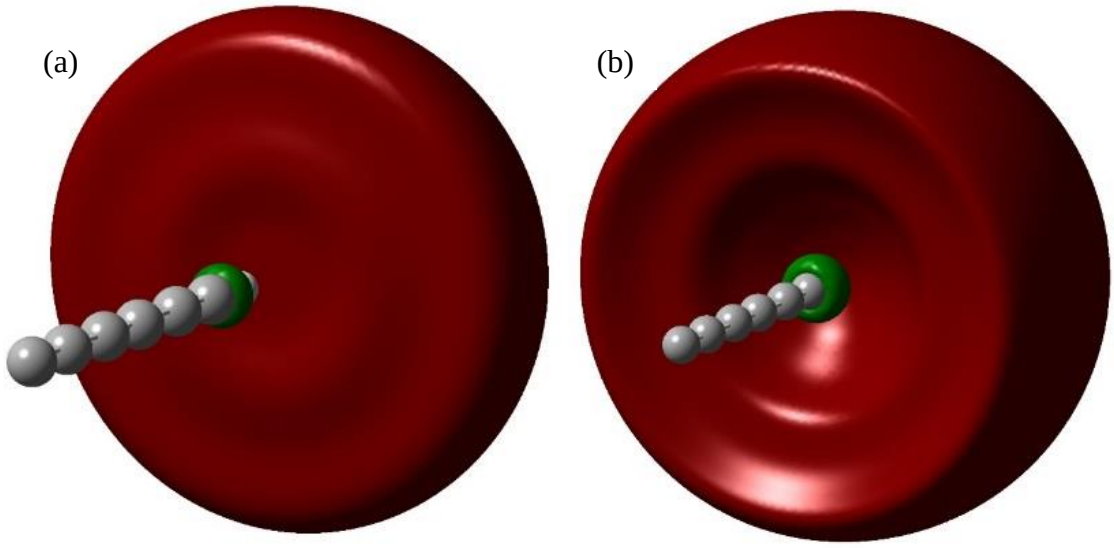

Figure 3.19: Population analysis of $[C_6H]^-$ using MP2/aug-cc-pVQZ level of theory. Both figures are the lowest unoccupied molecular orbital of the anion. (a) LUMO IsoValue = 0.015 (b) LUMO IsoValue = 0.008.

3.13 Pressure Dependence

The accuracy of the results and bond energy dissociations obtained from threshold energy resolved collision induced dissociation experiments is a function of the pressure of neutrals in the collision cell and if indeed the single collision criteria is the case. Often this would not be practical and that is when the extrapolation to zero pressure is necessary. That requires one to do the experiment at a few different pressure and then extrapolate the intensities to zero pressure (perhaps a linear extrapolation would work). Below is an example of this procedure for trans 2,2́,6,6́-tetrafluoroazobenzene. We performed the experiment at 35 and 52 microTorr and linearly extrapolated the result for precursor ion intensity to zero pressure. Doing so would make sure the obtained results are due to single collisions which is the basics of any deconvolution program such as Crunch program. Each and every collision in multiple collision scheme can deposit some energy

in the precursor ion (and also in neutral gas in the collision cell) and the threshold energy resulting from this experiment would not be reliable to obtain the dissociation energy.

Collision cell pressure can also influence the fragment ion intensities as well. In theory if a fragment ion is due the multiple-collision process, its intensity should increase by increasing the pressure of neutral gas in the collision cell. Below we presented an example of how the intensity of precursor and fragment ions change by changing the pressure. Without removing the contribution from multipole collisions, the measured threshold will be too small.[1]

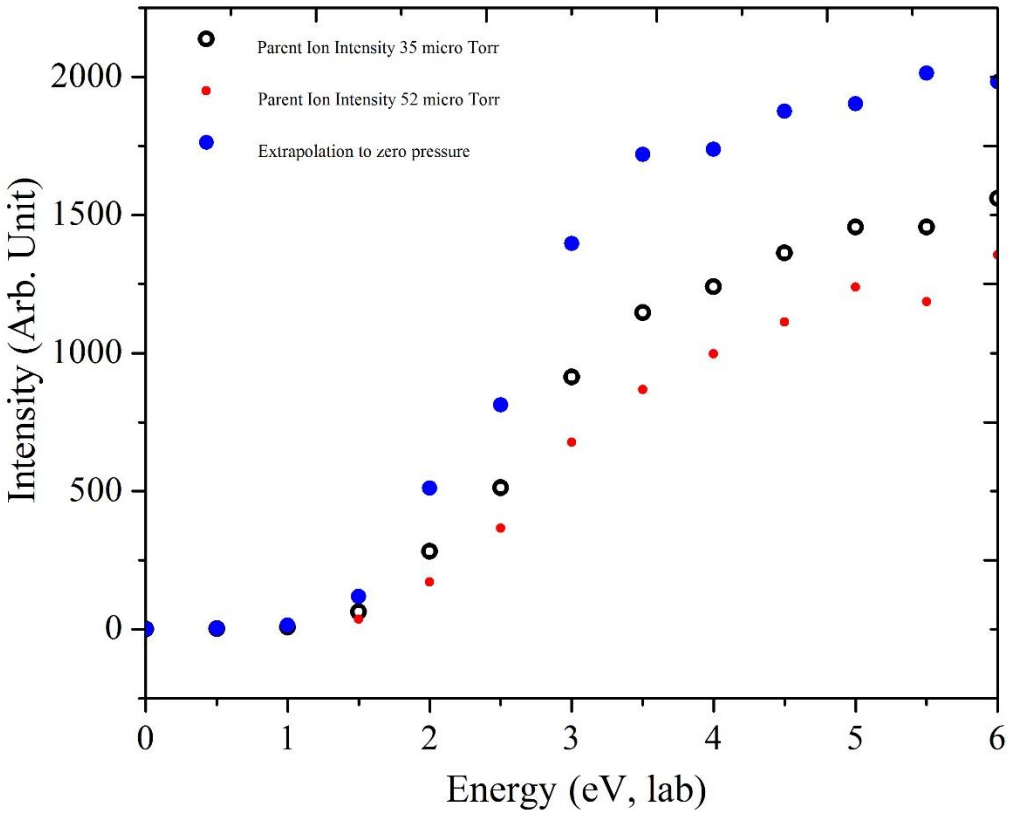

Figure 3.20: zero pressure extrapolation for the 2,2́,6,6́-tetrafluoroazobenzene precursor ion. We can see the effect of pressure on the precursor ion intensity.

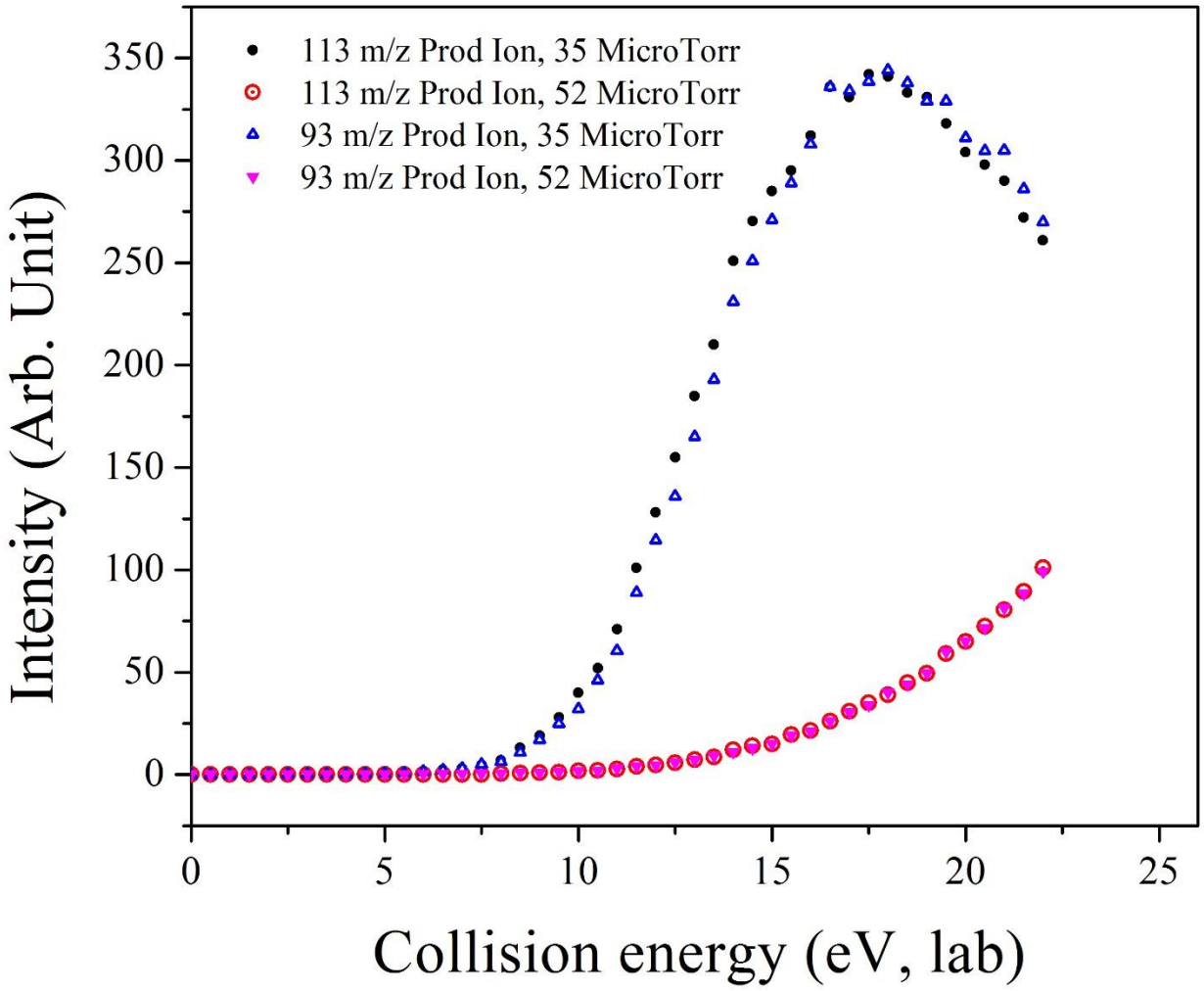

Figure 3.21: Pressure dependence of product ions 113 m/z and 93 m/z from the 2,2́,6,6́-tetrafluoroazobenzene CID experiment. The intensity of products in 35 and 52 micro Torr shows they are almost identical which means there is no multiple collisions (or pressure dependence).

3.14 Collision Induced dissociation of azobenzene experiment:

Azobenzene was the original sample investigated in this research. We tried electro-spray ionization (ESI) method to ionize azobenzene but was not unable to generate negative ion of azobenzene. Then we changed the ionization method to atmospheric pressure chemical ionization APCI which is slightly harder method comparing to ESI and it was able to produce parent negative ions. Figure 20 shows the azobenzene precursor anion intensity as a function of collision energy in the laboratory frame. We have not observed any fragment ion with significant intensity for analysis. There are two peaks at m/z = 154 and m/z = 168. The m/z =154 is biphenyl negative ion and we are not sure at this point about the nature of this anion since our computational investigations showed this anion might be stable and exist and the experimental intensity is extremely weak. Further investigation on this subject is currently ongoing and the confirmation requires more experimental and precision computations. For the completeness here we provide a few results regarding the biphenyl negative ion which was observed with extremely weak intensity in our experimental results here. The CID experiments were carried out using an AB Sciex QSTAR Elite Hybrid LC/MS/MS apparatus which is a hybrid quadruple/time-of-flight mass spectrometer equipped with an atmospheric pressure chemical ionization (APCI) ion source. Negative ions are generated under atmospheric pressure conditions at high temperature, 573 K, using a corona discharge. Low energy electron attachment to the molecule is followed by collisional stabilization in a bath gas. Anions are introduced to the instrument using nitrogen as the curtain gas. A major source of uncertainty here is the fact that the internal energies of the anions are not well characterized. Azobenzene solution in methanol with 2 μg/ml concentration was used.

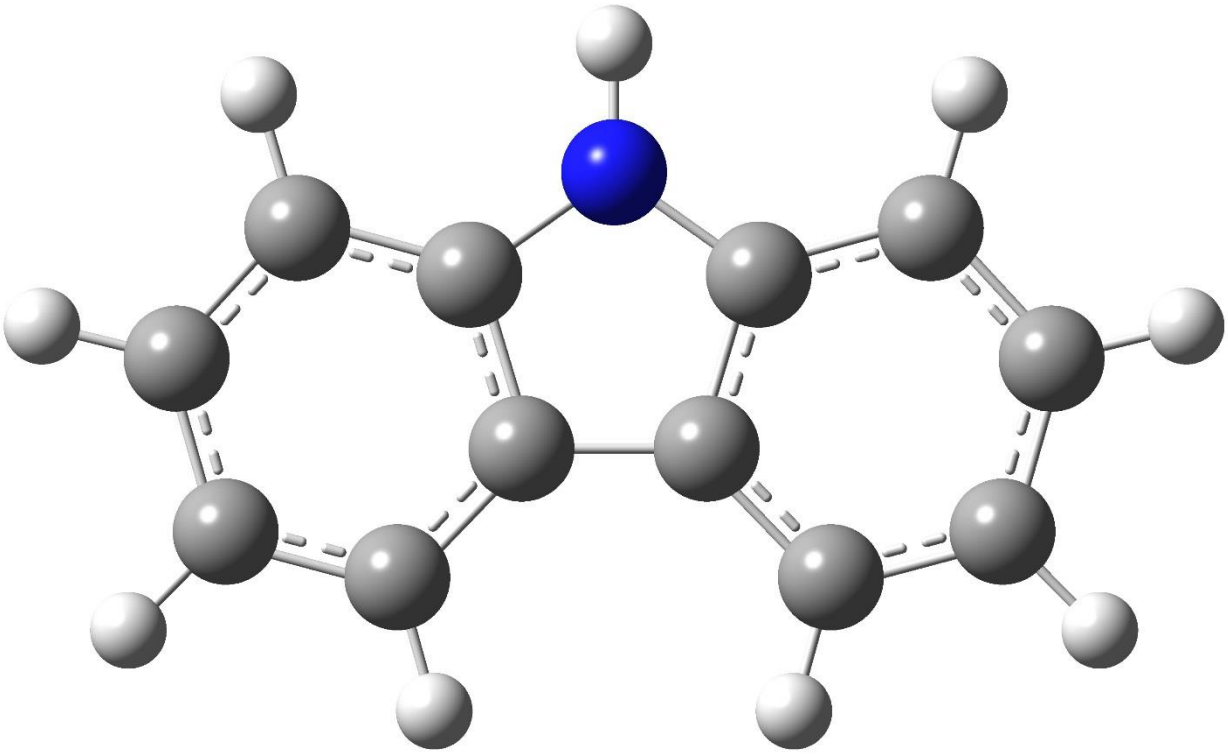

Figure 3.22: The optimized structure of $C_{12}H_{10}N$; m/z = 168; which we have observed as very weak signal. The calculations in B3LYP level of theory along with 6-311++G(d,p) yields -0.14 eV for its adiabatic electron affinity which means it is not a bond structure.

As we can infer the these results provided in Table 3.8, only B3LYP level of theory by considering the zero point energy does yield a bound state for the negative ion of biphenyl. All other calculations also showed that no bound state can form. This matter is under further investigations at this moment. Even though we have done different type of calculations for the biphenyl anion (which we have observed a very weak signal for it in the dissociation spectrum), only B3LYP level of theory with bigger basis set size such as 6-311++G(d,p) and larger than that resulted in a weakly bound state (in the order of ~30 meV) and that occurred by adding the ZPE to the calculated energy at 0 K. This matter is still under investigation but high level calculation such CBS multilevel method did not result a bound state. The unbound state is extremely weak as well (~0.1 eV).

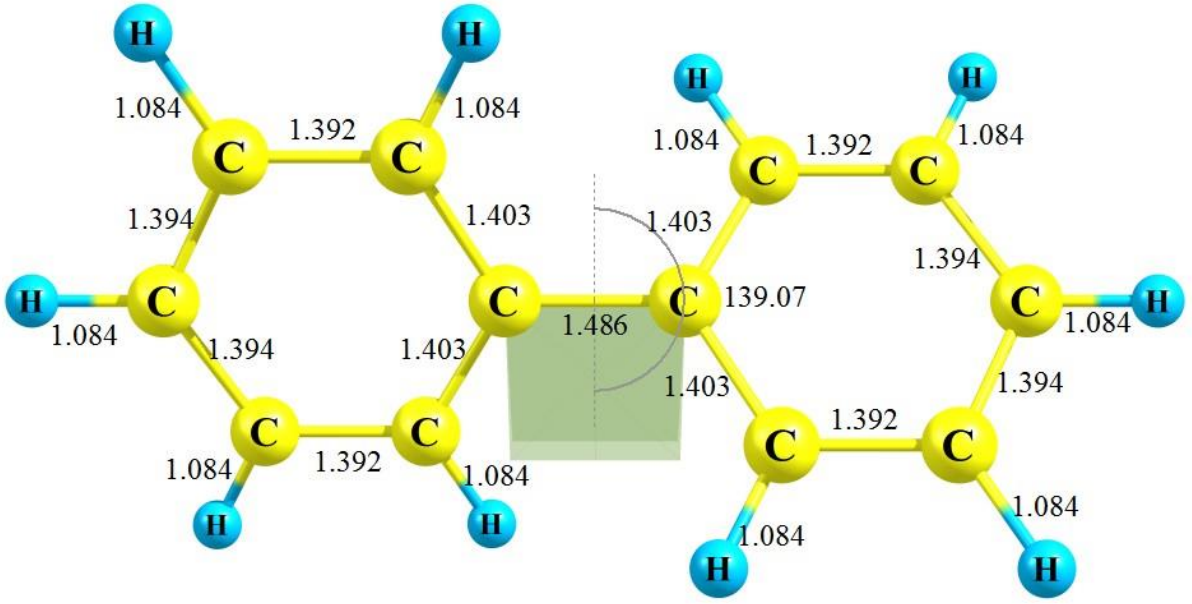

(a)

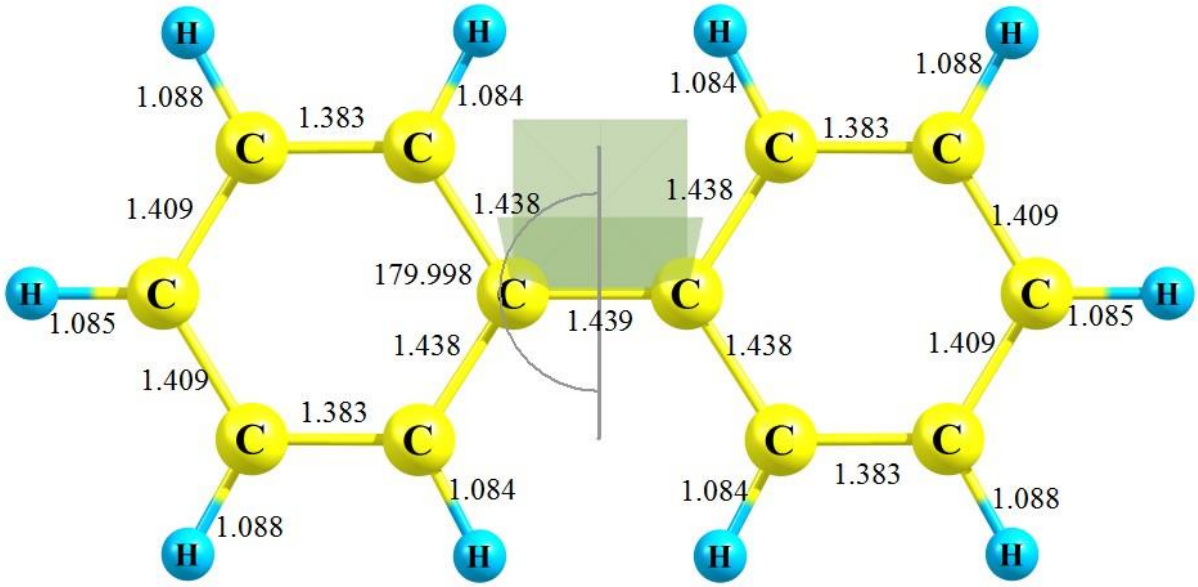

(b)

Figure 3.23: Optimized geometry of Biphenyl (a) neutral and (b) negative ion, in B3LYP level of theory with 6-311++G(d,p). The CCCC dihedral is shown which is 179.998 for the negative ion and 139.07 for the neutral. Only B3LYP type calculations resulted in a weakly bond structure for the negative ion.

Table 3.8: Summary of energy calculations for the Biphenyl and its potentially possible anion. (a) Sum of electronic and zero-point Energies (b) Sum of electronic and thermal energies (c) Sum of electronic and thermal enthalpies (d) Sum of electronic and thermal free energies. Dipole moments are in Debye and adiabatic electron affinities (AEA) are in eV.

	NEUT					NI					
Method/Basis set	(a)	(b)	(c)	(d)	Dipole	(a)	(b)	(c)	(d)	Dipole	AEA
B3LYP/6-311++G(d,p)	-463.2421	-463.2331	-463.2322	-463.2768	0.00	-463.2434	-463.2347	-463.2337	-463.2779	0.00	0.035
B3LYP/6-311++G(2d,2p)	-463.2595	-463.2506	-463.2497	-463.2929	0.00	-463.2607	-463.2512	-463.2502	-463.2971	0.00	0.033
B3LYP/aug-cc-pVTZ	-463.2893	-463.2804	-463.2795	-463.3239	0	-463.2907	-463.2812	-463.2802	-463.327	0.00	0.038
wB97XD/6-311++G(d,p)	-463.0685	-463.0596	-463.0587	-463.103	0.00	-463.0621	-463.0526	-463.0517	-463.0984	0.00	-0.174
wB97XD/aug-cc-pVDZ	-463.0094	-463.0005	-462.9996	-463.0440	0.00	-463.0037	-462.9945	-462.9936	-463.0392	0.00	-0.155
MP2(Full)/aug-cc-pVDZ	-461.7763	-461.7671	-461.7662	-461.8106	0	-461.7487	-461.7394	-461.7385	-461.7843	0.00	-0.751
CBS-QB3	-462.4144	-462.4054	-462.4044	-462.4491	0.00	-462.4080	-462.3984	-462.3974	-462.4441	0.00	-0.174

Figure 3.24: Population analysis of biphenyl negative ion using B3LY level of theory with 6-311++G(2d,2p) basis set. (a) LUMO + 1 (b) LUMO (c) HOMO (d) HOMO -1. IsoValue is 0.02 and Density is 0.0004.

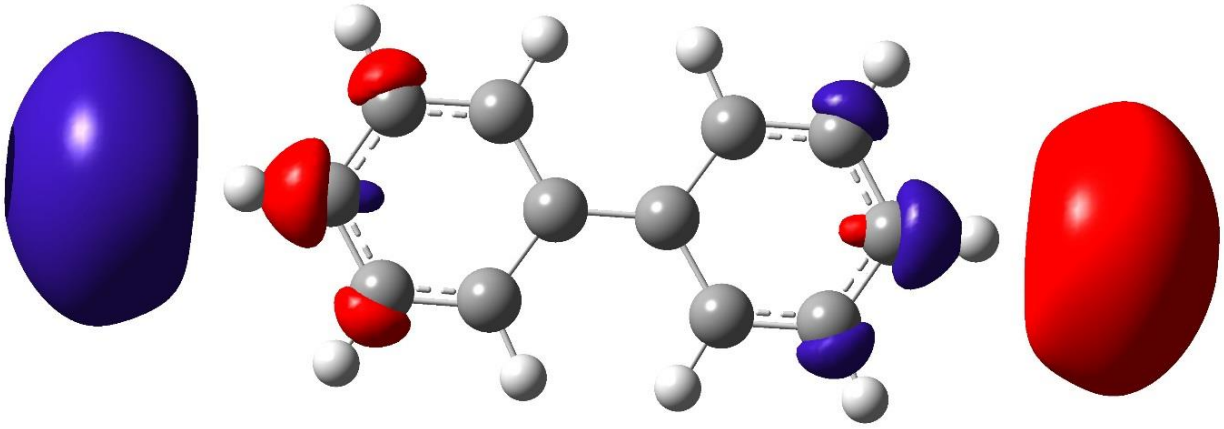

(a)

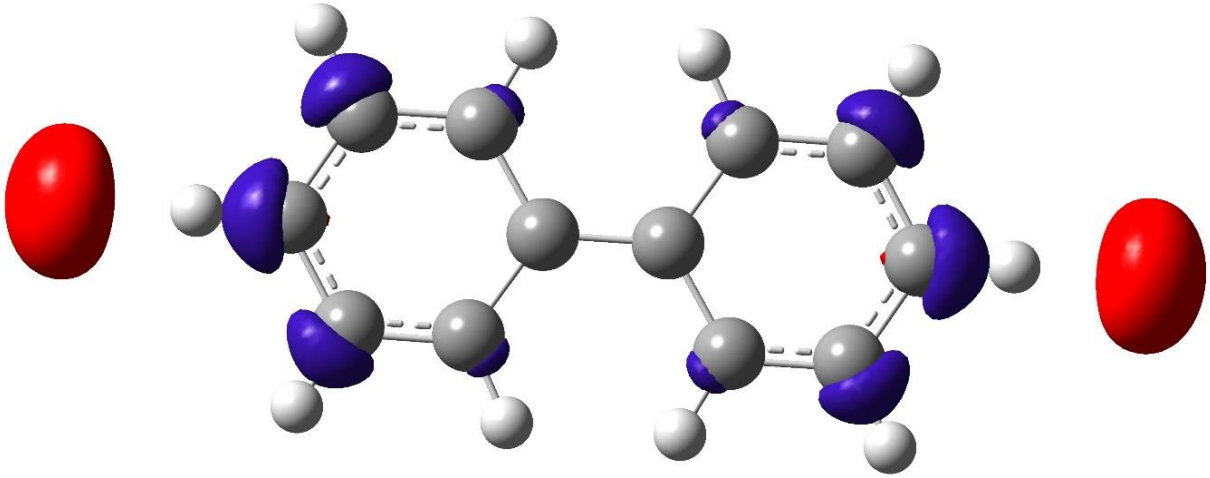

(b)

Figure 3.24: Continued

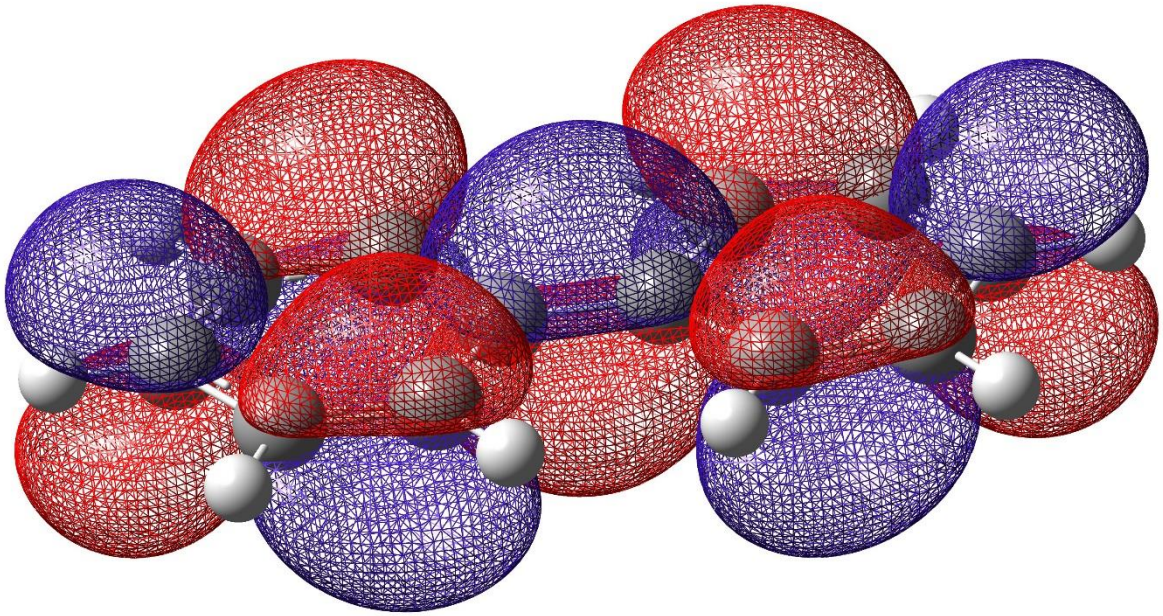

(c)

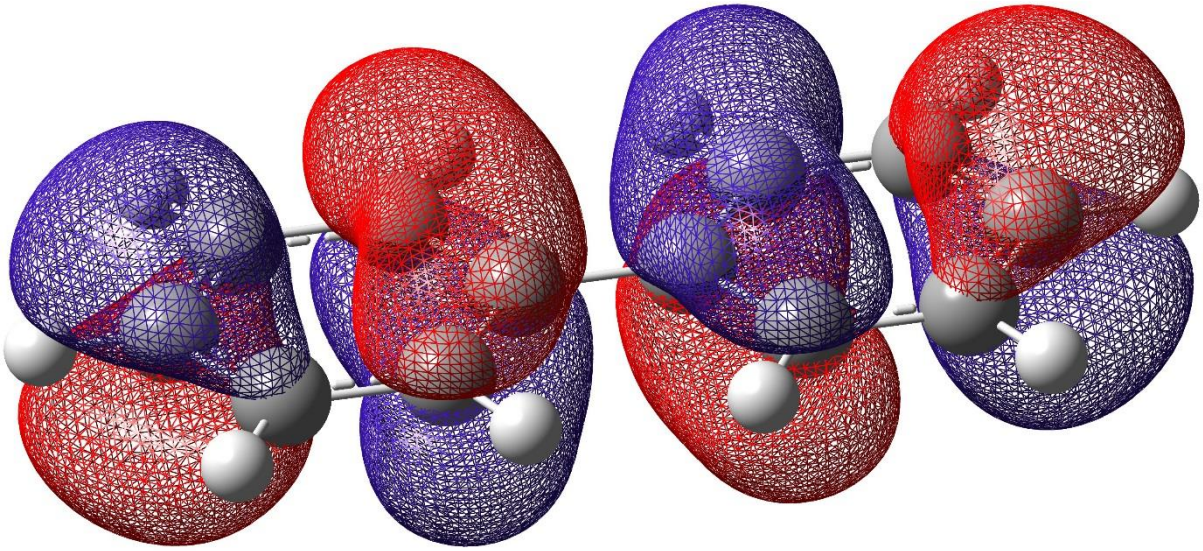

(d)

Figure 3.24: Continued

Besides our experiments in negative mode and looking for azobenzene anion, we have performed this experiment in positive mode and we found that the protonated azobenzene makes a positive ion with extremely high intensity of the precursor ion. This totally make sense since according to our calculations the proton affinity is in the order of ~10 eV. The major product ion is m/z =77 which is $[C_6H_5]^+$; phenyl cation; breaking of the C-N bond. We have not yet had the chance to perform quantitative analysis on the cross sections from energy resolved dissociation measurements to obtain the physical value for the threshold energy required for this bond dissociation. Preliminary results shows rearrangement in the neutral fragment. For the qualitative purposes and the completeness of the results we provided the mass spectrums of this dissociation experiment in different collision energies below. We have presented the data related to proton affinity of azobenzene in the computational sections. This experiment has been performed using the APCI source and each one of data points for each collision energy has been averaged over 1 minutes of data acquisition. The concentration is 2 μg/ml in methanol.

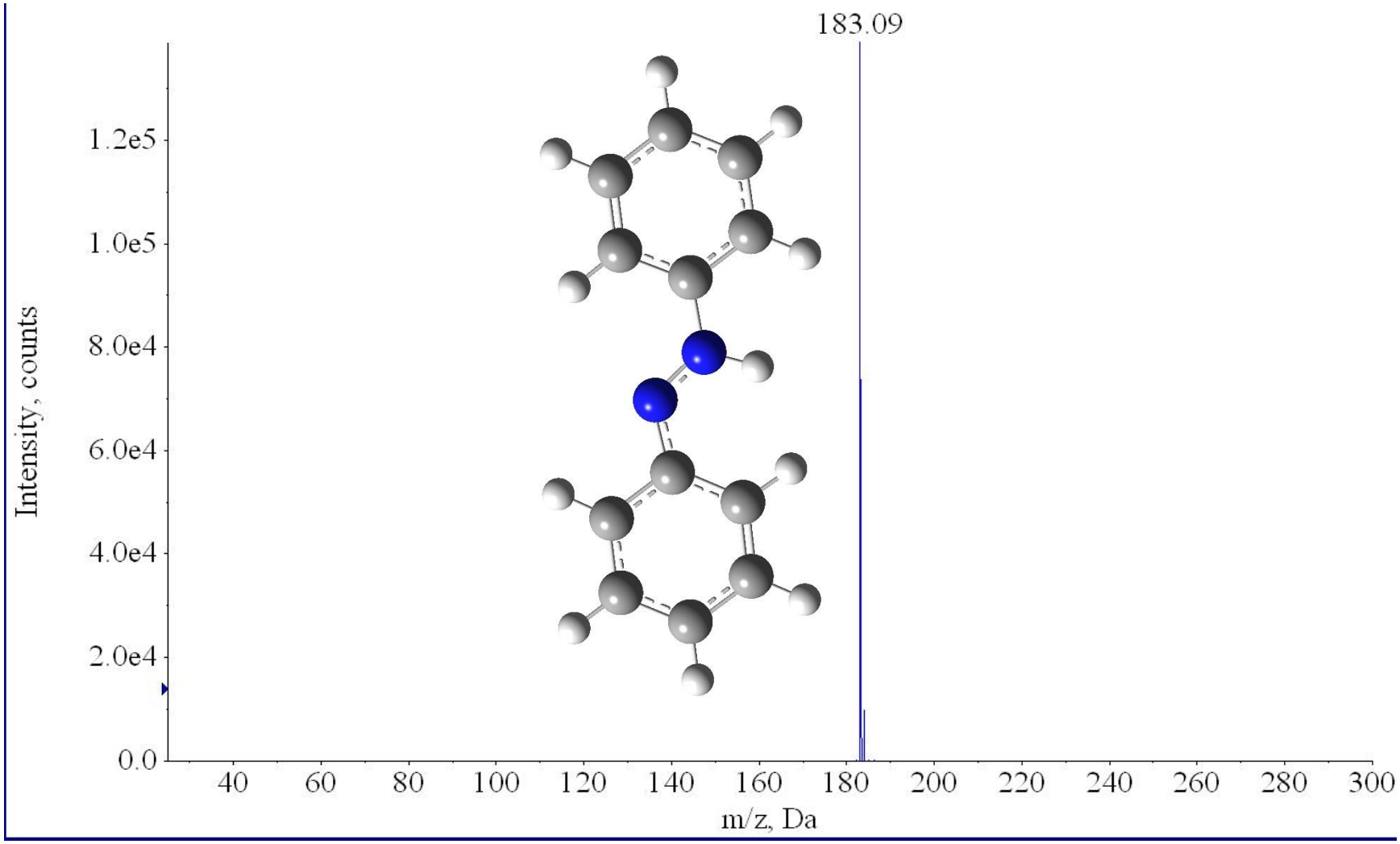

Figure 3.25: Mass spectrum (positive mode) of trans azobenzene ($C_{12}H_{10}N_2$, parent neutral Molecular Weight: 182.22 Da) at **2 eV** translational collision energy in the laboratory frame (CID experiment) and the parent cation is illustrated. This is in positive mode.

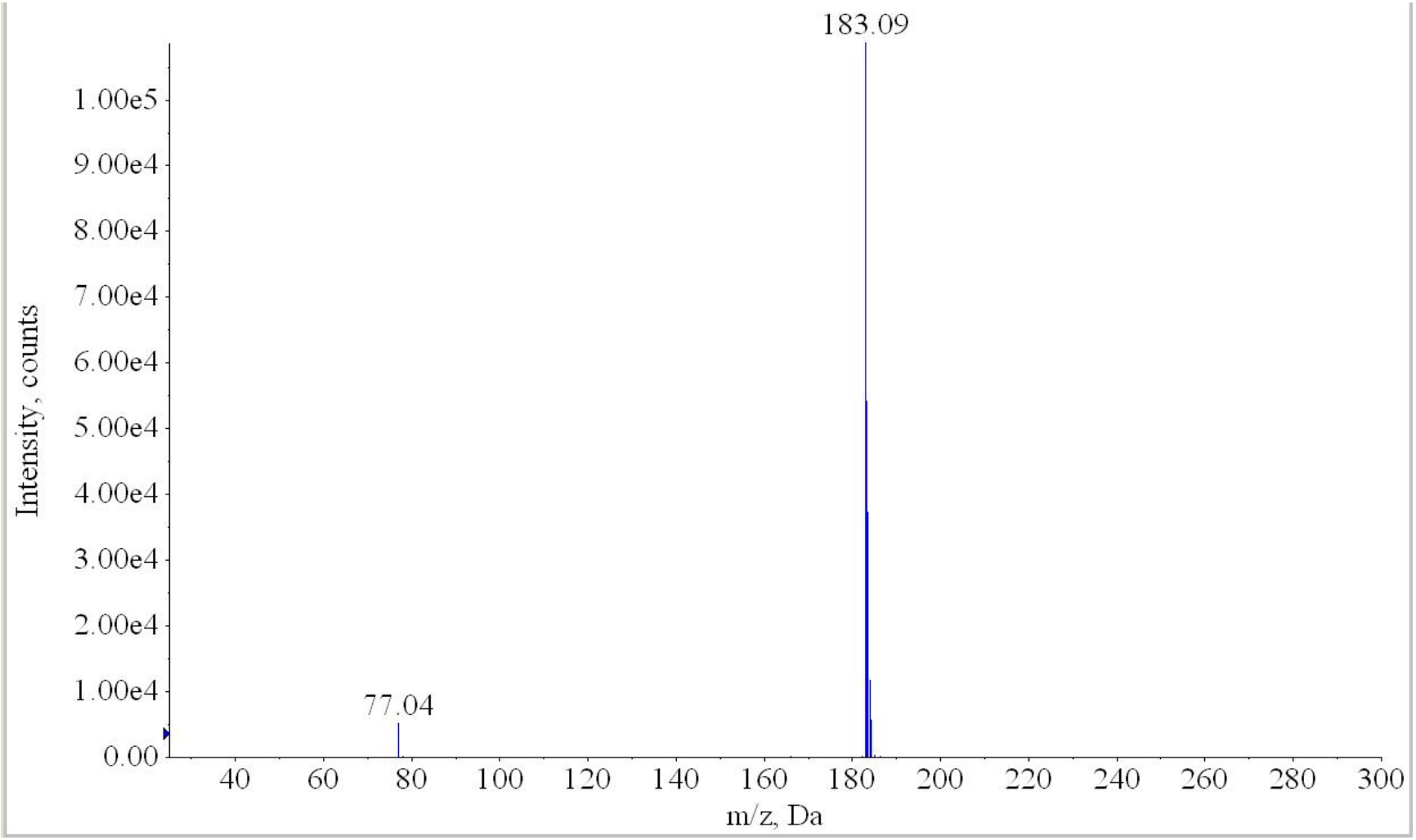

Figure 3.26: Mass spectrum (positive mode) of trans azobenzene at **8 eV** translational collision energy in the laboratory frame. Notice the intensity of the precursor ion is extremely high especially in compare to the negative ion case.

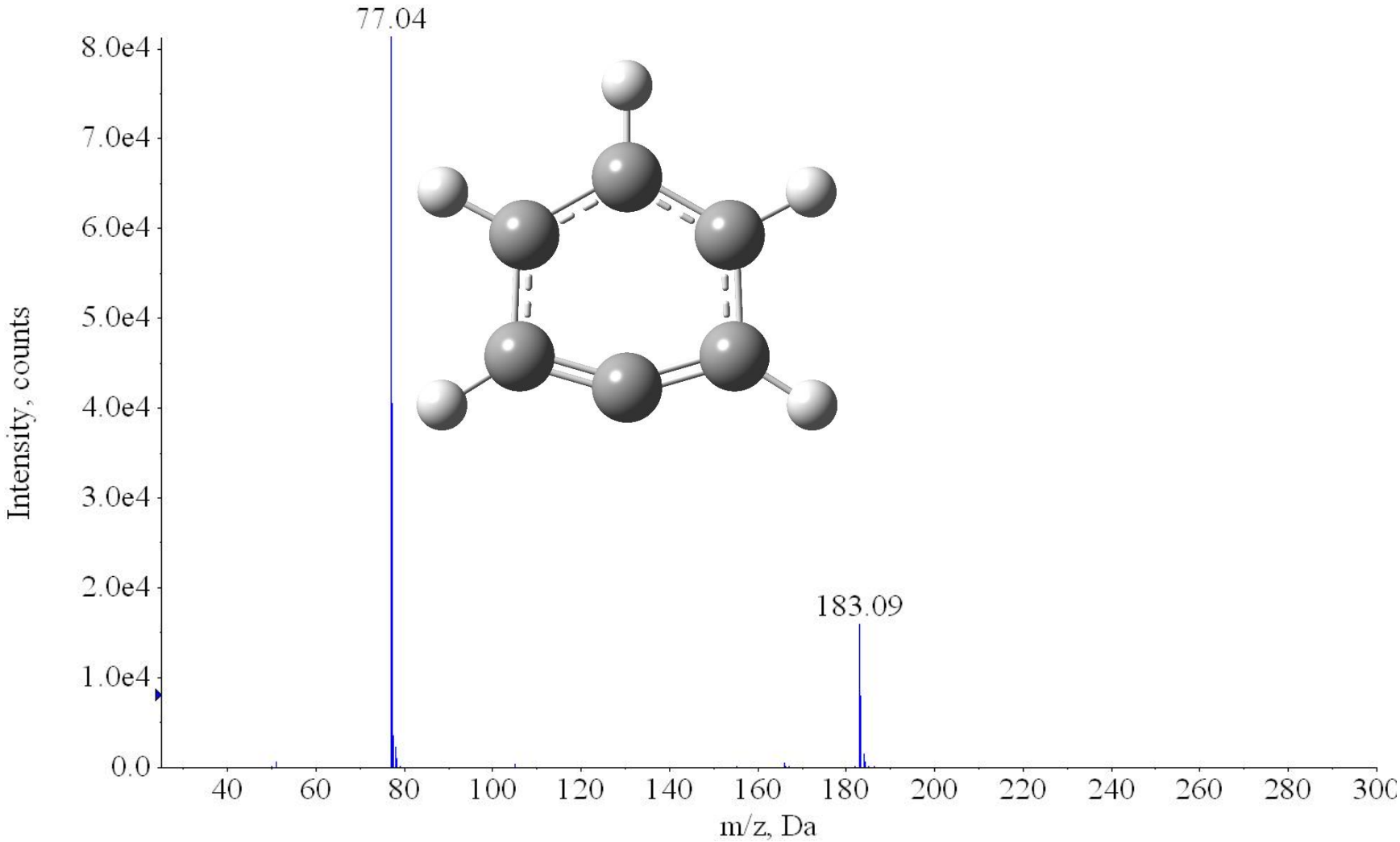

Figure 3.27: Mass spectrum (positive mode) of trans azobenzene at **15 eV** translational collision energy in the laboratory frame. The first fragment ion which its intensity starts increasing is m/z =77 C_6H_5 which is illustrated.

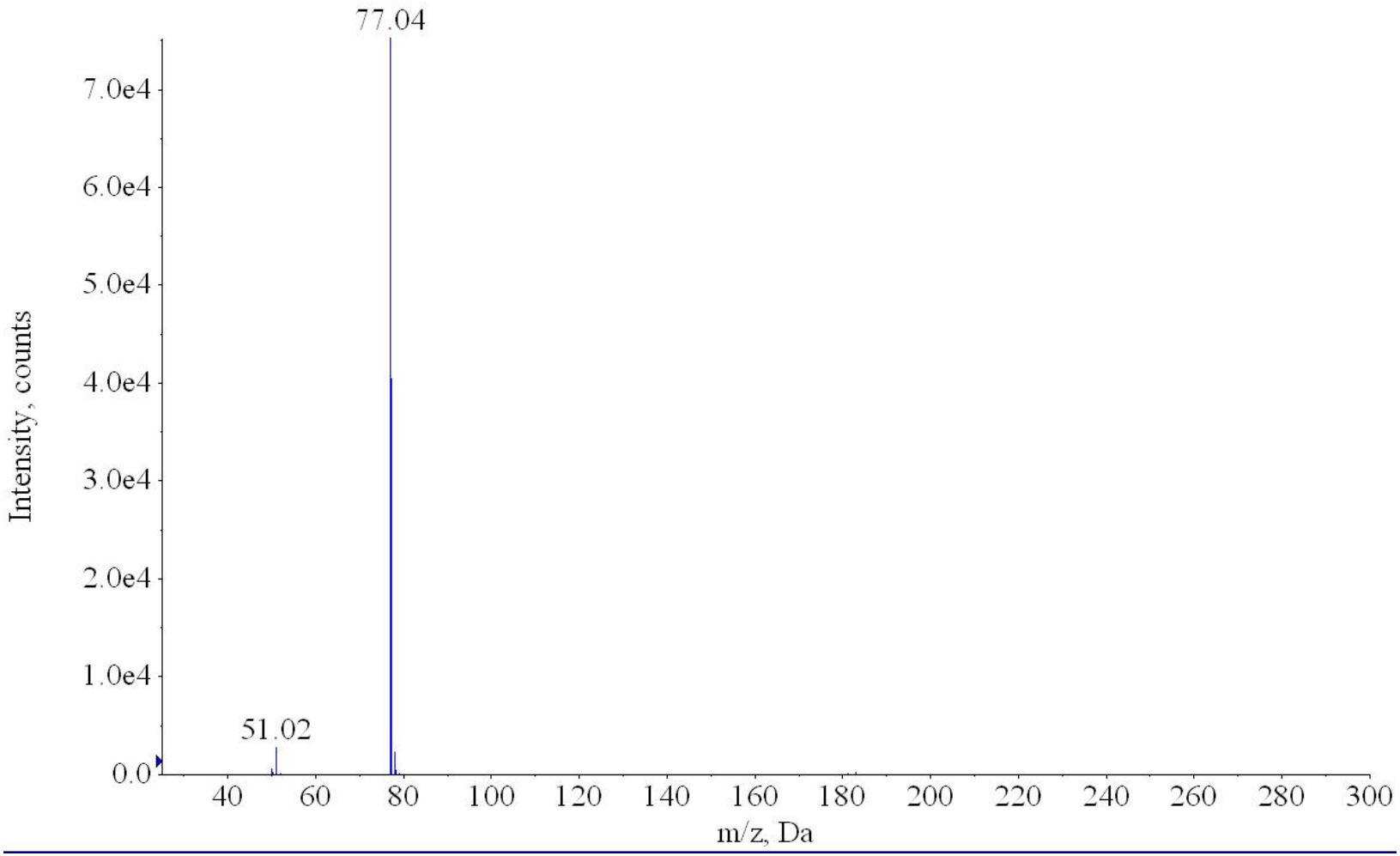

Figure 3.28: Mass spectrum (positive mode) of trans azobenzene at **22** eV translational collision energy in the laboratory frame. The fragment ion m/z =51.02 is possibly C_4H_3.

References

1. P. Armentrout, in *Modern Mass Spectrometry* (Springer, 2003), pp. 233-262.
2. J. Simons and K. D. Jordan, Chemical Reviews **87** (3), 535-555 (1987).
3. R. J. Bartlett and G. D. Purvis III, Phys Scripta **21** (3-4), 255 (1980).
4. G. D. Purvis III and R. J. Bartlett, The Journal of Chemical Physics **76** (4), 1910-1918 (1982).
5. J. Pople, R. Krishnan, H. Schlegel and J. Binkley, Int J Quantum Chem **14** (5), 545-560 (1978).
6. G. E. Scuseria, C. L. Janssen and H. F. Schaefer Iii, The Journal of Chemical Physics **89** (12), 7382-7387 (1988).
7. G. E. Scuseria and H. F. Schaefer III, The Journal of Chemical Physics **90** (7), 3700-3703 (1989).
8. J. A. Pople, M. Head-Gordon and K. Raghavachari, The Journal of chemical physics **87** (10), 5968-5975 (1987).
9. J. Gauss and D. Cremer, Chemical physics letters **150** (3), 280-286 (1988).
10. E. Salter, G. W. Trucks and R. J. Bartlett, The Journal of Chemical Physics **90** (3), 1752-1766 (1989).
11. J. A. Pople, M. Head-Gordon, D. J. Fox, K. Raghavachari and L. A. Curtiss, The Journal of Chemical Physics **90** (10), 5622-5629 (1989).
12. L. A. Curtiss, K. Raghavachari, G. W. Trucks and J. A. Pople, The Journal of chemical physics **94** (11), 7221-7230 (1991).
13. L. A. Curtiss, P. C. Redfern and K. Raghavachari, The Journal of chemical physics **126** (8), 084108 (2007).
14. L. A. Curtiss, P. C. Redfern and K. Raghavachari, The Journal of chemical physics **127** (12), 124105 (2007).
15. L. A. Curtiss, P. C. Redfern and K. Raghavachari, Chemical Physics Letters **499** (1), 168-172 (2010).
16. M. R. Nyden and G. A. Petersson, J Chem Phys **75** (4), 1843-1862 (1981).
17. G. Petersson and M. A. Al-Laham, The Journal of chemical physics **94** (9), 6081-6090 (1991).
18. G. Petersson, T. G. Tensfeldt and J. Montgomery Jr, The Journal of chemical physics **94** (9), 6091-6101 (1991).

19. J. Montgomery Jr, J. Ochterski and G. Petersson, The Journal of chemical physics **101** (7), 5900-5909 (1994).

20. S. Parthiban and J. M. Martin, The Journal of Chemical Physics **114** (14), 6014-6029 (2001).

21. J. M. Martin and G. de Oliveira, The Journal of chemical physics **111** (5), 1843-1856 (1999).

22. A. Frisch, *Gaussian 09: User's Reference*. (Gaussian, 2009).

23. L. A. Curtiss, K. Raghavachari, P. C. Redfern, V. Rassolov and J. A. Pople, The Journal of Chemical Physics **109** (18), 7764-7776 (1998).

24. C. J. Cramer, *Essentials of computational chemistry: theories and models*. (John Wiley & Sons, 2013).

25. P. Hohenberg and W. Kohn, Phys Rev **136** (3B), B864 (1964).

26. J.-L. Calais, Int J Quantum Chem **47** (1), 101-101 (1993).

27. J.-D. Chai and M. Head-Gordon, Phys Chem Chem Phys **10** (44), 6615-6620 (2008).

28. J.-D. Chai and M. Head-Gordon, The Journal of chemical physics **128** (8), 084106 (2008).

29. Y. Zhao and D. Truhlar, Theor Chem Account **120** (1-3), 215-241 (2008).

30. S. Lias, J. Bartmess, J. Liebman, J. Holmes, R. Levin and W. Mallard, National Institute of Standards and Technology, Gaithersburg MD **20899** (2003).

31. S. Lias, J. Phys. Chem. Ref. Data **17** (1988).

32. S. G. Lias, J. Phys. Chem. Ref Data **17** (1) (1988).

33. J. Simons, *An introduction to theoretical chemistry*. (Cambridge University Press, 2003).

34. I. U. o. P. a. A. Chemistry, (2002).

35. M. Venturi, P. Vogel, H. Wong and H. Yamamoto, Combinatorial Chemistry **279** (2007).

36. N. A. Wazzan, P. R. Richardson and A. C. Jones, Photochemical & Photobiological Sciences **9** (7), 968-974 (2010).

37. E. Britannica, INC. Yayınları, C **9** (2000).

38. E. Mitscherlich, Annalen der Pharmacie **9** (1), 39-48 (1834).

39. T. A. Singleton, K. S. Ramsay, M. M. Barsan, I. S. Butler and C. J. Barrett, The Journal of Physical Chemistry B **116** (32), 9860-9865 (2012).

40. J. Garcia-Amoros and D. Velasco, Beilstein journal of organic chemistry **8**, 1003-1017 (2012).

41. G. Hartley, Nature **140**, 281 (1937).

42. S. Samanta, T. M. McCormick, S. K. Schmidt, D. S. Seferos and G. A. Woolley, Chemical Communications **49** (87), 10314-10316 (2013).

43. R. Siewertsen, H. Neumann, B. Buchheim-Stehn, R. Herges, C. Nather, F. Renth and F. Temps, Journal of the American Chemical Society **131** (43), 15594-15595 (2009).

44. A. Emoto, E. Uchida and T. Fukuda, Polymers **4** (1), 150-186 (2012).

45. S. Sawada, N. Kato and K. Kaihatsu, Current pharmaceutical biotechnology **13** (14), 2642-2648 (2012).

46. A. Goulet-Hanssens and C. J. Barrett, J Polym Sci Pol Chem **51** (14), 3058-3070 (2013).

47. Z. Mahimwalla, K. G. Yager, J.-i. Mamiya, A. Shishido, A. Priimagi and C. J. Barrett, Polymer bulletin **69** (8), 967-1006 (2012).

48. L. Rocha, C.-M. Păiuş, A. Luca-Raicu, E. Resmerita, A. Rusu, I.-A. Moleavin, M. Hamel, N. Branza-Nichita and N. Hurduc, Journal of Photochemistry and Photobiology A: Chemistry **291**, 16-25 (2014).

49. S. K. Yesodha, C. K. S. Pillai and N. Tsutsumi, Progress in Polymer Science **29** (1), 45-74 (2004).

50. O. S. Bushuyev, A. Tomberg, T. Friščić and C. J. Barrett, Journal of the American Chemical Society **135** (34), 12556-12559 (2013).

51. S. Gan, A. Yuvaraj, M. Lutfor, M. Mashitah and H. Gurumurthy, RSC Advances **5** (9), 6279-6285 (2015).

52. R. H. El Halabieh, O. Mermut and C. J. Barrett, Pure and applied chemistry **76** (7-8), 1445-1465 (2004).

53. S. M. Bachrach, *Computational organic chemistry*. (John Wiley & Sons, 2007).

54. P. Armentrout, The Journal of chemical physics **126** (23), 234302 (2007).

55. M. Rodgers, K. M. Ervin and P. Armentrout, The Journal of chemical physics **106** (11), 4499-4508 (1997).

56. S. Narancic, A. Bach and P. Chen, The Journal of Physical Chemistry A **111** (30), 7006-7013 (2007).

57. T. Baer and W. L. Hase, *Unimolecular reaction dynamics: theory and experiments*. (Oxford university press New York, 1996).

58. K. M. Ervin and P. Armentrout, Journal of mass spectrometry **39** (9), 1004-1015 (2004).

59. M. Rodgers and P. Armentrout, Mass spectrometry reviews **19** (4), 215-247 (2000).

60. G. F. Clifford Dykstra, Kwang Kim, Gustavo Scuseria, (Elsevier).

61. M. J. Frisch, G. W. Trucks, H. B. Schlegel, G. E. Scuseria, M. A. Robb, J. R. Cheeseman, G. Scalmani, V. Barone, B. Mennucci, G. A. Petersson, H. Nakatsuji, M. Caricato, X. Li, H. P. Hratchian, A. F. Izmaylov, J. Bloino, G. Zheng, J. L. Sonnenberg, M. Hada, M. Ehara, K. Toyota, R. Fukuda, J. Hasegawa, M. Ishida, T. Nakajima, Y. Honda, O. Kitao, H. Nakai, T. Vreven, J. A. Montgomery Jr., J. E. Peralta, F. Ogliaro, M. J. Bearpark, J. Heyd, E. N. Brothers, K. N. Kudin, V. N. Staroverov, R. Kobayashi, J. Normand, K. Raghavachari, A. P. Rendell, J. C. Burant, S. S. Iyengar, J. Tomasi, M. Cossi, N. Rega, N. J. Millam, M. Klene, J. E. Knox, J. B. Cross, V. Bakken, C. Adamo, J. Jaramillo, R. Gomperts, R. E. Stratmann, O. Yazyev, A. J. Austin, R. Cammi, C. Pomelli, J. W. Ochterski, R. L. Martin, K. Morokuma, V. G. Zakrzewski, G. A. Voth, P. Salvador, J. J. Dannenberg, S. Dapprich, A. D. Daniels, Ö. Farkas, J. B. Foresman, J. V. Ortiz, J. Cioslowski and D. J. Fox, (Gaussian, Inc., Wallingford, CT, USA, 2009).

62. A. Hinchliffe, *Molecular modelling for beginners*. (John Wiley & Sons, 2005).

63. E. Lewars, *Computational chemistry: introduction to the theory and applications of molecular and quantum mechanics*. (Springer Science & Business Media, 2010).

64. R. S. Mulliken, The Journal of Chemical Physics **23** (10), 1833-1840 (1955).

65. W. K. Jurgen Popp, Encyclopedia of Analytical Chemistry, Online © 2006 John Wiley & Sons, Ltd.

66. D. Young, *Computational chemistry: a practical guide for applying techniques to real world problems*. (John Wiley & Sons, 2004).

67. B. Mennucci, in *Computational Spectroscopy* (Wiley-VCH Verlag GmbH & Co. KGaA, 2010), pp. 151-171.

68. B. Valeur and M. N. Berberan-Santos, *Molecular fluorescence: principles and applications*. (John Wiley & Sons, 2012).

69. A. J. Adler, N. J. Greenfield and G. D. Fasman, Methods in enzymology **27**, 675-735 (1973).

70. A. J. Adler, N. J. Greenfield and G. D. Fasman, Methods in enzymology **27**, 675-735 (1972).

71. N. M. O'boyle, A. L. Tenderholt and K. M. Langner, J Comput Chem **29** (5), 839-845 (2008).

72. K. M. Tait, J. A. Parkinson, S. P. Bates, W. J. Ebenezer and A. C. Jones, Journal of Photochemistry and Photobiology A: Chemistry **154** (2), 179-188 (2003).

73. J. M. Wittbrodt and H. B. Schlegel, The Journal of chemical physics **105** (15), 6574-6577 (1996).

74. E. C. Barnes, G. A. Petersson, J. A. Montgomery Jr, M. J. Frisch and J. M. Martin, Journal of Chemical Theory and Computation **5** (10), 2687-2693 (2009).

75. J. Cioslowski, *Quantum-mechanical prediction of thermochemical data*. (Springer Science & Business Media, 2002).

76. J. C. Rienstra-Kiracofe, G. S. Tschumper, H. F. Schaefer, S. Nandi and G. B. Ellison, Chemical reviews **102** (1), 231-282 (2002).

77. J. E. Bartmess.

78. Y. Bouteiller, C. Desfrancois, J. Schermann, Z. Latajka and B. Silvi, The Journal of chemical physics **108** (19), 7967-7972 (1998).

79. I. Alecu, J. Zheng, Y. Zhao and D. G. Truhlar, Journal of Chemical Theory and Computation **6** (9), 2872-2887 (2010).

80. L. A. Curtiss, K. Raghavachari, P. C. Redfern and J. A. Pople, The Journal of Chemical Physics **112** (17), 7374-7383 (2000).

81. P. D. Joseph W. Ochterski, (2000).

82. M. R. Nyden and G. Petersson, The Journal of Chemical Physics **75** (4), 1843-1862 (1981).

83. R. Krishnan, J. S. Binkley, R. Seeger and J. A. Pople, The Journal of Chemical Physics **72** (1), 650-654 (1980).

84. J. A. Montgomery Jr, M. J. Frisch, J. W. Ochterski and G. A. Petersson, The Journal of chemical physics **110** (6), 2822-2827 (1999).

85. J. A. Montgomery Jr, M. J. Frisch, J. W. Ochterski and G. A. Petersson, The Journal of Chemical Physics **112** (15), 6532-6542 (2000).

86. E. T. Denisov and T. Denisova, *Handbook of antioxidants: bond dissociation energies, rate constants, activation energies, and enthalpies of reactions*. (CRC press, 1999).

87. P. Armentrout, J Am Soc Mass Spectr **13** (5), 419-434 (2002).

88. P. Armentrout, Journal of analytical atomic spectrometry **19** (5), 571-580 (2004).

89. P. B. Armentrout, *The encyclopedia of mass spectrometry*. (Elsevier Science, 2003).

90. L. Sleno and D. A. Volmer, Journal of mass spectrometry **39** (10), 1091-1112 (2004).

91. J. M. Wells and S. A. McLuckey, Methods in enzymology **402**, 148-185 (2005).

92. K. K. Murray, R. K. Boyd, M. N. Eberlin, G. J. Langley, L. Li and Y. Naito, Pure and Applied Chemistry **85** (7), 1515-1609 (2013).

93. R. Cooks, J. Koskinen and P. Thomas, Journal of mass spectrometry **34** (2), 85-92 (1999).

94. K. Hiraoka, *Fundamentals of Mass Spectrometry*. (Springer, 2013).

95. L. Wu, J. W. Denault, R. G. Cooks, L. Drahos and K. Vékey, J Am Soc Mass Spectr **13** (12), 1388-1395 (2002).

96. V. Romanov, U. H. Verkerk, C. K. Siu, A. C. Hopkinson and K. W. Siu, Anal Chem **81** (16), 6805-6812 (2009).

97. P. Armentrout, Int J Mass Spectrom **200** (1), 219-241 (2000).

98. P. Armentrout and M. Rodgers, The Journal of Physical Chemistry A **104** (11), 2238-2247 (2000).

99. A. A. Shvartsburg, K. M. Ervin and J. H. Frederick, The Journal of chemical physics **104** (21), 8458-8469 (1996).

100. J. B. Griffin and P. Armentrout, J Chem Phys **107** (14), 5345-5355 (1997).

101. J. Xu, M. Rodgers, J. Griffin and P. Armentrout, J Chem Phys **108** (22) (1998).

102. P. Armentrout, Int J Mass Spectrom **227** (3), 289-302 (2003).

103. P. Armentrout, K. M. Ervin and M. Rodgers, The Journal of Physical Chemistry A **112** (41), 10071-10085 (2008).

104. K. Holbrook, Chemical Society reviews **12** (2), 163-211 (1983).

105. W. Forst, *Unimolecular reactions: a concise introduction*. (Cambridge University Press, 2003).

106. G. Luo, I. Marginean and A. Vertes, Analytical chemistry **74** (24), 6185-6190 (2002).

107. T. Baercor and P. M. Mayerfn, J Am Soc Mass Spectr **8** (2), 103-115 (1997).

108. P. Chantry, The Journal of Chemical Physics **55** (6), 2746-2759 (1971).

109. M. E. Weber, J. L. Elkind and P. B. Armentrout, The Journal of Chemical Physics **84** (3), 1521-1529 (1986).

110. V. F. DeTuri and K. M. Ervin, The Journal of Physical Chemistry A **103** (35), 6911-6920 (1999).

111. S. J. Blanksby and G. B. Ellison, Accounts of chemical research **36** (4), 255-263 (2003).

112. J. W. Ochterski, Gaussian Inc, Pittsburgh, PA, 1-17 (2000).

113. W. A. Chupka, The Journal of Chemical Physics **30** (1), 191-211 (1959).

114. H. M. Rosenstock, M. Wallenstein, A. Wahrhaftig and H. Eyring, Proceedings of the National Academy of Sciences of the United States of America **38** (8), 667 (1952).

115. M. Ben-Nun and T. J. Martínez, Chemical Physics **259** (2), 237-248 (2000).

116. M. Ben-Nun, J. Quenneville and T. J. Martínez, The Journal of Physical Chemistry A **104** (22), 5161-5175 (2000).

117. J. Quenneville, M. Ben-Nun and T. J. Martınez, Journal of Photochemistry and Photobiology A: Chemistry **144** (2), 229-235 (2001).

118. F. Muntean and P. Armentrout, The Journal of Chemical Physics **115** (3), 1213-1228 (2001).

119. M. McCarthy, C. Gottlieb, H. Gupta and P. Thaddeus, The Astrophysical Journal Letters **652** (2), L141 (2006).

120. A. Murakami, K. Kawaguchi and S. Saito, Publications of the Astronomical Society of Japan **39**, 189 (1987).

121. P. Skurski, M. Gutowski and J. Simons, Int J Quantum Chem **80** (4-5), 1024-1038 (2000).

122. D. Feller, J Comput Chem **17** (13), 1571-1586 (1996).

123. J. Simons, (2015).

124. N. Kawatsuki, E. Uchida and H. Ono, Appl Phys Lett **83** (22), 4544-4546 (2003).

125. T. K. Roy Dennington, and John Millam, Semichem Inc., Shawnee Mission, KS, 2009.

126. J. Foster and F. Weinhold, Journal of the American Chemical Society **102** (24), 7211-7218 (1980).

127. A. E. Reed and F. Weinhold, The Journal of Chemical Physics **78** (6), 4066-4073 (1983).

128. A. E. Reed, R. B. Weinstock and F. Weinhold, The Journal of Chemical Physics **83** (2), 735-746 (1985).

129. J. Carpenter and F. Weinhold, Journal of Molecular Structure: THEOCHEM **169**, 41-62 (1988).

130. A. E. R. E. D. Glendening, J. E. Carpenter3, and F. Weinhold

131. E. Glendening, Chem. Rev **88**, 899-926 (1988).

Appendix

Appendix A

A.1 Collision Induced Dissociation of the negative ion of (2,2',6,6') tetramethyl-(4,4') dinitro-azobenzene ($C_{16}H_{16}N_4O_4$):

In this section experiments are discussed involving the threshold for collision induced dissociation for the (2,2',6,6') tetramethyl-(4,4') dinitro-azobenzene anion into various fragments. In order to prepare the anions, 1 mg of the sample is dissolved in 1 milliliter of methanol and the 100 μg/ml solution was diluted twice to make a 2 μg/mL solution. The instrument used for the energy resolved mass spectroscopy was the QSTAR Elite triple quadrupole mass spectrometer (ABSciex) and the ions are made using APCI heated nebulizer ion source. The declustering potential (DP) is -50 V and focusing potential (FP) is -160 V, the declustering potential 2 (DP2) is -15 V, collision gas pressure was 3.5×10^{-5} Torr. The collision cell properties have been discussed in the tetra-fluoroazobenzene experimental section. The scan type used is the product ion and the selected mass is 238. The polarity is on negative ion since we were able to detect negative ions for this sample. The ion release delay (IRD) and ion release widths (IRW) are 6.0 and 5.0, respectively. Each data point has been acquired over a one minute period and under 120 cycles of data accumulation. The collision energy has been varied and scanned over a region from 1.5 eV to 30 eV in the laboratory frame using 0.5 eV increment (in negative mode). In the energy areas in which the product ion intensity was increasing rapidly (i.e., threshold) increments of 0.1 eV was used to obtain higher accuracy. The ion source temperature was 300 ºC and the curtain gas used to introduce the ion into the instrument was nitrogen at atmospheric pressure. The flow rate employed to insert the sample is 20 μL/min. The Q1 resolution (first MS) is on low. The voltage on the corona discharge needle (the APCI head) is -4.2 KV. The acquired data was saved and manipulated using MDS (SCIEX Instruments). Computational results using the B3LYP level of theory along with the 6-311++G(d,p) basis set shows that the first product ion which is a result of loss of an NO cannot be a simple bond cleavage, which means the transition state is tight and includes rearrangements. Here we presented the mass spectrum in several collision energy and we can see the precursor and the product ions. The loss of NO is common phenomena which we have seen for other samples as well.

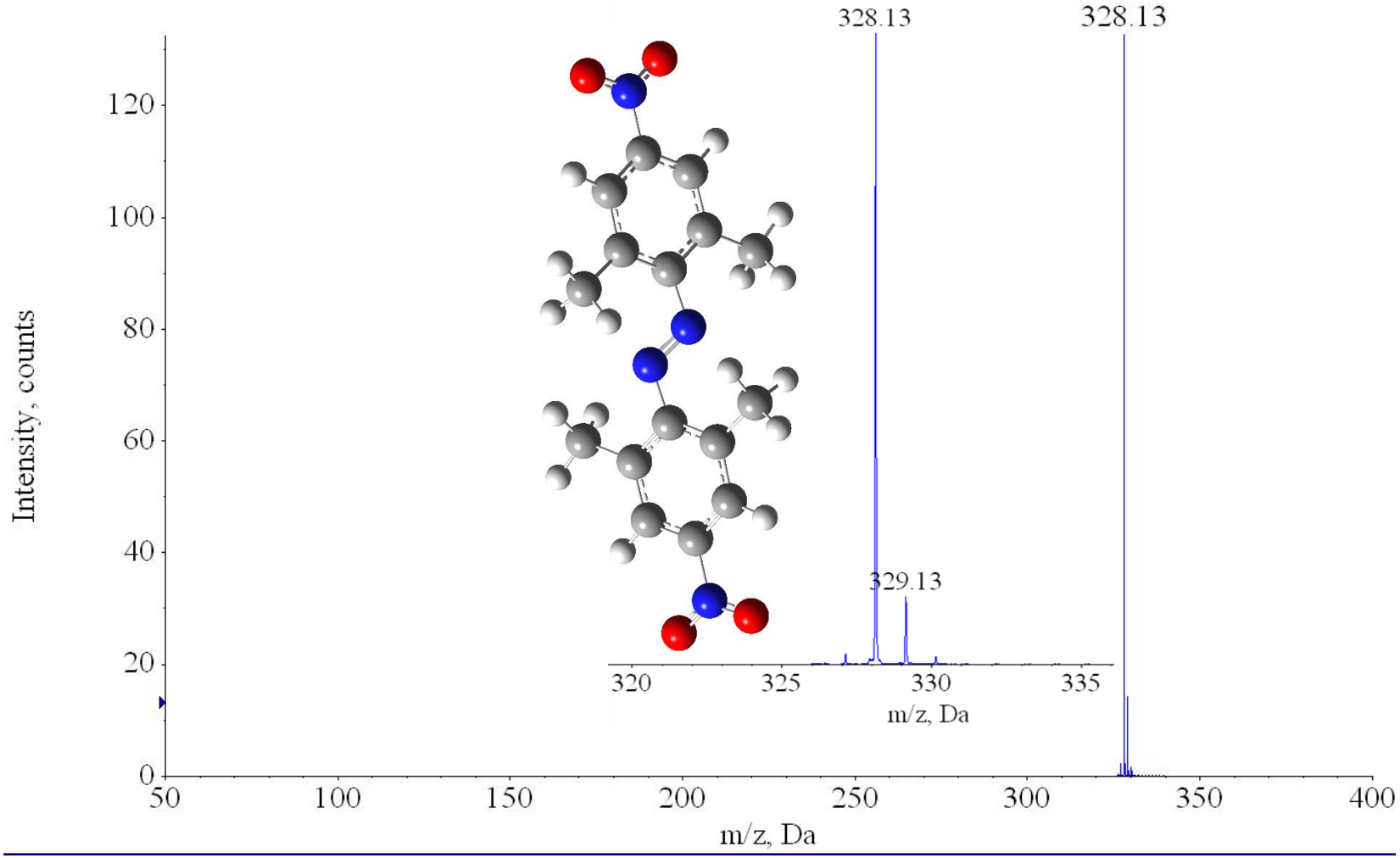

Figure A.1: Negative ion mass spectrum of **(2,2',6,6') tetramethyl-(4,4') dinitro-azobenzene ($C_{16}H_{16}N_4O_4$**, parent neutral Molecular Weight: 328.32 Da) at **2 eV** kinetic collision energy in the laboratory frame (CID experiment) and the parent **neutral** is illustrated.

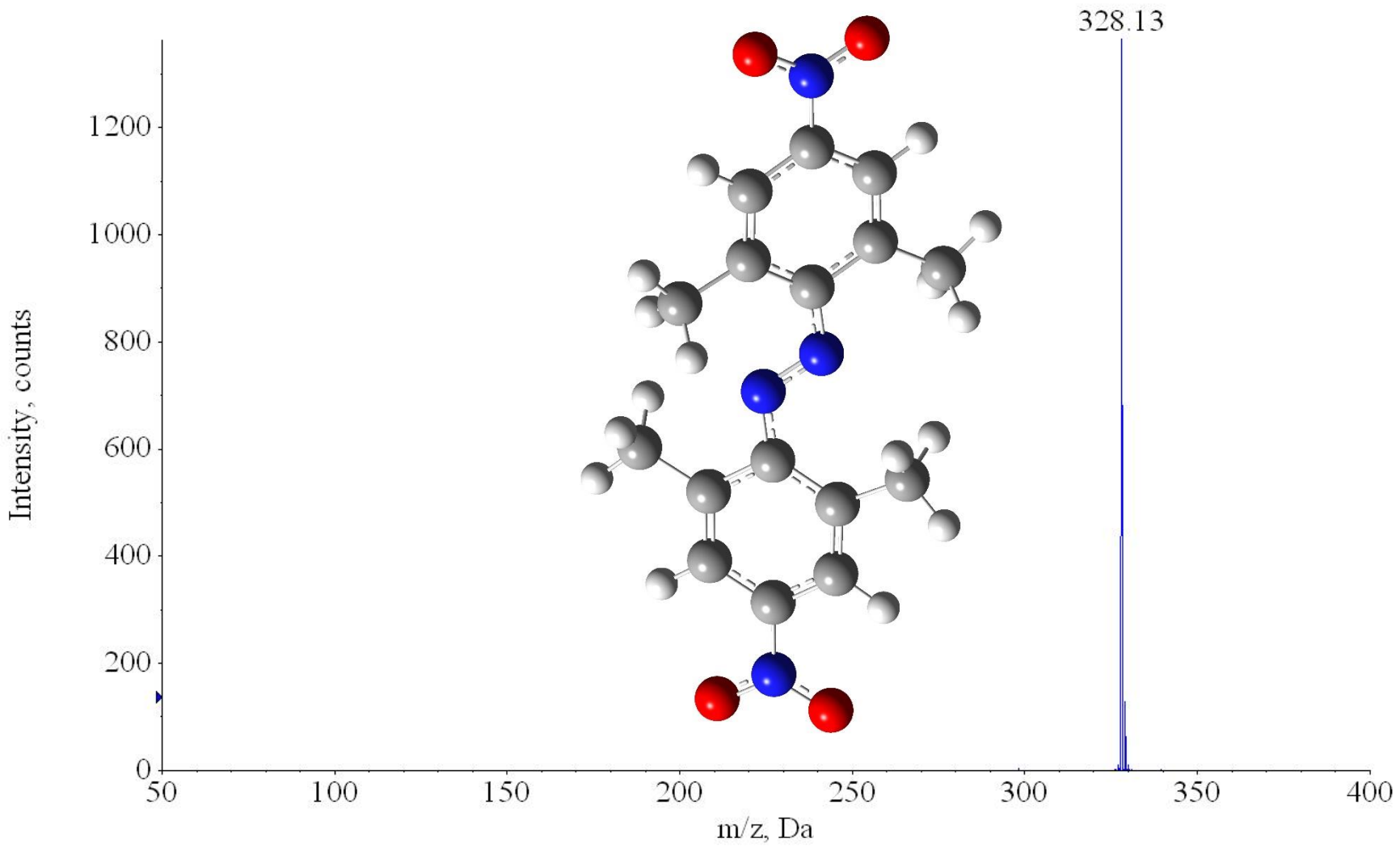

Figure A.2: Negative ion mass spectrum of (2,2',6,6') tetramethyl-(4,4') dinitro-azobenzene at **10 eV** collision energy in the laboratory frame (CID experiment) and the precursor ion is illustrated.

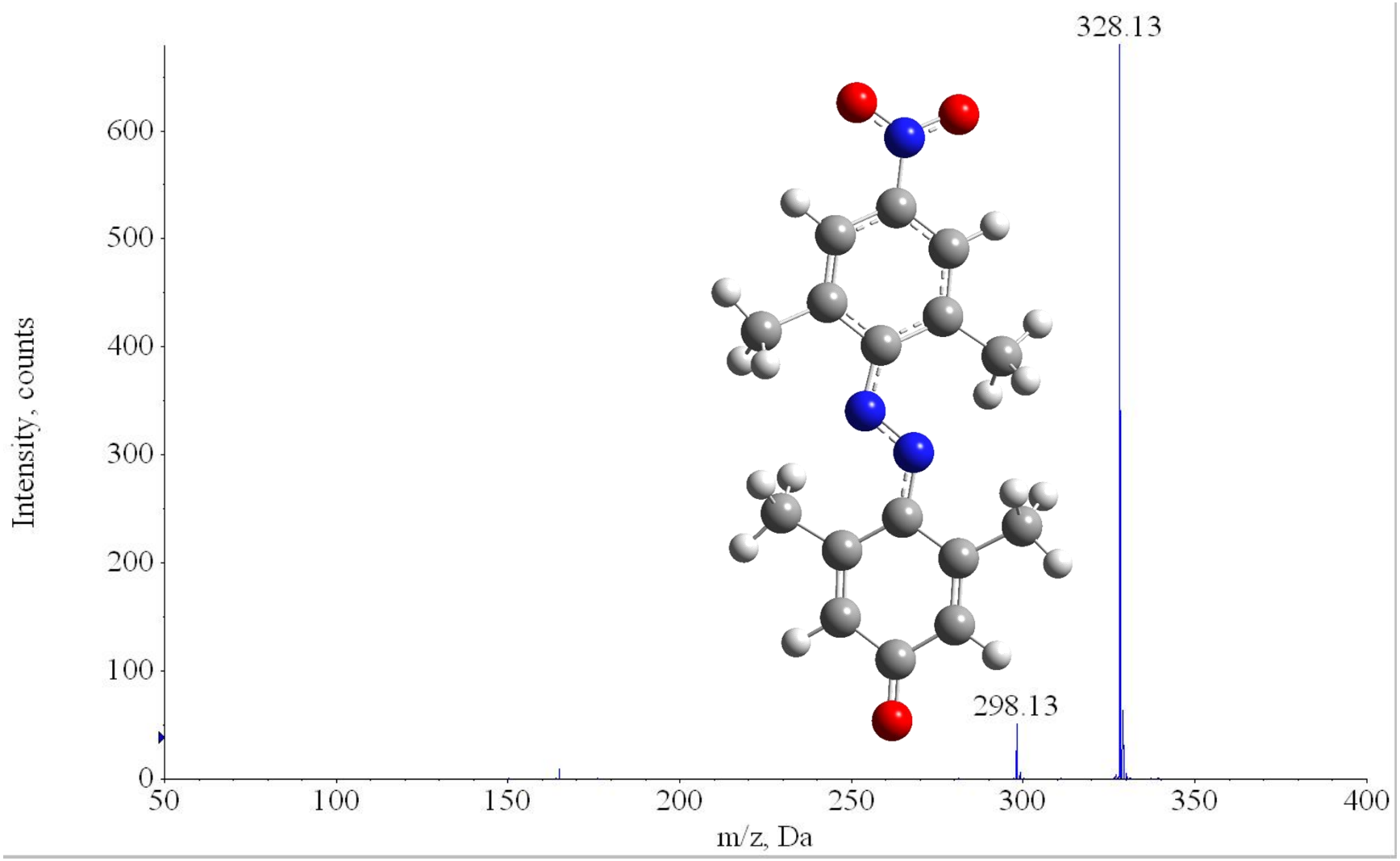

Figure A.3: Negative ion mass spectrum of (2,2',6,6') tetramethyl-(4,4') dinitro-azobenzene at **15 eV** collision energy in the laboratory frame (CID experiment). The fragment ion m/z= 298.13 is illustrated.

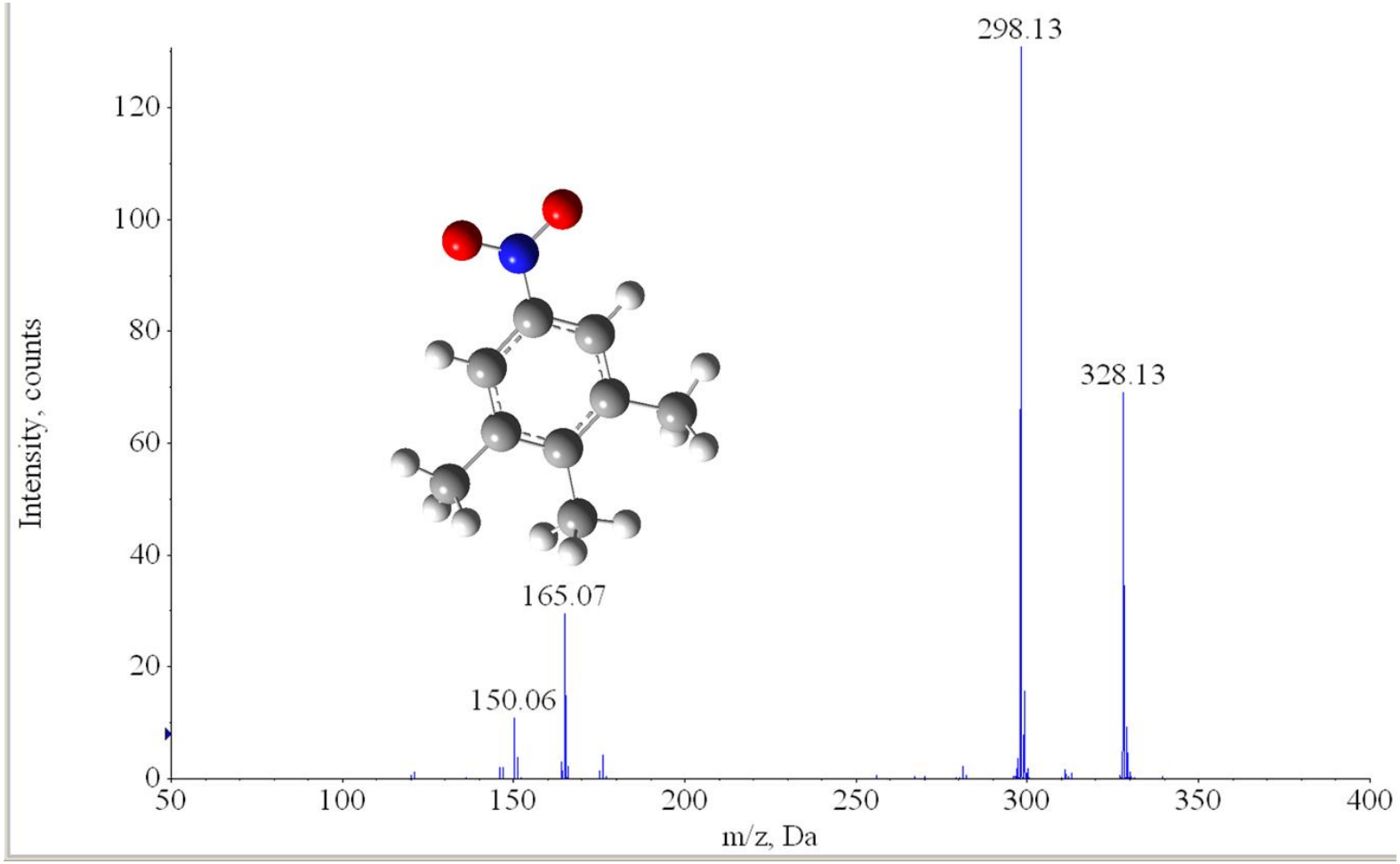

Figure A.4: Negative ion mass spectrum of (2,2',6,6') tetramethyl-(4,4') dinitro-azobenzene at **20 eV** collision energy in the laboratory frame (CID experiment) and the fragment ion m/z= 165.07 is illustrated.

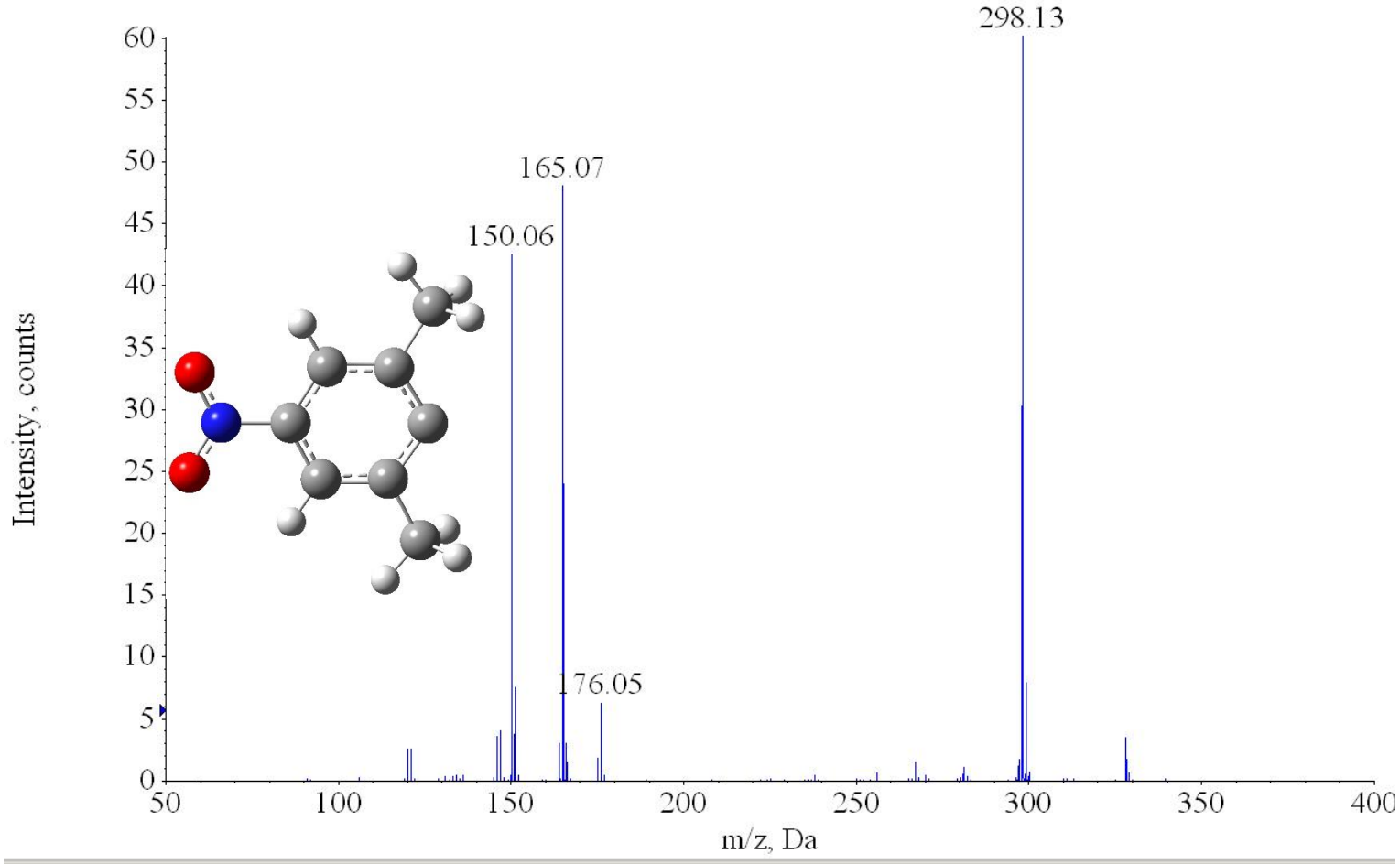

Figure A.5: Mass spectrum (negative mode) of (2,2',6,6') tetramethyl-(4,4') dinitro-azobenzene at **25 eV** translational collision energy in the laboratory frame (CID experiment) and the fragment ion m/z= 150.06 is illustrated.

A.2 Collision induced dissociation of the negative ion of (4,4') dinitro-azobenzene ($C_{12}H_8N_4O_4$):

In this section experiments on CID of the (4,4') dinitro-azobenzene ($C_{12}H_8N_4O_4$) anion are described. The experimental results are very similar to those reported in the above section. The collision energy in the laboratory frame here changes from 0 to 30 eV (in negative mode). The energy in region near threshold region (less than 1 eV) was varied in increments of 0.1 eV in order to obtain the true zero energy of the instrument. The very first negative product ion which shows up in the CID mass spectrum is $[C_{12}H_8N_3O_3]^-$. Similar to the results for previous samples the loss of NO is observed. This reaction again has an energy barrier, has a tight transition state and involves rearrangements. Even in this case (tight transition) we still can use the CRUNCH program for the deconvolution process in order to obtain the threshold for the dissociation reaction. Our calculations using B3LYP level of theory along with the 6-311++G(d,p) Pople basis set resulted in 2.95 eV for the adiabatic electron affinity of this molecule. As a result of this high electron affinity we can see higher intensity of parent ion comparing to the other samples we studied. Below we can see the mass spectrum in different collision energies and what product ions this precursor produce. The cross sections analysis for this sample is still being carried out.

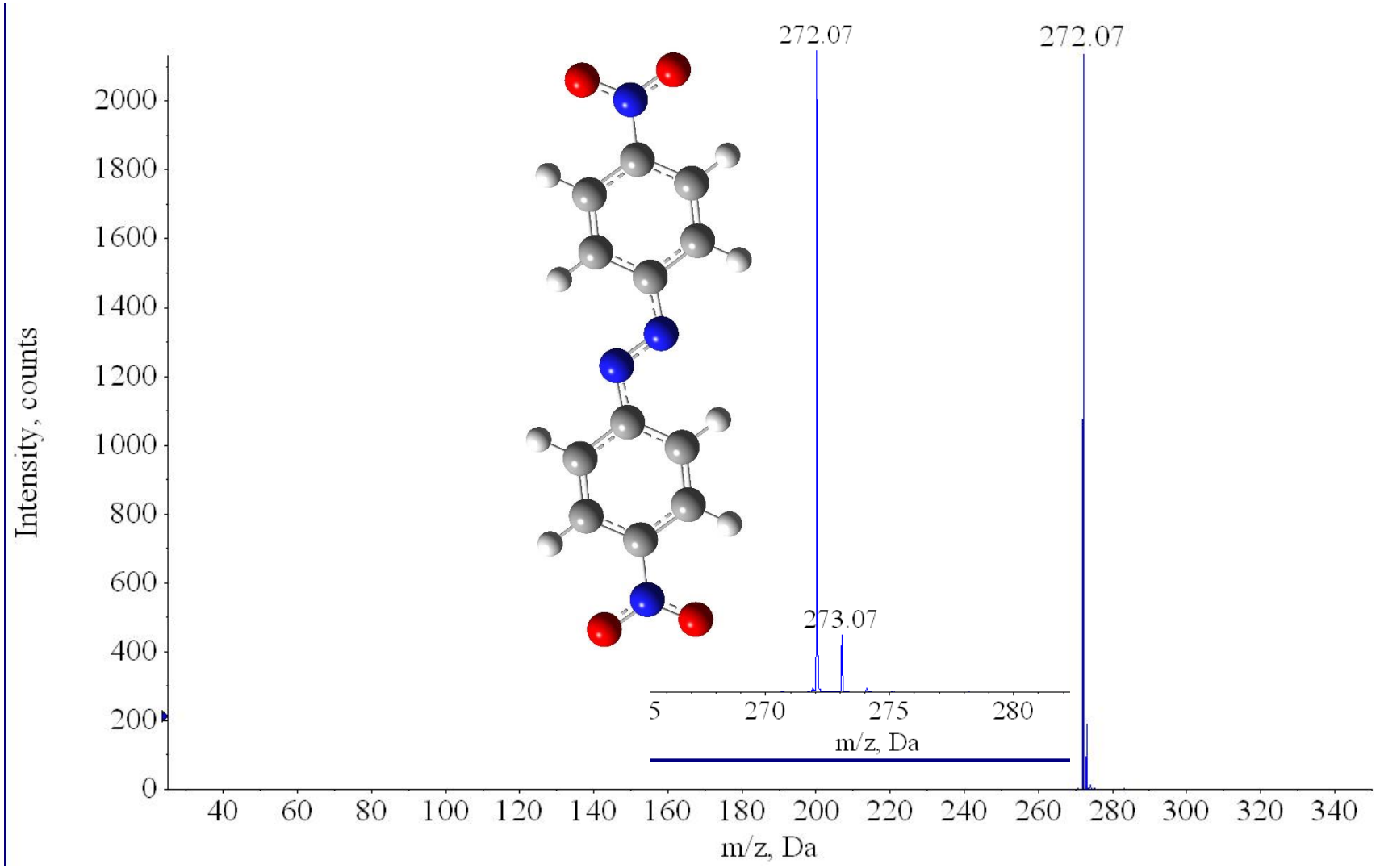

Figure A.6: Negative ion mass spectrum of **(4,4') dinitro-azobenzene ($C_{12}H_8N_4O_4$**, parent neutral Molecular Weight: **272.2 Da**) at **2 eV** translational collision energy in the laboratory frame (CID experiment) and the parent **anion** is illustrated.

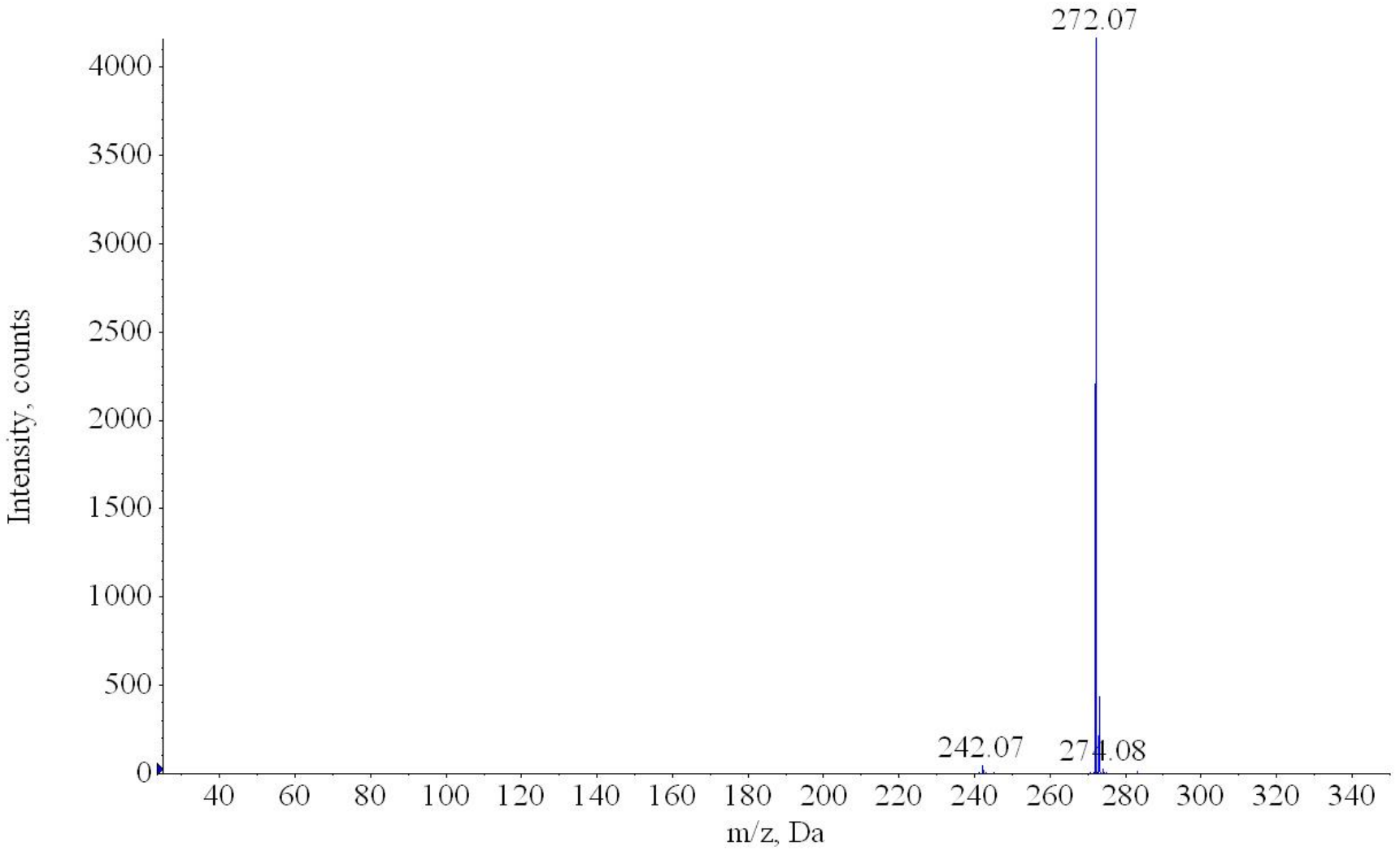

Figure A.7: Negative ion mass spectrum of (4,4') dinitro-azobenzene at **10 eV** translational collision energy in the laboratory frame (CID experiment).

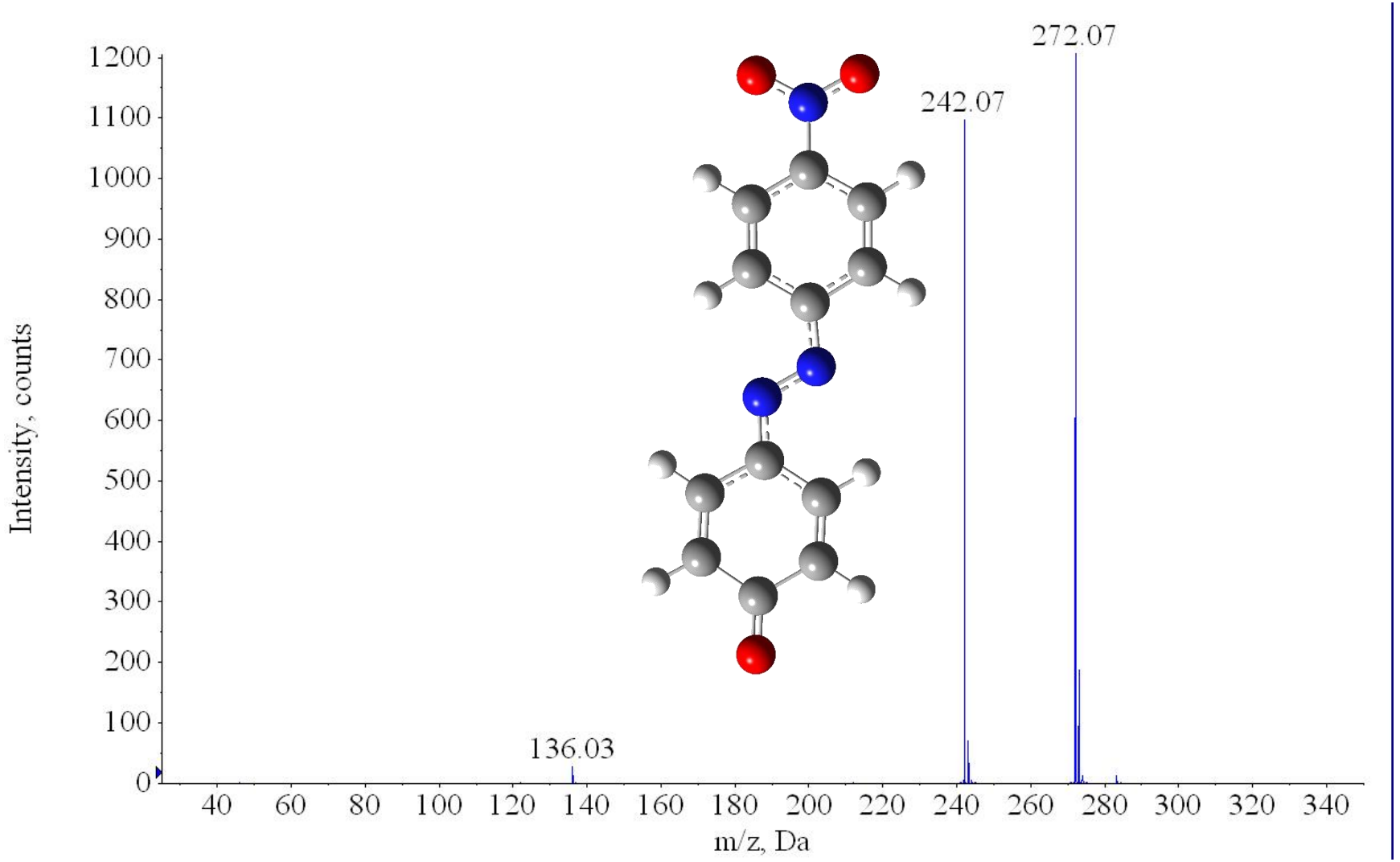

Figure A.8: Negative ion mass spectrum of (4,4') dinitro-azobenzene at **15 eV** translational collision energy in the laboratory frame (CID experiment) and the fragment ion m/z = 242 which is simply loss of NO is illustrated.

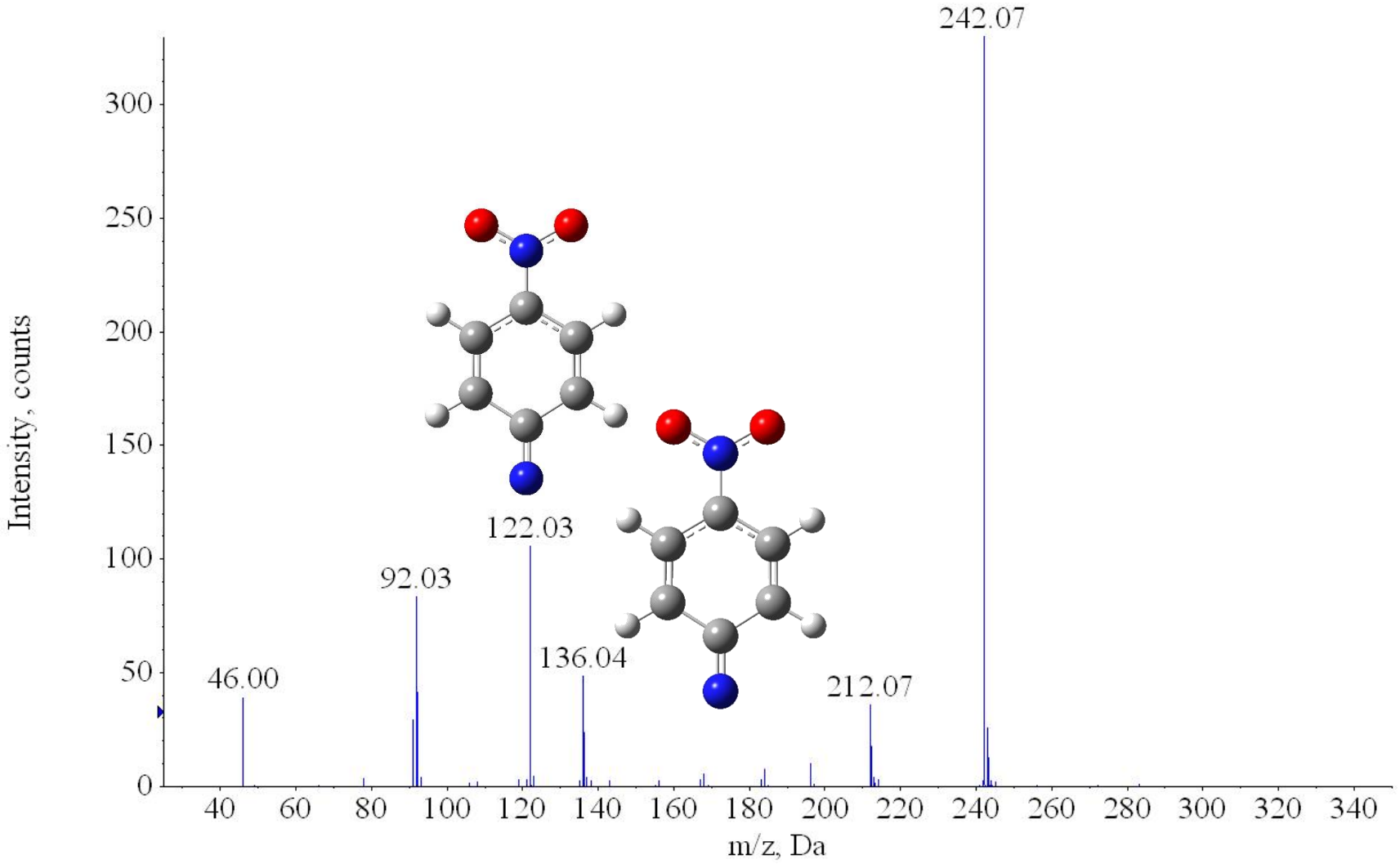

Figure A.9: Mass spectrum of (4,4') dinitro-azobenzene at **20 eV** translational collision energy in the laboratory frame (CID experiment) and the fragment ions m/z = 136.04 and m/z= 122.03 are illustrated.

A.3 Collision induced dissociation of the protonated ion of 2,2',6,6' tetramethylazobenzene ($C_{16}H_{18}N_2$):

2,2',6,6' tetramethylazobenzene, **$C_{16}H_{18}N_2$**, did not produce any negative ions under APCI conditions therefore studies of the positive ions was studied, In the positive ion mode under APCI the protonated cation of this ion was produced. Our calculations by using B3LP level of theory and 6-311++G(d,p) basis set yield 1.17 eV for the adiabatic electron affinity and 9.8 eV for the proton affinity. Calculations show that a proton can attach to one of the N atoms in the N-N bond making the protonated cation. The collision induced dissociation experiment has been performed using atmospheric pressure chemical ionization method and 300 ºC was the initial ion source temperature. Preliminarily results shows the first product ion is simply the loss of one the methyl groups as one can predict. A simple preliminary bond dissociation energy calculation using results calculated at the B3LYP level of theory yields 3.88 eV for the bond dissociation energy. Details of the CID experiment is very similar to what we have described before.

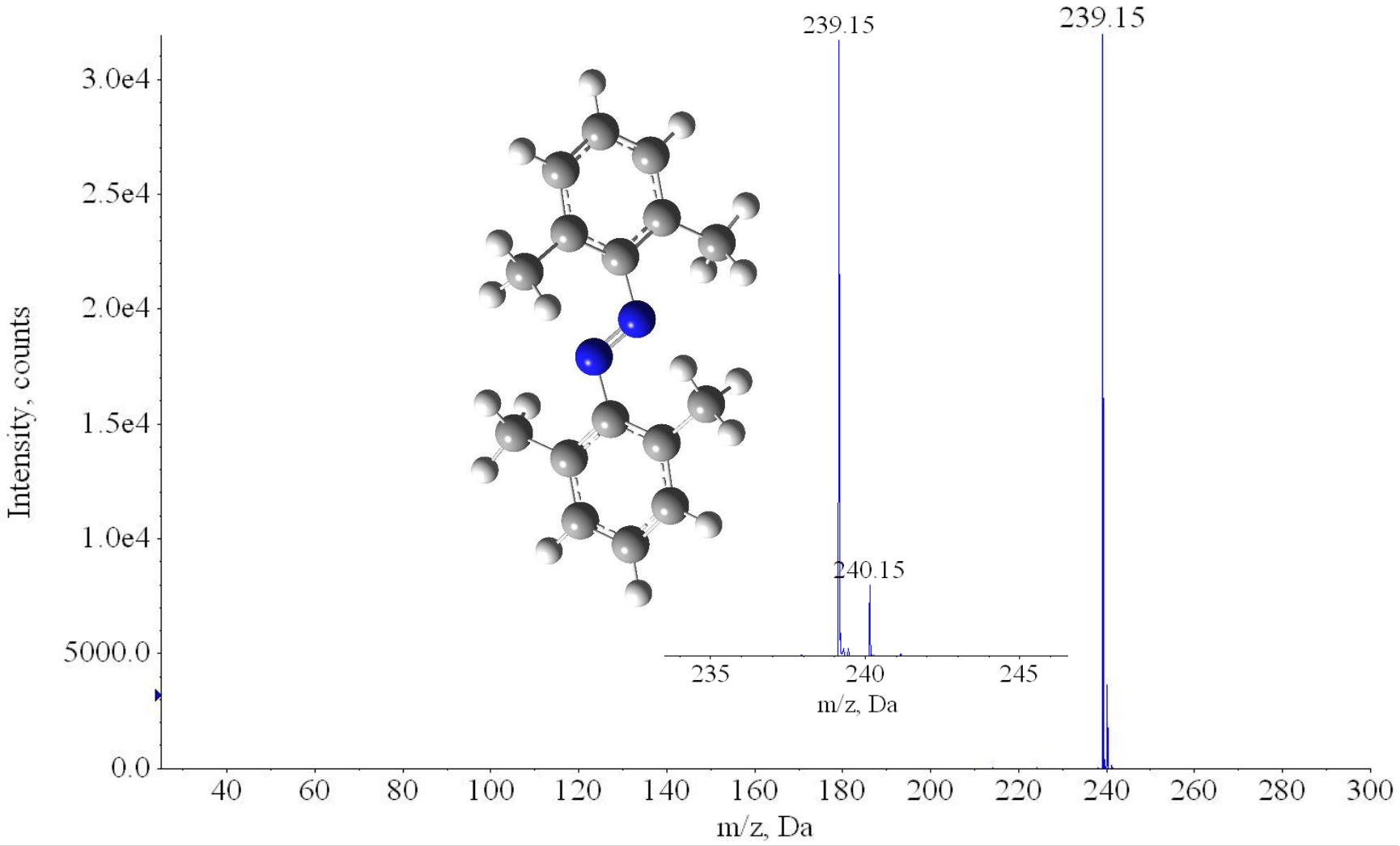

Figure A.10: Positive ion mass spectrum of **2,2',6,6' tetramethylazobenzene ($C_{16}H_{18}N_2$**, parent neutral Molecular Weight: **238.33Da**) at **2 eV** translational collision energy in the laboratory frame (CID experiment) and the parent **neutral** is illustrated.

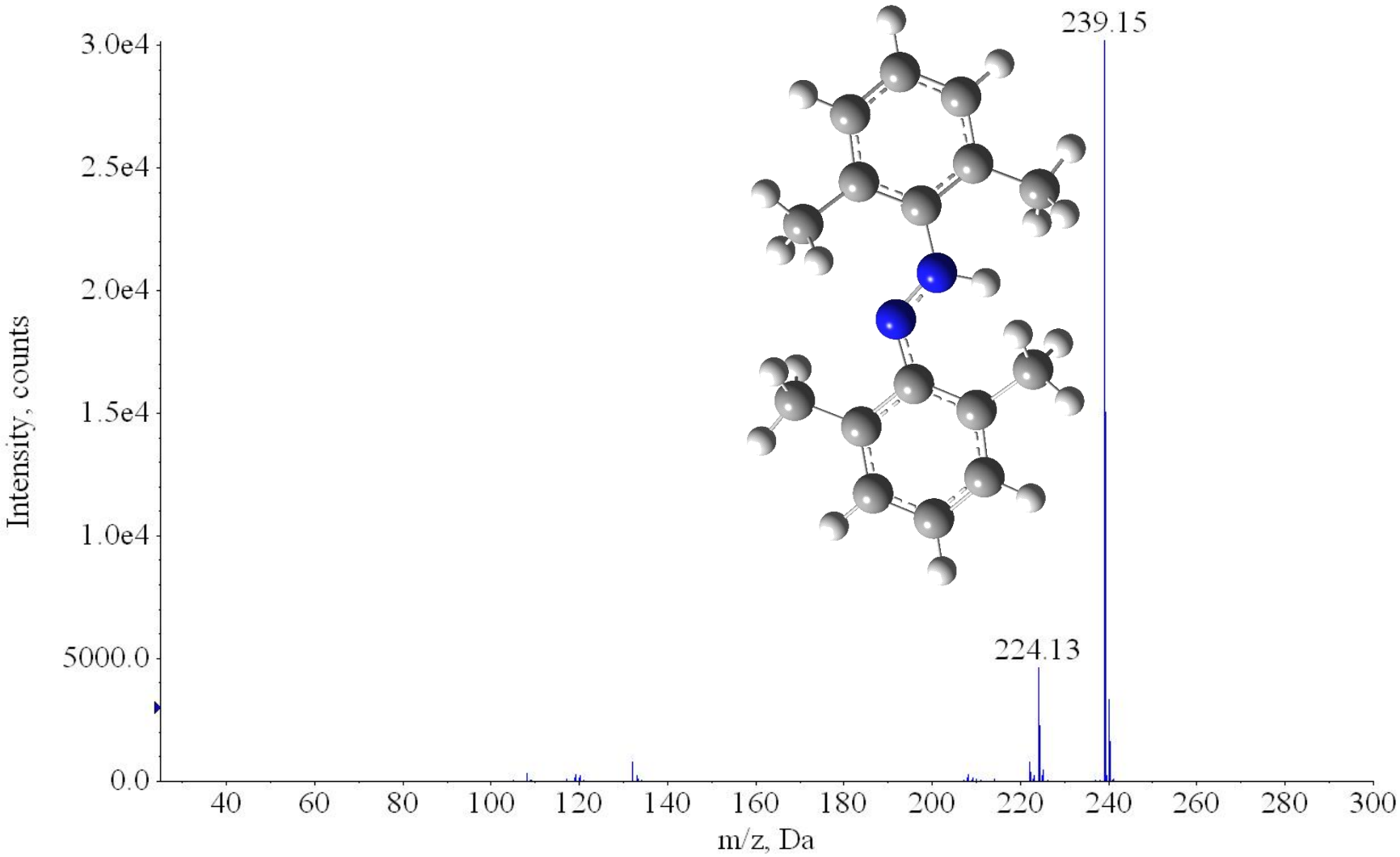

Figure A.11: Positive ion mass spectrum of **2,2',6,6' tetramethylazobenzene** at **10 eV** translational collision energy in the laboratory frame (CID experiment) and the precursor cation is illustrated. This is in positive mode and the precursor ion is formed as a result of proton attachment.

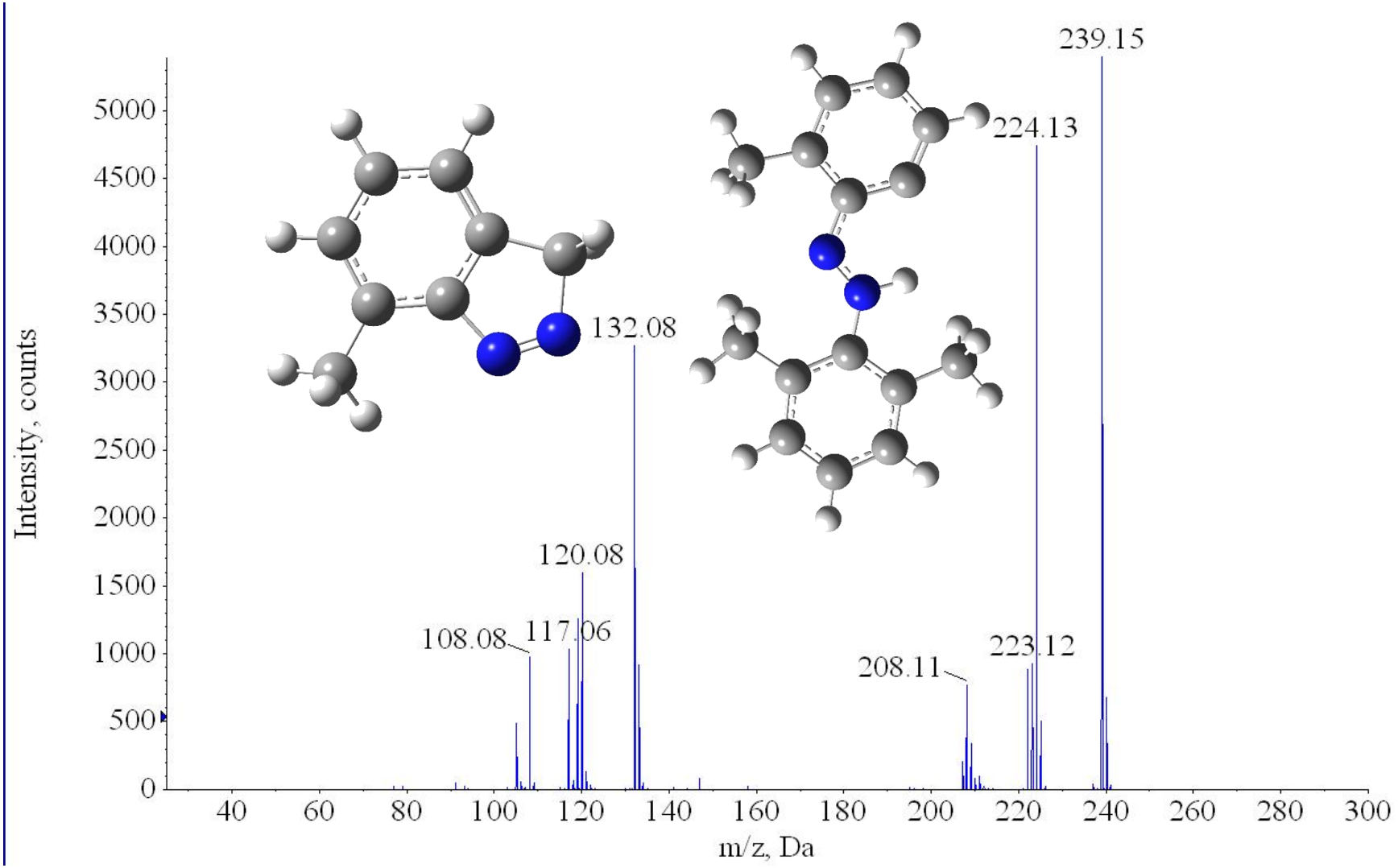

Figure A.12: Positive ion mass spectrum of **2,2',6,6' tetramethylazobenzene** at **15 eV** translational collision energy in the laboratory frame (CID experiment) and the fragment ions m/z = 224.13 and m/z = 132.08 are illustrated.

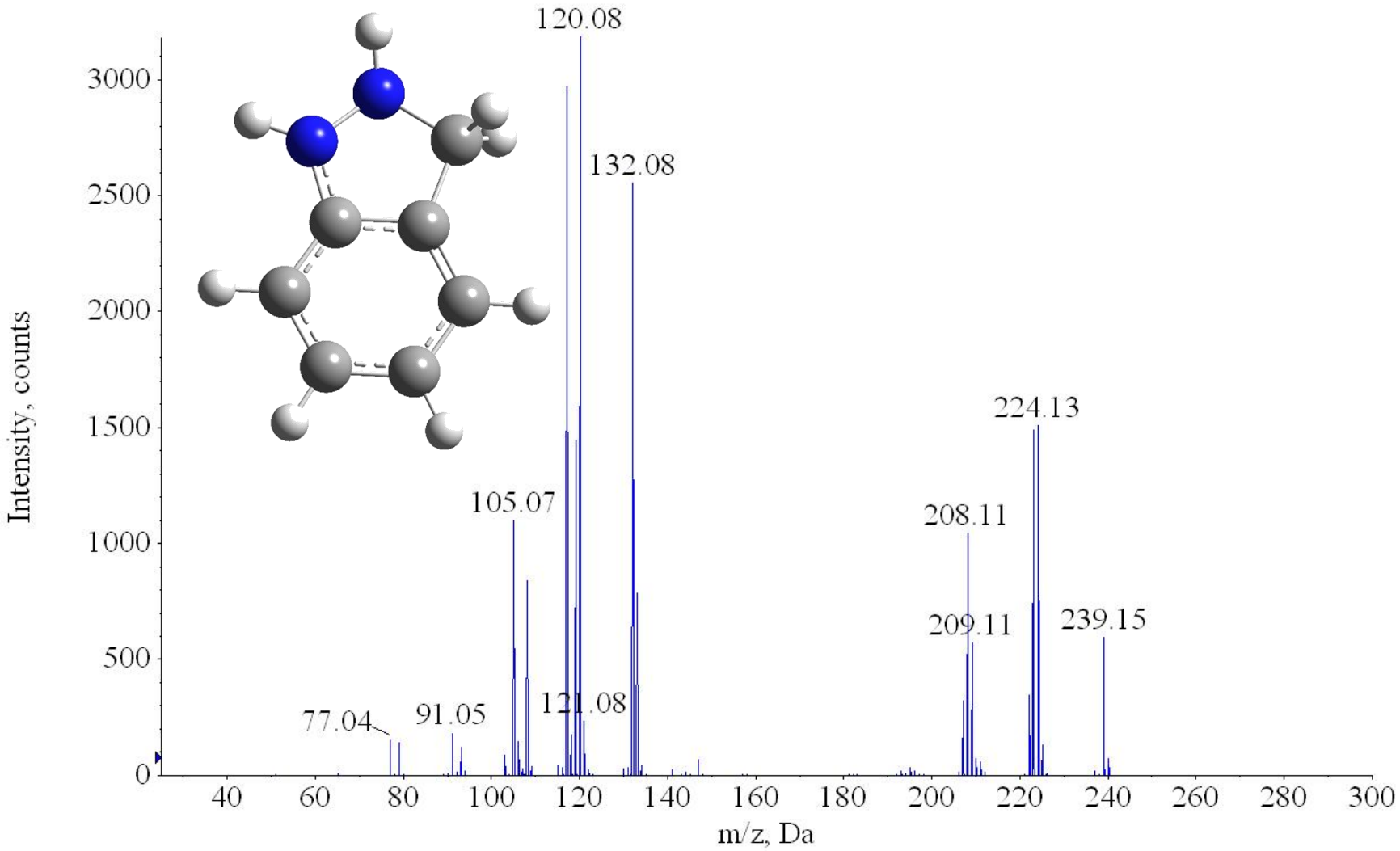

Figure A.13: Positive ion mass spectrum of **2,2',6,6' tetramethylazobenzene** at **20 eV** translational collision energy in the laboratory frame (CID experiment) and the fragment ion m/z = 120.08 is illustrated.

A.4 Collision induced dissociation of the protonated cation of 4-Dimethylamino-2-methylazobenzene ($C_{15}H_{17}N_3$):

4-Dimethylamino-2-methylazobenzene, $C_{15}H_{17}N_3$, (also known as N,N-Dimethyl-4-phenylazo-m-toluidine) was purchased from the Sigma Aldrich company and was used in these experiments without any further purification. Calculations using the B3LYP level of theory along with the 6-311++G(d,p) basis set resulted in 1.0 eV for the electron affinity of this molecule as well as 10.4 eV for the proton affinity. Our experiments and efforts to detect the negative ion of this sample was not fruitful but the positive ion signal was intense and was sufficient to produce collision induced dissociation spectrum of the protonated 4-dimethylamino-2-methylazobenzene cation. Details of the experiment has been explained before. Since this sample didn't generate negative ion which is our primary interest, we tried the positive mode and the positive ion intensity is fairly high. This is in consistent with our theoretical calculation results since the proton affinity is 10.54 eV (computation has been perform at wB97XD level of theory along with a 6-311++G(d,p) basis set). Below we can see the kinetic energy resolved mass spectrum for different collision energies and we can see the precursor and product ion intensities and how these varies by increasing the collision energy. The precursor cation is formed by attaching a proton to one of the nitrogen in N-N bond.

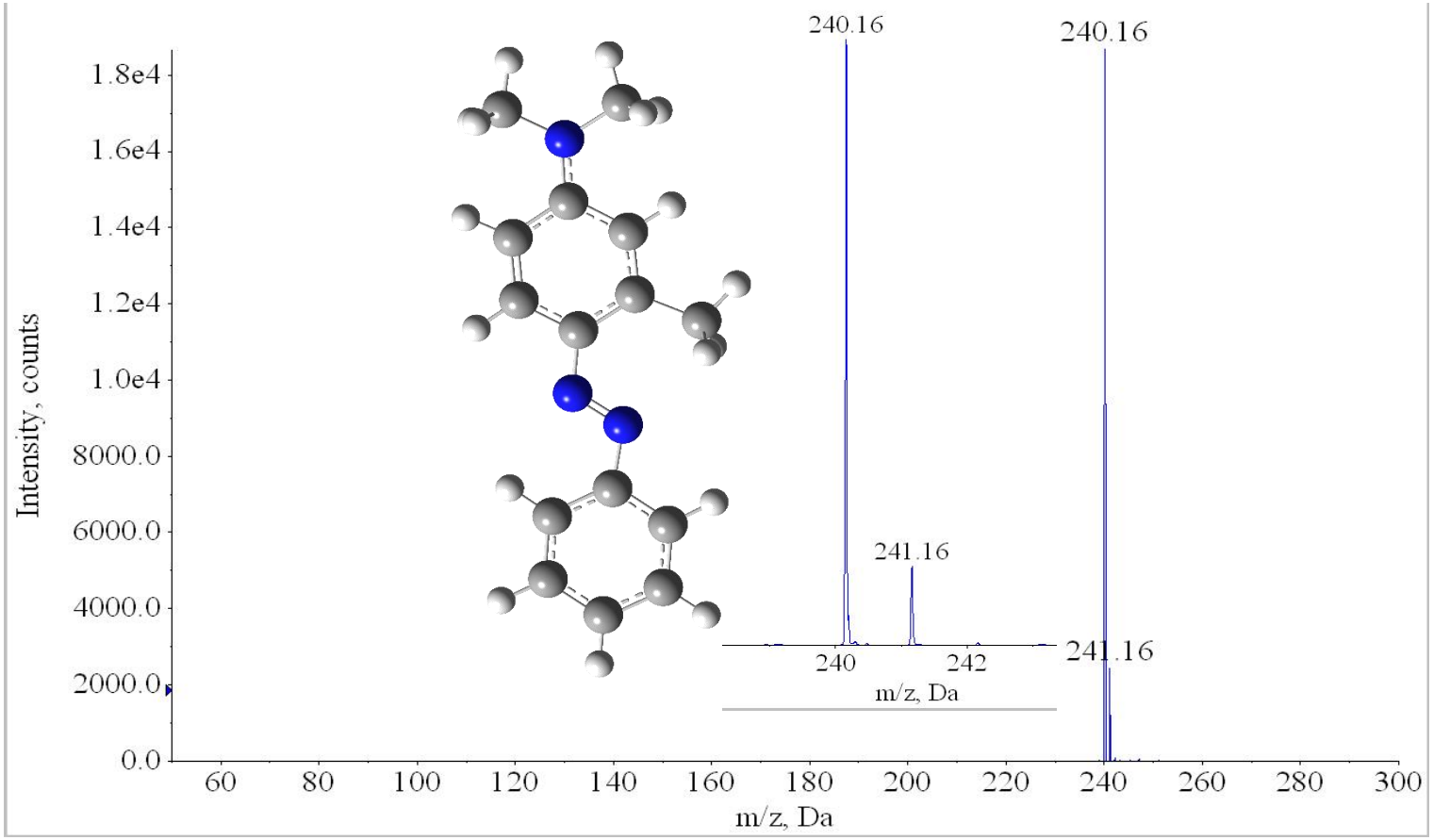

Figure A.14: Positive ion mass spectrum of 4-Dimethylamino-2-methylazobenzene ($C_{15}H_{17}N_3$, parent neutral Molecular Weight: 239.3 Da) at 2 eV translational collision energy in the laboratory frame (CID experiment) and the **parent neutral** is illustrated. This is in positive mode and the parent ion is positive.

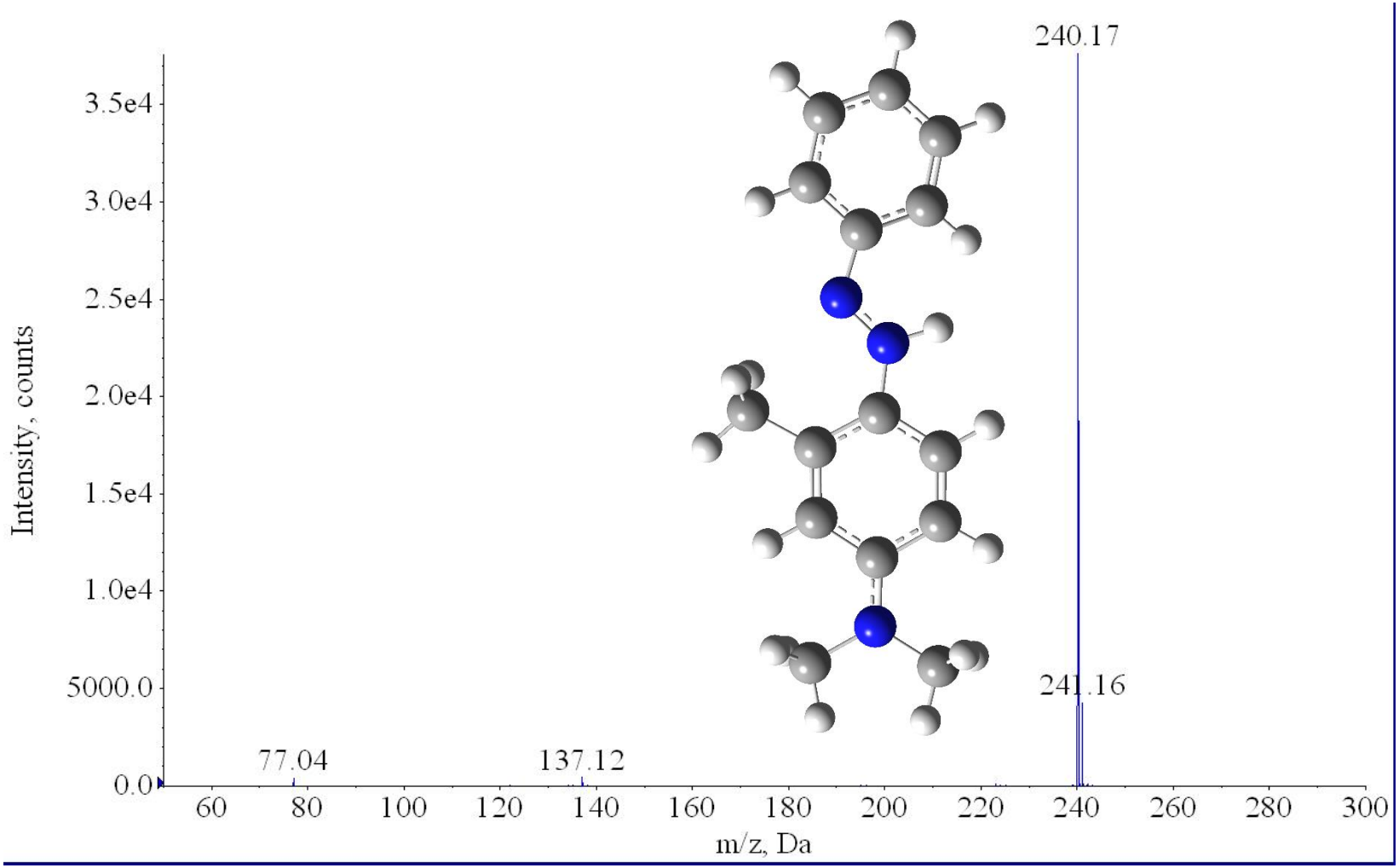

Figure A.15: Positive ion mass spectrum of 4-Dimethylamino-2-methylazobenzene ($C_{15}H_{17}N_3$, parent neutral Molecular Weight: 239.3 Da) at **10 eV** translational collision energy in the laboratory frame (CID experiment) and the **parent cation** is illustrated.

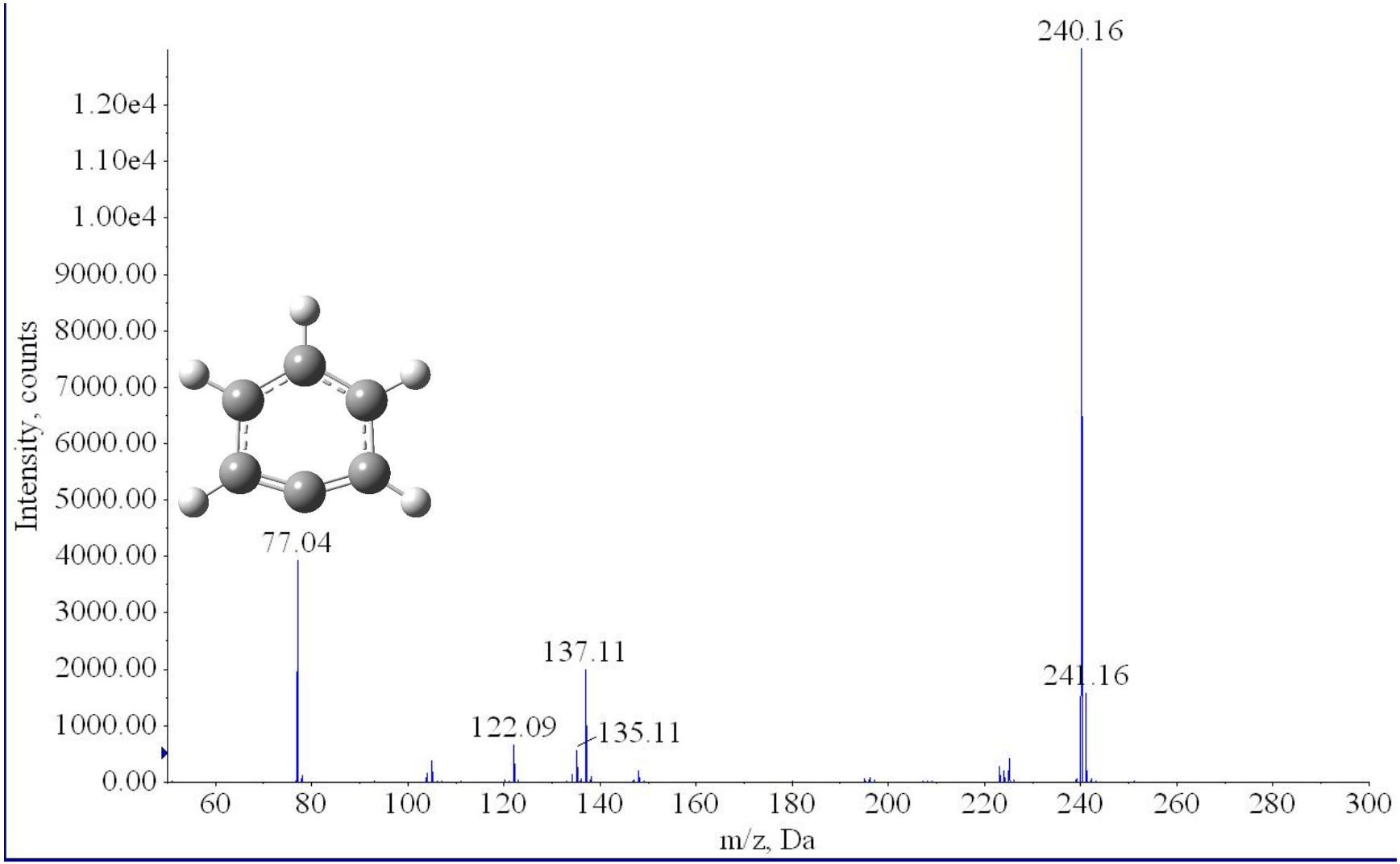

Figure A.16: Positive ion mass spectrum of 4-Dimethylamino-2-methylazobenzene ($C_{15}H_{17}N_3$, parent neutral Molecular Weight: 239.3 Da) at 15 eV translational collision energy in the laboratory frame (CID experiment)

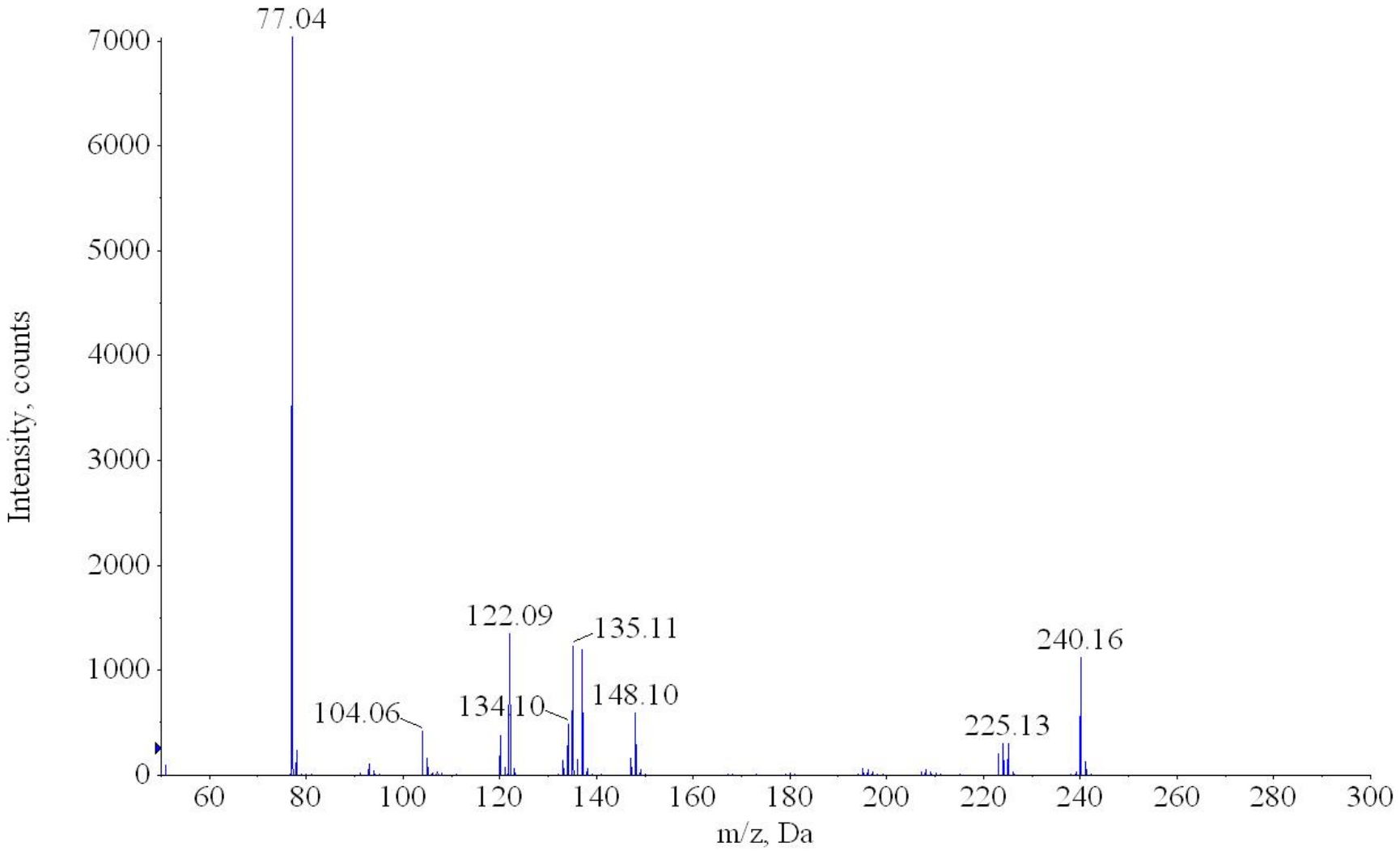

Figure A.17: Positive ion mass spectrum of 4-Dimethylamino-2-methylazobenzene ($C_{15}H_{17}N_3$, parent neutral Molecular Weight: 239.3 Da) at 20 eV translational collision energy in the laboratory frame (CID experiment)

A.5 Collision induced dissociation of 4-Methoxyazobenzene ($C_{13}H_{12}N_2O$):

4-Methoxyazobenzene ($C_{13}H_{12}N_2O$) with Molecular weight of 212.25 g/mol was purchased from the Sigma-Aldrich Company and the purity is better than 99%. The sample was studied without any further purification. Unfortunately, this sample did not generate negative ions, at least at low concentration. However, very intense positive ion signal was recorded. Calculations at the B3LYP/6-311++G(d,p) level of theory resulted in a value of 1.19 eV for the adiabatic electron affinity and 9.91 eV for the proton affinity. To produce the positive ions 2 μg/ml solution in methanol was prepared and injected into the instrument at 20 μl/min rate. The ion source was the APCI and ions are made at 300 ºC. The intensity of the precursor ion is strong and the collision energy is scanned from 0 to 25 eV in the laboratory frame. The main product ion in this experiment was the 77 m/z peak. Details of the CID experiments is the same as we have explained before in experimental sections. Fragments ions and precursor ion and the mass spectrums in different collision energies are shown in figures below. Details of cross section analysis of this CID experiment is still under investigation. 4-Methoxyazobenzene has very interesting applications in science and technology and applications such as stable pure polarization grating in a polymer film comprised of it had been reported.[124]

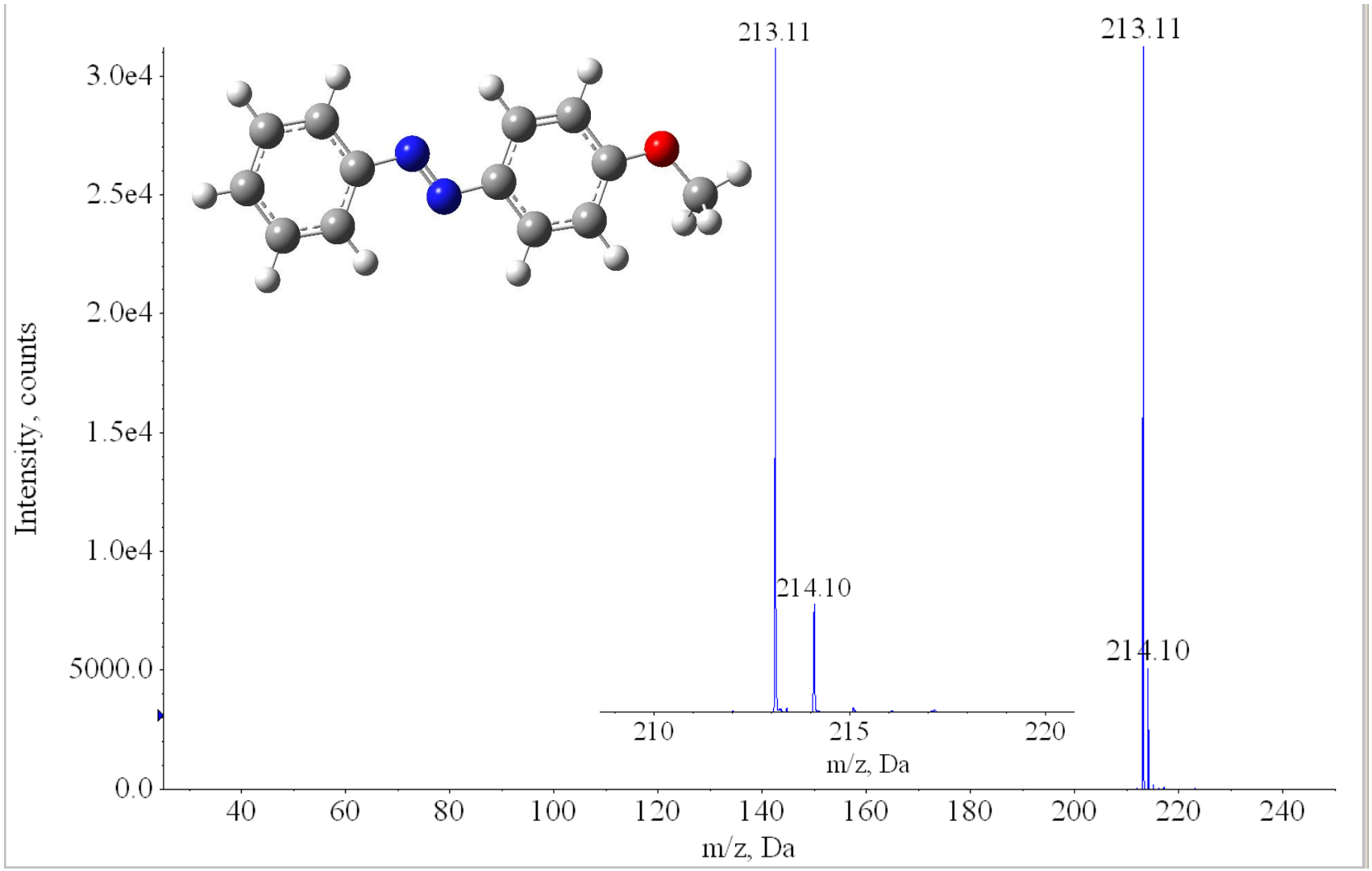

Figure A.18: Positive ion mass spectrum of 4-Methoxyazobenzene ($C_{13}H_{12}N_2O$, parent neutral Molecular Weight: 212.25 Da) at 2 eV translational collision energy in the laboratory frame and the parent neutral molecule is illustrated.

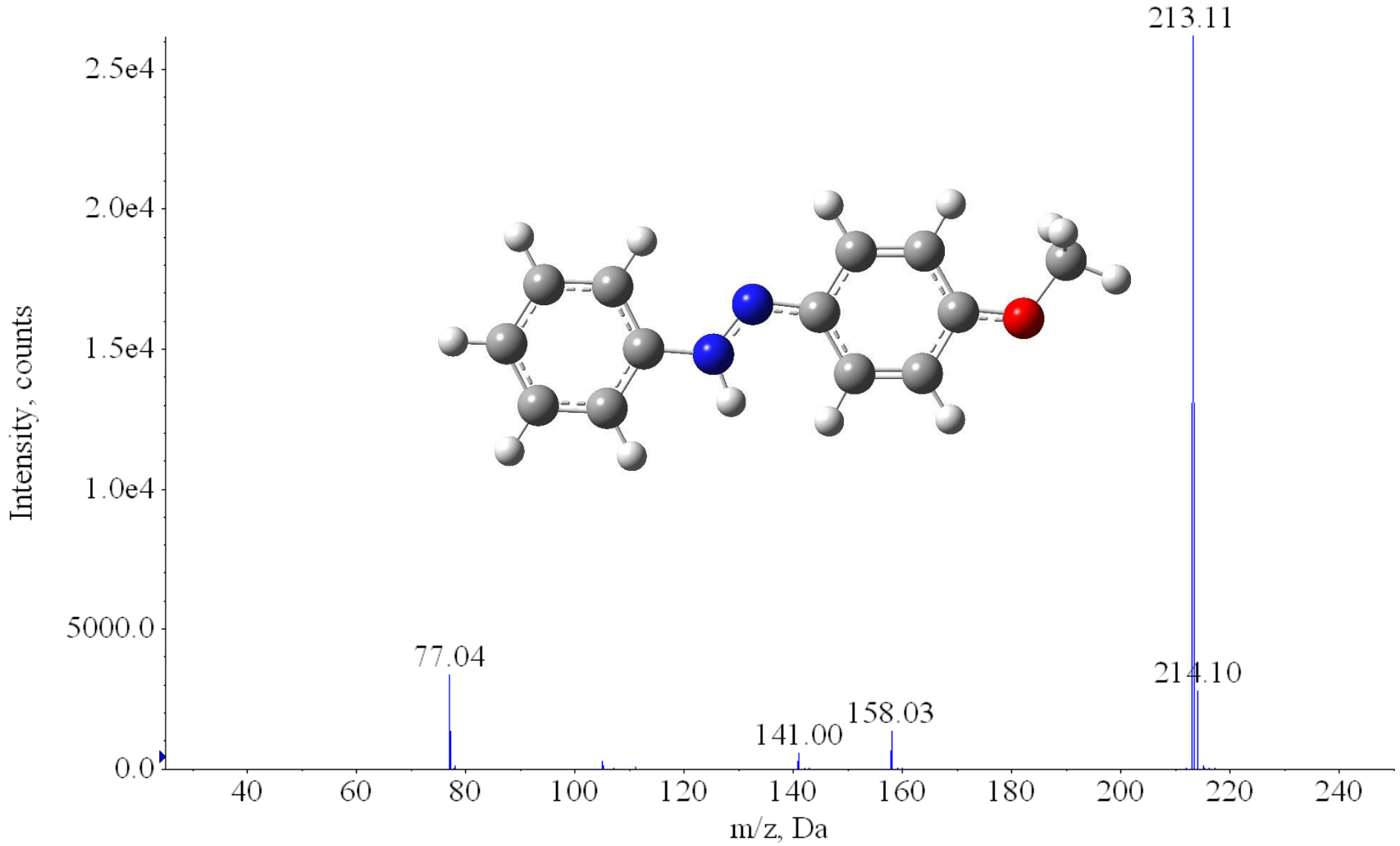

Figure A.19: Positive ion mass spectrum of 4-Methoxyazobenzene ($C_{13}H_{12}N_2O$, parent neutral Molecular Weight: 212.25 Da) at **10 eV** translational collision energy in the laboratory frame (CID experiment) and the parent cation is illustrated.

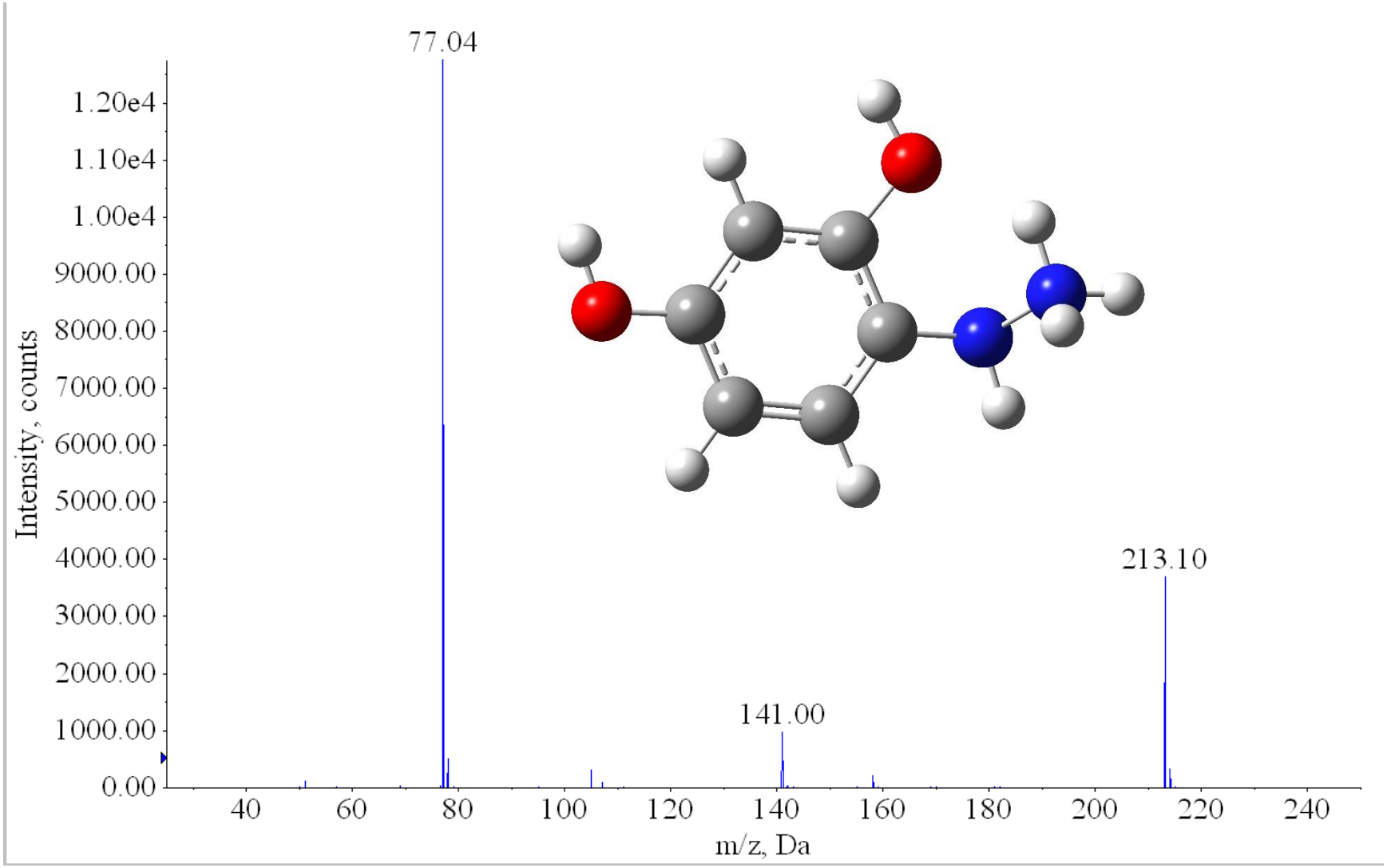

Figure A.20: Mass spectrum of 4-Methoxyazobenzene ($C_{13}H_{12}N_2O$, parent neutral Molecular Weight: 212.25 Da) at **15 eV** translational collision energy in the laboratory frame (CID experiment) and the fragment ion m/z = 141 is illustrated.

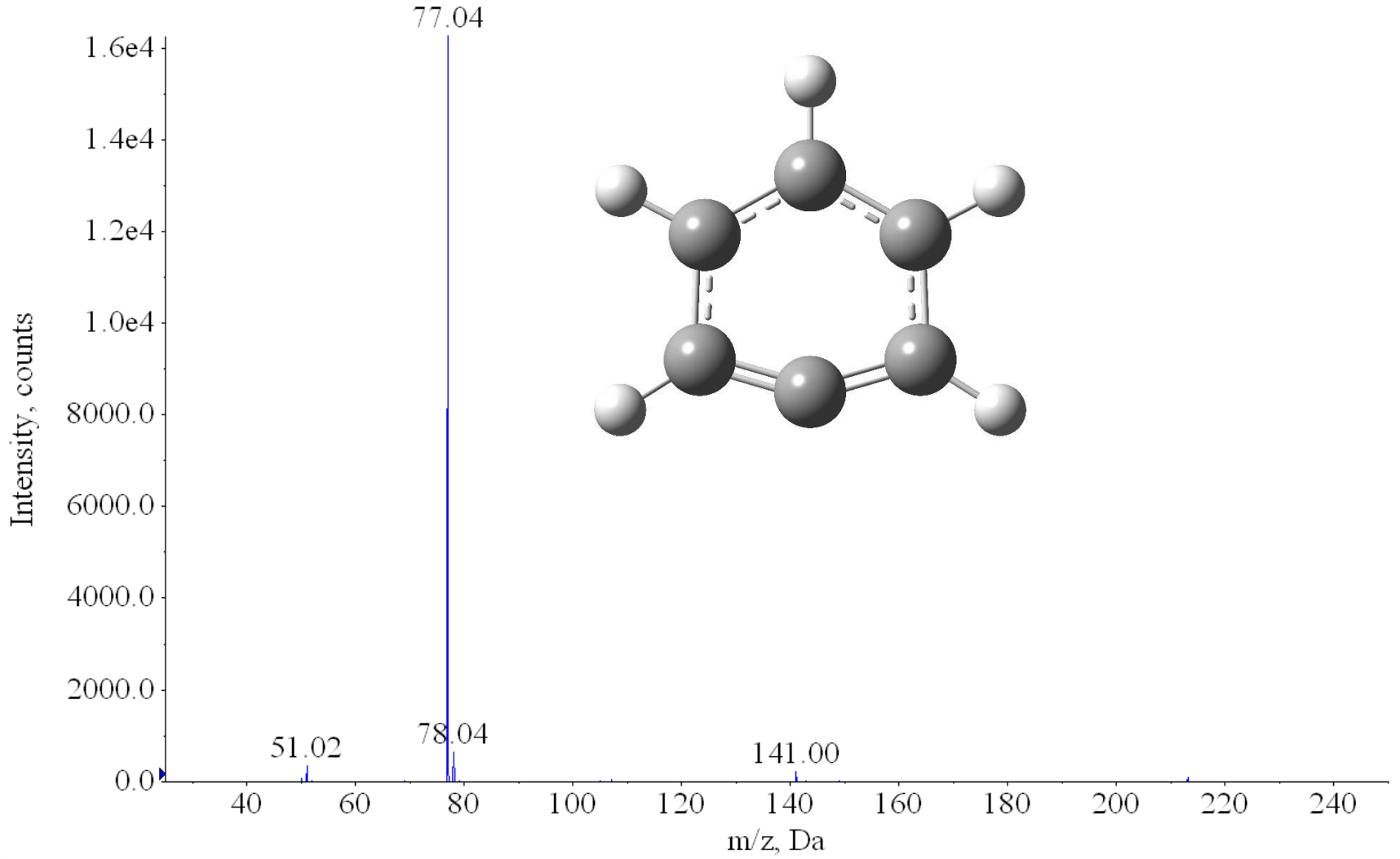

Figure A.21: Mass spectrum of 4-Methoxyazobenzene (C13H12N2O, parent neutral Molecular Weight: 212.25 Da) at **20 eV** translational collision energy in the laboratory frame (CID experiment) and the fragment ion m/z = 77.04 is illustrated.

A.6 Collision induced dissociation of 2,4-Dihydroxyazobenzene,4-(Phenylazo) resorcinol ($C_{12}H_{10}N_2O_2$):

The electron affinity for 2,4-Dihydroxyazobenzene,4-(Phenylazo)resorcinol has been calculated to be 1.04 eV using B3LYP level of theory and 6-311+G(d,p) and the proton affinity is 10.28 eV. According to calculations the extra proton is attached to the N-N bond and the precursor ion intensity is very intense (~10^4). The collision induced spectrum of this sample is interesting since in low collision energy region 3 major fragment peaks appear which are all related to the precursor ion. Since we are looking at positive ions made by this sample (negative ion mode did not result any significant precursor ion signal) 215 and 216 m/z peaks are just the protonated sample but the 214 m/z peal is the sample parent ion corresponding to the loss of an electron. This is the only sample in which we have seen the positive ion formed by two different mechanism simultaneously, loss of an electron and protonation. Details of the CID experiments is the similar to what we have explained before in experimental sections.

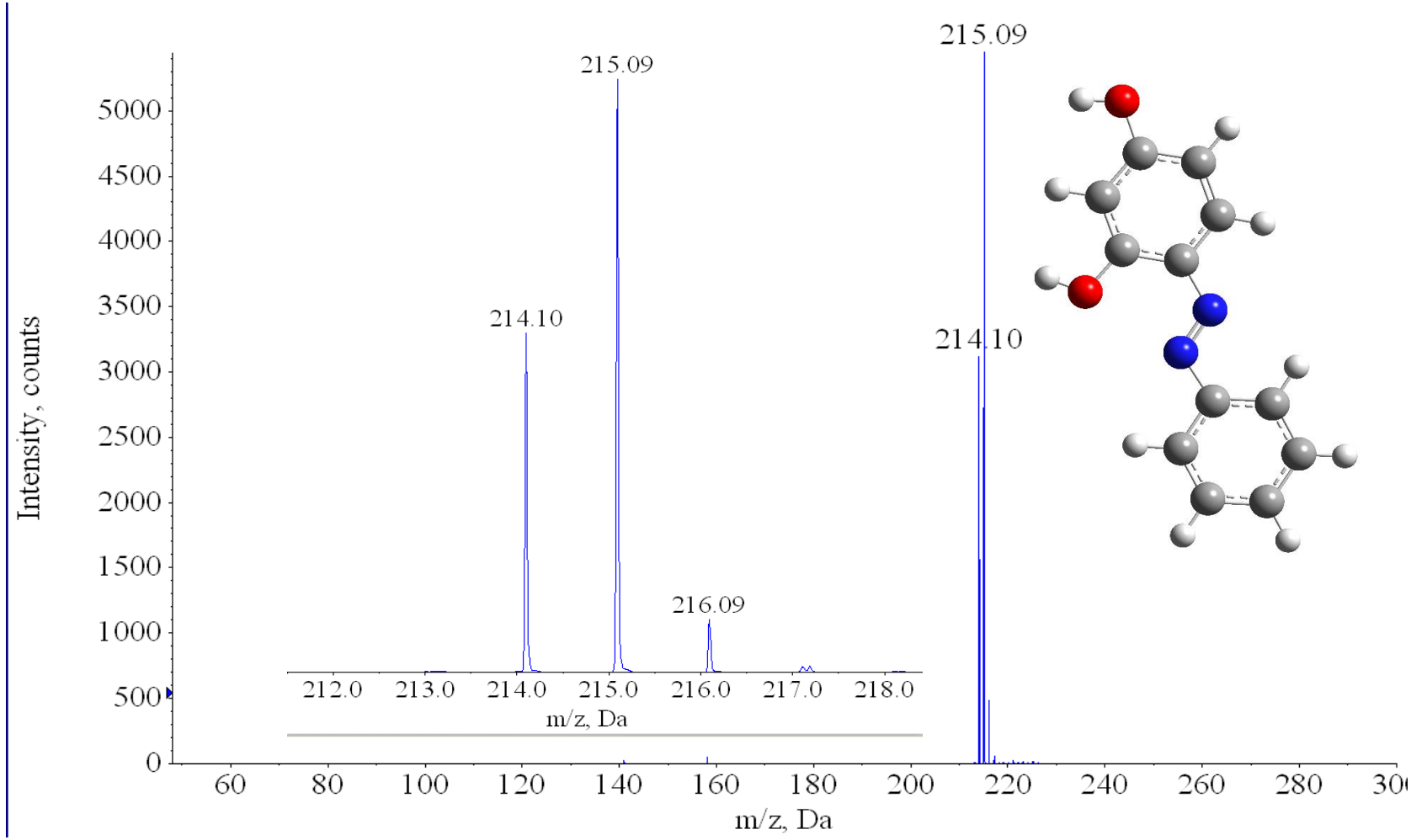

Figure A.22: Positive ion mass spectrum of 2,4-Dihydroxyazobenzene,4-(Phenylazo) resorcinol ($C_{12}H_{10}N_2O_2$, parent neutral Molecular Weight: 214.22 Da) at **2 eV** translational collision energy in the laboratory frame (CID experiment) and the parent neutral is illustrated. There are 2 different type of cations generated from this sample, loss of an electron and proton attachment.

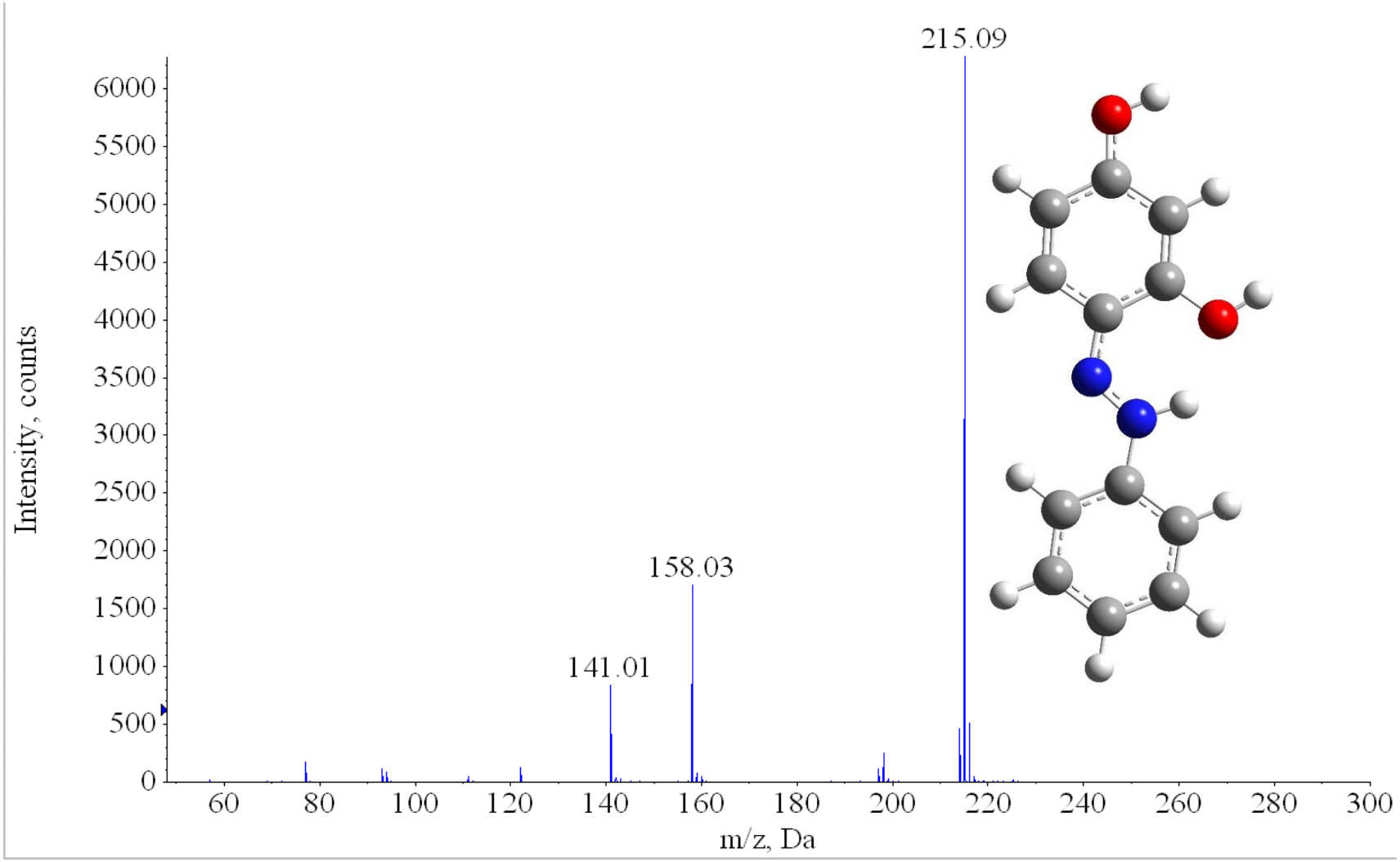

Figure A.23: Positive ion mass spectrum of 2,4- Dihydroxyazobenzene,4 - (Phenylazo) resorcinol ($C_{12}H_{10}N_2O_2$, parent neutral Molecular Weight: 214.22 Da) at **10 eV** translational collision energy in the laboratory frame (CID experiment) and the parent cation is illustrated.

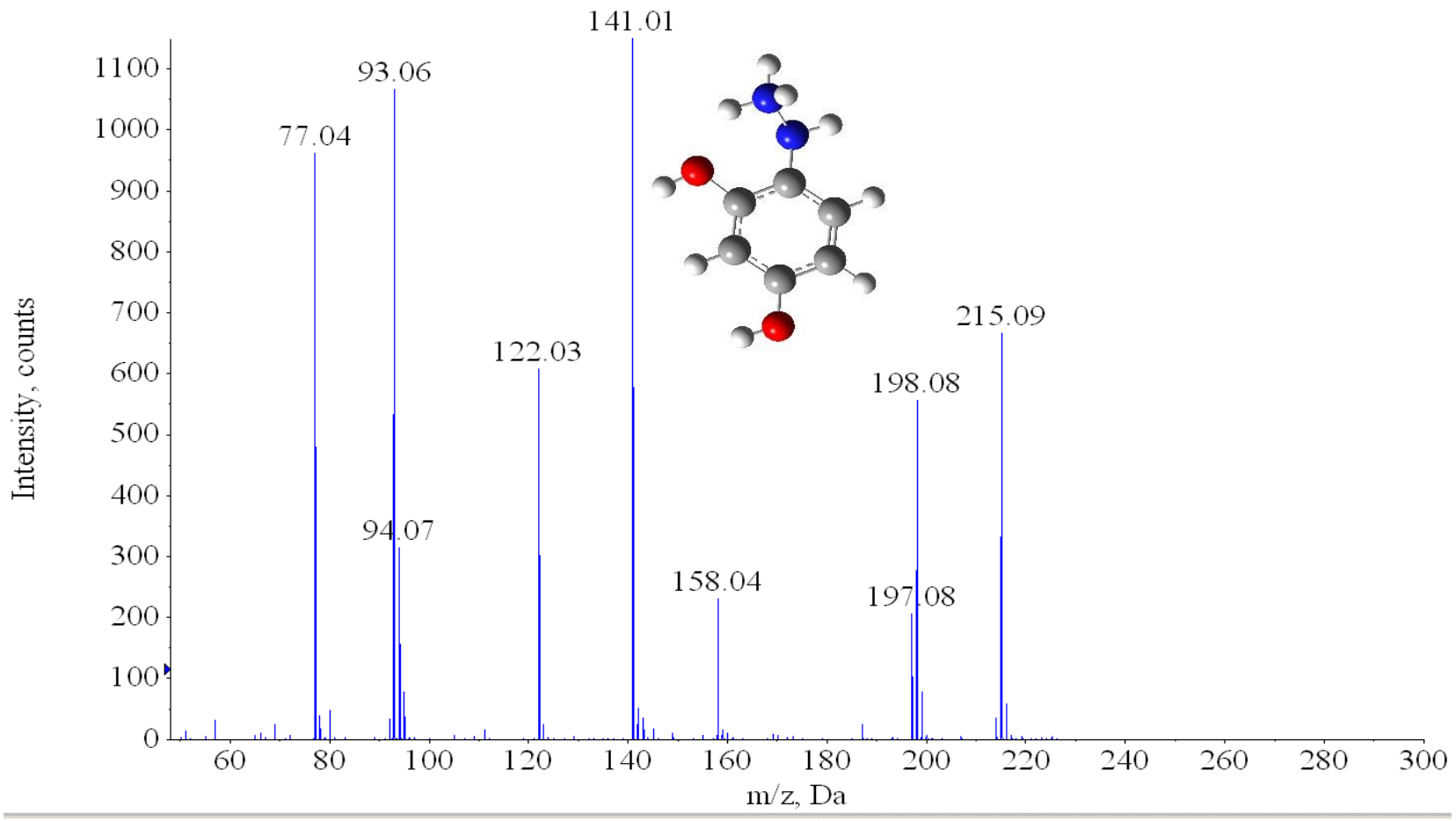

Figure A.24: Positive ion mass spectrum of 2,4- Dihydroxyazobenzene, 4 - (Phenylazo) resorcinol ($C_{12}H_{10}N_2O_2$, parent neutral Molecular Weight: 214.22 Da) at 15 eV translational collision energy in the laboratory frame (CID experiment) and the fragment cation m/z=141.0 is illustrated. As we can see this sample generated several fragment cations.

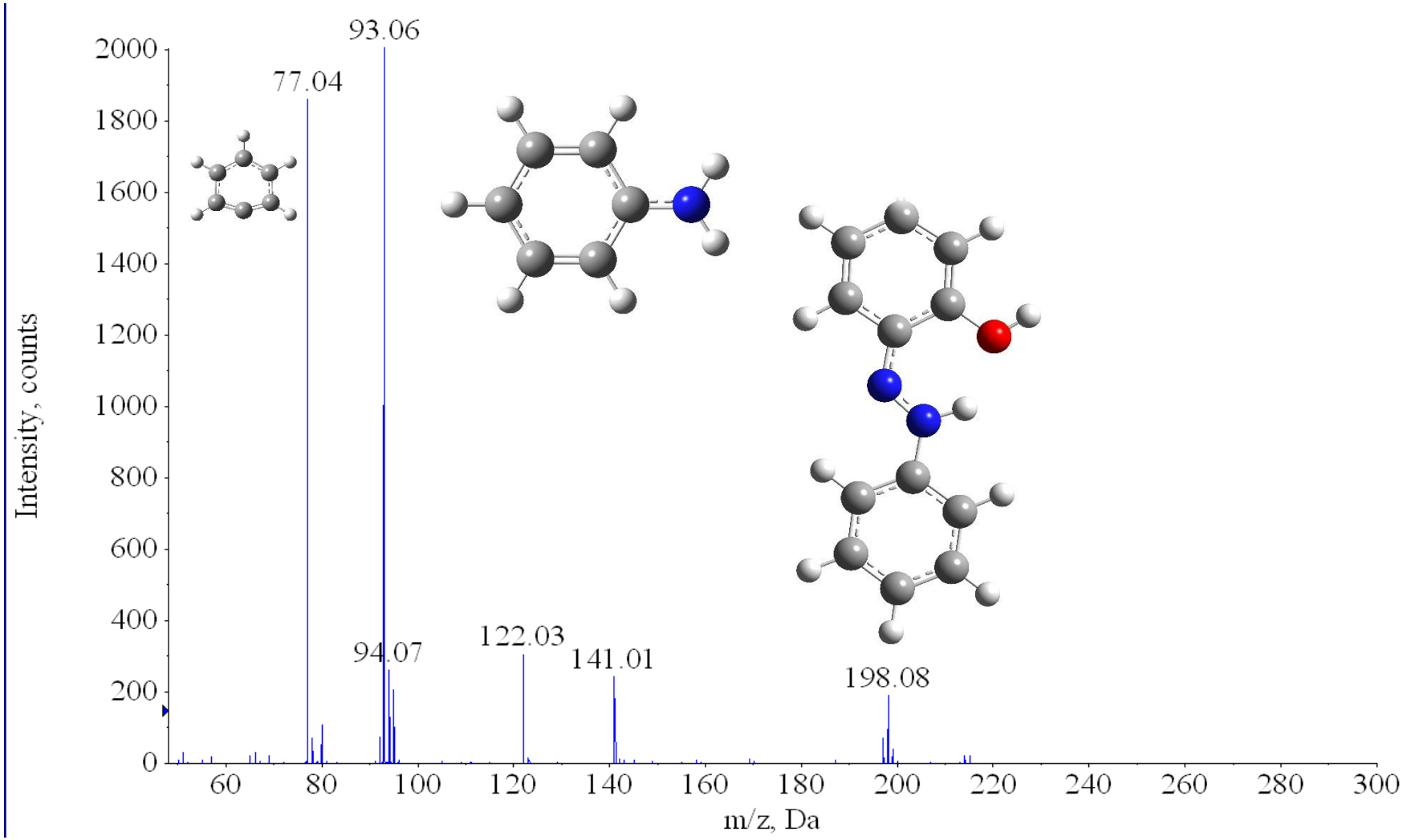

Figure A.25: Positive ion mass spectrum of 2,4- Dihydroxyazobenzene,4 - (Phenylazo) resorcinol ($C_{12}H_{10}N_2O_2$, parent neutral Molecular Weight: 214.22 Da) at **20 eV** translational collision energy in the laboratory frame (CID experiment) and the fragment cation m/z = 198.08, 93.06 and 77.04 are illustrated.

Appendix B

B.1 Azobenzene

These results are calculated for the trans azobenzene **anion** in **B3LYP** level of theory and by utilizing **6-311++G(2d,2p)** basis set. The natural bonding orbital analysis has been performed and the results visualized using GaussView[125] 5.09. Here we have performed natural population analysis.[126-129] The natural analysis is an alternative to conventional Mulliken population analysis, and seems to exhibit improved numerical stability and to better describe the electron distribution in compounds of high ionic character.[128] Natural Bond Orbital (NBO) analysis is done to obtain these results. NBOs are more useful to understand the chemical properties of a molecule comparing to conventional canonical orbitals. The Keyword SCF=NoVarAcc was used in all of our calculations and to make the integrals more precise we used the keyword Int=UltraFine.

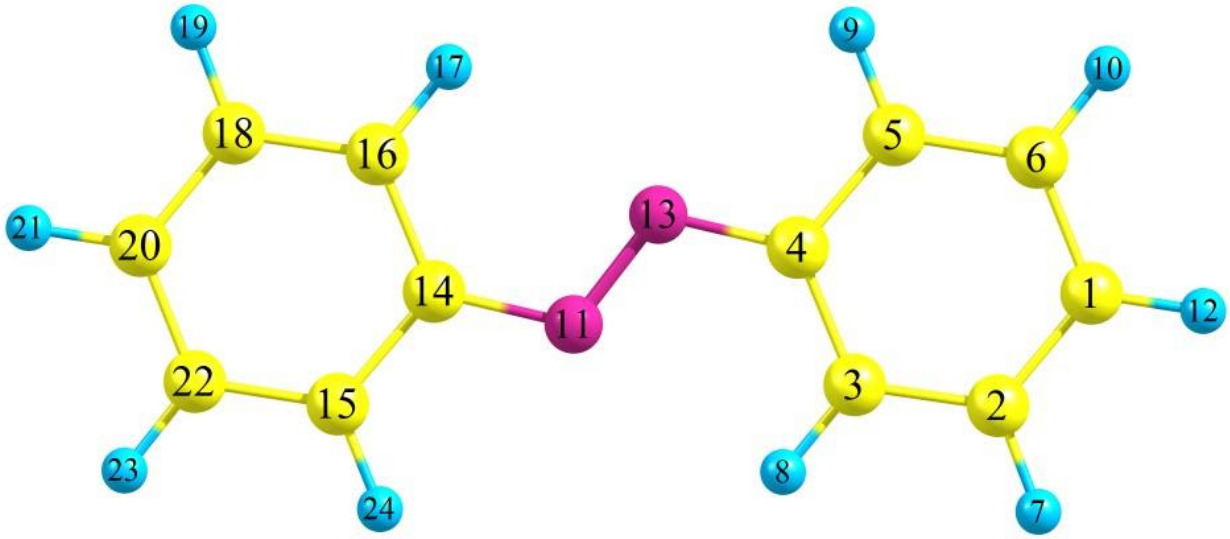

Figure B.1: Optimized Geometry of trans azobenzene anion using B3LYP level of theory along with 6-311++G(2d,2p) basis set.

! Optimized Parameters !

! (Angstroms and Degrees) !

! Name	Definition	Value	Derivative Info.	
R1	R(1,2)	1.3984	-DE/DX =	0.0 !
R2	R(1,6)	1.4006	-DE/DX =	0.0 !
R3	R(1,12)	1.0824	-DE/DX =	0.0 !
R4	R(2,3)	1.3856	-DE/DX =	0.0 !
R5	R(2,7)	1.085	-DE/DX =	0.0 !
R6	R(3,4)	1.4218	-DE/DX =	0.0 !
R7	R(3,8)	1.0791	-DE/DX =	0.0 !
R8	R(4,5)	1.4174	-DE/DX =	0.0 !
R9	R(4,13)	1.3721	-DE/DX =	0.0 !
R10	R(5,6)	1.3837	-DE/DX =	0.0 !
R11	R(5,9)	1.0826	-DE/DX =	0.0 !
R12	R(6,10)	1.0842	-DE/DX =	0.0 !
R13	R(11,13)	1.3251	-DE/DX =	0.0 !
R14	R(11,14)	1.3721	-DE/DX =	0.0 !
R15	R(14,15)	1.4174	-DE/DX =	0.0 !
R16	R(14,16)	1.4218	-DE/DX =	0.0 !
R17	R(15,22)	1.3837	-DE/DX =	0.0 !
R18	R(15,24)	1.0826	-DE/DX =	0.0 !
R19	R(16,17)	1.0791	-DE/DX =	0.0 !
R20	R(16,18)	1.3856	-DE/DX =	0.0 !
R21	R(18,19)	1.085	-DE/DX =	0.0 !
R22	R(18,20)	1.3984	-DE/DX =	0.0 !
R23	R(20,21)	1.0824	-DE/DX =	0.0 !
R24	R(20,22)	1.4006	-DE/DX =	0.0 !
R25	R(22,23)	1.0842	-DE/DX =	0.0 !

A1	A(2,1,6)	118.3974	-DE/DX = 0.0	!
A2	A(2,1,12)	120.7985	-DE/DX = 0.0	!
A3	A(6,1,12)	120.8041	-DE/DX = 0.0	!
A4	A(1,2,3)	121.4898	-DE/DX = 0.0	!
A5	A(1,2,7)	119.3772	-DE/DX = 0.0	!
A6	A(3,2,7)	119.133	-DE/DX = 0.0	!
A7	A(2,3,4)	120.7565	-DE/DX = 0.0	!
A8	A(2,3,8)	121.1694	-DE/DX = 0.0	!
A9	A(4,3,8)	118.0741	-DE/DX = 0.0	!
A10	A(3,4,5)	116.9711	-DE/DX = 0.0	!
A11	A(3,4,13)	125.7088	-DE/DX = 0.0	!
A12	A(5,4,13)	117.3201	-DE/DX = 0.0	!
A13	A(4,5,6)	121.6004	-DE/DX = 0.0	!
A14	A(4,5,9)	117.5368	-DE/DX = 0.0	!
A15	A(6,5,9)	120.8628	-DE/DX = 0.0	!
A16	A(1,6,5)	120.7848	-DE/DX = 0.0	!
A17	A(1,6,10)	119.776	-DE/DX = 0.0	!
A18	A(5,6,10)	119.4392	-DE/DX = 0.0	!
A19	A(13,11,14)	114.4709	-DE/DX = 0.0	!
A20	A(4,13,11)	114.4709	-DE/DX = 0.0	!
A21	A(11,14,15)	117.3201	-DE/DX = 0.0	!
A22	A(11,14,16)	125.7088	-DE/DX = 0.0	!
A23	A(15,14,16)	116.9711	-DE/DX = 0.0	!
A24	A(14,15,22)	121.6004	-DE/DX = 0.0	!
A25	A(14,15,24)	117.5368	-DE/DX = 0.0	!
A26	A(22,15,24)	120.8628	-DE/DX = 0.0	!
A27	A(14,16,17)	118.0741	-DE/DX = 0.0	!
A28	A(14,16,18)	120.7565	-DE/DX = 0.0	!
A29	A(17,16,18)	121.1694	-DE/DX = 0.0	!
A30	A(16,18,19)	119.133	-DE/DX = 0.0	!

A31	A(16,18,20)	121.4898	-DE/DX = 0.0	!
A32	A(19,18,20)	119.3772	-DE/DX = 0.0	!
A33	A(18,20,21)	120.7985	-DE/DX = 0.0	!
A34	A(18,20,22)	118.3974	-DE/DX = 0.0	!
A35	A(21,20,22)	120.8041	-DE/DX = 0.0	!
A36	A(15,22,20)	120.7848	-DE/DX = 0.0	!
A37	A(15,22,23)	119.4392	-DE/DX = 0.0	!
A38	A(20,22,23)	119.776	-DE/DX = 0.0	!
D1	D(6,1,2,3)	0.0	-DE/DX = 0.0	!
D2	D(6,1,2,7)	180.0	-DE/DX = 0.0	!
D3	D(12,1,2,3)	180.0	-DE/DX = 0.0	!
D4	D(12,1,2,7)	0.0	-DE/DX = 0.0	!
D5	D(2,1,6,5)	0.0	-DE/DX = 0.0	!
D6	D(2,1,6,10)	180.0	-DE/DX = 0.0	!
D7	D(12,1,6,5)	180.0	-DE/DX = 0.0	!
D8	D(12,1,6,10)	0.0	-DE/DX = 0.0	!
D9	D(1,2,3,4)	0.0	-DE/DX = 0.0	!
D10	D(1,2,3,8)	180.0	-DE/DX = 0.0	!
D11	D(7,2,3,4)	180.0	-DE/DX = 0.0	!
D12	D(7,2,3,8)	0.0	-DE/DX = 0.0	!
D13	D(2,3,4,5)	0.0	-DE/DX = 0.0	!
D14	D(2,3,4,13)	180.0	-DE/DX = 0.0	!
D15	D(8,3,4,5)	180.0	-DE/DX = 0.0	!
D16	D(8,3,4,13)	0.0	-DE/DX = 0.0	!
D17	D(3,4,5,6)	0.0	-DE/DX = 0.0	!
D18	D(3,4,5,9)	180.0	-DE/DX = 0.0	!
D19	D(13,4,5,6)	180.0	-DE/DX = 0.0	!
D20	D(13,4,5,9)	0.0	-DE/DX = 0.0	!
D21	D(3,4,13,11)	0.0	-DE/DX = 0.0	!
D22	D(5,4,13,11)	180.0	-DE/DX = 0.0	!

D23	D(4,5,6,1)	0.0	-DE/DX = 0.0	!
D24	D(4,5,6,10)	180.0	-DE/DX = 0.0	!
D25	D(9,5,6,1)	180.0	-DE/DX = 0.0	!
D26	D(9,5,6,10)	0.0	-DE/DX = 0.0	!
D27	D(14,11,13,4)	180.0	-DE/DX = 0.0	!
D28	D(13,11,14,15)	180.0	-DE/DX = 0.0	!
D29	D(13,11,14,16)	0.0	-DE/DX = 0.0	!
D30	D(11,14,15,22)	180.0	-DE/DX = 0.0	!
D31	D(11,14,15,24)	0.0	-DE/DX = 0.0	!
D32	D(16,14,15,22)	0.0	-DE/DX = 0.0	!
D33	D(16,14,15,24)	180.0	-DE/DX = 0.0	!
D34	D(11,14,16,17)	0.0	-DE/DX = 0.0	!
D35	D(11,14,16,18)	180.0	-DE/DX = 0.0	!
D36	D(15,14,16,17)	180.0	-DE/DX = 0.0	!
D37	D(15,14,16,18)	0.0	-DE/DX = 0.0	!
D38	D(14,15,22,20)	0.0	-DE/DX = 0.0	!
D39	D(14,15,22,23)	180.0	-DE/DX = 0.0	!
D40	D(24,15,22,20)	180.0	-DE/DX = 0.0	!
D41	D(24,15,22,23)	0.0	-DE/DX = 0.0	!
D42	D(14,16,18,19)	180.0	-DE/DX = 0.0	!
D43	D(14,16,18,20)	0.0	-DE/DX = 0.0	!
D44	D(17,16,18,19)	0.0	-DE/DX = 0.0	!
D45	D(17,16,18,20)	180.0	-DE/DX = 0.0	!
D46	D(16,18,20,21)	180.0	-DE/DX = 0.0	!
D47	D(16,18,20,22)	0.0	-DE/DX = 0.0	!
D48	D(19,18,20,21)	0.0	-DE/DX = 0.0	!
D49	D(19,18,20,22)	180.0	-DE/DX = 0.0	!
D50	D(18,20,22,15)	0.0	-DE/DX = 0.0	!
D51	D(18,20,22,23)	180.0	-DE/DX = 0.0	!
D52	D(21,20,22,15)	180.0	-DE/DX = 0.0	!

D53 D(21,20,22,23) 0.0 -DE/DX = 0.0 !

Summary of Natural Population Analysis:

Natural Population

Atom	No	Natural Charge	Core	Valence	Rydberg	Total
C	1	-0.28722	1.99915	4.26239	0.02569	6.28722
C	2	-0.21166	1.99915	4.19186	0.02065	6.21166
C	3	-0.25173	1.99905	4.23024	0.02243	6.25173
C	4	0.13149	1.99901	3.84040	0.02910	5.86851
C	5	-0.22117	1.99906	4.20022	0.02189	6.22117
C	6	-0.22664	1.99914	4.20634	0.02116	6.22664
H	7	0.17813	0.00000	0.81939	0.00249	0.82187
H	8	0.21474	0.00000	0.78086	0.00440	0.78526
H	9	0.19411	0.00000	0.80265	0.00324	0.80589
H	10	0.17935	0.00000	0.81810	0.00255	0.82065
N	11	-0.37924	1.99939	5.33511	0.04475	7.37924
H	12	0.17985	0.00000	0.81757	0.00259	0.82015
N	13	-0.37924	1.99939	5.33511	0.04475	7.37924
C	14	0.13149	1.99901	3.84040	0.02910	5.86851
C	15	-0.22117	1.99906	4.20022	0.02189	6.22117
C	16	-0.25173	1.99905	4.23024	0.02243	6.25173
H	17	0.21474	0.00000	0.78086	0.00440	0.78526
C	18	-0.21166	1.99915	4.19186	0.02065	6.21166
H	19	0.17813	0.00000	0.81939	0.00249	0.82187
C	20	-0.28722	1.99915	4.26239	0.02569	6.28722

H	21	0.17985	0.00000	0.81757	0.00259	0.82015
C	22	-0.22664	1.99914	4.20634	0.02116	6.22664
H	23	0.17935	0.00000	0.81810	0.00255	0.82065
H	24	0.19411	0.00000	0.80265	0.00324	0.80589

==========

* Total *	-1.00000	27.98791	68.61024	0.40186	97.00000

Natural Population

Core	27.98791 (99.9568% of 28)
Valence	68.61024 (99.4351% of 69)
Natural Minimal Basis	96.59814 (99.5857% of 97)
Natural Rydberg Basis	0.40186 (0.4143% of 97)

Figure B.2: Natural Bond Orbital analysis for the trans azobenzene anion. (a) LUMO +1 (b) LUMO (c) HOMO (d) HOMO – 1. IsoValue = 0.02 and the Density = 0.0004.

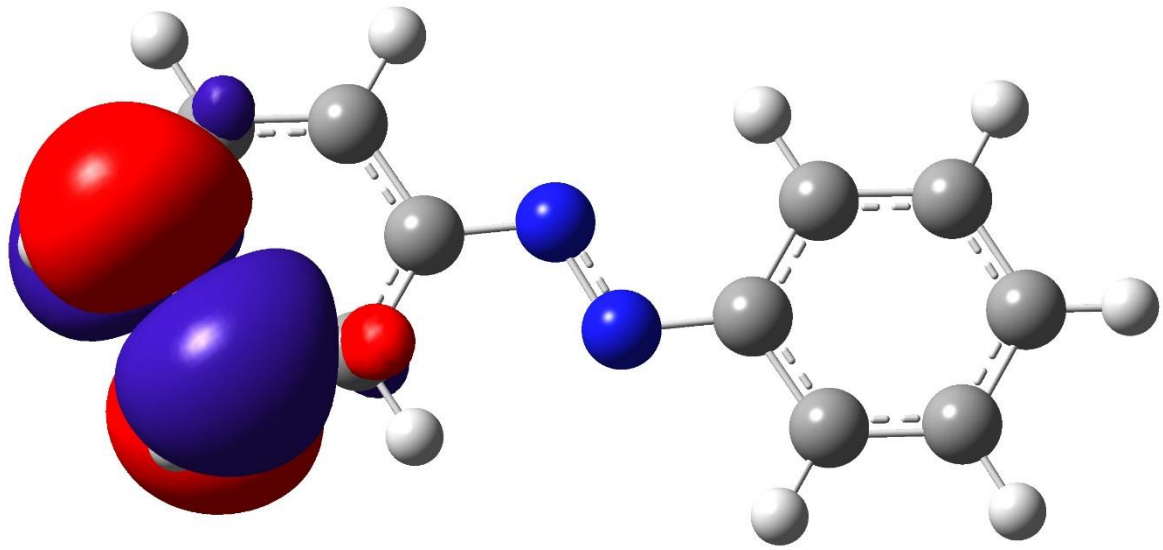

(a)

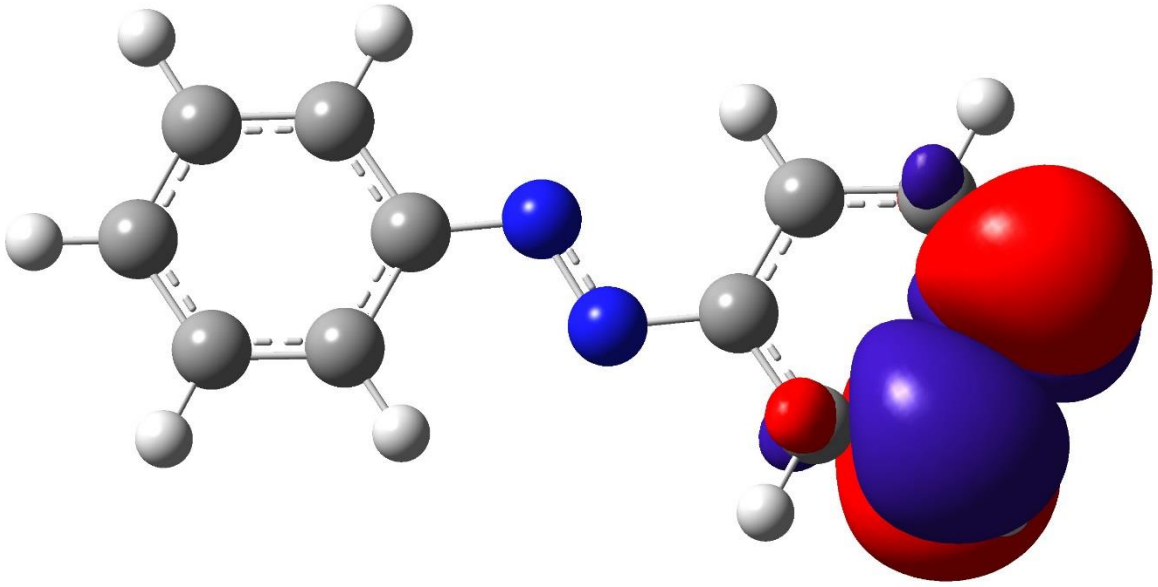

(b)

Figure B.2: Continued

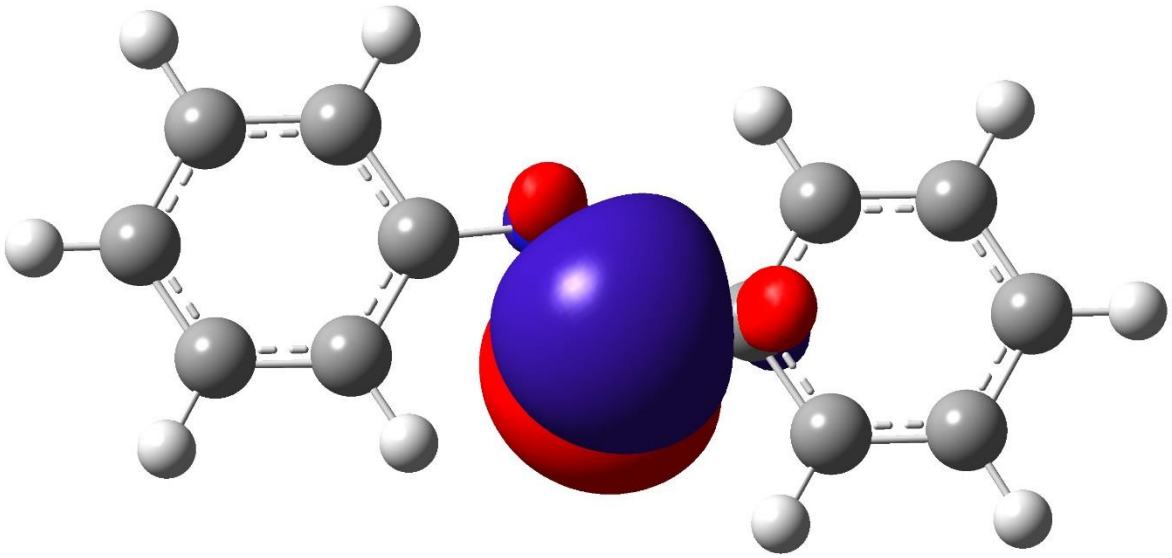

(c)

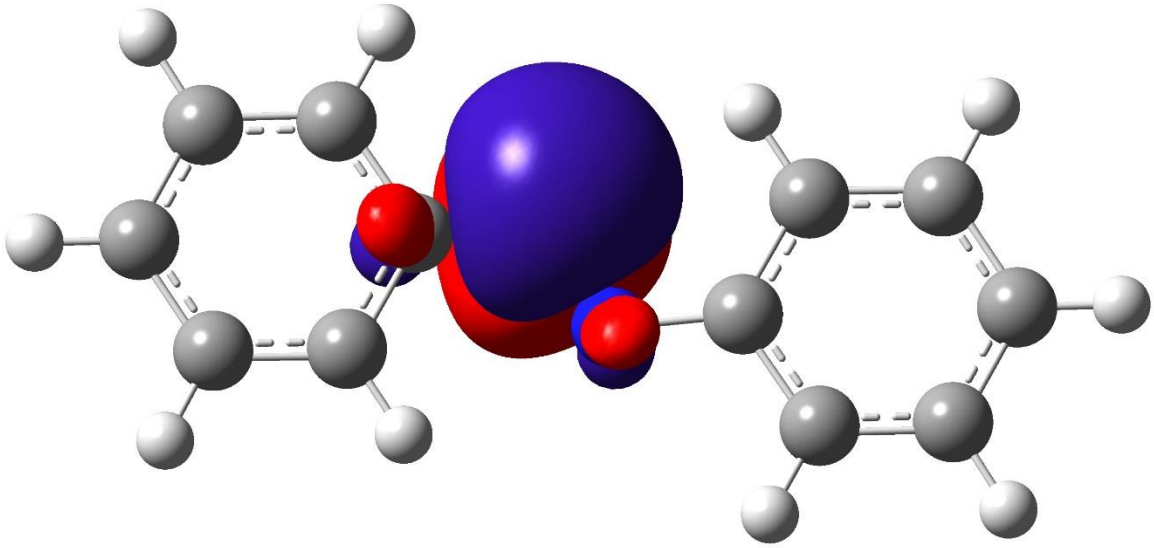

(d)

Figure B.2: Continued

Natural Bond Orbitals (Summary):

NBO	Occupancy	Energy	Principal Delocalizations (geminal,vicinal,remote)
Molecular unit 1 ($C_{12}H_{10}N_2$)			
1. BD (1) C 1 - C 2	0.98909	-0.55703	452(g),450(g),462(v),456(v) 94(v),161(v),96(v),160(v) 451(g),453(g)
2. BD (2) C 1 - C 2	0.87343	-0.12096	460(v),455(v),162(v),95(v) 449(g)
3. BD (1) C 1 - C 6	0.98878	-0.55521	459(g),448(g),453(v),461(v) 139(v),73(v),72(v),451(g) 462(g),138(v)
4. BD (1) C 1 - H 12	0.99041	-0.38886	452(v),459(v),160(v),72(v) 165(v),77(v),448(g),209(r) 450(g),182(r)
5. BD (1) C 2 - C 3	0.98890	-0.56191	458(v),448(g),454(g),451(v) 52(v),116(v),456(g),117(v) 50(v),453(g)
6. BD (1) C 2 - H 7	0.98980	-0.38277	454(v),450(v),94(v),50(v) 56(v),452(g),240(r),182(g)
7. BD (1) C 3 - C 4	0.98743	-0.52872	457(g),452(g),453(v),461(v) 73(v),458(g),138(v),72(v) 456(g),251(v),107(g)
8. BD (2) C 3 - C 4	0.78240	-0.09689	449(v),460(v),140(v),76(v) 455(g),252(v),250(v)
9. BD (1) C 3 - H 8	0.98828	-0.36538	448(v),457(v),116(v),72(v) 120(v),452(g),78(v),454(g)

453(v)

10. BD (1) C 4 - C 5 0.98651 -0.52960 463(v),454(g),459(g),462(v)
456(v),161(v),458(g),160(v)
251(v),96(v),461(g),94(v)
202(v)

11. BD (1) C 4 - N 13 0.99144 -0.63827 464(v),454(g),459(v),457(g)
218(v),452(v),138(v),94(v)

12. BD (1) C 5 - C 6 0.98915 -0.56647 450(g),458(v),457(g),451(v)
117(v),52(v),50(v),461(g)
462(g),201(v)

13. BD (2) C 5 - C 6 0.89959 -0.12265 455(v),449(v),51(v)

14. BD (1) C 5 - H 9 0.98931 -0.37284 450(v),454(v),116(v),160(v)
459(g),458(v),462(v),124(v)

15. BD (1) C 6 - H 10 0.98995 -0.38593 457(v),448(v),138(v),50(v)
143(v),459(g),209(g),240(r)
56(v)

16. BD (1) N 11 - N 13 0.99188 -0.68648 117(v),272(v),457(v),465(v)
116(v),271(v),458(g),464(g)

17. BD (1) N 11 - C 14 0.99144 -0.63827 458(v),467(g),468(v),465(g)
249(v),471(v),293(v),315(v)

18. BD (1) C 14 - C 15 0.98651 -0.52960 463(v),467(g),468(g),478(v)
470(v),410(v),464(g),408(v)
220(v),317(v),469(g),315(v)
441(v)

19. BD (2) C 14 - C 15 0.77811 -0.09847 477(v),472(v),221(v),316(v)
412(v)

20. BD (1) C 14 - C 16 0.98743 -0.52872 465(g),471(g),473(v),469(v)
347(v),464(g),293(v),346(v)

470(g),220(v),328(g)

21. BD (1) C 15 - C 22 0.98915 -0.56647 476(g),464(v),465(g),475(v)
272(v),379(v),378(v),469(g)
478(g),440(v)

22. BD (1) C 15 - H 24 0.98931 -0.37284 476(v),467(v),271(v),408(v)
468(g),464(v),478(v),279(v)

23. BD (1) C 16 - H 17 0.98828 -0.36538 474(v),465(v),271(v),346(v)
275(v),471(g),352(v),467(g)
473(v)

24. BD (1) C 16 - C 18 0.98890 -0.56191 464(v),474(g),467(g),475(v)
379(v),271(v),470(g),272(v)
378(v),473(g)

25. BD (2) C 16 - C 18 0.89246 -0.11824 466(v),477(v),377(v),472(g)

26. BD (1) C 18 - H 19 0.98980 -0.38277 467(v),476(v),315(v),378(v)
383(v),471(g),399(r),368(g)

27. BD (1) C 18 - C 20 0.98909 -0.55703 471(g),476(g),478(v),470(v)
315(v),410(v),317(v),408(v)
475(g),473(g)

28. BD (1) C 20 - H 21 0.99041 -0.38886 471(v),468(v),408(v),346(v)
413(v),351(v),474(g),430(r)
476(g),368(r)

29. BD (1) C 20 - C 22 0.98878 -0.55521 468(g),474(g),473(v),469(v)
294(v),347(v),346(v),475(g)
478(g),293(v)

30. BD (2) C 20 - C 22 0.86026 -0.12047 472(v),466(v),348(v),477(g)
295(v),297(v)

31. BD (1) C 22 - H 23 0.98995 -0.38593 465(v),474(v),293(v),378(v)
298(v),468(g),430(g),399(r)

383(v)

32. CR (1) C 1 0.99958 -9.89182 73(v),161(v),452(v),459(v)
33. CR (1) C 2 0.99958 -9.89478 96(v),52(v),454(v),450(v)
34. CR (1) C 3 0.99953 -9.87914 117(v),73(v),448(v),458(v)
457(v)
35. CR (1) C 4 0.99951 -9.91219 139(v),96(v),459(v),452(v)
463(v),457(g),253(v)
36. CR (1) C 5 0.99953 -9.88383 161(v),117(v),450(v),116(v)
454(v),458(v)
37. CR (1) C 6 0.99957 -9.89503 52(v),139(v),457(v),138(v)
448(v)
38. CR (1) N 11 0.99969 -13.98960 271(v),251(v),467(v),458(v)
465(v)
39. CR (1) N 13 0.99969 -13.98960 116(v),220(v),454(v),464(v)
457(v)
40. CR (1) C 14 0.99951 -9.91219 294(v),317(v),468(v),471(v)
463(v),465(g),222(v)
41. CR (1) C 15 0.99953 -9.88383 410(v),272(v),476(v),271(v)
467(v),464(v)
42. CR (1) C 16 0.99953 -9.87914 272(v),347(v),474(v),464(v)
465(v)
43. CR (1) C 18 0.99958 -9.89478 317(v),379(v),467(v),476(v)
44. CR (1) C 20 0.99958 -9.89182 347(v),410(v),471(v),468(v)
45. CR (1) C 22 0.99957 -9.89503 379(v),294(v),465(v),293(v)
474(v)
46. LP (1) N 11 0.97296 -0.22526 467(v),249(v),271(v),218(g)
223(g),251(v),274(v),222(g)
255(v),457(r),238(g),465(v)

			254(v),269(v),452(r),444(r)
			224(g),231(g),463(g),229(g)
47. LP (2) N	11	0.75957	-0.05298 466(v),250(v),276(v),256(v)
			472(r),273(v)
48. LP (1) N	13	0.97296	-0.22526 454(v),218(v),116(v),249(g)
			254(g),220(v),119(v),253(g)
			224(v),465(r),269(g),457(v)
			223(v),238(v),471(r),205(r)
			255(g),262(g),463(g),260(g)
49. LP (2) N	13	0.75957	-0.05298 455(v),219(v),121(v),225(v)
			118(v)

Bonds labels are according to BD for 2-center bond, CR for 1-center core pair, LP for 1-center valence lone pair, RY* for 1-center Rydberg, and BD* for 2-center antibond, the unstarred and starred labels corresponding to Lewis and non-Lewis NBOs, respectively.[130, 131]

B.2 2,2́,6,6́ - tetrafluoroazobenzene

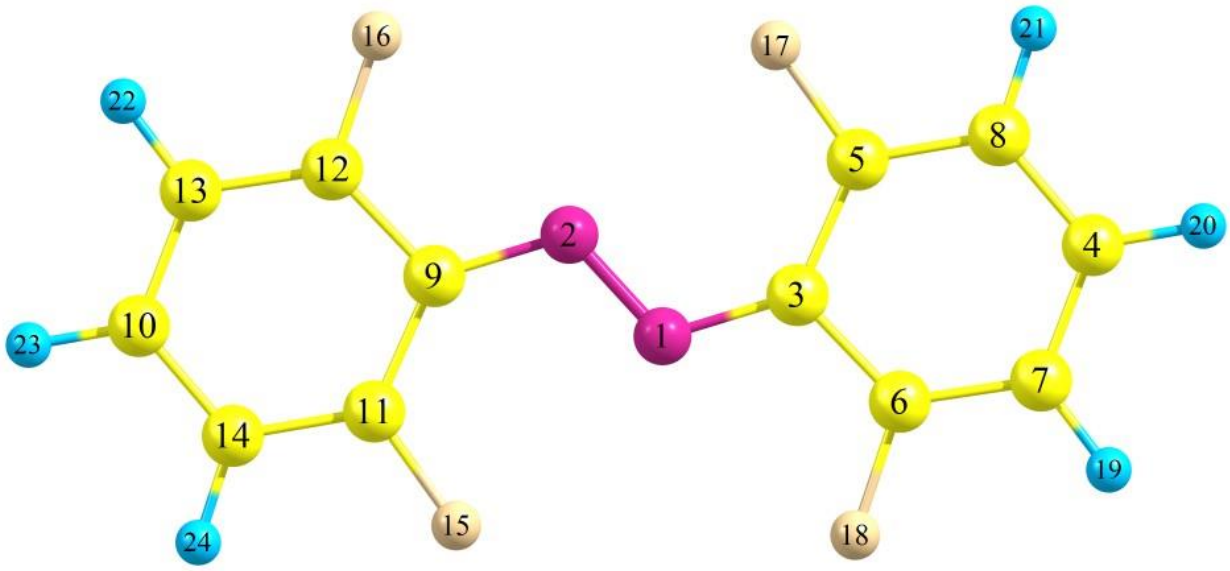

Figure B.3: Optimized Geometry of trans 2,2́,6,6́ - tetrafluoroazobenzene anion using B3LYP level of theory along with 6-311++G(2d,2p) basis set.

! Optimized Parameters !

! (Angstroms and Degrees) !

! Name	Definition	Value	Derivative Info.
R1	R(1,2)	1.3273	-DE/DX = 0.0 !
R2	R(1,3)	1.3606	-DE/DX = 0.0 !
R3	R(2,9)	1.3606	-DE/DX = 0.0 !
R4	R(3,5)	1.4289	-DE/DX = 0.0 !
R5	R(3,6)	1.4253	-DE/DX = 0.0 !
R6	R(4,7)	1.3976	-DE/DX = 0.0 !
R7	R(4,8)	1.3933	-DE/DX = 0.0 !
R8	R(4,20)	1.0805	-DE/DX = 0.0 !

R9	R(5,8)	1.382	-DE/DX = 0.0	!
R10	R(5,17)	1.354	-DE/DX = 0.0	!
R11	R(6,7)	1.3756	-DE/DX = 0.0	!
R12	R(6,18)	1.3569	-DE/DX = 0.0	!
R13	R(7,19)	1.0811	-DE/DX = 0.0	!
R14	R(8,21)	1.0817	-DE/DX = 0.0	!
R15	R(9,11)	1.4289	-DE/DX = 0.0	!
R16	R(9,12)	1.4253	-DE/DX = 0.0	!
R17	R(10,13)	1.3976	-DE/DX = 0.0	!
R18	R(10,14)	1.3933	-DE/DX = 0.0	!
R19	R(10,23)	1.0805	-DE/DX = 0.0	!
R20	R(11,14)	1.382	-DE/DX = 0.0	!
R21	R(11,15)	1.354	-DE/DX = 0.0	!
R22	R(12,13)	1.3756	-DE/DX = 0.0	!
R23	R(12,16)	1.3569	-DE/DX = 0.0	!
R24	R(13,22)	1.0811	-DE/DX = 0.0	!
R25	R(14,24)	1.0817	-DE/DX = 0.0	!
A1	A(2,1,3)	115.5833	-DE/DX = 0.0	!
A2	A(1,2,9)	115.5833	-DE/DX = 0.0	!
A3	A(1,3,5)	130.9379	-DE/DX = 0.0	!
A4	A(1,3,6)	116.8429	-DE/DX = 0.0	!
A5	A(5,3,6)	112.2192	-DE/DX = 0.0	!
A6	A(7,4,8)	118.5109	-DE/DX = 0.0	!
A7	A(7,4,20)	120.7727	-DE/DX = 0.0	!
A8	A(8,4,20)	120.7164	-DE/DX = 0.0	!
A9	A(3,5,8)	123.7381	-DE/DX = 0.0	!
A10	A(3,5,17)	120.3202	-DE/DX = 0.0	!
A11	A(8,5,17)	115.9417	-DE/DX = 0.0	!
A12	A(3,6,7)	125.2687	-DE/DX = 0.0	!
A13	A(3,6,18)	117.6193	-DE/DX = 0.0	!

A14	A(7,6,18)	117.1121	-DE/DX = 0.0	!
A15	A(4,7,6)	119.5233	-DE/DX = 0.0	!
A16	A(4,7,19)	121.8824	-DE/DX = 0.0	!
A17	A(6,7,19)	118.5943	-DE/DX = 0.0	!
A18	A(4,8,5)	120.7398	-DE/DX = 0.0	!
A19	A(4,8,21)	121.4812	-DE/DX = 0.0	!
A20	A(5,8,21)	117.779	-DE/DX = 0.0	!
A21	A(2,9,11)	130.9379	-DE/DX = 0.0	!
A22	A(2,9,12)	116.8429	-DE/DX = 0.0	!
A23	A(11,9,12)	112.2192	-DE/DX = 0.0	!
A24	A(13,10,14)	118.5109	-DE/DX = 0.0	!
A25	A(13,10,23)	120.7727	-DE/DX = 0.0	!
A26	A(14,10,23)	120.7164	-DE/DX = 0.0	!
A27	A(9,11,14)	123.7381	-DE/DX = 0.0	!
A28	A(9,11,15)	120.3202	-DE/DX = 0.0	!
A29	A(14,11,15)	115.9417	-DE/DX = 0.0	!
A30	A(9,12,13)	125.2687	-DE/DX = 0.0	!
A31	A(9,12,16)	117.6193	-DE/DX = 0.0	!
A32	A(13,12,16)	117.1121	-DE/DX = 0.0	!
A33	A(10,13,12)	119.5233	-DE/DX = 0.0	!
A34	A(10,13,22)	121.8824	-DE/DX = 0.0	!
A35	A(12,13,22)	118.5943	-DE/DX = 0.0	!
A36	A(10,14,11)	120.7398	-DE/DX = 0.0	!
A37	A(10,14,24)	121.4812	-DE/DX = 0.0	!
A38	A(11,14,24)	117.779	-DE/DX = 0.0	!
D1	D(3,1,2,9)	180.0	-DE/DX = 0.0	!
D2	D(2,1,3,5)	-0.0001	-DE/DX = 0.0	!
D3	D(2,1,3,6)	179.9999	-DE/DX = 0.0	!
D4	D(1,2,9,11)	-0.0001	-DE/DX = 0.0	!
D5	D(1,2,9,12)	179.9999	-DE/DX = 0.0	!

D6	D(1,3,5,8)	-180.0	-DE/DX = 0.0	!
D7	D(1,3,5,17)	0.0	-DE/DX = 0.0	!
D8	D(6,3,5,8)	0.0	-DE/DX = 0.0	!
D9	D(6,3,5,17)	180.0	-DE/DX = 0.0	!
D10	D(1,3,6,7)	180.0	-DE/DX = 0.0	!
D11	D(1,3,6,18)	0.0	-DE/DX = 0.0	!
D12	D(5,3,6,7)	0.0	-DE/DX = 0.0	!
D13	D(5,3,6,18)	-180.0	-DE/DX = 0.0	!
D14	D(8,4,7,6)	0.0	-DE/DX = 0.0	!
D15	D(8,4,7,19)	180.0	-DE/DX = 0.0	!
D16	D(20,4,7,6)	180.0	-DE/DX = 0.0	!
D17	D(20,4,7,19)	0.0	-DE/DX = 0.0	!
D18	D(7,4,8,5)	0.0	-DE/DX = 0.0	!
D19	D(7,4,8,21)	-180.0	-DE/DX = 0.0	!
D20	D(20,4,8,5)	-180.0	-DE/DX = 0.0	!
D21	D(20,4,8,21)	0.0	-DE/DX = 0.0	!
D22	D(3,5,8,4)	0.0	-DE/DX = 0.0	!
D23	D(3,5,8,21)	180.0	-DE/DX = 0.0	!
D24	D(17,5,8,4)	-180.0	-DE/DX = 0.0	!
D25	D(17,5,8,21)	0.0	-DE/DX = 0.0	!
D26	D(3,6,7,4)	0.0	-DE/DX = 0.0	!
D27	D(3,6,7,19)	180.0	-DE/DX = 0.0	!
D28	D(18,6,7,4)	-180.0	-DE/DX = 0.0	!
D29	D(18,6,7,19)	0.0	-DE/DX = 0.0	!
D30	D(2,9,11,14)	-180.0	-DE/DX = 0.0	!
D31	D(2,9,11,15)	0.0	-DE/DX = 0.0	!
D32	D(12,9,11,14)	0.0	-DE/DX = 0.0	!
D33	D(12,9,11,15)	180.0	-DE/DX = 0.0	!
D34	D(2,9,12,13)	180.0	-DE/DX = 0.0	!
D35	D(2,9,12,16)	0.0	-DE/DX = 0.0	!

D36	D(11,9,12,13)	0.0	-DE/DX =	0.0 !
D37	D(11,9,12,16)	-180.0	-DE/DX =	0.0 !
D38	D(14,10,13,12)	0.0	-DE/DX =	0.0 !
D39	D(14,10,13,22)	180.0	-DE/DX =	0.0 !
D40	D(23,10,13,12)	180.0	-DE/DX =	0.0 !
D41	D(23,10,13,22)	0.0	-DE/DX =	0.0 !
D42	D(13,10,14,11)	0.0	-DE/DX =	0.0 !
D43	D(13,10,14,24)	-180.0	-DE/DX =	0.0 !
D44	D(23,10,14,11)	-180.0	-DE/DX =	0.0 !
D45	D(23,10,14,24)	0.0	-DE/DX =	0.0 !
D46	D(9,11,14,10)	0.0	-DE/DX =	0.0 !
D47	D(9,11,14,24)	180.0	-DE/DX =	0.0 !
D48	D(15,11,14,10)	-180.0	-DE/DX =	0.0 !
D49	D(15,11,14,24)	0.0	-DE/DX =	0.0 !
D50	D(9,12,13,10)	0.0	-DE/DX =	0.0 !
D51	D(9,12,13,22)	180.0	-DE/DX =	0.0 !
D52	D(16,12,13,10)	180.0	-DE/DX =	0.0 !
D53	D(16,12,13,22)	0.0	-DE/DX =	0.0 !

Summary of Natural Population Analysis:

		Natural Population				
	Natural	----------				
Atom	No	Charge	Core	Valence	Rydberg	Total
N	1	-0.34775	1.99938	5.30449	0.04387	7.34775
N	2	-0.34775	1.99938	5.30449	0.04387	7.34775
C	3	0.02715	1.99888	3.94564	0.02833	5.97285
C	4	-0.25426	1.99918	4.23182	0.02325	6.25426

C	5	0.38507	1.99848	3.58704	0.02941	5.61493
C	6	0.41077	1.99848	3.56312	0.02762	5.58923
C	7	-0.30416	1.99904	4.28322	0.02190	6.30416
C	8	-0.29080	1.99906	4.27027	0.02147	6.29080
C	9	0.02715	1.99888	3.94564	0.02833	5.97285
C	10	-0.25426	1.99918	4.23182	0.02325	6.25426
C	11	0.38507	1.99848	3.58704	0.02941	5.61493
C	12	0.41077	1.99848	3.56312	0.02762	5.58923
C	13	-0.30416	1.99904	4.28322	0.02190	6.30416
C	14	-0.29080	1.99906	4.27027	0.02147	6.29080
F	15	-0.35146	1.99992	7.34080	0.01074	9.35146
F	16	-0.36131	1.99992	7.35075	0.01064	9.36131
F	17	-0.35146	1.99992	7.34080	0.01074	9.35146
F	18	-0.36131	1.99992	7.35075	0.01064	9.36131
H	19	0.20028	0.00000	0.79704	0.00268	0.79972
H	20	0.18685	0.00000	0.81053	0.00262	0.81315
H	21	0.19961	0.00000	0.79765	0.00274	0.80039
H	22	0.20028	0.00000	0.79704	0.00268	0.79972
H	23	0.18685	0.00000	0.81053	0.00262	0.81315
H	24	0.19961	0.00000	0.79765	0.00274	0.80039

==========

* Total *	-1.00000	35.98470	92.56476	0.45054	129.00000

Natural Population

Core	35.98470 (99.9575% of 36)
Valence	92.56476 (99.5320% of 93)
Natural Minimal Basis	128.54946 (99.6507% of 129)

Natural Rydberg Basis 0.45054 (0.3493% of 129)

Atom	No	Natural Electron Configuration
N	1	[core]2S(1.40)2p(3.90)3S(0.02)3p(0.01)3d(0.01)
N	2	[core]2S(1.40)2p(3.90)3S(0.02)3p(0.01)3d(0.01)
C	3	[core]2S(0.86)2p(3.09)3p(0.02)3d(0.01)
C	4	[core]2S(0.94)2p(3.29)3p(0.02)
C	5	[core]2S(0.84)2p(2.75)3p(0.02)3d(0.01)
C	6	[core]2S(0.84)2p(2.73)3p(0.02)3d(0.01)
C	7	[core]2S(0.95)2p(3.33)3p(0.01)
C	8	[core]2S(0.95)2p(3.32)3p(0.01)
C	9	[core]2S(0.86)2p(3.09)3p(0.02)3d(0.01)
C	10	[core]2S(0.94)2p(3.29)3p(0.02)
C	11	[core]2S(0.84)2p(2.75)3p(0.02)3d(0.01)
C	12	[core]2S(0.84)2p(2.73)3p(0.02)3d(0.01)
C	13	[core]2S(0.95)2p(3.33)3p(0.01)
C	14	[core]2S(0.95)2p(3.32)3p(0.01)
F	15	[core]2S(1.83)2p(5.51)
F	16	[core]2S(1.83)2p(5.52)
F	17	[core]2S(1.83)2p(5.51)
F	18	[core]2S(1.83)2p(5.52)
H	19	1S(0.80)
H	20	1S(0.81)
H	21	1S(0.80)
H	22	1S(0.80)
H	23	1S(0.81)
H	24	1S(0.80)

Figure B.4: Natural Bond Orbital analysis for the trans 2,2́,6,6́-tetrafluoroazobenzene anion. (a) LUMO +1 (b) LUMO (c) HOMO (d) HOMO – 1. IsoValue = 0.02 and the Density = 0.0004.

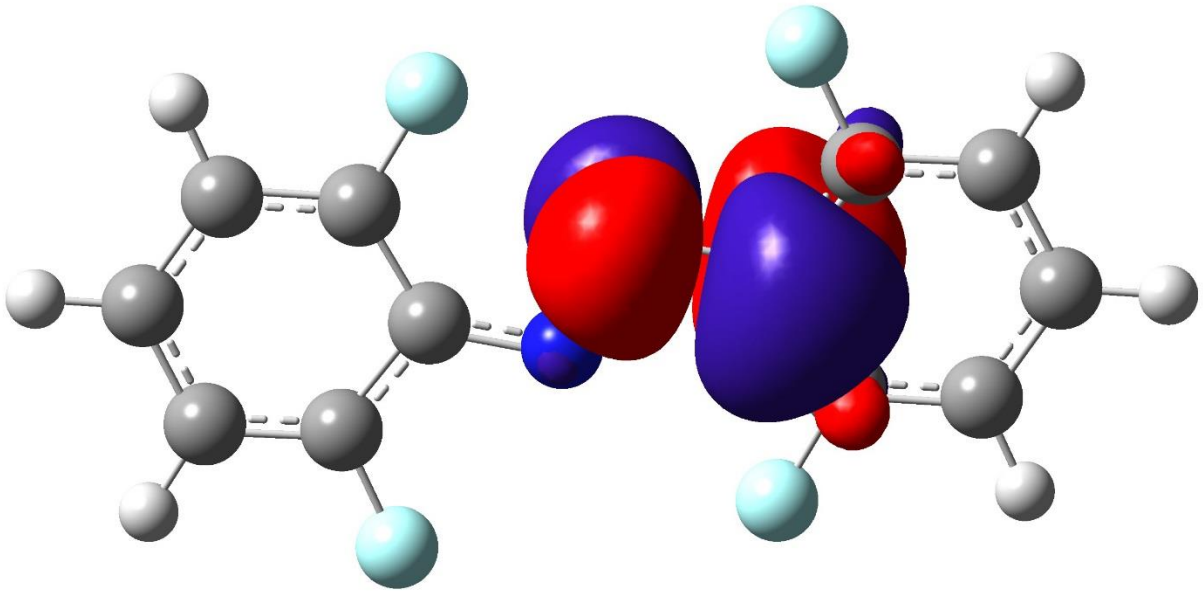

(a)

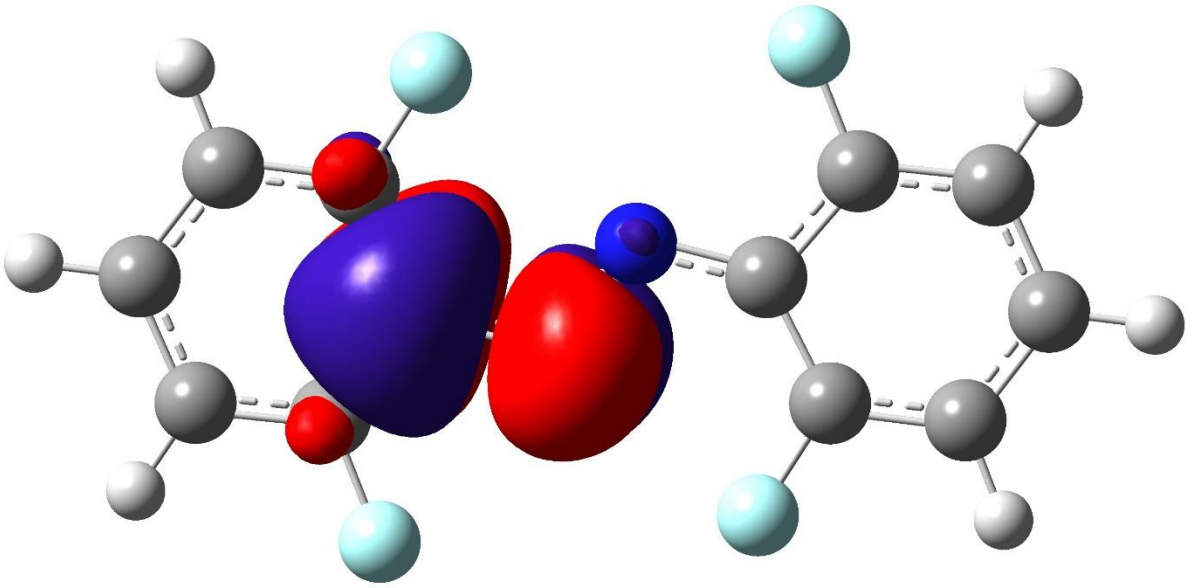

(b)

Figure B.4: Continued

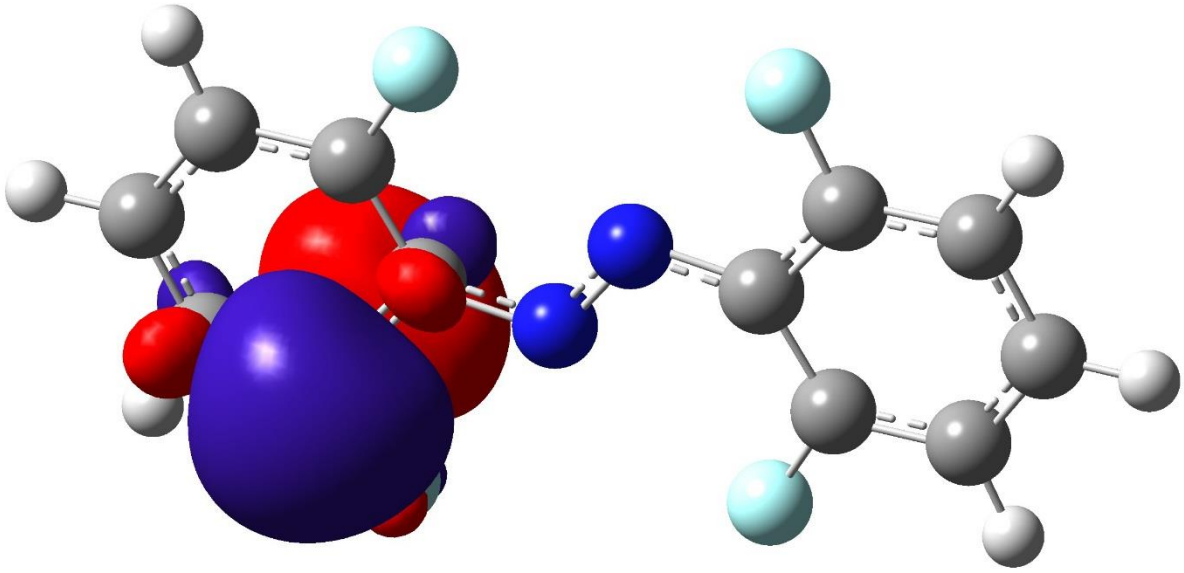

(c)

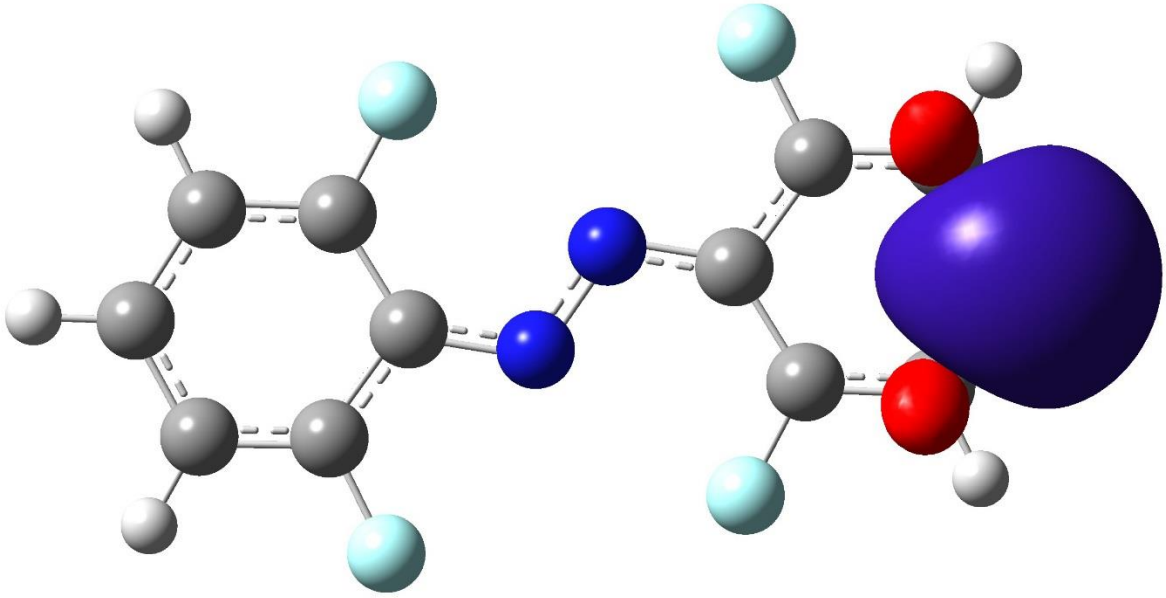

(d)

Figure B.4: Continued

Molecular orbitals energy levels in eV:

1	-668.281248804	Occupied	B	1 -668.273901672	Occupied B
2	-668.280976688	Occupied	A	2 -668.273901672	Occupied A
3	-668.125326336	Occupied	B	3 -668.109271492	Occupied B
4	-668.125326336	Occupied	A	4 -668.109271492	Occupied A
5	-385.770417604	Occupied	A	5 -385.6223865	Occupied A
6	-385.763342588	Occupied	B	6 -385.614495136	Occupied B
7	-275.629833908	Occupied	B	7 -275.575682824	Occupied A
8	-275.629833908	Occupied	A	8 -275.575682824	Occupied A
9	-275.620581964	Occupied	B	9 -275.57323378	Occupied B
10	-275.620581964	Occupied	A	10 -275.57323378	Occupied A
11	-274.259185616	Occupied	B	11 -274.276873156	Occupied B
12	-274.2589135	Occupied	A	12 -274.27660104	Occupied A
13	-273.72012382	Occupied	B	13 -273.661074648	Occupied B
14	-273.72012382	Occupied	A	14 -273.661074648	Occupied A
15	-273.625155336	Occupied	B	15 -273.644747688	Occupied A
16	-273.625155336	Occupied	A	16 -273.644747688	Occupied A
17	-273.618352436	Occupied	?A	17 -273.637400556	Occupied B
18	-273.618352436	Occupied	?A	18 -273.63712844	Occupied A
19	-29.808675104	Occupied	A	19 -29.789354868	Occupied A
20	-29.808130872	Occupied	B	20 -29.788810636	Occupied B
21	-29.696835428	Occupied	A	21 -29.660644	Occupied A
22	-29.695202732	Occupied	B	22 -29.65928342	Occupied B
23	-23.11489362	Occupied	A	23 -22.820464108	Occupied A
24	-20.38965188	Occupied	B	24 -20.316996908	Occupied B
25	-20.017125076	Occupied	A	25 -19.953177816	Occupied A
26	-18.555862156	Occupied	B	26 -18.402388732	Occupied B
27	-17.133239708	Occupied	A	27 -17.091878076	Occupied A

28	-17.128613736	Occupied	B	28	-17.086707872	Occupied	B
29	-16.865477564	Occupied	A	29	-16.79499952	Occupied	A
30	-15.423262764	Occupied	B	30	-15.208019008	Occupied	B
31	-13.860772692	Occupied	A	31	-13.794376388	Occupied	A
32	-13.56226144	Occupied	B	32	-13.537498884	Occupied	B
33	-13.450421764	Occupied	A	33	-13.419944772	Occupied	A
34	-12.842242504	Occupied	B	34	-12.769859648	Occupied	B
35	-11.77309874	Occupied	A	35	-11.738540008	Occupied	A
36	-11.629149376	Occupied	B	36	-11.582345424	Occupied	B
37	-10.991309472	Occupied	A	37	-10.946954564	Occupied	A
38	-10.768446468	Occupied	B	38	-10.748309884	Occupied	B
39	-10.176594168	Occupied	A	39	-10.165437412	Occupied	A
40	-9.919716664	Occupied	B	40	-9.89277718	Occupied	B
41	-9.896042572	Occupied	A	41	-9.869103088	Occupied	A
42	-9.727058536	Occupied	B	42	-9.711275808	Occupied	B
43	-9.543380236	Occupied	A	43	-9.402424148	Occupied	A
44	-9.43970404	Occupied	B	44	-9.325687436	Occupied	B
45	-9.064728192	Occupied	B	45	-8.953160632	Occupied	B
46	-9.058197408	Occupied	A	46	-8.948806776	Occupied	A
47	-8.908805724	Occupied	A	47	-8.844586348	Occupied	A
48	-8.566755912	Occupied	B	48	-8.543626052	Occupied	B
49	-8.506890392	Occupied	A	49	-8.481311488	Occupied	A
50	-7.571083468	Occupied	B	50	-7.545504564	Occupied	B
51	-7.361282032	Occupied	A	51	-7.353118552	Occupied	A
52	-7.223591336	Occupied	A	52	-6.871473232	Occupied	A
53	-6.895963672	Occupied	A	53	-6.863037636	Occupied	B
54	-6.886711728	Occupied	B	54	-6.766980688	Occupied	B
55	-6.795824984	Occupied	B	55	-6.74983738	Occupied	A

56	-6.514729156	Occupied	A	56	-6.492959876	Occupied	A
57	-6.461122304	Occupied	B	57	-6.317989288	Occupied	B
58	-6.105738808	Occupied	A	58	-5.84641226	Occupied	B
59	-6.004511656	Occupied	B	59	-5.750627428	Occupied	A
60	-4.429776364	Occupied	B	60	-4.104325628	Occupied	B
61	-3.493425208	Occupied	A	61	-3.383218228	Occupied	B
62	-3.493153092	Occupied	B	62	-3.37968072	Occupied	A
63	-2.694220516	Occupied	A	63	-2.206316528	Occupied	A
64	-1.965493868	Occupied	A	64	-1.776645364	Occupied	A
65	-0.249802488	Occupied	B	65	1.465616776	Unoccupied	B
66	2.186179944	Unoccupied	A	66	2.184275132	Unoccupied	A
67	2.186996292	Unoccupied	B	67	2.18509148	Unoccupied	B

B.3 2,2',6,6' tetramethyl - (4,4') dinitro-azobenzene

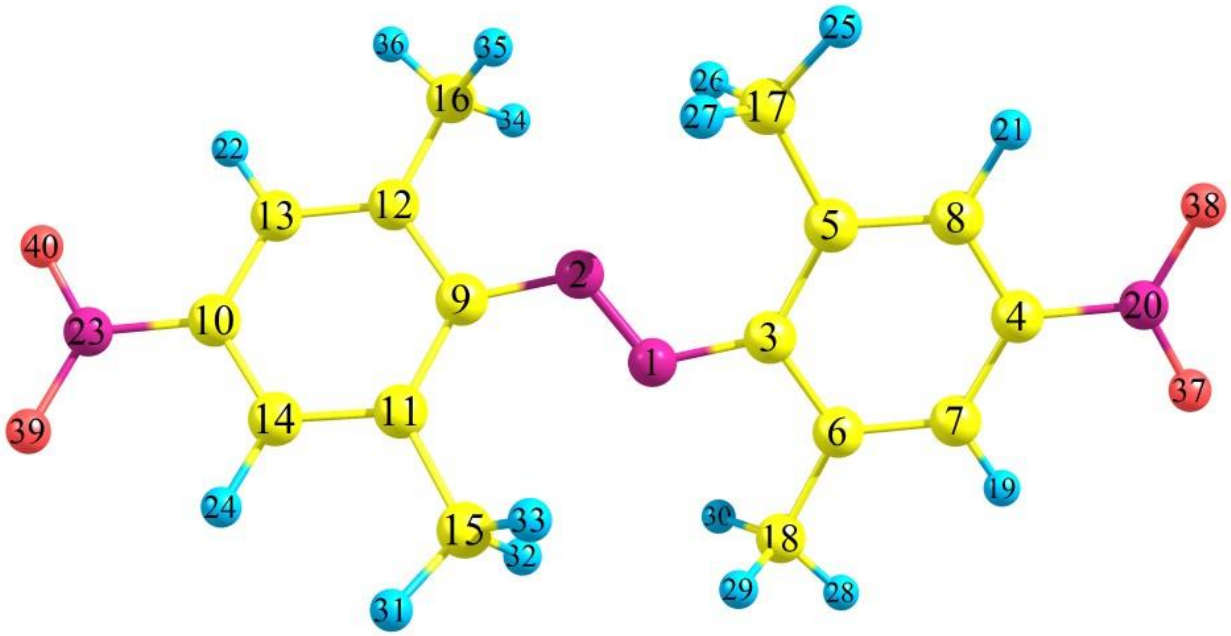

Figure B.5: Optimized Geometry of trans 2,2',6,6' tetramethyl - (4,4') dinitro-azobenzene anion using B3LYP level of theory along with 6-311++G(2d,2p) basis set.

! Optimized Parameters !

! (Angstroms and Degrees) !

! Name	Definition	Value	Derivative Info.	
R1	R(1,2)	1.3059	-DE/DX = 0.0	!
R2	R(1,3)	1.3704	-DE/DX = 0.0	!
R3	R(2,9)	1.3704	-DE/DX = 0.0	!
R4	R(3,5)	1.4392	-DE/DX = 0.0	!
R5	R(3,6)	1.4361	-DE/DX = 0.0	!
R6	R(4,7)	1.3994	-DE/DX = 0.0	!
R7	R(4,8)	1.3976	-DE/DX = 0.0	!

R8	R(4,20)	1.4293	-DE/DX =	0.0	!
R9	R(5,8)	1.3819	-DE/DX =	0.0	!
R10	R(5,17)	1.5091	-DE/DX =	0.0	!
R11	R(6,7)	1.3762	-DE/DX =	0.0	!
R12	R(6,18)	1.5071	-DE/DX =	0.0	!
R13	R(7,19)	1.0787	-DE/DX =	0.0	!
R14	R(8,21)	1.0792	-DE/DX =	0.0	!
R15	R(9,11)	1.4392	-DE/DX =	0.0	!
R16	R(9,12)	1.4361	-DE/DX =	0.0	!
R17	R(10,13)	1.3994	-DE/DX =	0.0	!
R18	R(10,14)	1.3976	-DE/DX =	0.0	!
R19	R(10,23)	1.4293	-DE/DX =	0.0	!
R20	R(11,14)	1.3819	-DE/DX =	0.0	!
R21	R(11,15)	1.5091	-DE/DX =	0.0	!
R22	R(12,13)	1.3762	-DE/DX =	0.0	!
R23	R(12,16)	1.5071	-DE/DX =	0.0	!
R24	R(13,22)	1.0787	-DE/DX =	0.0	!
R25	R(14,24)	1.0792	-DE/DX =	0.0	!
R26	R(15,31)	1.0909	-DE/DX =	0.0	!
R27	R(15,32)	1.088	-DE/DX =	0.0	!
R28	R(15,33)	1.089	-DE/DX =	0.0	!
R29	R(16,34)	1.0903	-DE/DX =	0.0	!
R30	R(16,35)	1.0902	-DE/DX =	0.0	!
R31	R(16,36)	1.0898	-DE/DX =	0.0	!
R32	R(17,25)	1.0909	-DE/DX =	0.0	!
R33	R(17,26)	1.088	-DE/DX =	0.0	!
R34	R(17,27)	1.089	-DE/DX =	0.0	!
R35	R(18,28)	1.0898	-DE/DX =	0.0	!
R36	R(18,29)	1.0902	-DE/DX =	0.0	!
R37	R(18,30)	1.0903	-DE/DX =	0.0	!

R38	R(20,37)	1.2451	-DE/DX = 0.0	!
R39	R(20,38)	1.2449	-DE/DX = 0.0	!
R40	R(23,39)	1.2449	-DE/DX = 0.0	!
R41	R(23,40)	1.2451	-DE/DX = 0.0	!
A1	A(2,1,3)	117.6045	-DE/DX = 0.0	!
A2	A(1,2,9)	117.6045	-DE/DX = 0.0	!
A3	A(1,3,5)	127.5795	-DE/DX = 0.0	!
A4	A(1,3,6)	113.8614	-DE/DX = 0.0	!
A5	A(5,3,6)	118.5228	-DE/DX = 0.0	!
A6	A(7,4,8)	120.0056	-DE/DX = 0.0	!
A7	A(7,4,20)	120.0239	-DE/DX = 0.0	!
A8	A(8,4,20)	119.9667	-DE/DX = 0.0	!
A9	A(3,5,8)	118.8403	-DE/DX = 0.0	!
A10	A(3,5,17)	123.8106	-DE/DX = 0.0	!
A11	A(8,5,17)	117.3121	-DE/DX = 0.0	!
A12	A(3,6,7)	120.5827	-DE/DX = 0.0	!
A13	A(3,6,18)	120.0128	-DE/DX = 0.0	!
A14	A(7,6,18)	119.3983	-DE/DX = 0.0	!
A15	A(4,7,6)	120.2697	-DE/DX = 0.0	!
A16	A(4,7,19)	118.8976	-DE/DX = 0.0	!
A17	A(6,7,19)	120.8327	-DE/DX = 0.0	!
A18	A(4,8,5)	121.7521	-DE/DX = 0.0	!
A19	A(4,8,21)	118.2276	-DE/DX = 0.0	!
A20	A(5,8,21)	120.0182	-DE/DX = 0.0	!
A21	A(2,9,11)	127.5795	-DE/DX = 0.0	!
A22	A(2,9,12)	113.8614	-DE/DX = 0.0	!
A23	A(11,9,12)	118.5228	-DE/DX = 0.0	!
A24	A(13,10,14)	120.0056	-DE/DX = 0.0	!
A25	A(13,10,23)	120.0239	-DE/DX = 0.0	!
A26	A(14,10,23)	119.9667	-DE/DX = 0.0	!

A27	A(9,11,14)	118.8403	-DE/DX =	0.0	!
A28	A(9,11,15)	123.8106	-DE/DX =	0.0	!
A29	A(14,11,15)	117.3121	-DE/DX =	0.0	!
A30	A(9,12,13)	120.5827	-DE/DX =	0.0	!
A31	A(9,12,16)	120.0128	-DE/DX =	0.0	!
A32	A(13,12,16)	119.3983	-DE/DX =	0.0	!
A33	A(10,13,12)	120.2697	-DE/DX =	0.0	!
A34	A(10,13,22)	118.8976	-DE/DX =	0.0	!
A35	A(12,13,22)	120.8327	-DE/DX =	0.0	!
A36	A(10,14,11)	121.7521	-DE/DX =	0.0	!
A37	A(10,14,24)	118.2276	-DE/DX =	0.0	!
A38	A(11,14,24)	120.0182	-DE/DX =	0.0	!
A39	A(11,15,31)	109.4681	-DE/DX =	0.0	!
A40	A(11,15,32)	111.8942	-DE/DX =	0.0	!
A41	A(11,15,33)	111.6526	-DE/DX =	0.0	!
A42	A(31,15,32)	108.799	-DE/DX =	0.0	!
A43	A(31,15,33)	108.9176	-DE/DX =	0.0	!
A44	A(32,15,33)	105.9948	-DE/DX =	0.0	!
A45	A(12,16,34)	111.4592	-DE/DX =	0.0	!
A46	A(12,16,35)	111.2539	-DE/DX =	0.0	!
A47	A(12,16,36)	110.2671	-DE/DX =	0.0	!
A48	A(34,16,35)	106.3584	-DE/DX =	0.0	!
A49	A(34,16,36)	108.7571	-DE/DX =	0.0	!
A50	A(35,16,36)	108.6125	-DE/DX =	0.0	!
A51	A(5,17,25)	109.4681	-DE/DX =	0.0	!
A52	A(5,17,26)	111.8942	-DE/DX =	0.0	!
A53	A(5,17,27)	111.6526	-DE/DX =	0.0	!
A54	A(25,17,26)	108.799	-DE/DX =	0.0	!
A55	A(25,17,27)	108.9176	-DE/DX =	0.0	!
A56	A(26,17,27)	105.9948	-DE/DX =	0.0	!

A57	A(6,18,28)	110.2671	-DE/DX = 0.0	!
A58	A(6,18,29)	111.2539	-DE/DX = 0.0	!
A59	A(6,18,30)	111.4592	-DE/DX = 0.0	!
A60	A(28,18,29)	108.6125	-DE/DX = 0.0	!
A61	A(28,18,30)	108.7571	-DE/DX = 0.0	!
A62	A(29,18,30)	106.3584	-DE/DX = 0.0	!
A63	A(4,20,37)	118.6044	-DE/DX = 0.0	!
A64	A(4,20,38)	118.7879	-DE/DX = 0.0	!
A65	A(37,20,38)	122.6077	-DE/DX = 0.0	!
A66	A(10,23,39)	118.7879	-DE/DX = 0.0	!
A67	A(10,23,40)	118.6044	-DE/DX = 0.0	!
A68	A(39,23,40)	122.6077	-DE/DX = 0.0	!
D1	D(3,1,2,9)	-175.0719	-DE/DX = 0.0	!
D2	D(2,1,3,5)	16.791	-DE/DX = 0.0	!
D3	D(2,1,3,6)	-165.4536	-DE/DX = 0.0	!
D4	D(1,2,9,11)	16.791	-DE/DX = 0.0	!
D5	D(1,2,9,12)	-165.4537	-DE/DX = 0.0	!
D6	D(1,3,5,8)	178.7303	-DE/DX = 0.0	!
D7	D(1,3,5,17)	1.0061	-DE/DX = 0.0	!
D8	D(6,3,5,8)	1.0667	-DE/DX = 0.0	!
D9	D(6,3,5,17)	-176.6575	-DE/DX = 0.0	!
D10	D(1,3,6,7)	-179.8039	-DE/DX = 0.0	!
D11	D(1,3,6,18)	1.1059	-DE/DX = 0.0	!
D12	D(5,3,6,7)	-1.8284	-DE/DX = 0.0	!
D13	D(5,3,6,18)	179.0813	-DE/DX = 0.0	!
D14	D(8,4,7,6)	0.3557	-DE/DX = 0.0	!
D15	D(8,4,7,19)	-179.604	-DE/DX = 0.0	!
D16	D(20,4,7,6)	179.6431	-DE/DX = 0.0	!
D17	D(20,4,7,19)	-0.3166	-DE/DX = 0.0	!
D18	D(7,4,8,5)	-1.1275	-DE/DX = 0.0	!

D19	D(7,4,8,21)	178.3507	-DE/DX = 0.0	!
D20	D(20,4,8,5)	179.5847	-DE/DX = 0.0	!
D21	D(20,4,8,21)	-0.9372	-DE/DX = 0.0	!
D22	D(7,4,20,37)	0.0894	-DE/DX = 0.0	!
D23	D(7,4,20,38)	-179.936	-DE/DX = 0.0	!
D24	D(8,4,20,37)	179.3771	-DE/DX = 0.0	!
D25	D(8,4,20,38)	-0.6484	-DE/DX = 0.0	!
D26	D(3,5,8,4)	0.3827	-DE/DX = 0.0	!
D27	D(3,5,8,21)	-179.0863	-DE/DX = 0.0	!
D28	D(17,5,8,4)	178.2546	-DE/DX = 0.0	!
D29	D(17,5,8,21)	-1.2144	-DE/DX = 0.0	!
D30	D(3,5,17,25)	168.8439	-DE/DX = 0.0	!
D31	D(3,5,17,26)	-70.4642	-DE/DX = 0.0	!
D32	D(3,5,17,27)	48.1597	-DE/DX = 0.0	!
D33	D(8,5,17,25)	-8.9124	-DE/DX = 0.0	!
D34	D(8,5,17,26)	111.7795	-DE/DX = 0.0	!
D35	D(8,5,17,27)	-129.5967	-DE/DX = 0.0	!
D36	D(3,6,7,4)	1.1221	-DE/DX = 0.0	!
D37	D(3,6,7,19)	-178.919	-DE/DX = 0.0	!
D38	D(18,6,7,4)	-179.782	-DE/DX = 0.0	!
D39	D(18,6,7,19)	0.1768	-DE/DX = 0.0	!
D40	D(3,6,18,28)	178.1401	-DE/DX = 0.0	!
D41	D(3,6,18,29)	-61.2836	-DE/DX = 0.0	!
D42	D(3,6,18,30)	57.2454	-DE/DX = 0.0	!
D43	D(7,6,18,28)	-0.9609	-DE/DX = 0.0	!
D44	D(7,6,18,29)	119.6154	-DE/DX = 0.0	!
D45	D(7,6,18,30)	-121.8557	-DE/DX = 0.0	!
D46	D(2,9,11,14)	178.7303	-DE/DX = 0.0	!
D47	D(2,9,11,15)	1.0061	-DE/DX = 0.0	!
D48	D(12,9,11,14)	1.0667	-DE/DX = 0.0	!

D49	D(12,9,11,15)	-176.6575	-DE/DX = 0.0	!
D50	D(2,9,12,13)	-179.8039	-DE/DX = 0.0	!
D51	D(2,9,12,16)	1.1058	-DE/DX = 0.0	!
D52	D(11,9,12,13)	-1.8284	-DE/DX = 0.0	!
D53	D(11,9,12,16)	179.0813	-DE/DX = 0.0	!
D54	D(14,10,13,12)	0.3557	-DE/DX = 0.0	!
D55	D(14,10,13,22)	-179.604	-DE/DX = 0.0	!
D56	D(23,10,13,12)	179.6431	-DE/DX = 0.0	!
D57	D(23,10,13,22)	-0.3166	-DE/DX = 0.0	!
D58	D(13,10,14,11)	-1.1275	-DE/DX = 0.0	!
D59	D(13,10,14,24)	178.3507	-DE/DX = 0.0	!
D60	D(23,10,14,11)	179.5846	-DE/DX = 0.0	!
D61	D(23,10,14,24)	-0.9372	-DE/DX = 0.0	!
D62	D(13,10,23,39)	-179.936	-DE/DX = 0.0	!
D63	D(13,10,23,40)	0.0894	-DE/DX = 0.0	!
D64	D(14,10,23,39)	-0.6484	-DE/DX = 0.0	!
D65	D(14,10,23,40)	179.3771	-DE/DX = 0.0	!
D66	D(9,11,14,10)	0.3827	-DE/DX = 0.0	!
D67	D(9,11,14,24)	-179.0863	-DE/DX = 0.0	!
D68	D(15,11,14,10)	178.2546	-DE/DX = 0.0	!
D69	D(15,11,14,24)	-1.2144	-DE/DX = 0.0	!
D70	D(9,11,15,31)	168.8439	-DE/DX = 0.0	!
D71	D(9,11,15,32)	-70.4642	-DE/DX = 0.0	!
D72	D(9,11,15,33)	48.1597	-DE/DX = 0.0	!
D73	D(14,11,15,31)	-8.9124	-DE/DX = 0.0	!
D74	D(14,11,15,32)	111.7794	-DE/DX = 0.0	!
D75	D(14,11,15,33)	-129.5967	-DE/DX = 0.0	!
D76	D(9,12,13,10)	1.1221	-DE/DX = 0.0	!
D77	D(9,12,13,22)	-178.919	-DE/DX = 0.0	!
D78	D(16,12,13,10)	-179.782	-DE/DX = 0.0	!

D79	D(16,12,13,22)	0.1768	-DE/DX =	0.0	!
D80	D(9,12,16,34)	57.2454	-DE/DX =	0.0	!
D81	D(9,12,16,35)	-61.2836	-DE/DX =	0.0	!
D82	D(9,12,16,36)	178.1401	-DE/DX =	0.0	!
D83	D(13,12,16,34)	-121.8557	-DE/DX =	0.0	!
D84	D(13,12,16,35)	119.6154	-DE/DX =	0.0	!
D85	D(13,12,16,36)	-0.9609	-DE/DX =	0.0	!

Figure B.6: Population analysis for the trans 2,2',6,6' tetramethyl - (4,4') dinitro-azobenzene anion. Calculations has been performed in B3LYP level of theory along with 6-311++G(2d,2p) basis set. (a) LUMO +1 (b) LUMO (c) HOMO (d) HOMO – 1. IsoValue = 0.02 and the Density = 0.0004.

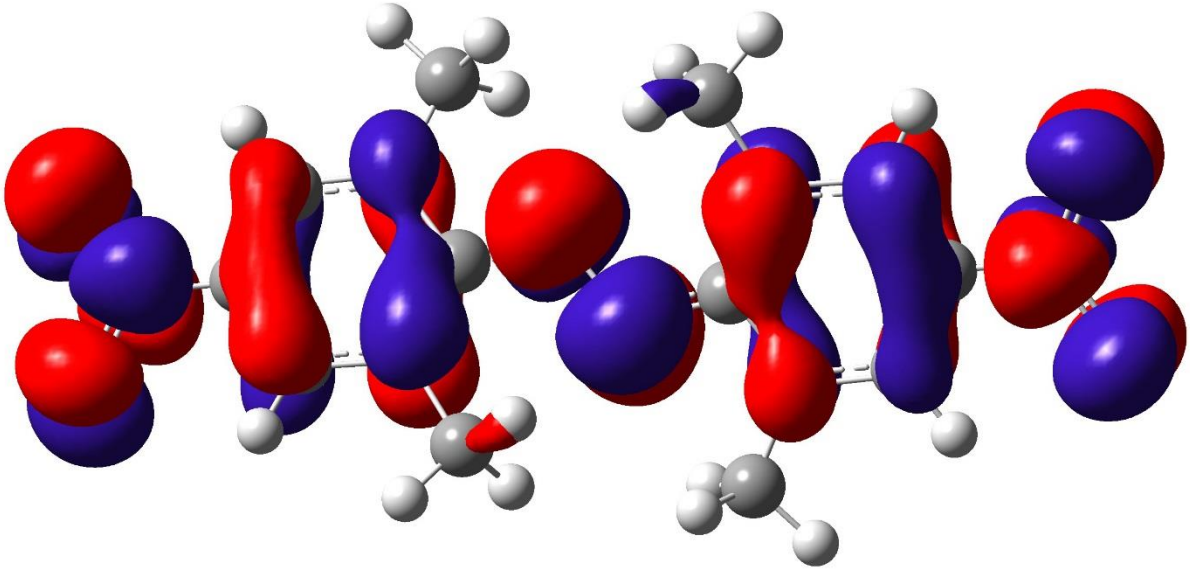

(a)

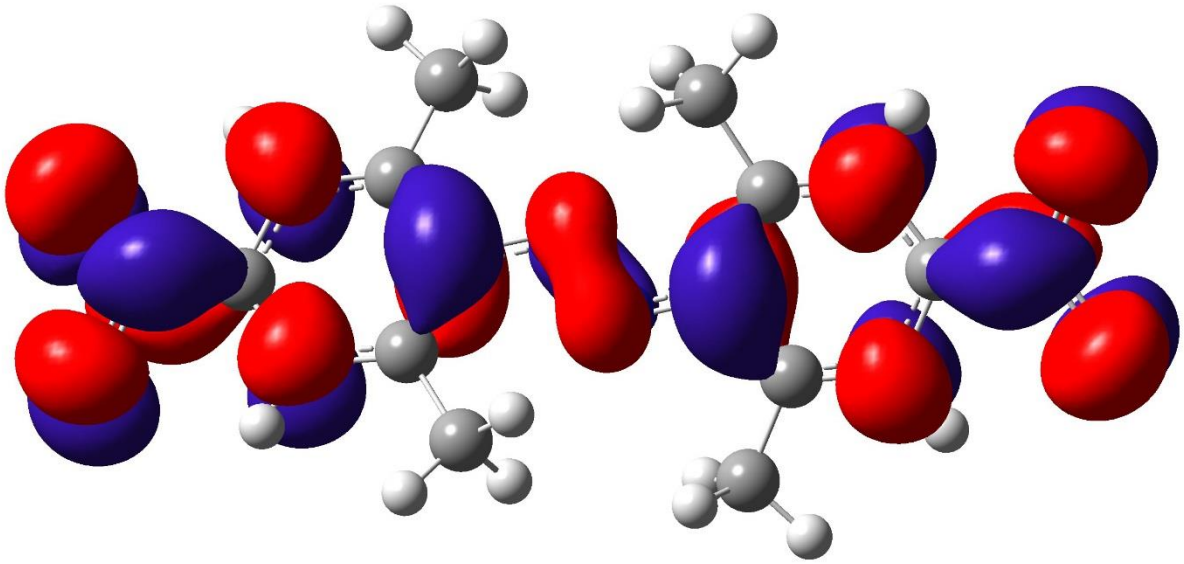

(b)

Figure B.6: Continued

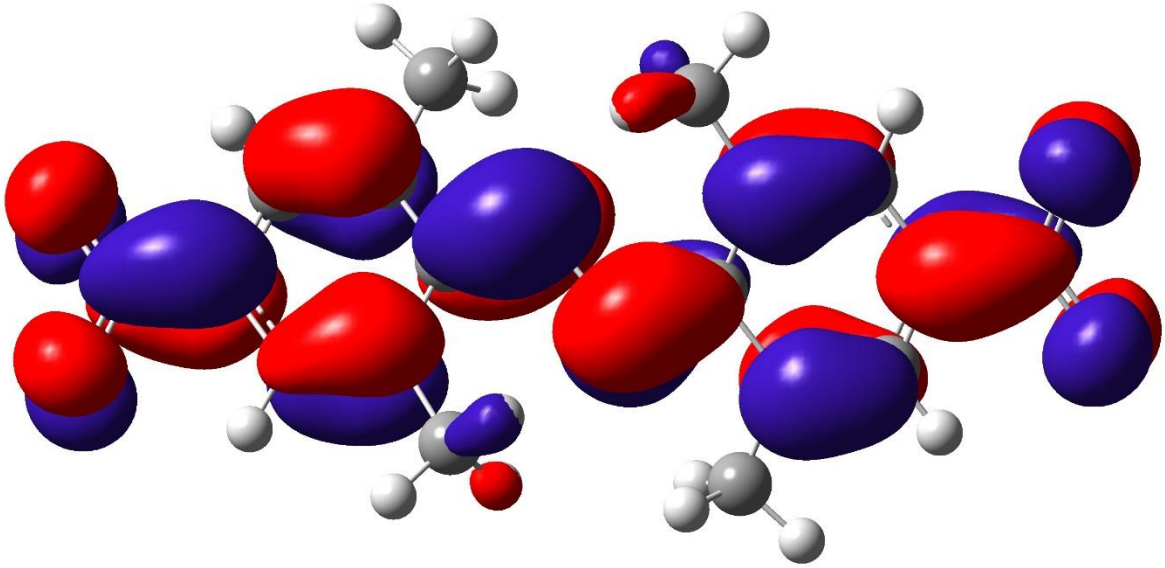

(c)

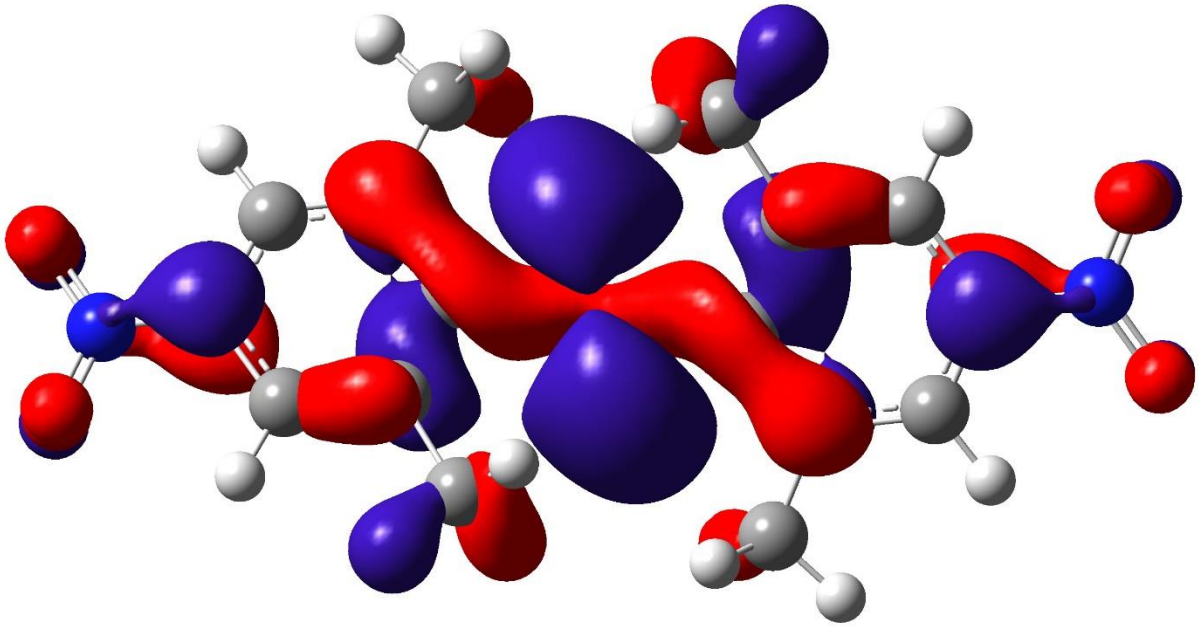

(d)

Figure B.6: Continued

B.4 4,4' dinitro - azobenzene

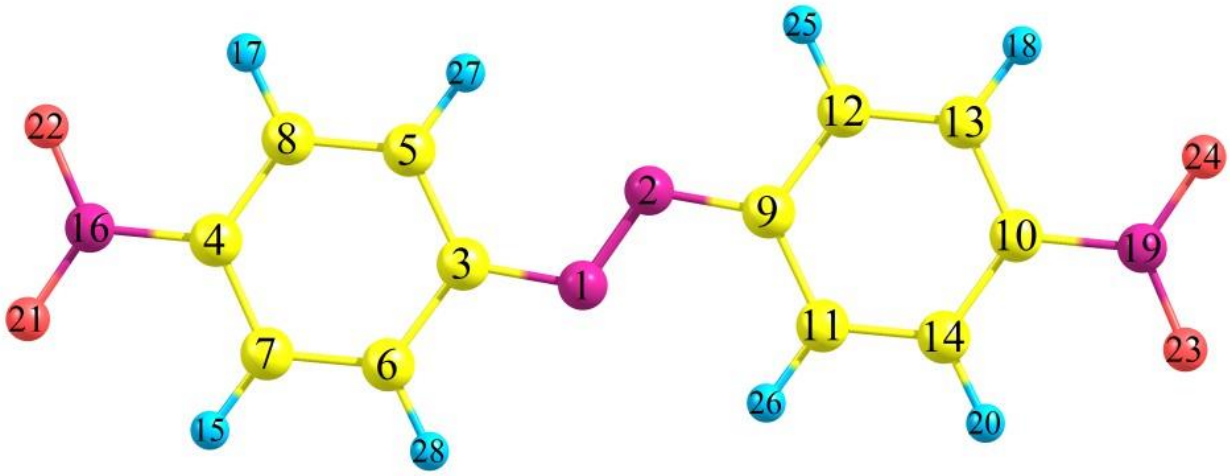

Figure B.7: Optimized Geometry of trans 4,4' dinitro - azobenzene anion using B3LYP level of theory along with 6-311++G(2d,2p) basis set.

! Optimized Parameters !

! (Angstroms and Degrees) !

! Name	Definition	Value	Derivative Info.
! R1	R(1,2)	1.3043	-DE/DX = 0.0 !
! R2	R(1,3)	1.371	-DE/DX = 0.0 !
! R3	R(2,9)	1.371	-DE/DX = 0.0 !
! R4	R(3,5)	1.4214	-DE/DX = 0.0 !
! R5	R(3,6)	1.4166	-DE/DX = 0.0 !
! R6	R(4,7)	1.4037	-DE/DX = 0.0 !
! R7	R(4,8)	1.4047	-DE/DX = 0.0 !
! R8	R(4,16)	1.4301	-DE/DX = 0.0 !
! R9	R(5,8)	1.3741	-DE/DX = 0.0 !
! R10	R(5,27)	1.0784	-DE/DX = 0.0 !

! R11	R(6,7)	1.3748	-DE/DX = 0.0	!
! R12	R(6,28)	1.0811	-DE/DX = 0.0	!
! R13	R(7,15)	1.0784	-DE/DX = 0.0	!
! R14	R(8,17)	1.079	-DE/DX = 0.0	!
! R15	R(9,11)	1.4214	-DE/DX = 0.0	!
! R16	R(9,12)	1.4166	-DE/DX = 0.0	!
! R17	R(10,13)	1.4037	-DE/DX = 0.0	!
! R18	R(10,14)	1.4047	-DE/DX = 0.0	!
! R19	R(10,19)	1.4301	-DE/DX = 0.0	!
! R20	R(11,14)	1.3741	-DE/DX = 0.0	!
! R21	R(11,26)	1.0784	-DE/DX = 0.0	!
! R22	R(12,13)	1.3748	-DE/DX = 0.0	!
! R23	R(12,25)	1.0811	-DE/DX = 0.0	!
! R24	R(13,18)	1.0784	-DE/DX = 0.0	!
! R25	R(14,20)	1.079	-DE/DX = 0.0	!
! R26	R(16,21)	1.244	-DE/DX = 0.0	!
! R27	R(16,22)	1.2439	-DE/DX = 0.0	!
! R28	R(19,23)	1.2439	-DE/DX = 0.0	!
! R29	R(19,24)	1.244	-DE/DX = 0.0	!
! A1	A(2,1,3)	114.9694	-DE/DX = 0.0	!
! A2	A(1,2,9)	114.9694	-DE/DX = 0.0	!
! A3	A(1,3,5)	125.4611	-DE/DX = 0.0	!
! A4	A(1,3,6)	116.618	-DE/DX = 0.0	!
! A5	A(5,3,6)	117.9209	-DE/DX = 0.0	!
! A6	A(7,4,8)	120.2228	-DE/DX = 0.0	!
! A7	A(7,4,16)	119.8899	-DE/DX = 0.0	!
! A8	A(8,4,16)	119.8873	-DE/DX = 0.0	!
! A9	A(3,5,8)	120.7203	-DE/DX = 0.0	!
! A10	A(3,5,27)	118.4668	-DE/DX = 0.0	!
! A11	A(8,5,27)	120.8129	-DE/DX = 0.0	!

! A12	A(3,6,7)	121.4948	-DE/DX =	0.0 !
! A13	A(3,6,28)	117.7699	-DE/DX =	0.0 !
! A14	A(7,6,28)	120.7353	-DE/DX =	0.0 !
! A15	A(4,7,6)	119.4875	-DE/DX =	0.0 !
! A16	A(4,7,15)	119.0174	-DE/DX =	0.0 !
! A17	A(6,7,15)	121.4951	-DE/DX =	0.0 !
! A18	A(4,8,5)	120.1537	-DE/DX =	0.0 !
! A19	A(4,8,17)	118.6572	-DE/DX =	0.0 !
! A20	A(5,8,17)	121.1891	-DE/DX =	0.0 !
! A21	A(2,9,11)	125.4611	-DE/DX =	0.0 !
! A22	A(2,9,12)	116.618	-DE/DX =	0.0 !
! A23	A(11,9,12)	117.9209	-DE/DX =	0.0 !
! A24	A(13,10,14)	120.2228	-DE/DX =	0.0 !
! A25	A(13,10,19)	119.8899	-DE/DX =	0.0 !
! A26	A(14,10,19)	119.8873	-DE/DX =	0.0 !
! A27	A(9,11,14)	120.7203	-DE/DX =	0.0 !
! A28	A(9,11,26)	118.4668	-DE/DX =	0.0 !
! A29	A(14,11,26)	120.8129	-DE/DX =	0.0 !
! A30	A(9,12,13)	121.4948	-DE/DX =	0.0 !
! A31	A(9,12,25)	117.7699	-DE/DX =	0.0 !
! A32	A(13,12,25)	120.7353	-DE/DX =	0.0 !
! A33	A(10,13,12)	119.4875	-DE/DX =	0.0 !
! A34	A(10,13,18)	119.0174	-DE/DX =	0.0 !
! A35	A(12,13,18)	121.4951	-DE/DX =	0.0 !
! A36	A(10,14,11)	120.1537	-DE/DX =	0.0 !
! A37	A(10,14,20)	118.6572	-DE/DX =	0.0 !
! A38	A(11,14,20)	121.1891	-DE/DX =	0.0 !
! A39	A(4,16,21)	118.6085	-DE/DX =	0.0 !
! A40	A(4,16,22)	118.7133	-DE/DX =	0.0 !
! A41	A(21,16,22)	122.6782	-DE/DX =	0.0 !

```
! A42   A(10,19,23)        118.7133       -DE/DX =    0.0            !
! A43   A(10,19,24)        118.6085       -DE/DX =    0.0            !
! A44   A(23,19,24)        122.6782       -DE/DX =    0.0            !
 ! D1    D(3,1,2,9)         180.0         -DE/DX =    0.0            !
 ! D2    D(2,1,3,5)          0.0          -DE/DX =    0.0            !
 ! D3    D(2,1,3,6)         180.0         -DE/DX =    0.0            !
 ! D4    D(1,2,9,11)         0.0          -DE/DX =    0.0            !
 ! D5    D(1,2,9,12)        180.0         -DE/DX =    0.0            !
 ! D6    D(1,3,5,8)         180.0         -DE/DX =    0.0            !
 ! D7    D(1,3,5,27)         0.0          -DE/DX =    0.0            !
 ! D8    D(6,3,5,8)          0.0          -DE/DX =    0.0            !
 ! D9    D(6,3,5,27)        180.0         -DE/DX =    0.0            !
 ! D10   D(1,3,6,7)         180.0         -DE/DX =    0.0            !
 ! D11   D(1,3,6,28)          0.0         -DE/DX =    0.0            !
 ! D12   D(5,3,6,7)           0.0         -DE/DX =    0.0            !
 ! D13   D(5,3,6,28)        180.0         -DE/DX =    0.0            !
 ! D14   D(8,4,7,6)           0.0         -DE/DX =    0.0            !
 ! D15   D(8,4,7,15)        180.0         -DE/DX =    0.0            !
 ! D16   D(16,4,7,6)        180.0         -DE/DX =    0.0            !
 ! D17   D(16,4,7,15)         0.0         -DE/DX =    0.0            !
 ! D18   D(7,4,8,5)           0.0         -DE/DX =    0.0            !
 ! D19   D(7,4,8,17)        180.0         -DE/DX =    0.0            !
 ! D20   D(16,4,8,5)        180.0         -DE/DX =    0.0            !
 ! D21   D(16,4,8,17)         0.0         -DE/DX =    0.0            !
 ! D22   D(7,4,16,21)         0.0         -DE/DX =    0.0            !
 ! D23   D(7,4,16,22)       180.0         -DE/DX =    0.0            !
 ! D24   D(8,4,16,21)       180.0         -DE/DX =    0.0            !
 ! D25   D(8,4,16,22)         0.0         -DE/DX =    0.0            !
 ! D26   D(3,5,8,4)           0.0         -DE/DX =    0.0            !
 ! D27   D(3,5,8,17)        180.0         -DE/DX =    0.0            !
```

```
 ! D28   D(27,5,8,4)         180.0         -DE/DX =    0.0             !
 ! D29   D(27,5,8,17)         0.0         -DE/DX =    0.0             !
 ! D30   D(3,6,7,4)           0.0         -DE/DX =    0.0             !
 ! D31   D(3,6,7,15)        180.0         -DE/DX =    0.0             !
 ! D32   D(28,6,7,4)         180.0         -DE/DX =    0.0             !
 ! D33   D(28,6,7,15)          0.0         -DE/DX =    0.0             !
 ! D34   D(2,9,11,14)        180.0         -DE/DX =    0.0             !
 ! D35   D(2,9,11,26)          0.0         -DE/DX =    0.0             !
 ! D36   D(12,9,11,14)         0.0         -DE/DX =    0.0             !
 ! D37   D(12,9,11,26)       180.0         -DE/DX =    0.0             !
 ! D38   D(2,9,12,13)        180.0         -DE/DX =    0.0             !
 ! D39   D(2,9,12,25)          0.0         -DE/DX =    0.0             !
 ! D40   D(11,9,12,13)         0.0         -DE/DX =    0.0             !
 ! D41   D(11,9,12,25)       180.0         -DE/DX =    0.0             !
 ! D42   D(14,10,13,12)        0.0         -DE/DX =    0.0             !
 ! D43   D(14,10,13,18)      180.0         -DE/DX =    0.0             !
 ! D44   D(19,10,13,12)      180.0         -DE/DX =    0.0             !
 ! D45   D(19,10,13,18)        0.0         -DE/DX =    0.0             !
 ! D46   D(13,10,14,11)        0.0         -DE/DX =    0.0             !
 ! D47   D(13,10,14,20)      180.0         -DE/DX =    0.0             !
 ! D48   D(19,10,14,11)      180.0         -DE/DX =    0.0             !
 ! D49   D(19,10,14,20)        0.0         -DE/DX =    0.0             !
 ! D50   D(13,10,19,23)      180.0         -DE/DX =    0.0             !
 ! D51   D(13,10,19,24)        0.0         -DE/DX =    0.0             !
 ! D52   D(14,10,19,23)        0.0         -DE/DX =    0.0             !
 ! D53   D(14,10,19,24)      180.0         -DE/DX =    0.0             !
 ! D54   D(9,11,14,10)         0.0         -DE/DX =    0.0             !
 ! D55   D(9,11,14,20)       180.0         -DE/DX =    0.0             !
 ! D56   D(26,11,14,10)      180.0         -DE/DX =    0.0             !
 ! D57   D(26,11,14,20)        0.0         -DE/DX =    0.0             !
```

! D58	D(9,12,13,10)	0.0	-DE/DX =	0.0 !
! D59	D(9,12,13,18)	180.0	-DE/DX =	0.0 !
! D60	D(25,12,13,10)	180.0	-DE/DX =	0.0 !
! D61	D(25,12,13,18)	0.0	-DE/DX =	0.0 !

Summary of Natural Population Analysis:

Natural Population

Atom	No	Natural Charge	Core	Valence	Rydberg	Total
N	1	-0.31045	1.99938	5.26830	0.04276	7.31045
N	2	-0.31045	1.99938	5.26830	0.04276	7.31045
C	3	0.14215	1.99902	3.82985	0.02898	5.85785
C	4	0.04395	1.99883	3.93421	0.02302	5.95605
C	5	-0.22208	1.99905	4.20289	0.02013	6.22208
C	6	-0.19607	1.99907	4.17685	0.02015	6.19607
C	7	-0.19668	1.99906	4.17608	0.02154	6.19668
C	8	-0.18200	1.99907	4.16201	0.02092	6.18200
C	9	0.14215	1.99902	3.82985	0.02898	5.85785
C	10	0.04395	1.99883	3.93421	0.02302	5.95605
C	11	-0.22208	1.99905	4.20289	0.02013	6.22208
C	12	-0.19607	1.99907	4.17685	0.02015	6.19607
C	13	-0.19668	1.99906	4.17608	0.02154	6.19668
C	14	-0.18200	1.99907	4.16201	0.02092	6.18200
H	15	0.22680	0.00000	0.77046	0.00273	0.77320
N	16	0.46056	1.99938	4.48968	0.05038	6.53944
H	17	0.22554	0.00000	0.77177	0.00269	0.77446
H	18	0.22680	0.00000	0.77046	0.00273	0.77320

N	19	0.46056	1.99938	4.48968	0.05038	6.53944
H	20	0.22554	0.00000	0.77177	0.00269	0.77446
O	21	-0.46115	1.99980	6.44010	0.02125	8.46115
O	22	-0.45979	1.99980	6.43883	0.02116	8.45979
O	23	-0.45979	1.99980	6.43883	0.02116	8.45979
O	24	-0.46115	1.99980	6.44010	0.02125	8.46115
H	25	0.20743	0.00000	0.79009	0.00248	0.79257
H	26	0.22179	0.00000	0.77385	0.00436	0.77821
H	27	0.22179	0.00000	0.77385	0.00436	0.77821
H	28	0.20743	0.00000	0.79009	0.00248	0.79257

==========

* Total *	-1.00000	39.98495	100.44995	0.56510	141.00000

Natural Population

Core	39.98495	(99.9624% of 40)
Valence	100.44995	(99.4554% of 101)
Natural Minimal Basis	140.43490	(99.5992% of 141)
Natural Rydberg Basis	0.56510	(0.4008% of 141)

Figure B.8: Natural Bond Orbital analysis for the trans 4,4' dinitro-azobenzene anion. (a) LUMO +1 (b) LUMO (c) HOMO (d) HOMO – 1. IsoValue = 0.02 and the Density = 0.0004.

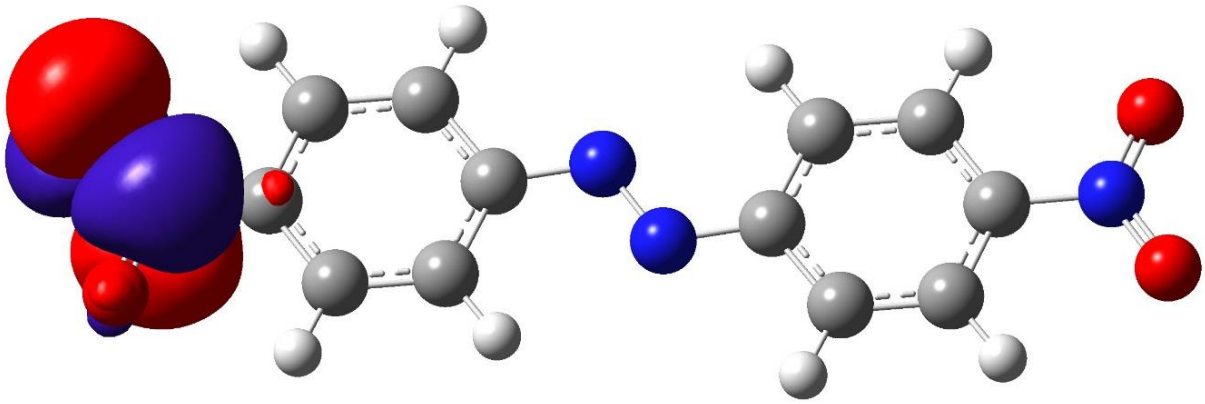

(a)

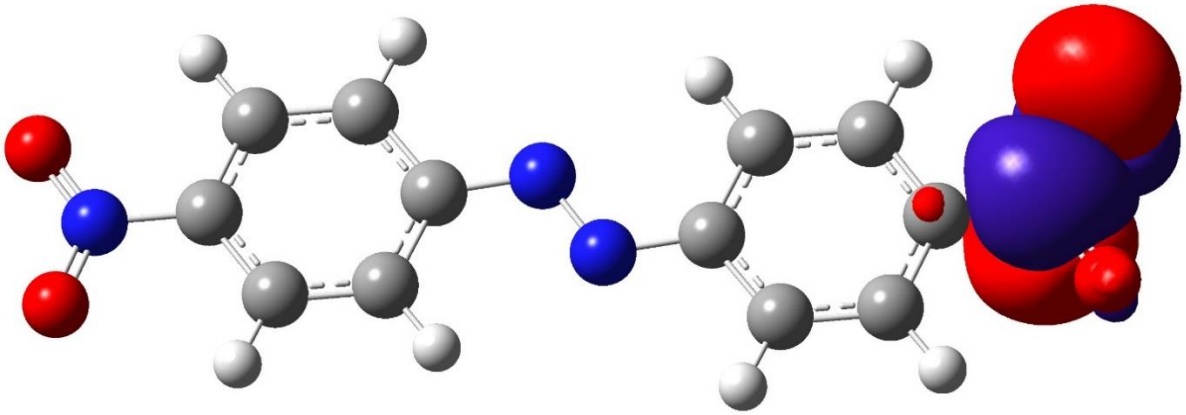

(b)

Figure B.8: Continued

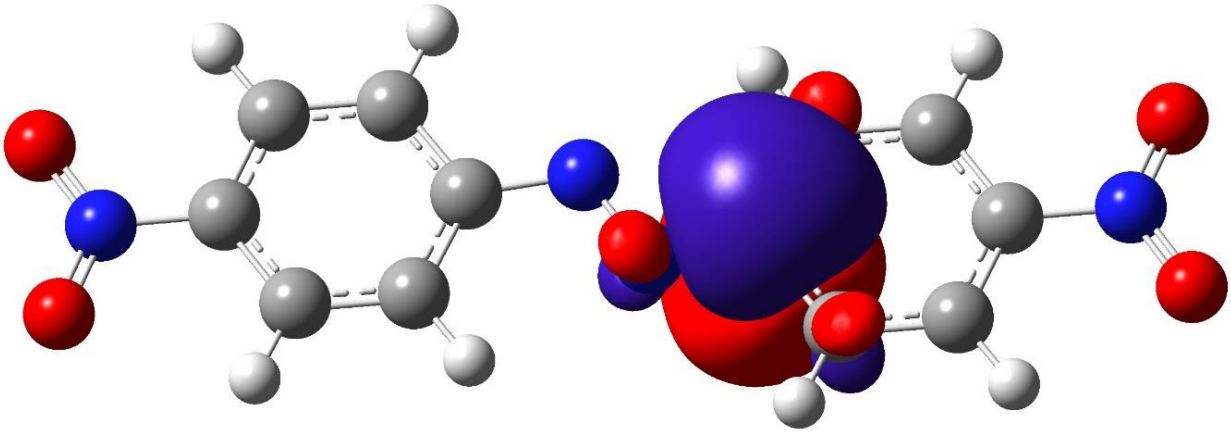

(c)

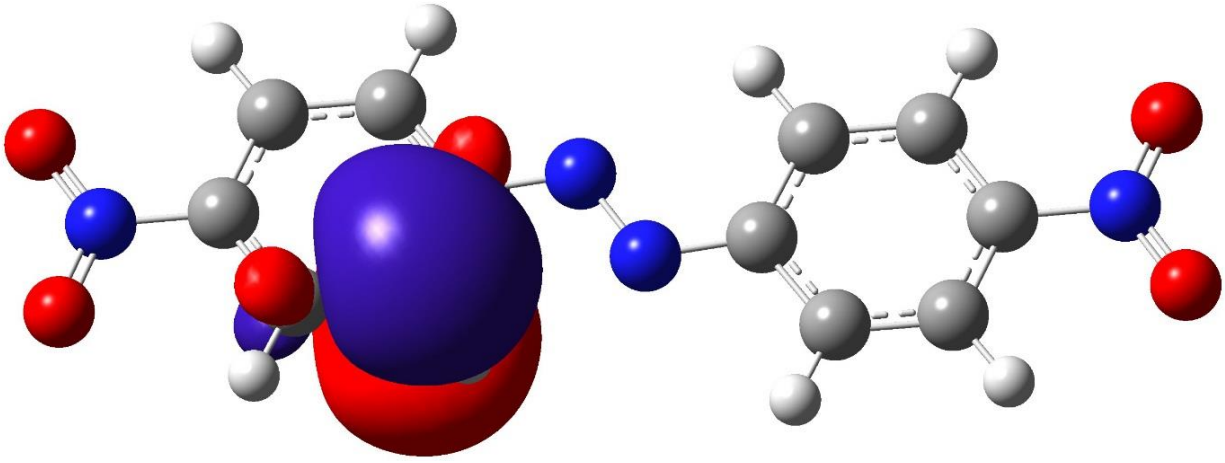

(d)

Figure B.8: Continued

B.5 2,2',6,6' tetramethyl-azobenzene

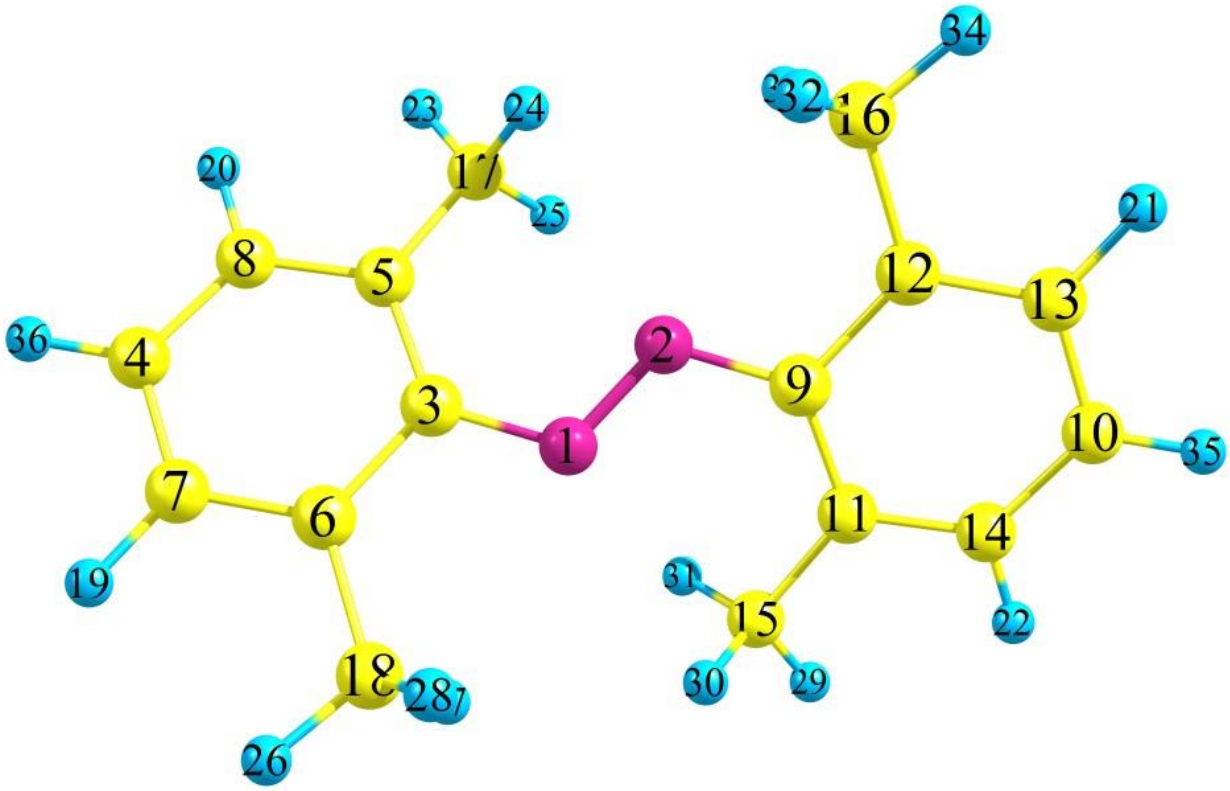

Figure B.9: Optimized Geometry of trans 2,2',6,6' tetramethyl-azobenzene anion using B3LYP level of theory along with 6-311++G(2d,2p) basis set.

Optimized Parameters

(Angstroms and Degrees)

! Name	Definition	Value	Derivative Info.	
! R1	R(1,2)	1.3284	-DE/DX =	0.0 !
! R2	R(1,3)	1.3722	-DE/DX =	0.0 !
! R3	R(2,9)	1.3722	-DE/DX =	0.0 !

! R4	R(3,5)	1.4379	-DE/DX =	0.0	!
! R5	R(3,6)	1.4352	-DE/DX =	0.0	!
! R6	R(4,7)	1.3958	-DE/DX =	0.0	!
! R7	R(4,8)	1.3924	-DE/DX =	0.0	!
! R8	R(4,36)	1.0823	-DE/DX =	0.0	!
! R9	R(5,8)	1.3929	-DE/DX =	0.0	!
! R10	R(5,17)	1.5109	-DE/DX =	0.0	!
! R11	R(6,7)	1.3851	-DE/DX =	0.0	!
! R12	R(6,18)	1.5067	-DE/DX =	0.0	!
! R13	R(7,19)	1.0847	-DE/DX =	0.0	!
! R14	R(8,20)	1.0852	-DE/DX =	0.0	!
! R15	R(9,11)	1.4379	-DE/DX =	0.0	!
! R16	R(9,12)	1.4352	-DE/DX =	0.0	!
! R17	R(10,13)	1.3958	-DE/DX =	0.0	!
! R18	R(10,14)	1.3924	-DE/DX =	0.0	!
! R19	R(10,35)	1.0823	-DE/DX =	0.0	!
! R20	R(11,14)	1.3929	-DE/DX =	0.0	!
! R21	R(11,15)	1.5109	-DE/DX =	0.0	!
! R22	R(12,13)	1.3851	-DE/DX =	0.0	!
! R23	R(12,16)	1.5067	-DE/DX =	0.0	!
! R24	R(13,21)	1.0847	-DE/DX =	0.0	!
! R25	R(14,22)	1.0852	-DE/DX =	0.0	!
! R26	R(15,29)	1.0937	-DE/DX =	0.0	!
! R27	R(15,30)	1.0887	-DE/DX =	0.0	!
! R28	R(15,31)	1.0893	-DE/DX =	0.0	!
! R29	R(16,32)	1.0915	-DE/DX =	0.0	!
! R30	R(16,33)	1.0916	-DE/DX =	0.0	!
! R31	R(16,34)	1.0921	-DE/DX =	0.0	!
! R32	R(17,23)	1.0937	-DE/DX =	0.0	!
! R33	R(17,24)	1.0887	-DE/DX =	0.0	!

! R34	R(17,25)	1.0893	-DE/DX = 0.0	!
! R35	R(18,26)	1.0921	-DE/DX = 0.0	!
! R36	R(18,27)	1.0916	-DE/DX = 0.0	!
! R37	R(18,28)	1.0915	-DE/DX = 0.0	!
! A1	A(2,1,3)	116.9727	-DE/DX = 0.0	!
! A2	A(1,2,9)	116.9727	-DE/DX = 0.0	!
! A3	A(1,3,5)	128.0774	-DE/DX = 0.0	!
! A4	A(1,3,6)	114.3388	-DE/DX = 0.0	!
! A5	A(5,3,6)	117.5538	-DE/DX = 0.0	!
! A6	A(7,4,8)	118.2549	-DE/DX = 0.0	!
! A7	A(7,4,36)	120.9703	-DE/DX = 0.0	!
! A8	A(8,4,36)	120.7701	-DE/DX = 0.0	!
! A9	A(3,5,8)	118.9739	-DE/DX = 0.0	!
! A10	A(3,5,17)	123.613	-DE/DX = 0.0	!
! A11	A(8,5,17)	117.3559	-DE/DX = 0.0	!
! A12	A(3,6,7)	120.8232	-DE/DX = 0.0	!
! A13	A(3,6,18)	119.4631	-DE/DX = 0.0	!
! A14	A(7,6,18)	119.7086	-DE/DX = 0.0	!
! A15	A(4,7,6)	121.4139	-DE/DX = 0.0	!
! A16	A(4,7,19)	119.7822	-DE/DX = 0.0	!
! A17	A(6,7,19)	118.8039	-DE/DX = 0.0	!
! A18	A(4,8,5)	122.9554	-DE/DX = 0.0	!
! A19	A(4,8,20)	119.0712	-DE/DX = 0.0	!
! A20	A(5,8,20)	117.969	-DE/DX = 0.0	!
! A21	A(2,9,11)	128.0774	-DE/DX = 0.0	!
! A22	A(2,9,12)	114.3388	-DE/DX = 0.0	!
! A23	A(11,9,12)	117.5538	-DE/DX = 0.0	!
! A24	A(13,10,14)	118.2549	-DE/DX = 0.0	!
! A25	A(13,10,35)	120.9703	-DE/DX = 0.0	!
! A26	A(14,10,35)	120.7701	-DE/DX = 0.0	!

! A27	A(9,11,14)	118.9739	-DE/DX = 0.0	!
! A28	A(9,11,15)	123.613	-DE/DX = 0.0	!
! A29	A(14,11,15)	117.3559	-DE/DX = 0.0	!
! A30	A(9,12,13)	120.8232	-DE/DX = 0.0	!
! A31	A(9,12,16)	119.4631	-DE/DX = 0.0	!
! A32	A(13,12,16)	119.7086	-DE/DX = 0.0	!
! A33	A(10,13,12)	121.4139	-DE/DX = 0.0	!
! A34	A(10,13,21)	119.7822	-DE/DX = 0.0	!
! A35	A(12,13,21)	118.8039	-DE/DX = 0.0	!
! A36	A(10,14,11)	122.9554	-DE/DX = 0.0	!
! A37	A(10,14,22)	119.0712	-DE/DX = 0.0	!
! A38	A(11,14,22)	117.969	-DE/DX = 0.0	!
! A39	A(11,15,29)	109.4687	-DE/DX = 0.0	!
! A40	A(11,15,30)	112.3383	-DE/DX = 0.0	!
! A41	A(11,15,31)	111.6598	-DE/DX = 0.0	!
! A42	A(29,15,30)	108.758	-DE/DX = 0.0	!
! A43	A(29,15,31)	108.8283	-DE/DX = 0.0	!
! A44	A(30,15,31)	105.6523	-DE/DX = 0.0	!
! A45	A(12,16,32)	111.4026	-DE/DX = 0.0	!
! A46	A(12,16,33)	111.424	-DE/DX = 0.0	!
! A47	A(12,16,34)	110.4694	-DE/DX = 0.0	!
! A48	A(32,16,33)	105.8633	-DE/DX = 0.0	!
! A49	A(32,16,34)	108.8879	-DE/DX = 0.0	!
! A50	A(33,16,34)	108.6389	-DE/DX = 0.0	!
! A51	A(5,17,23)	109.4687	-DE/DX = 0.0	!
! A52	A(5,17,24)	112.3383	-DE/DX = 0.0	!
! A53	A(5,17,25)	111.6598	-DE/DX = 0.0	!
! A54	A(23,17,24)	108.758	-DE/DX = 0.0	!
! A55	A(23,17,25)	108.8283	-DE/DX = 0.0	!
! A56	A(24,17,25)	105.6523	-DE/DX = 0.0	!

! A57	A(6,18,26)	110.4694	-DE/DX = 0.0	!
! A58	A(6,18,27)	111.424	-DE/DX = 0.0	!
! A59	A(6,18,28)	111.4026	-DE/DX = 0.0	!
! A60	A(26,18,27)	108.6389	-DE/DX = 0.0	!
! A61	A(26,18,28)	108.8879	-DE/DX = 0.0	!
! A62	A(27,18,28)	105.8633	-DE/DX = 0.0	!
! D1	D(3,1,2,9)	-175.4279	-DE/DX = 0.0	!
! D2	D(2,1,3,5)	17.6791	-DE/DX = 0.0	!
! D3	D(2,1,3,6)	-164.3812	-DE/DX = 0.0	!
! D4	D(1,2,9,11)	17.6791	-DE/DX = 0.0	!
! D5	D(1,2,9,12)	-164.3813	-DE/DX = 0.0	!
! D6	D(1,3,5,8)	179.2591	-DE/DX = 0.0	!
! D7	D(1,3,5,17)	2.0881	-DE/DX = 0.0	!
! D8	D(6,3,5,8)	1.3765	-DE/DX = 0.0	!
! D9	D(6,3,5,17)	-175.7945	-DE/DX = 0.0	!
! D10	D(1,3,6,7)	-179.9281	-DE/DX = 0.0	!
! D11	D(1,3,6,18)	0.8901	-DE/DX = 0.0	!
! D12	D(5,3,6,7)	-1.7573	-DE/DX = 0.0	!
! D13	D(5,3,6,18)	179.0609	-DE/DX = 0.0	!
! D14	D(8,4,7,6)	0.5453	-DE/DX = 0.0	!
! D15	D(8,4,7,19)	-179.5003	-DE/DX = 0.0	!
! D16	D(36,4,7,6)	179.7717	-DE/DX = 0.0	!
! D17	D(36,4,7,19)	-0.2739	-DE/DX = 0.0	!
! D18	D(7,4,8,5)	-0.926	-DE/DX = 0.0	!
! D19	D(7,4,8,20)	178.3004	-DE/DX = 0.0	!
! D20	D(36,4,8,5)	179.846	-DE/DX = 0.0	!
! D21	D(36,4,8,20)	-0.9276	-DE/DX = 0.0	!
! D22	D(3,5,8,4)	-0.0613	-DE/DX = 0.0	!
! D23	D(3,5,8,20)	-179.2957	-DE/DX = 0.0	!
! D24	D(17,5,8,4)	177.2862	-DE/DX = 0.0	!

! D25	D(17,5,8,20)	-1.9482	-DE/DX = 0.0	!
! D26	D(3,5,17,23)	168.122	-DE/DX = 0.0	!
! D27	D(3,5,17,24)	-70.9471	-DE/DX = 0.0	!
! D28	D(3,5,17,25)	47.5448	-DE/DX = 0.0	!
! D29	D(8,5,17,23)	-9.0914	-DE/DX = 0.0	!
! D30	D(8,5,17,24)	111.8394	-DE/DX = 0.0	!
! D31	D(8,5,17,25)	-129.6687	-DE/DX = 0.0	!
! D32	D(3,6,7,4)	0.8091	-DE/DX = 0.0	!
! D33	D(3,6,7,19)	-179.1457	-DE/DX = 0.0	!
! D34	D(18,6,7,4)	179.9889	-DE/DX = 0.0	!
! D35	D(18,6,7,19)	0.0341	-DE/DX = 0.0	!
! D36	D(3,6,18,26)	178.1086	-DE/DX = 0.0	!
! D37	D(3,6,18,27)	-61.0323	-DE/DX = 0.0	!
! D38	D(3,6,18,28)	56.9483	-DE/DX = 0.0	!
! D39	D(7,6,18,26)	-1.0825	-DE/DX = 0.0	!
! D40	D(7,6,18,27)	119.7767	-DE/DX = 0.0	!
! D41	D(7,6,18,28)	-122.2427	-DE/DX = 0.0	!
! D42	D(2,9,11,14)	179.2591	-DE/DX = 0.0	!
! D43	D(2,9,11,15)	2.0881	-DE/DX = 0.0	!
! D44	D(12,9,11,14)	1.3765	-DE/DX = 0.0	!
! D45	D(12,9,11,15)	-175.7945	-DE/DX = 0.0	!
! D46	D(2,9,12,13)	-179.9281	-DE/DX = 0.0	!
! D47	D(2,9,12,16)	0.8901	-DE/DX = 0.0	!
! D48	D(11,9,12,13)	-1.7573	-DE/DX = 0.0	!
! D49	D(11,9,12,16)	179.0609	-DE/DX = 0.0	!
! D50	D(14,10,13,12)	0.5453	-DE/DX = 0.0	!
! D51	D(14,10,13,21)	-179.5003	-DE/DX = 0.0	!
! D52	D(35,10,13,12)	179.7717	-DE/DX = 0.0	!
! D53	D(35,10,13,21)	-0.2739	-DE/DX = 0.0	!
! D54	D(13,10,14,11)	-0.926	-DE/DX = 0.0	!

! D55	D(13,10,14,22)	178.3004	-DE/DX = 0.0	!
! D56	D(35,10,14,11)	179.846	-DE/DX = 0.0	!
! D57	D(35,10,14,22)	-0.9276	-DE/DX = 0.0	!
! D58	D(9,11,14,10)	-0.0613	-DE/DX = 0.0	!
! D59	D(9,11,14,22)	-179.2957	-DE/DX = 0.0	!
! D60	D(15,11,14,10)	177.2862	-DE/DX = 0.0	!
! D61	D(15,11,14,22)	-1.9482	-DE/DX = 0.0	!
! D62	D(9,11,15,29)	168.1221	-DE/DX = 0.0	!
! D63	D(9,11,15,30)	-70.9471	-DE/DX = 0.0	!
! D64	D(9,11,15,31)	47.5449	-DE/DX = 0.0	!
! D65	D(14,11,15,29)	-9.0914	-DE/DX = 0.0	!
! D66	D(14,11,15,30)	111.8395	-DE/DX = 0.0	!
! D67	D(14,11,15,31)	-129.6686	-DE/DX = 0.0	!
! D68	D(9,12,13,10)	0.8091	-DE/DX = 0.0	!
! D69	D(9,12,13,21)	-179.1457	-DE/DX = 0.0	!
! D70	D(16,12,13,10)	179.9889	-DE/DX = 0.0	!
! D71	D(16,12,13,21)	0.0341	-DE/DX = 0.0	!
! D72	D(9,12,16,32)	56.9484	-DE/DX = 0.0	!
! D73	D(9,12,16,33)	-61.0322	-DE/DX = 0.0	!
! D74	D(9,12,16,34)	178.1087	-DE/DX = 0.0	!
! D75	D(13,12,16,32)	-122.2426	-DE/DX = 0.0	!
! D76	D(13,12,16,33)	119.7768	-DE/DX = 0.0	!
! D77	D(13,12,16,34)	-1.0824	-DE/DX = 0.0	!

Figure B.10: Population analysis for the trans 2,2',6,6' tetramethyl - azobenzene anion. Calculations has been performed in B3LYP level of theory along with 6-311++G(2d,2p) basis set. (a) LUMO +1 (b) LUMO (c) HOMO (d) HOMO – 1. IsoValue = 0.02 and the Density = 0.0004.

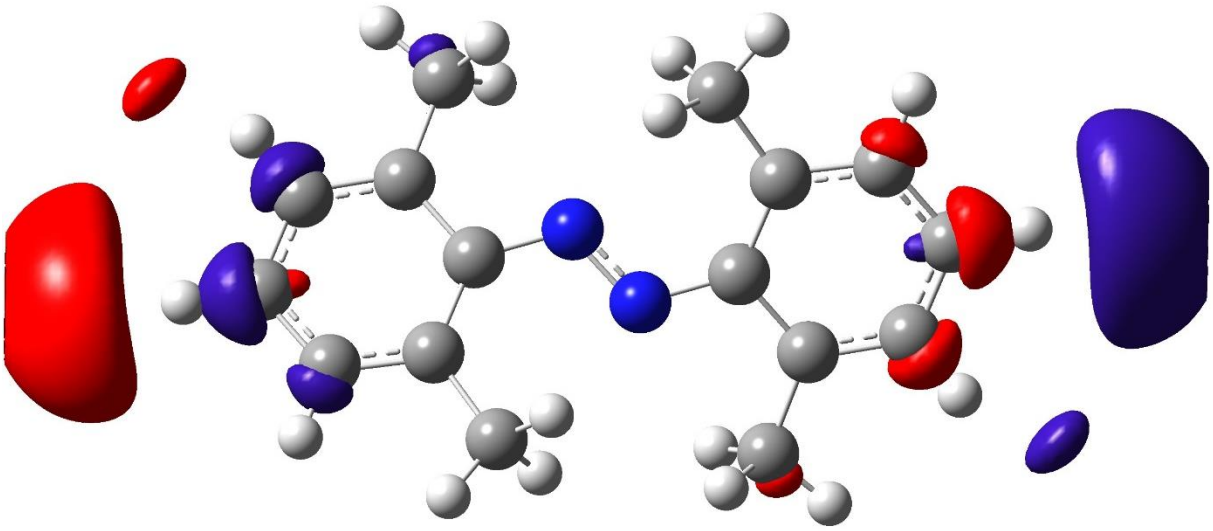

(a)

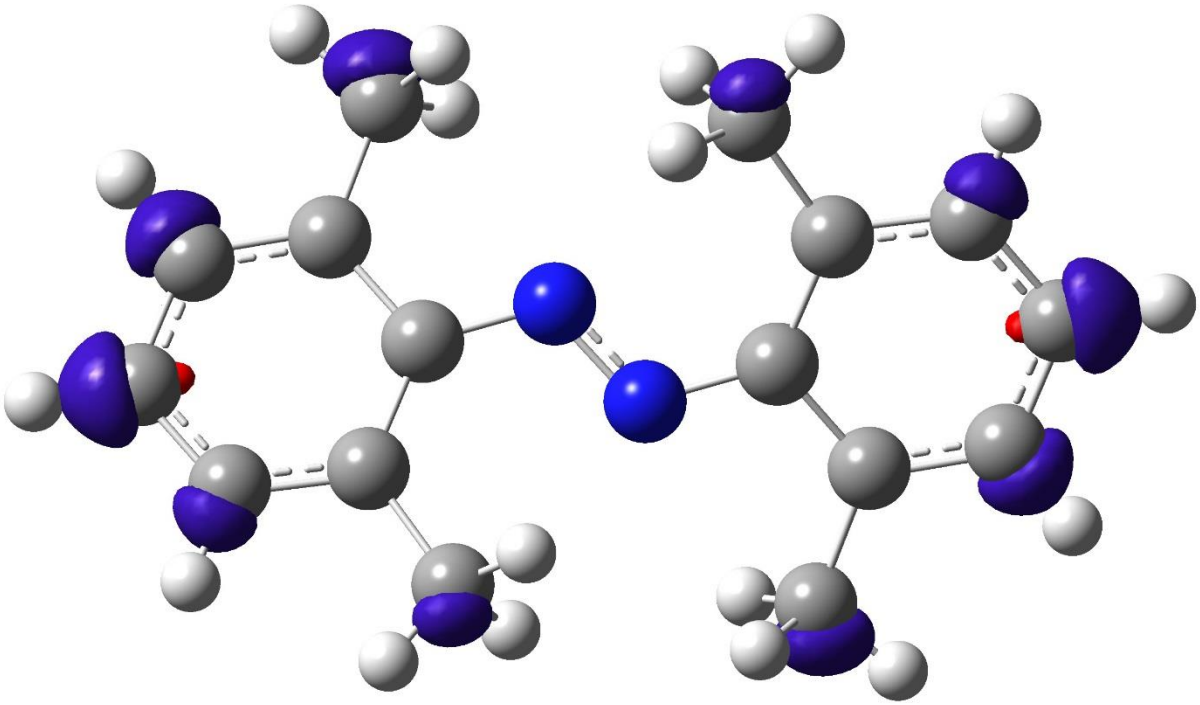

(b)

Figure B.10: Continued

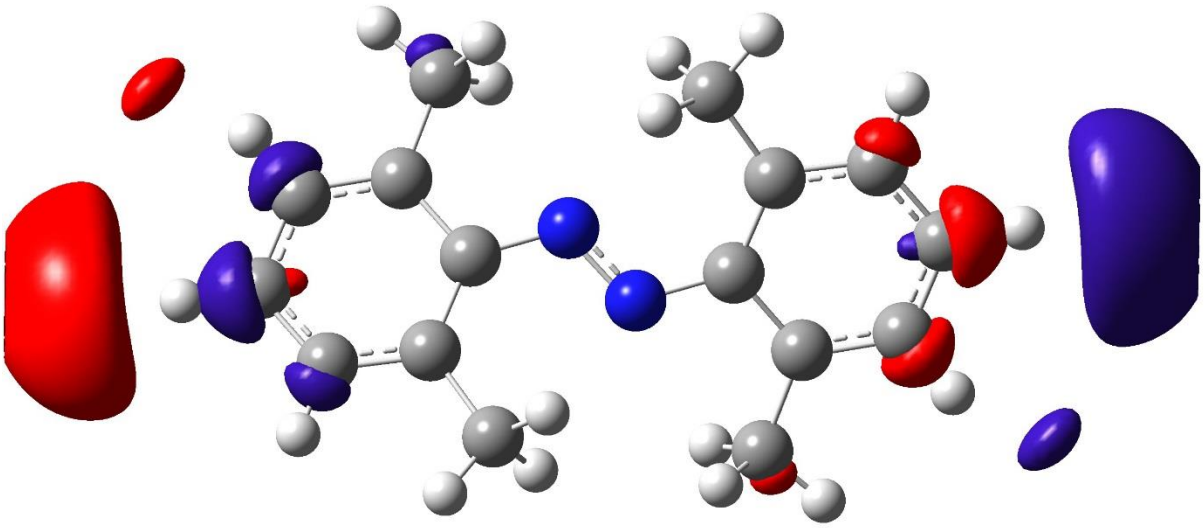

(c)

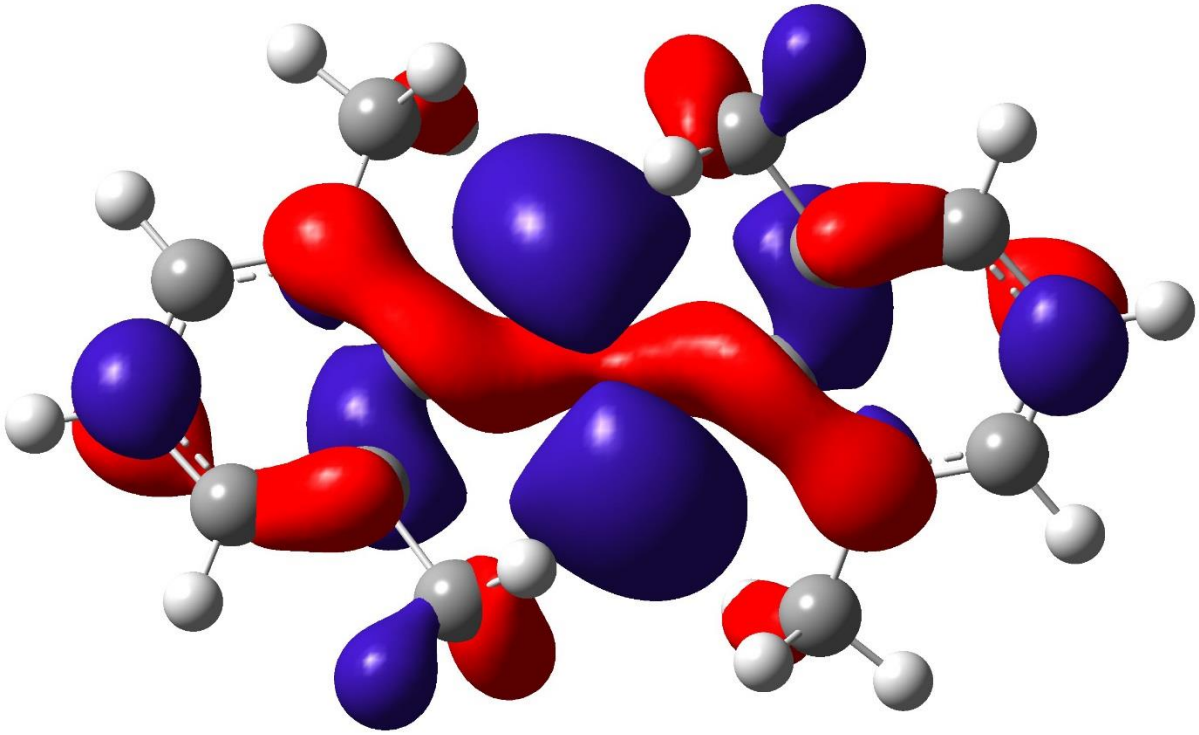

(d)

Figure B.10: Continued

B.6 4-Methoxyazobenzene ($C_{13}H_{12}N_2O$)

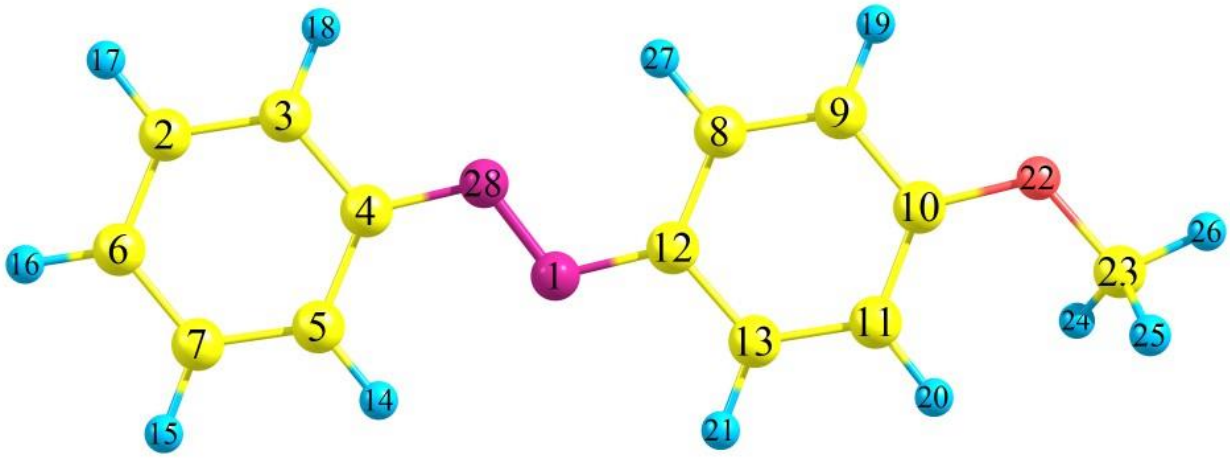

Figure B.11: Optimized Geometry of trans 4-Methoxyazobenzene anion using B3LYP level of theory along with 6-311++G(2d,2p) basis set.

Optimized Parameters

(Angstroms and Degrees)

Name	Definition	Value	Derivative Info.	
! R1	R(1,12)	1.3741	-DE/DX = 0.0	!
! R2	R(1,28)	1.3265	-DE/DX = 0.0	!
! R3	R(2,3)	1.3835	-DE/DX = 0.0	!
! R4	R(2,6)	1.4012	-DE/DX = 0.0	!
! R5	R(2,17)	1.0843	-DE/DX = 0.0	!
! R6	R(3,4)	1.4182	-DE/DX = 0.0	!
! R7	R(3,18)	1.0827	-DE/DX = 0.0	!
! R8	R(4,5)	1.4228	-DE/DX = 0.0	!
! R9	R(4,28)	1.3706	-DE/DX = 0.0	!

! R10	R(5,7)	1.3856	-DE/DX = 0.0	!
! R11	R(5,14)	1.0791	-DE/DX = 0.0	!
! R12	R(6,7)	1.3985	-DE/DX = 0.0	!
! R13	R(6,16)	1.0824	-DE/DX = 0.0	!
! R14	R(7,15)	1.0852	-DE/DX = 0.0	!
! R15	R(8,9)	1.3829	-DE/DX = 0.0	!
! R16	R(8,12)	1.4222	-DE/DX = 0.0	!
! R17	R(8,27)	1.079	-DE/DX = 0.0	!
! R18	R(9,10)	1.3969	-DE/DX = 0.0	!
! R19	R(9,19)	1.0834	-DE/DX = 0.0	!
! R20	R(10,11)	1.3966	-DE/DX = 0.0	!
! R21	R(10,22)	1.3918	-DE/DX = 0.0	!
! R22	R(11,13)	1.3901	-DE/DX = 0.0	!
! R23	R(11,20)	1.0807	-DE/DX = 0.0	!
! R24	R(12,13)	1.411	-DE/DX = 0.0	!
! R25	R(13,21)	1.0823	-DE/DX = 0.0	!
! R26	R(22,23)	1.4073	-DE/DX = 0.0	!
! R27	R(23,24)	1.0956	-DE/DX = 0.0	!
! R28	R(23,25)	1.0956	-DE/DX = 0.0	!
! R29	R(23,26)	1.0887	-DE/DX = 0.0	!
! A1	A(12,1,28)	114.2434	-DE/DX = 0.0	!
! A2	A(3,2,6)	120.8271	-DE/DX = 0.0	!
! A3	A(3,2,17)	119.4101	-DE/DX = 0.0	!
! A4	A(6,2,17)	119.7628	-DE/DX = 0.0	!
! A5	A(2,3,4)	121.6443	-DE/DX = 0.0	!
! A6	A(2,3,18)	120.8242	-DE/DX = 0.0	!
! A7	A(4,3,18)	117.5315	-DE/DX = 0.0	!
! A8	A(3,4,5)	116.8728	-DE/DX = 0.0	!
! A9	A(3,4,28)	117.4063	-DE/DX = 0.0	!
! A10	A(5,4,28)	125.7209	-DE/DX = 0.0	!

! A11	A(4,5,7)	120.7885	-DE/DX =	0.0 !
! A12	A(4,5,14)	118.0789	-DE/DX =	0.0 !
! A13	A(7,5,14)	121.1326	-DE/DX =	0.0 !
! A14	A(2,6,7)	118.3292	-DE/DX =	0.0 !
! A15	A(2,6,16)	120.8362	-DE/DX =	0.0 !
! A16	A(7,6,16)	120.8346	-DE/DX =	0.0 !
! A17	A(5,7,6)	121.5382	-DE/DX =	0.0 !
! A18	A(5,7,15)	119.1032	-DE/DX =	0.0 !
! A19	A(6,7,15)	119.3587	-DE/DX =	0.0 !
! A20	A(9,8,12)	121.1983	-DE/DX =	0.0 !
! A21	A(9,8,27)	120.7461	-DE/DX =	0.0 !
! A22	A(12,8,27)	118.0556	-DE/DX =	0.0 !
! A23	A(8,9,10)	121.0332	-DE/DX =	0.0 !
! A24	A(8,9,19)	120.6135	-DE/DX =	0.0 !
! A25	A(10,9,19)	118.3533	-DE/DX =	0.0 !
! A26	A(9,10,11)	119.1046	-DE/DX =	0.0 !
! A27	A(9,10,22)	116.2196	-DE/DX =	0.0 !
! A28	A(11,10,22)	124.6758	-DE/DX =	0.0 !
! A29	A(10,11,13)	119.9	-DE/DX =	0.0 !
! A30	A(10,11,20)	121.0898	-DE/DX =	0.0 !
! A31	A(13,11,20)	119.0102	-DE/DX =	0.0 !
! A32	A(1,12,8)	125.7268	-DE/DX =	0.0 !
! A33	A(1,12,13)	117.7865	-DE/DX =	0.0 !
! A34	A(8,12,13)	116.4866	-DE/DX =	0.0 !
! A35	A(11,13,12)	122.2772	-DE/DX =	0.0 !
! A36	A(11,13,21)	119.9799	-DE/DX =	0.0 !
! A37	A(12,13,21)	117.7429	-DE/DX =	0.0 !
! A38	A(10,22,23)	117.3402	-DE/DX =	0.0 !
! A39	A(22,23,24)	111.9146	-DE/DX =	0.0 !
! A40	A(22,23,25)	111.9146	-DE/DX =	0.0 !

```
! A41   A(22,23,26)          106.4067        -DE/DX =    0.0             !
! A42   A(24,23,25)          108.4868        -DE/DX =    0.0             !
! A43   A(24,23,26)          109.0198        -DE/DX =    0.0             !
! A44   A(25,23,26)          109.0198        -DE/DX =    0.0             !
 ! A45   A(1,28,4)           114.5335        -DE/DX =    0.0             !
  ! D1    D(28,1,12,8)         0.0          -DE/DX =    0.0            !
 ! D2    D(28,1,12,13)        180.0          -DE/DX =    0.0             !
 ! D3    D(12,1,28,4)         180.0          -DE/DX =    0.0             !
  ! D4    D(6,2,3,4)           0.0          -DE/DX =    0.0            !
 ! D5    D(6,2,3,18)          180.0          -DE/DX =    0.0             !
 ! D6    D(17,2,3,4)          180.0          -DE/DX =    0.0             !
 ! D7    D(17,2,3,18)         0.0          -DE/DX =    0.0             !
  ! D8    D(3,2,6,7)           0.0          -DE/DX =    0.0            !
 ! D9    D(3,2,6,16)          180.0          -DE/DX =    0.0             !
 ! D10   D(17,2,6,7)          180.0          -DE/DX =    0.0             !
 ! D11   D(17,2,6,16)         0.0          -DE/DX =    0.0             !
  ! D12   D(2,3,4,5)           0.0          -DE/DX =    0.0            !
 ! D13   D(2,3,4,28)          180.0          -DE/DX =    0.0             !
 ! D14   D(18,3,4,5)          180.0          -DE/DX =    0.0             !
 ! D15   D(18,3,4,28)         0.0          -DE/DX =    0.0             !
  ! D16   D(3,4,5,7)           0.0          -DE/DX =    0.0            !
 ! D17   D(3,4,5,14)          180.0          -DE/DX =    0.0             !
 ! D18   D(28,4,5,7)          180.0          -DE/DX =    0.0             !
 ! D19   D(28,4,5,14)         0.0          -DE/DX =    0.0             !
 ! D20   D(3,4,28,1)          180.0          -DE/DX =    0.0             !
  ! D21   D(5,4,28,1)          0.0          -DE/DX =    0.0            !
  ! D22   D(4,5,7,6)           0.0          -DE/DX =    0.0            !
 ! D23   D(4,5,7,15)          180.0          -DE/DX =    0.0             !
 ! D24   D(14,5,7,6)          180.0          -DE/DX =    0.0             !
 ! D25   D(14,5,7,15)         0.0          -DE/DX =    0.0             !
```

```
 ! D26   D(2,6,7,5)          0.0          -DE/DX =    0.0              !
 ! D27   D(2,6,7,15)         180.0        -DE/DX =    0.0              !
 ! D28   D(16,6,7,5)         180.0        -DE/DX =    0.0              !
 ! D29   D(16,6,7,15)         0.0         -DE/DX =    0.0              !
 ! D30   D(12,8,9,10)         0.0         -DE/DX =    0.0              !
 ! D31   D(12,8,9,19)         180.0       -DE/DX =    0.0              !
 ! D32   D(27,8,9,10)         180.0       -DE/DX =    0.0              !
 ! D33   D(27,8,9,19)         0.0         -DE/DX =    0.0              !
 ! D34   D(9,8,12,1)          180.0       -DE/DX =    0.0              !
 ! D35   D(9,8,12,13)         0.0         -DE/DX =    0.0              !
 ! D36   D(27,8,12,1)         0.0         -DE/DX =    0.0              !
 ! D37   D(27,8,12,13)        180.0       -DE/DX =    0.0              !
 ! D38   D(8,9,10,11)         0.0         -DE/DX =    0.0              !
 ! D39   D(8,9,10,22)         180.0       -DE/DX =    0.0              !
 ! D40   D(19,9,10,11)        180.0       -DE/DX =    0.0              !
 ! D41   D(19,9,10,22)        0.0         -DE/DX =    0.0              !
 ! D42   D(9,10,11,13)        0.0         -DE/DX =    0.0              !
 ! D43   D(9,10,11,20)        180.0       -DE/DX =    0.0              !
 ! D44   D(22,10,11,13)       180.0       -DE/DX =    0.0              !
 ! D45   D(22,10,11,20)       0.0         -DE/DX =    0.0              !
 ! D46   D(9,10,22,23)        180.0       -DE/DX =    0.0              !
 ! D47   D(11,10,22,23)       0.0         -DE/DX =    0.0              !
 ! D48   D(10,11,13,12)       0.0         -DE/DX =    0.0              !
 ! D49   D(10,11,13,21)       180.0       -DE/DX =    0.0              !
 ! D50   D(20,11,13,12)       180.0       -DE/DX =    0.0              !
 ! D51   D(20,11,13,21)       0.0         -DE/DX =    0.0              !
 ! D52   D(1,12,13,11)        180.0       -DE/DX =    0.0              !
 ! D53   D(1,12,13,21)        0.0         -DE/DX =    0.0              !
 ! D54   D(8,12,13,11)        0.0         -DE/DX =    0.0              !
 ! D55   D(8,12,13,21)        180.0       -DE/DX =    0.0              !
```

! D56	D(10,22,23,24)	61.011	-DE/DX =	0.0	!
! D57	D(10,22,23,25)	-61.011	-DE/DX =	0.0	!
! D58	D(10,22,23,26)	180.0	-DE/DX =	0.0	!

Summary of Natural Population Analysis:

Natural Population

Atom	No	Natural Charge	Core	Valence	Rydberg	Total
N	1	-0.04427	0.99969	2.52326	0.02132	3.54427
C	2	-0.12841	0.99957	2.11846	0.01037	3.12841
C	3	-0.07329	0.99953	2.06324	0.01052	3.07329
C	4	0.05699	0.99951	1.92926	0.01423	2.94301
C	5	-0.06589	0.99952	2.05652	0.00984	3.06589
C	6	-0.07603	0.99957	2.06509	0.01136	3.07603
C	7	-0.12971	0.99958	2.11975	0.01038	3.12971
C	8	-0.05042	0.99953	2.04183	0.00906	3.05042
C	9	-0.14963	0.99953	2.14004	0.01006	3.14963
C	10	0.18909	0.99936	1.80006	0.01149	2.81091
C	11	-0.17465	0.99952	2.16617	0.00896	3.17465
C	12	0.03722	0.99950	1.94929	0.01399	2.96278
C	13	-0.05404	0.99954	2.04395	0.01055	3.05404
H	14	0.10506	0.00000	0.39269	0.00225	0.39494
H	15	0.08931	0.00000	0.40943	0.00126	0.41069
H	16	0.08756	0.00000	0.41118	0.00126	0.41244
H	17	0.08977	0.00000	0.40894	0.00129	0.41023
H	18	0.09528	0.00000	0.40305	0.00167	0.40472
H	19	0.09672	0.00000	0.40172	0.00157	0.40328
H	20	0.09552	0.00000	0.40315	0.00134	0.40448
H	21	0.09555	0.00000	0.40259	0.00186	0.40445
O	22	-0.27557	0.99986	3.26585	0.00986	4.27557

C	23	-0.09682	0.99961	2.08880	0.00841	3.09682
H	24	0.07889	0.00000	0.41923	0.00188	0.42111
H	25	0.07889	0.00000	0.41923	0.00188	0.42111
H	26	0.08502	0.00000	0.41399	0.00099	0.41498
H	27	0.10674	0.00000	0.39096	0.00230	0.39326
N	28	-0.06890	0.99969	2.54761	0.02160	3.56890

==========

* Total *	0.00000	15.99312	39.79534	0.21154	56.00000

Natural Population

Core	15.99312 (99.9570% of 16)
Valence	39.79534 (99.4883% of 40)
Natural Minimal Basis	55.78846 (99.6222% of 56)
Natural Rydberg Basis	0.21154 (0.3778% of 56)

Figure B.12: Natural Bond Orbital analysis for the trans 4-Methoxyazobenzene anion. (a) LUMO +1 (b) LUMO (c) HOMO (d) HOMO – 1. IsoValue = 0.02 and the Density = 0.0004.

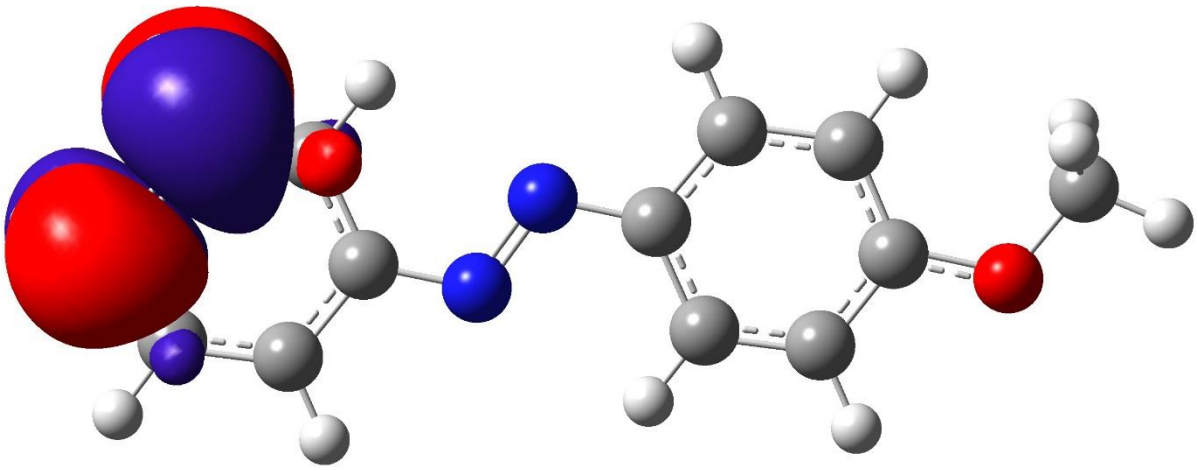

(a)

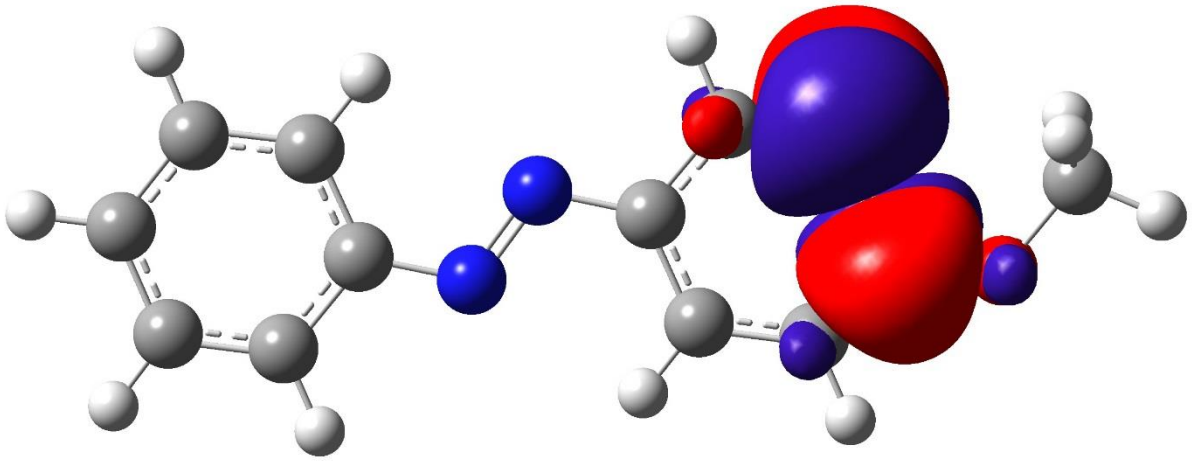

(b)

Figure B.12: Continued

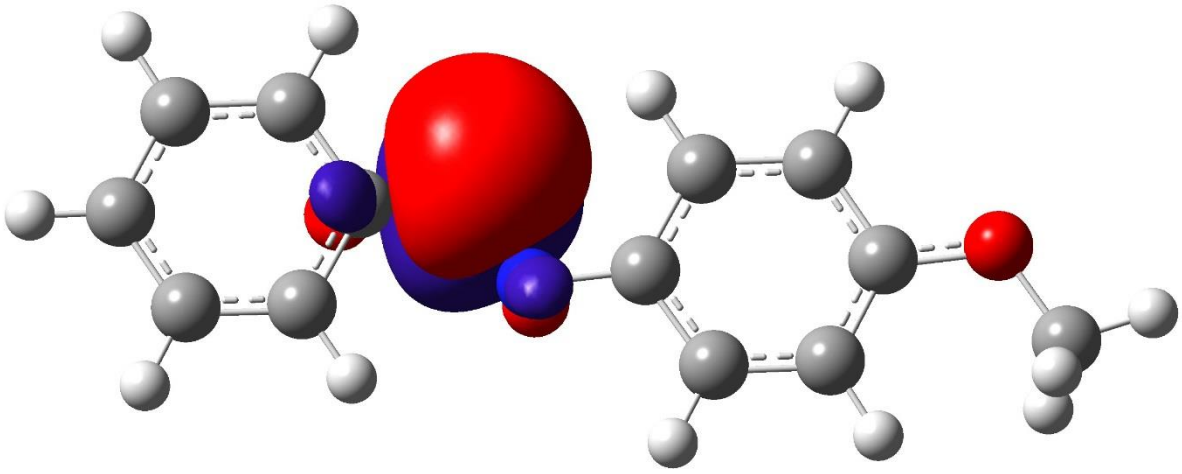

(c)

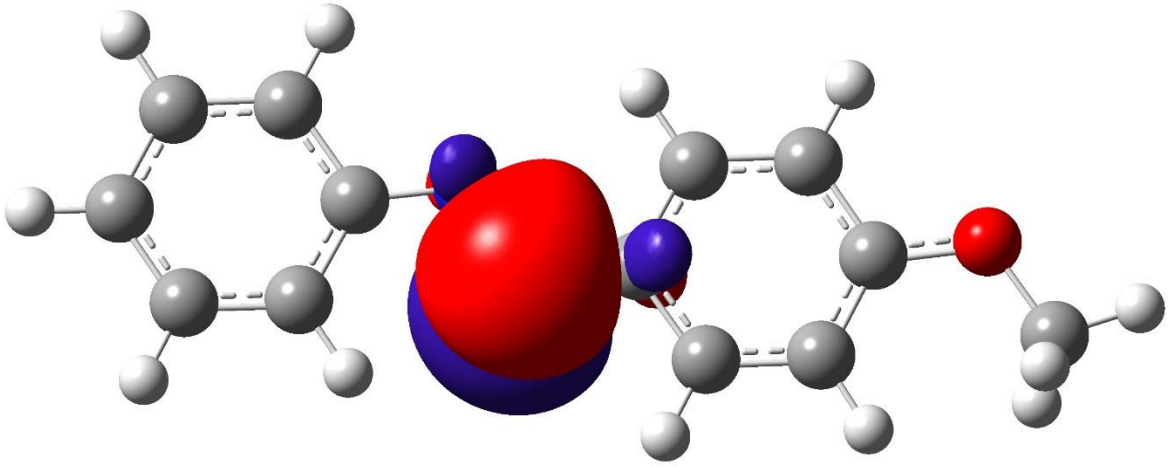

(d)

Figure B.12: Continued

B.7 2,4-Dihydroxyazobenzene,4-(Phenylazo) resorcinol

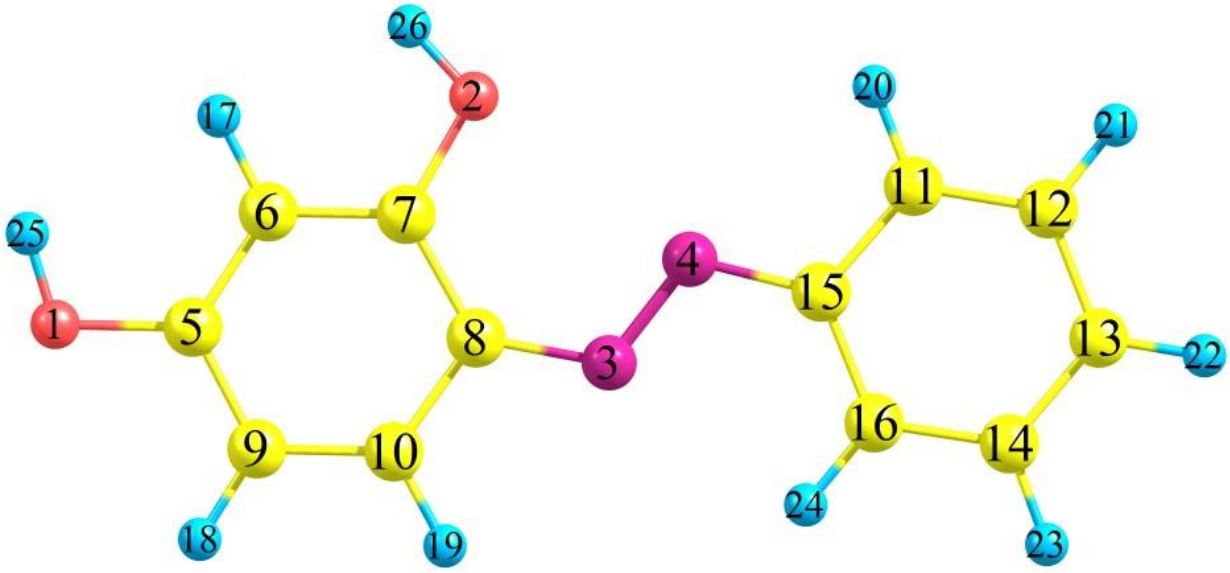

Figure B.13: Optimized Geometry of trans 2,4-Dihydroxyazobenzene,4-(Phenylazo) anion using B3LYP level of theory along with 6-311++G(2d,2p) basis set.

Optimized Parameters

(Angstroms and Degrees)

Name	Definition	Value	Derivative Info.	
! R1	R(1,5)	1.3935	-DE/DX = 0.0	!
! R2	R(1,25)	0.9601	-DE/DX = 0.0	!
! R3	R(2,7)	1.3754	-DE/DX = 0.0	!
! R4	R(2,26)	0.9625	-DE/DX = 0.0	!
! R5	R(3,4)	1.3252	-DE/DX = 0.0	!

! R6	R(3,8)	1.3697	-DE/DX = 0.0	!
! R7	R(4,15)	1.3703	-DE/DX = 0.0	!
! R8	R(5,6)	1.3921	-DE/DX = 0.0	!
! R9	R(5,9)	1.3889	-DE/DX = 0.0	!
! R10	R(6,7)	1.3945	-DE/DX = 0.0	!
! R11	R(6,17)	1.0886	-DE/DX = 0.0	!
! R12	R(7,8)	1.4335	-DE/DX = 0.0	!
! R13	R(8,10)	1.4196	-DE/DX = 0.0	!
! R14	R(9,10)	1.385	-DE/DX = 0.0	!
! R15	R(9,18)	1.0816	-DE/DX = 0.0	!
! R16	R(10,19)	1.0814	-DE/DX = 0.0	!
! R17	R(11,12)	1.3831	-DE/DX = 0.0	!
! R18	R(11,15)	1.4191	-DE/DX = 0.0	!
! R19	R(11,20)	1.0826	-DE/DX = 0.0	!
! R20	R(12,13)	1.402	-DE/DX = 0.0	!
! R21	R(12,21)	1.0845	-DE/DX = 0.0	!
! R22	R(13,14)	1.3988	-DE/DX = 0.0	!
! R23	R(13,22)	1.0825	-DE/DX = 0.0	!
! R24	R(14,16)	1.3855	-DE/DX = 0.0	!
! R25	R(14,23)	1.0854	-DE/DX = 0.0	!
! R26	R(15,16)	1.4239	-DE/DX = 0.0	!
! R27	R(16,24)	1.0792	-DE/DX = 0.0	!
! A1	A(5,1,25)	108.1538	-DE/DX = 0.0	!
! A2	A(7,2,26)	107.468	-DE/DX = 0.0	!
! A3	A(4,3,8)	117.3765	-DE/DX = 0.0	!
! A4	A(3,4,15)	113.9798	-DE/DX = 0.0	!
! A5	A(1,5,6)	122.0523	-DE/DX = 0.0	!
! A6	A(1,5,9)	118.9333	-DE/DX = 0.0	!
! A7	A(6,5,9)	119.0144	-DE/DX = 0.0	!
! A8	A(5,6,7)	122.1276	-DE/DX = 0.0	!

! A9	A(5,6,17)	119.4766	-DE/DX = 0.0	!
! A10	A(7,6,17)	118.3958	-DE/DX = 0.0	!
! A11	A(2,7,6)	118.7837	-DE/DX = 0.0	!
! A12	A(2,7,8)	120.5957	-DE/DX = 0.0	!
! A13	A(6,7,8)	120.6206	-DE/DX = 0.0	!
! A14	A(3,8,7)	130.1377	-DE/DX = 0.0	!
! A15	A(3,8,10)	115.2594	-DE/DX = 0.0	!
! A16	A(7,8,10)	114.6029	-DE/DX = 0.0	!
! A17	A(5,9,10)	119.0348	-DE/DX = 0.0	!
! A18	A(5,9,18)	119.8461	-DE/DX = 0.0	!
! A19	A(10,9,18)	121.119	-DE/DX = 0.0	!
! A20	A(8,10,9)	124.5997	-DE/DX = 0.0	!
! A21	A(8,10,19)	115.5529	-DE/DX = 0.0	!
! A22	A(9,10,19)	119.8474	-DE/DX = 0.0	!
! A23	A(12,11,15)	121.6689	-DE/DX = 0.0	!
! A24	A(12,11,20)	120.9405	-DE/DX = 0.0	!
! A25	A(15,11,20)	117.3906	-DE/DX = 0.0	!
! A26	A(11,12,13)	120.8567	-DE/DX = 0.0	!
! A27	A(11,12,21)	119.4068	-DE/DX = 0.0	!
! A28	A(13,12,21)	119.7365	-DE/DX = 0.0	!
! A29	A(12,13,14)	118.2896	-DE/DX = 0.0	!
! A30	A(12,13,22)	120.8623	-DE/DX = 0.0	!
! A31	A(14,13,22)	120.8481	-DE/DX = 0.0	!
! A32	A(13,14,16)	121.5671	-DE/DX = 0.0	!
! A33	A(13,14,23)	119.3346	-DE/DX = 0.0	!
! A34	A(16,14,23)	119.0983	-DE/DX = 0.0	!
! A35	A(4,15,11)	117.1484	-DE/DX = 0.0	!
! A36	A(4,15,16)	126.0419	-DE/DX = 0.0	!
! A37	A(11,15,16)	116.8097	-DE/DX = 0.0	!
! A38	A(14,16,15)	120.808	-DE/DX = 0.0	!

```
! A39   A(14,16,24)        121.0663       -DE/DX =    0.0             !
! A40   A(15,16,24)        118.1257       -DE/DX =    0.0             !
 ! D1    D(25,1,5,6)         0.0          -DE/DX =    0.0             !
 ! D2    D(25,1,5,9)       180.0          -DE/DX =    0.0             !
 ! D3    D(26,2,7,6)         0.0          -DE/DX =    0.0             !
 ! D4    D(26,2,7,8)       180.0          -DE/DX =    0.0             !
 ! D5    D(8,3,4,15)       180.0          -DE/DX =    0.0             !
 ! D6    D(4,3,8,7)          0.0          -DE/DX =    0.0             !
 ! D7    D(4,3,8,10)       180.0          -DE/DX =    0.0             !
 ! D8    D(3,4,15,11)      180.0          -DE/DX =    0.0             !
 ! D9    D(3,4,15,16)        0.0          -DE/DX =    0.0             !
 ! D10   D(1,5,6,7)        180.0          -DE/DX =    0.0             !
 ! D11   D(1,5,6,17)         0.0          -DE/DX =    0.0             !
 ! D12   D(9,5,6,7)          0.0          -DE/DX =    0.0             !
 ! D13   D(9,5,6,17)       180.0          -DE/DX =    0.0             !
 ! D14   D(1,5,9,10)       180.0          -DE/DX =    0.0             !
 ! D15   D(1,5,9,18)         0.0          -DE/DX =    0.0             !
 ! D16   D(6,5,9,10)         0.0          -DE/DX =    0.0             !
 ! D17   D(6,5,9,18)       180.0          -DE/DX =    0.0             !
 ! D18   D(5,6,7,2)        180.0          -DE/DX =    0.0             !
 ! D19   D(5,6,7,8)          0.0          -DE/DX =    0.0             !
 ! D20   D(17,6,7,2)         0.0          -DE/DX =    0.0             !
 ! D21   D(17,6,7,8)       180.0          -DE/DX =    0.0             !
 ! D22   D(2,7,8,3)          0.0          -DE/DX =    0.0             !
 ! D23   D(2,7,8,10)       180.0          -DE/DX =    0.0             !
 ! D24   D(6,7,8,3)        180.0          -DE/DX =    0.0             !
 ! D25   D(6,7,8,10)         0.0          -DE/DX =    0.0             !
 ! D26   D(3,8,10,9)       180.0          -DE/DX =    0.0             !
 ! D27   D(3,8,10,19)        0.0          -DE/DX =    0.0             !
 ! D28   D(7,8,10,9)         0.0          -DE/DX =    0.0             !
```

! D29	D(7,8,10,19)	180.0	-DE/DX = 0.0 !
! D30	D(5,9,10,8)	0.0	-DE/DX = 0.0 !
! D31	D(5,9,10,19)	180.0	-DE/DX = 0.0 !
! D32	D(18,9,10,8)	180.0	-DE/DX = 0.0 !
! D33	D(18,9,10,19)	0.0	-DE/DX = 0.0 !
! D34	D(15,11,12,13)	0.0	-DE/DX = 0.0 !
! D35	D(15,11,12,21)	180.0	-DE/DX = 0.0 !
! D36	D(20,11,12,13)	180.0	-DE/DX = 0.0 !
! D37	D(20,11,12,21)	0.0	-DE/DX = 0.0 !
! D38	D(12,11,15,4)	180.0	-DE/DX = 0.0 !
! D39	D(12,11,15,16)	0.0	-DE/DX = 0.0 !
! D40	D(20,11,15,4)	0.0	-DE/DX = 0.0 !
! D41	D(20,11,15,16)	180.0	-DE/DX = 0.0 !
! D42	D(11,12,13,14)	0.0	-DE/DX = 0.0 !
! D43	D(11,12,13,22)	180.0	-DE/DX = 0.0 !
! D44	D(21,12,13,14)	180.0	-DE/DX = 0.0 !
! D45	D(21,12,13,22)	0.0	-DE/DX = 0.0 !
! D46	D(12,13,14,16)	0.0	-DE/DX = 0.0 !
! D47	D(12,13,14,23)	180.0	-DE/DX = 0.0 !
! D48	D(22,13,14,16)	180.0	-DE/DX = 0.0 !
! D49	D(22,13,14,23)	0.0	-DE/DX = 0.0 !
! D50	D(13,14,16,15)	0.0	-DE/DX = 0.0 !
! D51	D(13,14,16,24)	180.0	-DE/DX = 0.0 !
! D52	D(23,14,16,15)	180.0	-DE/DX = 0.0 !
! D53	D(23,14,16,24)	0.0	-DE/DX = 0.0 !
! D54	D(4,15,16,14)	180.0	-DE/DX = 0.0 !
! D55	D(4,15,16,24)	0.0	-DE/DX = 0.0 !
! D56	D(11,15,16,14)	0.0	-DE/DX = 0.0 !
! D57	D(11,15,16,24)	180.0	-DE/DX = 0.0 !

Summary of Natural Population Analysis:

Natural Population

Atom	No	Natural Charge	Core	Valence	Rydberg	Total
O	1	-0.34721	0.99988	3.33644	0.01088	4.34721
O	2	-0.32015	0.99987	3.30722	0.01305	4.32015
N	3	-0.05628	0.99969	2.53478	0.02180	3.55628
N	4	-0.05498	0.99969	2.53402	0.02128	3.55498
C	5	0.20167	0.99935	1.78773	0.01125	2.79833
C	6	-0.20813	0.99949	2.19840	0.01024	3.20813
C	7	0.20679	0.99937	1.78114	0.01269	2.79321
C	8	0.01357	0.99947	1.97300	0.01397	2.98643
C	9	-0.17556	0.99951	2.16558	0.01048	3.17556
C	10	-0.03725	0.99956	2.02741	0.01028	3.03725
C	11	-0.07265	0.99953	2.06234	0.01078	3.07265
C	12	-0.12922	0.99957	2.11918	0.01046	3.12922
C	13	-0.07494	0.99957	2.06393	0.01144	3.07494
C	14	-0.13085	0.99958	2.12076	0.01051	3.13085
C	15	0.05696	0.99951	1.92889	0.01464	2.94304
C	16	-0.06582	0.99953	2.05648	0.00982	3.06582
H	17	0.08373	0.00000	0.41426	0.00202	0.41627
H	18	0.09882	0.00000	0.39992	0.00127	0.40118
H	19	0.09756	0.00000	0.40033	0.00211	0.40244
H	20	0.09606	0.00000	0.40217	0.00177	0.40394
H	21	0.08919	0.00000	0.40950	0.00131	0.41081
H	22	0.08700	0.00000	0.41173	0.00127	0.41300
H	23	0.08876	0.00000	0.40995	0.00129	0.41124
H	24	0.10369	0.00000	0.39357	0.00274	0.39631
H	25	0.22837	0.00000	0.26960	0.00203	0.27163
H	26	0.22087	0.00000	0.27684	0.00229	0.27913

==========

 * Total * 0.00000 15.99317 39.78517 0.22166 56.00000

Natural Population

Core	15.99317 (99.9573% of 16)
Valence	39.78517 (99.4629% of 40)
Natural Minimal Basis	55.77834 (99.6042% of 56)
Natural Rydberg Basis	0.22166 (0.3958% of 56)

Figure B.14: Natural Bond Orbital analysis for the trans 2,4-Dihydroxyazobenzene,4-(Phenylazo) resorcinol anion. (a) LUMO +1 (b) LUMO (c) HOMO (d) HOMO − 1. IsoValue = 0.02 and the Density = 0.0004.

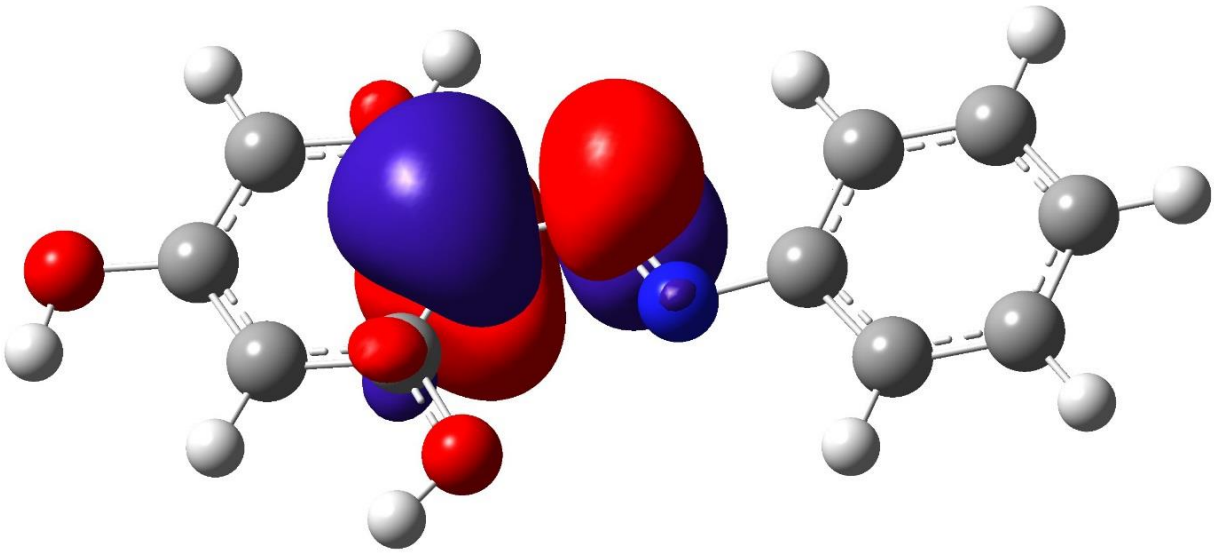

(a)

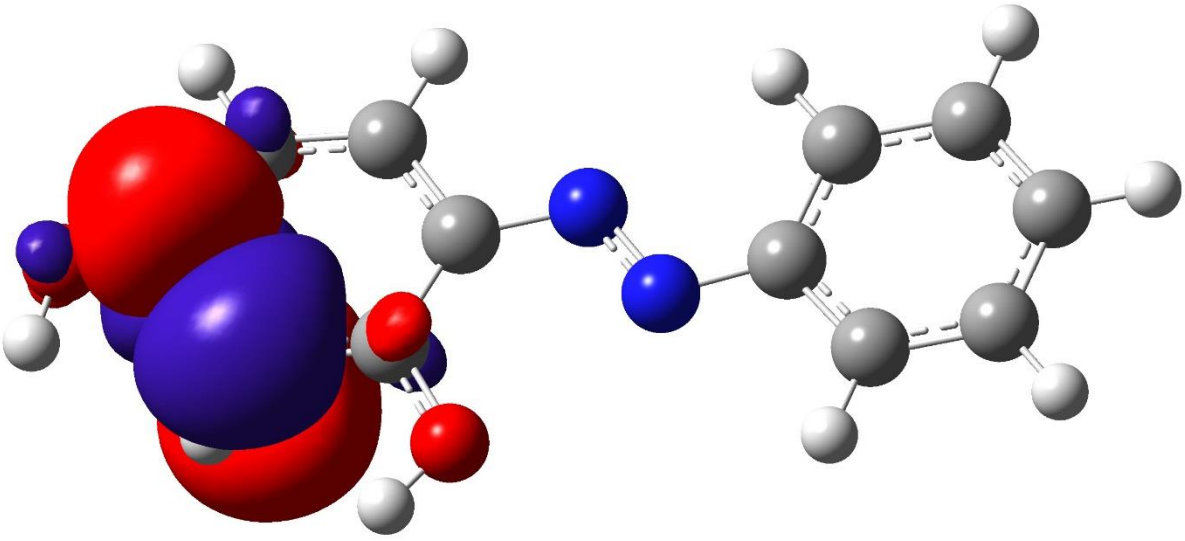

(b)

Figure B.14: Continued

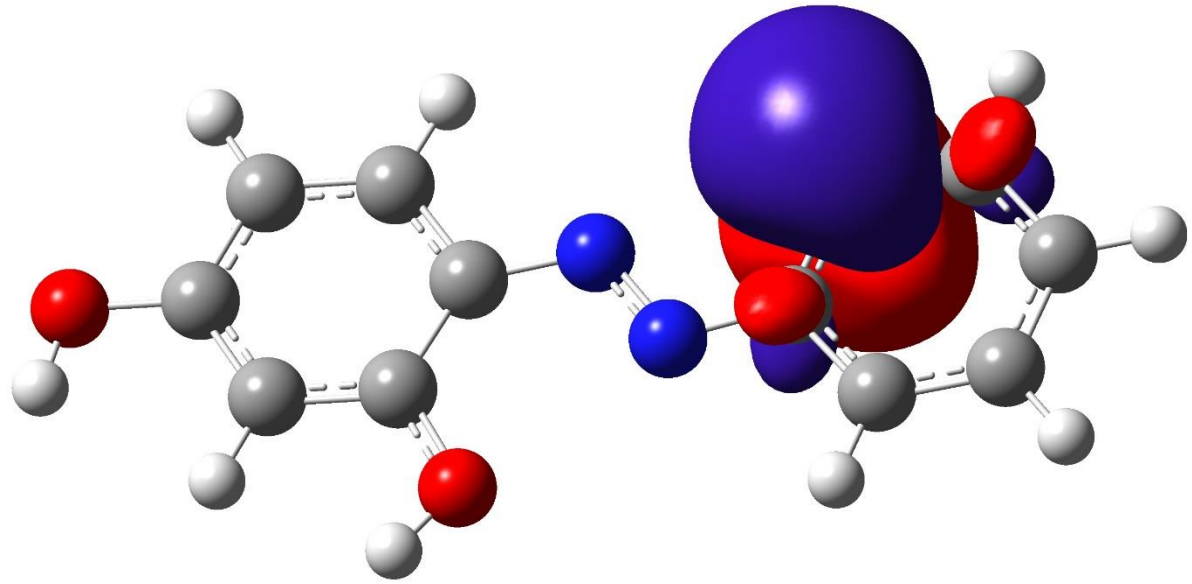

(c)

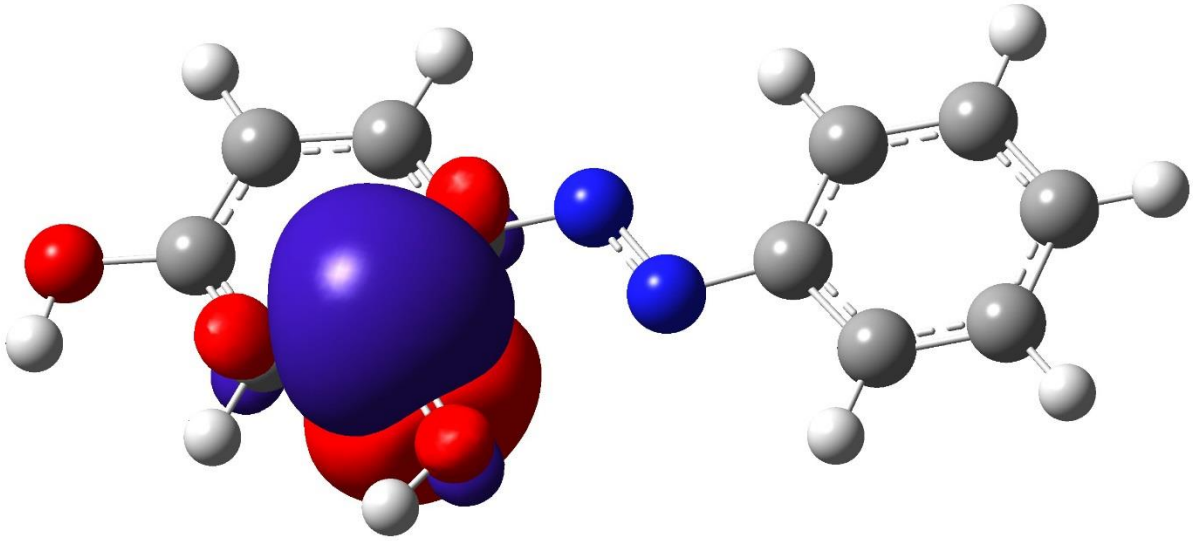

(d)

Figure B.14: Continued

B.8 4-Dimethylamino-2-methylazobenzene

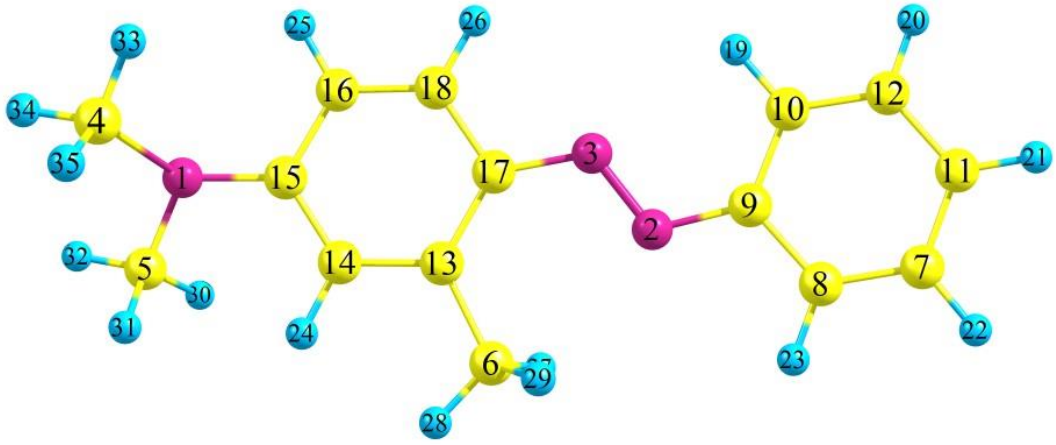

Figure B.15: Optimized Geometry of trans 4-Dimethylamino-2-methylazobenzene anion using B3LYP level of theory along with 6-311++G(2d,2p) basis set.

! Optimized Parameters !

! (Angstroms and Degrees) !

! Name	Definition	Value	Derivative Info.
! R1	R(1,4)	1.4583	-DE/DX = 0.0 !
! R2	R(1,5)	1.4486	-DE/DX = 0.0 !
! R3	R(1,15)	1.4367	-DE/DX = 0.0 !
! R4	R(2,3)	1.326	-DE/DX = 0.0 !
! R5	R(2,9)	1.3719	-DE/DX = 0.0 !
! R6	R(3,17)	1.3713	-DE/DX = 0.0 !
! R7	R(4,33)	1.0866	-DE/DX = 0.0 !
! R8	R(4,34)	1.0929	-DE/DX = 0.0 !
! R9	R(4,35)	1.1039	-DE/DX = 0.0 !
! R10	R(5,30)	1.0888	-DE/DX = 0.0 !

! R11	R(5,31)	1.1039	-DE/DX = 0.0	!
! R12	R(5,32)	1.092	-DE/DX = 0.0	!
! R13	R(6,13)	1.5101	-DE/DX = 0.0	!
! R14	R(6,27)	1.0893	-DE/DX = 0.0	!
! R15	R(6,28)	1.0938	-DE/DX = 0.0	!
! R16	R(6,29)	1.089	-DE/DX = 0.0	!
! R17	R(7,8)	1.3836	-DE/DX = 0.0	!
! R18	R(7,11)	1.401	-DE/DX = 0.0	!
! R19	R(7,22)	1.0843	-DE/DX = 0.0	!
! R20	R(8,9)	1.4184	-DE/DX = 0.0	!
! R21	R(8,23)	1.0827	-DE/DX = 0.0	!
! R22	R(9,10)	1.4228	-DE/DX = 0.0	!
! R23	R(10,12)	1.3854	-DE/DX = 0.0	!
! R24	R(10,19)	1.079	-DE/DX = 0.0	!
! R25	R(11,12)	1.3986	-DE/DX = 0.0	!
! R26	R(11,21)	1.0823	-DE/DX = 0.0	!
! R27	R(12,20)	1.0851	-DE/DX = 0.0	!
! R28	R(13,14)	1.3984	-DE/DX = 0.0	!
! R29	R(13,17)	1.4347	-DE/DX = 0.0	!
! R30	R(14,15)	1.3967	-DE/DX = 0.0	!
! R31	R(14,24)	1.0826	-DE/DX = 0.0	!
! R32	R(15,16)	1.4039	-DE/DX = 0.0	!
! R33	R(16,18)	1.3761	-DE/DX = 0.0	!
! R34	R(16,25)	1.0833	-DE/DX = 0.0	!
! R35	R(17,18)	1.4225	-DE/DX = 0.0	!
! R36	R(18,26)	1.0819	-DE/DX = 0.0	!
! A1	A(4,1,5)	111.2482	-DE/DX = 0.0	!
! A2	A(4,1,15)	114.3777	-DE/DX = 0.0	!
! A3	A(5,1,15)	116.3621	-DE/DX = 0.0	!
! A4	A(3,2,9)	114.1006	-DE/DX = 0.0	!

! A5	A(2,3,17)	117.361	-DE/DX = 0.0	!
! A6	A(1,4,33)	110.2244	-DE/DX = 0.0	!
! A7	A(1,4,34)	109.7089	-DE/DX = 0.0	!
! A8	A(1,4,35)	112.4314	-DE/DX = 0.0	!
! A9	A(33,4,34)	108.3153	-DE/DX = 0.0	!
! A10	A(33,4,35)	107.8646	-DE/DX = 0.0	!
! A11	A(34,4,35)	108.1811	-DE/DX = 0.0	!
! A12	A(1,5,30)	110.0085	-DE/DX = 0.0	!
! A13	A(1,5,31)	113.7316	-DE/DX = 0.0	!
! A14	A(1,5,32)	109.0087	-DE/DX = 0.0	!
! A15	A(30,5,31)	108.0659	-DE/DX = 0.0	!
! A16	A(30,5,32)	108.4455	-DE/DX = 0.0	!
! A17	A(31,5,32)	107.431	-DE/DX = 0.0	!
! A18	A(13,6,27)	111.8087	-DE/DX = 0.0	!
! A19	A(13,6,28)	109.7283	-DE/DX = 0.0	!
! A20	A(13,6,29)	111.8527	-DE/DX = 0.0	!
! A21	A(27,6,28)	108.9938	-DE/DX = 0.0	!
! A22	A(27,6,29)	105.2594	-DE/DX = 0.0	!
! A23	A(28,6,29)	109.0616	-DE/DX = 0.0	!
! A24	A(8,7,11)	120.8207	-DE/DX = 0.0	!
! A25	A(8,7,22)	119.4103	-DE/DX = 0.0	!
! A26	A(11,7,22)	119.769	-DE/DX = 0.0	!
! A27	A(7,8,9)	121.6583	-DE/DX = 0.0	!
! A28	A(7,8,23)	120.7217	-DE/DX = 0.0	!
! A29	A(9,8,23)	117.62	-DE/DX = 0.0	!
! A30	A(2,9,8)	117.3116	-DE/DX = 0.0	!
! A31	A(2,9,10)	125.8362	-DE/DX = 0.0	!
! A32	A(8,9,10)	116.8523	-DE/DX = 0.0	!
! A33	A(9,10,12)	120.7945	-DE/DX = 0.0	!
! A34	A(9,10,19)	118.0847	-DE/DX = 0.0	!

! A35	A(12,10,19)	121.1208	-DE/DX = 0.0	!
! A36	A(7,11,12)	118.3242	-DE/DX = 0.0	!
! A37	A(7,11,21)	120.8381	-DE/DX = 0.0	!
! A38	A(12,11,21)	120.8378	-DE/DX = 0.0	!
! A39	A(10,12,11)	121.5501	-DE/DX = 0.0	!
! A40	A(10,12,20)	119.0984	-DE/DX = 0.0	!
! A41	A(11,12,20)	119.3515	-DE/DX = 0.0	!
! A42	A(6,13,14)	117.3382	-DE/DX = 0.0	!
! A43	A(6,13,17)	123.8648	-DE/DX = 0.0	!
! A44	A(14,13,17)	118.7962	-DE/DX = 0.0	!
! A45	A(13,14,15)	123.9584	-DE/DX = 0.0	!
! A46	A(13,14,24)	116.8302	-DE/DX = 0.0	!
! A47	A(15,14,24)	119.2112	-DE/DX = 0.0	!
! A48	A(1,15,14)	123.6085	-DE/DX = 0.0	!
! A49	A(1,15,16)	119.261	-DE/DX = 0.0	!
! A50	A(14,15,16)	117.1206	-DE/DX = 0.0	!
! A51	A(15,16,18)	120.3921	-DE/DX = 0.0	!
! A52	A(15,16,25)	119.7102	-DE/DX = 0.0	!
! A53	A(18,16,25)	119.8873	-DE/DX = 0.0	!
! A54	A(3,17,13)	129.902	-DE/DX = 0.0	!
! A55	A(3,17,18)	113.8721	-DE/DX = 0.0	!
! A56	A(13,17,18)	116.2244	-DE/DX = 0.0	!
! A57	A(16,18,17)	123.4944	-DE/DX = 0.0	!
! A58	A(16,18,26)	120.2291	-DE/DX = 0.0	!
! A59	A(17,18,26)	116.2679	-DE/DX = 0.0	!
! D1	D(5,1,4,33)	-177.7376	-DE/DX = 0.0	!
! D2	D(5,1,4,34)	-58.5476	-DE/DX = 0.0	!
! D3	D(5,1,4,35)	61.88	-DE/DX = 0.0	!
! D4	D(15,1,4,33)	47.894	-DE/DX = 0.0	!
! D5	D(15,1,4,34)	167.0841	-DE/DX = 0.0	!

! D6	D(15,1,4,35)	-72.4884	-DE/DX =	0.0 !
! D7	D(4,1,5,30)	175.8416	-DE/DX =	0.0 !
! D8	D(4,1,5,31)	-62.7858	-DE/DX =	0.0 !
! D9	D(4,1,5,32)	57.0522	-DE/DX =	0.0 !
! D10	D(15,1,5,30)	-50.7686	-DE/DX =	0.0 !
! D11	D(15,1,5,31)	70.6039	-DE/DX =	0.0 !
! D12	D(15,1,5,32)	-169.5581	-DE/DX =	0.0 !
! D13	D(4,1,15,14)	115.6353	-DE/DX =	0.0 !
! D14	D(4,1,15,16)	-65.5418	-DE/DX =	0.0 !
! D15	D(5,1,15,14)	-16.3264	-DE/DX =	0.0 !
! D16	D(5,1,15,16)	162.4964	-DE/DX =	0.0 !
! D17	D(9,2,3,17)	-179.9226	-DE/DX =	0.0 !
! D18	D(3,2,9,8)	-179.9386	-DE/DX =	0.0 !
! D19	D(3,2,9,10)	0.0741	-DE/DX =	0.0 !
! D20	D(2,3,17,13)	-0.1671	-DE/DX =	0.0 !
! D21	D(2,3,17,18)	-179.6827	-DE/DX =	0.0 !
! D22	D(27,6,13,14)	121.2149	-DE/DX =	0.0 !
! D23	D(27,6,13,17)	-59.1321	-DE/DX =	0.0 !
! D24	D(28,6,13,14)	0.1565	-DE/DX =	0.0 !
! D25	D(28,6,13,17)	179.8095	-DE/DX =	0.0 !
! D26	D(29,6,13,14)	-121.0166	-DE/DX =	0.0 !
! D27	D(29,6,13,17)	58.6364	-DE/DX =	0.0 !
! D28	D(11,7,8,9)	0.0063	-DE/DX =	0.0 !
! D29	D(11,7,8,23)	179.9933	-DE/DX =	0.0 !
! D30	D(22,7,8,9)	-179.9908	-DE/DX =	0.0 !
! D31	D(22,7,8,23)	-0.0039	-DE/DX =	0.0 !
! D32	D(8,7,11,12)	-0.0012	-DE/DX =	0.0 !
! D33	D(8,7,11,21)	179.997	-DE/DX =	0.0 !
! D34	D(22,7,11,12)	179.9959	-DE/DX =	0.0 !
! D35	D(22,7,11,21)	-0.0059	-DE/DX =	0.0 !

! D36	D(7,8,9,2)	-179.9933	-DE/DX =	0.0 !
! D37	D(7,8,9,10)	-0.0048	-DE/DX =	0.0 !
! D38	D(23,8,9,2)	0.0194	-DE/DX =	0.0 !
! D39	D(23,8,9,10)	-179.9921	-DE/DX =	0.0 !
! D40	D(2,9,10,12)	179.9856	-DE/DX =	0.0 !
! D41	D(2,9,10,19)	-0.0098	-DE/DX =	0.0 !
! D42	D(8,9,10,12)	-0.0017	-DE/DX =	0.0 !
! D43	D(8,9,10,19)	-179.9972	-DE/DX =	0.0 !
! D44	D(9,10,12,11)	0.0068	-DE/DX =	0.0 !
! D45	D(9,10,12,20)	-179.9967	-DE/DX =	0.0 !
! D46	D(19,10,12,11)	-179.9978	-DE/DX =	0.0 !
! D47	D(19,10,12,20)	-0.0014	-DE/DX =	0.0 !
! D48	D(7,11,12,10)	-0.0054	-DE/DX =	0.0 !
! D49	D(7,11,12,20)	179.9982	-DE/DX =	0.0 !
! D50	D(21,11,12,10)	179.9965	-DE/DX =	0.0 !
! D51	D(21,11,12,20)	0.0	-DE/DX =	0.0 !
! D52	D(6,13,14,15)	-179.2774	-DE/DX =	0.0 !
! D53	D(6,13,14,24)	0.5598	-DE/DX =	0.0 !
! D54	D(17,13,14,15)	1.0514	-DE/DX =	0.0 !
! D55	D(17,13,14,24)	-179.1114	-DE/DX =	0.0 !
! D56	D(6,13,17,3)	-0.177	-DE/DX =	0.0 !
! D57	D(6,13,17,18)	179.3293	-DE/DX =	0.0 !
! D58	D(14,13,17,3)	179.4713	-DE/DX =	0.0 !
! D59	D(14,13,17,18)	-1.0225	-DE/DX =	0.0 !
! D60	D(13,14,15,1)	178.7562	-DE/DX =	0.0 !
! D61	D(13,14,15,16)	-0.09	-DE/DX =	0.0 !
! D62	D(24,14,15,1)	-1.0773	-DE/DX =	0.0 !
! D63	D(24,14,15,16)	-179.9235	-DE/DX =	0.0 !
! D64	D(1,15,16,18)	-179.7628	-DE/DX =	0.0 !
! D65	D(1,15,16,25)	-0.9351	-DE/DX =	0.0 !

! D66	D(14,15,16,18)	-0.8643	-DE/DX =	0.0 !
! D67	D(14,15,16,25)	177.9634	-DE/DX =	0.0 !
! D68	D(15,16,18,17)	0.8658	-DE/DX =	0.0 !
! D69	D(15,16,18,26)	179.7635	-DE/DX =	0.0 !
! D70	D(25,16,18,17)	-177.9598	-DE/DX =	0.0 !
! D71	D(25,16,18,26)	0.9379	-DE/DX =	0.0 !
! D72	D(3,17,18,16)	179.6922	-DE/DX =	0.0 !
! D73	D(3,17,18,26)	0.7543	-DE/DX =	0.0 !
! D74	D(13,17,18,16)	0.1064	-DE/DX =	0.0 !
! D75	D(13,17,18,26)	-178.8315	-DE/DX =	0.0 !

Summary of Natural Population Analysis:

Natural Population

Atom	No	Natural Charge	Core	Valence	Rydberg	Total
N	1	-0.54869	1.99938	5.51374	0.03557	7.54869
N	2	-0.38806	1.99939	5.34350	0.04518	7.38806
N	3	-0.37696	1.99938	5.33286	0.04472	7.37696
C	4	-0.33748	1.99929	4.32441	0.01378	6.33748
C	5	-0.34868	1.99932	4.33385	0.01551	6.34868
C	6	-0.57616	1.99927	4.56507	0.01181	6.57616
C	7	-0.22630	1.99914	4.20597	0.02118	6.22630
C	8	-0.22527	1.99906	4.20437	0.02185	6.22527

C	9	0.13089	1.99902	3.84046	0.02963	5.86911
C	10	-0.25538	1.99905	4.23386	0.02246	6.25538
C	11	-0.29188	1.99915	4.26664	0.02610	6.29188
C	12	-0.21105	1.99915	4.19119	0.02071	6.21105
C	13	-0.07115	1.99903	4.04863	0.02349	6.07115
C	14	-0.21461	1.99898	4.20251	0.01312	6.21461
C	15	0.10203	1.99894	3.87329	0.02573	5.89797
C	16	-0.25089	1.99903	4.23136	0.02050	6.25089
C	17	0.12264	1.99892	3.84885	0.02958	5.87736
C	18	-0.18942	1.99908	4.16847	0.02187	6.18942
H	19	0.21433	0.00000	0.78151	0.00416	0.78567
H	20	0.17759	0.00000	0.81991	0.00250	0.82241
H	21	0.17960	0.00000	0.81780	0.00260	0.82040
H	22	0.17886	0.00000	0.81858	0.00256	0.82114
H	23	0.19241	0.00000	0.80445	0.00314	0.80759
H	24	0.18063	0.00000	0.81670	0.00266	0.81937
H	25	0.18671	0.00000	0.81041	0.00288	0.81329
H	26	0.19743	0.00000	0.79931	0.00326	0.80257
H	27	0.21636	0.00000	0.77995	0.00369	0.78364
H	28	0.16591	0.00000	0.83152	0.00256	0.83409
H	29	0.21698	0.00000	0.77931	0.00371	0.78302
H	30	0.19688	0.00000	0.80054	0.00258	0.80312
H	31	0.15433	0.00000	0.84167	0.00400	0.84567
H	32	0.17685	0.00000	0.82063	0.00251	0.82315
H	33	0.19594	0.00000	0.80202	0.00204	0.80406
H	34	0.17037	0.00000	0.82700	0.00262	0.82963
H	35	0.15526	0.00000	0.84075	0.00399	0.84474

==========

* Total *	-0.99995	35.98459	92.52111	0.49426	128.99995

Natural Population

Core	35.98459 (99.9572% of 36)
Valence	92.52111 (99.4851% of 93)
Natural Minimal Basis	128.50570 (99.6168% of 129)
Natural Rydberg Basis	0.49426 (0.3831% of 129)

Figure B.16: Natural Bond Orbital analysis for the trans -Dimethylamino-2-methylazobenzene anion. (a) LUMO +1 (b) LUMO (c) HOMO (d) HOMO – 1. IsoValue = 0.02 and the Density = 0.0004.

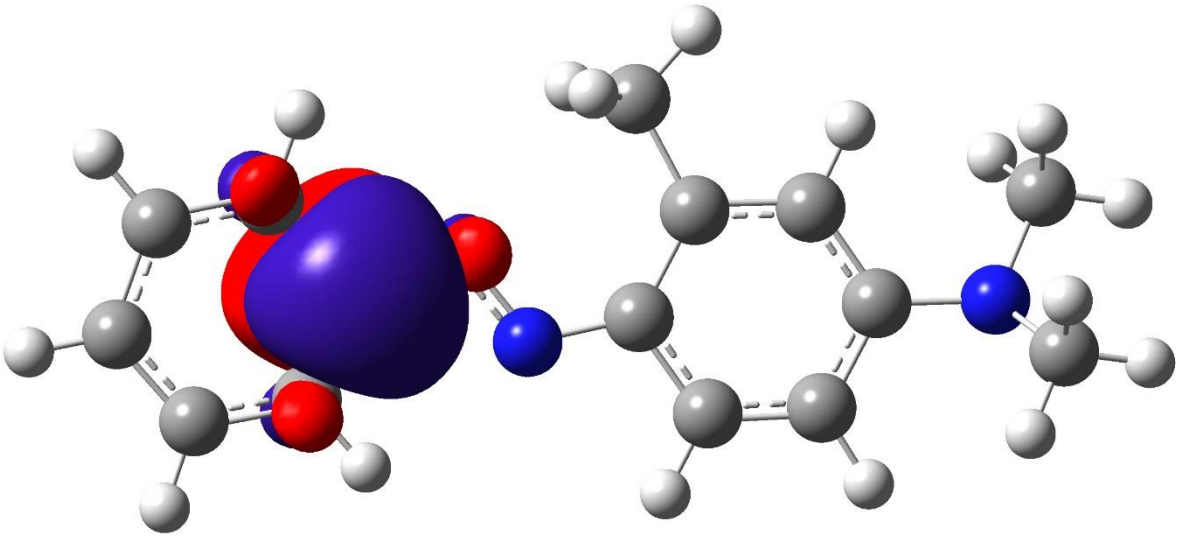

(a)

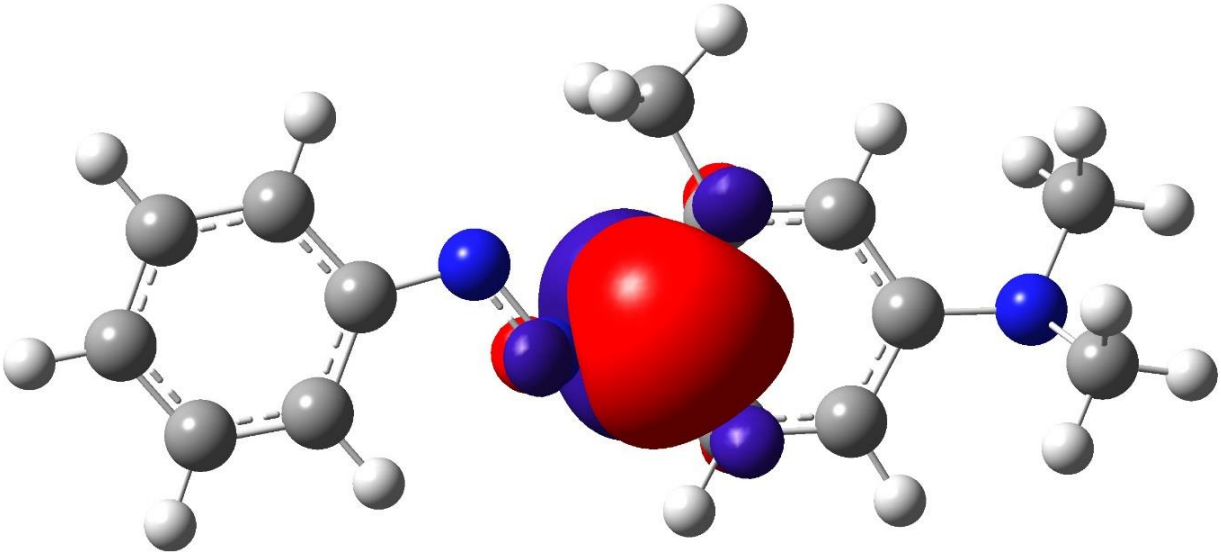

(b)

Figure B.16: Continued

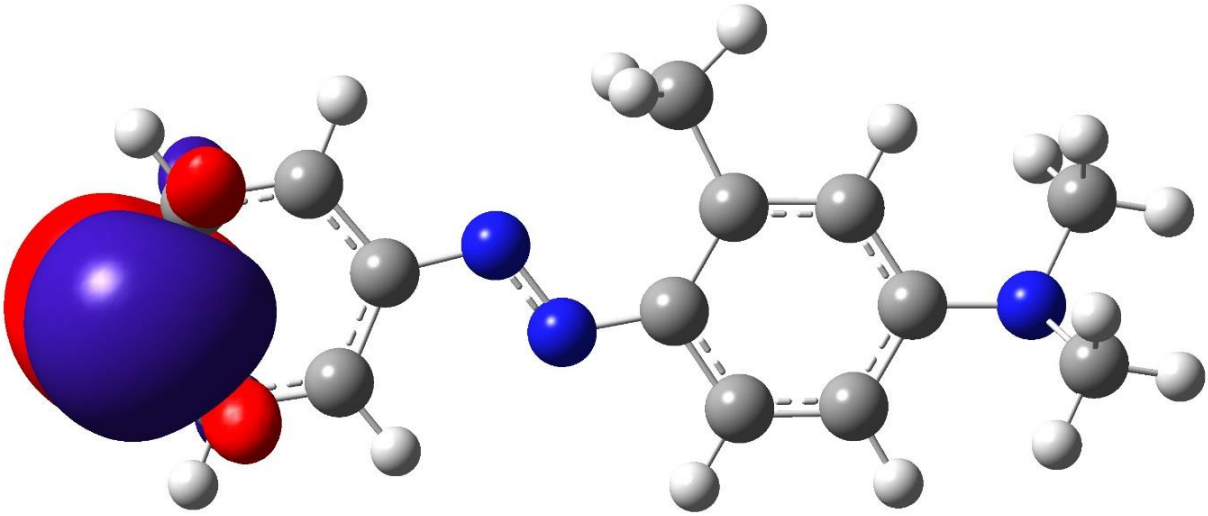

(c)

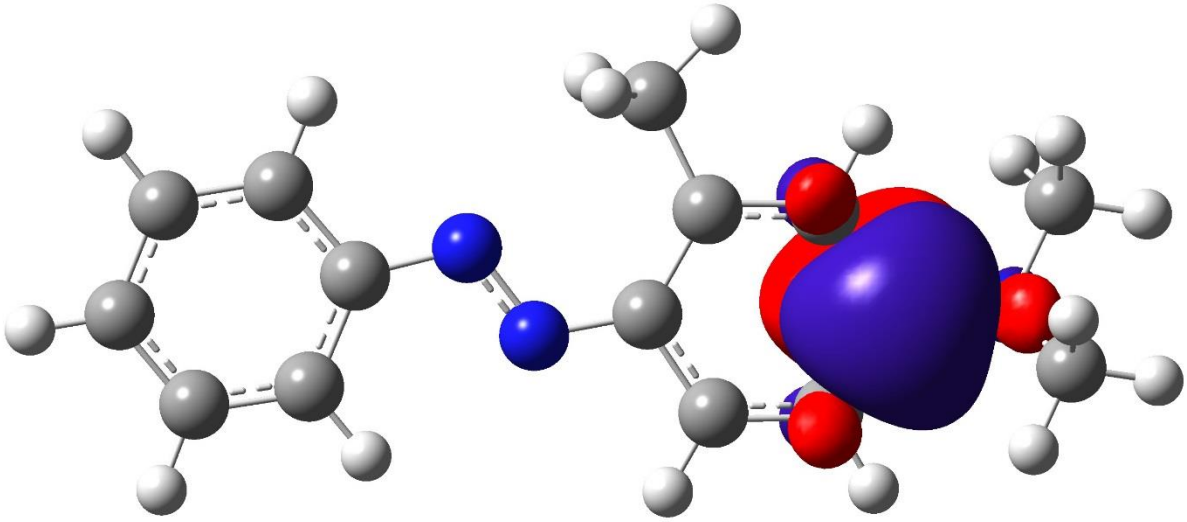

(d)

Figure B.16: Continued

Vita

Mohammadreza Rezaee was born in Babol, Iran on September 16, 1981. He graduated with a BSc in Atomic Physics from Shiraz University in 2005. He ranked 25th among 1028 nationwide participants in Matriculation exam for Master's degree held in 2005 in the field of Photonics and entered Laser and Plasma Research Institute, Shahid Beheshti University, Tehran, Iran. He graduated in 2008 with a Master's degree in Photonics. He started his PhD in Physics in University of Tennessee at Knoxville in 2010 and graduated in summer 2015.